BULLETIN 96

MAGMA GENESIS
1977

PROCEEDINGS OF THE AMERICAN GEOPHYSICAL UNION
CHAPMAN CONFERENCE ON PARTIAL MELTING
IN THE EARTH'S UPPER MANTLE

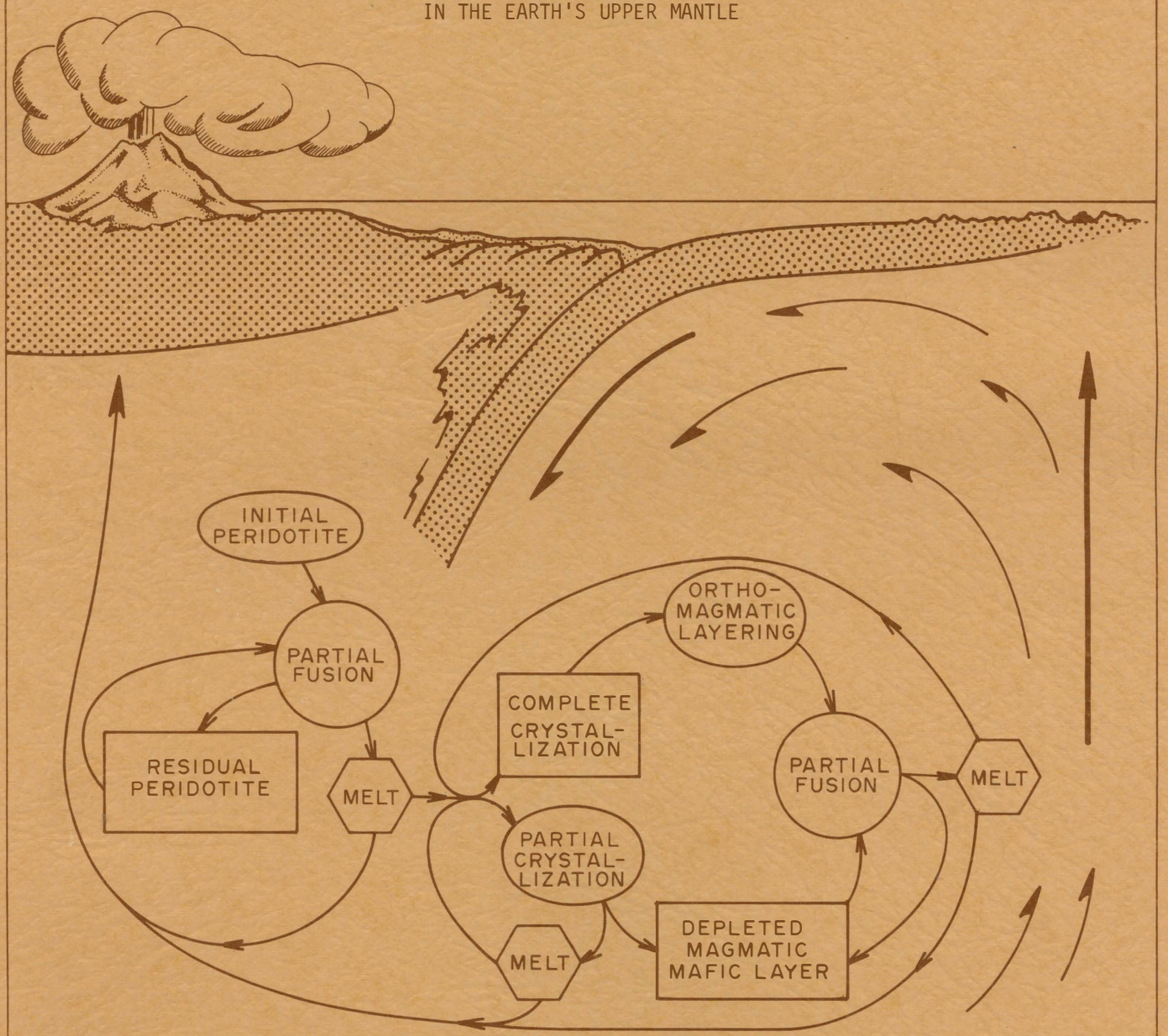

STATE OF OREGON
DEPARTMENT OF GEOLOGY AND MINERAL INDUSTRIES
RALPH S. MASON, STATE GEOLOGIST

STATE OF OREGON
DEPARTMENT OF GEOLOGY AND MINERAL INDUSTRIES
1069 State Office Building, Portland, Oregon 97201

BULLETIN 96

MAGMA GENESIS

PROCEEDINGS OF THE AMERICAN GEOPHYSICAL UNION
CHAPMAN CONFERENCE ON PARTIAL MELTING
IN THE EARTH'S UPPER MANTLE

Henry J. B. Dick, Editor
Woods Hole Oceanographic Institution

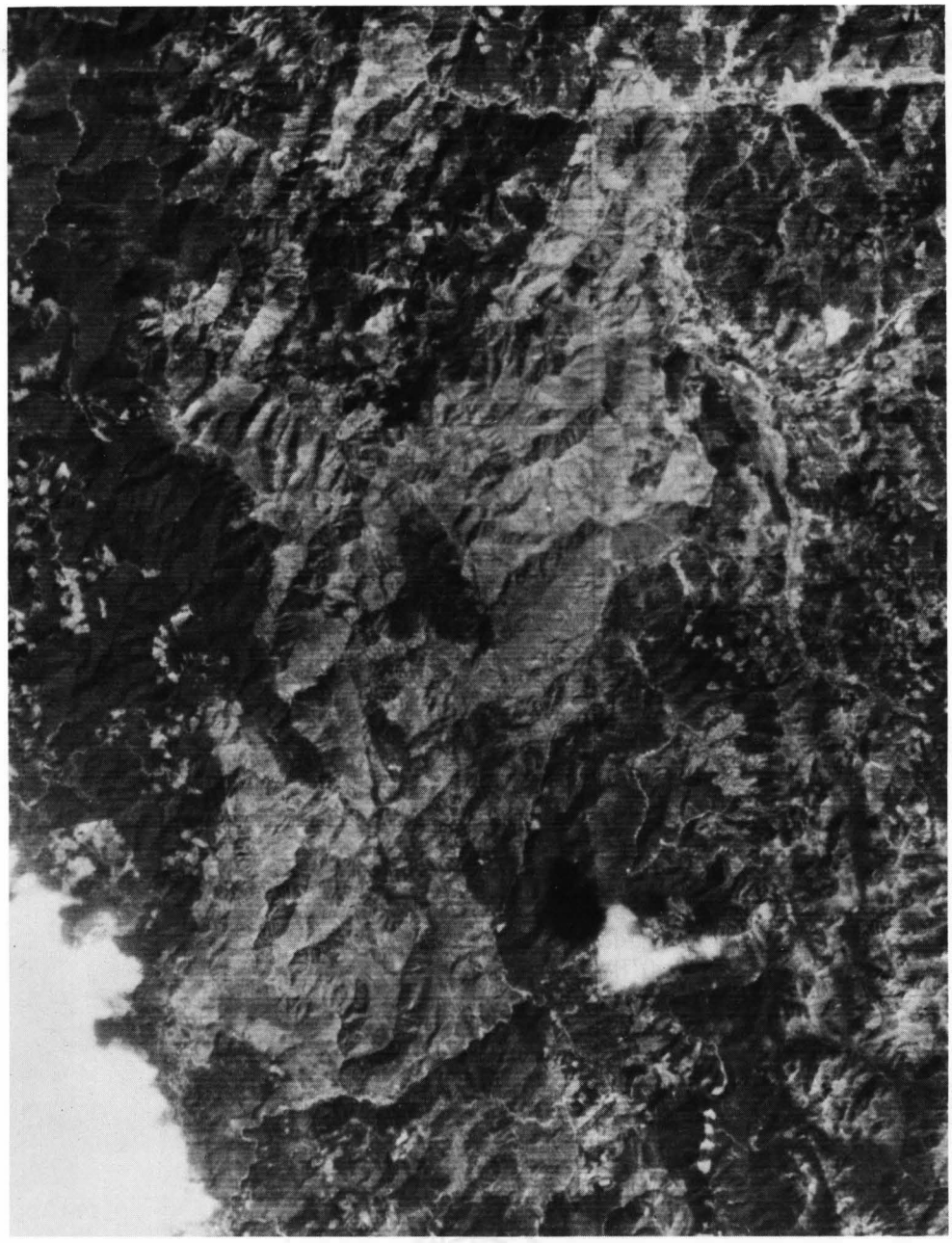

Frontispiece - Satellite view of the Josephine Peridotite, southwestern Oregon and northern California. The peridotite is plainly outlined by the more densely vegetated greywackes and volcanics surrounding it. The peridotite is an alpine-type harzburgite massif covering approximately 640 km^2. The peridotite was the location of the Chapman Conference on Partial Melting in the Earth's Upper Mantle, Sept. 10-14th 1976. The photograph is approximately 50 km across.

FOREWORD

The American Geophysical Union Chapman Conference on Partial Melting in the Earth's Upper Mantle was held September 10-14th, 1976 in southwestern Oregon. The conference included a one day meeting in Brookings Oregon and a 3 1/2 day field trip to the Josephine Peridotite. Fifty-two scientists and students from the U.S. and abroad attended and twenty-four papers were presented.

The purpose of the conference was to bring together scientists working on the processes involved in the formation of magmas in the laboratory with those workers who are looking for evidence of magma generation in the field. The Josephine Peridotite was chosen as the site for the conference as it consists of some 640 km^2 of relatively fresh upper mantle peridotite. This peridotite massif contains many features which may be products of the melting process, and has been studied in some detail by the convenor.

This volume presents the results of the Chapman Conference with the intent of providing a review of current and past research on magma generation. The papers cover a diversity of topics and should provide the reader with a fairly broad perspective on the problems involved in studying the origin of magmas.

ACKNOWLEDGEMENTS

The organizers of this conference would like to express their thanks to the numerous individuals who made the first AGU Chapman field conference a success. These include Mr. R. E. Corcoran of the Oregon Department of Geology and Mineral Industries, Dr. Fred Spilhaus and Cindy Beadling of the American Geophysical Union, Mr. Don Hinton of Wilderness Pack Trips, Mr. Russel Kahre, district ranger for the U.S. Forest Service, and Dr. Arthur Maxwell and Maureen Greenawalt of the Woods Hole Oceanographic Institution. A special note of thanks goes to Bob Coleman of the U.S. Geological Survey for an excellent discussion of the geology of the Oregon Coast Ranges which he presented to the conference during the field trip. Sandra Tonge of the Woods Hole Oceanographic Institution typed and prepared the photo-ready copy of all manuscripts for publication. The conference was supported by a grant from the National Science Foundation (EAR 76-22658).

* * * * *

The Oregon Department of Geology and Mineral Industries has agreed to publish these papers because the subject matter is consistent with the mission of the Department. The usual style and standards for this series have been modified to accommodate the style used by the editor of this bulletin. To facilitate timely distribution of information, camera-ready copy submitted by the editor has not been edited by the staff of the Department of Geology and Mineral Industries.

CONTENTS

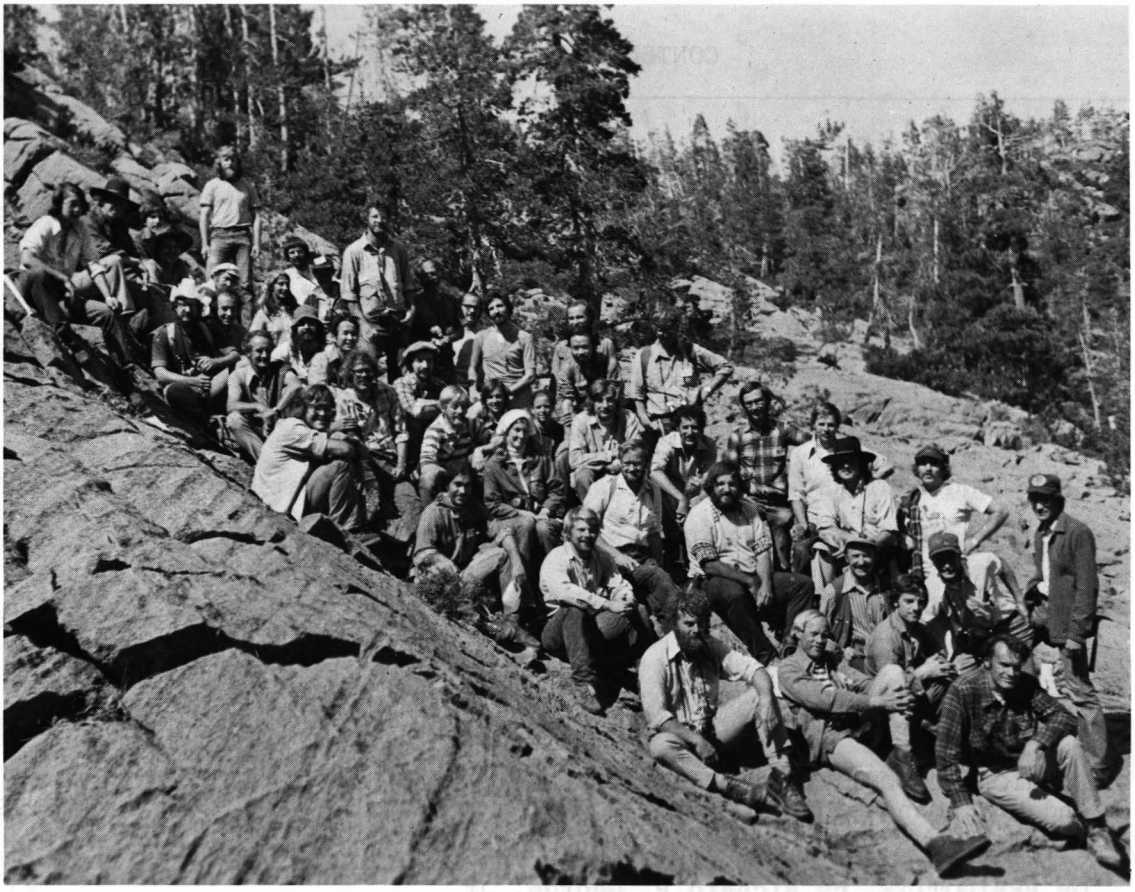

Chapman Conference for Partial Melting in the Earth's Upper Mantle standing on compositionally banded harzburgite of the Josephine Peridotite. Conference participants included: Jagan Akella, Richard J. Arculus, Rodey Batiza, Francoise Boudier, Robert G. Coleman, Donald J. DePaolo, Henry J.B. Dick, John S. Dickey, Mary M. Donato, Michael A. Dungan, David H. Eggler, Martin Engi, Bernard W. Evans, Russel Evarts, Mark Ferns, Patrick Fung, Richard P. George, H.W. Green, Jeffrey K. Greenberg, Rosalind Helz, Albrecht Hofmann, Neil Irvine, A.J. Irving, H.M. Iyer, David A. Johnston, M. Allan Kays, Charles H. Langmuir, William P. Leeman, Thomas D. Light, Nancy Lindsley-Griffin, L. Gordon Medaris, Martin Menzies, Peter J. Michael, Maw Suen Ma, Ellen D. Mullen, A.V. Murali, Dennis O. Nelson, Masaaki Obata, Michael J. O'Hara, Philip M. Orville, Elaine R. Padovani, Norman Peterson, Chandra Shekhar Rai, Len Ramp, John B. Reid, John R. Sans, Motoaki Sato, Thomas J. Shankland, Dennis M. Shaw, John M. Sinton, and Geoffrey Woods.

1. EXPERIMENTAL MELTING STUDIES

SOLUBILITY OF VOLATILES IN SILICATE MELTS UNDER THE PRESSURE AND TEMPERATURE CONDITIONS OF PARTIAL MELTING IN THE UPPER MANTLE

Bjørn O. Mysen
Geophysical Laboratory
Carnegie Institution of Washington
Washington, D.C. 20008

Abstract

Available data on the solubility of H_2O, CO_2, and SO_2 in silicate melts at high pressure are reviewed. It is emphasized that (1) the solubility of H_2O is several times greater than that of both CO_2 and SO_2; (2) the solubility of H_2O is essentially dependent only on pressure, whereas the solubilities of CO_2 and SO_2 probably depend on temperature and bulk composition in addition to pressure. The solubilities of carbon dioxide and sulfur dioxide increase with both increasing pressure and increasing temperature. The solubility of CO_2, and possibly that of SO_2, are also positively correlated with the basicity of the melt.

Because of the large difference in the solubility of H_2O, CO_2, and SO_2, partial melting of a volatile-bearing mantle will result in a residue that is most strongly enriched in the volatile component that is the least soluble in silicate melt. Such vapor fractionation becomes more effective the more acidic the magma.

Some models of partial melting and fractional crystallization in a volatile-bearing upper mantle are reviewed in the light of solubility mechanisms of H_2O and CO_2 in silicate melts and the different relative solubilities of the volatile components in the melts.

Introduction

Evidence from fluid inclusions in mantle-derived minerals and the presence of hydrous and carbonate minerals (see *Irving and Wyllie*, 1975, for review) indicate the presence of CO_2 and H_2O in the mantle. The predominant species in volcanic gases are H_2O, CO_2, and SO_2 (*Nordlie*, 1971; *Anderson*, 1975; *Gerlach and Nordlie*, 1975a,b,c), suggesting that SO_2, in addition to CO_2 and H_2O, may occur in the upper mantle.

Data on phase relations of volatile-bearing silicate systems relevant to partial melting in the upper mantle have led to the suggestion that H_2O and CO_2 may be important in controlling the compositions of partial melts of volatile-bearing peridotite at high pressure and temperature (*Kushiro, Yoder, and Nishikawa*, 1968; *Kushiro*, 1969, 1972, 1975; *Eggler*, 1973, 1974, 1975, 1976; *Mysen and Boettcher*, 1975a,b; *Huang and Wyllie*, 1974; *Wyllie and Huang*, 1975, 1976; *Brey and Green*, 1975). Data on the solubility of the volatiles in silicate melts and an understanding of the solubility mechanisms are necessary for evaluating models of magma

genesis in the upper mantle. This paper presents a review of recent data on the solubility of volatiles in such melts and gives comments on some models for magma generation (partial melting and fractional crystallization) in a volatile-bearing upper mantle.

Solubility Data

Recently, a considerable amount of data on the solubility of H_2O and CO_2 in both simple model and natural complex silicate melts has accumulated. The solubility of sulfur species at pressures and temperatures corresponding to the upper mantle has not been determined experimentally, largely because of severe experimental difficulties. Some very recent preliminary results (*B.O. Mysen and R.J. Arculus*, unpublished data) are presented and discussed. The main emphasis in this review, however, is on the solubility of H_2O and CO_2 under pressure and temperature conditions relevant to magma genesis in the upper mantle.

Water Solubility

The first data on H_2O solubility in natural rock melts at high pressures were published by *Goranson* (1931). *Hamilton, Burnham, and Osborn* (1964) found that their solubility data for basalt and andesite to P_{H_2O} = 6 kbar were consistent with the model of water solubility of *Wasserburg* (1957), who suggested that water dissolved in silicate melts by forming OH^- through interaction between H_2O and bridging oxygen in the silicate melt. On the basis of thermodynamic data on H_2O at high pressures and temperatures (*Burnham, Holloway, and Davis*, 1969) and on hydrous silicate melts to 10 kbar and 1100°C (*Burnham and Davis*, 1971, 1974), *Burnham* (1974, 1975) concluded that the simple concept of OH^- formation in the melt does not adequately explain the experimental data. *Burnham* (1974, 1975), therefore, proposed a new model for H_2O solubility in silicate melts at high pressure. *Burnham* (1974) found that for H_2O contents of melts up to 50 mole %, the solubility of H_2O (mole fraction of H_2O in melt, $x_{H_2O}^m$) was proportional to the square root of the water fugacity, f_{H_2O}. With $X_{H_2O}^m > 0.5$, the water solubility was found to vary exponentially with f_{H_2O} (Fig. 1). *Burnham* (1974) thus proposed the following two idealized solubility mechanisms for H_2O, using the system $NaAlSi_3O_8$-H_2O as example:

For $X_{H_2O}^m \leq 0.5$,

$$NaAlSi_3O_8(m) + H_2O(v) = AlSi_3O_7(OH)(m) + NaOH(m) \quad (1)$$

For $X_{H_2O}^m > 0.5$,

$$AlSi_3O_7(OH) + nH_2O(v) = AlSi_3O_7(OH)_{2n+1}(m) \quad (2)$$

This model was used successfully to predict H_2O solubility for a variety of silicate melts to at least 10 kbar pressure (*Burnham*, 1975). *Burnham* (1974) also showed that, provided the components of the melt are chosen appropriately, the molar solubility of H_2O does not depend on bulk composition of the silicate melt, at least within the pressure and temperature range studied by him and coworkers ($\leq$ 10 kbar and $\leq$ 1100°C). It is, however, possible that at pressures in excess of 10 kbar, water may also dissolve as molecular H_2O (*Hodges*, 1974).

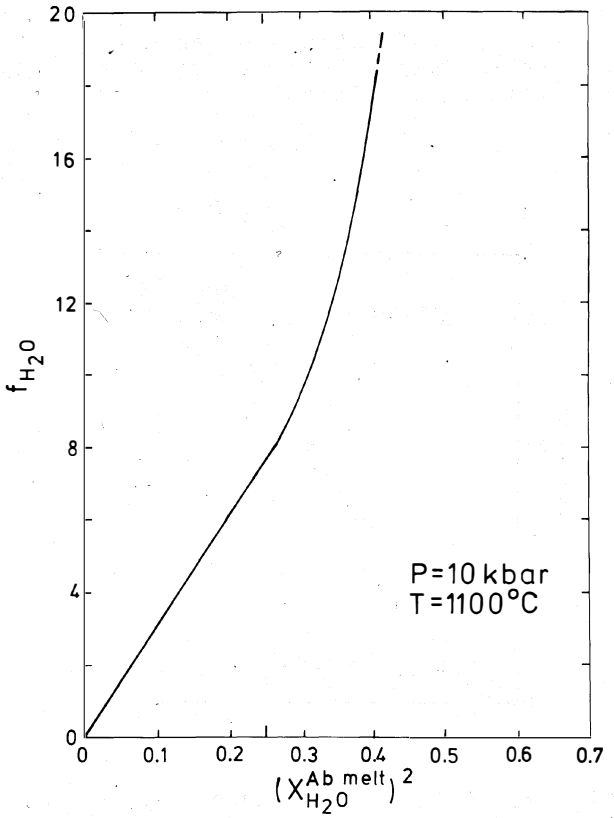

Fig. 1. Mole fraction of H_2O in albite melt ($X_{H_2O}^{Ab\ melt}$) as a function of f_{H_2O} at 10 kbar and 1100°C (data from *Burnham and Davis*, 1974).

Solution of H_2O, according to the model of *Burnham* (1974, 1975), greatly modifies the silicate melt structure by breaking up -O-(Al,Si)-O- polymers. Independent evidence in support of this idea has been obtained by determination of infrared spectra of H_2O-bearing melts quenched at high pressure (*Orlova*, 1964; *Velde and Kushiro*, 1976), by comparison of data on the viscosity of hydrous and dry silicate melts at high pressure (*Shaw*, 1963; *Burnham*, 1963; *Kushiro, Yoder, and Mysen*, 1976), and by determination of the effect of H_2O on shifts of critical liquidus boundaries in silicate systems relevant to rock-forming processes in the mantle (see *Kushiro*, 1975, for review).

Large quantities of H_2O can be dissolved under pressure conditions corresponding to those of the upper mantle. Data of *Boettcher and Wyllie* (1969), *Burnham and Davis* (1971, 1974), and *Rosenhauer and Eggler* (1975) showed that the solubility in typical melts may increase from about 10 wt. % near 10 kbar to about 30 wt. % at 30 kbar. On a weight basis, there is a compositional dependence of H_2O solubility (Fig. 2a), but recalculated to molar solubility using the method described by *Burnham* (1974), this compositional dependence becomes negligible (Fig. 2b). The temperature dependence of H_2O solubility in silicate melts is also small (*Kadik, Lebedev, and Khitarov*, 1971; *Burnham and Davis*, 1974) and apparently negative at pressures below 10 kbar and temperatures below 1100°C. At higher pressures and temperatures, the H_2O content of silicate melts may increase with increasing temperature (*Kadik*,

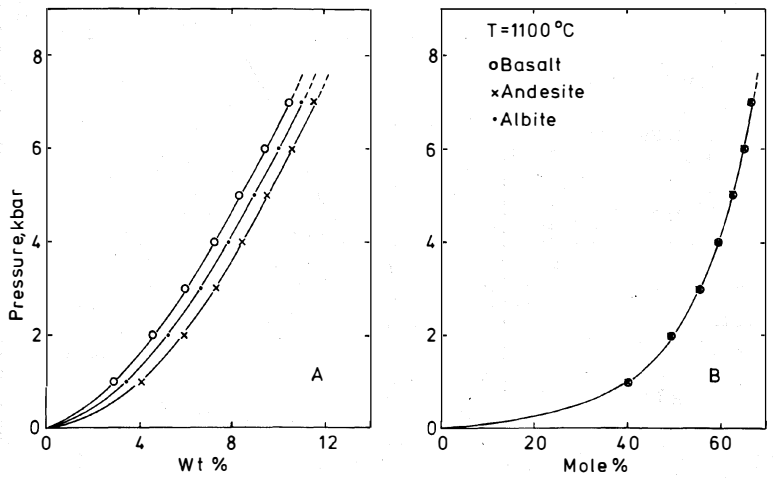

Fig. 2. Solubility of H_2O in basalt, andesite, and albite melts (data from *Hamilton, Burnham, and Osborn*, 1964; *Burnham and Davis*, 1974). (a) Wt. % H_2O; (b) mole % H_2O (calculated according to the scheme proposed by *Burnham*, 1974).

Lebedev, and Khitarov, 1971). Unfortunately, systematic studies of the temperature dependence of water solubility at P_{H_2O} > 10 kbar are scarce, making a detailed comparison with other volatiles difficult.

Carbon Dioxide Solubility

The importance of CO_2 with respect to the melting relations of mantle rocks has recently been realized (*Eggler*, 1973, 1974, 1975, 1976; *Mysen and Boettcher*, 1975a,b; *Brey and Green*, 1975; *Maaløe and Wyllie*, 1975; *Huang and Wyllie*, 1974; *Wyllie and Huang*, 1975, 1976). A considerable amount of data on CO_2 solubility in silicate melts has accumulated since then (*Eggler*, 1973; *Mysen*, 1975, 1976a,b; *Kadik and Eggler*, 1975; *Eggler, Mysen and Seitz*, 1974; *Mysen, Arculus, and Eggler*, 1975; *Mysen et al.*, 1976; *Holloway, Mysen and Eggler*, 1976). The solubility of CO_2, in contrast to that of H_2O depends strongly on bulk composition and temperature. Furthermore, the amount of CO_2 that can dissolve in a silicate melt is much smaller than that of H_2O at the same pressure and temperature (Fig. 3).

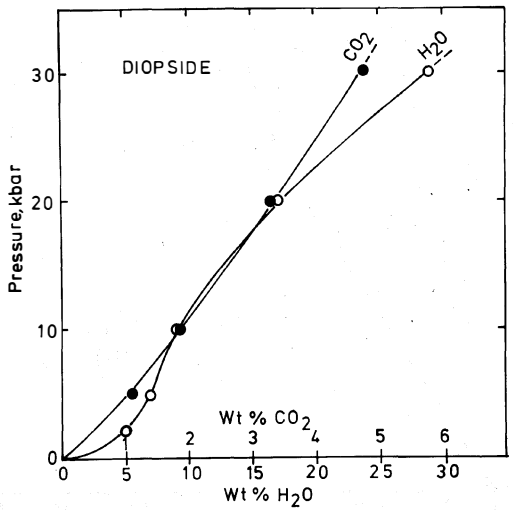

Fig. 3. Solubility of H_2O and CO_2 in $CaMgSi_2O_6$ melt to 30 kbar. H_2O data along the diopside solidus from *Rosenhauer and Eggler* (1975). CO_2 data at 1625°C from *Mysen et al.* (1976).

A comparison of CO_2 solubility in jadeite and diopside melt (Fig. 4) reveals a direct dependence on the bulk composition of the melt. A more dramatic illustration of this effect has been observed in melts in the compositional range 28-65 wt. % Mg_2SiO_4 along the join Ca_2SiO_4-Mg_2SiO_4 (Fig. 5). In analogy with the crystalline counterparts, melts along this join are probably polymerized only to a small degree. The solubility of CO_2 increases rapidly, however, as the larnite component of the melt increases. Carbon dioxide solubility is also positively correlated with the proportion of basic oxide of fixed composition (e.g., Na_2O) as shown in Fig. 6 for albite, jadeite, and nepheline melts. The solubility curves for melts with less than 14 mole % Na_2O (albite) are dashed because of lack of data.

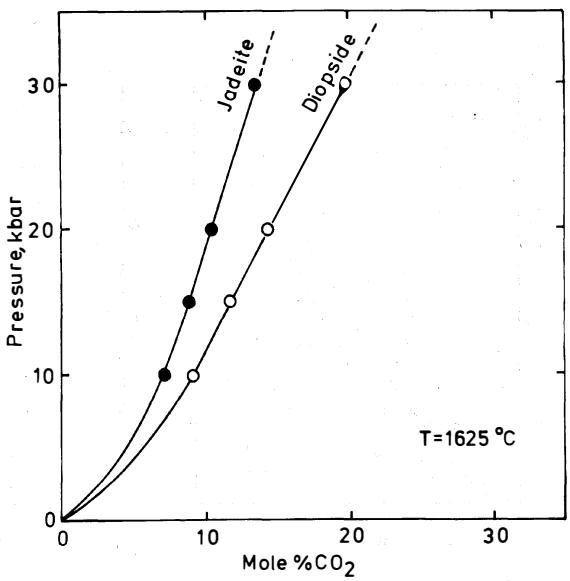

Fig. 4. Carbon dioxide solubility in $CaMgSi_2O_6$ and $NaAlSi_2O_6$ melts to 30 kbar at 1625°C (data from *Mysen et al.*, 1976; *Mysen*, 1975).

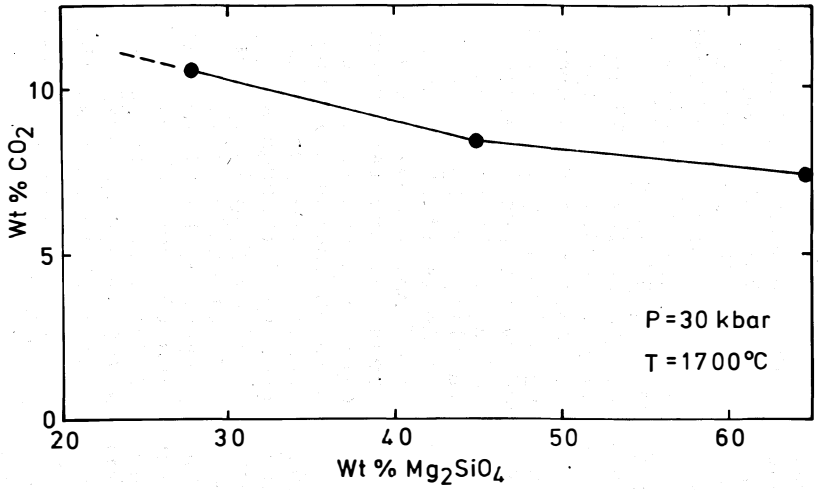

Fig. 5. Solubility of CO_2 along the join Ca_2SiO_4-Mg_2SiO_4 (data from *Holloway, Mysen, and Eggler*, 1976).

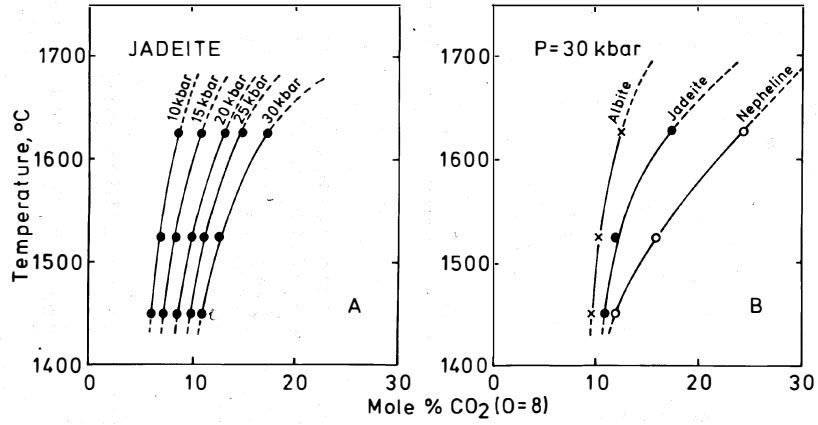

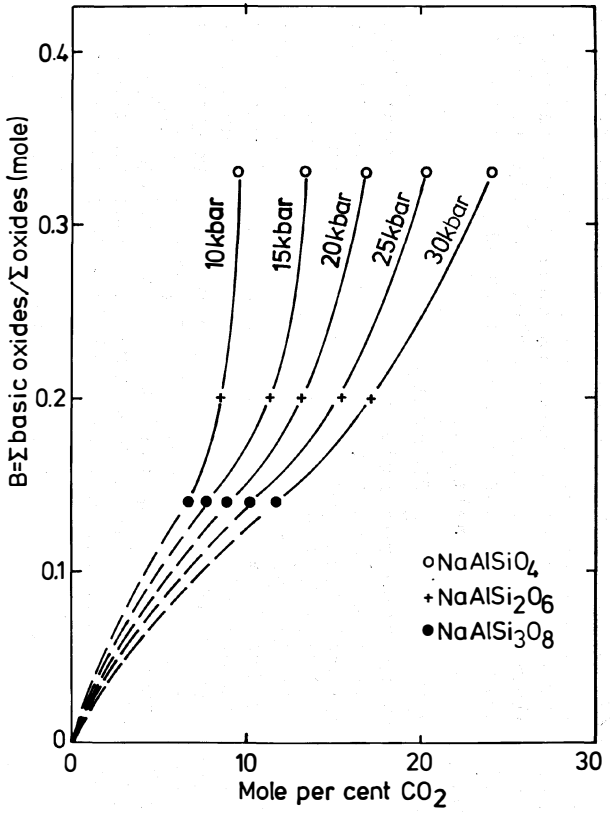

Fig. 6. CO_2 solubility (mole % with O = 8 in chemical formulae) as a function of basic oxide (Na_2O) at 1625°C (data from *Mysen*, 1975).

← Fig. 7. Temperature dependence of CO_2 solubility in silicate melts (a) as a function of pressure (*Mysen*, 1975), and (b) as a function of basicity of silicate melt (*Mysen*, 1975).

Carbon dioxide contents of all melts studied thus far show some increase with increasing temperature. In most cases, the rate of increase, $(dX_{CO_2}^{melt}/dT)_P$, increases with increasing pressure (Fig. 7a) -- that is $(d^2X_{CO_2}^{melt}/dTdP) > 0$. In general, $(dX_{CO_2}^{melt}/dT)_P$ and $(d^2X_{CO_2}^{melt}/dTdP)$ also increase with increasing basicity* of the melt (Fig. 7b). Increasing basicity of a silicate melt is usually correlated with a decreasing degree of polymerization. For example, jadeite melt is less polymerized than albite melt, and as can be seen from the data in Fig. 7b,

$$(dX_{CO_2}^{Jd\ melt}/dT)_P > (dX_{CO_2}^{Ab\ melt}/dT)_P \quad \text{and}$$

$$(d^2X_{CO_2}^{Jd\ melt}/dTdP) > (d^2X_{CO_2}^{Ab\ melt}/dTdP).$$

Holloway, Mysen, and Eggler (1976) have recently shown, however, that there is an upper limit to the positive temperature dependence of CO_2 solubility. Silicate melts approach a structural state of random disorder with increasing temperature (*Adam and Gibbs*, 1965). It has been proposed (*Holloway, Mysen, and Eggler*, 1976; *Mysen et al.*, 1976) that the positive temperature dependence of the solubility of carbon dioxide in silicate melts is caused by an increasing activity of the oxygen ion with increasing temperature. Therefore, the amount of carbonate in the melt increases with increasing temperature. After the melt is completely depolymerized, however, further increase in temperature may result in decreasing temperature dependence of the CO_2 solubility. This tendency is observed along certain portions of the join La-Fo and for natural olivine melilite nepheline (Fig. 8) at very high temperatures ($\geq$ 1700°C).

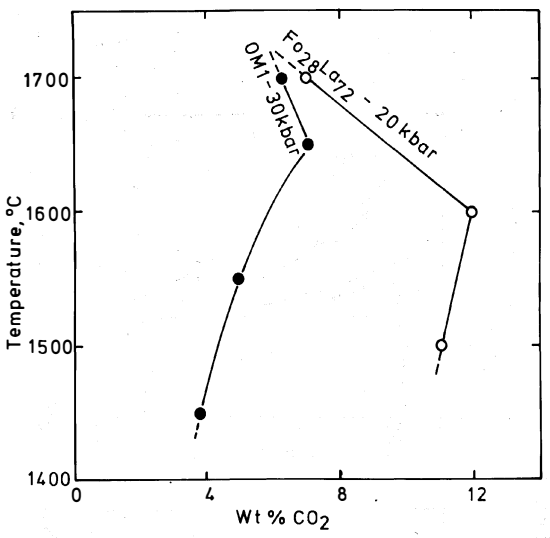

Fig. 8. Temperature inversions of CO_2 solubility. (Data on the Fo-La join from *Holloway, Mysen, and Eggler*, 1976. Data on natural olivine melilite nepheline (OM1) from *Mysen, Arculus, and Eggler*, 1975, and unpublished data.)

In all likelihood, partial melting in the upper mantle occurs in the presence of multicomponent volatiles (bound in minerals or as a separate vapor phase), as evidenced, for example, by the presence of both H_2O and CO_2 in volcanic gases (*Anderson*, 1975). Data on the solubility of CO_2 in hydrous silicate melts have been obtained by *Eggler* (1973, 1974); *Kadik and Eggler* (1975); *Mysen, Arculus, and Eggler* (1975); *Mysen et al.* (1976); and *Mysen* (1976b). All these data show that CO_2 solubility in melts is affected by the presence of dissolved H_2O. In Fig. 9a,b, the solubility of CO_2 in hydrous nepheline melts is shown as a function of molar $CO_2/(CO_2 + H_2O)$, pressure, and temperature. It is clear that dissolved H_2O results in an increase in the CO_2 solubility; the CO_2 solubility curves pass through a maximum as the f_{H_2O} is increased before the effect of dilution of the CO_2 vapor by H_2O lowers the saturation CO_2 content of the melt. In Fig. 10, both H_2O and CO_2 contents of albite melt in equilibrium with a $(CO_2 + H_2O)$-bearing vapor are shown. In contrast to the C-shaped CO_2 solubility curves, the H_2O solubility decreases continuously with increasing activity of CO_2

* Basicity is defined as molar proportion of basic oxide in the melt (*Pearce*, 1964).

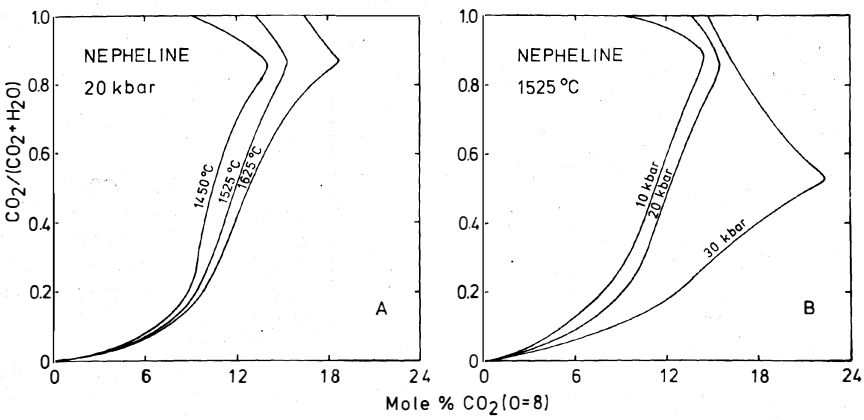

Fig. 9. Carbon dioxide solubility in hydrous $NaAlSiO_4$ melt (a) as a function of molar $CO_2/(CO_2 + H_2O)$ and temperature, and (b) as a function of molar $CO_2/(CO_2 + H_2O)$ and pressure (data from *Mysen*, 1975).

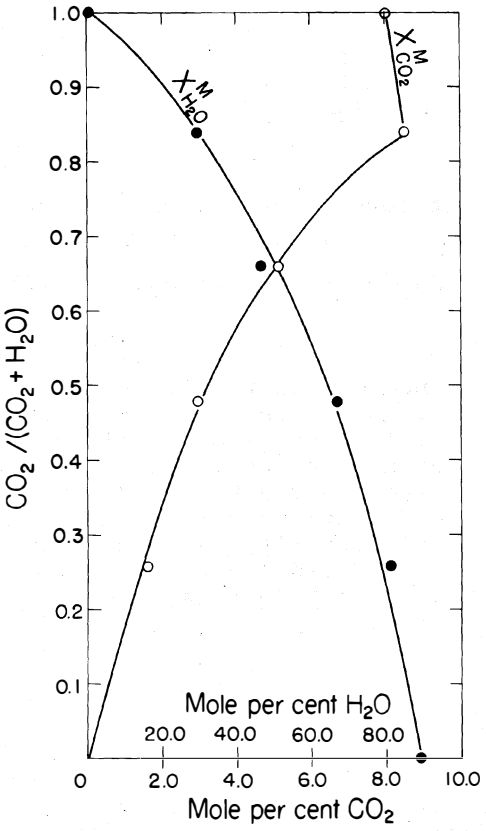

Fig. 10. CO_2 and H_2O solubilities in albite melt as a function of molar $CO_2/(CO_2 + H_2O)$ at 1450°C and 20 kbar (data from *Mysen*, 1975).

(decreasing activity of H_2O).

Three major types of silicate partial melts can be formed from a peridotite + H_2O + CO_2 source (*Mysen and Boettcher*, 1975b; *Eggler*, 1974, 1975). These melts are andesitic under H_2O-rich conditions, tholeiitic with approximately equal proportions of CO_2 and H_2O, and olivine nephelinitic (or olivine melilite nephelinitic) with molar CO_2 > molar H_2O. *Mysen, Arculus, and Eggler* (1975) measured the CO_2 solubilities in such melts under both H_2O-free and hydrous conditions. Some of their data are reproduced in Fig. 11, showing that the solubility of CO_2 in natural rock melts closely resembles that in simple systems such as those already discussed.

Albite melt may be used to illustrate the difference in solubility behavior of H_2O and CO_2 in silicate melts, and to explain the effect of H_2O on CO_2 solubility as well as the effect of CO_2 on H_2O solubility. By studying infrared spectra, it has been shown (*Mysen, Arculus, and Eggler*, 1975; *Mysen et al.*, 1976; *Mysen*, 1976a,b) that in both H_2O-free and hydrous silicate melts carbon dioxide dissolves both as molecular CO_2 and as CO_3^{2-} anion. The proportion of CO_3^{2-} increases with increasing temperature, increasing basicity, and decreasing pressure. *Mysen* (1976b) also noted that the proportion of carbonate in albite melt increases in hydrous melt relative to anhydrous melt. Bicarbonate was never observed.

Solution of H_2O in albite melt can be illustrated with equations (1) and (2). Solution of CO_2 in hydrous albite melt was illustrated by *Mysen* (1976b) by the equation

$$2NaAlSi_3O_8(m) + H_2O(v) + CO_2(v) = 2AlSi_3O_7(OH)(m) + Na_2CO_3(m) \quad (3)$$

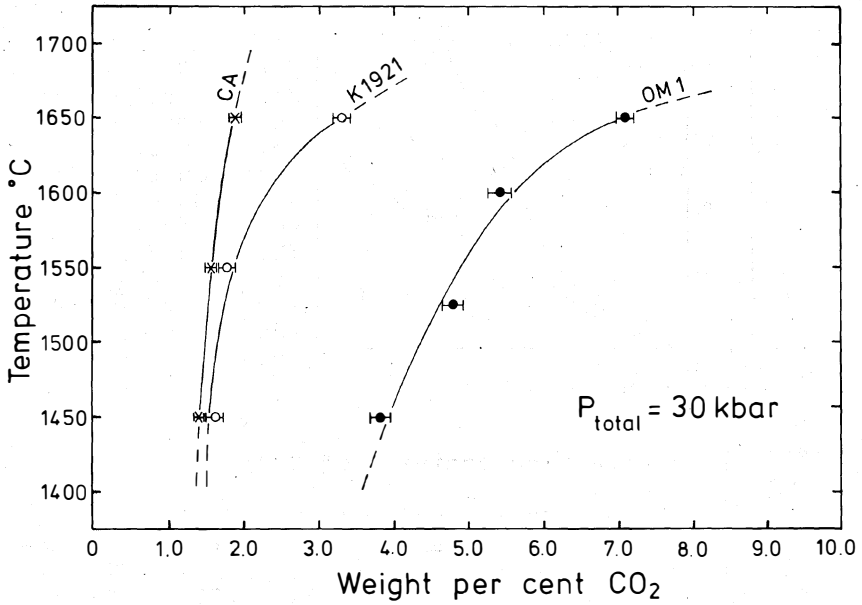

Fig. 11. CO_2 solubility in melts of andesite (CA), tholeiite (K1921), and olivine melilite nephelinite (OM1) compositions (data from *Mysen, Arculus, and Eggler*, 1975).

whereas solution of CO_2 in anhydrous albite melt (predominantly molecular CO_2) is approximated by the equation

$$Y NaAlSi_3O_8(m) + X CO_2(v) = Y NaAlSi_3O_8(m) + CO_2(m) + (X - 1)CO_2(v) \quad (4)$$

where $X > 1$ and $Y > 1$.

The formation of carbonate in the presence of H_2O results from the stabilization of $Na_2CO_3(m)$ by exchanging OH^- [eq. (1)] with carbonate. The maxima on the CO_2 solubility curves occur where all exchangeable cations (e.g., Na_2O; see also *Burnham*, 1975) have been used to stabilize carbonate (*Mysen*, 1976b). Even higher f_{H_2O} than that required to reach the maximum CO_2 solubility results in lowering of the CO_2 solubility because of the dilution effect on CO_2 of H_2O. Consequently, the solubility maximum seen in Fig. 9, as in all other hydrous silicate melts studied (*Eggler*, 1973, 1974; *Mysen*, 1975, 1976b; *Kadik and Eggler*, 1975; *Mysen, Arculus, and Eggler*, 1975; *Mysen et al.*, 1976), would be expected.

Sulfur Dioxide Solubility

The role of sulfurous gas species in the mantle is less well known than that of CO_2 and H_2O. Sulfides occur in peridotite nodules from kimberlite and alkali basalts (*White*, 1966; *Harris*, 1972; *Bishop, Smith, and Dawson*, 1975). The levels of f_{S_2} and f_{O_2} required to stabilize SO_2 relative to reduced sulfur species, however, are known only for pressure conditions near 1 atm (*Gerlach and Nordlie*, 1975c), where CO_2, SO_2, and H_2O appear to be the stable species in equilibrium with basaltic melts. In view of these observations, a few preliminary experiments on the solubility of SO_2 in albite melt have been carried out at 15-30 kbar pressure (*Mysen and Arculus*, unpublished data) using sulfur-35 as the source of beta particles for beta-track mapping of sulfur in quenched glasses (*Mysen and Seitz*, 1975).

The solubility data for SO_2 in albite melt are shown in Fig. 12 and compared with the solubilities of H_2O and CO_2 in similar melts and under similar conditions in Fig. 13. The SO2 solubility curves resemble

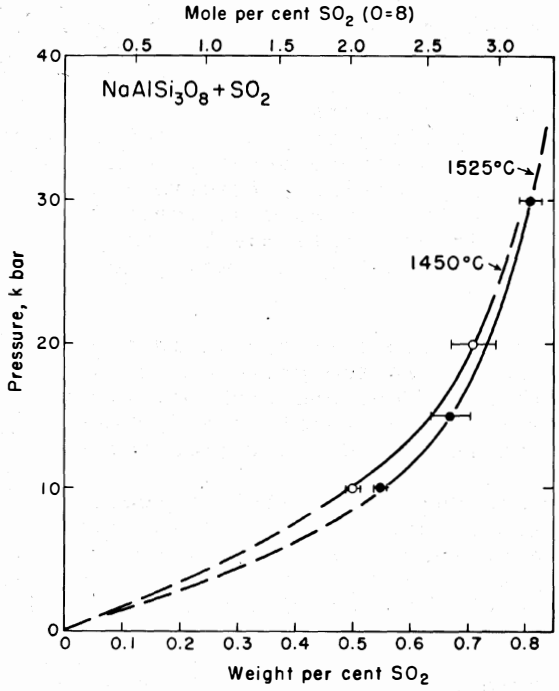

Fig. 12. SO_2 solubility in albite melt as a function of temperature and pressure (*Mysen and Arculus*, unpublished data).

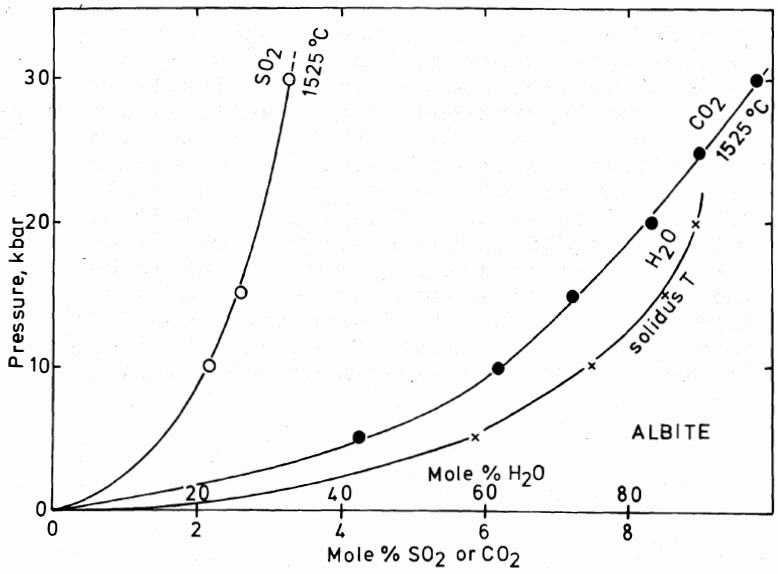

Fig. 13. Comparison of data on H_2O, CO_2, and SO_2 solubility in albite melt. CO_2 and SO_2 data at 1450°C (data from *Mysen*, 1975, and unpublished data by *Mysen and Arculus*). H_2O data along the albite-H_2O solidus (data from *Burnham and Davis*, 1974; *Boettcher and Wyllie*, 1969). Molar solubilities are calculated with 8 oxygens in chemical formulae.

those of CO_2; SO_2 contents increase with increasing temperature and with increasing pressure. The solubility of SO_2 is even lower than that of CO_2, probably reflecting the larger size of the SO_2 molecule.

Discussion

The different effects of H_2O and CO_2 on phase relations of peridotitic systems under upper mantle conditions can be understood by considering the different solubility mechanisms of the two components in silicate melts. Solution of H_2O results in breakage of bridging oxygens in tetrahedral polymers, whereas solution of CO_2 results in an increasing degree of polymerization of the silicate melt. Consequently, liquidus boundaries between two crystalline phases having different degrees of polymerization (e.g., olivine and orthopyroxene) will be shifted toward the silica-rich side of the system with increasing activity of H_2O. Increasing activity of CO_2 results in a shift toward the silica-poor side of the system. It has been observed that high H_2O activity in peridotite upper mantle results in melts of andesitic affinities, whereas CO_2-rich conditions yield melts of the nephelinitic type (*Mysen and Boettcher*, 1975b). These experimental observations are in accord with the inferred effects of dissolved volatiles on the silicate melt structures.

As a magma at high pressure ($\gtrsim$ 10 kbar) cools and precipitates minerals, the activity of CO_2 in the melt increases more rapidly than that of H_2O. This increase in CO_2 activity is caused by the rather

strong positive temperature dependence of the CO_2 solubility and by the lower solubility of CO_2 compared with H_2O. A consequence of this situation is that, if for example a (CO_2 + H_2O)-bearing magma (e.g., tholeiite) initially precipitates olivine, as the result of crystallization (even under near constant temperature conditions), rapidly increasing activity of CO_2 at high pressures may result in an abrupt change to orthopyroxene crystallization. Thus, the residual liquid may initially fractionate toward more silica-rich compositions and then trend toward silica undersaturation. *Eggler* (1974) suggested that this principle may be the cause of the evolution from tholeiitic to nephelinitic melts in Hawaii, for example.

Even though data on sulfur solubility are scarce, it is suggested that during partial melting in the upper mantle in the presence of H_2O, CO_2, and SO_2, the melt is richer in H_2O than in CO_2, and probably richer in CO_2 than in SO_2. The coexisting vapor will show relative enrichments opposite to those of the melt. This effect is called vapor fractionation.

Because CO_2 solubility (and perhaps SO_2 solubility) increases with increasing basicity, whereas the compositional effect on H_2O solubility is relatively small, the effectiveness of vapor fractionation will decrease the more basic the melt. For example, *Eggler* (1973) showed that at 20 kbar albite melt with molar $CO_2/(CO_2 + H_2O)$ = 0.05 could coexist with vapor of $CO_2/(CO_2 + H_2O)$ = 0.75. He also showed that diopside melt at the same pressure has a molar $CO_2/(CO_2 + H_2O)$ between 0.4 and 0.3 when coexisting with a vapor of 0.75. The actual CO_2 saturation contents of the two liquids were 0.9 and 3.5 wt. %, respectively, for albite and diopside melts. Nevertheless, vapor fractionation is significant in controlling the evolution of a melt-crystal-vapor system even for basic magmas such as nephelinite (CO_2 solubility is about 50% higher than in diopside melt under similar physical conditions).

A consequence of the principle of vapor fractionation is that partial melting of a (CO_2 + H_2O)-bearing peridotite mantle will result in enrichment in CO_2 in the residual mantle, whereas the melt itself is enriched in H_2O. This CO_2 is probably retained in the mantle as a carbonate (*Eggler*, 1976; *Eggler, Kushiro, and Holloway*, 1976). In fact, according to the latter authors, stabilization of carbonate in the residual mantle results in greater enrichment of H_2O over CO_2 in the partial melts than when in equilibrium with CO_2-rich vapor. Thus, partial melting results in preferential depletion of H_2O in the upper mantle. It would be expected that this process will result in an upper mantle that is heterogeneous with respect to vapor components. Some consequences of such a possibility for the evolution of magmas in island arcs have been discussed by *Mysen, Arculus, and Eggler* (1975). Similarly, *Mysen and Boettcher* (1975b) utilized this principle to model the genesis of nephelinitic magmas associated with kimberlite.

Acknowledgements

Reviews by Drs. D.H. Eggler, B. Watson, and H.S. Yoder, Jr., are appreciated.

References

Adam, G., and J.H. Gibbs, On the temperature dependence of cooperative relaxation properties in glass-forming liquids, *J. Chem. Phys., 43*, 139-146, 1965.

Anderson, A.T., Some basaltic and andesitic gases, *Rev. Geophys., 13*, 37-57, 1975.

Bishop, F.C., J.V. Smith, and J.B. Dawson, Pentlandite-magnetite intergrowth in deBeers spinel lherzolite: Review of sulfides in nodules, *Phys. Chem. Earth, 9*, 323-337, 1975.

Boettcher, A.L., and P.J. Wyllie, Phase relationships in the system $NaAlSiO_4$-SiO_2-H_2O to 35 kilobars pressure, *Am. J. Sci., 267*, 875-909, 1969.

Brey, G., and D.H. Green, The role of CO_2 in the genesis of olivine melilitite, *Contrib. Mineral. Petrol., 49*, 93-103, 1975.

Burnham, C.W., Viscosity of a water-rich pegmatite melt at high pressures (abstr.), *Geol. Soc. Am. Spec. Pap. 76*, 26, 1963.

Burnham, C.W., $NaAlSi_3O_8$-H_2O solutions: A thermodynamic model for hydrous magmas, *Bull. Soc. Fr. Mineral. Cristallogr., 97*, 223-230, 1974.

Burnham, C.W., Thermodynamics of melting in experimental silicate-volatile systems, *Geochim. Cosmochim. Acta, 39*, 1077-1084, 1975.

Burnham, C.W., and N.F. Davis, The role of H_2O in silicate melts. I. P-V-T relations in the system $NaAlSi_3O_8$-H_2O to 10 kilobars and 1000°C, *Am. J. Sci., 270*, 54-79, 1971.

Burnham, C.W., and N.F. Davis, The role of H_2O in silicate melts. II. Thermodynamic and phase relations in the system $NaAlSi_3O_8$-H_2O to 10 kilobars, 700° to 1100°C, *Am. J. Sci., 274*, 902-940, 1974.

Burnham, C.W., J.R. Holloway, and N.F. Davis, Thermodynamic properties of water to 1000°C and 10,000 bars, *Geol. Soc. Am. Spec. Pap. 132*, 96 p., 1969.

Eggler, D.H., Role of CO_2 in melting processes in the mantle, *Carnegie Inst. Washington Yearb. 72*, 457-467, 1973.

Eggler, D.H., Effect of CO_2 on the melting of peridotite, *Carnegie Inst. Washington Yearb. 73*, 215-224, 1974.

Eggler, D.H., Peridotite-carbonatite relations in the system CaO-MgO-SiO_2-CO_2, *Carnegie Inst. Washington Yearb. 74*, 468-474, 1975.

Eggler, D.H., Does CO_2 cause partial melting in the low velocity layer of the mantle?, *Geology, 2*, 69-72, 1976.

Eggler, D.H., I. Kushiro, and J.R. Holloway, Stability of carbonate minerals in a hydrous mantle, *Carnegie Inst. Washington Yearb. 75*, 631-636, 1976.

Eggler, D.H., B.O. Mysen, and M.G. Seitz, The solubility of CO_2 in silicate liquids and crystals, *Carnegie Inst. Washington Yearb. 73*, 226-228, 1974.

Gerlach, T.M., and B.E. Nordlie, The C-O-H-S gaseous system. Part I. Composition limits and trends of basaltic gases, *Am. J. Sci.*, *275*, 353-376, 1975a.

Gerlach, T.M., and B.E. Nordlie, The C-O-H-S gaseous system. Part II. Temperature, atomic composition, and molecular equilibria in volcanic gases, *Am. J. Sci.*, *275*, 377-394, 1975b.

Gerlach, T.M., and B.E. Nordlie, The C-O-H-S gaseous system. Part III. Magmatic gases compatible with oxides and sulfides in basaltic magmas, *Am. J. Sci.*, *275*, 395-410, 1975c.

Goranson, R.W., The solubility of water in granite magmas, *Am. J. Sci.*, *5th ser.*, *22*, 481-502, 1931.

Hamilton, D.L., C.W. Burnham, and E.F. Osborn, The solubility of water and effects of oxygen fugacity and water content on crystallization in mafic magmas, *J. Petrol.*, *5*, 21-39, 1964.

Harris, J.W., Black material on mineral inclusions and in internal fractures in diamond, *Contrib. Mineral. Petrol.*, *35*, 22-33, 1972.

Hodges, F.N., The solubility of H_2O in silicate melts, *Carnegie Inst. Washington Yearb. 73*, 251-255, 1974.

Holloway, J.R., B.O. Mysen, and D.H. Eggler, The solubility of CO_2 in liquids on the join CaO-MgO-SiO_2-CO_2, *Carnegie Inst. Washington Yearb. 75*, 626-630, 1976.

Huang, W.-L., and P.J. Wyllie, Eutectic between wollastonite II and calcite contrasted with thermal barrier in MgO-SiO_2-CO_2 at 30 kilobars with applications to kimberlite-carbonatite petrogenesis, *Earth Planet. Sci. Lett.*, *24*, 305-310, 1974.

Irving, A.J., and P.J. Wyllie, Subsolidus and melting relations for calcite, magnesite on the join $CaCO_3$-$MgCO_3$ to 36 kb, *Geochim. Cosmochim. Acta*, *39*, 35-53, 1975.

Kadik, A.A., and D.H. Eggler, Melt-vapor relations on the join $NaAlSi_3O_8$-H_2O-CO_2, *Carnegie Inst. Washington Yearb. 74*, 479-484, 1975.

Kadik, A.A., E.B. Lebedev, and N.J. Khitarov, The water in magmatic melts (in Russian), *"Nauka" Publishers, Moscow*, 265 p., 1971.

Kushiro, I., The system forsterite-diopside-silica with and without water at high pressures, *Am. J. Sci.*, *267-A*, 269-294, 1969.

Kushiro, I., Effect of water on the composition of magmas formed at high pressures, *J. Petrol.*, *13*, 311-334, 1972.

Kushiro, I., On the nature of silicate melts and its significance in magma genesis: Regularities in the shift of liquidus boundaries involving olivine, pyroxene and silica minerals, *Am. J. Sci.*, *275*, 411-431, 1975.

Kushiro, I., H.S. Yoder, Jr., and B.O. Mysen, Viscosities of basalt and andesite melts at high pressures, *J. Geophys. Res.*, *81*, 6351-6356, 1976.

Kushiro, I., H.S. Yoder, Jr., and M. Nishikawa, Effect of water on the melting of enstatite, *Geol. Soc. Am. Bull., 79*, 1685-1692, 1968.

Maaløe, S., and P.J. Wyllie, The join grossularite-calcite through the system $CaO-Al_2O_3-SiO_2-CO_2$ at 30 kilobars: Crystallization ranges of silicates and carbonates on the liquidus, *Earth Planet. Sci. Lett., 28*, 205-208, 1975.

Mysen, B.O., Solubility of volatiles in silicate melts at high pressure and temperature: The role of carbon dioxide and water in feldspar, pyroxene and feldspathoid melts, *Carnegie Inst. Washington Yearb. 74*, 454-468, 1975.

Mysen, B.O., Coordination changes of aluminum in silicate melts: Evidence from data on carbon dioxide solubility in albite melt, *Carnegie Inst. Washington Yearb. 75*, 621-623, 1976a.

Mysen, B.O., The role of volatiles in silicate melts: Solubility of carbon dioxide and water in feldspar, pyroxene and feldspathoid melts to 30 kbar and 1625°C, *Am. J. Sci., 276*, 969-996, 1976b.

Mysen, B.O., R.J. Arculus, and D.H. Eggler, Solubility of carbon dioxide in natural nephelinite, tholeiite and andesite melts to 30 kbar pressure, *Contrib. Mineral. Petrol., 53*, 227-239, 1975.

Mysen, B.O., and A.L. Boettcher, Melting of a hydrous mantle. I. Phase relations of natural peridotite at high pressures and temperatures with controlled activities of water, carbon dioxide and hydrogen, *J. Petrol., 16*, 520-548, 1975a.

Mysen, B.O., and A.L. Boettcher, Melting of a hydrous mantle. II. Geochemistry of crystals and liquids formed by anatexis of mantle peridotite at high pressures and high temperatures as a function of controlled activities of water, hydrogen and carbon dioxide, *J. Petrol., 16*, 549-590, 1975b.

Mysen, B.O., D.H. Eggler, M.G. Seitz, and J.R. Holloway, Carbon dioxide in silicate melts and crystals. I. Solubility measurements, *Am. J. Sci., 276*, 455-479, 1976.

Mysen, B.O., and M.G. Seitz, Trace element partitioning determined by beta-track mapping -- an experimental study using carbon and samarium as examples, *J. Geophys. Res., 80*, 2627-2635, 1975.

Nordlie, B.E., The composition of magmatic gases of Kilauea in the near surface environment, *Am. J. Sci., 271*, 417-463, 1971.

Orlova, G.P., The solubility of water in albite melts, *Int. Geol. Rev., 6*, 254-258, 1964.

Pearce, M.L., Solubility of carbon dioxide and variation of oxygen ion activity in soda-silica melts, *J. Am. Ceram. Soc., 47*, 342-347, 1964.

Rosenhauer, M., and D.H. Eggler, Solution of H_2O and CO_2 in diopside melt, *Carnegie Inst. Washington Yearb. 74*, 474-479, 1975.

Shaw, H.R., Obsidian-H_2O viscosities at 1000 and 2000 bars in the temperature range 700°-900°C, *J. Geophys. Res., 68*, 6337-6343, 1963.

Velde, B., and I. Kushiro, Infrared spectra of high-pressure quenched silicate liquids, *Carnegie Inst. Washington Yearb. 75*, 618-620, 1976.

Wasserburg, G.J., The effects of H_2O in silicate systems, *J. Geol.*, *65*, 15-23, 1957.

White, R.W., Ultramafic inclusions in basaltic rocks from Hawaii, *Contrib. Mineral. Petrol.*, *12*, 245-314, 1966.

Wyllie, P.J., and W.-L. Huang, Influence of mantle CO_2 in the generation of carbonatites and kimberlites, *Nature*, *257*, 297-299, 1975.

Wyllie, P.J., and W.-L. Huang, Carbonation and melting reactions in the system $CaO-MgO-SiO_2-CO_2$ at mantle pressures with geophysical and petrological applications, *Contrib. Mineral. Petrol.*, *54*, 79-107, 1976.

PARTIAL MELTING OF PERIDOTITE IN THE PRESENCE OF H_2O and CO_2: PRINCIPLES AND REVIEW

David H. Eggler
Geophysical Laboratory
Carnegie Institution of Washington
Washington, D.C. 20008*

John R. Holloway
Geochemistry Division
Department of Chemistry
Arizona State University
Tempe, Arizona 85281

Abstract

The principal volatile species in the upper mantle, H_2O and CO_2, have been observed, in experimental studies, to have large opposing effects upon composition of partial melts of peridotite. Hydrous liquids are more silica-saturated than liquids produced in the absence of volatiles, whereas CO_2-saturated liquids are less silica-saturated. These studies have been conducted using relatively large amounts of volatiles. Volatiles are thought to be present in the mantle, however, in small amounts (< 0.5 wt. %). For such small volatile contents, sub-soldius peridotite mineral assemblages containing hydrous or carbonate minerals exist in *zones of invariant vapor composition* (ZIVC). Because vapor is, isobarically and isothermally, invariant in composition, isobaric melting of peridotite occurs at the same temperature, forming the same liquid composition, regardless of the ratio of CO_2 to H_2O in the peridotite source region.

Isobaric $\underline{T}$-$\underline{X}_{CO_2}$ sections at 15 and 30 kbar for a total H_2O + CO_2 content of 0.1 wt %, constructed using principles derived from simple systems, are presented as examples of ZIVC-type melting. Amphibole peridotite (+ vapor) at 15 kbar melts at about 1100°C to a nephelinitic liquid. Andesitic liquid can be produced only if CO_2 is absent. Dolomite-phlogopite peridotite (with or without vapor) at 30 kbar melts at about 1025°C to a melilititic liquid. The presence of CO_2 is critical to the development of such primary alkaline magmas. The amount of liquid produced of either nephelinitic or melilititic composition would be small (< 5%), and would be produced within about 50°C of the solidus temperature. For higher degrees of melting, the amounts of volatiles present would be insufficient to saturate the melt, and hence the effects of those volatiles would diminish, until, at temperatures 300°-500°C above the solidus, nearly volatile-free theoleiitic melts would be produced.

Introduction

The principle volatile species in the upper mantle are thought to be CO_2 and H_2O (for reviews see *Mysen and Boettcher*, 1975a; *Mysen et al.*,

* Now at Department of Geosciences, Pennsylvania State University, University Park, Pennsylvania 16802.

1976). These volatiles can have a large effect upon the composition of liquids produced by partial melting of peridotite if the liquids are saturated or nearly saturated with volatiles. Saturated liquids contain about 5-30 wt. % H_2O and CO_2 (*Eggler and Rosenhauer*, 1977). By contrast, the total amount of volatiles in the upper mantle is believed to be small, on the order of a few tenths of a percent. Consequently, volatile-saturated or nearly-saturated liquids can only be produced by relatively small degrees of partial melting, at temperatures not greatly in excess of the solidus. As a corollary, volatiles are only influential in the first few percent melting of peridotite. That first few percent melt should not be considered insignificant, however, for it represents the liquid in the low-velocity zone; the liquid that, if removed, can fundamentally alter the trace and minor-element composition of a peridotite source region; and the liquid parental to rare but important igneous rocks.

The thesis of this paper is that near-solidus peridotite phase relations are sufficiently complicated that few of the experiments conducted on melting of peridotite in the presence of an excess of volatiles can be applied directly to a mantle peridotite-H_2O-CO_2 system where the total volatile content is very small. This paper, therefore, begins with principles of melting of peridotite in the presence of volatiles.

Principles of Melting in Peridotite-Volatile Systems

Eggler (1973a) has analyzed simple, model systems to clarify some of the principles of stability of volatile-bearing phases. That analysis is extended here to systems of increasing complexity that model phase relations of peridotite containing volatile-bearing phases.

The System A-H_2O

The binary model A-H_2O involves a relatively refractory component A, the volatile component H_2O, a hydrous phase H, and liquid L. The geometry of the phase relations (Fig. 1) is characterized by variable composition of the liquid phase. The liquid composition is variable because silicate melts can dissolve more H_2O at high pressure than at low pressure and because vapor-absent liquids contain less H_2O than liquids in equilibrium with vapor. In order to clarify the reactions, liquids containing less H_2O than H are called L_1 and liquids containing more H_2O than H, L_2. Although the relations in Fig. 1 are general, the geometry was designed for the behavior of amphibole.

The phase relations of interest in Fig. 1 arise because the dehydration reaction, (L), intersects the melting reaction, (H). At pressures above that point, I_1, the hydrous phase disappears, with increasing temperature, because it *melts*. Between I_1 and S_1, the melting reaction is $H = L_1 + V$, because the vapor-saturated liquid L_1 contains less H_2O than H. At S_1, the vapor-saturated liquid contains as much H_2O as H, and at higher pressures, more H_2O than H; above S_1, the vapor-present solidus reaction is $H + V = L_2$. (This vapor-saturated solidus is shown to change from negative to positive slope with increase in pressure. Such a change is possible because of the reduced molar volume of H_2O vapor at high pressures, but for most silicate compositions the slope actually changes because of phase changes in the crystalline phases (*Boettcher and Wyllie*, 1969)). At pressures above S_1, H alone melts by a vapor-absent reaction at a

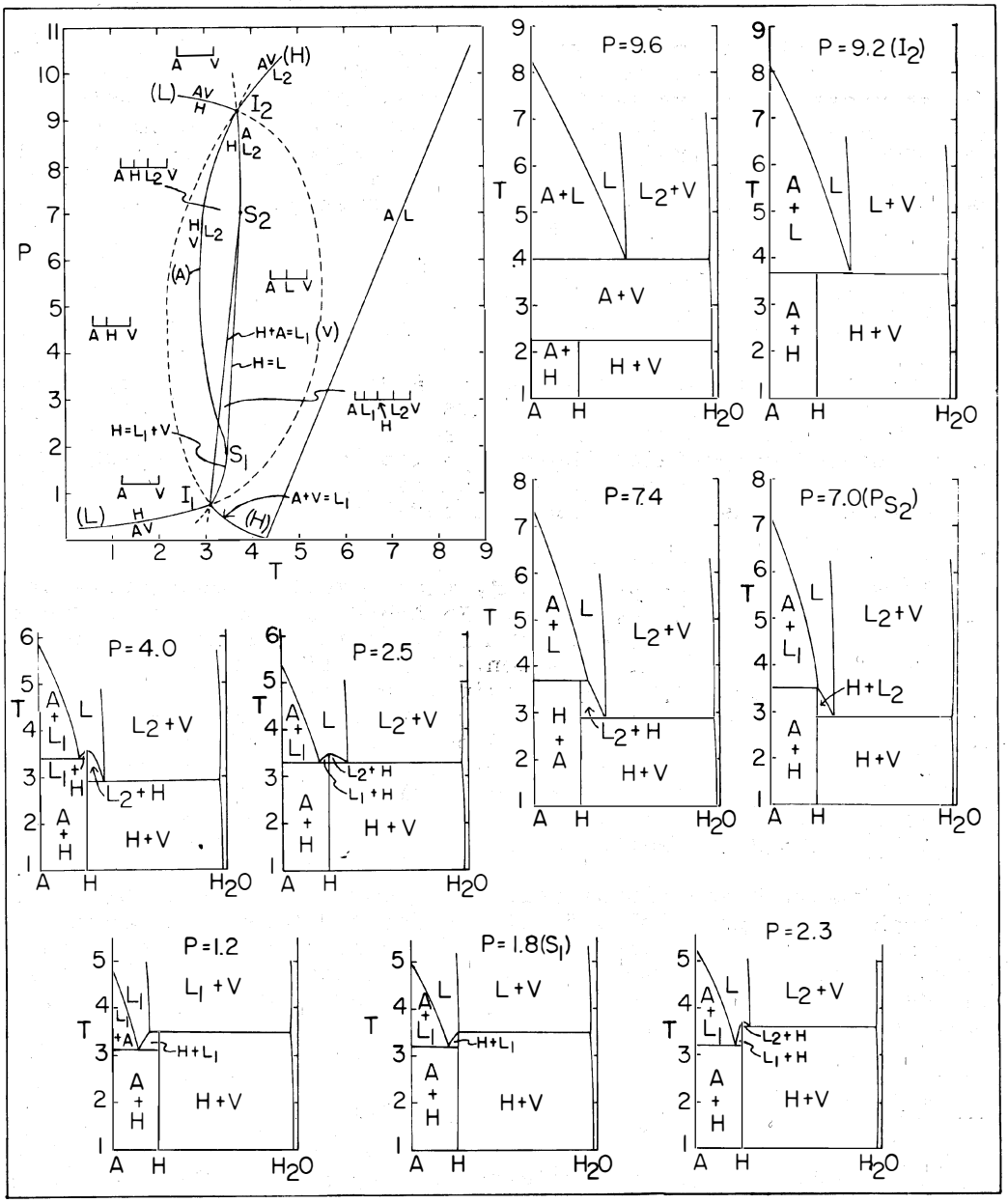

Fig. 1. Phase relations in the model system A-H_2O, including a P-T projection and isobaric T-composition sections. Solid lines refer to stable univariant reactions; dashed lines, to metastable reactions. Univariant reactions have been arranged according to Schreinemaker's rules and are labeled by the phase (x) not participating in a reaction. Phases include a refractory silicate A, a hydrous phase H, liquid L, and vapor V. P, T, and composition scales are arbitrary. The system is theoretical, but has been modeled after melting behavior of an amphibole peridotite.

temperature higher than the vapor-present solidus reaction. Between S_1 and S_2, H has a maximum temperature stability limit (e.g., P = 4.0), which occurs at a *restricted univariant reaction* (*Ricci*, 1951, p. 29), H = L. For this simple system, the restricted univariant reaction is a congruent

reaction, generated by compositional coincidence of H and L.

At pressures above singular point S_2, all liquids coexisting with H contain more H_2O than H; hence H melts incongruently and has no temperature maximum of stability (e.g., the section at P = 7.4, Fig. 1). Finally, at I_2, the vapor-absent melting reaction intersects the vapor-saturated solidus, so that at high pressures H is stable only in the subsolidus region (e.g., the section at P = 9.6).

The System A-B-H_2O

This system (Fig. 2) contains an additional refractory component B. Liquids containing increasing amounts of H_2O are called L_1, L_2, and L_3 to define three separate vapor-absent reactions, as indicated in the inset in Fig. 2. Liquid compositions have been labeled on diagrams where they unambiguously conform to the labeling convection. As in Fig. 1, isobaric sections have been constructed, in this case (Fig. 2) for a pseudobinary join.

It was shown in A-H_2O (Fig. 1) that H melted congruently or incongruently, depending upon pressure. In A-B-H_2O, H melts by a congruent-like reaction (as at P = 5.0, Fig. 2) or by an incongruent-like reaction (as at P = 8.4, Fig. 2). The congruent-like melting of H is not truly congruent, because the temperature maximum in this system (and in all systems with more than one refractory component) occurs at a restricted univariant reaction that is restricted by virtue of collinearity of phase composition, not by virtue of compositional coincidence, as in Fig. 1. Such maxima have been found in systems involving melting of zoisite (*Boettcher*, 1970), phlogopite (*Yoder and Kushiro*, 1969; *Modreski and Boettcher*, 1972), and pargasite (*Holloway*, 1973).

Systems with additional refractory components could be constructed. Inasmuch as the principles developed for A-H_2O are also found in A-B-H_2O, they should, however, also be found in systems with more refractory components. Indeed, the simple pseudobinary joins in Fig. 2 closely model melting features of rocks containing variable amounts of H_2O (e.g., *Robertson and Wyllie*, 1971).

The System A-H_2O-CO_2

A-H_2O-CO_2 with one volatile-containing phase. This system (Fig. 3) is built upon the principles established previously. With addition of CO_2, there are two phases of variable composition, liquid and vapor. The distribution of volatiles between liquid and vapor is modeled after crystal-liquid-vapor relations determined for a number of silicate compositions (*Eggler*, 1973b, 1975a; *Kadik and Eggler*, 1975; *Eggler and Rosenhauer*, 1977).

Phase relations for the subsystem A-H_2O are the same as in Fig. 1, except that relations involving the low-pressure singular point S_1 (Fig. 1) are omitted for simplification. Points analogous to S_1 probably occur below 2 kbar (e.g., *Yoder and Kushiro*, 1969, for phlogopite; or *Holloway*, 1973, for pargasite), pressures not relevant to peridotite melting in the mantle. An example of a system without a low-pressure singular point is $KAlSi_3O_8$-Al_2O_3-H_2O (*Huang, Robertson and Wyllie*, 1973).

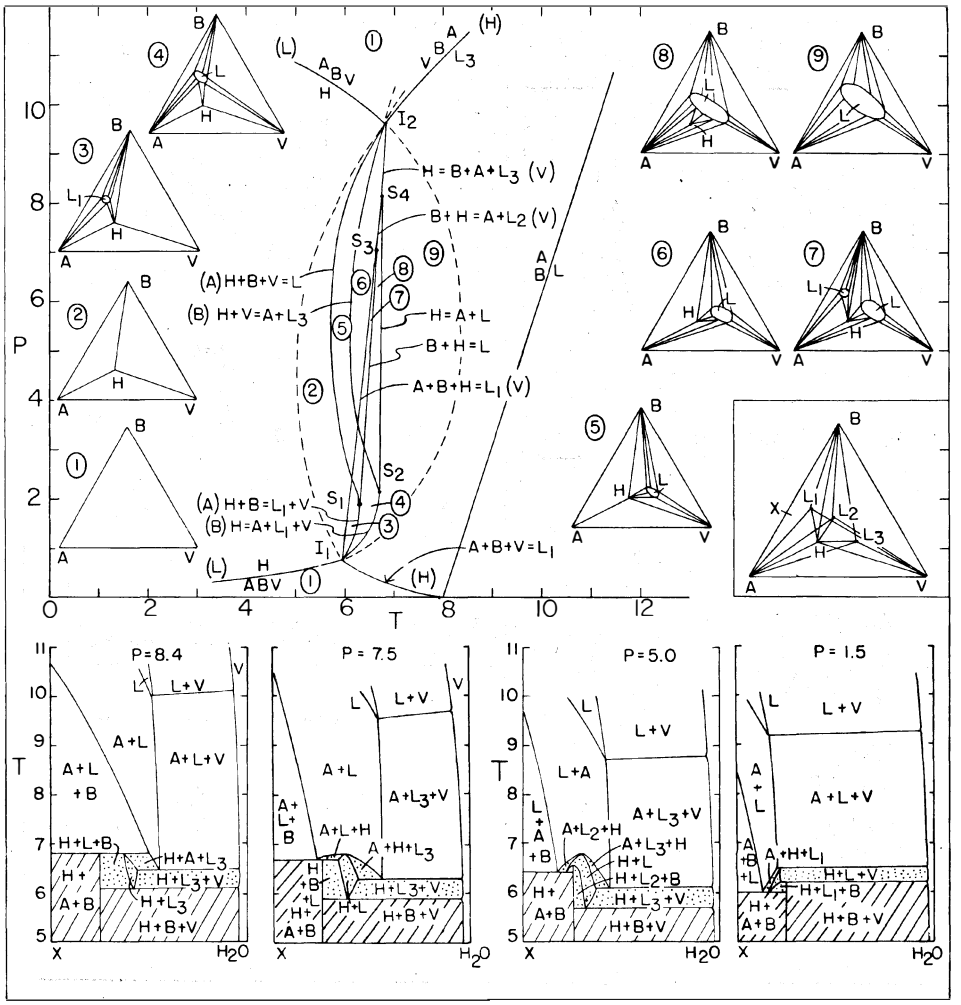

Fig. 2. Phase relations in the model system A-B-H_2O, including a P-T projection; isothermal, isobaric sections; and T-composition sections for the pseudobinary join x-H_2O, where x is a composition on the A-B join. P, T, and composition scales are arbitrary. Lined areas in sections are subsolidus regions, and stippled areas are regions where hydrous phase H coexists with liquid. There is continuous solution between liquid fields L_1, L_2, and L_3 at appropriate temperatures; those liquids have been labeled to separate vapor-absent reactions. The system is theoretical but has been modeled after melting behavior of an amphibole peridotite.

The subsolidus assemblage A + H + V is key to an understanding of the ternary melting relations. Such an assemblage has been called a *zone of invariant vapor composition* (ZIVC) (*Eggler*, 1977). We define a ZIVC as the region in P-T-X space in which a volatile-bearing mineral coexists with a multicomponent vapor and with its breakdown products in a reaction relation that buffers the vapor composition. The subsolidus section at P = 6, T = 1 (Fig. 3) is illustrative. Within a three-phase triangle, H coexists with A and vapor, V. For compositions within that triangle, insufficient

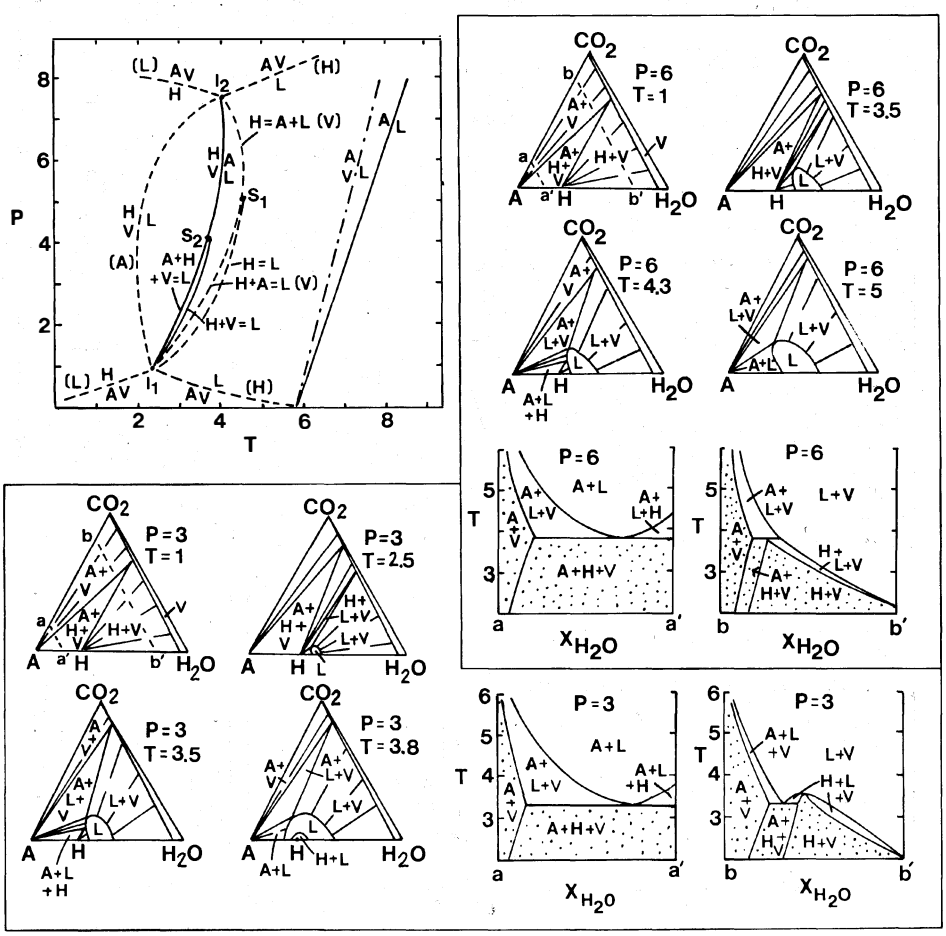

Fig. 3. Phase relations in the model system A-H_2O-CO_2 containing a hydrous phase. In the P-T projection, short-dashed lines refer to univariant reactions in A-H_2O; dot-dash line, to the univariant reaction in A-CO_2; and solid lines, to univariant reactions in A-H_2O-CO_2. Metastable extensions are not shown. The abscissa in the pseudobinary joins (a-a' and b-b') denotes the $CO_2/(CO_2 + H_2O)$ of the bulk composition, not the vapor composition. Subsolidus regions are stippled. The system is theoretical but is modeled after melting behavior of an amphibole peridotite, showing congruent-like melting at lower pressure and incongruent-like melting at higher pressure.

H_2O is available to completely hydrate the assemblage, in this case to react all A to H by the reaction A + H_2O = H. Moreover, because A and H coexist with a H_2O-CO_2 vapor, the assemblage is, at any P and T, invariant, and the vapor composition is invariant. In other words, vapor composition is buffered, its composition kept constant by variation in the relative amounts of the hydrous mineral and its breakdown products. For bulk compositions sufficiently rich in H_2O to react all A to H (the assemblage H + V), however, vapor composition can no longer be buffered by reaction of A to H. Therefore, H can coexist with a vapor of *variable* composition, and the assemblage H + V lies outside the ZIVC.

There are two ternary univariant melting reactions for the assemblage A + H + V, which are separate from reactions in A-H_2O. They have been arranged in P-T projection (Fig. 3) analogously to the vapor-absent melting reactions in A-H_2O, with a singular point S_2. Two sets of pseudobinary joins have been drawn, one set (a-a') for compositions containing a small amount of volatiles and one set (b-b') for compositions containing a relatively large amount of volatiles.

The differences in melting behavior between sections a-a' and b-b' follow directly from the ZIVC concept. Because vapor composition within a ZIVC is, at any P and T, invariant, all compositions melt at a single temperature (i.e., the subsolidus assemblage A + H + V, sections a-a'). On the other hand, bulk compositions outside a ZIVC (i.e., the assemblage H + V, sections b-b') melt at different temperatures, depending upon the volatile composition. Perhaps more important to mantle melting, the liquid produced at the solidus in the sections a-a' is the same, whatever the volatile composition, whereas liquids produced at the solidi in the sections b-b' are variable, depending upon the volatile composition.

A-H_2O-CO_2 with two volatile-containing phases. This model system (Fig. 4) has been designed specifically for a dolomite-phlogopite peridotite at pressures above about 27 kbar, a pressure regime in the model above about P = 4. Relations in the subsystem A-H_2O are after Fig. 1. Relations in the subsystem A-CO_2, about invariant point I_2, are modeled after relations in the system CaO-MgO-SiO_2-CO_2 (*Eggler*, 1976a); although A in effect represents a mantle mineralogy (forsterite + orthopyroxene + clinopyroxene), rather than a single refractory phase, only variation of volatile content in liquid composition can be shown in ternary sections. There are in addition five ternary reactions about I_3; the sequence of these reactions follows directly from the assumption that H and C melt to liquids containing more volatiles than the vapor-absent assemblage A + H + C (incongruent-like); this assumption is justified for the dolomite-phlogopite peridotite in a later section.

The implications of the pseudobinary sections are reiterative of points previously stressed: (1) Melting in the presence of two volatiles takes place by a different set of reactions than in the presence of H_2O or CO_2 alone. (2) In the presence of a small amount of volatiles (a-a'), peridotite compositions melt pseudoinvariantly. In this model, the ZIVC assemblage is C + H + V; the assemblage A + C + H is also pseudoinvariant, but is a special case in which no vapor is present (*Holloway and Eggler*, 1976). (3) In the presence of large amounts of volatiles (b-b'), peridotite compositions melt pseudounivariantly, and a range of liquid compositions can be produced, depending upon the volatile composition.

Relations for a model system A-B-H_2O-CO_2 have been worked out but cannot be presented here for lack of space. It is hoped that the reader is convinced that principles established for simple systems apply also to systems with additional refractory components. It is encouraging, in this regard, that section a-a' (Fig. 4) perfectly mimics the near-solidus melting behavior of dolomite-phlogopite peridotite at 30 kbar deduced by *Holloway and Eggler* (1976) from phase equilibrium experiments.

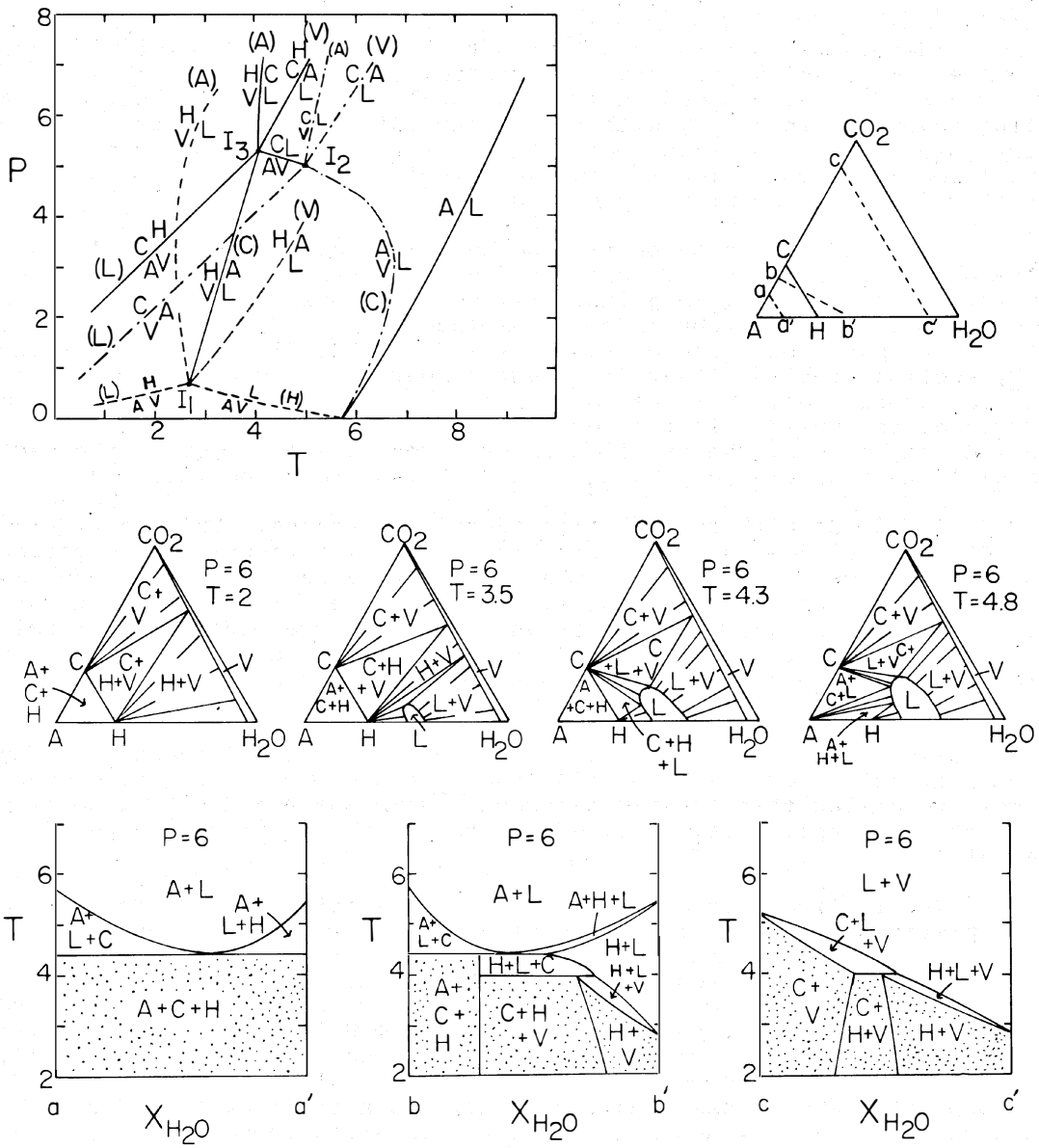

Fig. 4. Phase relations in the model system A-H_2O-CO_2 containing a hydrous phase and a carbonate phase (C). In the P-T projection, short-dashed lines refer to univariant reactions in A-H_2O; dot-dash lines, to univariant reactions in A-CO_2; and solid lines, to univariant reactions in A-H_2O-CO_2. Metastable extensions are not shown. The abscissa of the pseudobinary joins denotes the $CO_2/(CO_2 + H_2O)$ bulk composition, not the vapor composition. The system is theoretical but is modeled after the presumed behavior of a dolomite-phlogopite peridotite.

Studies of Peridotite-H_2O Melting

Synthetic systems. The large effect of H_2O upon the composition of the partial melt of peridotite at high pressures was discovered by *Kushiro, Yoder, and Nishikawa* (1968) in the system MgO-SiO_2-H_2O. They found that liquid in equilibrium with H_2O vapor and peridotite phases contained much more silica than liquid formed in the absence of volatiles and was, in fact, quartz-normative at pressures as high as 20 kbar. This conclusion has been largely substantiated in subsequent studies (in which liquid composition was established by phase relations) on systems of ever-increasing complexity -- CaO-MgO-SiO_2-H_2O (*Kushiro*, 1969), CaO-MgO-Al_2O_3-SiO_2-H_2O (*Ford and O'Hara*, 1972; *Ford*, 1976), Na_2O-MgO-Al_2O_3-SiO_2-H_2O (*Kushiro*, 1972), Na_2O-CaO-MgO-Al_2O_3-SiO_2-H_2O (*Kushiro*, 1972, 1974), K_2O-Na_2O-CaO-MgO-Al_2O_3-SiO_2-H_2O (*Kushiro*, 1974), and K_2O-CaO-MgO-Al_2O_3-SiO_2-H_2O (*Bravo and O'Hara*, 1975) -- and has led to the theory that some andesites can be produced by direct partial melting of peridotite (e.g., *Yoder*, 1969). An example of a join that has been determined is presented in Fig. 5.

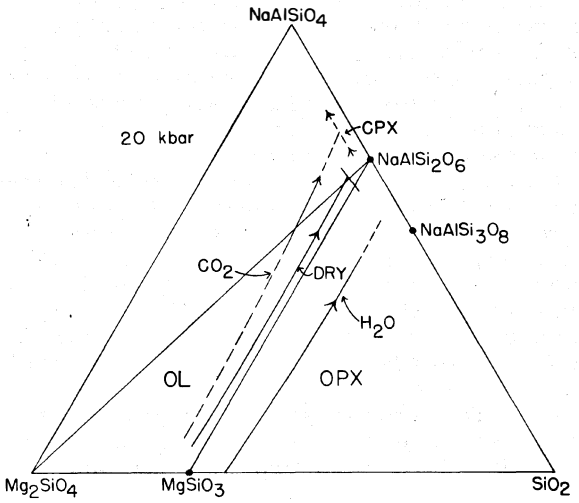

Fig. 5. Phase relations in the join $NaAlSiO_4$-Mg_2SiO_4-SiO_2 at 20 kbar pressure under conditions of CO_2 vapor-saturation (*Eggler*, 1974), H_2O vapor-saturation (*Kushiro*, 1972), and in the absence of volatiles (*Kushiro*, 1968). Reproduced with permission of the Carnegie Institution of Washington.

Bravo and O'Hara (1975) also determined, by an iterative series of experiments, the composition of liquid in equilibrium with H_2O vapor and phlogopite-garnet peridotite at 30 kbar in the K_2O-CaO-MgO-Al_2O_3-SiO_2 system. This liquid composition is unusual, but could be characterized as a potash-rich olivine tholeiite. *Howells* (1976) found that H_2O-saturated liquid at 25 kbar in the system Na_2O-CaO-MgO-Al_2O_3-SiO_2-H_2O was olivine tholeiitic.

Studies of the stability of phlogopite in peridotite assemblages, succeeding *Yoder and Kushiro's* (1969) determination of the stability of phlogopite itself, include *Modreski and Boettcher's* (1972, 1973) investigations in the systems K_2O-MgO-Al_2O_3-SiO_2-H_2O and K_2O-CaO-MgO-Al_2O_3-SiO_2-H_2O to 35 kbar in the presence *and in the absence* of H_2O vapor, the study by *Bravo and O'Hara* (1975) cited above, and the investigation of *Holloway and Eggler* (1976) in the system K_2O-CaO-MgO-CoO-Al_2O_3-SiO_2-H_2O at 30 kbar in the absence of vapor.

Natural compositions. The solidi of various peridotite compositions in the presence of H_2O vapor have been determined by *Kushiro, Syono, and Akimoto* (1968); *Kushiro* (1970); *Green* (1973a); *Millhollen, Irving, and Wyllie* (1974); and *Mysen and Boettcher* (1975a). These solidi lie within a

band about 50°C in width, except for the solidi determined by *Mysen and Boettcher* (1975a), which are 100°-140°C lower in temperature than the rest.

The solidus of a natural, volatile-bearing peridotite in the absence of vapor has been determined only by *Green* (1973a) for a pyrolite (minus 40% olivine) composition + 0.2 wt. % H_2O at pressures to 40 kbar. He observed that the solidus was also essentially the "amphibole-out" curve and that the solidus lay at higher temperatures than the vapor-present solidus. The general configuration of the vapor-absent solidus had been predicted by *Green* (1970) and *Wyllie* (1971); theory of the vapor-absent solidus can be traced in more detail with Figs. 1 and 2 of this paper.

The upper pressure limit of amphibole stability in H_2O-saturated melt has been determined by *Kushiro* (1970); *Green* (1973a); *Millhollen, Irving, and Wyllie* (1974); and *Mysen and Boettcher* (1975a). These results vary from about 22 to 29 kbar. Some of the variation may be due to compositional differences in the samples investigated.

The composition of H_2O-saturated partial melts of peridotite was first determined directly by *Kushiro et al.* (1972), who analyzed very silica-rich glasses in runs on spinel and garnet lherzolite. These analyses may not represent the equilibrium liquid. Several authors (e.g., *Cawthorn et al.*, 1973) have pointed out that liquids formed by small degrees of partial melting commonly quench to a mixture of quenched crystals (olivine, pyroxenes, amphiboles) plus siliceous glass. The quenched crystals may be discrete or may be very thin overgrowths on stable crystals. On the other hand, where sufficiently large volumes of glass are present, glass composition in areas not near overgrown grains is unaffected by quenching, and glass compositions can represent equilibrium liquids. *Kushiro* (1974) found excellent agreement between liquid compositions determined by phase equilibria and by analysis in the system Na_2O-CaO-Al_2O-MgO-SiO_2-H_2O, where a relatively large volume (> 75%) of glass was analyzed. *Mysen and Boettcher* (1975b) analyzed smaller, but significant, volumes of glass (> 20%) and argued that the glasses represent equilibrium liquids. These liquids were andesitic at pressures to 22 kbar. On the other hand, *Green* (1973a) claimed that 20-30% volumes of liquid could not be quenched to glass. He calculated the composition of liquids in runs with H_2O vapor, using analyzed compositions of stable phases, the olivine-liquid Mg-Fe partitioning coefficient (with an allowance for iron loss from the charge to Pd-Ag capsules), and a visual or X-ray estimate of the proportions of phases present. Large errors may be introduced in this procedure (*Mysen and Boettcher*, 1975b). *Green* (1973a) argued that H_2O-saturated partial melts can be andesitic to quartz tholeiitic at 10 kbar but are olivine tholeiitic at 20 kbar.

Compositions of liquids in equilibrium with peridotite phases have also been inferred by an opposite approach -- experiments are performed on igneous rocks that are assumed to have been primary magmas, and a P and T are assigned for an appropriate configuration of liquidus or near-liquidus phases. It is further assumed that the experimentalist can separate out any effects due to fractionation or to reaction relationships between the peridotite phases and the liquid. These difficult assumptions notwithstanding, a number of workers have studied rock compositions, only a few of which can be cited here. *Nicholls and Ringwood* (1973) and *Nicholls* (1974) determined liquidus phases for H_2O-saturated andesites and tholeiites (plus varying amounts of olivine) and concluded that partial melts of peridotite are andesitic at 10 kbar, but at higher pressure, up to about 17 kbar, are quartz tholeiitic. These results generally agree with the peridotite-H_2O experiments of *Green* (1973a), but differ in detail from the peridotite-H_2O experiments of *Mysen and Boettcher* (1975b) and from some of the results on

synthetic systems (preceding section). Although the disagreements have been aired (*Mysen et al.*, 1974), areas of agreement should also be noted: It is now accepted that partial melts of peridotite in equilibrium with H_2O vapor can be quartz-normative; the differences of opinion concern the degree of silica saturation and the upper pressure limit of production of quartz-normative liquid.

Compositions of H_2O-undersaturated liquids are reviewed in the section on peridotite-H_2O-CO_2.

Studies of Peridotite-CO_2 Melting

Synthetic systems. The solubility of CO_2 in silicate melts (*Eggler*, 1973b; *Mysen et al.*, 1976) is reviewed in this volume by Mysen. Peridotite-CO_2 phase relations were studied by *Eggler* (1974, 1977) in the system Na_2O-CaO-MgO-Al_2O_3-SiO_2-CO_2 to 30 kbar. He found that liquids formed in the presence of CO_2 are more silica-poor and more alkali-rich than liquids derived in the absence of volatiles or in the presence of H_2O, and that extremely silica-undersaturated nephelinites can be derived from peridotite, in the presence of CO_2, in the pressure range 15-30 kbar. The primary cause is expansion of the phase field of orthopyroxene, relative to olivine, in the presence of CO_2. An example is the join in Fig. 5. From phase equilibrium experiments in the system CaO-MgO-SiO_2-CO_2 (*Eggler*, 1975b, 1976a,b, 1977), it was found that at pressure in excess of about 28 kbar, CO_2 has a larger effect on phase relations than at lower pressures: The solidus temperature is significantly lowered, dolomite becomes a solidus phase, and partial melt compositions are carbonate-rich. The same major effects, in the CaO-MgO-SiO_2-CO_2 system, have been found by *Wyllie and Huang* (1975a,b, 1976a) with some minor differences (*Eggler, Holloway, and Mysen*, 1976; *Wyllie and Huang*, 1976b,c; *Eggler*, 1976c).

No natural compositions have been studied.

Studies of Peridotite-H_2O-CO_2 Melting

Synthetic systems. Crystal-liquid-vapor equilibria for several silicate-H_2O-CO_2 systems have been determined and have been applied to peridotite-liquid petrogenesis (*Eggler*, 1973b; *Kadik and Eggler*, 1975; *Eggler and Rosenhauer*, 1977). *Yoder* (1970) had previously examined the join phlogopite-H_2O-CO_2 at 10 kbar, with application to magmatic crystal-liquid relations.

Eggler (1973b, 1975a) studied the composition of liquid in equilibrium with forsterite and enstatite and various CO_2-H_2O vapors in the system MgO-SiO_2-H_2O-CO_2 at 20 kbar and found that liquid composition changes from quartz-normative at $CO_2/(CO_2 + H_2O) < 0.42$ (mol) to olivine-normative at $CO_2/(CO_2 + H_2O) > 0.42$.

Holloway and Eggler (1976) determined the solidus and the phlogopite melting interval of a garnet-phlogopite peridotite in the system K_2O-CaO-MgO-CoO-Al_2O_3-SiO_2-H_2O-CO_2.

Natural compositions. *Mysen and Boettcher* (1975a,b) studied the melting of a spinel peridotite from Hawaii in the presence of relatively large amounts of H_2O and CO_2 and analyzed glass compositions. They found that, in the pressure range 10-15 kbar, with increase in $CO_2/(CO_2 + H_2O)$,

the solidus temperature increased, and the composition of partial melts changed from quartz-normative through olivine-hypersthene normative and olivine-nepheline normative to nepheline-larnite normative. (The change from quartz-normative to olivine-normative occurred at $CO_2/(CO_2 + H_2O)$ (mol) between 0.5 and 0.4, nearly the same result as in the system MgO-SiO_2-CO_2-H_2O (*Eggler*, 1975a), confirming that the orthopyroxene reaction relation seen in synthetic systems is a dominant reaction in natural compositions.)

Experiments on "primary magma" compositions (see above) have been applied to peridotite-H_2O-CO_2 problems. *Bultitude and Green* (1967), *Green* (1973b), and *Arculus* (1975) have noted the absence of orthopyroxene on the liquidus of olivine nephelinite and basanite compositions. According to results of *Eggler* (1974, 1977), CO_2 should expand the primary phase field of orthopyroxene. Indeed, *Brey and Green* (1975) have now found olivine, orthopyroxene, clinopyroxene, and garnet as liquidus or near-liquidus phases for a Tasmanian olivine melilitite at 30 kbar in the presence of CO_2-H_2O. They have claimed that the melilitite composition can be a primary melt (for comment see *Eggler and Mysen*, 1976; *Eggler*, 1977). The study of *Brey and Green* (1975) supports an interpretation (*Eggler*, 1974) of experiments of *Bultitude and Green* (1967) and *Green* (1973b), conducted with small amounts of H_2O in graphite capsules: Expansion of the field of orthopyroxene must have been due to the presence of CO_2 (produced by reaction of H_2O with graphite), not to the presence of H_2O, as claimed by *Green*. Note should be made, however, that in experiments of *Merrill and Wyllie* (1975) on a Kakanui eclogite (basanite composition) in the presence of H_2O *but no* CO_2, orthopyroxene was found as a liquidus or subliquidus phase at pressures of 18-25 kbar.

A Structural Explanation of Peridotite-H_2O-CO_2 Melting Patterns

The experimental results can be rationalized by considering a polymerization reaction, where O^{2-}, O^-, and O^0 represent free oxygen ions, oxygens bonded to one silicon (nonbridging oxygens), and oxygens bonded to two silicons (bridging oxygens), respectively (*Toop and Samis*, 1962):

$$2(O^-)_L = (O^0)_L + (O^{2-})_L. \quad (1)$$

Solution of H_2O can be written as the reaction (*Eggler and Rosenhauer*, 1977)

$$(O^0)_L + (H_2O)_V = 2(O^-H^+)_L. \quad (2)$$

If (1) and (2) are combined,

$$2(O^-)_L + (H_2O)_V = (O^{2-})_L + 2(O^-H^+)_L, \quad (3)$$

it can be seen that the result of H_2O solution is an increase in O^{2-}/O^-, representing a net depolymerization. If it is assumed that less-polymerized melts crystallize less-polymerized minerals (*Kushiro*, 1975), then olivine crystallization should be promoted at the expense of orthopyroxene. Reference to Fig. 5 should convince the reader that liquid produced at invariant-like points will be more silica-saturated than in the absence of volatiles. Solution of CO_2 can be written (*Eggler and Rosenhauer*, 1977):

$$2(O^-)_L + (CO_2)_V = (O^0)_L + (CO_3^{2-})_L. \quad (4)$$

The result is an increase in O^0/O^-, representing a net polymerization. It follows that such invariant-like liquids should be less silica-saturated than in the absence of volatiles.

Melting of a Model Mantle Composition

It has been argued above, on a semitheoretical basis, that the melting of peridotite in the presence of small amounts of volatiles is quite different from that in the presence of large amounts of volatiles, and that the former case is more applicable to the mantle than the latter. In this section, two examples of how peridotite is believed to melt in the mantle are presented for a specific mantle composition.

TABLE 1. Chemical Composition of a Peridotite Used in Construction of Isobaric Sections.

SiO_2	43.70
TiO_2	0.25
Al_2O_3	2.75
Cr_2O_3	0.28
Fe_2O_3	1.38
FeO	8.81
MnO	0.13
MgO	37.22
CaO	3.26
Na_2O	0.45
K_2O	0.05
$\Sigma(H_2O + CO_2)$	0.10
	98.38

The refractory portion of the composition (Table 1) is essentially the composition of nodule 1611 (*Nixon and Boyd*, 1973), a fertile garnet peridotite from a Lesotho kimberlite pipe. However, the K content has been lowered from 1160 ppm to what is considered a more reasonable level of 400 ppm, and the Na content has been slightly raised. A hypothetical volatile content of 0.1 wt. % has been added to this composition. Choice of this volatile content is intended only to be illustrative; for each section constructed, the range of applicable volatile contents is indicated.

The Melting Reactions

Melting and mineral stability curves selected from the papers reviewed and relevant to the constructions are shown in Fig. 6. The pressures chosen for isobaric sections are 15 and 30 kbar (Figs. 7 and 8).

The 15 kbar section. At 15 kbar, amphibole is the only volatile-containing phase that participates in a solidus reaction. The decarbonation reaction (Fig. 6) occurs at subsolidus temperatures. Phlogopite is not found (*Green*, 1973a; *Mysen and Boettcher*, 1975a) because K is incorporated in amphibole. The bulk composition (Table 1) can contain a maximum of about 15% amphibole when fully hydrated, representing an H_2O content of 0.37 wt. %, which exceeds the 0.1% available. Thus, for any volatile content from 0.01 to 0.37 wt. %, the ZIVC principle applies.

A ZIVC-type isobaric section can be constructed (Fig. 7), equivalent to a model section a-a' (Fig. 3). The "vapor-out" curve is calculated

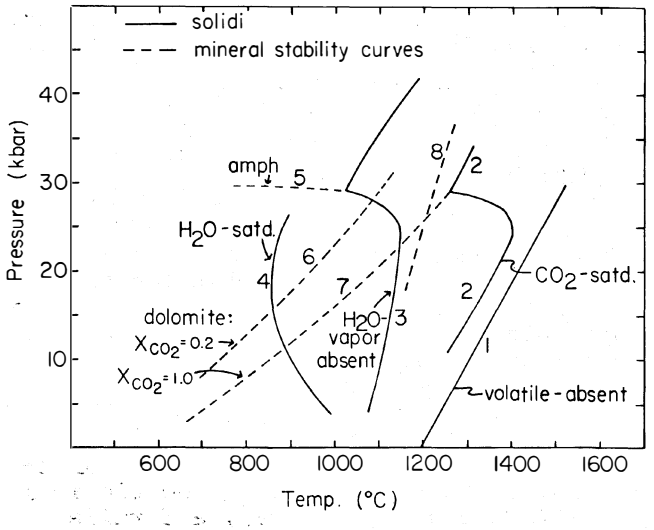

Fig. 6. A compilation of solidus and mineral stability curves for peridotite. (1) Volatile-absent solidus (*Kushiro, Syono, and Akimoto*, 1968; (2) CO_2 vapor-saturated solidus (*Eggler*, 1976a, determined in the system CaO-MgO-SiO_2-CO_2 and adjusted by about -150°C below 25 kbar to allow for other components); (3) vapor-absent pyrolite-H_2O solidus (*Green*, 1973a), also the approximate upper stability of amphibole; (4) H_2O vapor-saturated solidus (*Mysen and Boettcher*, 1975a); (5) upper pressure limit of amphibole stability (*Green*, 1973a); (6,7) upper stability limit of dolomite in peridotite phase assemblages (by the reaction enstatite + dolomite = diopside + olivine + CO_2) in the presence of vapors of $CO_2/(CO_2 + H_2O)$ = 0.2 and of $CO_2/(CO_2 + H_2O)$ = 1.0 (*Eggler, Kushiro, and Holloway*, 1976; (8) melting of phlogopite in a phlogopite-peridotite (*Holloway and Eggler*, 1976).

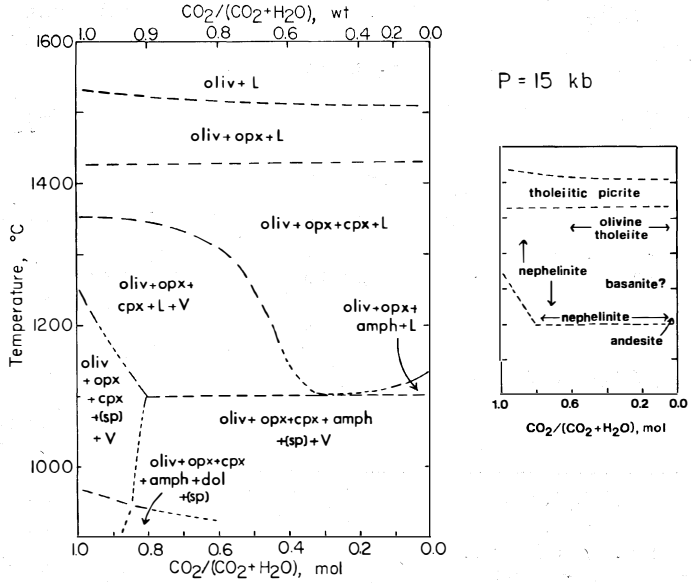

Fig. 7. Phase relations of a peridotite containing 0.1 wt. % volatiles (H_2O + CO_2) as a function of the $CO_2/(CO_2$ + $H_2O)$ volatile composition, at 15 kbar pressure. The near-solidus relations apply to volatile contents up to 0.37%. The abscissa does not denote vapor composition; vapor composition for the assemblage olivine + clinopyroxene (cpx) + orthopyroxene (opx) + amphibole (amph) + spinel (sp) is in fact invariant (at any P and T) because the assemblage is in a ZIVC. Estimated compositions of liquids in the various phase fields are shown in the inset. Phase boundaries and liquid compositions are estimated from several sources, as explained in the text. Solid lines denote well-determined boundaries; long-dashed lines, extrapolated boundaries; and short-dashed lines, estimated boundaries. Hypersolidus relations for spinel have not been estimated.

from diopside-CO_2-H_2O data of *Eggler and Rosenhauer* (1977), and the subsolidus dolomite fields are estimated from *Eggler, Kushiro, and Holloway* (1976). The temperature of melting of amphibole in the absence of vapor and of CO_2, 1115°C, is from *Green* (1973a). The solidus temperature can be bracketed between 1115° and 1050°C; a temperature at which amphibole was

stable in the CO_2-H_2O vapor-saturated experiments of *Mysen and Boettcher* (1975a), because the ZIVC solidus is also the maximum stability limit of amphibole in the presence of CO_2-H_2O vapor for incongruent-like amphibole melting behavior (compare sections a-a' and b-b', P = 6, Fig. 3). The solidus also coincides with that for a vapor composition of $CO_2/(CO_2 + H_2O)$ (mol) = 0.8 (*Mysen and Boettcher*, 1975a), as described below. The solidus reaction probably actually occurs over a small temperature interval because of solid solutions, principally Fe-Mg in olivine and pyroxenes and Na in clinopyroxene. The phase boundaries above 1400°C are estimated from the melting data of *Mysen and Kushiro* (1976) on rock 1611 in the absence of volatiles.

The compositions of liquids as a function of temperature (Fig. 7) have been estimated. Liquid formed at temperatures immediately above the solidus must be of the same composition for all volatile compositions from $CO_2/(CO_2 + H_2O)$ = 0.01 to 0.8, because for all these compositions the subsolidus phase assemblage is in a ZIVC. Moreover, the vapor composition must be the value at the left-hand side of the ZIVC, that is, 0.8. (Refer to the section at P = 6, T = 1, Fig. 3, for a visualization of this principle.) The particular value of 0.8 is not known precisely, but it must be greater than 0.75, because *Mysen and Boettcher* (1975a) found amphibole in equilibrium with liquid and vapor of $CO_2/(CO_2 + H_2O)$ = 0.75 in their excess-vapor experiments. The composition of liquid in equilibrium with vapor of $CO_2/(CO_2 + H_2O)$ = 0.8 is probably nephelinitic, judging from the data of *Eggler* (1974, 1977) and *Mysen and Boettcher* (1975b). Only for vapor consisting solely of H_2O, and therefore outside the ZIVC, is the liquid andesitic. The persistence of the nephelinite field above the solidus is due to the persistence of CO_2-rich vapor to hypersolidus temperatures. Because vapor becomes more CO_2-rich as temperature is increased (*Eggler and Rosenhauer*, 1977; *Eggler*, 1977), liquid composition must be at least as silica-undersaturated as nephelinite. At temperatures above the vapor-present field, the volatile contents of liquids will decrease as temperature increases. At temperatures approaching the volatile-absent solidus (1360°C at 15 kbar, Fig. 5), the effect of volatiles is minimal, because at these temperatures, the amount of melt increases dramatically (*Wyllie*, 1971). Below these temperatures, the amount of melt is probably less than 5% (*Mysen and Kushiro*, 1976). Thus, the fields for olivine tholeiite and tholeiitic picrite can be extrapolated with some confidence from the liquid compositions determined in the absence of volatiles by *Mysen and Kushiro* (1976).

The 30 kbar section. Above about 27 kbar, phlogopite succeeds amphibole as a solidus hydrous phase (*Green*, 1973a; *Modreski and Boettcher*, 1972), and dolomite is a solidus carbonate phase (*Holloway and Eggler*, 1976; *Eggler, Kushiro, and Holloway*, 1976). For the peridotite composition (Table 1), a completely hydrated phlogopite-peridotite will contain 0.44 wt. % phlogopite or 0.02 wt. % H_2O. A completely carbonated peridotite will contain about 10 wt. % dolomite, or 5% CO_2. Thus, an isobaric section for a dolomite-phlogopite peridotite with only 0.1 wt. % volatiles (Fig. 8) is analogous to section b-b' (Fig. 4) in the model A-H_2O-CO_2, inasmuch as compositions are, at subsolidus conditions, always undersaturated with respect to dolomite, but either saturated or undersaturated with respect to phlogopite, depending on volatile composition. The hypersolidus configuration of Fig. 8 up to about 1400°C is probably applicable to volatile contents of 0 to about 5 wt. %.

Most of the sources used in construction of the isobaric section are listed in the figure caption. The line separating the two invariant subsolidus assemblages lies at $CO_2/(CO_2 + H_2O)$ = 0.6 because at that point the bulk composition contains 0.02 wt. % H_2O, the maximum amount that can

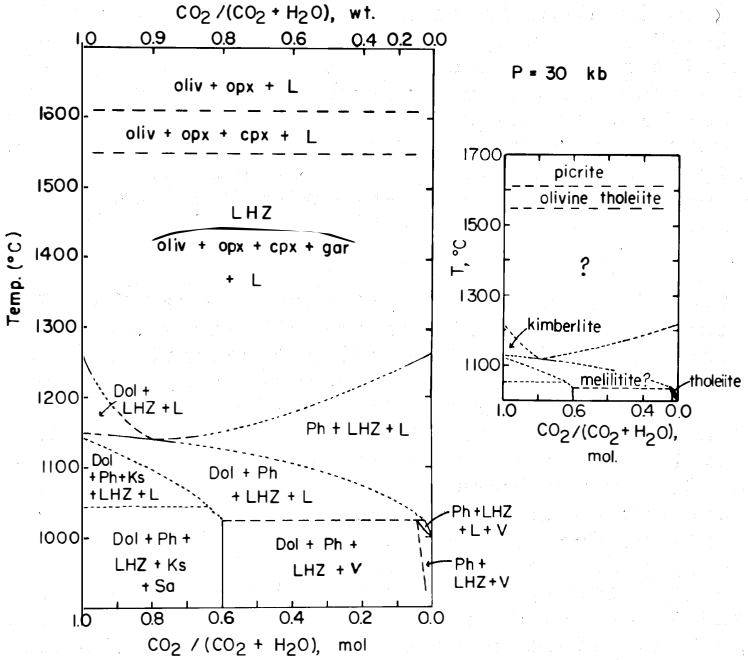

Fig. 8. Phase relations of a peridotite containing 0.1 wt. % volatiles (H_2O + CO_2) as a function of the $CO_2/(CO_2 + H_2O)$ volatile composition. The abscissa does not denote vapor composition. Dol, dolomite; Ph, phlogopite; Ks, kalsilite; Sa, sanidine; LHZ, oliv + opx + cpx + garnet (gar). Solid lines denote well-determined boundaries; long-dashed lines, extrapolated boundaries; and short-dashed lines, estimated boundaries. The boundaries between Ph + LHZ + L and LHZ + L and between Dol + Ph + LHZ + L and LHZ + L are after *Holloway and Eggler* (1976); the boundary between Dol + LHZ + L and LHZ + L is after *Eggler* (1976a); the boundary between Dol + Ph + LHZ + V and Dol + Ph + LHZ + L (the ZIVC solidus) was calculated from the decarbonation curve of *Eggler, Kushiro, and Holloway* (1976) and the peridotite solidus of *Kushiro, Syono, and Akimoto* (1968) (contours of equal X_{H_2O} must intersect at the ZIVC solidus). Phase relations above 1500°C are extrapolated from *Mysen and Kushiro* (1976). Estimated compositions of liquids in the various phase fields are shown in the inset. The low-temperature tholeiite field is after *Bravo and O'Hara* (1975), the kimberlite field after *Eggler* (1976a), and the high-temperature theoleiite and picrite fields after *Mysen and Kushiro* (1976).

be contained in phlogopite. The temperature interval between the solidus and the volatile-absent solidus (1510°C, Fig. 5) is 400°C, over which the amount of liquid must be small (probably < 2%). Above 1510°C, the amount of liquid will increase rapidly, and phase relations (and liquid compositions) interpolated from *Mysen and Kushiro* (1976) will be essentially correct. The composition of the near-solidus liquid has been estimated to be larnite-normative, on the basis of experiments of *Brey and Green* (1975) and *Eggler* (1977). (The rock name for the liquid is melilitite, although it should be noted that not all larnite-normative rocks contain modal melilite (*Velde and Yoder*, 1976).) Liquid in the Dol + LHZ + L field will be more carbonate-rich (kimberlitic), because Dol melts over that temperature interval. The composition of liquid in equilibrium with LHZ + Ph + H_2O-rich vapor is assumed to be the potash-rich olivine tholeiite determined by *Bravo and O'Hara* (1975).

Petrologic Conclusions

The following conclusions can be reached from inspection of Figs. 7 and 8. It should be kept in mind that the figures are constructed for specific ranges of volatile compositions, as indicated above.

1. In experiments on peridotite-H_2O-CO_2 systems carried out with relatively large amounts of volatiles (*Mysen and Boettcher*, 1975a; *Eggler*, 1975a), it has been found that the solidus temperature and liquid composition vary with $CO_2/(CO_2 + H_2O)$, because excess vapor, of varying composition, is present. For mantle compositions containing relatively small amounts of volatiles, where a hydrous or carbonate mineral is present, the vapor composition is (at any $\underline{P}$ and $\underline{T}$) invariant (for most $CO_2/(CO_2 + H_2O)$ compositions) within a ZIVC. Such mantle compositions melt (isobarically), whatever the $CO_2/(CO_2 + H_2O)$, at a common temperature to a common liquid.

2. At 15 kbar pressure, amphibole peridotite (plus vapor) containing small amounts of $CO_2 + H_2O$ melts at about 1100°C to a nephelinitic liquid, because the coexisting, invariant vapor has $CO_2/(CO_2 + H_2O) \approx 0.8$. Only a small amount of nephelinitic liquid can be produced, however, if the amount of volatiles in the source region is small ($\sim$ 0.1 wt. %). For larger degrees of melting, liquids will contain smaller amounts of volatiles and their compositions will be less affected by the volatiles, until at temperatures near the volatile-absent solidus (1510°C), liquid compositions will be similar to those of liquids produced in the absence of volatiles (tholeiites). If partial melting is fractional, melting will cease at the point at which the volatile-containing liquid fraction is removed from the source region, and will not resume unless the temperature rises to that of the volatile-absent solidus. An exception is the hypersolidus field containing both liquid and vapor: If vapor is not removed with the liquid fraction, melting will not cease. Moreoever, the liquid composition will be strongly controlled by vapor fractionation (*Eggler*, 1974; *Mysen, Arculus, and Eggler*, 1975), becoming even less silica-saturated than nephelinite. (Note that under no circumstances can andesite be produced by partial melting, except if CO_2 is entirely lacking in the source region.)

3. At 30 kbar pressure, dolomite-phlogopite peridotite (with or without vapor) containing small amounts of CO_2 and H_2O melts at about 1025°C to a liquid that is probably melilititic. Such melilititic primary melts can be produced only in the presence of CO_2 (*Eggler*, 1974; *Brey and Green*, 1975). For *very* high $H_2O/(H_2O + CO_2)$, the liquid is olivine tholeiitic. The composition of liquid produced in the absence of H_2O is kimberlitic or carbonatitic (*Eggler*, 1975b, 1976a; *Wyllie and Huang*, 1975b). Dolomite or phlogopite persists to temperatures about 100°C above the solidus, but the amount of liquid produced is probably only a few percent until temperatures about 350°C above the solidus are reached. The same principles of fractional melting discussed above apply to the 30 kbar section, with the exception that within the hypersolidus fields containing either dolomite or phlogopite, removal of the liquid fraction will not cause melting to cease. Rather, melting will proceed, but on a radically different course, inasmuch as the source region will then contain only CO_2 or H_2O, depending on whether dolomite or phlogopite is the residual phase.

Acknowledgements

Analysis of the theoretical H_2O-CO_2 systems has been stimulated by discussions with Dean Presnall, B.J. Hensen, and A.B. Thompson. Reviews of the paper by B.O. Mysen, D.M. Burt, R.F. Wendlandt, N.T. Arndt, and H.S. Yoder, Jr., are appreciated. The initiative of Henry Dick in organizing the Partial Melting Conference resulted in this new analysis of peridotite melting. The research was supported by the National Science Foundation, Earth Sciences Section, Grant DES 73-00266A01.

Note added in proof: *Wyllie* (1977) has developed a concept very similar to the ZIVC developed here, that is, a mantle vapor composition buffered by reaction. His discussion is, however, limited to a carbonated peridotite.

References

Arculus, R.J., Melting behavior of two basanites in the range 10-35 kbar and the effect of TiO_2 on the olivine-diopside reactions at high pressures, *Carnegie Inst. Washington Yearb. 74*, 512-515, 1975.

Boettcher, A.L., The system $CaO-Al_2O_3-SiO_2-H_2O$ at high pressures and temperatures, *J. Petrol., 11*, 337-379, 1970.

Boettcher, A.L., and P.J. Wyllie, Phase relationships in the system $NaAlSiO_4-SiO_2-H_2O$ to 35 kilobars pressure, *Am. J. Sci., 267*, 875-909, 1969.

Bravo, M.S., and M.J. O'Hara, Partial melting of phlogopite-bearing synthetic spinel- and garnet-lherzolites, *Phys. Chem. Earth, 9*, 845-854, 1975.

Brey, G., and D.H. Green, The role of CO_2 in the genesis of olivine melilitite, *Contrib. Mineral. Petrol., 49*, 93-103, 1975.

Bultitude, R.J., and D.H. Green, Experimental study at high pressures on the origin of olivine nephelinite and olivine melilite nephelinite magmas, *Earth Planet. Sci. Lett., 3*, 325-337, 1967.

Cawthorn, R.G., C.E. Ford, G.M. Biggar, M.S. Bravo, and D.B. Clarke, Determination of the liquid composition in experimental samples: discrepancies between microprobe analysis and other methods, *Earth Planet. Sci. Lett., 21*, 1-5, 1973.

Eggler, D.H., Principles of melting of hydrous phases in silicate melt, *Carnegie Inst. Washington Yearb. 72*, 491-495, 1973a.

Eggler, D.H., Role of CO_2 in melting processes in the mantle, *Carnegie Inst. Washington Yearb. 72*, 457-467, 1973b.

Eggler, D.H., Effect of CO_2 on the melting of peridotite, *Carnegie Inst. Washington Yearb. 73*, 215-224, 1974.

Eggler, D.H., CO_2 as a volatile component of the mantle: the system $Mg_2SiO_4-SiO_2-H_2O-CO_2$, *Phys. Chem. Earth, 9*, 869-881, 1975a.

Eggler, D.H., Peridotite-carbonate relations in the system $CaO-MgO-SiO_2-CO_2$, *Carnegie Inst. Washington Yearb. 74*, 468-474, 1975b.

Eggler, D.H., Does CO_2 cause partial melting in the low-velocity layer of the mantle?, *Geology, 4*, 69-72, 1976a.

Eggler, D.H., Composition of the partial melt of carbonated peridotite in the system $CaO-MgO-SiO_2-CO_2$, *Carnegie Inst. Washington Yearb. 75*, 623-626, 1976b.

Eggler, D.H., Does CO_2 cause partial melting in the low-velocity layer of the mantle?: reply, *Geology, 4*, 787-789, 1976c.

Eggler, D.H., Carbon dioxide in silicate melts: III. The effect of CO_2 upon partial melting of peridotite in the system Na_2O-CaO-Al_2O_3-MgO-SiO_2-CO_2-H_2O to 35 kbar pressure, *Am. J. Sci.*, in press, 1977.

Eggler, D.H., J.R. Holloway, and B.O. Mysen, High CO_2 solubilities in mantle magmas: comment, *Geology, 4*, 198-199, 1976.

Eggler, D.H., I. Kushiro, and J.R. Holloway, Stability of carbonate minerals in a hydrous mantle, *Carnegie Inst. Washington Yearb. 75*, 631-636, 1976.

Eggler, D.H., and B.O. Mysen, The role of CO_2 in the genesis of olivine melilitite: discussion, *Contrib. Mineral. Petrol., 55*, 231-236, 1976.

Eggler, D.H., and M. Rosenhauer, Carbon dioxide in silicate melts: II. Solubilities of CO_2 and H_2O in $CaMgSi_2O_6$ (diopside) liquids and vapors at pressures to 40 kb, *Am. J. Sci.*, in press, 1977.

Ford, C.E., Phase relations in the system CaO-MgO-Al_2O_3-SiO_2-H_2O, in *Progress in Experimental Petrology*, vol. 3, London, Nat. Environment Res. Council, Publ. Ser. D., no. 6, 266-272, 1976.

Ford, C.E., and M.J. O'Hara, The system $MgSiO_3$-$Ca_3Al_2Si_3O_2$-H_2O, in *Progress in Experimental Petrology*, vol. 2, London, Nat. Environment Res. Council, Publ. Ser. D, no. 2, 151-153, 1972.

Green, D.H., Compositions of basaltic magmas as indicators of conditions of origin: application to oceanic volcanism, *Philos. Trans. R. Soc. London, 268*, 707-721, 1970.

Green, D.H., Experimental melting studies on a model upper mantle composition at high pressure under water-saturated and water-undersaturated conditions, *Earth Planet. Sci. Lett., 19*, 37-53, 1973a.

Green, D.H., Conditions of melting of basanite magma from garnet peridotite, *Earth Planet. Sci. Lett., 17*, 456-465, 1973b.

Holloway, J.R., The system pargasite-H_2O-CO_2: a model for melting of a hydrous mineral with a mixed-volatile fluid: I. Experimental results to 8 kbar, *Geochim. Cosmochim. Acta, 37*, 651-666, 1973.

Holloway, J.R., and D.H. Eggler, Fluid-absent melting of peridotite containing phlogopite and dolomite, *Carnegie Inst. Washington Yearb. 75*, 636-639, 1976.

Howells, S., An investigation into the possibility of obtaining nepheline-normative liquids in the system CaO-MgO-Al_2O_3-SiO_2-Na_2O-H_2O at high pressure, in *Progress in Experimental Petrology*, vol. 3, London, Nat. Environment Res. Council, Publ. Ser. D, no. 6, 279-280, 1976.

Huang, W.L., J.K. Robertson, and P.J. Wyllie, Melting relations of muscovite to 30 kilobars in the system $KAlSi_3O_8$-Al_2O_3-H_2O, *Am. J. Sci., 273*, 415-427, 1973.

Kadik, A.A., and D.H. Eggler, Melt-vapor relations on the join $NaAlSi_3O_8$-H_2O-CO_2, *Carnegie Inst. Washington Yearb. 74*, 479-484, 1975.

Kushiro, I., Compositions of magmas formed by partial zone melting of the earth's upper mantle, *J. Geophys. Res., 73*, 619-634, 1968.

Kushiro, I., The system forsterite-diopside-silica with and without water at high pressures, *Am. J. Sci., 267A*, 269-294, 1969.

Kushiro, I., Stability of amphibole and phlogopite in the upper mantle, *Carnegie Inst. Washington Yearb. 68*, 245-247, 1970.

Kushiro, I., Effect of water on the composition of magmas formed at high pressures, *J. Petrol., 13*, 311-334, 1972.

Kushiro, I., Melting of hydrous upper mantle and possible generation of andesitic magma: an approach from synthetic systems, *Earth Planet. Sci. Lett., 22*, 294-299, 1974.

Kushiro, I., On the nature of silicate melt and its significance in magma genesis: regularities in the shift of the liquidus boundaries involving olivine, pyroxene, and the silica minerals, *Am. J. Sci., 275*, 411-431, 1975.

Kushiro, I., N. Shimizu, Y. Nakamura, and S. Akimoto, Compositions of co-existing liquid and solid phases formed upon melting of natural garnet and spinel lherzolites at high pressures: a preliminary report, *Earth Planet. Sci. Lett., 14*, 19-25, 1972.

Kushiro, I., Y. Syono, and S. Akimoto, Melting of a peridotite nodule at high pressures and high water pressures, *J. Geophys. Res., 73*, 6023-6029, 1968.

Kushiro, I., H.S. Yoder, Jr., and M. Nishikawa, Effect of water on the melting of enstatite, *Geol. Soc. Am. Bull., 79*, 1685-1692, 1968.

Merrill, R.B., and P.J. Wyllie, Kaersutite and kaersutite eclogite from Kakanui, New Zealand -- water-excess and water-deficient melting to 30 kilobars, *Geol. Soc. Am. Bull., 86*, 555-570, 1975.

Millhollen, G.L., A.J. Irving, and P.J. Wyllie, Melting interval of peridotite with 5.7 percent water to 30 kilobars, *J. Geol., 82*, 575-587, 1974.

Modreski, P.J., and A.L. Boettcher, The stability of phlogopite + enstatite at high pressures: a model for micas in the interior of the earth, *Am. J. Sci., 272*, 852-869, 1972.

Modreski, P.J., and A.L. Boettcher, Phase relationships in the system K_2O-MgO-CaO-Al_2O_3-H_2O to 35 kilobars: a better model for micas in the interior of the earth, *Am. J. Sci., 273*, 385-515, 1973.

Mysen, B.O., R.J. Arculus, and D.H. Eggler, Solubility of carbon dioxide in melts of andesite, tholeiite, and olivine nephelinite composition to 30 kbar pressure, *Contrib. Mineral. Petrol., 53*, 227-239, 1975.

Mysen, B.O., and A.L. Boettcher, Melting of a hydrous mantle. I. Phase relations of natural peridotite at high pressures and temperatures with controlled activities of water, carbon dioxide, and hydrogen, *J. Petrol., 16*, 520-548, 1975a.

Mysen, B.O., and A.L. Boettcher, Melting of a hydrous mantle. II. Geochemistry of crystals and liquids formed by anatexis of mantle peridotite at high pressures and high temperatures as a function of controlled activities of water, hydrogen, and carbon dioxide, *J. Petrol., 16*, 549-590, 1975b.

Mysen, B.O., D.H. Eggler, M.G. Seitz, and J.R. Holloway, Carbon dioxide in silicate melts and crystals. I. Solubility measurements, *Am. J. Sci., 276*, 455-479, 1976.

Mysen, B.O., and I. Kushiro, Compositional variation of coexisting phases with degree of melting of peridotite under upper mantle conditions, *Carnegie Inst. Washington Yearb. 75*, 546-555, 1976.

Mysen, B.O., I. Kushiro, I.A. Nicholls, and A.E. Ringwood, A possible mantle origin for andesitic magmas: discussion of a paper by Nicholls and Ringwood, *Earth Planet. Sci. Lett., 21*, 221-229, 1974.

Nicholls, I.A., Liquids in equilibrium with peridotitic mineral assemblages at high water pressures, *Contrib. Mineral. Petrol., 45*, 289-316, 1974.

Nicholls, I.A., and A.E. Ringwood, Production of silica-saturated tholeiitic magmas in island arcs, *Earth Planet. Sci. Lett., 17*, 243-246, 1973.

Nixon, P.H., and F.R. Boyd, Petrogenesis of the granular and sheared ultrabasic nodule suite in kimberlite, in *Lesotho Kimberlites*, edited by P.H. Nixon, Lesotho National Development Corporation, Maseru, Lesotho, 48-56, 1973.

Ricci, J.E., *The Phase Rule and Heterogeneous Equilibrium*, D. Van Nostrand Company, Inc., New York, 1951.

Robertson, J.K., and P.J. Wyllie, Rock-water systems, with special reference to the water-deficient region, *Am. J. Sci., 271*, 252-277, 1971.

Toop, G.W., and C.S. Samis, Activities of ions in silicate melts, *Trans. Metall. Soc. AIME, 224*, 878-887, 1962.

Velde, D., and H.S. Yoder, Jr., The chemical composition of melilite-bearing eruptive rocks, *Carnegie Inst. Washington Yearb. 75*, 574-580, 1976.

Wyllie, P.J., The role of water in magma generation and initiation of diapiric uprise in the mantle, *J. Geophys. Res., 76*, 1328-1338, 1971.

Wyllie, P.J., Mantle fluid compositions buffered by carbonates in peridotite-H_2O-CO_2, *J. Geology, 85*, 187-207, 1977.

Wyllie, P.J., and H.L. Huang, Influence of mantle CO_2 in the generation of carbonatites and kimberlites, *Nature, 257*, 297-299, 1975a.

Wyllie, P.J., and H.L. Huang, Peridotite, kimberlite, and carbonatite explained in the system CaO-MgO-SiO_2-CO_2, *Geology, 3*, 621-624, 1975b.

Wyllie, P.J., and W.L. Huang, Carbonation and melting reactions in the system $CaO-MgO-SiO_2-CO_2$ at mantle pressures with geophysical and petrological applications, *Contrib. Mineral. Petrol.*, *54*, 79-107, 1976a.

Wyllie, P.J., and W.L. Huang, High CO_2 solubilities in mantle magmas: reply, *Geology*, *4*, 199-200, 1976b.

Wyllie, P.J., and W.L. Huang, Does CO_2 cause partial melting in the low-velocity layer of the mantle?: comment, *Geology*, *4*, 712-713, 1976c.

Yoder, H.S., Jr., Calcalkaline andesites: experimental data bearing on the origin of their assumed characteristics, in *Proceedings of the Andesite Conference*, edited by A.R. McBirney, Oreg. Dept. Geol. Miner. Ind. Bull. 65, 77-89, 1969.

Yoder, H.S., Jr., Phlogopite-H_2O-CO_2: an example of the multicomponent gas problem, *Carnegie Inst. Washington Yearb. 68*, 236-240, 1970.

Yoder, H.S., Jr., and I. Kushiro, Melting of a hydrous phase: phlogopite, *Am. J. Sci.*, *267A*, 558-582, 1969.

EQUILIBRIUM AND MIXING IN A PARTIALLY MOLTEN MANTLE

Albrecht W. Hofmann and Mordeckai Magaritz
Carnegie Institution of Washington
Department of Terrestrial Magnetism
5241 Broad Branch Road N.W.
Washington, D.C. 20015

The volume of rock that will attain chemical and isotopic equilibrium during partial melting depends on (a) the reaction rate between solid and melt, (b) the rate of mixing due to convective movement of the melt or the solid-melt aggregate, (c) the rate of transport due to diffusion, and (d) the duration of the process.

Effect (a) has been reviewed by *Hofmann and Hart* (1977), who summarized the available diffusion data for mantle minerals (olivine, pyroxene, phlogopite) and estimated that $D=10^{-13}cm^2s^{-1}$ is a lower limit for diffusivities at temperatures above 1000°C. This means that crystals of 1 cm diameter or less will reach essentially complete (> 99%) equilibrium with the surrounding melt phase in less than $4x10^4$ years. Unfortunately, the experimental data on diffusion in crystalline silicates are incomplete and in many cases open to question. Therefore, the above conclusion should be regarded as a current best estimate only. However, for the purpose of this discussion, we shall assume that solid-melt equilibration is sufficiently rapid so that the partially molten aggregate may be regarded as being in local equilibrium, in the sense that the melt is everywhere in equilibrium with the nearest solid phases.

Effect (b) is difficult to assess because the dynamics of mantle convection is poorly understood. Quantitative estimates might be obtained for certain probable processes such as diapiric intrusion of a crystal-melt mush, or two-phase flow during upwelling at the mid-ocean ridge (*Turcotte and Ahern*, 1977). *Hofmann and Hart* (1977) reviewed the Sr isotopic data on oceanic basalts, which are relatively uniform for ocean floor rocks and much more heterogeneous for ocean islands. We suggest that the relative uniformity of the ocean floor rocks is the result of convective mixing within a well defined reservoir in the mantle which undergoes only limited mixing with the source mantle of the oceanic islands. The length scale of mixing between these two reservoirs can be estimated from the length of the transition zones between the two types of material. Although it is not *a priori* clear that these transition zones must be a result of mixing rather than a primary feature of the underlying mantle, such an interpretation is plausible, for example, if the islands are derived from a deep-mantle plume. Such transition zones, interpreted as regions of mixing between two mantle-derived components, have been studied on the Reykjanes Ridge by *Schilling* (1973), *Hart et al.* (1973) and *Sun et al.* (1975), and on the Azores platform by *Schilling* (1975), *White et al.* (1976) and *White* (1977). The length of the transition zone is about 400 km in the Reykjanes Ridge and about 1000 km in the ridge segment south of the Azores platform. Despite this relatively large overall scale of mixing, the isotopic composition shows smaller fluctuations on a scale of tens of kilometers or less along both ridge segments. This must reflect the length

scale of the convective motions involved.

Effect (c) can be measured with more confidence from available experimental data on diffusion in silicate melts. Figure 1 is a compilation of results for diffusion in melts of basaltic composition. *Hofmann and Magaritz* (1977) have argued that these diffusivities would not be drastically increased by the addition of volatiles to the basalt. These arguments are based in part on the low cation mobility in a water-saturated basalt - rhyolite couple (*Yoder*, 1973). Thus, although the addition of water can increase the reaction rates in silicates by several orders of magnitude, the effect on the diffusion rates in silicate melts appears to be much smaller. The similarities of diffusivities of a wide variety of ionic species makes it possible to estimate transport rates in a partially molten mantle, assuming that the composition of the melt phase is similar to basalt. In multiphase aggregates, the diffusion transport is a complex process when considered in detail. However, the assumptions normally applied to diffusion metasomatism in metamorphic rocks should also apply to partially molten rocks. Following *Korzhinskii* (1970), we assume local equilibrium between liquid and solid phases and diffusional transport through a standing pore liquid, which is everywhere interconnected. The diffusion equation (for one dimension) may then be written

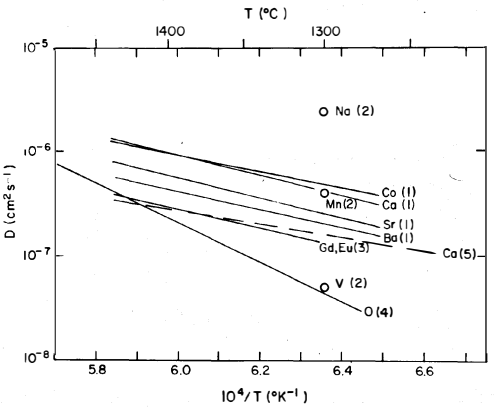

Fig. 1. Diffusion coefficients in molten basalt as a function of inverse absolute temperature. Sources of data are given by number in parentheses: (1) *Hofmann and Magaritz* (1977); (2) *Hofmann and Brown* (1976); (3) *Magaritz and Hofmann* (1977a); (4) *Muehlenbachs and Kushiro* (1974); (5) *Medford* (1973). (1), (2) and (3) are tracer diffusion studies on olivine tholeiite basalt (*Kilauea*, 1921); (4) is a tracer diffusion study on (unspecified) basalt; (5) is a study of chemical diffusion from a mugearite, artificially enriched in CaO, into normal mugearite.

$$\frac{\partial c}{\partial t} = \frac{\beta D_{melt}}{\tau[k(1-\beta)+\beta]} \frac{\partial^2 c}{\partial x^2} \qquad (1)$$

where c is the concentration of the diffusing component in the melt, t is the time, τ is the coefficient related to the tortuosity of the diffusion path, β is the fractional porosity, D is the diffusion coefficient, k is the bulk partition coefficient given by k = s/c, where s is the concentration in the solid phases and k is assumed constant, x is the distance in the direction of diffusion. Equation (1) may be derived, for example, from equation 14.3 given by *Crank* (1975). Thus, an effective diffusion coefficient can be defined for the partially molten rock

$$D_{rock} = \frac{\beta D_{melt}}{\tau[(1-\beta(k+\beta]}$$

The dependence of D_{rock}/D_{melt} on the melt fraction β is shown on Fig. 2 for different values of K. The value of τ is assumed to be unity. This illustrates the difference in diffusion behavior between major elements ($k > 0.1$) and incompatible trace elements ($k < 0.1$). For large values of k and moderate degrees of melting, the effective diffusion coefficient of the rock is given by $D_{rock} \approx D_{melt}(\beta/k)$, and D_{rock} is therefore smaller than

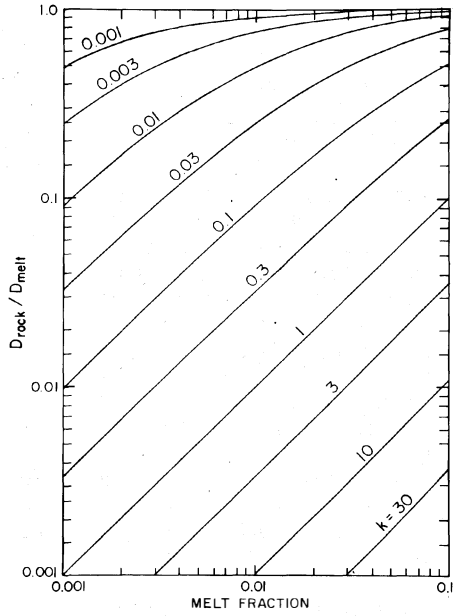

Fig. 2. Relative effective diffusion coefficient of the partially molten rock, D(rock/D(melt), as a function of the melt fraction of the rock, for different values of the bulk partition coefficient k = 0.001 to k = 30. The melt is assumed to be interconnected and the effect of path tortuosity negligible. All transport is assumed to occur in the melt phase, which is everywhere in local equilibrium with the solid phases.

D_{melt} by one or several orders of magnitude. For very small values of k, D_{rock} becomes approximately equal to D_{melt}, except when the degree of melting is also very small. Consequently, the incompatible elements, such as Ba and the light REE, will in general diffuse more rapidly through a partially molten mantle than do the major elements, such as Ca, or trace elements such as Co that have relatively large partition coefficients. For example, if the bulk partition coefficients for Sr and Ca are k = 0.01 and k = 1.0 respectively, the effective diffusion coefficients in a rock with one per cent melt at 1300°C will be D_{rock} (Sr) = 1 x 10^{-7} and D_{rock} (Ca) = 4 x 10^{-9} cm^2s^{-1}, even though D_{melt} (Ca) is greater than D_{melt}(Sr).

The order of magnitude of equilibration distances is most conveniently estimated by the relation $X = (Dt)^{1/2}$. Consideration of examples with specific initial and boundary conditions yields results that are surprisingly similar to those obtained from this simple estimate (*Magaritz and Hofmann*, 1977b; *Hofmann and Magaritz*, 1977). Using D = 10^{-6} cm^2s^{-1} as an upper limit for most of the effective diffusion coefficients, we obtain distances of 5.6 cm for one year, 56 cm for 100 years, 56 m for 10^6 years, and 3.8 km for 4.5 x 10^9 years. Thus, diffusion is very efficient in equilibrating a partially molten mantle on a small scale, but any mixing on a scale greater than a few kilometers can only be accomplished by convection.

The persistence of relatively small-scale isotopic inhomogeneities along the Mid-Atlantic ridge shows that convective mixing did not reduce the size of these inhomogeneities sufficiently for complete diffusive homogenization to take place. Thus it appears that diffusive and convective mixing do not interact efficiently in the source regions of midocean ridges, and it should therefore be possible to set a lower limit for the size of the small mantle-convection cells that have recently been advocated (*Richter and Parsons*, 1975; *Parsons and McKenzie*, 1977).

In contrast with these heterogeneities along the midocean ridge, many individual volcanoes and several entire oceanic islands are quite uniform in isotopic composition (*O'Nions and Pankhurst*, 1974; *Hofmann and Hart*, 1977). These must be derived from reservoirs that are internally well mixed by combined convection and diffusion. It seems plausible that the necessary small-scale convection is related to the intrusion process itself.

The effect of time (d) can be estimated from the relation $X = (Dt)^{1/2}$ for diffusion processes. Because of the square root relation, errors in the time estimate are demagnified in the estimate of diffusion distance. Estimates for the duration of convection depend strongly on the particular convection process. Thus the time for convective turnover

of a large oceanic plate may be estimated from the rate of sea floor spreading to be on the order of 10^8 to 10^9 years. Times for magma ascent can be estimated from the viscosity of the magma and the size of xenoliths transported by the magma. *Kushiro et al.* (1976) estimated times of several days for tholeiitic magmas and hours for alkalic magmas, if inclusions of 10 cm diameter are transported by magma with Newtonian behavior. *Sparks et al.* (1977) discussed the possibility of a slower ascent on the order of 100 days because of the yield strength of magmas. In contrast with these comparatively rapid ascent rates, the rise of hot viscous diapirs or "blobs" will be much slower, if there is no crack or pre-existing conduit. *Marsh* (1977) has estimated the ascent rate of a blob that heats its wall as it rises to be about 10^{-6} m s^{-1}, or about 3×10^3 yr per 100 km.

The conclusion drawn from the above observations is that the three processes which cause homogenization and equilibrium in the mantle have different characteristic length scales: for solid-solid and solid-melt reactions the scale is on the order of 1 cm or less; for convective mixing it is hundreds of kilometers, except in intrusive processes where it is sufficiently small so that convection interacts with diffusion in the melt to produce nearly complete homogenization. Diffusion in a partially molten homogenizes the rock on a scale of meters to kilometers for times between 10^6 and 10^9 years. Incompatible trace elements tend to diffuse faster than major elements (despite lower diffusion coefficients) because their mobility is less retarded by reaction with solid phases.

Acknowledgements

We thank D.C. Presnall for reviewing the manuscript and suggesting several improvements. The National Science Foundation Grant No. EAR 73-00255 A02 provided financial support.

References

Crank, J., *The Mathematics of Diffusion, Second Edition*, Oxford University Press, 1975.

Hart, S.R., J.-G. Schilling, and J.L. Powell, Basalts from Iceland and along the Reykjanes Ridge: Sr isotope geochemistry, *Nature Phys. Sci., 246*, 155, 104-107, 1973.

Hofmann, A.W., and L. Brown, Diffusion measurements using fast deuterons for *in situ* production of radioactive tracers, *Carnegie Inst. Yearbook 75*, 259-262, 1976.

Hofmann, A.W., and S.R. Hart, An assessment of local and regional isotopic equilibrium in the mantle, *Earth Planet. Sci. Lett.*, 1977, in press.

Hofmann, A.W., and M. Magaritz, Diffusion of Ca, Sr, Ba and Co in a basalt melt: Implications for the geochemistry of the mantle, *Jour. Geophys. Res.*, 1977, in press.

Korzhinskii, D.S., *Theory of Metasomatic Zoning*, Oxford University Press, 162 p., 1970.

Kushiro, I., H.S. Yoder, and B.O. Mysen, Viscosities of basalt and andesite melts at high pressures, *J. Geophys. Res.*, *81*, 6351-6356, 1977.

Magaritz, M., and A.W. Hofmann, Cation diffusion in natural silicate melts, *Carnegie Inst. Washington Yearbook 76*, 1977a, in press.

Magaritz, M., and A.W. Hofmann, Diffusion of Sr, Ba, and Na in obsidian, *Geochim. et Cosmochim. Acta*, 1977b,(ms. submitted).

Marsh, B., Ascent of a hot viscous blob (abst.), *EOS*, *58*, 535, 1977.

Medford, G.A., Calcium diffusion in a mugearite melt, *Can. J. Earth Sci.*, *10*, 394-402, 1973.

Muehlenbachs, K., and I. Kushiro, Oxygen isotope exchange and equilibrium of silicates with CO_2 or O_2, *Carnegie Inst. Washington Yearbook 73*, 232-236, 1974.

O'Nions, R.K., and R.J. Pankhurst, Petrogenetic significance of isotope and trace element variations in volcanic rocks from the Mid-Atlantic, *J. Petrology*, *15*, 603-634, 1974.

Parsons, B., and D. McKenzie, Mantle convection and the thermal structure of the plates (abst.), *EOS*, *58*, 499, 1977.

Richter, F.M., and B. Parsons, On the interaction of two scales of convection in the mantle, *J. Geophys. Res.*, *80*, 2529-2541, 1975.

Schilling, J.-G., Iceland Mantle Plume: geochemical evidence along Reykjanes Ridge, *Nature*, *242*, 565-571, 1973.

Schilling, J.-G., Azores mantle blob: rare-earth evidence, *Earth Planet. Sci. Lett.*, *25*, 103-115, 1975.

Sparks, R.S.J., H. Pinkerton, and R. MacDonald, The transport of xenoliths in magmas, *Earth Planet. Sci. Lett.*, *35*, 234-238, 1977.

Sun, S.S., M. Tatsumoto, and J.-G. Schilling, Mantle mixing along the Reykjanes Ridge axis: lead isotopic evidence, *Science*, *190*, 143-147, 1975.

Turcotte, D.L., and J.L. Ahern, A porous flow model for magma migration in the asthenosphere (abst.), *EOS*, *58*, 535, 1977.

White, W.M., Geochemistry of igneous rocks from the central North Atlantic: the Azores and the mid-Atlantic ridge, *Ph.D. Dissertation*, *University of Rhode Island*, 1977.

White, W.M., J.-G. Schilling, and S.R. Hart, Evidence for the Azores mantle plume from strontium isotope geochemistry of the Central North Atlantic, *Nature*, *263*, 659-663, 1976.

Yoder, H.S., Jr., Contemporaneous basaltic and rhyolitic magmas, *Amer. Mineral.*, *58*, 153-171, 1973.

2. FIELD EVIDENCE OF PARTIAL MELTING

NON-EQUILIBRIUM PARTIAL FUSION DUE TO DECOMPRESSION AND THERMAL EFFECTS IN CRUSTAL XENOLITHS

Elaine R. Padovani
Department of Earth and Planetary Sciences
Massachusetts Institute of Technology
Cambridge, Massachusetts 02139

James L. Carter
University of Texas at Dallas
Program for Geosciences
Box 688
Richardson, Texas 75080

Abstract

Variable amounts of partial fusion both within cracks in minerals and along grain boundaries have been observed in crustally derived granulite facies xenoliths from Kilbourne Hole maar, south central New Mexico. The fusion occurred rapidly enough to have had little effect on the homogeneity of major phases. The melt produced was quenched producing either inhomogeneous interstitial glasses or symplectites of either: 1) orthopyroxene-spinel-glass around garnet margins, or 2) olivine-glass around orthopyroxene margins. Lack of mixing of liquids on a microscale has been observed where fusion occurred between adjacent ilmenite and sanidine grains. Partial fusion in anorthosite and charnockite produced glasses rich in P_2O_5 (up to 10 oxide weight percent) due to the presence of locally abundant apatite. Interstitial melting most frequently occurs adjacent to ferromagnesian phases; such liquids, however, do not represent the first melts that would be produced by equilibrium fusion of the xenolith. The reactions involved have not reached equilibrium and, therefore, cannot give indications of temperature, oxygen fugacity or pressure attained by the xenolith either before incorporation into the vent or during transport to the surface.

Introduction

We have found variable amounts of glass and its cooling products in a suite of lower crustal xenoliths from Kilbourne Hole maar in south central New Mexico. The xenoliths have been previously described (*Padovani*, 1977; *Padovani and Carter*, 1977) and appear to represent lower crustal material which was incorporated into ascending magmas during the explosive volcanic eruptions which formed the maar. The xenolith glasses and their products are chemically unlike the host alkali olivine basalt and evidently represent partial melts of the xenoliths preserved *in situ* by quenching.

Xenolith Mineralogy

The lower crustal xenoliths consist of anhydrous quartzofeldspathic garnet granulites, two pyroxene granulites, charnockite and anorthosite in decreasing abundance (*Padovani*, 1977; *Padovani and Carter*, 1977). The mineralogy and chemistry of these xenoliths is outlined in *Padovani and Carter* (1977) and described in detail in *Padovani* (1977), but, in general, garnet, feldspars, sillimanite, pyroxene and ilmenite are the principal phases.

Partial Fusion Products

The xenoliths most affected by the fusion process are the quartzofeldspathic garnet granulites (Plates 1 and 2). Two pyroxene granulite, charnockite and anorthosite also display effects of partial fusion, but melts in these rock types are much less extensively developed. Garnet is the principal phase most affected by the partial fusion process (Plates 1a, 1b and 1c). Moderate amounts of partial fusion appear to have not affected the homogeneity of major phases such as garnet, as demonstrated by electron microprobe analyses which indicate no observable zonation with respect to major and minor elements (*Padovani and Carter*, 1973, 1977). Ilmenite, when extensively fused, develops ulvospinel rims or quench-like crystals of ulvospinel of variable composition along its margins (*Padovani*, 1977). Often, hercynitic spinel is found nucleating on the ulvospinel rims (*Padovani*, 1977). Ulvospinel lamellae of uniform composition are found in the interiors of ilmenite grains which have undergone small amounts of fusion. With progressive fusion, the rims develop at the expense of the lamellae, which eventually disappear.

Interstitial glass is an ubiquitous component in the garnet-rich regions of the quartzofeldspathic granulites and it is also observed in regions rich sillimanite, feldspars and quartz (Plates 1d and 2). Glasses produced from the partial fusion of ilmenite are typically purple in color, those produced from the partial fusion of garnet are pale yellow and those produced from the partial fusion of potassium feldspar (sanidine) are colorless. These differences are accentuated where glasses produced by partial fusion of garnet, ilmenite and sanidine have formed but have not been thoroughly mixed (Plate 2a). Plate 2 illustrates various types of incipient fusion. Estimates of the percent of glass and its contained quench products determined by point counting demonstrate that interconnection of intergranular melt pockets is slight until greater than 40 to 50 percent trapped melt is present in the garnet granulites. Locally, initial melts tend to reflect adjacent mineralogies. A few xenoliths have a frothy texture with dark glassy material along formerly garnet-rich layers, which now are separated from one another by regions of lighter colored glass containing partially digested and/or unaltered grains of plagioclase, sillimanite and quartz (Plate 1d).

Glassy alkali olivine basalt forms partial or complete crusts around the xenoliths. The contact between the interstitial glass formed within the xenolith and the basalt crust is sharp except where fractures, extending to the surface of the xenolith, have acted as pathways for entry of magma. Where this basaltic glass and its quench products is observed within a xenolith, its presence is distinctive because of its dark brown color, vesicular nature and the presence of olivine and/or pyroxene phenocrysts.

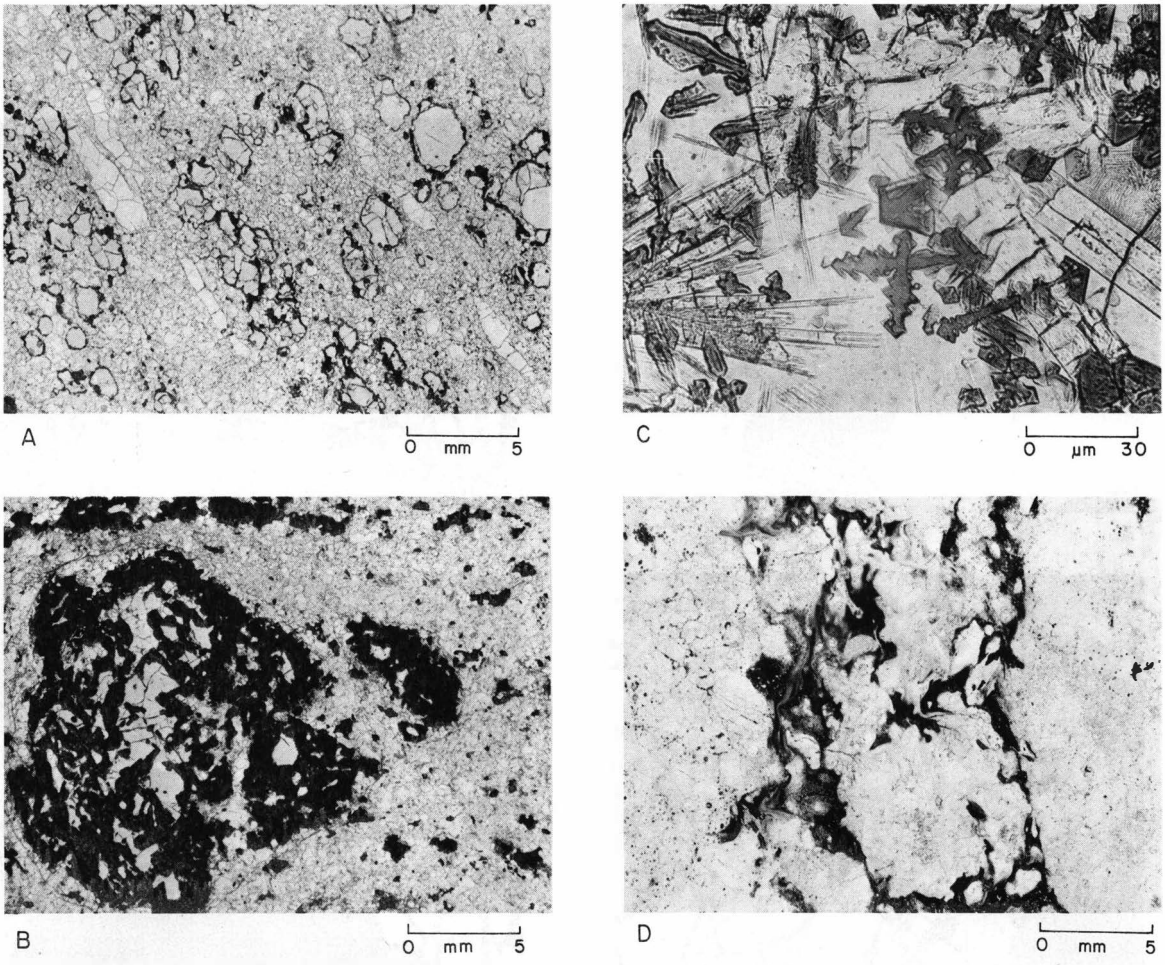

Plate 1. a. Garnet granulite with about 7% partial melt (established by point counting) seen in this photomicrograph as dark rims around garnet and ilmenite. Principal minerals are garnet, quartz, sillimanite, potassium feldspar (sanidine perthite), plagioclase and ilmenite. Accessory minerals are rutile and zircon. b. Garnet granulite with about 30% partial melt seen as dark patches which are composed of glass, orthopyroxene and spinel symplectites. The symplectites have partially replaced the large garnet in the central and lefthand portions of the photomicrograph and have totally replaced the smaller garnets in the righthand side. Mineral assemblage is the same as in Plate 1a. c. Detail of symplectite associated with garnet. Cruciform, medium gray hercynitic spinel and lath-like pale gray orthopyroxene occur as quench-like crystals in glass. d. Garnet granulite which has undergone greater than 50% fusion. Garnet can no longer be recognized as a discrete phase, but its presence can be inferred by patches of symplectite. Lines of flow in melt are seen as light and dark areas of poorly mixed interstitial glasses of variable composition. Mineral residue consists of quartz, sillimanite, potassium feldspar and plagioclase.

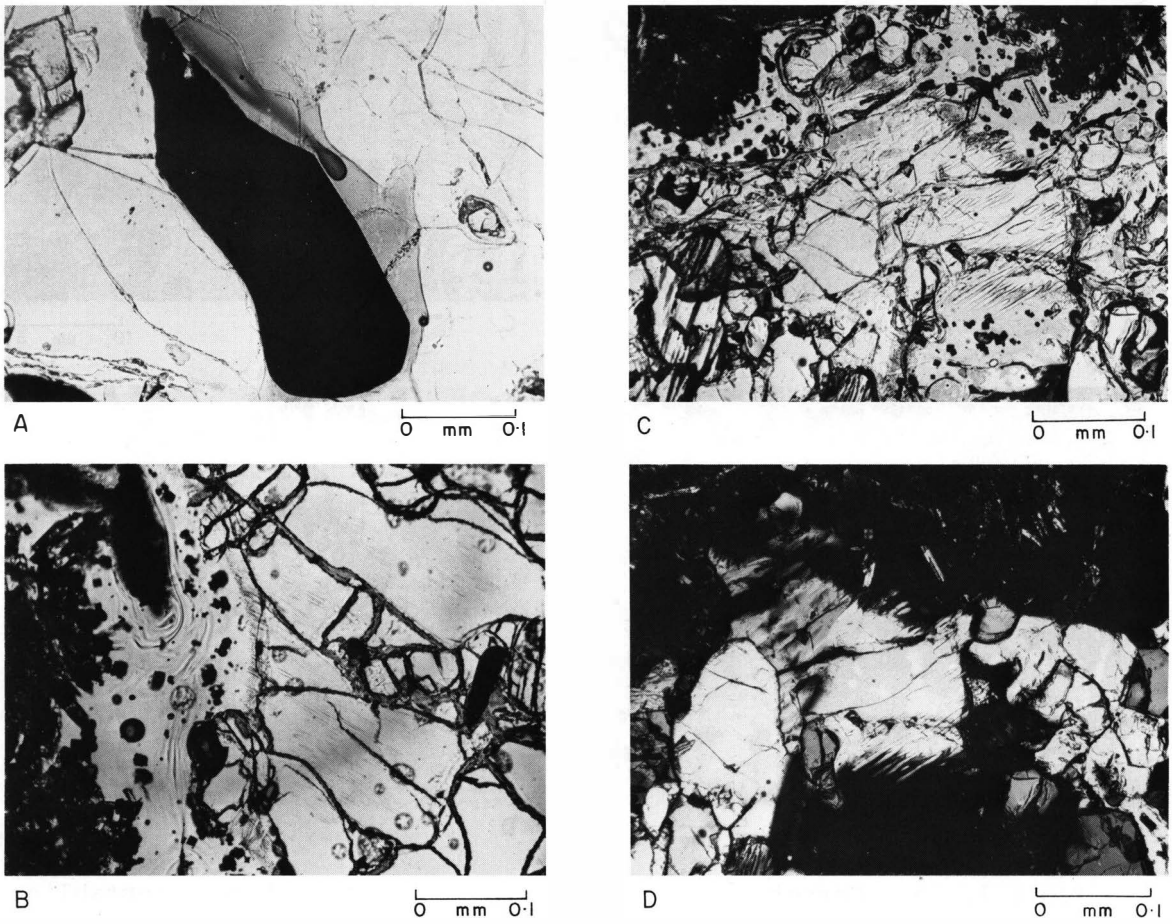

Plate 2. a. Example of apparent lack of mixing between melts, now seen as glasses, of Fe, Ti-rich, Si-poor (ilmenite rich) composition (elongated dark blob above black ilmenite grain) and K, Si-rich (sanidine-rich) composition (seen as pale gray glass surrounding the dark blob). Garnet occupies the lefthand portion of the photomicrograph, while sanidine occupies the righthand side. b. Flow lines in glass within symplectite seen in lefthand portion of photomicrograph. Black minerals in glass are hercynite and orthopyroxene. Minerals in righthand portion of photomicrograph are potassium feldspar (sanidine perthite). Perthite can be seen extending into glass along margin of sanidine host. c. Area within a garnet granulite which has undergone approximately 30% fusion. Potassium feldspar is the mineral in the center, with sillimanite grains to the left of it. Note that perthite lamellae have been left stranded in glass on either side of the partially melted sanidine host, in the same optical orientation as those within the host. d. Same photomicrograph as in Plate 2c but with crossed nicols. Stranded perthite lamellae can be seen extending from the margins of the sanidine host into the isotropic glass.

Electron microprobe analyses of the glasses suggest that the glass compositions are essentially reflecting adjacent mineralogies and that thorough mixing did not occur between melts of variable compositions within a given xenolith (Tables 1 and 2). Multiple electron microprobe analyses of glassy areas within individual thin sections show the influence of garnet and potassium feldspar on the glass compositions, which can vary from silica undersaturated to silica oversaturated within several millimeters (Fig. 1). As seen in this figure, garnet clearly influences the aluminum, iron and magnesium contents of the coexisting glasses. Trends within each sample are nearly linear between garnet and glass for these elements. Potassium feldspar appears to be the main contributor to the sodium and potassium contents in the glasses, but these trends are more complex.

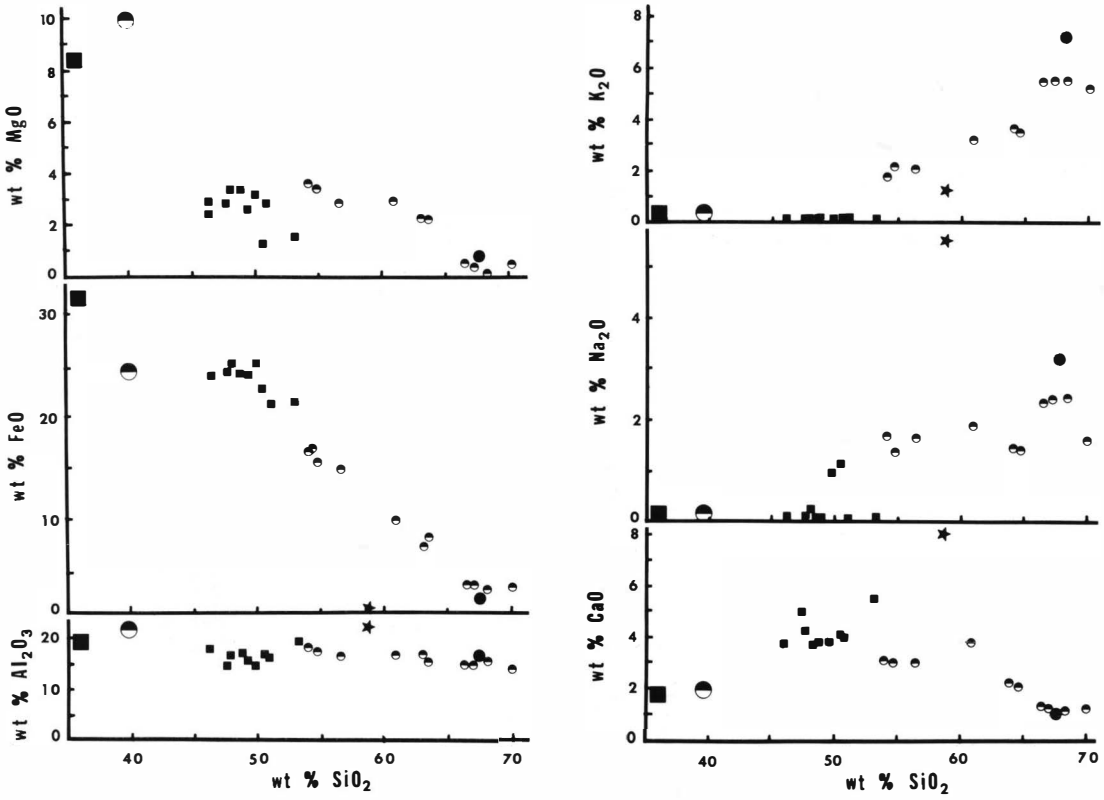

Fig. 1. Electron microprobe analyses of glass compositions from garnet granulites compared with analyses of major phases. Small squares and half-circles represent the range of compositions of glasses from two xenoliths representing group 1 and group 2 garnet granulites respectively (*Padovani*, 1977). The large square and half-circle represent the average composition of garnet from the same samples. The star and closed circle, respectively, represent co-existing plagioclase and potassium feldspar compositions.

The role of texture is important and appears to control the extent of melting in the xenoliths. The amount of melt produced and the extent of its interconnection from one region to another is largley influenced by the

TABLE 1. Representative Glass Analyses From Kilbourne Hole Garnet Granulite K9

Wt. %	9/1a	9/1b	9/1c	9/1d	9/2a	9/2b	9/2c	9/2d	9/2e	9/3a	9/3d	9/4c
SiO_2	64.28	63.89	60.92	62.35	54.57	53.71	56.30	52.85	52.79	68.01	67.31	69.49
TiO_2	2.14	2.09	2.12	2.06	1.54	1.61	1.71	1.87	0.91	1.80	2.02	1.50
Al_2O_3	15.82	15.84	16.70	15.74	17.40	17.34	17.76	17.49	17.87	15.41	15.27	14.24
FeO	8.76	8.99	10.29	10.16	15.95	16.92	15.10	16.71	17.10	3.85	4.26	3.97
MnO	0.13	0.12	0.15	0.12	0.27	0.32	0.30	0.31	0.33	nd	0.02	0.03
MgO	2.39	2.40	3.01	2.71	3.78	3.79	2.99	3.49	3.38	0.62	0.61	0.64
CaO	2.12	2.22	2.69	2.18	3.00	3.10	3.00	3.30	3.42	1.25	1.31	1.43
Na_2O	1.41	1.71	1.87	1.69	1.58	1.53	1.61	1.38	1.56	2.48	2.53	2.54
K_2O	3.59	3.63	3.30	3.40	2.17	1.87	2.15	1.80	1.81	5.58	5.23	5.25
TOTAL	100.64	100.68	100.85	100.40	100.27	100.19	99.92	99.18	99.17	99.00	98.96	99.19

Sample K9 has the following mineralogy: garnet, plagioclase, potassium feldspar, quartz, ilmenite, rutile and zircon. nd = not determined. Total iron expressed as FeO. Glasses in Table 1 range from colorless to yellowish brown with increasing iron content.

TABLE 2. Glass Analyses From Garnet Granulite K33, Anorthosite and Charnockite

Wt. %	33/4b	33/1	33/5a	33/5e	33/6d	33/6f	33/6h	33/3h	20/1	6/1	6/3	6/2
SiO_2	45.96	48.74	57.60	49.02	49.44	50.32	50.80	52.84	48.73	46.99	48.76	48.87
TiO_2	1.78	2.11	2.13	1.62	2.76	2.82	2.59	0.88	2.20	4.08	3.54	3.54
Al_2O_3	18.43	15.71	16.31	17.07	14.88	16.76	14.04	19.13	14.21	12.59	12.57	12.30
Cr_2O_3	nd	nd	nd	nd	nd	nd	nd	nd	nd	0.01	0.02	0.06
FeO	25.22	24.67	26.62	25.87	26.71	22.98	24.86	21.68	13.93	13.05	12.68	10.99
MnO	nd	0.77	nd	nd	nd	nd	nd	nd	0.26	0.62	0.66	0.64
MgO	2.60	2.87	3.57	2.56	3.47	1.42	2.45	1.71	2.58	4.87	4.64	4.90
CaO	3.72	3.91	4.27	4.15	3.83	4.05	3.45	5.55	9.68	2.20	2.34	2.21
Na_2O	0.05	nd	0.29	0.31	0.92	1.11	1.11	0.01	3.31	1.46	1.64	2.02
K_2O	0.06	nd	0.29	0.18	0.25	0.08	0.08	0.05	1.83	2.61	2.78	2.94
P_2O_5	nd	nd	nd	nd	nd	nd	nd	nd	5.06	11.03	10.55	10.98
TOTAL	97.81	98.78	100.88	100.78	102.25	99.53	99.39	101.85	101.79	99.41	100.18	99.49

Sample K33 has the following mineralogy: garnet, plagioclase, quartz, orthopyroxene, ilmenite; Sample 20 is anorthosite with less than 1% orthopyroxene and apatite as a minor phase; Sample 6 is charnockite with orthopyroxene, clinopyroxene, sanidine, plagioclase, ilmenite and apatite as a minor phase. nd = not determined. Total iron expressed as FeO. Glasses in Table 2 are dark colored. Those in sample 33 are pale brown to dark purplish brown; those in samples 6 and 20 are dark brown or black.

concentration of mafic minerals. An isolated garnet will produce a given volume of melt, which, itself, will be isolated. Such a melt may or may not connect with other partial melts depending on the proximity of phases such as ilmenite and sanidine. In the garnet granulites, where mafic minerals (garnet and ilmenite) tend to be isolated, large amounts of partial fusion (greater than 40%, established by point counting) are necessary before extensive interconnection of melt is achieved. In contrast, partial melts in layers of mafic minerals, such as in two pyroxene granulite and charnockite, may exhibit greater interconnection of melt at small melt fractions because of the proximity of mafic phases.

Quench crystals of orthopyroxene and spinel are not abundant in the glass formed from the initial stages of melting (1 to 3% of the rock). With an increase in the percent of melt, orthopyroxene and spinel quench crystals increase in abundance in glasses produced by garnet melting. The variability of cooling rates appears to have affected these quench products and their textures and may also have influenced the extent of crystallization of spinel and orthopyroxene.

Quench and Crystallization Products

Symplectites of quench-like crystals of orthopyroxene and spinel occur in glass at garnet margins in many of the garnet granulites. Garnets, in the xenoliths which do not have such symplectites, may instead have thin borders of yellowish glass or, more rarely, are in direct contact with the surrounding minerals with no evidence of fusion at all. Electron microprobe analyses of the symplectic phases show that the orthopyroxene is ferrohypersthene and that the spinel is hercynite (*Padovani*, 1977; *Padovani and Carter*, 1977).

The orthopyroxene occurs either as pale green laths or as stubby subhedral green pleochroic grains which often are zoned. Electron microprobe analyses of such a zoned grain are plotted in Fig. 2. In this example, iron enrichment is accompanied by a decrease in alumina content.

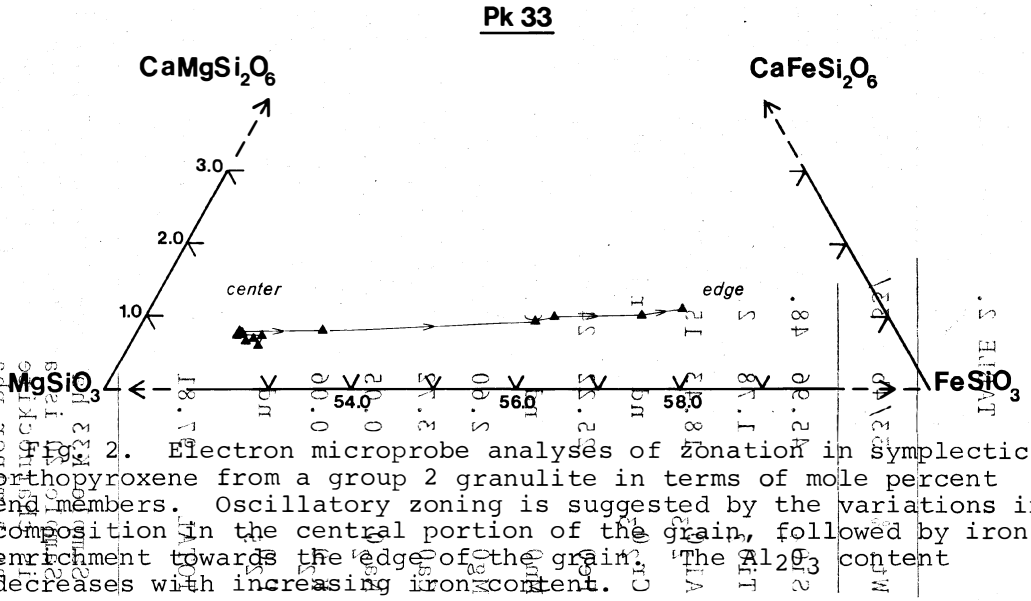

Fig. 2. Electron microprobe analyses of zonation in symplectic orthopyroxene from a group 2 granulite in terms of mole percent end members. Oscillatory zoning is suggested by the variations in composition in the central portion of the grain, followed by iron enrichment towards the edge of the grain. The Al_2O_3 content decreases with increasing iron content.

from center to rim. The alumina content of the orthopyroxene is high and ranges from 7 to 14 oxide weight percent (Fig. 3). Orthopyroxene occurs also as a primary phase along with garnet and plagioclase in one type of garnet granulite, in charnockite and in anorthosite (*Padovani and Carter*, 1977).

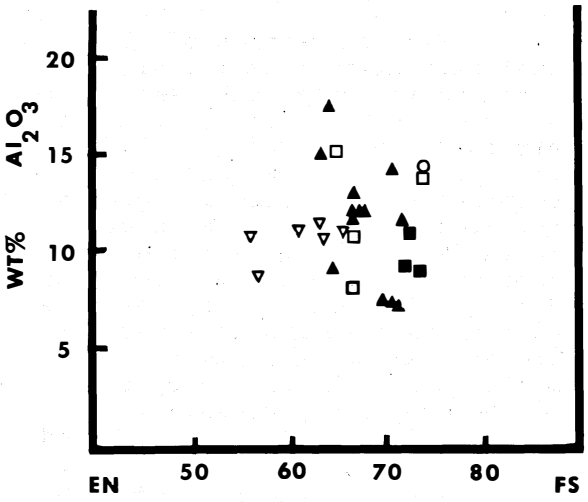

Fig. 3. Weight percent Al_2O_3 plotted versus mole percent ferrosilite in symplectic orthopyroxene from quartzfeldspathic garnet granulites. Squares and circles represent samples from group 1 granulites, while triangles represent samples from group 2 granulites.

Cruciform green or purple hercynite ($FeAl_2O_4$), 1 to 35 microns in maximum dimensions, has nucleated along the margins and skeletal interiors of orthopyroxene in the symplectites (Plate 1c). It has been observed also along garnet margins and as isolated crystals in glass bordering garnet and ilmenite. The purple spinels are found in glass bordering ilmenite, while the green spinels are found in glass bordering garnet. Semiquantitative electron microprobe analyses indicate that the purple color is probably due to a greater concentration of titanium (approximately 0.3 to 0.5 weight percent TiO_2) than that observed in the green spinel (up to about 0.3 weight percent TiO_2 (*Padovani*, 1977.

In two pyroxene granulite, charnockite and anorthosite, partial fusion of orthopyroxene is characterized by symplectites of quench-like skeletal olivine in glass along its margins. Apatite, when present as a minor phase in charnockite and anorthosite, occurs as discrete anhedral grains and as subhedral to euhedral inclusions in plagioclase and can contribute up to 10 oxide weight percent P_2O_5 to the glass compositions within such xenoliths (Table 2) (*Padovani*, 1977).

Discussion

The mineral assemblages present in the garnet granulites, the composition of the garnets, and the absence of the hydrous phase biotite indicate that these granulites formed at pressures greater than those required for the breakdown of cordierite and that the equilibrium temperature had to be greater than that required for the breakdown of biotite (*Holdaway and Lee*, 1977). This suggests minimum equilibrium P-T conditions of 5.4 kilobars and 700°C. Equilibrium temperatures of 750° to 1000°C are indicated from feldspar geothermometry (*Stormer*, 1975; *Padovani*, 1977; *Padovani and Carter*, 1977). Application of geobarometry to the garnet-plagioclase equilibrium yields a pressure range corresponding to depths of 22 to 28 kilometers (*Ghent*, 1976; *Padovani*, 1977; *Padovani and Carter*, 1977). This is equivalent to a geothermal gradient of approximately 30°/km in this depth range beneath the southern Rio Grande Rift.

The percent rock melted (established by point counting) was plotted versus the range in temperature to determine whether or not there is a correlation between the amount of fusion within the xenoliths and the calculated temperature. It can be seen from Fig. 4 that the lowest equilibration temperature (sample 54) correlates with the most extensive fusion, so there appears to be no direct relationship between visible melt and calculated temperature.

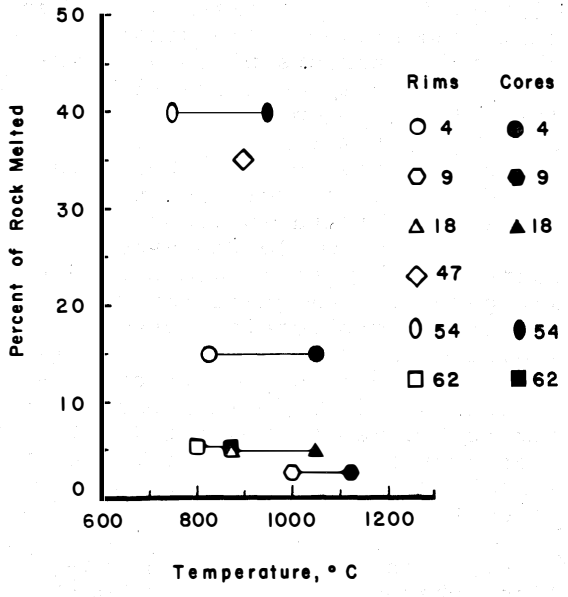

Fig. 4. Percent of rock melted, as established by point counting, versus its temperature range calculated by using the method of *Stormer* (1975). Open and closed symbols, respectively, represent temperatures calculated from electron microprobe analyses of the rims and cores of potassium feldspar (*Padovani*, 1977).

The composition of ulvospinel exsolution from ilmenite may be used to indicate both temperature and oxygen fugacity at the time of their formation (*Buddington and Lindsley*, 1964). However, the ulvospinel rims on ilmenite grains within the xenoliths have reacted with the surrounding melt and are inhomogeneous with respect to major and minor elements. Thus, the rims cannot be used to indicate temperature and oxygen fugacity at the time the xenolith was incorporated into the eruptive process. In contrast, ulvospinel lamellae found in the interiors of ilmenite grains are homogeneous and may be used to indicate conditions at the onset of fusion. Electron microprobe analyses of lamellae and host from one sample indicate a temperature of about 1000°C and oxygen pressure of about 10^{-12} atmosphere (*Buddington and Lindsley*, 1964; *Padovani and Carter*, 1977).

Melts in this suite of rocks formed under anhydrous conditions and in many xenoliths the initial stages of melting have been preserved. The apparent lack of mixing of melts, now seen as glasses, of Fe, Ti-rich, Si-poor (ilmenite-rich) composition and K, Si-rich (sanidine-rich) composition may be due to metastable immiscibility (Plate 2a). *Irvine* (1976) has demonstrated experimentally that large regions of metastable immiscibility exist in the system Mg_2SiO_4-Fe_2SiO_4-$CaAl_2Si_2O_8$-$KAlSi_3O_8$-SiO_2. Given the appropriate intermediate to basic melt compositions and the presence of fusable components such as Fe-rich pyroxene, ilmenite, potassium feldspar and apatite, the potential for immiscibility is enhanced because of the proximity of the low temperature cotectics between plagioclase and the mafic minerals to the region of immiscibility. *Powell et al.* (1975) noted the presence of immiscible Fe-rich (Si-poor) and Si, K-rich glasses in mesostasis in Apollo 16 feldspathic melt rocks. The melts in these rocks were formed by rapid disequilibrium fusion and quenching of the melt products, a process comparable to that which produced the melts in the xenoliths. An alternative explanation for the apparent lack of mixing of melts in the xenoliths may have been simply insufficient time for diffusive mixing. With advanced melting and the appearance of orthopyroxene and spinel as crystallization products, mixing appears to become more efficient (Plate 1d, Plate 2b).

The lack of thorough mixing of melts of different compositions, the existence of melts of variable composition within small regions within a xenolith, and the presence of melt crystallization products suggest that these melts formed under disequilibrium conditions. In addition, the compositions of the melts formed do not resemble those compositions predicted by either equilibrium fusion or fractional fusion of a lower crust of intermediate composition. (Figs. 5 and 6) (*Presnall and Bateman*, 1973).

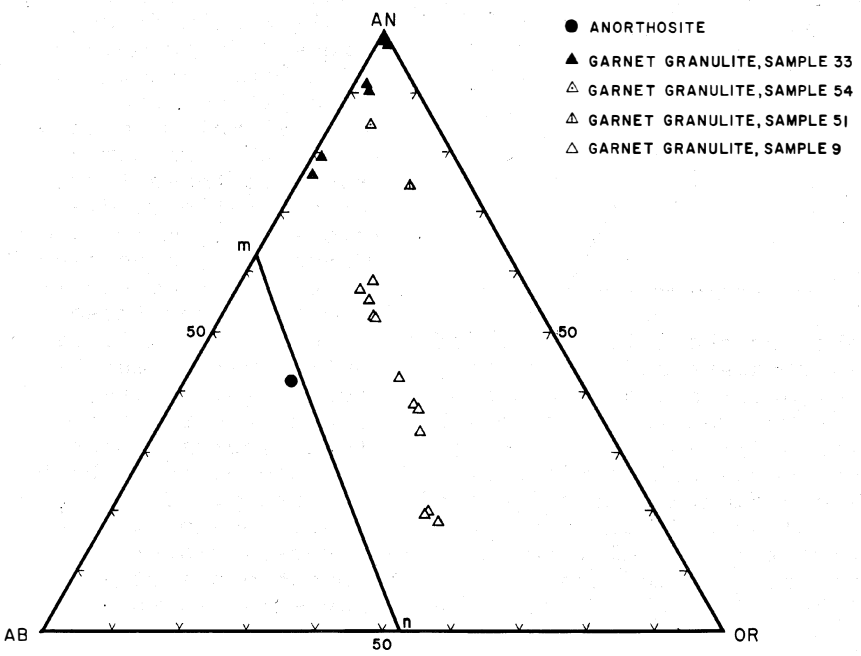

Fig. 5. Normative proportions of AB, AN and OR normalized to 100 percent of glasses from Kilbourne Hole granulite facies xenoliths. Triangles represent glass compositions from garnet granulites, while the circle represents a glass composition from anorthosite. The line m-n shows the approximate trend of Sierra Nevada rock compositions (*Presnall and Bateman*, 1973). Note that the trend exhibited by open triangles is derived from a single thin section and its contained variability of glass compositions.

The fusion textures observed in the Kilbourne Hole xenoliths provide some limits to the disaggregation of material of this composition at depth. During the initial formation of melt, the melt is restricted to the boundary of and/or to cracks within the phase being melted. The shape of the developing melt pocket reflects the shape of the adjacent grains which are not undergoing melting. Thus, the shape of the pocket is highly variable depending upon local geometries between the melt phase and its non-melting matrix. The interconnection of melt in the xenoliths at low melt fractions is highly dependent on the abundance and proximity of garnet, ilmenite and sanidine in the quartzofeldspathic granulites and of pyroxenes and ilmenite in the two pyroxene granulites and charnockites.

Yoder (1976) notes that little data is available on the determination of what quantities of melt are required before the bridging structure of crystals collapses under conditions of load or stress at depth. In theory, approximately 50 percent melt is required for the initiation of the collapse of an *undisturbed* crystalline aggregate (*Yoder*, 1976). The melt textures in the garnet granulites support this theory since greater than 40 percent melt formed before any extensive interconnection of melt and disaggregation of the parent material was produced (Plate 1d). Melt

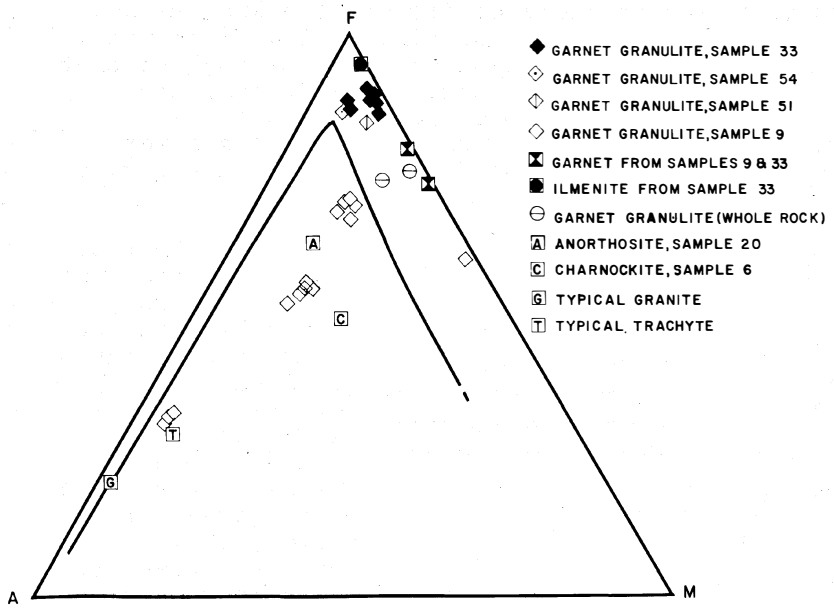

Fig. 6. AFM diagram showing the relationship of glass compositions to major phases and estimated whole rock compositions of quartzofeldspathic and mafic granulites. Skaergaard trend of iron enrichment is shown for comparison (*Wager and Mitchell*, 1951). Diamonds represent glass compositions from garnet granulites, while the squares enclosing the letters A and C represent glass compositions from anorthosite and charnockite respectively. Whole rock compositions of "typical granite" and "typical trachyte" are taken from *Turner and Verhoogen* (1960).

textures within the pyroxene granulites also reflect the abundance and distribution of mafic phases but exhibit less extensive melting. In general, when hydrous phases are present, there is greater interconnection of melt at smaller melt fractions than is observed in the garnet granulites. The partial melts in the xenoliths are comparable to those formed under static conditions where melts are formed due to heating in undisturbed conditions. Under these circumstances, it is unlikely that anhydrous felsic melts could move far from their source region because of their high viscosity. Under conditions of load or stress, "disturbed" conditions such as may exist in the lower crust, the possibility of filter pressing and buoyancy of crystal-liquid mushes must be considered. The extent of melting that must be obtained before migration of melts occurs under conditions of load or stress in the lower crust has not yet been determined for rocks of this composition.

The experimental data of *Keesman et al.* (1971) can be used to place upper limits on the amount of heat added to the xenoliths to produce the observed symplectites associated with garnet. At temperatures above 1088°C and pressures up to 10 kilobars, almandine melts incongruently to hercynite-cordierite-liquid and hercynite-quartz liquid, respectively. At temperatures between 1150° and 1200°C and at pressures of 1 atmosphere to 12 kilobars, almandine melts incongruently to hercynite-liquid. Since quartz and cordierite are absent from the crystallization products produced by garnet melting and since equilibrium temperatures of 750° to 1000°C are indicated for the garnet granulites, the experimental data of *Keesman et al.* (1971) suggest that the xenoliths may have experienced an increase of not more than 200° to 400°C because of the general lack of fusion (*Padovani*, 1977). Furthermore, the high alumina contents of orthopyroxene in the garnet breakdown assemblages suggests an upper limit of 1100°C for its occurrence (*Anastasiou and Seifert*, 1972; *Stahle*, 1975).

The mineralogies and textures observed in the interstitial glasses and their quench products are similar to those reported by *Stahle* (1975) in rocks of similar composition which have undergone rapid fusion in response to meteorite impact shock melting. He found aluminous ferro-hypersthene, spinel and glass as phases of a shock-induced breakdown assemblage of almandine garnet in gneiss fragments from the Ries Crater, Germany. In contrast to the Kilbourne Hole garnet granulites, the garnet gneisses from the Ries Crater are strongly shocked and contain isotropic glasses of silica and plagioclase composition. In addition, the highly zoned garnets from the Ries Crater exhibit multiple sets of planar deformation features, which are not observed in the garnets from Kilbourne Hole, and the latter show no observable zonation with respect to major elements. High alumina contents (up to 10 oxide weight percent) are characteristic of the orthopyroxene in the Ries Crater assemblages similar to those observed in the xenoliths. The Ries Crater assemblages containing garnet and its breakdown products are considered to have formed at high post-shock temperatures and rapidly diminishing pressures directly after the passage of shock waves (*Stahle*, 1975).

From the lack of shock induced features, it can be inferred that the glasses in the Kilbourne Hole granulites were not produced by impact melting. One hypothesis for the origin of the glasses in the xenoliths invokes heating in, or in the vicinity of, basaltic magma at depth and subsequently cooling them on the earth's surface after rapid transport during explosive volcanic eruptions. *McGetchin* (1975) has calculated that flow velocities in kimberlite pipes averaged 30 meters/second at depth and accelerated to 300 to 400 meters/second near the surface due to gas expansion. The preferred hypothesis, suggested by the observations of *Stahle* (1975), is that the xenoliths melted largely due to decompression at close to their wall rock temperatures. Since the percent of melting within any given xenolith is uniformly distributed throughout the xenolith, decompression may have had greater effect on melting relative to heating by the basaltic magma. This model satisfies the requirement that the xenoliths undergo partial melting but not total fusion, and that the melt so produced be quenched before either complete diffusion between melts of different compositions has occurred or before extensive crystallization has occurred in the melt and/or glass.

Conclusions

1) The partial fusion which affected the Kilbourne Hole garnet granulites, two pyroxene granulites, charnockites and anorthosite was of a disequilibrium nature as evidenced by the lack of complete mixing of melts on a microscale, the varied chemistries of the melt crystallization products and by the variability in the amount of melt produced.

2) The partial fusion appears to represent disequilibrium melting during transport to the earth's surface in alkali basalt magma.

3) The melts so produced were quenched after rapid transport to the earth's surface.

4) Incipient melting reflects adjacent mineralogies with garnet, pyroxenes, sanidine and ilmenite the phases most often affected.

5) Continuous interconnection of melt has not been observed in anhydrous quartzofeldspathic garnet granulites until greater than 40% melting has occurred. In two pyroxene granulites and charnockites, greater interconnection of melt at smaller melt fractions is observed and reflects the abundance and distribution of mafic phases.

Acknowledgements

This work was supported by NSF grnnt DES 74-14532. Contribution No. 334 of the Program for Geosciences at the University of Texas at Dallas. The comments of H. Dick are gratefully acknowledged as is the assistance of M. Padovani with preparation of the illustrations.

References

Anastasiou, P., and F. Seifert, Solid solubility of Al_2O_3 in enstatite at high temperatures and 1-5 kbars water pressure, *Contrib. Mineral. Petrol., 34*, 272, 1972.

Buddington, A.F., and D.H. Lindsley, Iron-titanium oxide minerals and synthetic equivalents, *J. Petrology, 5*, 310-357, 1964.

Ghent, E.D., Plagioclase-garnet-Al_2SiO_5-quartz: a potential geobarometer-geothermometer, *Am. Mineral., 61*, 710-714, 1976.

Holdaway, M.J., and S.M. Lee, Significance of Fe-Mg cordierite stability relations on temperature, pressure and water pressure in cordierite granulites, in *The Earth's Crust, Geophys. Mongr. Ser. 20*, edited by J.G. Heacock, AGU, Washington, D.C., in press, 1977.

Irvine, T.N., Metastable liquid immiscibility and MgO-FeO-SiO_2 fractionation patterns in the system Mg_2SiO_4-Fe_2SiO_4-$CaAl_2Si_2O_8$-$KAlSi_3O_8$-SiO_2, *Carneg. Inst. Yrbk., 1975-1976*, 597-611, 1976.

Keesman, I., S. Matthes, W. Schreyer, and F. Seifert, Stability of almandine in the system FeO-(Fe_2O_3)-Al_2O_3-SiO_2-(H_2O) at elevated pressures, *Contrib. Mineral. Petrol., 31*, 132, 1971.

McGetchin, T.R., The mechanism of caldera-forming ash blast eruptions, *Trans. Am. Geophys. Un., 56*, 461, 1975.

Padovani, E.R., Granulite facies xenoliths from Kilbourne Hole maar and their bearing on deep crustal evolution, *Ph.D. Dissertation, Univ. Texas at Dallas, Richardson, Texas*, 1977.

Padovani, E.R., and J.L. Carter, Mineralogy and mineral chemistry of a suite of anhydrous, quartzofeldspathic garnet-bearing granulites from Kilbourne Hole maar, New Mexico, *G.S.A. Abs. Progr., 5*, 761-762, 1973.

Padovani, E.R., and J.L. Carter, Aspects of the deep crustal evolution beneath south central New Mexico, in *The Earth's Crust, Geophys. Monogr. Ser., 20*, edited by J.G. Heacock, AGU, Washington, D.C., in press, 1977.

Powell, B.N., M.A. Dungan, and P.W. Weiblen, Apollo 16 feldspathic melt rocks: clues to the magmatic history of the lunar crust, *Proc. Lun. Sci. Conf. 6th*, 415-433, 1975.

Presnall, D.C., and P.C. Bateman, Fusion relations in the system $NaAlSi_3O_8$-$CaAl_2Si_2O_8$-SiO_2-H_2O and generation of granitic magmas in the Sierra Nevada batholith, *G.S.A. Bull., 84*, 3181-3202, 1973.

Stahle, V., Natural shock behavior of almandite in metamorphic rocks from the Ries Crater, Germany, *Earth Planet. Sci. Let., 25*, 71-81, 1975.

Stormer, J.C., A practical two-feldspar geothermometer, *Amer. Mineral., 60*, 667-674, 1975.

Turner, F.J., and J. Verhoogen, *Igneous and Metamorphic Petrology*, McGraw-Hill, New York, 694 p., 1960.

Wager, L.R., and R.L. Mitchell, The distribution of trace elements during strong fractionation of basic magma - a further study of the Skaergaard intrusion, East Greenland, *Geochim. Cosmochim. Acta, 1*, 129-208, 1951.

Yoder, H.S., *Generation of Basaltic Magma*, National Academy of Sciences, Washington, D.C., 236 p., 1976.

EVIDENCE OF PARTIAL MELTING IN THE JOSEPHINE PERIDOTITE

Henry J.B. Dick*
Yale University
New Haven, Connecticut 06520

(Extended Abstract)

The Josephine Peridotite is an alpine-type peridotite, 640 km^2 in area, located on the western edge of the Klamath Mountains of southwestern Oregon and northern California. The peridotite massif is an eastward dipping thrust sheet which overlies the Rogue volcanics and Illinois River Gabbro. *Dick* (1976, 1977) has suggested that the peridotite may have been emplaced from a marginal basin to the east over an area of active late Jurassic island-arc volcanism represented by the gabbro and volcanics.

The peridotite is largely harzburgite (> 95%) with scattered patches of dunite (< 5%), and irregular seams of orthopyroxenite and olivine websterite. The average harzburgite modal composition is 78 $\pm$ 6% olivine, 20 $\pm$ 5% orthopyroxene, 1.3 $\pm$ 1.3% diopside and 0.6 $\pm$ 0.3% chromian spinel. In the harzburgite, olivine ranges from $Fo_{89.5}$ to $Fo_{91.2}$ while the orthopyroxene ranges from $En_{90.3}$ to $En_{91.9}$. Accessory spinel, unlike the silicates, has a large range of composition in the harzburgite with Cr/(Cr+Al) ratios from 0.18 to 0.76.

The ultramafic rocks in layered intrusions, the only crustal ultramafic bodies comparable to alpine-type peridotites, differ significantly from the Josephine Peridotite. Whereas gabbroic rocks associated with layered intrusions greatly exceed in volume the ultramafic portion, the proportion of gabbroic to ultramafic rocks in the vicinity of the Josephine Peridotite is approximately 1:1. No layered intrusion is known to contain a thickness of ultramafic rock comparable to the kilometer thick exposed section of the Josephine Peridotite. Layered intrusions are characterized by diverse lithologies and mineralogies and typically have large systematic ranges of silicate compositions with restricted spinel compositions.

Fractional crystallization and partial fusion are not simply the opposite of one another: fractional crystallization produces diverse lithologies and a large range of mineral compositions while partial fusion is expected to leave a solid residue of nearly uniform composition and mineralogy (*Presnall*, 1969; *Dick*, 1977). The Josephine Peridotite, then, has all the features of a residue of partial fusion. As might be expected, olivine-spinel geothermometry indicates nearly uniform crystallization temperatures across the peridotite, which is to be expected for the residue of partial fusion (rather than the range of temperatures found in layered intrusions and expected for fractional crystallization).

---

* Present address: Department of Geology and Geophysics, Woods Hole Oceanographic Institution, Woods Hole, Massachusetts 02543

Fig. 1. Irregular seams of olivine websterite in harzburgite. The larger seam at the center has been partially replaced by dunite. The high chrome content in the pyroxene of the olivine-websterite has resulted in chromite enrichment (black specks) where it has been replaced. The pyroxene in the harzburgite and olivine websterite stands out as it is more resistant than the olivine to weathering.

Fig. 2. Tabular orthopyroxenite, one of a parallel set in the harzburgite, crosscutting dunite.

The minerals in the Josephine Peridotite show systematic variations in composition (Fe, Al, Ca depletion, Mg, Cr enrichment) from pyroxene-rich to more refractory pyroxene-poor harzburgites consistent with a limited variation in the degree of fusion and melt removal (*Dick*, 1977, 1976).

Olivine websterite, orthopyroxenite, dunite and chromitite together constitute a very small proportion of the peridotite with very important petrogenetic significance. Olivine websterite occurs as irregular seams and layers locally in the peridotite (Fig. 1). The modal composition of these layers plots in the Ol-Opx-Cpx ternary diagram in a linear manner which mimics the position of the high pressure olivine-forsterite cotectic in much the same manner as granite compositions plot near a ternary eutectic minimum-melt composition. The olivine-websterites then are thought to represent the congruently crystallized products of pockets of trapped melt in the harzburgite.

Dunite and chromitite occur together in the harzburgite, with the chromitites invariably enclosed in dunite. The dunite occurs as irregular patches, tabular bodies, and pods ranging in size from a few cm^3 to thousands of cubic meters. Dunite is found cross-cutting and replacing the olivine websterite and harzburgite on all scales (Fig. 1). It can be clearly shown that the formation of the dunite occurred *in situ* and involved the replacement reaction: pyroxene → olivine + spinel + liquid. On the other hand, many of the larger bodies of dunites contain cumulus chromitite ore bodies which range in size from a few kilograms to thousands of metric tons. These ore bodies clearly fractionally crystallized from a melt. As their enclosing dunites crosscut layering in the harzburgite country rock, both dunite and chromitite are thought to be lag deposits precipitated from relatively large bodies of melt which were passing through the mantle to the crust. This is to be expected of such melts as the field of olivine contracts on the basalt liquidus at low pressures (*O'Hara*, 1968). The dunites, such as are shown in Figs. 1 and 2, however, probably did not form in this manner. It is evident that there are many generations of dunite in the Josephine Peridotite (*Himmelburg and Loney*, 1973; *Dick*, 1976) and there appears to be a complete gradation from the small irregular dunite patch replacing pyroxenite (Fig. 1) up to the huge dunite bodies encompassing a major cumulus ore deposit. The smaller dunites have probably formed, then, due to late stage incongruent melting of the peridotite and leaching of pryoxene from wall rocks due to the movement of melt through the peridotite.

Formation of the dunites by desilicification of the peridotite by water vapor is unlikely for three reasons: 1) The chromitites within the small dunites have formed at high temperatures (*Dick*, 1977). Thus the introduction of water would cause the peridotite to melt anyway. 2) There are cumulus chromitites in many dunites indicating precipitation from a melt. 3) Dunite is ubiquitous in the peridotite; its formation due to desilicification by water vapor requires the penetrative flow of an enormous volume of water vapor through the peridotite, for which evidence, other than the dunites, such as hydrous phases, is completely lacking.

Orthopyroxenite occurs as tabular dikes in the harzburgite. These bodies are often aligned with one another as though they were following a joint pattern. Many of them contain euhedral chromite and crosscut dunites. They may represent late stage crystallization of melt sweated out along joints, by the reaction melt + wall rock olivine → enstatite, at the end of partial fusion and cooling of the peridotite.

The observations at the Josephine Peridotite may put some limits on models for magma generation. *Dick* (1977) has pointed out that some melt must have been trapped in the peridotite throughout the course of partial fusion. The presence of many generations of dunite, with cumulus chromitite ores in the peridotite indicates, however, that significant bodies of melt did segregate *within* the mantle and rise to the crust. The range of ore compositions (*Dick*, 1976) indicates that a range of magma compositions was produced, while the varying degrees of deformation of the dunite residues suggests this occurred over a range of depths. The impression one receives, then, is that magma generation in the mantle must have occurred by fractional fusion with incomplete removal of melt at any one time (a residue = solid + trapped melt). Magmas were evidently produced at a range of depths with a range of compositions, probably reflecting increasing degrees of depletion of the source rock during upward ascent of the mantle.

References

Dick, H.J.B., The origin and emplacement of the Josephine Peridotite of Southwestern Oregon, *Ph.D. Thesis, Yale University, University Microfilms, Ann Arbor, Michigan*, 1976.

Dick, H.J.B., Partial melting in the Josephine Peridotite I, the effect on mineral composition and its consequence for geobarometry and geothermometry, *Am. Jour. Sci., 277*, 801-832, 1977.

Himmelburg, G.R., and R.A. Loney, Petrology of the Vulcan Peak alpine-type peridotite, southwestern Oregon, *Geol. Soc. Am. Bull., 84*, 1585-1600, 1973.

O'Hara, M.J., Are ocean floor basalts primary magmas?, *Nature, 220*, 683-686, 1968.

Presnall, D.C., The geometrical analysis of partial fusion, *Am. Jour. Sci., 267*, 1178-1194, 1969.

STRUCTURAL CONTROLS ON PARTIAL MELTING IN THE LANZO PERIDOTITES

Francoise Boudier and Adolphe Nicolas
Laboratoire de Tectonophysique
Université de Nantes
BP 1044
44037 Nantes cedex, France

Abstract

The study deals with natural partial melting in the Lanzo lherzolite massif and with experimental melting performed on cores from this massif while a deviatoric stress was applied. The relations between plastic flow and simultaneous melting are investigated. During experiments the incipient melting appears at grain boundaries and cracks parallel to σ_1. In natural melting, feldspar lenses corresponding to about 5% melting in the lherzolite do or do not coalesce depending on the intensity of the plastic deformation. When it is intense, parallel lenses form; in the case of rotational shear flow, they parallel the inferred flow plane, which lies roughly 15° off the foliation plane. Feldspathic veinlets grade into gabbroic dikes which are commonly perpendicular to lineation in the host peridotite. Some gabbroic dikes have dunitic walls and were probably fed by extensive partial melting in the host peridotite along the margins of the dikes. Field observations show that the so-called dunitic "dikes" are probably the residua that remain after complete removal of gabbroic or pyroxenitic magma.

No difference is noticed in microstructures and mineral preferred orientations between unmelted lherzolites and those deformed in the presence of about 5% melt, suggesting that the plastic properties do not necessarily change with 5% melting.

INTRODUCTION

The problem of partial melting of peridotites, especially lherzolites, is of prime importance since there is now a consensus that basalts and gabbros derive from this process occurring in the upper mantle. The geochemical and petrological aspects of this problem have been dealt with considerably more care than the physical and mechanical ones. Questions such as: where the first molten products are generated, how they coalesce, and how they affect the mechanical and rheological properties of the rock have not received all the attention they deserve. Answering them would contribute to an understanding of what is softening the low velocity zone (*Goetze*, in preparation) or would provide a better basis for electrical conduction models in the mantle (*Chan et al.*, 1973; *Shankland and Waff*, in preparation). The studies in this field are mainly oriented toward explaining how partial melting affects seismic velocities and attenuation. They are theoretical (*Walsh*, 1969; *O'Connel and Budianski*, 1974) and experimental (*Stocker and Gordon*, 1975); a few have investigated how partial melting

affects the creep properties (*Auten et al.*, 1974; *Arzi*, 1974). Direct observations on the geometry of partial melts in naturally or experimentally deformed peridotites have not been reported yet.

The lherzolite massif of Lanzo (Western Alps) is a preferred place to study the process of partial melting. During its plastic flow emplacement into the continental crust, it equilibrated in the feldspar lherzolite facies. Since only some parts of it underwent partial fusion, the massif contains a range of structures corresponding to a range of fusion, from incipient melting to more than 25% melting (*Boudier*, 1976). The freshness of the rocks in the massif facilitates observations. The present study investigates the mechanics of melt coalescence during plastic flow of the host peridotite and complements previous work on the petrology and geochemistry of gabbroic partial fusion (*Boudier*, 1972; *Boudier and Nicolas*, 1972; *Menzies*, 1974; *Loubet*, 1976). We will report on evidence from the Lanzo massif but will include data from harzburgite massifs in Turkey and from deformation experiments on Lanzo peridotite conducted at hypersolidus temperatures.

Terminology and its background

A kinematic interpretation of textures and fabrics in the peridotites, and especially in the Lanzo massif was proposed by *Nicolas et al.* (1972, 1973) and reviewed in *Nicolas and Poirier* (1976). It was shown that, due to the homogeneous deformation of these rocks, it is possible to correlate the orientation of the principal strain axes determined from the study of penetrative field structures, with the orientation of the principal kinematic axes determined from the study of preferred lattice orientation in olivine and enstatite:

- principal strain axes ($X > Y > Z$)

X = direction of mineral elongation, parallel in the field to a spinel-aggregate lineation.

Z = perpendicular to the foliation plane (plane of mineral flattening).

Y = intermediate axis, perpendicular to X in the foliation plane.

- principal kinematic axes (a,b,c)

a = flow line approximated by the maximum of slip directions in olivine and enstatite: $[100]_{ol}$ and $[001]_{en}$.

c = normal to the flow plane approximated by the maximum of slip planes in olivine and enstatite: $(010)_{ol}$ (high temperature) or $(001)_{ol}$ (low temperature), and $(100)_{en}$.

b = perpendidular to a in the flow plane.

- relations between strain and kinematic axes

  - rotational shear flow (simple shear):

a oblique to X by an angle α[1] related to the shear angle θ by $\cot 2\alpha = 1/2 \tan \theta$

(1) A computer simulation of rotational shear flow has since indicated that the true flow line may be at an angle slightly larger than α from the X direction (*Etchecopar*, 1974, 1977).

b parallel to Y

c oblique to Z by α

- irrotational shear flow (pure shear): maxima of slip directions and planes respectively equated with the flow line and flow plane only for large strain.

- combination of these elementary flows: α is reduced in proportion of the percentage of irrotational shear component.

Feldspathic lenses and dikes

Boudier and Nicolas (1972) described in Lanzo feldspathic lenses (of regular shape) and veinlets (contorted and irregular) on the one hand, indigeneous (previously called "in situ") and intrusive gabbro dikes on the other. The mineral modes of the indigeneous and intrusive dikes remain remarkably constant at 60% labradorite, 30% diopside and 10% olivine, with the exception of special types of intrusive dikes observed only locally. Ill-defined boundaries preclude meaningful measurements of modes of feldspathic lenses and veinlets any thinner than one to two centimeters thick.

The feldspathic lenses and dikes are ubiquitous in the southern body and on the western margin of the central body of the tripartite massif (Fig. 1). Against and inside the serpentinite rim along the western margin of the central body, the indigeneous dikes are especially numerous and attain sizes of a few meters; here the indigeneous dikes are enclosed in dunites and strongly depleted lherzolites. The abundance of lenses and indigeneous dikes decreases rapidly to the east, and only intrusive dikes are present more than 1 km inside the western margin of the massif.

Feldspar Lenses and Veinlets

Two types of feldspar + pyroxene segregations can be distinguished on the basis of their shape and the structure of the enclosing lherzolite. The mildly deformed lherzolites from the center of the southern body contain feldspar veinlets that are thin and contorted with no preferred orientation. The veinlets are composed of slightly elongated poikilitic crystals of feldspar enclosing corroded olivine grains. Feldspar is not deformed (Fig. 2). The lherzolite is depleted in plagioclase and pyroxene in the vicinity of the veinlets, to the extent of being a dunite (Fig. 3). Exceptionally veinlets coalesce into indigeneous dikes the way roots converge in the stem of a tree.

Elsewhere in the massif the plastic flow has imprinted mineral preferred orientations, foliation and lineation; plagioclase + pyroxene segregations are then better developed, with a regular lense shape (0.5 - 2 cm in width, 10-20 cm in length) and aligned, but it is possible in the field to trace their origin to streaks of a few individual grains of feldspar oblique to the foliation. In thin section, it is no longer possible to observe any poikiloblastic texture of the feldspar grains which are strained. Evidence like that given in Fig. 4 indicates that the feldspar has grown from triple junctions and grain boundaries by corosion of the olivine neighbours. The corrosion is faster along grain boundaries and subboundaries.

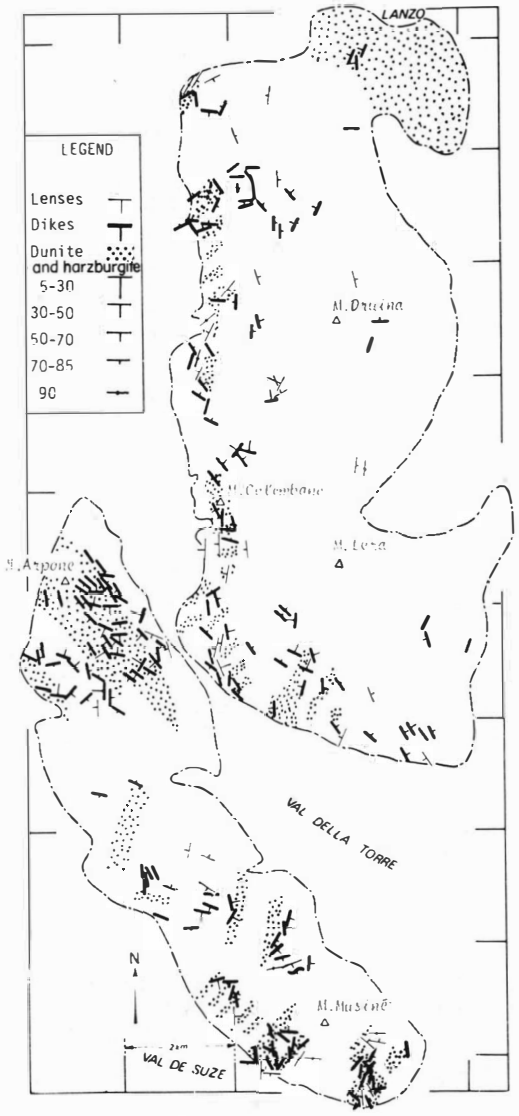

Fig. 1. Contours of the Lanzo massif showing the field distribution of feldspathic lense gabbro dikes and dunites.

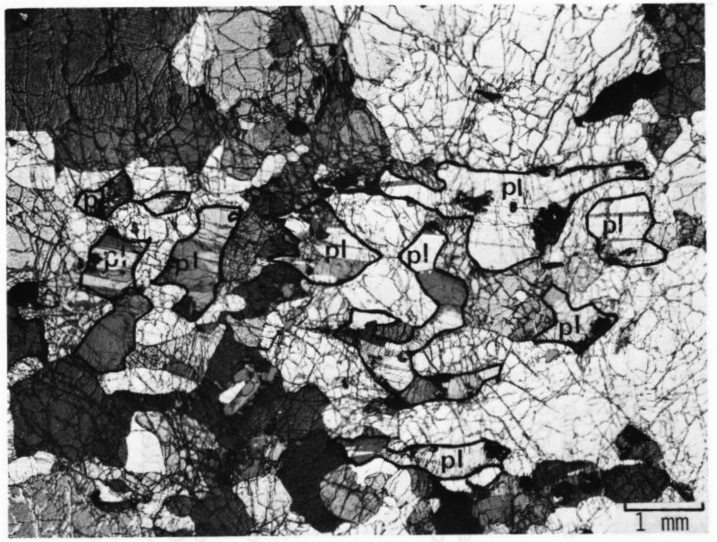

Fig. 2. Plagioclase grains in small lenses (PI, heavy contours). These poikilitic crystals are believed to have crystallized from the incipient melt, reacting with the surrounding olivine (Fig. 4). Micrograph, crossed polarizers.

Fig. 3. Contoured feldspathic lenses in dunites from an area of mild deformation (Mte. Arpone).

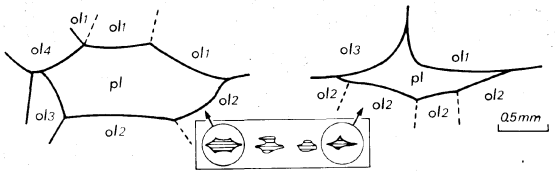

Fig. 4. Drawing after a micrograph comparable to that of Fig. 2. The plagioclase (Pl) has reacted with the olivine grains (Ol) from triple junctions and along grain boundaries. The corrosion is faster along grain boundaries and subboundaries (dotted lines) resulting in concave contours.

Assuming that the depletion in lherzolite next to the gabbro lenses is produced by the formation of these lenses, it is possible to estimate the amount of melt corresponding to these lenses. This was done by solving the overdeterminated system for major elements compositions: normal lherzolite = depleted lherzolite + minerals from gabbro (*Boudier*, 1976). A good fit was obtained for a melt corresponding to 5% partial fusion of the normal lherzolite.

Structural setting

The lenses are oblique with respect to the foliation, usually in a single direction and occasionally in two conjugate directions (Fig. 5 and 6). They are often *en echelon* (Fig. 5), and may give evidence of rotation

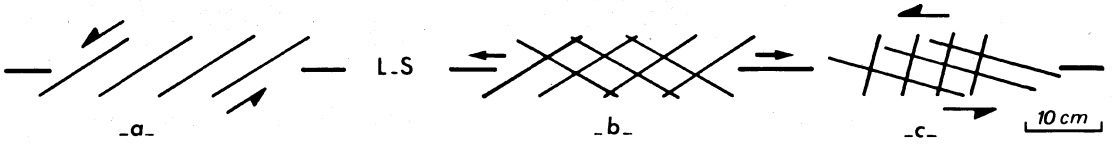

Fig. 5. Various patterns of lenses and veinlets observed in a plane parallel to the mineral lineation (L) and normal to the foliations (see also Figs. 6, 8 and 9).
a) en echelon pattern typical of rotational shear flow.
b) symmetrical conjugate set typical of irrotational shear flow.
c) asymmetrical conjugate set indicating a change from irrotational to rotational shear flow.

from their previous orientation (Figs. 5 and 8). *Boudier and Nicolas* (1972) interpreted the lenses as tension gashes; this interpretation must be revised. Fig. 7 gives the lenses orientation with respect to the foliation and aggregate lineation in the central body where the flow was rotational: the mean angle between the lenses and the foliation is only 15°. The angle should be larger in tension gashes and would increase in case of a rotation due to subsequent shear. Indeed this rotation occurs (Fig. 8) and explains departures toward angles larger than 15° on the net. Observations in thin section suggest that the lenses form in the plane containing the slip planes of olivine and enstatite and considered as the flow plane. Indeed in the central body of Lanzo this flow plane is usually inclined at about 15° to the foliation, *Boudier* (1976). The block diagram of Fig. 9 illustrates the relation between lenses, foliation and lineation, and flow plane. The lenses coinciding with the flow plane can be used to determine the shear sense in a rotational shear flow. The sense remains the same as in

Fig. 6. Oblique feldspathic lense in a lherzolite with a strong plastic deformation (Stura di Viu).

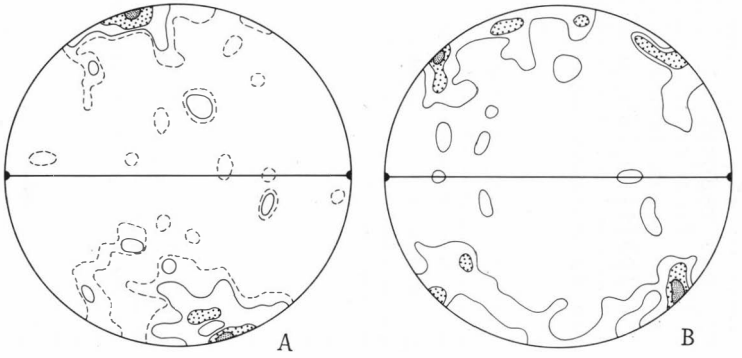

Fig. 7. Orientations of poles of feldspathic lenses and veinlets in Lanzo. Lower-hemisphere equal area projection, contours per 0.45% net area; structural reference system: foliation vertical EW, aggregate lineation horizontal EW. A and B are respectively for the central and southern bodies; A) 81 measurements, contours approximately at 1, 2, 4, 8%; B) 51 measurements, contours at 2, 4, 8%.

← Fig. 8. Oblique feldspathic veinlets: in the upper part of the picture a conjugate set of veinlets has been rotated with respect of the foliation. Some veinlets tend to grow into gabbro segregations (Rio Ordagna).

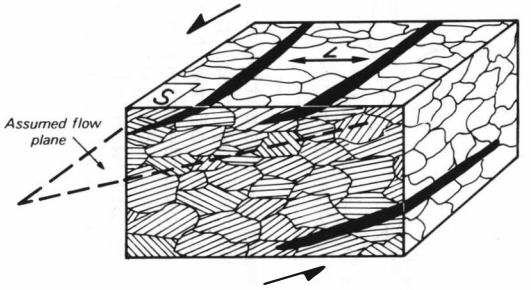

Fig. 9. Theoretical block diagram illustrating how the feldspar lenses (black) coalesce in the flow plane the orientation of which is assumed from slip orientations in olivine and enstatite (hatchings).

the previous interpretation (tension gashes) (*Boudier and Nicolas*, 1972). The conjugate sets of lenses have been observed mainly in one locality (Castello Camerletto) where no obliquity is reported between foliation and mineral preferred orientation (*Boudier*, 1976, p. 30). This latter fact suggests an irrotational flow in which case the two sets of lenses would coincide with the two shear planes associated with this flow regime.

The lenses and veinlets can locally grow into gabbroic segregations as illustrated by Fig. 10. As in the case of indigenous dikes, depleted lherzolites surround them but they do not have any continuity and there is no reason to consider them as transitional between lenses and indigenous dikes.

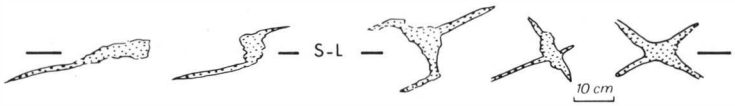

Fig. 10. Various patterns of coalescence of veinlets observed in a plane parallel to the mineral lineation and normal to the foliation. The surrounding lherzolite is locally depleted (sketches after pictures, see also Fig. 8).

GABBRO DIKES

Indigenous dikes and dunites

Although the indigenous dikes were probably fed in part by extraneous magma, their name is justified by the fact that they also have borrowed materials from their wall rocks. The typical indigenous dike is symmetrically bound by layers of dunite grading away into a lherzolite depleted in a plagioclase and diopside (Fig. 11); the thickness of the dunite band is proportional to that of the dike; there is a vague comb structure inside the dike; both the dike and the dunite walls can be folded and foliated; the contact of the dike and the dunite is interdigitated and close examination of it reveals a continuation of the dunite into the dike

Fig. 11. Indigenous gabbro dike with dunite walls (Mt. Arpone).

as olivine septa (Fig. 12) which seem to be oriented close to the foliation and hence could have a tectonic origin; a magmatic origin is also possible with the magma circulating parallel to the septa.

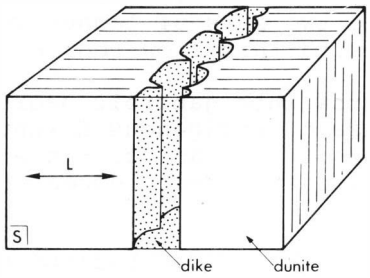

Fig. 12. Block diagram showing the olivine septa at the contact between the gabbro dike (dots) and its dunite wall (blank) and how they are oriented with respect to the foliation S and mineral lineation L.

The gabbro dike may have migrated out leaving behind the dunite and depleted lherzolite walls. This leads to the so called dunite "dikes". Their origin as partial melting residua is suggested when relics of the gabbro dike are left behind, and when the websteritic primary banding from the surrounding lherzolite can be traced into dunite as a seam of spinel + orthopyroxene grains (Fig. 13)(1). Such evidence has been observed in Lanzo, in the Hatay harzburgite massif in Turkey, in Josephine peridotite (*Dick*, 1977) and in Burro Mountain (with pyroxenes relicts). It is postulated here that the dunites observed in the tectonic peridotites are such residua; when they are parallel to the pyroxenitic layers, they may be part of an earlier layering transposed after a partial melting episode.

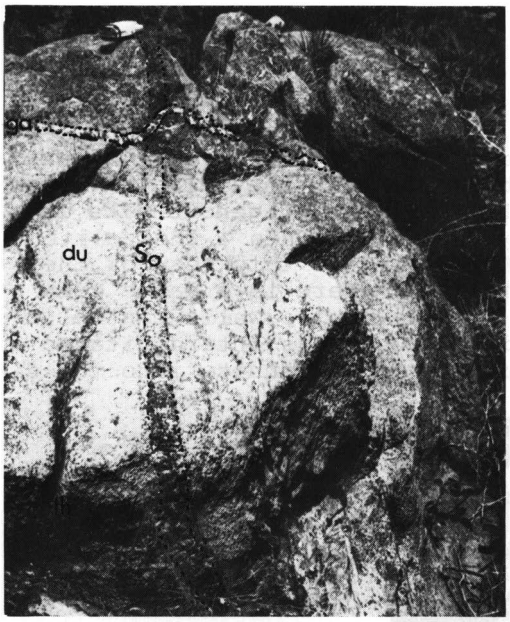

Fig. 13. Drawing after a photograph of deformed gabbro dyke (ga) cutting dunite (du). In the dunite, the primary banding (S_o) is preserved as a seam of spinel plus orthopyroxene. (Lh) = lherzolite.

Intrusive dikes

In Lanzo, three types of intrusive dikes have been observed. They all sharply cut the undepleted lherzolite. The most common type has the same composition as that of the indigenous dikes: they are 20 cm thick or more and internally layered with a comb structure at the margins and a more homogeneous and fine-grained structure in the center (Fig. 14). They may be slightly foliated and gently folded. Later dikes are either enstatite bearing, one centimeter thick and absolutely undeformed or andesine-augite-olivine bearing, a few decimeters thick and undeformed. The later dikes are restricted to specific areas and will not be discussed further in this study.

Intrusive dikes from the Antalya harzburgite massif in Turkey, considered below, are enstatite-bearing and strongly foliated and lineated (*Juteau*, 1974; *Juteau et al.*, 1977).

(1) Moreover olivine in the dunite has the same Fo content as in the adjacent lherzolite: Fo91 (*Boudier*, 1972).

Fig. 14. Intrusive gabbro dike, cross cutting the pyroxenitic layering (Castello Camerletto).

Origin of the Lanzo dikes

Earlier petrochemical calculations (*Boudier and Nicolas*, 1972; *Boudier*, 1976) have shown that the indigenous dikes crystallized from a composite magma formed by addition of an extraneous magma corresponding to a moderate (less than 5%) melting with one locally generated and corresponding to an extensive (up to 30%) melting. Should the composite magma be allowed to move into fresh lherzolites it would give birth to an intrusive dike. This interpretation is supported by the analogous range of bulk composition in the two sorts of dikes. Following a suggestion by Dickey, we believe that the extraneous magma was overheated due to its chemical equilibration with the lherzolite at a deeper level, and it reacted strongly with its lherzolite walls and triggered the extensive partial melting resulting in the formation of the indigenous dike. On the other hand, the composite magma if injected into the lherzolite penetrates it at 1250°C (*Boudier*, 1976) a temperature at which it is no longer reactive. The temperature of the overheated extraneous magma can be estimated from our experimental partial fusion on the Lanzo lherzolite. It indicates that the complete melting of enstatite leaving olivine-spinel residuum occurs around 1400°C. This was the situation at the walls of the indigenous dikes (dunite residuum); therefore this magma was at 1400°C or above.

Other possibilities have been suggested by *Coleman and Obata* (personal communications) to explain depleted margins without overheating. They call on the enrichment in a melting agent (CO_2 or H_2O). We discarded this possibility considering the absence of any hydrated phase in the gabbros.

Structural setting

As no difference appeared in the attitudes of the indigenous and intrusive dikes from Lanzo, they have been plotted together on the nets of Fig. 15 with respect to structural axes. The dikes tend to orient themselves perpendicular to the aggregate lineation.

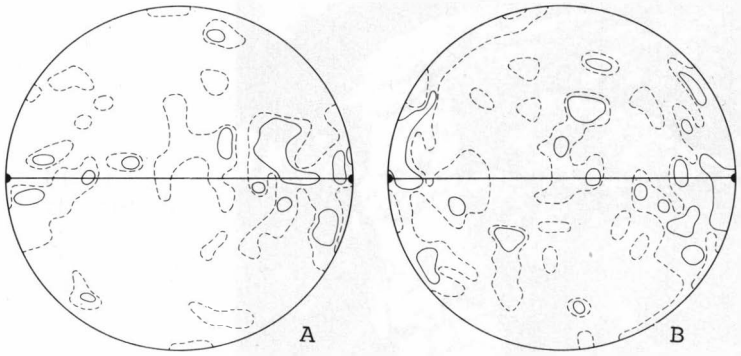

Fig. 15. Orientations of poles to gabbro dikes in Lanzo. Lower hemisphere, equal area projection, contours per 0.45% net area; structural reference system: foliation vertical EW, aggregate lineation horizontal EW. A and B are respectively for the central and southern bodies; A) 86 measurements, contours approximately at 1,2%; B) 102 measurements contours at 1,2%.

The intrusive dikes from Antalya are plotted on Fig. 16 with respect to geographic coordinates. The plot on the same net of the best computed axis for the spinel lineation and pole of foliation planes (*Juteau et al.*, in press) indicates that the gabbro dikes tend to be at various angles to the foliation but intersect with this plane parallel to the spinel lineation.

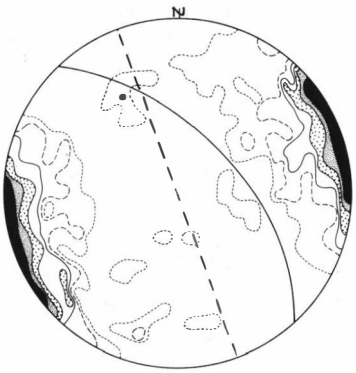

Fig. 16. Geographical orientations of gabbro dikes in Antalya. Lower hemisphere, equal area projection; 243 measurements, contours at 0.4, 0.8, 1.6, 2.5, 3.3 and 4% per 0.45% area. The solid line and the dot are respectively the best computed foliation and mineral lineation in the massif; the dashed line is the best computed dike orientation.

Experimental Melting Under Uniaxial Compressive Stress

Experimental conditions

Experiments of partial fusion have been conducted in a Griggs solid medium apparatus. A compressive stress was applied to investigate its influence on the melt coalescence. Cores from a Lanzo feldspar peridotite(1) were used directly, after dehydration at 100°C, in view to determine the nominal temperature at which each mineral phase disappears. The

(1) Modal composition: olivine = 64; orthopyroxene,= 17,5; clinopyroxene = 7,5; spinel = 1,5; plagioclase = 9,5.

cores were Pt jacketed and the sample assemblies were dry (Alsimag sleeves). Eight successful runs were performed at 7Kb and temperatures between 1150°C and 1600°C with a longitudinal temperature gradient between 50°C and 400°C. Runs varied in time from 1 to 10 hours.

Results

The complete melting of feldspar occurs within a few degrees above 1180°C. It results in pockets of tholeiitic melt with slightly different compositions(1) due to the temperature gradient and probably local departure from equilibrium. The melt pockets are connected by channels along which the other minerals suffer corrosion. Clinopyroxene disappears around 1250°C, and orthopyroxene between 1400°C and 1450°C. The initial amount of melt does not conspicuously exceed that of the former feldspar. The channels follow grain boundaries but can also follow cracks into grains (Fig. 17). They are more abundant, parallel to σ_1; melt products have also

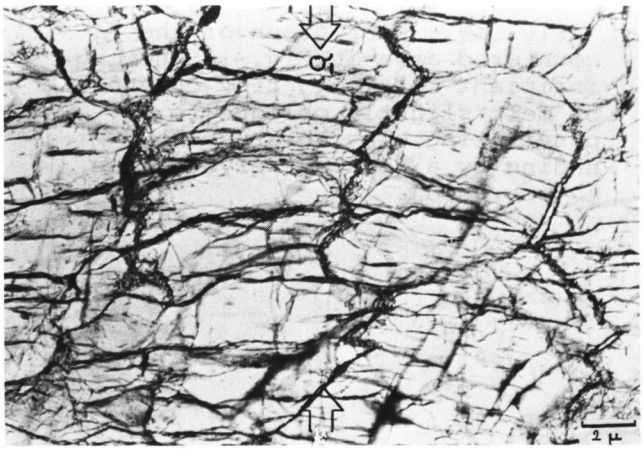

Fig. 17. Micrograph of experimental melting in a Lanzo lherzolite. The glass is concentrated at grain boundaries and cracks parallel to the σ_1 direction. Grain boundaries corroded by glass look darker and strained. The glass pockets (upper left, middle and lower right) look lighter.

been identified in oblique shear zones. Coalescence of melt in cracks and at grain boundaries parallel to σ_1 is more spectacular in a series of similar experiments conducted at 15 Kb with a spinel lherzolite, because it can be studied starting from an incipient melting lower than 1%; melting is then much more gradual (Fig. 18). In particular, tiny channels of melts have been observed penetrating into olivine crystals at a small angle to σ_1. Similar observations are reported by *Avé Lallemant and Carter* (1970) in experiments conducted with powders. The channels are initiated at grain boundaries, always pointing towards the warmer and more molten part of the specimen with, at their termination, a negative crystal due to corrosion (Fig. 19). For amounts of melting in the range of 20% and above, the melt pockets are moderately flattened perpendicular to σ_1.

(1) Glass microprobe analyses were performed by *M.H. Beeson*.

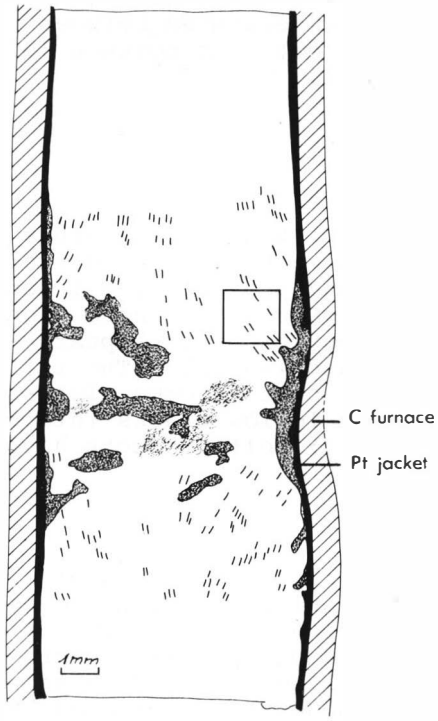

Fig. 18. Drawing after a picture of the experimental assemblage for partial melting experiments under stress. The melting in this spinel lherzolite is important in the central part of the specimen (gray decoration); at the colder ends the incipient melting (dashes) follow the stress trajectories.

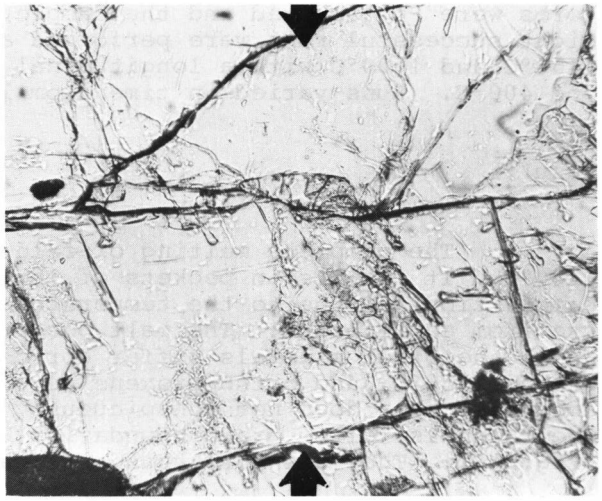

Fig. 19. Micrograph of the countered area in Fig. 18 showing incipient melting: tiny channels of melt slightly oblique to σ_1 penetrating olivine crystals, ending by a negative crystal due to corrosion.

Discussion

Time relation of partial melting and plastic deformation

The gabbro lenses and dikes in Lanzo were produced by partial melting as evidenced by the occurrence of residual dunite and depleted lherzolite at their contact. This partial melting event took place during the plastic deformation as deduced from the following evidences.

i) The lenses and dikes have special orientations with respect to the plastic deformation structures (foliation and lineation). These orientations cannot have been attained by rotation during the flow, in contrast to the dikes in Antalya where this is possible (see below).

ii) In the southern body, the indigenous dikes can be gently folded and the wall-dunites are foliated with a related olivine preferred orientation (*Boudier*, 1972). In the northern body where the deformation was active at temperatures well below the solidus, dikes are boudined and their minerals

always strained. At the crystal scale the same sort of conflicting observations are reported: in lenses the feldspar is strained but on the other hand this mineral reacts with olivine, presenting triple junctions involving a subboundary (Fig. 4); this indicates that the plastic flow substructure predates the corrosion. These conflicts are reconciled by considering that the melting occurred during the plastic flow.

iii) Mineral equilibrations in lherzolites affected by plastic deformation indicate maximum temperatures on the feldspar lherzolite dry solidus (*Boudier*, 1976, p. 106).

Coalescence at incipient melting

The incipient melting (< 1%) observed experimentally, impregnates grain boundaries and cracks parallel to σ_1 and shear zones oblique to σ_1; corrosion channels through olivine and again subparallel to σ_1 have been reported. Attributed to this stage in small lenses of naturally molten lherzolites are the feldspar grains reacting with olivine along grain boundaries and subboundaries, often starting from triple junctions.

Coalescence in feldspar lenses

Evidence from experiments supported by an approximate calculation shows that all the feldspar melts in a 10°C interval. This suggests that when the feldspar lenses formed in the Lanzo lherzolite the rock contained 5 to 10% melt. Where the deformation is weak the coalescence exceptionally exceeds the stage of producing monomineralic contorted veinlets (Fig. 3); where the deformation is strong the lenses readily attain one or two centimeters in thickness; at the same time they concentrate in the shear planes. In the case of rotational shear flow, they stand at some 15° from the foliation in the shear plane as it is defined by mineral preferred orientations (Fig. 9). From there they may rotate during flow subsequent to melt crystallization. They can also form an *en echelon* pattern. These orientations with respect to the foliation are readily used to specify the sense of shear. The veinlets can grow to become irregular gabbroic segregations developing a depleted area in the lherzolite around them. There is no evidence that these segregations represent transition towards indigenous dikes.

The question of how this 5 to 10% melt product concentrates in the shear planes (a single shear plane in rotational deformation, two conjugate shear planes in irrotational deformation) is not understood. Such a melt concentration in shear planes is observed at the incipient stage of melting in experiments conducted with an applied stress, together with another concentration in fractures parallel to the direction of the applied stress.

An important point is that the lherzolite microstructure and mineral preferred orientation in these areas where lenses are described differs in no conspicuous way from areas where traces of partial melting have not been found (compare in Boudier, 1976, p. 35-36 and p. 38). This suggests that the presence of 5-10% melt in the rock does not drastically change its plastic properties in keeping with some experimental evidence (*Arzi*, 1974).

The indigenous and intrusive dikes in Lanzo have the same composition and the same orientation in the field. This is explained in the following manner: an extraneous magma corresponding to a moderate peridotite melting at greater depth and overheated at 1400°C or more (or a fluid rich magma) is injected in the lherzolite the temperature of which is 1250°C. It triggers a local and extensive melting, leaving the dunite walls of the indigenous dikes as residua. If the composite magma thus generated remains there it will crystallize into an indigenous dike. If it is injected into an undepleted lherzolite it will constitute an intrusive dike, leaving behind the so-called dunite "dikes" which are indeed, in Lanzo and in other visited massifs, residua of partial melting.

In this interpretation the magmas responsible for the two kinds of dikes are both injected into the lherzolites over a short interval of time, thus explaining why they have the same composition and orientation in the field. They tend to gather at a large angle to the aggregate lineation (that is in a stretching orientation).

A different orientation has been recorded in Antalya where the intrusive dikes form various angles with the foliation but tend to contain the lineation. Considering their intense internal deformation and the dominant constrictive character of the strain in that massif (*Juteau et al.*, in press), their orientation can be explained by a rotation during the flow from any previous orientation towards that of the lineation; but other explanations cannot be ruled out.

Acknowledgements

We would like to express our appreciation to the Centre National de la Recherche Scientifique (E.R.A. 547, A.T.P. 32.41) and the U.S. Geological Survey in which laboratories these experiments were performed. These experiments were made possible thanks to E.D. Jackson, C.B. Raleigh, S.H. Kirby, and M.H. Beeson; J.L. Bouchez wrote the computer programs. The manuscript was revised taking into account comments by R.P. George.

References

Arzi, A., Partial melting in rocks: rheology, kinetics, water diffusion, *Ph.D. Thesis, Harvard University*, 1974.

Auten, T.A., R.B. Gordon, and R.L. Stocker, Q^{-1} and mantle creep, *Nature Phys. Sci.*, *250*, 317-318, 1974.

Ave'Lallemant, H.G., and N.L. Carter, Syntectonic recrystallization of olivine and modes of flow in the upper mantle, *Geol. Soc. Amer. Bull.*, *81*, 2203-2220, 1970.

Boudier, F., Relations lherzolites-gabbros-dunites dans le massif de Lanzo (Alpes piémontaises): Exemple de fusion partielle, *Thèse 3° cycle*, Nantes, 118 p., 1972.

Boudier, F., Le massif lherzolitique de Lanzo (Alpes piémontaises): Etude

structurale et pétrologique, *Thèse doct. Etat*, Nantes, 163 p., 1976.

Boudier, F., and A. Nicolas, Fusion partielle gabbroique dans la lherzolite de Lanzo (Alpes piémontaises), *Bull. Suisse Min. Petrog., 52*, 1, 39-56, 1972.

Chan, T., E. Nyland, and D.T. Gough, Partial melting and conductivity anomalies in the upper mantle, *Nature Phys. Sci., 244*, 89-90, 1973.

Dick, H.J.B., Partial melting in the Josephine peridotite: The effect on mineral composition and its consequence for geobarometry and geothermometry, *Am. Jour. Sci., 277*, 768-800.

Etchecopar, A., Simulation par ordinateur de la déformation progressive d'un agrégat polycristallin: Etude de développement de structures orientées par écrasement et cisail lement, *Thèse 3° cycle, Nantes*, 135 p., 1974.

Etchecopar, A., Plane kinematic model of progressive deformation in polycrystalline aggregates, *Tectonophysics, 39*, 121-139, 1977.

Goetze, C., A brief summary of our present day understanding of the effect of volatiles and partial melt on the mechanical properties of the upper mantle, *in preparation*.

Juteau, T., Les ophiolites des nappes d'Antalya (Taurides occidentales, Turquie): Pétrologie d'un fragment de l'ancienne croute océanique téthysienne, *Sci. de la Terre, Mem. 32*, 1-692, 1975.

Juteau, T., A. Nicolas, J. Dubessy, J.C. Fruchard, and J.L. Bouchez, The Antalya ophiolite complex (Western taurides, Turkey): Structural relationships between tectonites, cumulates and dykes: A possible model for an oceanic ridge, *Geol. Soc. Amer. Bull., in press*.

Loubet, M., Géochimie des Terres Rares dans les massifs de péridotites dits de "haute température": évolution du manteau terrestre, *Thèse Doct. Etat, Paris VII*, 357 p., 1976.

Menzies, M., Rare earth geochemistry of fused ophiolitic and alpine lherzolites: I. Othris, Lanzo and Troodos, *Geochimica et Cosmoch. Acta, 40*, 645-656, 1976.

Nicolas, A., J.L. Bouchez, and F. Boudier, Interprétation cinématique des déformations plastiques dans le massif de lherzolite de Lanzo (Alpes piémontaises), *Tectonophysics, 14*, 143-171, 1972.

Nicolas, A., F. Boudier, and A.M. Boullier, Mechanisms of flow in naturally and experimentally deformed peridotites, *Am. Jour. Sci., 273*, 853-876, 1973.

Nicolas, A., and F. Boudier, Kinematic interpretation of folds in alpine-type peridotites, *Tectonophysics, 25*, 233-260, 1975.

Nicolas, A., and J.P. Poirier, Crystalline plasticity and flow in metamorphic rocks, *J. Wiley and Sons Ltd., Interscience, London*, 444 p., 1976.

O'Connell, R.J., and B. Budiansky, Seismic velocities in dry and saturated cracked solids, *J. Geophys. Res.*, 5412-5426, 1974.

Shankland, T.J., and H.S. Waff, Partial melting and electrical conductivity anomalies in the upper mantle, *in preparation*.

Stocker, R.L., and R.B. Gordon, Velocity and internal friction in partial melts, *J. Geophys. Res.*, 4838-4836, 1975.

Walsh, J.B., A new analysis of attenuation in partially melted rock, *J. Geophys. Res.*, *74*, 4333-4337, 1969.

PARTIAL FUSION VERSUS FRACTIONAL CRYSTALLIZATION: HYPOTHESES FOR THE DIFFERENTIATION OF THE RONDA ULTRAMAFIC MASSIF OF SOUTHERN SPAIN

John S. Dickey, Jr., Masaaki Obata, and C. John Suen
Department of Earth and Planetary Sciences
Massachusetts Institute of Technology
Cambridge, Massachusetts 02139

Abstract

The Ronda ultramafic massif of southern Spain was differentiated into peridotite (85 to 90%) with mafic segregations before it was elevated to the crust from deep in the lithosphere. No primary igneous textures are preserved because of extensive metamorphism during elevation of the massif from the lower lithosphere. Some features can be identified, however, which apparently relate to the differentiation of the massif. These features, involving the forms, bulk compositions and phase equilibria of the mafic segregations, suggest that the differentiation process was a multi-stage process involving partial fusion and subsequent modification of the partial melts by crystal fractionation and, possibly, remelting.

Introduction

The surface of the earth contains a few places where masses of ultramafic and related rocks have penetrated the outer lithosphere as hot, solid intrusions. These high-temperature peridotite intrusions typically create substantial contact metamorphic aureoles, contain notably high concentrations of magmaphile elements (such as Si, Ti, Al, Fe, Ca and Na), and contain phases and textures which have developed along decreasing T-P gradients.

Several of these peridotite massifs contain segregations of mafic rocks, varying in mineralogy from garnet pyroxenites to olivine gabbros, and chemically approaching picritic basalts. How these segregations formed remains a mystery. *Carswell* (1968), *Kornprobst* (1969) and *Dickey* (1970) proposed that such segregations in the Almklovdalen, Beni Bouchera and Ronda peridotites, respectively, represent melts formed by partial fusion of mantle peridotite. As an explanation for the rocks partial fusion has several advantages over fractional crystallization: no ultramafic magma is required; the observed chemical uniformity of the host peridotite would be readily achieved; and the segregations are close to compositions from which basalts might be derived. Yet attempts to confirm the partial fusion hypothesis by geochemical tests have met with only marginal success, and in the case of the Ronda massif geochemical and experimental studies have demonstrated that fusion alone cannot explain the mafic segregations as they now exist.

Description of the Ronda Massif

The Ronda ultramafic massif is the world's largest high temperature peridotite intrusion, covering 300 km^2 near the south coast of Spain between Marbella and Estepona (Figure 1). This mass of peridotite and related rocks is a 1.5 km thick slab which has been thrust north from high density roots in the Alboran Sea (*Bonini et al.*, 1973). Surrounding the massif is a contact metamorphic aureole (part of which is also allochthonous) which indicates last equilibration temperatures of approximately 800°C at the contact (*Loomis*, 1972; *Dickey and Obata*, 1974).

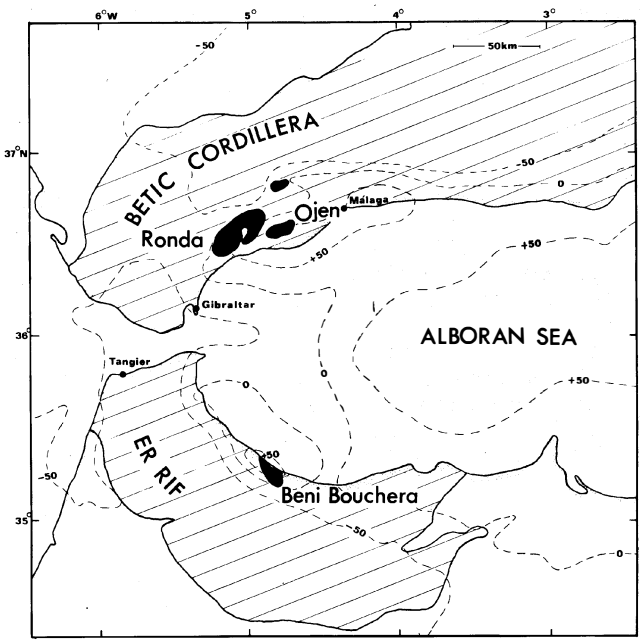

Figure 1. Locations of the major peridotite massifs in the Betic-Rif orocline. Bouger gravity anomalies (in mgal.), shown as dashed lines, are from *Bonini et al.* (1973). Positive anomalies as high as +110 mgal. occur within the +50 mgal. closure southeast of the Ronda massif. Petrological descriptions of the Ronda, Ojen and Beni Bouchera massifs can be found in *Dickey* (1970), *Hernandez-Pacheco* (1967) and *Kornprobst* (1969) respectively.

The Ronda massif is 85 to 90 percent peridotite. In addition the massif contains sheets of mafic rocks and a variety of discordant dikes. Some of the dikes may be indigenous to the massif; some may be related to exotic magma systems; and some may represent anatectic magmas formed by partial fusion of crustal rocks during the emplacement of the hot peridotite. There are also graphite- and cordierite-rich dikes which apparently originated by intrusion and metamorphism of hydrocarbon-charged mud during the final emplacement of the massif (*Dickey and Obata*, 1974).

Mafic segregations occur within the peridotite as sharply bounded layers, from 1 cm to 3 m thick, in which are concentrated (relative to the host peridotite) such magmaphile elements as Si, Al, Fe, Ca and Na. These mafic layers have fairly uniform chemical compositions (average: 47% SiO_2, 14% Al_2O_3, 7% Fe as FeO, 17% MgO, 12% CaO, 1% Na_2O and less than 0.01% K_2O); however, they vary in lithology from eclogites to gabbros and are defined in terms of 3 major groups characterized by the presence or absence of garnet and olivine:

Group I Garnet Pyroxenites

a. Cpx + Gar + Plag
b. Cpx + Opx + Gar
c. Cpx + Gar

Group I Garnet Pyroxenites (continued)

d. Cpx + Gar + Plag + Qz
e. Cpx + Opx + Gar + green Sp (ceylonite)

Group II Pyroxenites

a. Cpx + Opx + green Sp
b. Cpx + Opx + green Sp + Plag
c. Cpx

Group III Olivine Gabbros

a. Cpx + Ol + Plag + Opx + brown Sp (picotite)
b. Cpx + Ol + Plag + Opx + opaque Sp (chromite)

Ultramafic rocks in the Ronda massif vary from garnet peridotite to spinel peridotite and plagioclase peridotite. Lherzolite is most abundant, followed by harzburgite and dunite. From the distribution of the types of mafic layers and of the garnet-, spinel- and plagioclase-peridotites it is possible to subdivide the massif into 4 mineral facies zones (Figure 2):

I. Garnet Lherzolite Facies
II. Ariegite Subfacies of the Spinel Lherzolite Facies
III. Seiland Subfacies of the Spinel Lherzolite Facies
IV. Plagioclase Lherzolite Facies

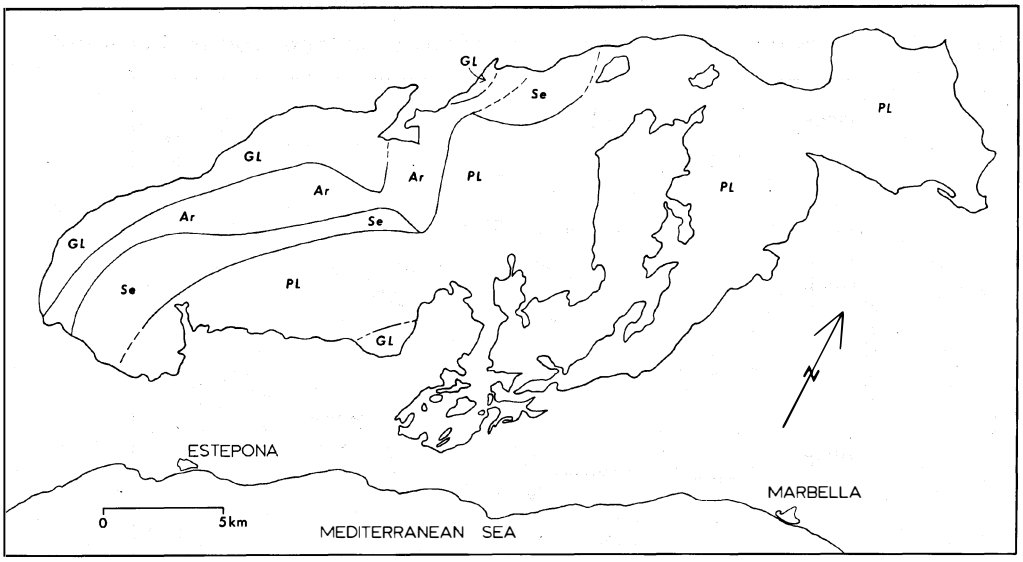

Figure 2. Distribution of mineral facies in the Ronda peridotite massif. GL Garnet lherzolite facies. AR Ariegite subfacies of the spinel lherzolite facies. SE Seiland subfacies of the spinel lherzolite facies. PL Plagioclase lherzolite facies. These facies are defined in the sense of *O'Hara* (1967).

Most of the mineralogical characteristics of the massif, including the distribution of mineral facies zones, were established by subsolidus reactions in response to decompression and cooling after the mafic

segregations were established in the mass of peridotite. Many of the mafic segregations have complex textures due to incomplete decompression metamorphism. Over most of the massif the rocks re-equilibrated to low pressure mineral assemblages (Group III), but in certain regions, particularly near the north west contact, metamorphism was inhibited, and the rocks retained higher pressure mineral assemblages (Groups I and II).

Conditions of Equilibration

The pressures and temperatures at which the rocks of the garnet lherzolite facies equilibrated can be estimated from the compositions of coexisting garnet and pyroxenes. Using "primary" (core) compositions of enstatite porphyroclasts and experimental data by *Mori and Green* (1975) and *Akella* (1976), *Obata* (1976, 1977) demonstrated that the garnet peridotite once equilibrated at temperatures and pressures of at least 1100°C and 22 kbar. This corresponds to depths of 70 to 75 km. Compositions of pyroxene neoblasts in the garnet peridotite indicate that it was later metamorphosed at 800° to 900°C and 15 kbar (50 km). Mafic layer R127, a plagioclase garnet clinopyroxenite within the garnet peridotite, was completely recrystallized at 800° to 900°C and more than 10 kbar (*Obata and Dickey*, 1976). Although layer R127 preserves no record of higher pressures or temperatures this mafic segregation must have formed before the garnet peridotite equilibrated at 22 kbar. Between 10 and 22 kbar the dry solidus of R127 rises from 1210°C to 1300°C (Figure 3). If R127 had formed at such temperatures after the massif rose from 70 to 75 km, the pyroxenes in the garnet peridotite would have completely recrystallized. We conclude, therefore, that the Ronda massif existed in its differentiated form (that is, with mafic segregations) when it was part of the lower lithosphere.

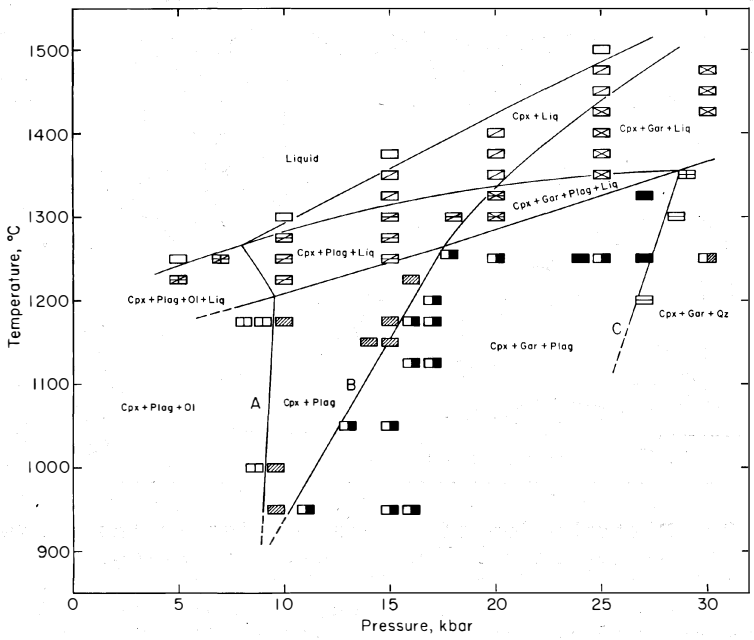

Figure 3. Pressure-temperature diagram for the composition of plagioclase-garnet clinopyroxenite R127. Experiments run in graphite crucibles under dry conditions. See *Obata and Dickey* (1976) for detailed discussion of methods and results.

In order to understand how the Ronda massif became differentiated it is necessary to look beyond the effects of metamorphism and identify features which were established by the differentiation processes. We now recognize 6 pre-metamorphic features, related to the forms, major element compositions and trace element compositions of the mafic segregations, which constrain the possible hypotheses of differentiation.

1. The mafic layers typically have sharp contacts with the host peridotites.

These sharp contacts may have been created by differential movement between the mafic layers and the host peridotites. Nevertheless, there is no evidence suggesting that primary megascopic gradations existed between the mafic layers and the peridotites.

2. Modal variations exist within some thick mafic layers which may be due to crystal fractionation or to wallrock reactions.

Although pyroxene-rich schlieren are present within the peridotites these are not features which now resemble products of crystal fractionation.

3. The major element compositions of the mafic layers are richer than the host peridotites in magmaphile elements.

The mafic layer compositions (Table 1) are between basaltic and peridotitic. C.I.P.W. norms of these rocks contain 17 to 28 percent Ol (except for an orthopyroxenite which contain 8 percent Ol and 70 percent Hy).

High pressure norm calculations (*Dickey*, ms) indicate that in the lower lithosphere these rocks would exist as garnet pyroxenites with accessory quantities of such phases as quartz, olivine, spinel, kyanite and corundum.

4. Concentrations of K and P are vanishingly small (less than 0.01 percent) in both the mafic layers and in the host peridotites.

Such low concentrations of K and P suggest that, relative to basalt-producing mantle rocks, the parental material of the Ronda massif was already depleted in magmaphile elements. Alternatively, these elements may have been removed from the differentiated massif by some unknown process. No concentrations of K or P, which might be evidence for pegmatitic, hydrothermal or metasomatic migrations of these elements, have been found.

5. The liquid of one mafic layer composition (perhaps others) is not saturated with olivine at liquidus temperatures above 8 kbar and is not saturated with orthopyroxene under any conditions.

The results of a series of high T-P experiments on garnet plagioclase clinopyroxenite R127 (Figure 3) clearly indicate that liquids of this composition would not be in equilibrium with peridotite under lower lithosphere conditions. This means that either the mafic layer represents a liquid generated at less than 8 kbar, or that a reaction relationship existed between the liquid and the host peridotite, or that the layer represents a crystal cumulate rather than a liquid.

If layer R127 formed from a low pressure melt it must have been metamorphosed under increasing pressure after crystallization. There is no evidence for compressional metamorphism in the Ronda massif.

If layer R127 formed from a melt generated at pressures greater than 8 kbar it might have reacted with the peridotitic host rock upon cooling. Such reactions involving olivine, orthopyroxene and liquid have been documented in high T-P experiments by *Kushiro and Yoder* (1974) and by *O'Hara and Yoder* (1967). The creation of wallrock reaction zones, composed probably of clinopyroxene and spinel, would isolate the liquid and terminate the reactions. Some mafic layers have pyroxene-rich margins, but these are not yet recognized as reaction zones.

If the layer formed as a high pressure cumulate, consisting, for example, of garnet and clinopyroxene, it is difficult to explain the fine scale (cm) alternation of peridotite and mafic layers which is commonly observed. If the layer formed as a low pressure cumulate it also must have been metamorphosed under increasing pressure (for which there is no evidence) and it is difficult to explain the absence of chromitite layers, which are common magmatic cumulates in mafic plutons which have differentiated by fractional crystallization under crustal (<8 kbar) pressures (cf. *Thayer*, 1970). There are no chromitite layers in the Ronda massif.

6. Rare earth element (REE) concentrations (normalized to chondritic abundances) show higher REE concentrations in the mafic layers than in the peridotites, light rare earth element (LREE) depletion in all samples, and a Eu anomaly (positive) in only 1 sample.

Rare earth element abundances (Figure 4) were obtained by neutron activation analysis of rock powders for which major element compositions have previously been reported (*Dickey*, 1970) except for garnet peridotite R501.

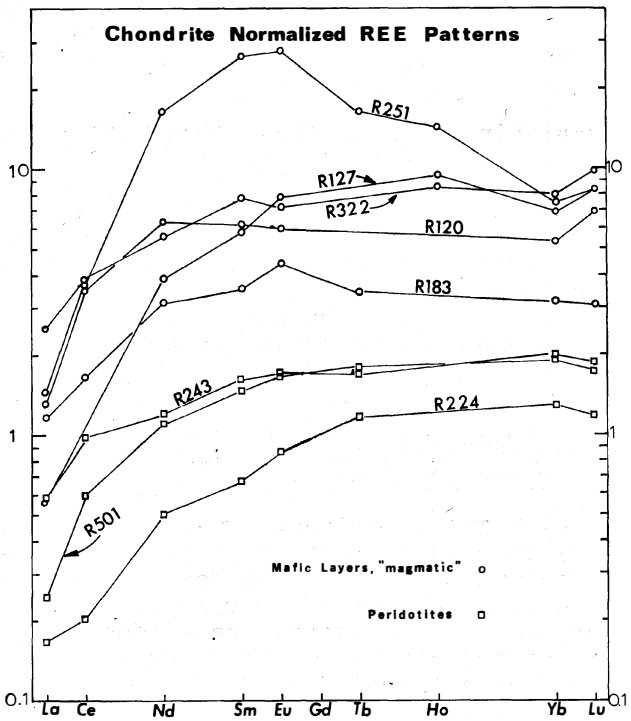

Figure 4. Concentrations of rare earth elements, relative to chondritic meteorites, in mafic layers and peridotites of the Ronda massif. R251, spinel pyroxenite. R127, plagioclase-garnet clinopyroxenite. R322, olivine gabbro. R120, olivine gabbro. R183, olivine gabbro. R243, spinel lherzolite. R224, spinel harzburgite. R501, garnet lherzolite.

The depletion of the peridotites in LREE is compatible with an origin as residues of a small degree (less than 10%) of partial melting of a near chondritic source. The absence of an Eu anomaly in the peridotite patterns precludes the possibility of partial melting in the plagioclase peridotite stability field. Similar patterns are recognized for many other mantle-derived peridotites (e.g., *Frey*, 1969; *Frey et al.*, 1971; *Loubet et al.*, 1975).

The REE patterns of the mafic layers are more varied than those of the peridotites. Some patterns resemble REE patterns of oceanic tholeiites, although the REE concentrations in the mafic layers are much lower than typical concentrations in oceanic tholeiites. One sample (R127) is as strongly depleted in LREE as some peridotites, while another sample (R251) has a convex pattern with a maximum around Sm and Eu. None of the analyzed mafic layers is as enriched in LREE as would be expected if the mafic layers are the unmodified products of small degrees of partial melting of the Ronda peridotites.

No single-step process is capable of explaining the REE distributions in the peridotites and mafic layers. The REE data suggest that the mafic layers and peridotites may be high pressure cumulates, or the mafic layers may be crystal fractionates from partial melt segregations, or the mafic layers may be residual material from repeated partial fusion of segregations which were originally formed by partial melting or by fractional crystallization.

Conclusions

Even with the constraints and implications of the 6 premetamorphic characteristics described above the history of the differentiation of the Ronda massif remains obscure. The field and chemical data appear to favor differentiation of a solid peridotite source by partial melting and melt segregation, but fractional crystallization of an ultramafic magma, perhaps at great depth, is also possible. What is not possible is a simple, single-step process. The data show that the differentiation process involved more than 1 stage and may have been very complex.

Figure 5 illustrates how partial fusion, crystallization and melt segregation could relate to one another in a process which is based upon partial fusion of solid peridotite. This flow diagram shows how complicated cycles could develop. The mafic segregations are divided into 2 classes: those which represent the compositions of their parent melts (orthomagmatic) and those which lack some part of their parent melts (depleted). Several generations of melts may be created by partial fusion of residual peridotite or of mafic layers. Orthomagmatic segregations may form from <u>any</u> of these melts. Their definitive characteristic is that their bulk compositions are the same as the compositions of their parent melts. Depleted layers can also form during any cycle. Furthermore, depleted layers can form in 2 ways: as crystal cumulates lacking some part of the parent melt, or as unmelted residues formed by partial fusion of mafic layers. In the absence of clear textural evidence these 2 kinds of depleted segregations are probably indistinguishable. Such is the case at Ronda where metamorphism has oblitterated the primary textures, but elsewhere it may be possible to distinguish partial fusion residues from cumulates.

Many of the details of the differentiation process can be determined by further study. There is, however, 1 step for which no

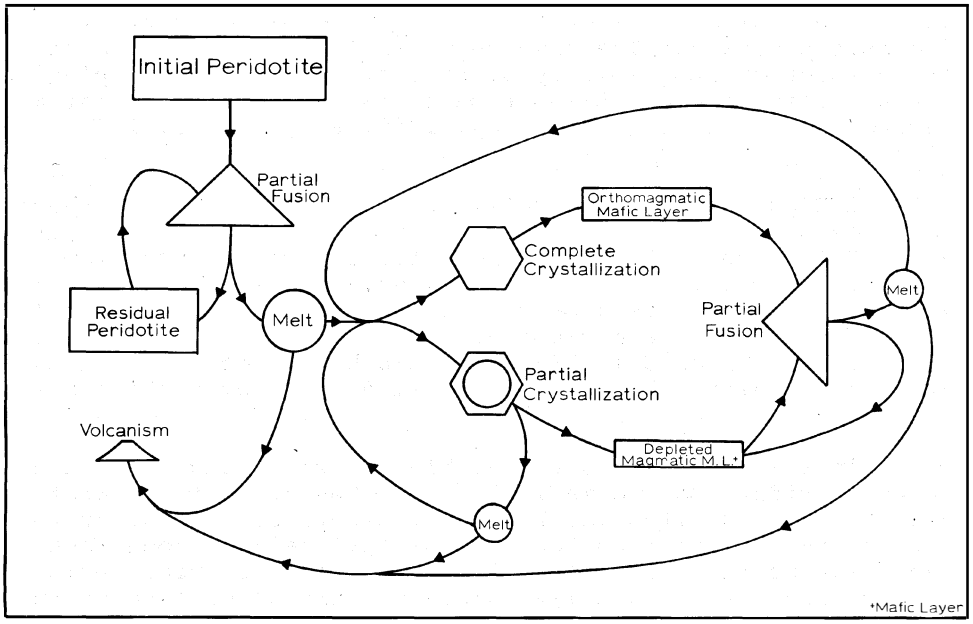

Figure 5. Flow diagram for the partial fusion model of the differentiation of the Ronda massif. Solid residues from fusion may be remelted. Liquids formed by partial fusion may be modified by crystal fractionation, liquid extraction, and remelting. Any magmatic layer which truly represents the composition of its parental melt is called an orthomagmatic mafic layer. All others are called depleted magmatic mafic layers.

evidence has yet been found: there are no known volcanic, pegmatitic or other igneous rocks within or adjacent to the Ronda massif which can be recognized as the fugitive constituents of the depleted mafic segregations. There are basic volcanics of Triassic age in the Nevado-Filabride complex, which lies between the Ronda and Ojen massifs, however (*Rondeel and Simon*, 1974), and future studies may show that these rocks represent the fugitive constituents of the Ronda massif.

However it formed the Ronda ultramafic massif demonstrates that a substantial part of the lower lithosphere is heterogeneous on a fine scale (cm to m) and that segregations of eclogitic material are present, as suggested, for example, by *Ringwood* (1958). Future investigations may resolve the process of differentiation. Other important questions which also may be answered are: when was the massif differentiated? where was the massif during differentiation? and do the mafic segregations bear any genetic relationships to basalts?

Acknowledgements

Research on the Ronda ultramafic massif is supported by the Earth Sciences Division of the National Science Foundation (grant numbers DES73-00264, DES75-02900 and EAR76-84067). The study of rare earth element distribution was guided by Professor F.A. Frey. Technical assistance was

TABLE 1. Compositions of Mafic Layers in the Ronda Massif (Dickey, 1970)

	Sample						
	R127	R251	R183	R120	R322	R343	R349
SiO_2	47.73	44.09	46.67	46.68	48.33	48.91	53.21
TiO_2	0.73	1.12	0.24	0.19	0.31	0.06	0.09
Al_2O_3	16.16	14.51	17.71	12.91	11.83	11.61	5.17
Cr_2O_3	0.00	0.06	0.09	0.25	0.47	0.35	0.82
Fe_2O_3	0.94	2.47	0.96	0.99	0.48	0.53	0.63
FeO	7.84	4.97	6.15	5.43	4.43	5.81	5.42
MnO	0.15	0.14	0.14	0.17	0.12	0.15	0.14
MgO	9.88	14.80	12.16	20.81	22.38	20.01	29.81
CaO	14.15	16.44	14.16	10.33	9.86	11.27	3.92
Na_2O	1.89	0.89	1.30	0.96	0.77	0.53	0.18
K_2O	<0.01	0.01	<0.01	0.00	0.01	0.00	0.00
H_2O+	0.35	0.24	0.37	1.03	0.52	0.56	0.33
H_2O-	0.06	0.09	0.06	0.10	0.11	0.09	0.11
P_2O_5	0.00	0.00	0.00	0.00	0.00	0.00	0.00
NiO	<0.01	0.03	0.03	0.08	0.11	0.06	0.02
$SO_3=$	0.00	0.04	0.00	0.12	0.06	0.00	0.05
Total	99.88	99.90	100.04	100.05	99.79	99.94	99.90
Or	--	--	--	--	0.06	--	--
Ab	15.76	--	11.00	7.34	6.12	4.48	1.20
An	35.61	35.74	42.49	31.34	29.00	29.30	13.47
Ne	0.12	3.94	--	--	--	--	--
Di	28.02	35.69	22.25	15.76	15.70	21.12	4.71
Hy	--	--	1.23	14.13	23.30	25.47	69.96
Ol	17.19	18.13	20.66	27.98	22.90	17.51	7.74
Mt	1.36	3.58	1.39	1.44	0.70	0.77	0.91
Chr	--	0.09	0.13	0.37	0.69	0.52	1.21
Ilm	1.39	2.13	0.46	0.36	0.59	0.11	0.17
Rest	0.35	0.50	0.37	1.24	0.63	0.56	0.42
Total	99.82	99.80	99.98	99.95	99.68	99.85	99.79

Modes:

R127 61% cpx, 23% plag, 5% gn, 11% kelyphite.
R251 81% cpx, 8% sp, 7% plag, 4% ol, less than 0.5% ilm.
R183 51% cpx, 30% plag, 15% ol, 3% sp, 0.6% chr, 0.4% opx.
R120 23% cpx, 33% plag, 27% ol, 3% sp, 12% opx, 2% secondary.
R322 35% cpx, 22% plag, 23% ol, 16% opx, 4% chr + sp, less than 0.5% secondary brown amphibole.
R343 15% cpx, 36% plag, 24% ol, 15% opx, less than 1% chr.
R349 79% opx, 9% ol, 7% cpx, 4% plag, 1% sp.

provided by Dr. A.S. Parkes. Assistance in the field was provided by Mr. Dorian Nicol. Obata's travel expenses to the Chapman Conference on Partial Melting were paid by the American Geophysical Union and the Department of Earth and Planetary Sciences at the Massachusetts Institute of Technology. Suen's field expenses were partially paid by the Geological Society of America. The Carnegie Institution of Washington provided materials and facilities for experimental studies. Dr. Ikuo Kushiro guided the experimental studies at the Geophysical Laboratory. Samples for instrumental neutron activation analysis were irradiated at the MIT Research Reactor. INAA work supported by NSF Grant DES75-02900.

References

Akella, J., Garnet pyroxene equilibria in the system $CaSiO_3$-$MgSiO_3$-Al_2O_3 and in a natural mineral mixture, *Am. Mineral.*, *61*, 589-598, 1976.

Bonini, W.E., T.P. Loomis, and J.D. Robertson, Gravity anomalies, ultramafic intrusions, and the tectonics of the region around the Strait of Gibraltar, *J. Geophys. Res.*, *78*, 1372-1382, 1973.

Carswell, D.A., Picritic magma - residual dunite relationships in garnet peridotite at Kalskaret near Tafjord, South Norway, *Contrib. Mineral. Petrology*, *19*, 97-124, 1968.

Dickey, J.S., Jr., Partial fusion products in alpine-type peridotites: Serrania de la Ronda and other examples, *Min. Soc. America Special Paper*, *3*, 33-49, 1970.

Dickey, J.S., Jr., (ms.), A norm for the lunar interior.

Dickey, J.S., Jr., and M. Obata, Graphitic hornfels dikes in the Ronda high-temperature peridotite massif, *Am. Mineral.*, *59*, 1183-1189, 1974.

Frey, F.A., Rare earth abundances in a high-temperature peridotite intrusion, *Geochim. Cosmochim. Acta*, *33*, 1429-1447, 1969.

Frey, F.A., L.A. Haskin, and M.A. Haskin, Rare earth abundances in some ultramafic rocks, *J. Geophys. Res.*, *76*, 2057-2070, 1971.

Hernandez-Pacheco, A., Estudio petrografico y geochimico del macizo ultramafico de Ojen (Malaga), *Estud. Geol.*, *23*, 85-143, 1967.

Kornprobst, J., Le massif ultrabasique des Beni Bouchera (Rif Interne, Maroc): etude des peridotites de haute temperature et de haute pression, et des pyroxénolites à grenat qui leur sont associées, *Contrib. Mineral. Petrol.*, *23*, 283-322, 1969.

Kushiro, I., and H.S. Yoder, Jr., Formation of eclogite from garnet lherzolite: liquidus relations in a portion of the system $MgSiO_3$-$CaSiO_3$-Al_2O_3 at high pressure, *Carnegie Inst. Washington Year Book*, *73*, 266-269, 1974.

Loomis, T.P., Contact metamorphism of pelitic rock by the Ronda ultramafic intrusion, southern Spain, *Geol. Soc. America Bull.*, *83*, 2449-2474, 1972.

Loubet, M., N. Shimizu, and C.J. Allegre, Rare earth elements in alpine peridotites, *Contrib. Mineral. Petrol.*, *53*, 1-12, 1975.

Mori, T., and D.H. Green, Subsolidus equilibria between pyroxenes in the CaO-MgO-SiO_2 system at high pressures and temperatures, *Am. Mineral.*, *61*, 616-625, 1976.

Obata, M., Pressure-temperature trajectories of the Ronda peridotite intrusion, southern Spain, *Abstracts with Programs*, *8*, 1033, 1976.

Obata, M., Petrology and petrogenesis of a high-temperature peridotite intrusion: Serrania de la Ronda, southern Spain, Ph.D. Thesis, Massachusetts Institute of Technology, 1977.

Obata, M., and J.S. Dickey, Jr., Phase relations of mafic layers in the Ronda peridotite, *Carnegie Inst. Washington Year Book*, *75*, 562-566, 1976.

O'Hara, M.J., Mineral paragenesis in ultrabasic rocks, in *Ultramafic and Related Rocks*, edited by P.J. Wyllie, pp. 393-401, John Wiley and Sons, Inc., New York, 1967.
O'Hara, M.J., and H.S. Yoder, Jr., Formation and fractionation of basic magmas at high pressures, *Scot. J. Geol.*, *3*, 67-117, 1967.
Ringwood, A.E., The constitution of the mantle - III. *Geochim. Cosmo. Acta*, *15*, 195-212, 1958.
Rondeel, H.E., and O.J. Simon, Betic Cordilleras, in *Mesozoic-Cenozoic Orogenic Belts*, edited by A.M. Spencer, pp. 23-35, Scottish Academic Press, Edinburgh, 1974.
Thayer, T.P., Chromite segregations as petrogenetic indicators, *Geol. Soc. . Africa Spec. Publ. 1*, 380-390, 1970.

COMPLEMENTARY META-GABBROS AND PERIDOTITES IN THE NORTHERN KLAMATH MOUNTAINS, U.S.A.

M.A. Kays, M. Ferns, and L. Beskow
Department of Geology
University of Oregon
Eugene, Oregon 97403

Abstract

Ultramafic rocks in some parts of the northern Klamath Mountains in Oregon and northern California are persistently associated with a complementary suite of gabbroic rocks. The ultramafic and gabbroic bodies are generally small, highly deformed, and metamorphosed. If the suite of gabbros and ultramafic rocks bear a product-residue relationship here, individual rock bodies may be the highly dismembered erosional remnants of one or more areally extensive ultramafic-mafic complexes. Because of the size, metamorphism and fragmentation of the ultramafic-mafic rock bodies, we cannot discount the possibility that they are tectonically emplaced, unrelated rock members. Nor can we discount entirely metasomatic modification of some members. Nevertheless, the association of serpentinized harzburgite and dunite with internally gradational wehrlite-clinopyroxenite-gabbro suggests a consanguineous suite.

In the western Paleozoic and Triassic belt, ultramafic-mafic rocks have a persistent association with areally extensive metamorphic terranes of higher grade than adjacent metavolcanic-metasedimentary rocks. In some places the ultramafic and higher grade rocks are clearly allochthonous. The metamorphosed rocks are mainly amphibolites and quartz-rich biotite schists and are tectonically interleaved and folded with ultramafic-mafic rocks. Potassium-argon determinations on the amphibolites in the ultramafic sequence and in associated metamorphosed rocks indicate grossly similar metamorphic age relations with allochthonous ultramafic and metamorphosed rocks over large areas in the Klamath Mountains and Coast Ranges in Oregon and northern California.

Introduction

Small but numerous bodies of ultramafic rocks have a close association with gneissic and schistose metamorphic rocks of clearly higher grade than surrounding more feebly metamorphosed metaclastic and metavolcanic rocks within the western Paleozoic and Triassic belt*. Metamorphosed ultramafic rocks and basic gneisses make up a sizeable part of this higher grade terrane. Some of the basic gneisses have textural, compositional, and mineralogical characters more consistent with plutonic intrusive rocks than effusive basalts. These same basic gneisses are in places gradational and interlayered with amphibole-and/or pyroxene-rich

---

* Hereafter referred to simply as WTrPz.

ultramafic rocks. Thus, an objective of this study is to learn more about the relationship of basic gneisses to ultramafic rocks; another objective is to learn more about the relations among metamorphosed members of the higher grade association. Here we focus attention on the relations determined between ultramafic and gneissic rocks in two areas within the WTrPz where field and petrographic relations are well known (Fig. 1).

In the Wrangle-Red Mountain area near the California-Oregon border ultramafic and higher grade metamorphic rocks are tectonically interleaved and separated by folded thrust faults. The highly fragmented, mélange-like character of the metamorphic and ultramafic rocks is consistent with an allochthonous occurrence. In the northernmost area, a part of the May Creek Schist belt, higher grade metamorphic and ultramafic rocks are tectonically interleaved but a large body of quartz diorite-granodiorite is approximately central to the metamorphic units.

Regional Relations

The relatively large volume of higher grade and more completely recrystallized metamorphic rocks in such close association with small discrete bodies of ultramafic rocks in the WTrPz is in strong contrast with the massive Josephine peridotite and Trinity ultramafic sheets in the adjacent western Jurassic and eastern Paleozoic belts (Fig. 1). In the latter, ultramafic rocks are of large areal extent and metamorphic rocks are minor or rare; metamorphic rocks are widespread, however, at the margins below these ultramafic sheets.

This close and frequently mélanged association of ultramafic rocks with higher-grade schists and gneisses is similar to certain occurrences in the Oregon and California Coast Ranges (*Coleman*, 1972; *Ramp*, 1976; *Ernst and others*, 1970). In contrast to the Coast Range mélanges, however, these rocks have affinities more consistent with a higher temperature facies (*Miyashiro*, 1961) than the high pressure-low temperature Franciscan association. However, the thrusted and in part allochthonous Stuart Fork Formation at the eastern margin of the WTrPz may contain glaucophane-lawsonite-bearing blueschists at its base (*Hotz*, 1973).

The abundance and size of "granitic" plutons in the WTrPz, and the higher temperature nature of these rocks may indicate some similarities with the group of formations collectively referred to as the central metamorphic belt (*Davis and Lipman*, 1962). Mapping in the central metamorphic belt indicates a generally greater coherence of metamorphic units than in the higher grade terranes of the WTrPz (*Davis and others*, 1965).

Nature of the Ultramafic and High Grade Metamorphic Association

Character and Occurrence

A variety of amphibole-bearing gneisses and schistose rocks occurs folded with, and in some places, interlayered with ultramafic rocks. In the Wrangle-Red Mountain area near the California-Oregon border, the ultramafic, gneissic, and schistose rocks constitute a separate terrane within the bounds of more feebly recrystallized metaclastic and metavolcanic rocks of the WTrPz (Fig. 1). In places, metamorphic and ultramafic rocks are

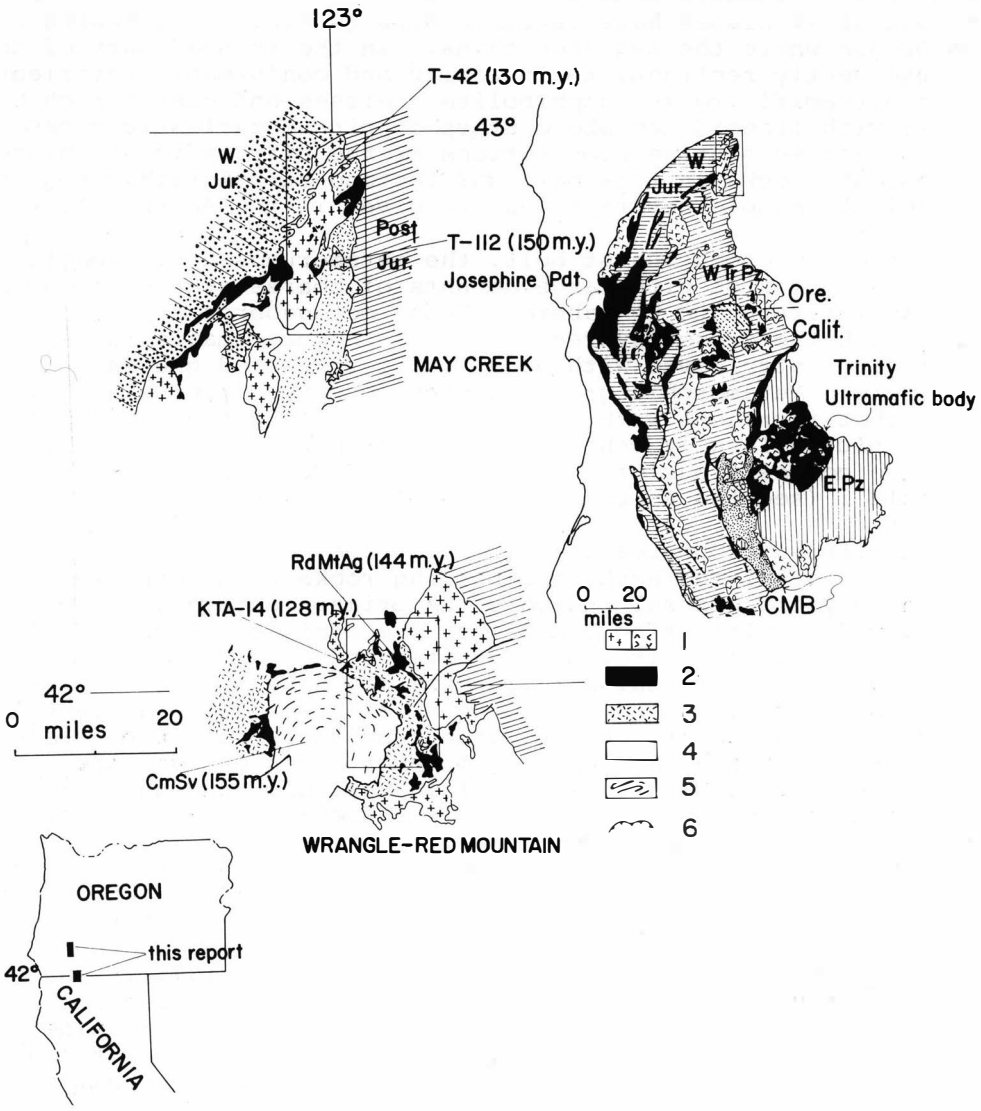

Fig. 1. Location map and distribution of ultramafic rocks and higher grade metamorphic terranes in some parts of the WTrPz. The Wrangle-Red Mountain area and the northern part of the May Creek Schist belt are outlined. The distribution of ultramafic complexes in the western Jurassic (W. Jur.), the western Paleozoic and Triassic (WTrPz), central metamorphic (CMB), and eastern Paleozoic (E.Pz) belts is after *Hotz* (1971) as are all regional relations. Metamorphic ages were determined by the potassium-argon method and are keyed to the analyses in Tables 1 and 2. The map symbols are: 1) plutonic intrusive rocks, 2) ultramafic rocks, 3) amphibole gneisses and schistose rocks, 4) undifferentiated low grade-feebly metamorphosed metavolcanic and metasedimentary rocks of the WTrPz, 5) the schists of Condrey Mountain, 6) thrust fault with sawteeth on the upper plate.

separated by folded thrust faults (*Hotz*, 1967). Here, harzburgite-dunite and wehrlite intergradational with clinopyroxenite and lesser gabbro are all part of the ultramafic sequence. Folding of the sequence is frequently recumbent but axial planes have variable dips generally flattening northward into Oregon where the sequence thins. In the thinned part of the sequence, the gently reclined, tectonically and conformably interleaved sequence of ultramafic rocks, amphibolite gneisses and quartz-rich biotite schists rest with discordance above steep dipping metaclastic rocks of lower grade. Representative compositions of the ultramafic and higher grade metamorphic rocks in this mélanged tectono-stratigraphic sequence are given in Table 1 (sample descriptions are given in the Appendix).

In the May Creek Schist belt, the metamorphosed ultramafic rocks are in close association with large amounts of coarse-grained metabasic rocks that we interpret to be gabbro. These metagabbros appear to be conformable with the gross-layered aspect of the ultramafic rocks but both are tectonically interleaved with genetically unrelated gneissic and schistose rocks. Metamorphic grade changes abruptly forming a zonal arrangement that increases with proximity to the large quartz diorite-granodiorite pluton largely central to the metamorphic belt (*Kays*, 1970). Representative compositions of ultramafic and metamorphic rock units are given in Table 1 (see the Appendix for sample descriptions).

The ultramafic bodies of this study are metamorphosed to a variety of serpentine-, talc-, and amphibole-bearing rocks with persistent relict minerals that may, in places, indicate the primary nature of the rocks. Although individual ultramafic bodies have recognizable layers up to several meters thick of dunite, harzburgite, and a variety of pyroxenites, and gabbros, whatever internal stratigraphy may have existed on a regional basis prior to deformation and metamorphism is now largely destroyed. Dunites and harzburgites are recognizable from their relict minerals, and their antigorite-rich and talc-bearing metamorphosed equivalents. Pyroxenites contain varying combinations of talc, amphibole, and chlorite as well as serpentine minerals, but also have relict assemblages. Clinopyroxenites and clinopyroxene-bearing peridotite seem to be especially abundant in some areas. These features form a strong contrast to those of the larger coherent peridotite sheets (e.g., the Josephine peridotite) where possible trapped, early cotectic melting products such as olivine websterite or other clinopyroxene-enriched peridotites are of minor importance in comparison to widespread harzburgite and dunite (*Dick*, 1975). The peridotites of this study are apparently more like those of the central ophiolite zone of the Dinarides in Bosnia, Yugoslavia in which clinopyroxene-rich rocks, gabbros, and amphibolites occur interstratified with ultramafic masses, and the alternating layers of harzburgite-dunite are not so abundant or widespread (*Pamić and others*, 1973).

There are two separate associations of amphibole-rich gneisses with ultramafic rocks in the higher grade metamorphic complexes of this study. In one association, coarsely crystalline, granular to poorly gneissic and foliated amphibolites occur in close association with the ultramafic rocks and may be gradational with those that are pyroxene-rich. The mineralogical and compositional features of these amphibolitic rocks also suggest a close genetic connection with the ultramafic rocks. In other places, usually fine-grained amphibolite gneisses are interlayered with metasedimentary rocks; in this case, the association with ultramafic rocks is tectonic. Mapping is underway in some areas to determine more precisely the proportions of the different rock types in the ultramafic-mafic association.

TABLE 1. Selected analyses from the ultramafic-mafic sequence and associated high grade schists and gneisses

	SiO_2	TiO_2	Al_2O_3	MgO	FeO	Fe_2O_3	CaO	Na_2O	K_2O	P_2O_5	MnO	Ignition Loss	Total
A. Wrangle-Red Mountain Area													
(1) TA-10-74	40.56	0.05	0.31	38.02		11.77*	0.04	0.65	b.d.**	b.d.	0.15	7.32	98.87
(2) KTA-12-75	47.66	0.04	0.86	27.27		9.42*	12.58	0.03	b.d.	b.d.	0.21	1.35	99.41
(3) KTA-7-75	55.54	0.02	2.27	23.71		5.00*	10.72	0.31	0.01	b.d.	0.17	0.87	98.62
(4) OBPKPXT	48.89	0.11	3.50	19.58	8.29	0.92	16.78	0.12	0.03	0.02	0.16	0.39	98.79
(5) KTA-11-75	53.46	0.47	7.85	13.10		8.26*	11.82	1.52	0.51	0.08	0.20	0.84	98.11
(6) KTA-14-71	45.76	0.43	14.12	11.75	8.36	0.93	15.46	0.21	0.17	0.15	0.14	0.99	98.47
(7) RDMTAG	46.82	1.06	20.38	3.27	10.38	1.16	10.66	3.27	0.43	0.12	0.21	0.64	98.40
(8) KTA-3-71	67.74	0.88	12.90	3.34	5.87	0.65	0.49	1.31	4.81	0.05	0.13	2.20	100.37
B. May Creek Schist Belt													
(9) T-113-71	39.25	0.07	1.17	38.25	7.01	0.78	0.24	0.01	0.02	b.d.	0.12	12.8	99.72
(10) T-112-71	50.59	0.36	7.58	16.81	8.08	0.90	11.64	1.40	0.11	0.07	0.19	1.1	98.83
(11) T-115-71	46.88	1.67	15.28	4.55	9.03	1.01	16.52	2.57	0.35	0.38	0.12	0.74	99.10
(12) T-42-68	48.53	0.64	20.43	5.39	6.33	0.71	11.05	3.35	0.69	0.10	0.25	0.79	98.26

* Total iron oxide as Fe_2O_3 ** b.d. = below detection *Note:* Sample descriptions and relations among samples are given in the Appendix.

Compositional relations

The ultramafic-mafic rocks including peridotites, pyroxenites and closely associated, coarse-grained "gabbroic" amphibolites have a trend on the AFM diagram that shows increasing total iron oxide and only moderate alkali enrichment (Fig. 2A). Separation of the rocks of the ultramafic-mafic sequence on an Al_2O_3-CaO-MgO plot is shown in Fig. 2B. Wehrlites-clinopyroxenites show a rather continuous compositional variation with

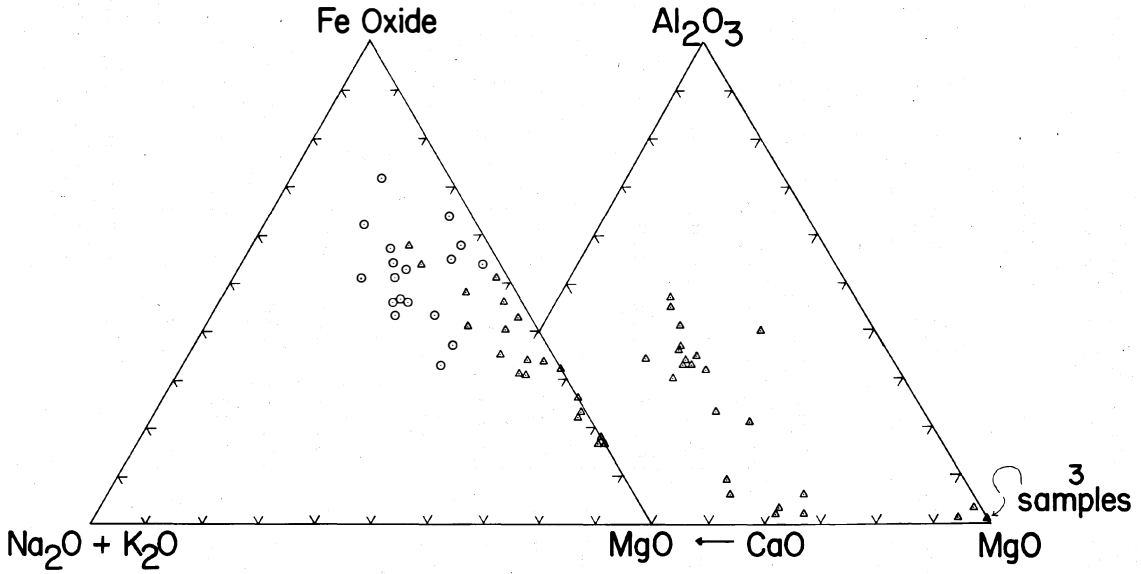

Fig. 2. (A) AFM ($Na_2O + K_2O$- total iron oxide as Fe_2O_3-MgO) and (B) CaO-Al_2O_3-MgO plots of ultramafic and metamorphic rocks from the Wrangle-Red Mountain area and the May Creek Schist belt. In the AFM diagram the triangles are ultramafic rocks and closely associated pyroxenites-gabbros; the circles are other amphibolites of volcanic (and/or sedimentary) origin. In the CaO - Al_2O_3 - MgO plot only the peridotites, pyroxenites, and gabbros are represented.

"gabbroic" gneisses and are well separated from harzburgites-dunites. These rocks cannot be confused with eastern Mediterranean aluminous or plagioclase lherzolites (*Menzies and Allen*, 1974). Although mafic "metavolcanic" amphibolites have greater total iron-oxide and alkali enrichment than members of the ultramafic association, their trend on an AFM diagram is congruent with the sequence of ultramafic-mafic rocks. On the basis of bulk rock compositions there is a clear chemical distinction between the association of amphibolitized pyroxenites and gabbros and the amphibolitized rocks of volcanic affinity (Fig. 3, Table 1). Clearly MgO-deficient and Al_2O_3 + Na_2O + K_2O-enriched, the "metavolcanic" amphibolites are also distinguished from those of the peridotitic association on the basis of CaO and the SI index (Figs. 3 and 4). Some "metavolcanic" amphibolites may also be CaO-rich but these rocks are distinguished by their relatively low SI index. There is a general increase in TiO_2 contents with SI consistent with increased iron oxide throughout the ultramafic-mafic sequence and "metavolcanic" association (Fig. 5).

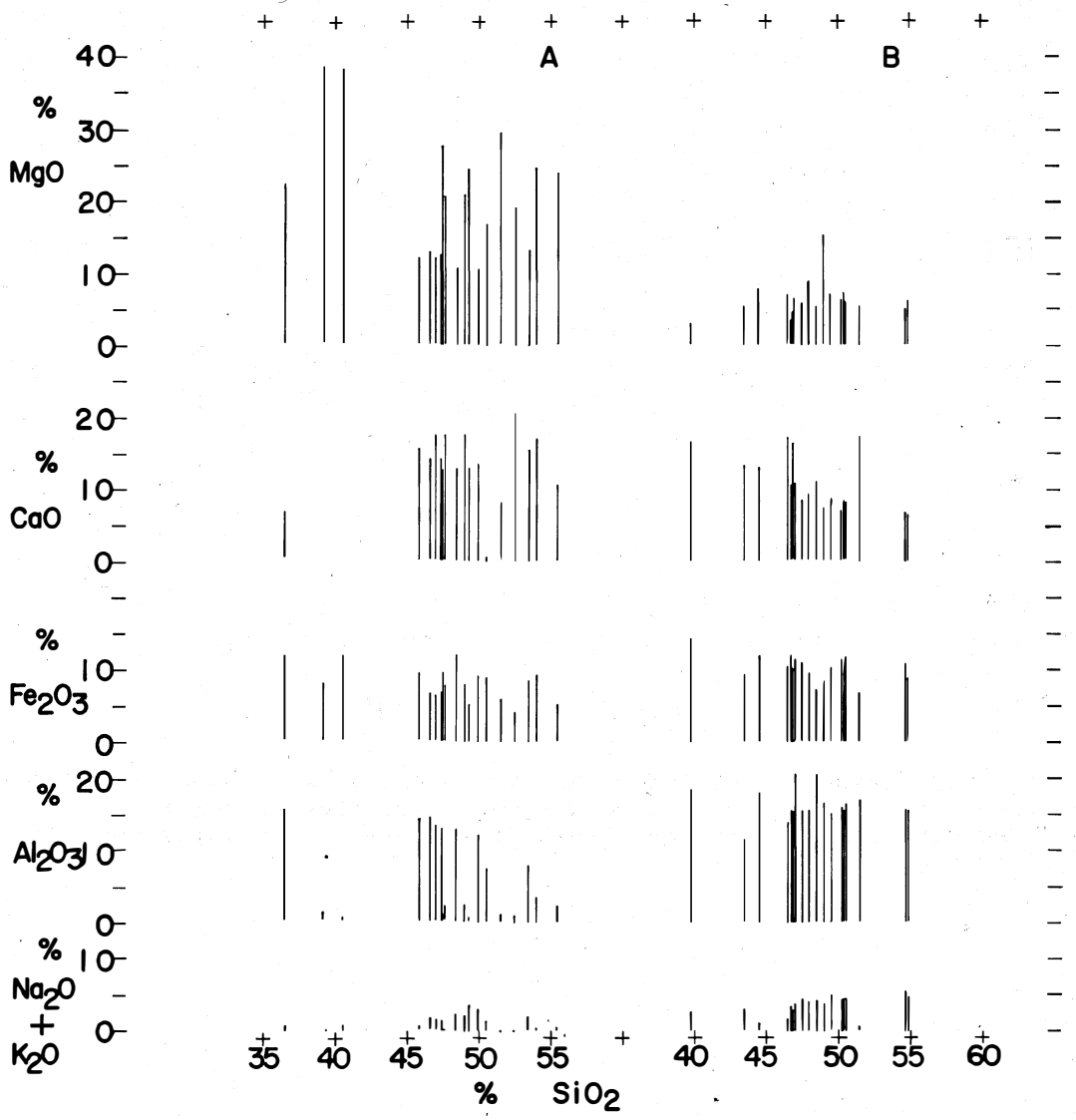

Fig. 3. Bulk rock chemical compositions of A. ultramafic rocks, and amphibolitized pyroxenites-gabbros and B. the amphibolitized rocks of volcanic affinity. All values are given in weight percent of the oxides.

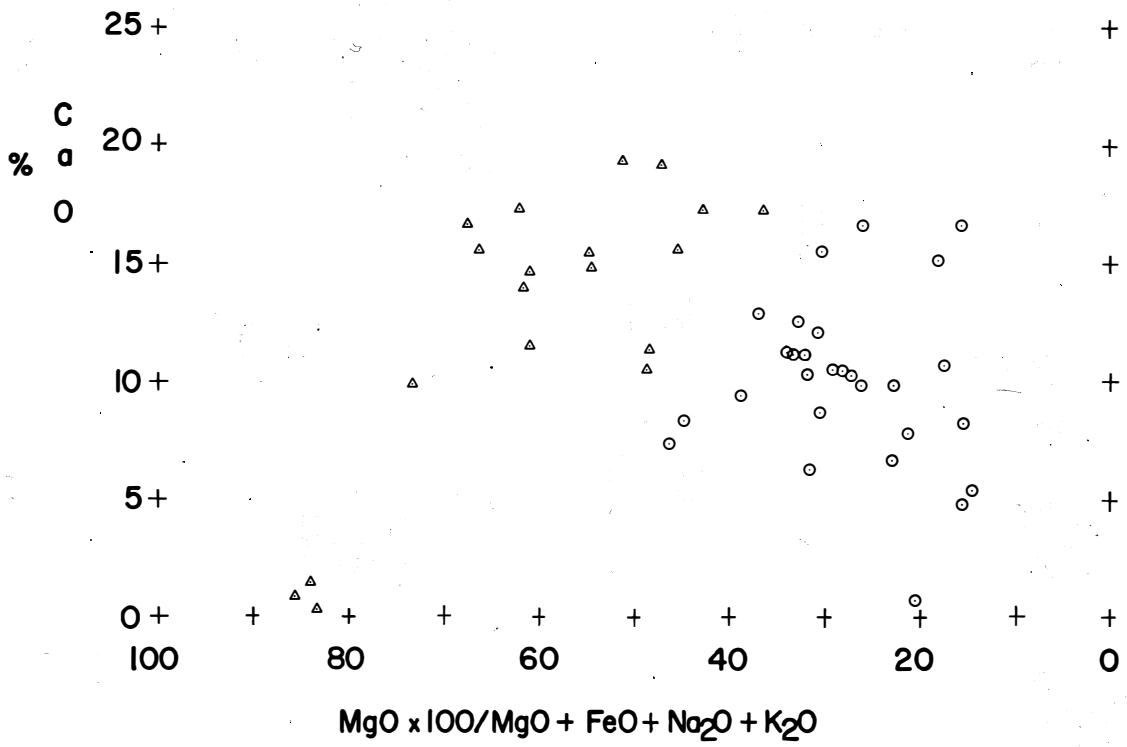

Fig. 4. CaO versus the SI index (MgO/MgO + FeO + CaO + Na_2O + K_2O) for ultramafic-mafic (triangles) and metavolcanic (circles) rocks from the Wrangle-Red Mountain area and May Creek Schist belt. The value for FeO is total iron oxide.

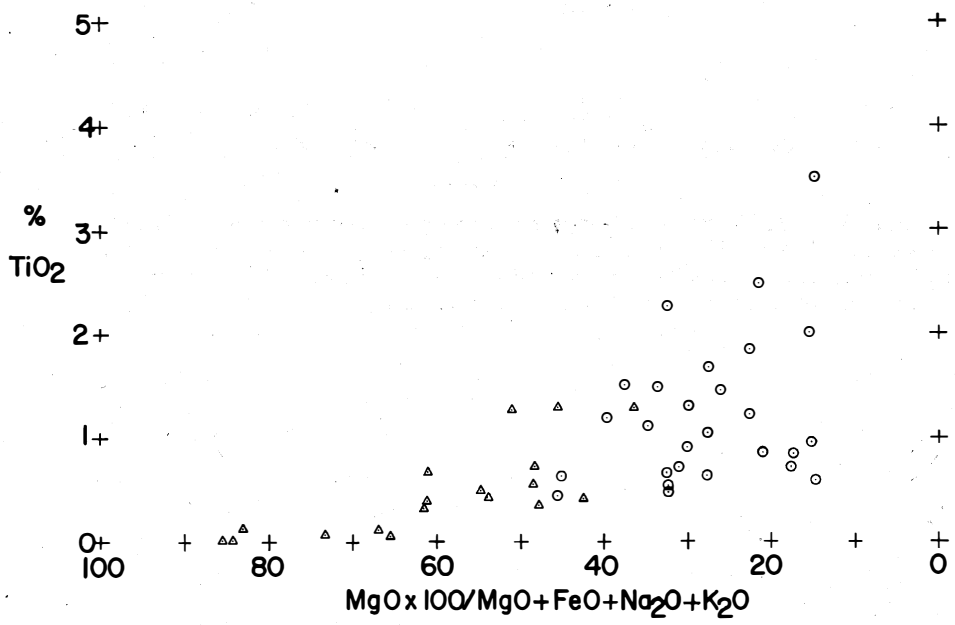

Fig. 5. TiO_2 versus the SI index for the two rock associations as described in Fig. 4.

Although use of "gabbroic" and "metavolcanic" in reference to chemically distinct amphibolites infers genesis, the terms are applied on the basis of occurrence. To our knowledge, none of the "gabbroic" amphibolites occur interstratified with biotite schists whereas the interstratified association of "metavolcanic" amphibolites is always clear. This does not imply that modification of the primary compositions couldn't occur prior to, during or after metamorphic differentiation. However, such modification, if it occurred, must have acted to amplify the primary character. For example, the rocks of the ultramafic association always have high MgO frequently coupled with high CaO (greater than 10 and up to 20 wt. %, respectively) whereas the alkalies are always low (generally less than 1 wt. %). For a comparable range in SiO_2 contents, rocks of the "metavolcanic" association have only moderate MgO contents and in those specimens where CaO contents are high (about 17 wt. %) MgO contents are even lower (less than 8 wt. % generally, and as low as 4 wt. %). Where CaO is high in the ultramafic association, total iron oxide is moderate to low, whereas where CaO is high in the "metavolcanic" association, total iron oxide is moderate to high (Fig. 3). These characteristics, and the appreciably higher alkalies and TiO_2 contents of the "metavolcanic" rocks, we believe reflect the primary character of the two rock associations. Metamorphic differentiation and metasomatic change appear to have only amplified the primary chemical character. Furthermore, the "gabbroic" and "metavolcanic" amphibolites are not small or local segregations and though affected by metamorphic differentiation are of large enough dimensions to be recognizable in their field association.

Metamorphic ages

Older K-Ar ages from hornblendes of isolated blocks and larger bodies of amphibolite gneiss from the Coast Range formations (Franciscan and Otter Point mélanges, Great Valley Sequence and Dothan Formation), and the western Jurassic belt are largely coincident with the amphibolite ages of this study ($\sim$ 150 m.y.) (Tables 2 and 3). The older K-Ar ages from amphiboles of glaucophane schists that occur as isolated tectonic blocks in the Franciscan and Otter Point mélange also have an upward termination of roughly 150 m.y. (*Coleman and Lanphere*, 1971). The remarkable similarity of ages and the widespread distribution of basic metamorphic rocks suggests a thermal event of regional proportions in the Klamath Mountains and Coast Ranges. The fact that the metamorphic rocks occur frequently within mélanged terranes or are in thrust relation with overlying or interlayered peridotite sheets suggests further that the older (150 m.y.) metamorphism developed in close relation to or culminated in thrust faulting of regional scale.

Metamorphic ages were determined by the potassium-argon method using hornblende concentrates from four samples of amphibolite gneiss; two samples are from the Wrangle-Red Mountain area and two from the May Creek Schist belt (Fig. 1). All potassium-argon analytical work was done for us by Henry Dick at Yale University. The sample descriptions, nature of occurrence and determined ages are given in Table 2. Samples KTA-14-71 and T-42-68 are amphibole-rich gneisses marginal to intrusions of "granitic" rocks in the Wrangle-Red Mountain area and the May Creek Schist belt, respectively. Both samples show the effects of thermal overprinting and have relatively young ages in the range 128-130 m.y. The mode of occurrence of the two samples is quite different. Sample KTA-14-71 is interlayered with peridotite and is likely to have been a part of the ultramafic complex prior to metamorphism. Sample T-42-68 is clearly metavolcanic and interlayered with schistose metasedimentary rocks. Away from the influence of the intrusion of "granitic" rocks, concentrates of hornblende from the

TABLE 2. Potassium-argon ages and analytical data

Sample No.	Age M.Y.	Wt. % K	$^{40}Ar\ 10^{-6}$ STP (% Air Correction)	General Location
KTA-14-71	128 ± 8	0.14	83.04(27)	Wrangle-Red Mtn.
RdMtAg	144 ± 3	0.38	56.40(11)	Wrangle-Red Mtn.
T-42-68	130 ± 3	0.66	36.57(09)	May Creek Schist Belt
T-112-70	150 ± 11	0.08	84.90(98)	May Creek Schist Belt
CMSV*	155 ± 3	2.04	13.15(18)	Condrey Mtn.

* Whole rock analysis: from *Suppe and Armstrong* (1972); all other analyses are from hornblende separates, this paper.

Sample Descriptions: KTA-14-71: S.C. SE1/4 NW1/4 Sec. 12, T41S, R2W, Talent quadrangle, Oregon; amphibolite gneiss: tight-folded together with serpentinized peridotite and injected by quartz diorite: brown-green to olive green-brown hornblende is dominant; plagioclase and clinozoisite form thin bands.

RdMtAg: W.C. NE1/4 NE1/4 Sec. 32, T40S, R1W, Talent quadrangle, Oregon; amphibolite gneiss: tight-folded, narrow band in serpentinized peridotite: brown-green hornblende dominant but plagioclase is relatively abundant; clinoziosite is minor.

T-42-68: E.C. Sec. 25, T30S, R3W, Days Creek quadrangle, Oregon; amphibolite gneiss intruded by quartz diorite; hornblende is abundant along with plagioclase; some epidote; plagioclase has poorly developed concentric zoning; interlayered with biotite-garnet schists.

T-112-70: N.C. NE1/4 Sec. 27, T32S, R3W, Days Creek quadrangle, Oregon; amphibolite gneiss with hornblende dominant containing rare pyroxene cores; plagioclase is not as abundant; texture, especially that of hornblende, suggests cumulate growth of pyroxene with intercumulus plagioclase; the rock is interlayered with serpentinized peridotite and is locally crushed and sheared.

CMSV(6): Location given as 122°57'44"W, 41°50'58"N, Condrey Mtn. quadrangle, by *Suppe and Armstrong* (1972): quartz-muscovite-chlorite-albite schist. This sample is from the schists of Condrey Mountain south of the Wrangle-Red Mountain area.

TABLE 3. Correlation of older ages of amphibolites and other basic rocks, and high-grade blueschists from the Klamath Mountains and Coast Ranges.

Calculated Age (M.Y.)	Mineral	Source	Sample Number	Location and Occurrence
151 ± 6	hornblende	(1)	54-65	Big Craggies klippe, resting on Dothan Fm. rocks; Collier Butte quad., Oregon.
148 ± 6	hornblende	(1)	P-1064	Pickett Peak, tectonic block in Franciscan Fm., Pickett Peak quad., California.
149 ± 5	hornblende	(1)	9-70	Crevison Peak, tectonic block in Franciscan Fm., Crevison Peak quad., 7 1/2', California.
144	hornblende	(2)	J82-8	Amphibolite gneiss just north of Madstone Cabin, at northern contact below Josephine peridotite, Chetco Peak quad., Oregon.
148	hornblende	(2)	J87-6	Amphibolite gneiss just west of Chetco Lake, in thrust contact below Josephine peridotite, Chetco Peak quad., Oregon.
150	hornblende	(2)	J89-1	Amphibolite gneiss just north of Vulcan Lake, structurally below the Josephine peridotite, Chetco Peak Quad., Oregon.
153	hornblende	(2)	J57-19	Hornblende diorite in Rogue Fm., west of Josephine Mtn., Cave Junction quad., Oregon.
146	hornblende	(2)	J45B	Dikes, mostly dioritic that intrude the Josephine
146			J37H	peridotite, Cave Junction quad. (J45B, J37H, 541D) and
150			J41D	Chetco Peak (J123-2, J57-6) quad., Oregon.
152			J123-2	
159			J57-6	

TABLE 3. (Continued)

Calculated Age (M.Y.)	Mineral	Source	Sample Number	Location and Occurrence
144 ± 3	hornblende	(3)	RdMtnAg	Narrow dike-like amphibolite gneiss body within the Red Mtn. ultramafic body, Wrangle-Red Mountain area, WTrPz, Talent quad., Oregon.
150 ± 11	hornblende	(3)	T-112-71	Hornblende-rich "gabbroic" gneiss interlayered and folded with peridotite, south of Devils Flat, May Creek Schist belt. WTrPz, Days Creek quad., Oregon.
155 ± 3	Whole rock	(4)	CMSV	Quartz-muscovite-chlorite-albite schist, schist of Condrey Mtn., Condrey Mountain quad., California.
Basic glaucophane schists				
145 ± 8	glaucophane	(1)	94-67	Garnetiferous glaucophane schist, Tupper Rock jetty quarry, Otter Point Fm., Bandon, Bandon quad., Oregon.
150 ± 6	glaucophane	(1)	55-cZ-59	Garnetiferous glaucophane schist, Ward Creek, Franciscan Fm., Cazadero quad., 7 1/2', California.

(1) *Coleman and Lanphere* (1971)

(2) *Dick* (1976), see also *Dick* (1973)

(3) *Kays et al.*, this paper

(4) *Suppe and Armstrong* (1972)

amphibolite gneisses yield ages in the range 143-151 m.y. Sample RdMtAg from the Wrangle-Red Mountain area has texture, composition and mode of occurrence indicative of formation as a near-surface intrusive rock or as a flow subsequently folded with the ultramafic rocks. Sample T-112-70 from the May Creek Schist belt is also folded with peridotite, but has relict cumulate texture and a composition which suggests that it formed as gabbro interlayered with the ultramafic rocks.

Summary and Conclusions

The occurrence of relatively high grade gneisses and schists in close proximity with ultramafic rocks is peculiar in that the association in the Wrangle-Red Mountain area is completely separated by faults from metavolcanic and metaclastic rocks of lower grade. In a structural sense, metamorphism is shown to increase toward thrust planes generally bounded by ultramafic rocks. The change in grade of metamorphism may not be great, but there is always a strong improvement in the metamorphic fabrics and the degree of recrystallization toward the tectonic boundary between the ultramafic and metamorphic rocks. Although the metamorphism is of different character, the allochthonous occurrence may be similar in a structural sense to the "upside-down" association of blueschists and ultramafic rocks in the California Coast Ranges (*Blake, Irwin, and Coleman*, 1967; *Ernst and others*, 1970). A later metamorphism is associated with intrusion of granitic rocks and has produced recognizable thermal zonation (*Kays*, 1970) in the May Creek Schist belt. There is no mélanging evident here, although the WTrPz in this area is in thrust contact with the underlying Jurassic Galice Formation; the metasedimentary-metavolcanic rock units are continuous and traceable.

There is persistent association of ultramafic rocks and high grade "gabbroic" gneisses. Undoubtedly, a strong deformation and metamorphism has had a profound effect on the primary character of these rocks. Our own field and petrographic studies indicate that the ultramafic and metamorphosed rocks of the mélanged association on the California-Oregon border may have had quite a complicated history. *Hotz* (1967, and personal communications) indicates that thrust faults separating ultramafic and metamorphosed rocks of this association are folded; the evidence suggests that the rocks were folded and metamorphosed after mélanging. Thus, all of the rocks of this association could have been modified through metamorphic differentiation. In addition, *Coleman* (1967) has shown that metasomatic change during metamorphism of ultramafic rocks can be appreciable. Nevertheless, for reasons already stated, we believe that most change associated with metamorphic differentiation or metasomatism is recognizable as such, and that it is unlikely that the compositional relations reflect only later modification of the rocks.

Thus, we interpret features such as persistent field association of ultramafic rocks and "gabbroic" gneisses and their interlayered nature locally in the WTrPz, and the occasional relict cumulate textures among pyroxenites and gabbroic rocks to be compatible with differentiation of gabbroic magmas. In this case, differentiation resulted in iron-enrichment with only moderate alkali gain. The ultramafic-"gabbroic" rock association showing iron-enrichment and increasing TiO_2 with FeO/MgO seems clearly indicative of magmas of tholeiitic affinity (*Miyashiro and others*, 1970). These rocks are, therefore, compatible with liquids derived from partial melting of the upper mantle that ultimately leave behind "depleted" bodies of predominantly harzburgite-dunite, such as the Josephine peridotite complex (*Dick*, 1976). We suggest that the compositionally intergradational suite of gabbros, clinopyroxenites, and wehrlites represent parts of the

constructional pile of an ophiolite sequence. However, it is not clear, and perhaps impossible to judge on the basis of these data, whether the environment for differentiation was ocean floor or island arc setting. On the other hand, the field associations, low to moderate pressure metamorphic facies, and the abundance of granite series plutonic rocks make a rising island arc basement setting an attractive possibility. Some of the "metavolcanic" amphibolites have compositions which are consistent with liquids formed late from the same magma stem that produced the association of ultramafic and gabbroic rocks. No direct field evidence has been found to indicate that the "metavolcanic" amphibolites are related to the ultramafic rock and "gabbroic" gneiss sequence. However, a similar association of ultramafic-mafic and volcanic rocks has been recognized in other complexes, e.g., Troodos (*Bear*, 1969; *Gass and Masson-Smith*, 1963), Bay of Islands (*Williams*, 1973; *Williams, Malpas, and Comeau*, 1972), Canyon Mountain (*Brown and Thayer*, 1966; *Thayer and Himmelberg*, 1968). The widespread and close association of fragmented "metavolcanic" amphibolites and peridotites here as well as in the Coast Ranges, the western Jurassic belt, and beneath the Trinity ultramafic sheet suggests that their occurrence together is not fortuitous.

Acknowledgements

We would like to thank John M. Sinton and Robert G. Coleman for critical review of the manuscript. Discussions of the geology of the Klamath Mountains with Preston Hotz have been most helpful, as have conversations with Gordon Medaris on the petrology of ultramafic rocks. All whole rock compositions were determined by an XRF method by the authors at the University of Oregon; we acknowledge with thanks the help of Gary Cunningham in doing this work.

Appendix

Notes on Stratigraphic Relations

Wrangle-Red Mountain Area

Samples 1-6 occur as bands within larger complexes of ultramafic rocks. In general the ultramafic complexes occur as folded, sheet-like bodies above samples 7-8; the basal parts of the ultramafic-mafic complexes are highly sheared and the immediately underlying rocks have tight recumbent folds. "Gabbroic" amphibolites are not so abundant but clinopryxoene-rich ultramafic rocks are widespread. Biotite schists dominate in the interlayered sequence over amphibolite gneisses.

May Creek Schist Belt

Samples 9-10 are interlayered and folded together in an ultramafic-mafic complex that rests above sample 11; sample 12 is intruded by quartz diorite and interlayered with pelitic schistose rocks. Amphibolite gneisses may have coarse-grained, poorly banded and perhaps relict, gabbroic texture and occur immediately adjacent to ultramafic rocks, and in places may be interlayered with them. Amphibolite gneisses interlayered with biotite schists have a mapped distribution that is of greater areal extent than "gabbroic" amphibolites; however, in the latter case the mapped distribution is as much as one-half that of associated ultramafic bodies.

General

Samples 7-8, 11-12 are parts of the interlayered metasedimentary-metavolcanic sequence beneath ultramafic sheets in the WTrPz.

Sample Descriptions

(1) Highly serpentinized, amphibole-bearing peridotite.

(2) Olivine-bearing clinopyroxenite or wehrlite.

(3) Tremolite schist interlayered and folded with amphibolite; contains relict clinopyroxene, orthopyroxene, and olivine.

(4) Clinopyroxenite with exsolved patches and lamellae of orthopyroxene in clinopyroxene. Minor amphibole.

(5) Amphibolitized clinopyroxene-olivine-bearing metagabbro in peridotite. Amphibole is twinned grunerite-cumingtonite.

(6) Tight-folded amphibolite gneiss containing clinozoisite-chlorite interlayered with serpentinized peridotite.

(7) Fine-grained, tight-folded hornblende-rich amphibolite gneiss with plagioclase and epidote.

(8) Tight-folded, fine-grained quartz-rich, garnetiferous mica schist.

(9) Serpentinized talc-amphibole-bearing peridotite with relict olivine and orthopyroxene.

(10) Amphibole-rich metagabbro with relict clinopyroxene and plagioclase; has possible relict cumulate fabric.

(11) Feldspathic-epidote amphibolite with CO_3 and pyroxene; interlayered with pelite.

(12) Feldspathic amphibolite gneiss with concentrically zoned plagioclase. Interlayered with pelitic schist.

References

Bear, L.M., The evolution and petrogenesis of the Troodos Complex, Cyprus, *Geol. Survey Dept. Ann. Rept. 1965*, 26-37, 1966.

Blake, M.C., Jr., W.P. Irwin, and R.G. Coleman, Upside-down metamorphic zonation, blueschist facies, along a regional thrust in California and Oregon, *U.S. Geol. Survey Prof. Paper 575-C*, 1-19, 1967.

Brown, C.E., and T.P. Thayer, Geologic map of the Canyon City Quadrangle, northeastern Oregon, *U.S. Geol. Survey Mineral Inv. Field Studies Map 1-447*, 1966.

Coleman, R.G., The Colebrook Schist of southwestern Oregon and its relation to the tectonic evolution of the region, *U.S. Geol. Survey Bull. 1339*, 61 p., 1972.

Coleman, R.G., Low-temperature reaction zones and alpine ultramafic rocks of California, Oregon, and Washington, *U.S. Geol. Survey Bull. 1247*, 49 p., 1967.

Coleman, R.G., and M.A. Lanphere, Distribution of high-grade blueschists, associated eclogites, and amphibolites from Oregon and California, *Geol. Soc. America Bull., 82*, 2397-2412, 1971.

Davis, G.A., M.J. Holdaway, P.W. Lipman, and W.D. Romey, Structure, metamorphism, and plutonism in the south-central Klamath Mountains, California, *Geol. Soc. America Bull., 76*, 933-976, 1965.

Davis, G.A., and P.W. Lipman, Revised structural sequence of pre-Cretaceous metamorphic rocks in the southern Klamath Mountains, California, *Geol. Soc. America Bull., 73*, 1547-1552, 1962.

Dick, H.J.B., Notes for field trip to the Josephine Peridotite sheet, Chapman Conference: Partial melting in the Earth's upper mantle, *Guidebook, Amer. Geophys. Union*, 39-55, 1976.

Dick, H.J.B., The Josephine peridotite, a refractory residue of the generation of andesite, *Trans. Amer. Geophys. Union, 56*, 464, 1975.

Dick, H.J.B., K-Ar dating of intrusive rocks in the Josephine peridotite and Rogue Formation west of Cave Junction, southwestern Oregon, *in Abstracts of Cordilleran section of Geol. Soc. America Mtgs., 5*, 33-34, 1973.

Ernst, W.G., Y. Seki, A. Onuki, and M.C. Gilbert, Comparative study of low-grade metamorphism in the California Coast Ranges and the outer metamorphic belt of Japan, *Geol. Soc. America Mem. 124*, 276 p., 1970.

Gass, I.G., and D. Masson-Smith, The geology and gravity anomalies of the Troodos Massif, Cyprus, *Philos. Trans. Royal Soc. London, Series A, 255*, p. 417-467, 1963.

Hotz, P.E., Blueschist metamorphism in the Yreka-Fort Jones area, Klamath Mountains, California, *Jour. Research, U.S. Survey*, 53-61, 1973.

Hotz, P.E., Geology of lode gold districts in the Klamath Mountains, California and Oregon, *U.S. Geol. Survey Bull. 1290*, 91 p., 1971.

Kays, M.A., Mesozoic metamorphism, May Creek Schist belt, Klamath Mountains, Oregon, *Geol. Soc. America Bull., 81*, 2743-2758, 1970.

Miyashiro, A., Evolution of metamorphic belts, *Jour. Petrology, 2*, 277-311, 1961.

Miyashiro, A., F. Shido, and M. Ewing, Crystallization and differentiation in abyssal tholeiites and gabbros from mid-oceanic ridges, *Earth Sci. and Planet. Letters, 7*, 361-365, 1970.

Pamić, J., S. Sćavnicar, and S. Medjimorec, Mineral assemblages of amphibolites associated with alpine-type ultramafics in the Dinaride ophiolite zone (Yugoslavia), *Jour. Pet., 14*, Part 1, 133-157, 1973.

Menzies, M., and C. Allen, Plagioclase lherzolite-residual mantle relationships within two Eastern Mediterranean ophiolites, *Contr. Mineral. and Petrol., 45*, 197-213, 1974.

Ramp, L., Geology and mineral resources of the Upper Chetco drainage area, Oregon, *State of Oregon Dept. of Geol. and Min. Industries Bull. 88*, 47 p., 1975.

Suppe, J., and R.L. Armstrong, Potassium-argon dating of Franciscan metamorphic rocks, *American Jour. Sci., 272*, 217-233, 1972.

Thayer, T.P., and G.R. Himmelberg, Rock succession in the alpine-type mafic complex at Canyon Mountain, Oregon, *XXIII International Geol. Cong., 1*, 175-186, 1968.

Williams, H., Bay of Islands map-area, Newfoundland, *Canada Geol. Surv. Pap. 72-34 (map)*, 1973.

Williams, H., J. Malpas, and R. Comeau, Bay of Islands map-area, New Foundland, *Canada Geol. Surv. Pap. 72-1*, part A, 14-17, 1972.

FORMATION OF SMALL DUNITE BODIES BY METASOMATIC TRANSFORMATION OF HARZBURGITE IN THE CANYON MOUNTAIN OPHIOLITE, NORTHEAST OREGON

Michael A. Dungan
Geology Branch
NASA Johnson Space Center
Houston, Texas 77058

Hans G. Avé Lallemant
Department of Geology
Rice University
Houston, Texas 77001

Abstract

Canyon Mountain tectonic peridotites are crosscut by late-stage tabular dunite bodies that postdate the peridotite foliation. The dunites resemble veins or dikes (1-50 cm in width) and typically occur as anastomosing swarms cutting the foliation at all angles. Despite this discordance, the dunite and harzburgite share identical fabrics characteristic of syntectonic recrystallization. Spinel foliation does not deviate upon passing from the host peridotites through the dunite. These structural relationships indicate an origin for the dunites by *in situ* transformation of the peridotite.

One occurrence of dunite in harzburgite has been studied petrographically and with the microprobe. Near the margins of the dunite, amphibole has partially replaced orthopyroxene and clinopyroxene in the harzburgite along grain boundaries and as microveinlets. Chromian spinels within the dunite are rimmed by alteration assemblages of ferrian chromite + Cr-chlorite or, less commonly, magnetite + FeNi-metal. With the exception of minor alteration within 1 cm of the contact with dunite, the ferrian chromite+chlorite assemblage is absent from the harzburgite.

Dunite-formation is inferred to be the result of a metasomatic reaction produced by aqueous vapor percolating along a system of brittle fractures at subsolidus temperatures. The new-formed olivine grew by incongruent breakdown of unstable pyroxene which resulted in the solution and transport of Si and Ca. Olivine increased in size at the expense of pyroxene by secondary grain growth, thus preserving the original fabric.

Introduction

Dunite is one of the rock types that occurs in most alpine-type peridotites and in the ultramafic zones of ophiolite complexes. At least five hypotheses have been proposed to explain the origin of dunite: (1) Igneous dunites occurring in the basal cumulates of ophiolite complexes may form by gravitational settling of olivine from mafic magmas (*Jackson and others*, 1975). (2) Within the tectonite peridotite portion of ophiolites, dunite layers, oriented parallel to the tectonic foliation, are generally

explained as the result of metamorphic or tectonic differentiation (*Himmelberg and Loney*, 1973). (3) Tabular bodies of dunite which transect the country rock peridotite foliation in the Burro Mountain, Vulcan Peak and New Caledonia peridotites have been interpreted as igneous intrusions (*Page*, 1967; *Loney, Himmelberg and Coleman*, 1971; *Himmelberg and Loney*, 1973; *Guillon*, 1975). (4) On the basis of phase equilibria constraints *O'Hara* (1968) has suggested that dunite bodies might form as cumulates from primitive basaltic melts formed by *in situ* melting of host peridotites. *Boudier* (1972) and *Dick* (1976) have argued that some dunites in peridotites are residues of extreme ($\gtrsim$ 60%) localized partial melting. (5) *Bowen and Tuttle* (1949) proposed that dunite bodies might form by metasomatism: specifically, they suggested that an aqueous vapor phase percolating through fractures in peridotites might be capable of removing Ca and Si, thereby transforming an olivine and pyroxene assemblage to 100% olivine.

There is considerable interest in the harburgite-dunite portions of ophiolite and alpine peridotite complexes as representatives of the refractory residues of the partial melting episode that formed the associated plutonic and volcanic rocks (*Carswell*, 1968; *Dickey*, 1970; *Boudier and Nicolas*, 1972; *Menzies and Allen*, 1974; *Menzies*, 1973; *Dick*, 1977). Hypotheses 1 and 2 produce dunite that defines mineralogical layers in peridotite, whereas dunites formed by mechanisms described in 3, 4 and 5 could result in crosscutting bodies. The purpose of the present study is to examine alternate hypotheses 3, 4 and 5 for the origin of tabular dunite bodies, as they apply specifically to occurrences in the Canyon Mountain ophiolite, Oregon. *Avé Lallemant* (1976) has studied numerous occurrences of dunite bodies in the course of field work in the Canyon Mountain Complex and we have chosen one well-developed example (53B) for a detailed petrofabric, modal and structural analysis by H.G.A.L. in conjunction with petrologic and microprobe studies by M.A.D.

Regional Setting and General Geology of Canyon Mountain Complex

The Canyon Mountain Complex in east central Oregon is one of the few well preserved ophiolites of western North America (*Thayer*, 1956, 1963a, b, 1974; *Thayer and Himmelberg*, 1968; *Avé Lallemant*, 1976). The age of formation of the ophiolite is inferred to be Permo-Triassic. It contains, in ascending sequence, a basal zone of tectonite peridotites overlain by an ultramafic-mafic complex consisting of minor peridotite, pyroxenite, gabbro and volcanic rocks.

The peridotite zone consists primarily of tectonite harzburgite and minor amounts of lherzolite and dunite. Pyroxenite veins and dikes are abundant, whereas gabbro and gabbro-pegmatite dikes are rare. Well developed tectonic foliations and lineations are present in all peridotites and dunites, and in some of the overlying pyroxenites, gabbros and pegmatites. Isoclinal folds defined by mineral layering have foliations parallel to their axial planes and lineations parallel to their fold axes. Macroscopically the foliations and lineations are expressed by flattened and elongate xenomorphic grains of spinel and pyroxene. Rare layers and rods of peridotite strongly enriched in spinel and pyroxene occur parallel to the foliation and lineation respectively (*Avé Lallemant*, 1976).

Dunite has four modes of occurrence.

1. Within the transition zone between the peridotite zone and ultramafic-mafic complex.

The dunite occurs as bands in the basal portions of layered dunite-peridotite-pyroxenite-gabbro sequences. Although these dunites may have been formed by cumulus processes, some now have tectonite fabrics.

2. Thin layers oriented parallel to the foliation of the tectonite peridotite.

These are characteristic of the harzburgite throughout the peridotite and may have formed by the process described in hypothesis 2.

3. Large irregular masses.

These enigmatic bodies are found in many alpine peridotites. The association of layered chromite segregations with these units suggests that in some instances they may be related to magmatic processes (*Thayer*, 1970; *Dickey*, 1975; *Dick*, 1977).

4. Small crosscutting tabular bodies within the tectonite harzburgite zone.

This paper is concerned with the origin of this fourth mode of occurrence.

Structural Relations of the Crosscutting Dunite Bodies

The tectonite peridotite of the Canyon Mountain Complex is crosscut by many irregular and branching tabular dunite bodies (Fig. 1). Although these bodies resemble dikes and veins, these terms are not used here in order to avoid the genetic implications. The dunite weathers to a light, dun-colored smooth surface in low relief relative to the darker peridotite, which has an irregular surface expression due to differential weathering of pyroxene and olivine. Spinel, which defines the foliation in outcrop, weathers in high relief relative to the associated silicate phases in both peridotite and dunite. Weathered surfaces on spinel in the peridotite are dull black whereas those in the dunite exhibit a metallic luster.

Contacts between dunite and peridotite are generally sharp but may be gradational over the distance of a few centimeters. Gradational contacts are irregular in detail and characterized by pyroxene-rich layers that continue into the dunite. Fig. 2 is an example of a typical irregular contact showing embayments of dunite in the peridotite host. The crosscutting dunite bodies intersect the foliation at all angles. Thus, the linear trains of spinel present in the harzburgite cut the dunite-peridotite contacts at various angles. In general the spinel foliation crosses the dunite bodies without deviating in orientation. Two subgroups of dunite are recognized. The first typically consists of conjugate sets of tabular dunite bodies that intersect the tectonite foliation at small angles (e.g., Fig. 1a). The second (Fig. 1b) generally occurs as irregular branching clusters of dunite bodies or narrow (1-5 cm) straight dunite veinlets.

The preferred orientations of olivine in the peridotite and in an adjacent dunite body are indistinguishable (Fig. 3). In both rocks strong Z = [100] - olivine maxima occur parallel to the lineation; X = [010] - and Y = [001] - olivine form girdles around the lineation. These fabrics have orthorhombic symmetry and are homotactic (*Avé Lallemant*, 1976).

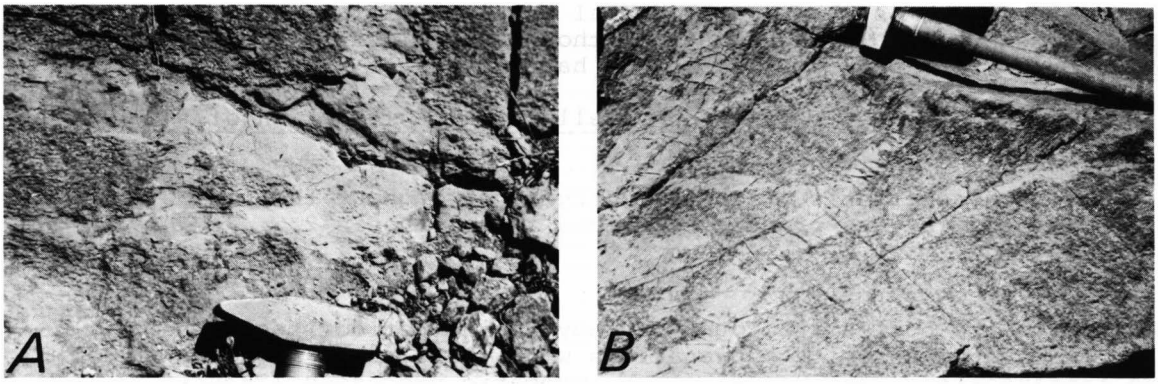

Fig. 1. Photographs of field relations of tabular dunite bodies. Dunites are characterized by smooth-weathering light colored surface in contrast to harzburgite which has a rough surface expression due to differential weathering of olivine and pyroxene. (1A) Sample 53B was taken from this outcrop. Note triangular-shaped remnant of harzburgite within dunite. Foliation (roughly horizontal in this photo) in the country rock harzburgite and the isolated remnant are identical in orientation. (1B) An example of the narrow, anastomosing morphology of a swarm of interconnected dunite bodies. Foliation trends from lower left to upper right.

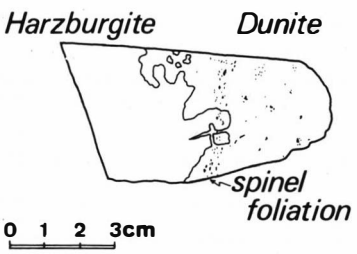

Fig. 2. Sketch of sample 53B which shows the slightly irregular contact between harzburgite and dunite. The thin section used for microprobe analysis was taken from the center of this specimen. Distribution of spinels within dunite is shown. Spinels within harzburgite are not portrayed due to the difficulty of observing them in the different lithology.

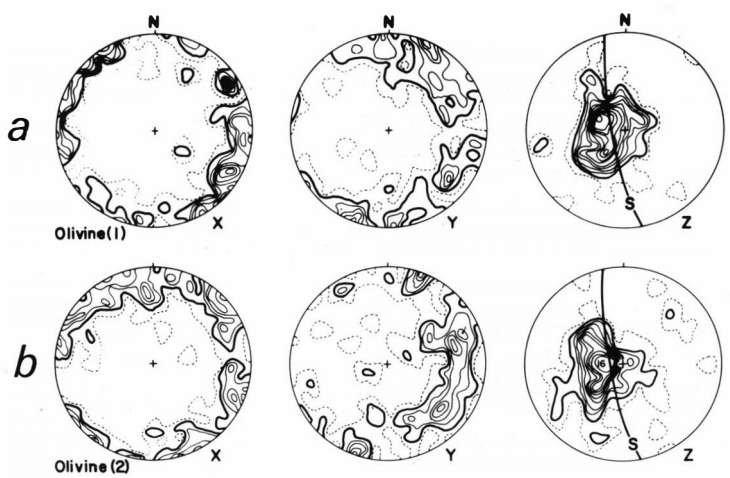

Fig. 3. Fabric relations in 53B. a - harzburgite, b - dunite. Data on 100 olivine grains were taken from dunite 53B and adjacent harzburgite and plotted on an equal-area net, lower hemisphere; contours are at intervals of 1 percent per 1 percent area; 1 percent contour is dashed line; 2 percent contour is heavy line. Where contour lines could not be drawn, the maximum percentage is indicated.

Structural Interpretation

The orthorhombic symmetry of the olivine fabrics of the peridotite and dunite and their associated structures was probably formed by flattening rather than by simple shear deformation inasmuch as the latter generally results in a monoclinic fabric. Laboratory experiments in which syntectonic recrystallization of olivine has occurred (*Avé Lallemant*, 1975) yield fabrics similar to those shown in Fig. 3. Thus, it is probable that the mechanism that produced the preferred orientation in the Canyon Mountain ultramafic rocks was also syntectonic recrystallization. The olivine fabrics in the dunite and peridotite are virtually indistinguishable, seemingly indicating that their preferred mineral orientations formed simultaneously. However, the dunite bodies show little evidence of having been folded. In fact, to the contrary, they are randomly oriented, irregular in morphology, and clearly post-tectonic in that individual tabular bodies intersect the spinel foliation at various angles. At several localities, small dunite bodies cut layering in deformed pyroxene-rich cumulates that occur within tectonite harzburgites. These structural relationships are incompatible with dunite formation prior to syntectonic recrystallization because dunite and peridotite have different mechanical properties, and the dunite bodies would be tightly folded had they been in existence at the time the foliation and preferred mineral orientations developed. We suggest, therefore, that the dunites formed *in situ*, by metasomatic transformation of the parent peridotite. Percolation of the inferred fluid phase along a system of brittle fractures is suggested by the irregular branching pattern of the dunites, their narrow linear morphology, and their relatively sharp boundaries. The larger grain size of the olivines in the dunite can be explained as secondary grain growth during the transformation, preserving the fabric relationships and the orientation of the spinel foliation. Petrologic evidence supporting this hypothesis is presented below.

Petrography and Mineral Chemistry

Petrography of the Primary Assemblages

The peridotite (53B) studied here in detail is a harzburgite according to the classification of *Thayer and Jackson* (1972). The primary constituents are olivine (77%), enstatite (15%), calcic augite (8%), and Cr-spinel (< 1%). The rock exhibits a pronounced foliation and lineation in both outcrop and thin section defined by a general parallelism of the longest dimension of the mineral grains. The average grain size of olivine is 2 mm. The pyroxene has generally similar dimensions but some grains are as long as 1 cm. Spinels are variable in size but are generally less than 0.5 mm in diameter. The dunite consists of olivine plus minor spinel (< 1%) and a trace of small grains of clinopyroxene. The dunite displays the same structures as the harzburgite but the olivine in the dunite is considerably more coarse-grained (5 mm) than in the harzburgite.

Spinel grains within both harzburgite and dunite are characterized by similar morphologies. They range from roughly equant anhedral grains to highly irregular branching shapes. Most grains are slightly elongate parallel to the foliation. Olivine in the dunite tends to be xenomorphic granular giving rise to straight grain boundaries and 120° triple point intersections. Textural relations among silicates in the harzburgite are

contrasting in that the pyroxenes are highly irregular in shape. Grain boundaries are embayed or even cuspate. Clinopyroxene and orthopyroxene tend to be spatially associated. Spinel is generally in contact only with olivine but some grains are partly enclosed by both orthopyroxene and olivine.

Alteration of Primary Minerals

Two stages of alteration of the primary mineral assemblages are recognized. The more recent is post-emplacement serpentinization which has resulted in lizardite-chrysotile pseudomorphs after olivine and orthopyroxene. The sample studied in detail is approximately 50% serpentinized; a feature which tends to obscure many details of primary and secondary textural relationships. The earlier stage of alteration is represented by two hydration reactions which may be related to dunite formation. These reactions are (1) the alteration of primary chromian spinel within the dunites and (2) replacement of pyroxenes in the adjacent harzburgite by calcic amphibole. These two hydration reactions are discussed separately below.

Alteration of Primary Chromian Spinel

Primary disseminated chromian spinel grains in the dunite are in part rimmed by Fe-rich, Al-poor ferrian chromite (Fig. 4) or an intergrowth of Cr-magnetite and FeNi-metal. Iron-nickel sulfide is also associated with the magnetite-metal assemblage although it was not observed in all cases. In the harzburgite near the contact with the dunite, these alteration parageneses are sporadically present in small amounts but in general the spinels within the country rock harzburgite are not altered (Fig. 4a). This relationship is obvious in outcrop as a result of the metallic luster imparted to altered spinel grains in the dunites. Where a substantial portion of an individual spinel grain has been replaced by ferrian-chromite, a rim of chromian-chlorite also surrounds the grain (Fig. 4c,d).

Veinlets of serpentine which crosscut broken spinel grains also cut the alteration overgrowths suggesting that the latter are pre-serpentinization features. The association of ferrian chromite with the assemblage magnetite + NiFe native metal has not been completely resolved in genetic terms. However, the lower oxygen fugacity implied by the magnetite + native metal assemblage may be the result of local equilibration with associated sulfide (*Eckstrand*, 1975). Alternatively, these phases may represent the further alteration of ferrian chromite during later serpentinization. Alteration of primary spinel grains in the dunite may have occurred most readily where they were in contact with pyroxene whereas spinels which were included in the stable olivine were less affected. This is corroborated by the work of *Evans and Frost* (1975) and *Onyeagocha* (1974) who found that the formation of ferrian chromite and chlorite is an enstatite-consuming reaction.

Alteration of Pyroxenes in the Harzburgite

Pale green anhedral amphibole occurs as small (0.1-0.5 mm) grains in harzburgite adjacent to the dunite bodies. Amphibole is also relatively well developed around the ragged, partially resorbed pyroxenes that occur at the harzburgite-dunite contacts although it never exceeds one percent

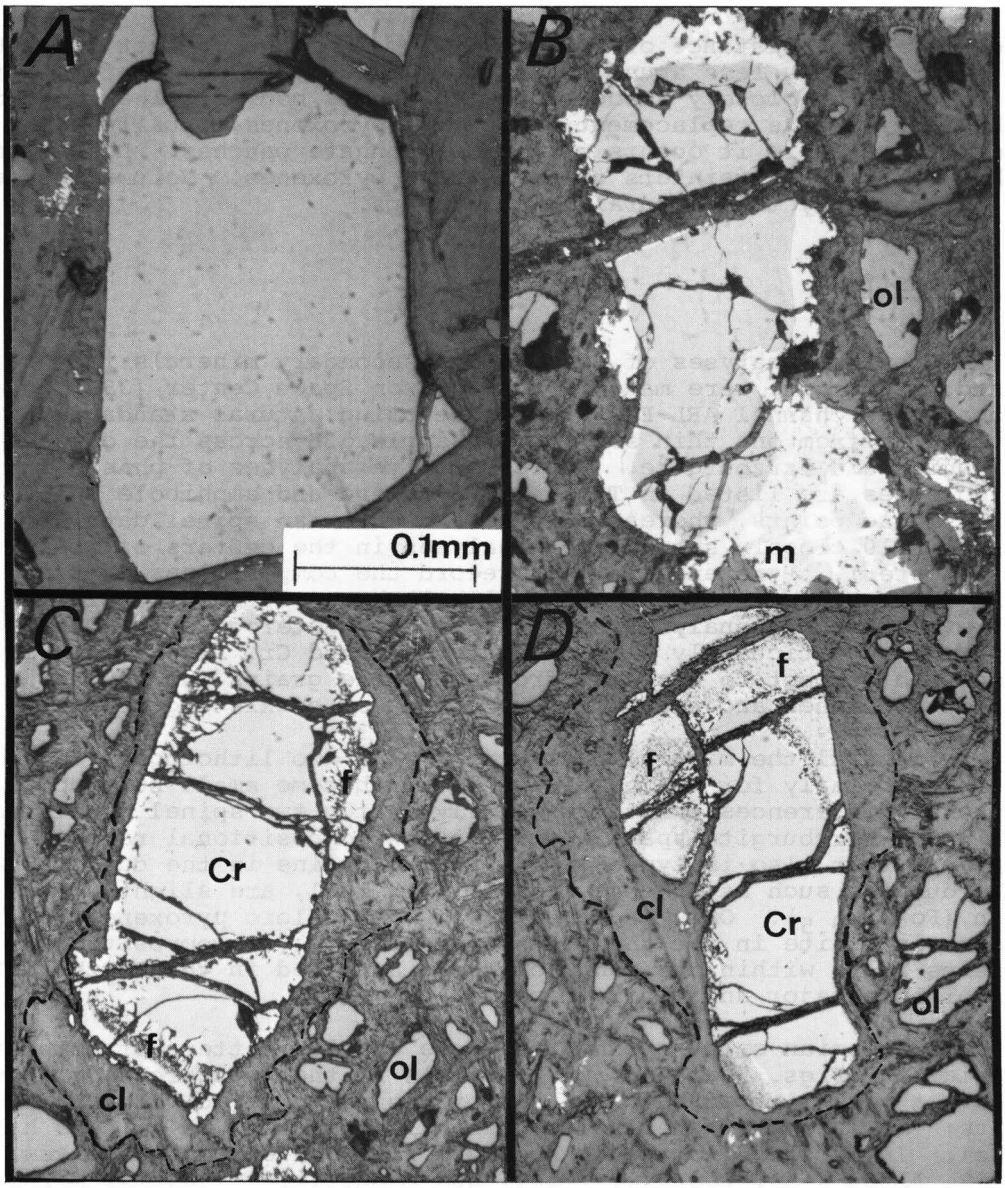

Fig. 4. Reflected light photomicrographs of spinels from harzburgite and dunite in sample 53B. (A) Typical unaltered spinel of harzburgite lacks ferrian chromite rim. (B) Altered spinel from dunite showing one of two alteration parageneses. The rim of high reflectance (m) around the unaltered core consists of an irregular intergrowth of magnetite and more highly reflectant FeNi-metal. (C,D) Spinels (Cr) with rims of ferrian chromite (f) surrounded by chlorite (cl). Note that the width of the chlorite halo is approximately proportional to ferrian chromite rim. All chromite grains in 53B are fractured as the result of late serpentinization. The serpentine filled fractures generally cut both unaltered cores and alteration rims without producing a substantial alteration zone.

in abundance. At a distance of 0.5 and 3.0 cm from the contact, amphibole becomes progressively less abundant and it generally is absent from harzburgite that is not closely associated with dunite bodies. The amphibole invariably occurs as a replacement product of pyroxenes, usually along grain boundaries where it occurs as narrow elongate patches. Less commonly it is observed in microveinlets cross-cutting pyroxenes. Volume changes are not indicated by the textural relationships.

Mineral Chemistry

Microprobe analyses of primary and secondary minerals in the dunite and harzburgite were made in the Johnson Space Center (JSC) laboratory on a three channel ARL-EMX microprobe using natural standards. The data were taken from one thin section of sample 53B across the contact between dunite and harzburgite. Representative analyses of phases from both lithologies are listed in Table 1. Pyroxene and amphibole analyses represent single points, whereas olivine and chromian spinel data are averages of 5-10 closely spaced spot analyses in the centers of grains (100 μm diameter). Pyroxene analyses record the compositions of rims which, in contrast to the cores, generally lack exsolution lamellae. However, even the host analyses demonstrate some heterogeneity within and between grains, particularly with respect to Al and Cr. No systematic variation with respect to distance from amphibole grains was found. Analyses of pyroxenes and amphiboles were made on coexisting grains.

In general the mineral chemistry of the two lithologies is quite similar (particularly for the olivines) although some small but important compositional differences exist, especially in the two spinel populations. Olivine in the harzburgite spans a very narrow compositional range ($Fo_{89.4-89.6}$) that also is typical of analyzed grains in the dunite. Some grains in dunite, such as the one listed in Table 1, are slightly more magnesian ($Fo_{90-90.5}$). Only two small grains of calcic pyroxene (150 μm) are present in dunite in the thin section studied. The composition of these grains falls within the range of those analyzed in the harzburgite in terms of both major and minor elements.

The chromian spinels exhibit a more complex pattern of compositional variation (Figs. 5 and 6). The spinels in the harzburgite are unzoned and have a very limited compositional range as compared with spinels in the dunite; they are characterized by slightly lower Cr/(Cr+Al) and higher Mg/(Mg+Fe). In addition to the conspicuous rims of ferrian chromite[1] (MgO < 10%, Al_2O_3 < 5%, FeO_{total} > 50%) and magnetitite + native metal, spinels in the dunite exhibit cryptic compositional zoning which is characterized by an increase in Fe, Fe^{+3}/Fe^{+2}, Ti and Cr from core to rim. Near the rims the chemical zoning becomes very irregular, making accurate analysis difficult. The composition of one spinel rim from a grain which lacks optical zoning is plotted on Figs. 5 and 6.

Ten amphibole grains from four areas in section 53B were analyzed by electron microprobe. A representative analysis is included in Table 1. These amphiboles are intermediate members of the solid solution series between tremolite and pargasite. The Fe/(Fe+Mg) of the analyzed grains ranges from 0.08 to 0.11 and (Al+Na)/4 ranges from 0.60 to 0.65 (see *Ernst*, 1968; Fig. 10). The concentrations of chromium (1.1-1.7 wt. % Cr_2O_3),

---

[1] Quantitative analyses of ferrian chromite are not reported due to their extreme inhomogeneity, poor polish and an unidentified silicate phase which was sporadically present.

TABLE 1

	Hz OPX	Hz CPX	Dun. CPX	Hz Amph.	Hz Oliv.	Hz Spin.	Dun. Oliv.	Dun. Spin.
SiO_2	55.3	52.9	53.1	47.8	40.4	n.d.	40.9	n.d.
TiO_2	0.05	0.23	0.32	0.57	n.d.	0.15	n.d.	0.30
Al_2O_3	2.9	3.3	2.1	11.5	n.d.	36.17	n.d.	33.62
Cr_2O_3	0.52	1.03	0.61	1.4	n.d.	29.91	n.d.	30.70
Fe_2O_3	n.d.	n.d.	n.d.	n.d.	n.d.	3.39	n.d.	4.41
FeO	6.8	2.2	2.1	3.3	10.2	17.13	9.2	18.13
MnO	0.17	0.12	0.04	0.08	0.15	0.24	0.14	0.25
MgO	33.3	17.3	17.8	19.5	48.5	13.50	49.3	12.54
CaO	0.72	23.2	24.4	11.2	0.03	n.d.	0.006	n.d.
NiO	n.d.	n.d.	n.d.	n.d.	0.27	n.d.	0.29	n.d.
Na_2O	0.00	0.19	0.15	2.1	n.d.	n.d.	n.d.	n.d.
K_2O	n.d.	n.d.	n.d.	0.17	n.d.	n.d.	n.d.	n.d.
Total	100.50	99.80	100.60	97.57	99.60	100.49	99.80	99.95
Si	1.923	1.912	1.922	6.688	0.998	-	1.002	-
Ti	0.001	0.006	0.009	0.060	-	0.026	-	0.054
Al	0.117	0.142	0.089	1.896	-	9.971	-	9.487
Cr	0.014	0.030	0.017	0.155	-	5.529	-	5.809
Fe^{+3}	-	-	-	-	-	0.598	-	0.795
Fe^{+2}	0.198	0.068	0.064	0.386	0.210	3.349	0.188	3.630
Mn	0.005	-	0.001	0.009	0.003	0.047	0.003	0.051
Mg	1.724	0.930	0.962	4.067	1.785	4.704	1.803	4.473
Ca	0.027	0.898	0.947	1.679	0.001	-	0.000	-
Ni	-	-	-	-	0.006	-	0.006	-
Na	-	0.013	0.010	0.570	-	-	-	-
K	-	-	-	0.029	-	-	-	-
Total	4.002	4.010	4.021	15.540	3.003	24.224	3.002	24.298
Wo	1.4	47.4	48.0					
En	88.5	49.0	48.7					
Fs	10.2	3.6	3.3					
Fo					89.4		90.5	
Cr/Cr+Al						0.544		0.503
Mg/Mg+Fe						0.357		0.380

n.d. = not determined, Fe^{+3} in spinel calculated on the assumption of charge balance and stoichiometry. Cations calculated on the basis of 6,23,4 and 32 oxygens for pyroxene, oliv., amph. and spinel.

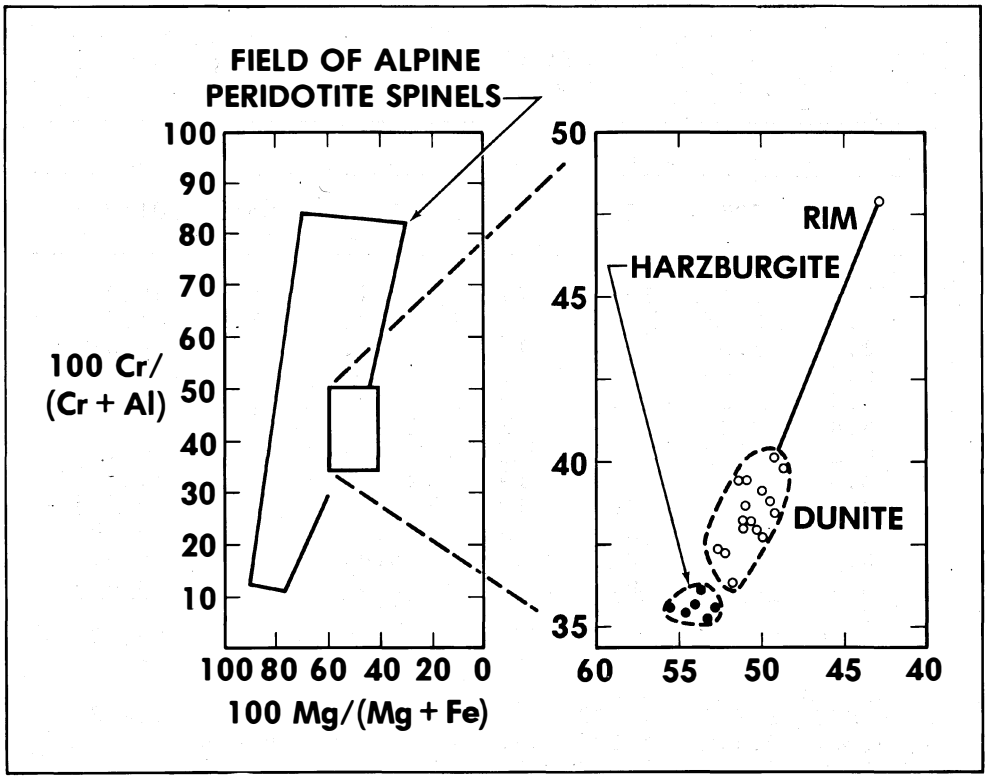

Fig. 5. Compositional variation in chromian spinels. Field of alpine peridotite spinels after *Irvine and Findlay* (1972). Note the larger range of chemical variation in the dunite which trends toward the rim composition.

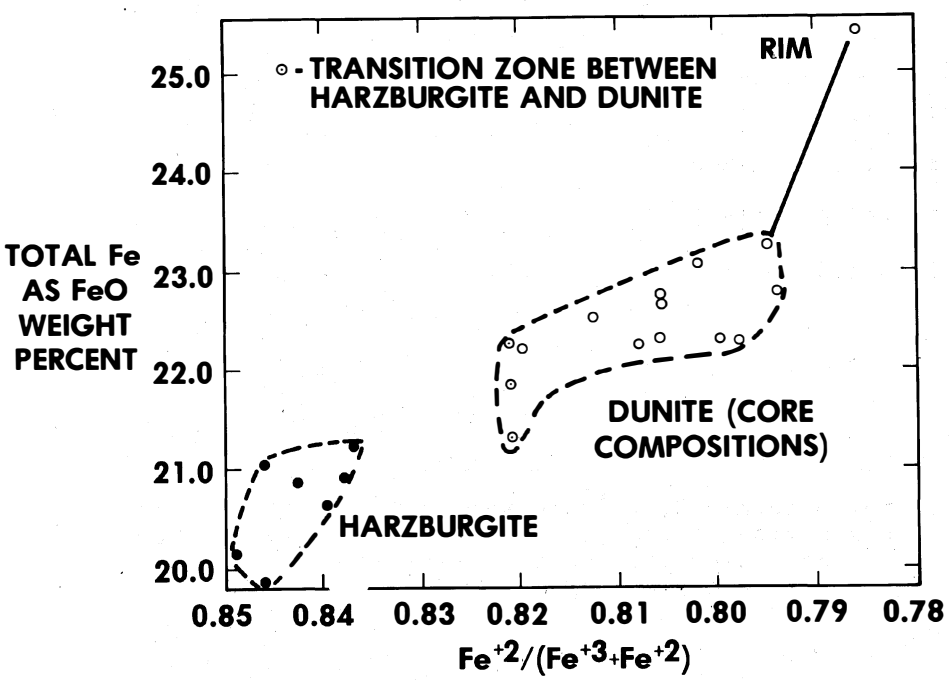

Fig. 6. FeO vs. $Fe^{+2}/(Fe^{+2} + Fe^{+3}$ in chromian spinels. Spinels in dunite and in the transition zone between dunite and harzburgite are more strongly oxidized than those within the harzburgite.

sodium (1.9-2.2 wt. % Na_2O) and titanium (0.56-0.88 wt. % TiO_2) are all markedly higher in the amphibole than in the pyroxene that it has replaced.

Interpretation of the Mineral Chemistry

The similarity of spinel and clinopyroxene compositions in harzburgite and dunite suggests that in the dunite these two phases are relics that have survived transformation without substantial chemical change. However, the relationships are somewhat obscured as the result of slight modification of the primary spinel chemistry due possibly to partial reequilibration during metasomatism or later serpentinization. This view is consistent with observations of spinel segregations and ghosts of pyroxene concentrations that extend into the dunite from the host peridotite.

Evans and Frost (1975), *Onyeagocha* (1974) and *Bliss and MacLean* (1975) examined textural and compositional relations between primary chromian spinel and alteration products, magnetite and ferrian chromite (or ferritchromite). These authors are in agreement that magnetitite or Cr-magnetite is a typical product of spinel alteration during lizardite-chrysotile serpentinization whereas ferrian chromite + chlorite is characteristic of relatively high temperature metamorphism (greenschist to upper amphibolite facies). *Evans and Frost* (1975) and *Bliss and MacLean* (1975) emphasize the complexity of these alteration parageneses and the diverse controls on the composition of metamorphic Cr-spinel. In general, however, compositional change with falling temperature (in the presence of H_2O) tends to involve a decrease in the $MgAl_2O_4$ component of the spinel with the accompanying formation of chlorite; the specific reaction depending on the coexisting silicate phases. *Evans and Frost* (1975) recognize five reactions corresponding to equilibria between spinel, chlorite and coexisting magnesium silicate minerals. The highest grade reaction appears to be directly applicable to the Canyon Mountain example:

$$\text{chlorite} \rightleftarrows 2 \text{ enstatite} + \text{olivine} + MgAl_2O_4 + 4H_2O$$

It is possible that the ferrian chromite alteration rims and the apparently metastable trend toward higher Cr/(Cr+Al) in dunite spinels can be explained by this reaction. Trends towards higher Fe^{+3}/Fe^{+2} ratios and higher TiO_2 observed in the Canyon Mountain dunite spinels are another characteristic feature of the alteration of primary chromian spinel (*Onyeagocha*, 1974).

Partial melting of spinel peridotite accompanied by extraction of the resulting melt produces systematic changes in the proportions and compositions of the residual phases (*Carter*, 1970; *Dick*, 1977). Compositional trends expected in melt-residue systems include an increasing Cr/(Cr+Al) in residual spinel due to extreme preferential partitioning of chromium into spinel while coexisting olivine becomes more magnesian. The final mineral chemistry is a complex function of the degree of partial melt extracted as well as T, P and f_{O_2} and reequilibration during cooling (*Irvine*, 1967; *Hill and Roedder*, 1974; *Mysen*, 1975; *Dick*, 1977). Petrogenetic processes which could produce widely varying Cr/(Cr+Al) in harzburgite spinels include sensitivity of the spinel to degree of partial melting and reactions involving variable amounts of trapped melt subsequent to the fusion event. The small compositional difference between spinels in harzburgite and adjacent dunite (cores) in the Canyon Mountain peridotite is trivial compared with the total range of spinel compositions found in individual harzburgite bodies (Fig. 5). In contrast to this limited Cr/(Cr+Al) trend there is a relatively large decrease in Mg/(Mg+Fe) in spinel with little or no change in olivine composition from harzburgite to

dunite. Thus, aside from the evidence that the compositional differences between harzburgite and dunite spinels are the result of subsolidus alteration, the olivine-spinel compositions in the dunite are not wholly consistent with an origin by partial melting of parental harzburgite.

The equivalence of olivine compositions in dunite and harzburgite can be explained only if the petrogenetic process that produced the dunite preserved the bulk Mg/Fe of the harzburgite. The nearly identical Mg/(Mg+Fe) of the coexisting olivine and orthopyroxene in the harzburgite indicates that this constraint would be satisfied by a metasomatic transformation if the reaction was essentially an incongruent breakdown of pyroxenes (to form olivine) such that Si and Ca (plus minor Cr, Al, Ti and alkalies) were removed from the original assemblage. The more magnesian olivine may have formed because iron was preferentially partitioned into ferrian chromite (or magnetite-metal) or because of the breakdown of clinopyroxene, which has a high Mg/(Mg+Fe) ratio relative to olivine and orthopyroxene.

Discussion of Amphibole Chemistry in Relation to Other Occurrences

Amphiboles in ultramafic rocks supposedly derived from the upper mantle have been discussed in many papers. A few ultramafic xenoliths have been interpreted as fragments of undepleted mantle in which the amphibole is a primary phase (*Varne*, 1968; *Erlank and Finger*, 1970). Another group of occurrences containing kearsutitic to pargasitic amphibole are interpreted as the result of crystallization of hydrous basaltic melt as megacrysts (*Kesson and Price*, 1972), as intercumulus phases in deep-seated magma chambers (*Best*, 1974), and as the result of reaction between trapped hydrous melt and residual mantle (*Conquéré*, 1971a,b; *Wilshire and Trask*, 1971; *Best*, 1974; *Frey and Green*, 1974; *Francis and Dickey*, 1974).

Pargasitic amphiboles broadly similar in composition to those analyzed in this study, occur as an interstitial phase in several xenolith suites (*White*, 1966; *Boyd*, 1971; *Wilshire and Trask*, 1971; *Aoki and Shiba*, 1973; *Smith et al.*, 1973; *Griffen*, 1973; *Best*, 1974; and *Francis and Dickey*, 1976). They differ from the Canyon Mountain amphibole in that they are generally more Cr, Al, Ti and alkali-rich. In most of these examples the formation of amphibole can be directly related to the breakdown of a chromian phase or phases in the presence of H_2O-vapor. The high alkali-contents of the amphiboles (and associated phlogopite) relative to the parental assemblages requires addition of Na and K by the vapor.

Rare, magnesian pargasitic tremolites from the Twin Sisters dunite, Washington are similar in general character to those discussed above (*Onyeagocha*, 1973). Several lines of evidence indicate that the amphiboles in the Twin Sisters formed by reaction between primary phases in the peridotite and alkali-rich vapor. Like the Canyon Mountain peridotite the Twin Sisters is a depleted harzburgite-dunite. If one accepts that hydrous minerals are part of the low-melting fraction of mantle lherzolites, and are therefore lost during partial melting, pargasitic amphibole and rare associated phlogopite are not primary constituents. The alkalies and H_2O bound in these phases are best explained as having been introduced subsequent to an earlier episode of very extensive partial melting and extraction of liquid. *Onyeagocha* (1973) has established that both orthopyroxene and clinopyroxene reacted with vapor to produce amphibole and olivine.

Additional Examples of Dunite Formed by Metasomatism

Irvine (1967b) has recognized large crosscutting dunite bodies in pyroxene-rich cumulates of the Duke Island layered complex. He attributes their origin to metasomatic transformation on the basis of field relations that demonstrate that relict primary layering continues into the dunite without disruption. In addition, these bodies occur with coarse-grained pegmatoids and coarse recrystallized zones that crosscut cumulus layering. Thus, this occurrence supports the concept that dunites may be formed by metasomatic transformation of pyroxene-bearing peridotites at subsolidus temperatures.

Within the Bushveld Complex there are irregular columnar-shaped mineralized bodies (pipes) composed principally of olivine. The localization of mineralization, the way in which chromite seams pass through the pipes (albeit somewhat disturbed), and the direct replacement of orthopyroxene by olivine plus associated iron-rich dunite veinlets and associated hornblende-diallage-olivine pegmatoid, all suggest a replacement origin (*Heckroodt*, 1959).

Another example of dunite bodies crosscutting layered cumulates has been described in detail by *Hess* (1960) from the lower Ultramafic Zone of the Stillwater Complex. These bodies occur as both large irregular masses and as small veins and dike-like tabular bodies that cut primary cumulus layering in the country-rock harzburgites and bronzitites at various angles. As in the Canyon Mountain dunite bodies, olivine is coarser than in the adjacent cumulates, chromian spinel is rimmed by magnetite and pyroxenes within harzburgite at the margin of dunites are partially replaced by colorless calcic amphibole. Olivine directly replaces bronzite at dunite margins. Sharp-bordered remnants of harzburgite within the dunites are unrotated, indicating *in situ* formation of the dunite.

Temperature of Formation and Nature of the Vapor Phase

On the basis of the mineralogy of the host peridotite and the mineral assemblage of the dunite bodies, two possible temperature regimes involving separate phase equilibria are suggested. On the basis of equilibria derived from the study of progressively metamorphosed and dehydrated serpentinites, the upper temperature limit for dunite formation may be defined by the lower stability limit of the assemblage forsterite + enstatite + H_2O which is approximately 700°C at 2 kb (*Greenwood*, 1963). Instability of diopside + forsterite + H_2O occurs at still lower temperatures resulting in the formation of calcic amphibole + olivine (*Trommsdorff and Evans*, 1972). The presence of CO_2 in the vapor phase will slightly expand the olivine-enstatite stability field to lower temperatures (*Evans and Trommsdorff*, 1974). Temperatures of less than 700°C are compatible with the chromite alteration assemblage, ferrian chromite + chlorite (*Evans and Frost*, 1975; *Frost*, 1975).

Experimental studies by *Nakamura and Kushiro* (1974) in the system Mg_2SiO_4-SiO_2-H_2O indicate that enstatite becomes unstable in the presence of vapor at subsolidus temperatures much higher than 700°C. The vapor coexisting with forsterite and enstatite contains 18 weight percent SiO_2 at 1280°C. This high silica-solubility provides an efficacious mechanism

for removal of Si from a harzburgite in an open system in which vapor is migratory. *Nakamura and Kushiro* (1974) infer that the solubility of silica in H_2O-vapor will decrease with decreasing pressure. The presence of CO_2 in the vapor expands the Fo + En stability field by lowering Si-solubility (*Eggler*, 1975). The late-stage timing of the Canyon Mountain dunites indicates that they formed at lower pressures. However, if the 15 Kbar phase relations extend to lower pressures (and perhaps also lower temperatures) this work presents a more attractive alternative than the lower temperature model discussed above.

While calcic amphibole is probably stable in both temperature regimes discussed, it is unlikely that the spinel alteration assemblages are associated with the high temperature regime unless they represent a metastable retrograde effect. The contrasting spinel-alteration in the harzburgite and dunite may, therefore, be a function of serpentinization in different bulk systems not genetically related to the formation of the dunite.

High alkali-contents in secondary amphibole relative to pyroxene in the Canyon Mountain peridotite are typical of secondary amphibole in mantle peridotites and appear to indicate initially high alkali-concentrations in the metasomatic fluid. The presence of S in the metasomatic fluid is indicated by the minor sulfide intergrown with the magnetite-metal assemblage if indeed this alteration occurred during dunite-formation rather than during serpentinization. The removal of Ca in solution from ultramafic rocks during serpentinization is a very efficient process even though it occurs at low temperatures (*Barnes and O'Neil*, 1969). Thus there is no reason to assume that Ca could not be removed in solution during higher temperature metasomatism in the Canyon Mountain example.

Source of the Postulated Vapor Phase

If dunite-formation occurred in the high-temperature regime (as opposed to 700-800°C), then they may reflect reactions between residual peridotite and vapor associated with small amounts of trapped partial melt which were not effectively segregated. *Kay* (1975) has proposed that one possible consequence of cooling of the oceanic lithosphere is that volatile species such as aqueous vapor and alkalies could be trapped in the mantle below a progressively thickening slab of peridotite that is cooled to temperatures below its solidus. Deformation of this uppermost mantle could then create fracture systems along which the vapor might migrate upwards, in which case it could result in the production of hydrous melt by local remelting of partially depleted peridotites. At lower temperatures, subsolidus metasomatic reactions such as those postulated in this paper might occur. Post-tectonic intrusive bodies occur in the Canyon Mountain complex, but a spatial relationship between the intrusions and the dunite bodies is not observed. Therefore, there is no direct evidence linking dunite formation to late-stage magmatism. Derivation of the inferred vapor phase from the mantle is favored due to the demonstrated efficacy of mantle-metasomatism recorded in several xenolith suites and the need for a silica-undersaturated fluid.

An alternative mechanism is that of sea water circulating downward into the oceanic crust along fractures. Serpentinization of ultramafic rocks and alteration and metamorphism of volcanic and plutonic rocks of the seafloor is a widely accepted metamorphic process (see *Miyashiro*, 1973). However, detailed studies of metamorphic zonation in ophiolite complexes indicate that seawater penetration apparently does not extend to depths below the top of layer 3 (*Christensen and Salisbury*, 1975; *De Wit*

and Stern, 1975) except along major fracture zones where ultramafic rocks are exposed and serpentinized.

Post-emplacement metasomatism of hot peridotites by invasion of country-rock water has been suggested by *McTaggart* (1971) as a mechanism for producing cross-cutting dunite and pyroxenite bodies. This mode of origin is grossly compatible with structural relations in the Canyon Mountain complex but it is considered unlikely on petrologic grounds due to the difficulty of deriving a silica-undersaturated fluid from a crustal source.

Summary and Conclusions

Two independent lines of evidence have been combined in order to develop an integrated hypothesis for the origin of dunite bodies in the Canyon Mountain ophiolite; a hypothesis first suggested for dunite-formation by *Bowen and Tuttle* (1949). Critical structural relations indicating that the dunite bodies transect foliation in combination with fabric data demonstrating the preferred orientations in dunite and country rock harzburgite formed simultaneously are only reconcilable with post-tectonic, *in situ* transformation of parental harzburgite. Consideration of alternative petrogenetic mechanisms that might form small tabular crosscutting dunite bodies suggests that this type of *morphology* could result from intrusion of magmatic dunite or very localized post-tectonic anatexis. Aside from the prohibitive thermal constraints associated with these two hypothetical magmatic processes, structural relations of the Canyon Mountain dunites are incompatible with these modes of origin. In order for a magmatic origin to be consistent with the structural and fabric relations presented in this paper, the dunites must have been recrystallized in the same stress field as the country rock harzburgites *subsequent* to their formation. Inasmuch as the Canyon Mountain dunite bodies are in general undeformed, these requirements are not reasonably applied to the examples described above. Small dunite bodies that replace deformed cumulates are a further indication that the formation of the dunites occurred in the subsolidus. However, retention of the original fabric is consistent with secondary grain growth by preexisting olivine grains during transformation.

Direct evidence in support of the model of *in situ* transformation is found in the replacement of pyroxenes in the harzburgite adjacent to the dunite bodies by calcic amphibole. This amphibole provides evidence that a vapor phase was present and is consistent with a wide range of subsolidus temperatures. High concentrations of TiO_2, Al_2O_3, Cr_2O_3 and alkalies in the amphiboles relative to the pyroxenes they replace are compatible with their addition to the anhydrous assemblage by the vapor phase. The high alkali-contents are presumed to reflect initial high concentrations in the vapor while Cr and Al and perhaps Ti may be derived locally from the breakdown of pyroxenes.

The replacement of pyroxene by amphibole in the Canyon Mountain ophiolite is inferred to take place in response to a subsolidus reaction between the pyroxenes and H_2O-vapor. Secondary microfractures and disrupted grain boundaries along the margins of the dunites permitted minor amounts of vapor to escape the main fracture system and penetrate the country rock. If the alteration of chromian spinel to ferrian chromite within the dunites is related to their formation and not to a later episode of serpentinization, they also are indicative of the presence of a fluid phase. However, they are more likely to be compatible with the lower temperature regime ($\approx$ 600-700°C) and, therefore, are not necessarily a definitive criteria.

The source and chemistry of the vapor phase are poorly known but some inferrences have been made. The constancy of olivine compositions in harzburgite and dunite and the lack of evidence for volume change during dunite-formation imply an isovolumetric transformation at nearly constant Mg/(Mg+Fe). On the basis of these relationships it is suggested that pyroxene underwent incongruent breakdown with the result that Si, Al, Ti, Ca and alkalies were transported away in solution and some Mg was added. The high alkali-contents of the aforementioned secondary amphibole (relative to the pyroxenes they replace) is believed to reflect alkali-enriched vapor.

The irregular branching patterns defined by anastomosing swarms of small dunite bodies, their generally tabular shape, and their sharp contacts are all suggestive of control of vapor migration by systems of brittle fractures. In the case of early formed dunite, these bodies may have been slightly recrystallized (e.g., deformation lamellae are present in olivines). Narrow, linear, randomly oriented late-stage dunite veins are clearly undeformed. This study does not provide evidence with regard to the origin of the vapor but the high temperatures involved are more compatible with an upward transfer than with circulation of sea water or penetration of country rock water during emplacement. The metasomatic effects of mantle-derived alkali-rich vapors are recorded in numerous xenolith suites and a mantle origin for the vapor is favored here.

Acknowledgements

Field studies of the Canyon Mountain ophiolite by HGAL were greatly facilitated by the cooperation of Tom Thayer. The senior author thanks Ron Frost and Henry Dick for stimulating discussions of some of the problems discussed in this paper. The manuscript was greatly improved as the result of thorough reviews by Richard Arculus, T.N. Irvine and G.A. Medaris. Martin Menzies called attention to a number of similar occurrences and provided invaluable insights and a review of the manuscript. David Eggler pointed out the possible relationship of these occurrences to experimental studies by Nakamura and Kushiro. Financial support for this work was provided by a grant from the National Science Foundation (GA-25897).

References

Aoki, K., and I. Shiba, Pargasites in lherzolite and websterite inclusions from Itinome-gata, Japan, *J. Jap. Ass. Miner. Petrol. Econ. Geol.*, *68*, 303-310, 1973.

Avé Lallemant, H.G., Mechanisms of preferred orientations of olivine in tectonite peridotites, *Geology*, *3*, 653-656, 1975.

Avé Lallemant, H.G., Structure of the Canyon Mountain (Oregon) ophiolite complex and its implication for sea-floor spreading, *Geol. Soc. Amer. Spec. Paper 173*, 49 p., 1976.

Barnes, I., and J.R. O'Neil, The relationship between fluids in some fresh alpine type ultramafics and possible modern serpentinization, Western U.S., *Geol. Soc. Amer. Bull.*, *80*, 1947-1960, 1969.

Best, M.G., Mantle-derived amphibole within inclusions in alkali-basaltic lavas, *J. Geophys. Res.*, *79*, 2107-2113, 1974.

Bliss, N.W., and W.H. MacLean, The paragenesis of zoned chromite from central Manitoba, *Geochim. Cosmochim. Acta*, *39*, 973-990, 1975.

Boudier, F., Relations lherzolite-gabbro-dunite dans le massif de Lanzo (Alpes piemontaises): Exemple de fusion partielle, *University of Nantes, Dissertation*, 1972.

Boudier, F., and A. Nicolas, Fusion partielle gabbroique dans la lherzolite de Lanzo, *Schweiz. Mineral. Petrog. Mitt.*, *52*, 39-46, 1972.

Bowen, N.L., and O.F. Tuttle, The system MgO-SiO_2-H_2O, *Geol. Soc. Amer. Bull. 60*, 439-460, 1949.

Boyd, F.R., Pargasite-spinel xenolith from the Wesselton Mine, *Carnegie Inst. Washington Yearb. 70*, 138-142, 1971.

Carswell, D.A., Picritic magma-residual dunite relationships in garnet-peridotite at Kalskaret near Tafjord, South Norway, *Contrib. Mineral. Petrol.*, *19*, 97-124, 1968.

Carter, J.L., Mineralogy and chemistry of the earths upper mantle based on the partial fusion-partial crystallization model, *Geol. Soc. Amer. Bull. 81*, 2021-2034, 1970.

Christensen, N.I., and M.H. Salisbury, The petrologic nature of the layer 2 - Layer 3 boundary in the oceanic crust (abstr.), *Proc. Int. Conf. on the Nature of the Oceanic Crust*, 1975.

Conquéré, F., Les pyroxenolites à amphibole et les amphibolites associées aux lherzolite du gisement de Lherz (Ariège, France): Un example du role de l'eau en course de la cristallisation fractionée des liquids issus de la fusion partielle de lherzolite, *Contrib. Mineral. Petrol.*, *33*, 32-61, 1971a.

Conquéré, F., La lherzolite à amphibole du gisement de Caussou (Ariège, France), *Contrib. Mineral. Petrol.*, *30*, 296-313, 1971b.

De Wit, M.J., and C.R. Stern, Ocean floor metamorphism, seismic layering and magnetism (abstr.), *Proc. Int. Conf. on the Nature of the Oceanic Crust*, 1975.

Dickey, Jr., J.S., Partial fusion products in alpine-type peridotites: Serrania de la Ronda and other examples, *Min. Soc. Amer. Spec. Paper 3*, 33-49, 1970.

Dickey, Jr., J.S., A hypothesis of origin for podiform chromite deposits, *Geochim. Cosmochim. Acta*, *39*, 1061-1074, 1975.

Dick, H.J.B., The origin and emplacement of the Josephine peridotite, *Ph.D. Dissertation, Yale University*, New Haven, Conn., 1976.

Dick, H.J.B., Partial melting in the Josephine Peridotite. I. The effect on mineral composition and its consequence for geobarometry and geothermometry, *Am. J. Sci.*, *277*, 801-832, 1977.

Eckstrand, O.R., The Dumont Serpentinite: A model for control of nickel-iferous opaque mineral assemblages by alteration reactions in ultramafic rocks, *Econ. Geol.*, *70*, 183-201, 1975.

Eggler, D.H., CO_2 as a volatile component of the mantle: The system Mg_2SiO_4-SiO_2-H_2O-CO_2, *Phys. Chem. Earth, 9*, 869-881, 1975.

Erlank, A., and L.W. Finger, The occurrence of potassic richterite in a mica nodule from the Werselton kimberlite, South Africa, *Carnegie Inst. Washington Yearb. 68*, 320-324, 1970.

Ernst, W.G., *Amphiboles: Crystal Chemistry, Phase Relations and Occurrence*, Springer-Verlag, New York, Inc., 125 p., 1968.

Evans, B.W., and V. Trommsdorff, Stability of enstatite and talc and CO_2-metasomatism of metaperidotite, Val d'Efra, Lepontine Alps, *Am. J. Sci., 274*, 274-296, 1974.

Evans, B.W., and B.R. Frost, Chrome-spinel in progressive metamorphism - a preliminary analysis, *Geochim. Cosmochim. Acta, 39*, 959-972, 1975.

Francis, D.M., and J.S. Dickey, Jr., Amphibole lherzolites - Nunivak Island, Alaska (abstr.), *Geol. Soc. Amer. Abstracts with Programs 6*, 1037-1038, 1974.

Francis, D.M., and J.S. Dickey, Jr., The origin of amphibole in lherzolite xenoliths from Nunivak Island, Alaska, *J. Petrol., 17*, 357-378, 1976.

Frey, F.A., and D.H. Green, The mineralogy, geochemistry and origin of lherzolite inclusions in Victorian basanites, *Geochim. Cosmochim. Acta, 38*, 1023-1060, 1974.

Frost, B.R., Contact metamorphism of serpentinite, chloritic blackwall and rodingite at Paddy-Go-Easy Pass, Central Cascades, Washington, *J. Petrol., 16*, 272-313, 1975.

Greenwood, H.J., The synthesis and stability of anthophyllite, *J. Petrol., 4*, 317-351, 1963.

Griffin, W.L., Lherzolite nodules from the Fen Alkaline Complex, Norway, *Contrib. Mineral. Petrol., 38*, 135-146, 1973.

Guillon, J.H., Les massifs peridotitiques de nouvelle Calidonie, *ORSTOM Paris memoires No. 76*, 1975.

Heckroodt,R.O., The geology around the dunite pipe on Dreikop (Eastern Transvaal), *Geol. Soc. South Africa, Trans., 62*, 59-73, 1959.

Hess, H.H., Stillwater igneous complex, Montana, a quantitative mineralogical study, *Mem. Geol. Soc. Amer., 80*, 230 p., 1960.

Hill, R., and P. Roedder, The crystallization of spinel from basaltic liquid as a function of oxygen fugacity, *Jour. Geol., 82*, 709-729, 1974.

Himmelburg, G.R., and R.A. Loney, Petrology of the Vulcan Peak alpine-type peridotite, southwestern Oregon, *Geol. Soc. Amer. Bull. 84*, 1585-1600, 1973.

Irvine, T.N., The Duke Island ultramafic complex, southeastern Alaska, in *Ultramafic and Related Rocks*, edited by P.J. Wyllie, John Wiley & Sons, New York, 84-97, 1967a.

Irvine, T.N., Chromian spinel as a petrogenetic indicator, Part 2., *Canad. J. Earth Sci.*, 71-103, 1967b.

Irvine, T.N., and T.C. Findlay, Alpine-type peridotite with particular reference to the Bay of Islands igneous complex, in *The Ancient Oceanic Lithosphere*, Symposium, Ottawa, *Canada Dept. Energy, Mines and Resources Earth Physics Br. Publs.*, *42*, 97-128, 1972.

Jackson, E.D., H.W. Green III, and E.M. Moores, The Vourinos Ophiolite, Greece: Cyclic units of lineated cumulates overlying harzburgite tectonite, *Geol. Soc. Amer. Bull. 86*, 390-398, 1975.

Kay, R., Chemical zonation in the upper mantle (abstr.), *Trans. Am. Geophys. Union, 56*, 1077, 1975.

Kesson, S., and R.C. Price, The major and trace element chemistry of Kearsutite and its bearing on the petrogenesis of alkaline rocks, *Contrib. Mineral. Petrol.*, *35*, 119-124, 1972.

Loney, R.A., G.R. Himmelburg, and R.G. Coleman, Structure and petrology of the alpine-type peridotite at Burro Mountain, California, U.S.A., *J. Petrol.*, *12*, 245-309, 1971.

McTaggart, K.C., On the origin of ultramafic rocks, *Geol. Soc. Amer. Bull. 82*, 23-42, 1971.

Menzies, M., Mineralogy and partial melt textures within an ultramafic-mafic body, Greece, *Contrib. Mineral. Petrol.*, *42*, 273-285, 1973.

Menzies, M., and C. Allen, Plagioclase lherzolite-residual mantle relationships within two eastern Mediterranean ophiolites, *Contrib. Mineral. Petrol.*, *45*, 197-213, 1974.

Miyashiro, A., *Metamorphism and Metamorphic Belts*, Halstead Press, New York, 1973.

Mysen, B., Partitioning of iron and magnesium between crystals and partial melts in peridotite upper mantle, *Contrib. Mineral. Petrol.*, *52*, 69-76, 1975.

Nakamura, Y., and I. Kushiro, Composition of the gas phase in Mg_2SiO_4-SiO_2-H_2O at 15 Kbar, *Carnegie Inst. of Washington Yearbook 73*, 255-258, 1974.

O'Hara, M.J., The bearing of phase equilibria studies on the origin of and evolution of basic and ultrabasic rocks, *Earth Sci. Rev.*, *4*, 69-133, 1968.

Onyeagocha, A.C., Petrology and mineralogy of the Twin Sisters dunite, Washington, *Ph.D. Dissertation, University of Washington, Seattle*, 1973.

Onyeagocha, A.C., Alteration of chromite from the Twin Sisters dunite, Washington, *Am. Min.*, *59*, 608-612, 1974.

Page, N.J., Serpentinization at Burro Mountain, California, *Contrib. Mineral. Petrol.*, *14*, 321-342, 1967.

Smith, J.V., J.B. Dawson, and F.I. Bishop, Sulphide-oxide and silicate-oxide intergrowths in xenoliths of upper mantle peridotite, *Int. Conf. on Kimb., Cape Town (abstr.)*, 291-293, 1973.

Thayer, T.P., Preliminary geologic map of the John Day quadrangle, Oregon, *U.S. Geol. Survey Min. Inv. Field Map MP 51*, 1956.

Thayer, T.P., The Canyon Mountain Complex, Oregon, and the alpine mafic magma stem, *U.S. Geol. Survey Prof. Paper 475C*, C82-C85, 1963a.

Thayer, T.P., Flow-layering in alpine peridotite-gabbro complexes, *Min. Soc. Am. Spec. Paper 1*, 55-61, 1963b.

Thayer, T.P., Chromite segregations as petrogenetic indicators, *Geol. Soc. South Africa Spec. Publ. 1*, 380-390, 1970.

Thayer, T.P., Some implications of sheet dike swarms in ophiolite complexes, in *International Symposium on Ophiolites in the Earth's Crust, Akad. Nauk. SSSR Doklady, Moscow*, in press.

Thayer, T.P., and G.R. Himmelburg, Rock succession in the alpine-type mafic complex at Canyon Mountain, Oregon, *Int. Geol. Congress, 23rd, Prague, 1*, 175-186, 1968.

Thayer, T.P., and E.D. Jackson, A classification of igneous rocks by their history of crystallization and emplacement, *U.S. Geol. Survey Prof. Paper 800-B*, B74-B83, 1972.

Trommsdorff, V., and B.W. Evans, Progressive metamorphism of antigorite schist in the Bergell tonalite aureole (Italy), *Am. J. Sci., 272*, 423-437, 1972.

Varne, R., Hornblende lherzolite and the upper mantle, *Contrib. Mineral. Petrol., 27*, 451-51, 1968.

White, R.W., Ultramafic inclusions in basaltic rocks from Hawaii, *Contrib. Mineral. Petrol., 12*, 245-314, 1966.

Wilshire, H.G., and N.S. Trask, Structural and textural relationships of amphibole and phlogopite in peridotite inclusions, Dish Hill, California, *Am. Min., 56*, 240-255, 1971.

3. TRACE ELEMENT AND ISOTOPIC STUDIES OF PARTIAL MELTING

RESIDUAL ALPINE LHERZOLITES AND HARZBURGITES - GEOCHEMICAL AND ISOTOPIC CONSTRAINTS ON THEIR ORIGIN

Martin Menzies*
Department of Geology
University of California
Davis, California 95616

Abstract

Alpine lherzclites and harzburgites (Appendix A) occur as isolated masses in the world's orogenic belts or as metamorphic basement complexes to major ophiolites. In many cases the predominance of harzburgite, minor lherzolite with associated gabbroic segregations is best explained by a partial melting model. Such a model is compatible with: the widespread occurrence of harzburgite on a local and worldwide scale, the restricted chemistry of the olivines and orthopyroxenes, the Cr-Al variation in the spinels resulting from partial melting processes or contamination with the melt, the totally refractory nature of the harzburgites and dunites, the existence of segregations whose composition is similar to cotectic liquids, and the existence of lherzolites with a major and minor element and REE chemistry compatible with that of "pyrolite". The harzburgites contain 70-90% olivine and 10-30% orthopyroxene which contributes to a low total REE content (< 0.5x chondrite) and a light REE depleted profile. Such peridotites also have highly radiogenic isotopic compositions ($^{87}Sr/^{86}Sr$ = 0.706-0.727), a fact best explained by the radiogenic minerals and/or serpentinization. The lherzolites have a more confusing history, in that the major, minor and REE chemistry is similar to that of "pyrolite" but these lherzolites are depleted in Rb, Sr, Ba, K, Na, etc. All the analyzed alpine lherzolites have chondritic or light REE depleted profiles (0.5-3.0x chondrite). Partial melts computed from such sources have REE characteristics similar to oceanic tholeiites. Published $^{87}Sr/^{86}Sr$ data has to date negated any hypothesis which relates alpine peridotites and basalts unless one envokes disequilibrium melting processes. Recent studies of the constituent minerals in alpine lherzolites (*Menzies and Murthy*, 1976) indicate that in four alpine lherzolites, the clinopyroxenes have $^{87}Sr/^{86}Sr$ = 0.70228 - 0.70370. The isotopic composition of olivines and orthopyroxenes is 0.70290 - 0.70831 and 0.70265 - 0.70429, respectively. The highly radiogenic nature of olivine may, however, be the result of secondary processes. Alpine lherzolites and harzburgites represent the residua left after one or more melting episode(s). An initial small degree of melting depleted a "fertile" lherzolite of an alkali and light REE enriched fraction, possibly a nephelinitic or alkalic liquid. Subsequent melting episodes further depleted the lherzolites of a basaltic fraction, and ultimately produced a totally refractory harzburgite.

Introduction

Peridotites of presumed mantle origin occur throughout the world's mountain belts (*Benson*, 1926; *Hess*, 1955) (alpine peridotites) and as

* Present address: Department of Geology and Geophysics, 108 Pillsbury Hall, University of Minnesota, Minneapolis, Minnesota 55455

basement complexes to the major ophiolites (*Davies*, 1969; *Bezzi and Piccardo*, 1971). Since the pioneering work of *Steinmann* (1905, 1927) and *Benson* (1926) the origins of alpine peridotites have been the subject of controversy. Prior to their metamorphic history such peridotites originated via accumulation from a basaltic liquid or via partial fusion processes. The first hypothesis of fractional crystallization of a mafic liquid is advocated by *Thayer* (1963, 1964, 1967, 1969, 1970) and is based primarily on the presence of relict 'igneous' textures in chromitites. The second hypothesis requires that the harzburgite represents a refractory residue left after the partial fusion of a lherzolite and subsequent complete or incomplete removal of basaltic melt. This process was suggested for the origin of basaltic melts (*Ringwood*, 1962; *Green and Ringwood*, 1967) where the source material is believed to have a composition similar to that of "pyrolite" (*Ringwood*, 1966).

The purpose of this short paper is to summarize field evidence, major, trace and rare earth element data, and isotopic analyses (*Menzies and Murthy*, 1976a,b,c) which strongly indicate that the partial fusion hypothesis best explains the co-existence of lherzolite - harzburgite - gabbro etc. Dunite bodies, however, have a variety of origins, and may represent infolded cumulates, *in situ* cumulates shed from upwelling basaltic pockets, subsided cumulates from a ridge magma chamber, refractory dunites left after partial melting episodes, intrusive dunitic melts, or may be metasomatic in origin.

Alpine Tectonite Peridotites

Peridotites of presumed mantle origin and exhibiting partial melt textures exist under garnet (65-100 kms), spinel (35-70 kms), or plagioclase (15-35 kms) peridotite facies (*Green*, 1964; *Carswell*, 1968; *Kornprobst*, 1969; *Dickey*, 1970; *Boudier*, 1972; *Menzies*, 1973; *Menzies and Allen*, 1974; *Dick*, 1975; *Medaris*, 1972; *Upadhyay et al.*, 1971; *Loney et al.*, 1971; *Himmelberg and Loney*, 1973; *Malpas and Strong*, 1975; see Appendix A for other examples). Such a wealth of information exists on mantle peridotites from ophiolites and alpine massifs that some attempt will be made to summarize the relevant field and chemical data.

Field Observations

The majority of alpine and ophiolitic tectonite* peridotite massifs are dominated by harzburgite and dunite (*Carswell*, 1968, Norway; *Nicolas and Jackson*, 1972, Mediterranean; *Gass*, 1967, Cyprus; *Menzies*, 1973, 1974, Greece; *Dick*, 1975, Oregon; *Loney et al.*, 1971, California; *Himmelberg and Loney*, 1973, Oregon; *Upadhyay et al.*, 1971, Newfoundland). Lherzolite bearing massifs are restricted in distribution (*Nicolas and Jackson*, 1972) and predominantly occur in the Mediterranean (*Conquere*, 1971; *Dickey*, 1970). Small but significant amounts of lherzolite occur in what were previously believed to be harzburgite-dunite massifs (*Menzies and Allen*, 1974). Massifs in the United States are predominantly harzburgite and dunite although minor amounts of lherzolite have been reported

---

* The subsequent sections (a) to (g) will outline the field and chemical characteristics of non-cumulus peridotites. These peridotites have metamorphic structures and tectonite fabrics. This includes minor amounts of tectonites with gabbroic mineralogy (*Nicolas and Jackson*, 1972).

(*Medaris*, 1972; *Himmelberg and Coleman*, 1968; *James*, 1971; *Medaris and Dott*, 1970; *Moores*, 1970; *Raleigh*, 1965; *Lindsley Griffin et al.*, 1974; *Springer*, 1974; *Southwick*, 1974; *Ehrenberg*, 1975). Many of the above described massifs are variably serpentinized and or deformed.

Harzburgite-dunite - The complexities of alpine harzburgite-dunite massifs are adequately described by *Loney et al.* (1971) and *George* (1975). The harzburgite terrain contains dunite in a variety of different forms, (1) interlayered pyroxenitic and dunitic patches, (2) interfingered dunitic masses with strung out chromitite deposits, (3) cross-cutting anastomosing veins, tabular bodies and dikes of dunite, (4) tightly interfolded dunitic layers, (5) isolated pods of dunite within the harzburgite formed via cumulate processes, e.g., infolded cumulates from a magma chamber (*Dickey*, 1975; *George*, 1975). The important observation in all of these complexes is that the enclosing harzburgite is petrographically monotonous on a local and world-wide scale. Within these complexes there is a form of layering or, in some cases, tight isoclinal folding (*Loney et al.*, 1971). This layering, however, does not exhibit the cryptic and modal variations characteristic of major stratiform bodies. The rather constant ratio of olivine:orthopyroxene = 80:20 in the harzburgite implies uniform controls on the partial melting process.

The origin of the associated dunites, however, is not clear: (1) The presence of tiny euhedra of spinel which cluster parallel to contacts with enclosing harzburgite led *Menzies and Allen* (1974) to propose a cumulate origin for the dunites. Such a hypothesis has been proposed by *Thayer* (1970) for some time. (2) *Boudier* (1972) interpreted dunitic margins to gabbroic dikelets as a refractory residue generated by high temperatures of fusion. (3) *Loney et al.* (1971) proposed a magmatic origin for the cross-cutting dunites in the Burro mountain complex. (4) *Dungan and Avé Lallemant* (1977, this volume) propose a metasomatic origin for the dunitic dikes in the Canyon mountain. (5) *Sinton* (1976) believes that additional physical differentiation processes may have been associated with partial melting processes in the formation of harzburgite-dunite massifs.

Lherzolite - Lherzolite occurs as either islands (Troodos and Othris - *Menzies and Allen*, 1974) within the harzburgite or constitutes a significant portion of the massif (Lanzo - *Boudier*, 1972). The lherzolites are commonly five phase assemblages (olivine + orthopyroxene + clinopyroxene + spinel + plagioclase) whereas the harzburgites are primarily an olivine - orthopyroxene mix, with variable spinel and accessory diopside and plagioclase. The contact with the harzburgite is normally gradational and the lherzolite and harzburgite contain abundant segregations and dikes of gabbroic material. The veins contain feldspar + clinopyroxene + orthopyroxene + olivine and the segregations are dominated by feldspar. The magmatic layers within many of the complexes vary in type: magnesian spinel pyroxenite, garnet pyroxenite, amphibole pyroxenite, lherzolite, and gabbro (*Dickey*, 1970).

Lherzolite occurs as two or perhaps more types. In many of the complexes a lherzolite is observed where the diopside is an interstitial phase but in other bodies diopside and plagioclase seem to occur in 'segregations'. Perhaps these can be referred to as unsegregated and segregated lherzolites respectively. Because of the higher modal amounts of diopside and plagioclase within these lherzolites, they may be considered as more fertile ultramafic rocks. The intimate association of gabbroic dikes and segregations is of particular interest since the mineralogy of such dikes mimics the low melting fraction of the lherzolites. Clearly a partial fusion hypothesis best explains such associations.

Mineral Chemistry

Olivine - Many studies of alpine harzburgites and dunites have demonstrated the limited range in chemical composition of their constituent minerals (e.g., *Loney et al.*, 1971; *Himmelberg and Loney*, 1973). Olivines are typically rich in Mg and have a restricted range in forsterite content (Fo_{87-95}). Olivines from stratiform intrusions may be just as rich in Mg, but commonly have a greater composition range, when all the lithologies are considered. Olivines from alpine lherzolites (*Menzies*, 1973; *Boudier*, 1972) and from pyroxenite veinlets and segregations are more Fe rich (*Challis*, 1975; *Himmelberg and Coleman*, 1968), than those in associated harzburgites.

Enstatite - Enstatite is a dominant mineral in the harzburgites (approx. 20%) and tends to be restricted in compositional range around En_{90} (e.g. *Dick*, 1976). The enstatites from the lherzolites are similar in chemistry but tend to be richer in ferrosilite. The aluminum content of the enstatites can vary significantly (*Green*, 1964; *Challis*, 1965; *Medaris*, 1972; *Himmelberg and Coleman*, 1968; *Loney et al.*, 1971; *Jackson and Thayer*, 1972; *Dick*, 1976) and the range differs between the harzburgite (1.0-3.0%) and lherzolite (1.5-8.0%) sub-types (*Jackson and Thayer*, 1972).

Diopside - Clinopyroxene occurs as an accessory mineral in alpine harzburgites and orthopyroxenite veins. Occasionally it occurs in dunitic bodies and constitutes up to 25% of some alpine lherzolites (*Loney et al.*, 1971). Clinopyroxenes are primarily chromian diopsides exhibiting a considerable range in titanium and chromian content (*Menzies*, 1973), but a small range in aluminum (1.3-2.6%) (*Ross et al.*, 1954; *Green*, 1964; *Challis*, 1965).

Spinel - Spinels from alpine and ophiolitic peridotites vary significantly in Cr and Al (*Thayer*, 1946; *Irvine*, 1965, 1967; *Rogers*, 1973; *Menzies*, 1975; *Malpas and Strong*, 1975; *Sinton*, 1976; *Dick*, 1976). Ternary plots of Fe^{3+} - Cr^{3+} - Al^{3+} reveal a significant range in Cr^{3+} - Al^{3+} but very little range in Fe^{3+}. Alpine harzburgites tend to contain highly chromiferous spinels as a groundmass phase and highly aluminous spinels as exsolution lamellae in deformed pyroxenes (*Irvine*, 1967; *Malpas and Strong*, 1975). The highly chromiferous spinels are characterized by low Mg/(Mg+Fe) ratios. Amoeboid or euhedral spinels separated from alpine lherzolites tend to be more aluminous than the groundmass spinels from the harzburgites (*Menzies*, 1975; *Malpas and Strong*, 1975).

Dickey and Yoder (1972) proposed that the Cr-Al variation may be the result of interaction with migrating basaltic melt. *Menzies* (1975) reported Cr-Al variations in a suite of spinels from a lherzolite-harzburgite complex. He noted a correlation between the presence of segregations and gabbroic schlieren and the composition of the spinel. Menzies interpreted these segregations as in situ basaltic melt and believed that the spinel compositional variation resulted from (partial) equilibration with migrating basaltic melt in an environment of depleted harzburgite. *Irvine and Findley* (1972) and *Malpas and Strong* (1975) explained spinel compositional variations in a harzburgite-dunite alpine body in a similar fashion. Since many alpine peridotite complexes may contain mantle tectonite ultramafics (*Davies*, 1969; *Menzies and Allen*, 1974) subsided cumulates (*Dickey*, 1974; *Moores*, 1969) and refractory ultramafics (*Bezzi and Piccardo*, 1971; *Davies*, 1969) the Cr-Al variation may arise from fractional crystallization effects (*Henderson*, 1974) and/or fractional fusion effects.

Plagioclase - Plagioclase is commonly highly altered in alpine peridotites and occurs as a "rodingite" assemblage (hydrogarnet + zoisite +

epidote, etc.). Where fresh in plagioclase lherzolites or harzburgites (*Menzies and Allen*, 1974) it is highly calcic in composition: An_{93} in alpine harzburgites from Greece and An_{90} in the Lanzo lherzolite (*Menzies*, 1974; *Boudier*, 1972). Gabbroic dikelets and segregations contain plagioclase (An_{62-85}) which is much more albitic.

Petrochemistry (Table 1)

Harzburgite - Chemically this group is very homogenous, based on the consistent mineralogy outlined in the last section. The three dominant mineral phases produce a highly refractory assemblage with bulk ratios of Mg/(Mg+Fe) typically in the range 0.89-0.91 (*Menzies and Allen*, 1974) for the harzburgites and higher in the case of dunitic material (Mg/(Mg+Fe+Mn) = 0.92, *Loney et al.*, 1971). The total alkali content is less than 1000 ppm and the individual calcium and aluminum contents are both less than one percent. This highly refractory chemistry and the constant ratio of olivine to orthopyroxene = 80:20 imply uniform controls in the partial melting process and cast doubt on the plausibility that such peridotites are cumulate in origin.

Lherzolite - Relative to the harzburgites, alpine lherzolites contain significantly more diopside and plagioclase (or spinel) and as such are richer in aluminum, calcium and titanium. The slightly more iron rich nature of the olivines and pyroxenes (relative to harzburgite) is reflected by lower NiO and a lower Mg/Mg+Fe (Table 1). On first inspection the bulk rock composition of most alpine lherzolites bears some similarity to estimates of the composition of primary mantle (*Ringwood*, 1966). However, elements such as sodium, potassium, titanium and phosphorous are normally lower than pyrolite estimates. Such comparisons of alpine lherzolites and pyrolite may be questioned on the grounds that "pyrolite" is a hypothetical calculation and that these lherzolites may represent deformed cumulate peridotites. However, *Menzies and Allen* (1974) pointed out several differences between alpine lherzolites and cumulate five-phase assemblages from quasi-stratiform massifs. Apart from considerable modal variations over short distances the cumulates have lower Ni, Cr, S and RO/SiO_2, higher Na, K, Ti, and P; Mg/(Mg+Fe) less than 0.87 and tiny euhedral iron rich spinels (*Menzies and Allen*, 1974).

Dunite - The high modal amount of forsteritic olivine and relative absence of diopside and plagioclase characterize a highly magnesian dunite with an Mg/(Mg+Fe) ratio in excess of 0.90 (*Menzies and Allen*, 1974). Such dunites have high Cr and Ni contents and very low contents of Ti, Fe, Mn, and S. Differences in the Mg/(Mg+Fe) ratio may be related to changes in olivine composition.

Rare Earth Element Chemistry

Rare earth element studies of alpine peridotites (*Frey*, 1969, 1970; *Frey et al.*, 1971; *Garmann et al.*, 1975; *Menzies*, 1974; *Loubet et al.*, 1975; *Kay and Senechel*, 1975; *Menzies*, 1976; *Menzies et al.*, 1975) indicates that all the analyzed lherzolites, and lherzolites recalculated from mineral REE data (*Menzies et al.*, 1977a, 1977b), have either chondritic or light REE depleted abundance profiles relative to chondrites. The level of enrichment (i.e. ΣREE) varies dependent on the modal amount of diopside and the REE content of the diopside, since the olivine and orthopyroxene contribute very little to the REE content of these peridotites.

TABLE 1. Chemistry of Alpine Lherzolites and Harzburgites

	LHERZOLITES							HARZBURGITES		
	1	2	3	4	5	6	7	8	9	10
SiO_2	43.63	44.69	42.75	44.28	44.77	44.93	44.7	42.41	43.87	43.47
TiO_2	0.11	0.25	0.02	0.18	0.19	0.08	-	0.06	0.04	0.01
Al_2O_3	1.85	3.03	3.63	4.90	4.16	3.21	4.2	0.48	2.38	0.47
Cr_2O_3	0.42	0.26	0.65	0.33	0.40	0.45	0.4	0.48	0.01	0.39
Fe_2O_3	2.48	-	3.10	-	-	-	-	0.83	2.18	5.44
FeO	6.18	8.42*	5.49	8.66*	8.21*	7.58*	8.7*	7.53	6.54	3.24
MnO	0.16	0.12	0.18	0.13	0.11	0.14	-	0.16	0.14	0.15
NiO	0.28	0.10	0.25	0.23	0.24	0.26	-	0.30	0.08	0.27
MgO	42.58	37.84	40.34	36.65	39.22	40.03	39.3	46.95	41.11	45.72
CaO	2.15	2.20	3.46	4.29	2.42	2.99	2.7	0.74	0.87	0.77
Na_2O	0.14	0.18	0.06	0.35	0.22	0.18	-	0.05	0.04	0.006
K_2O	0.02	-	0.00	0.01	0.55	0.02	-	0.01	tr	0.002
S	0.01	-	0.03	-	-	-	-	0.00	-	0.019
Total	100.01	97.09	99.96	100.01	99.99	99.87	100.00	100.00	97.26	99.95

* Total Fe as FeO.
1. Othris (*Menzies and Allen*, 1974); 2. Lanzo (*Boudier*, 1972); 3. Troodos (*Menzies and Allen*, 1974); 4. Ronda (*Dickey*, 1970); 5. Lizard (*Green*, 1964); 6. Tinaquillo (*MacKenzie*, 1960); Oregon (*Medaris*, 1972); 8. Othris (*Menzies and Allen*, 1974); 9. Lanzo (*Boudier*, 1972). 80 Troodos (*Menzies and Allen*, 1974).

lherzolites can vary from 3.0x chondrite to 0.5x chondrite (Table 2). The harzburgites and dunites are either mildly or heavily depleted in light REE with a low total REE content (Table 2).

The chondritic nature of certain lherzolites and the light REE depleted nature of the harzburgites are compatible with the studies of *Schilling* (1975) who computed the source material of oceanic tholeiites from studies of basalt REE chemistry, and concluded that the range of potential source peridotites and refractory material is compatible with the REE data reported by various authors for alpine lherzolites. *Menzies et al.* (1977b), *Menzies* (1976), and *Loubet et al.* (1975) reported that partial melting of alpine lherzolites would produce liquids with the REE characteristics of an oceanic tholeiite. Studies of lherzolites from the Klamath Mountains and southern Oregon (*Helmke*, unpublished data; *Menzies et al.*, 1977a) reveal that these lherzolites are similar in REE characteristics to lherzolites from the Mediterranean area. The diopsides and consequently the lherzolites are more markedly depleted in light REE, somewhat similar to an oceanic lherzolite described by *Shimizu and Hart* (1974).

K, Rb, Ba and Sr Relative Abundances

Studies of diopsides, separated from alpine lherzolites, reveal low concentrations of K, Rb, Ba and Sr (*Menzies and Murthy*, 1977c, in press) that were significantly lower than those reported for similar alpine clinopyroxenes by *Griffin and Murthy* (1969). *Shimizu* (1973) reported similarly low concentrations in diopsides separated from kimberlite nodules.

Calculation of possible co-existing liquids (*Menzies and Murthy*, 1976a) by the application of partition coefficient data, indicates that the lherzolites may have equilibrated with a highly alkalic liquid, either as a partial melt or as intercumulus liquid. As such the lherzolites are considered to be residual after the loss of a small percent partial melt. *Menzies and Allen* (1974) commented on the "slightly more residual nature" of the lherzolites because of the low relative abundances of Na, K, Ti and P relative to "pyrolite". They proposed removal of a nepheline normative liquid (< 5% partial melt) to explain these discrepancies. Such an idea is compatible with the K, Rb, Ba and Sr data.

U Relative Abundance

Alpine and ophiolitic ultramafics from the Mediterranean (*Dostal et al.*, 1975) contain variable amounts of U (11-74 ppb) similar to that of oceanic ultramafics (*Seitz and Hart*, 1973; *Komarov et al.*, 1973; *Aumento and Hyndeman*, 1971). Much of this U may have been added via alteration processes since mineral analyses indicate an estimated original content of 1-10 ppb. Most of the U is concentrated in the clinopyroxene and as such lherzolites contain more U than harzburgites. Uranium liquid-solid partition studies reveal the past presence of a tholeiitic liquid in the harzburgites. Clearly these ultramafics are a refractory residue after the removal of a partial melt.

Strontium Isotope Geochemistry

Any interpretations of the origin of alpine peridotites, which were based on the previously documented field and geochemical data, involve

TABLE 2. Chemistry of Alpine Lherzolites and Harzburgites

	LHERZOLITES				HARZBURGITES			
	1	2	3	4	5	6	7	8
La	-	-	-	-	-	0.02	-	-
Ce	0.80	0.72	0.610	0.540	0.052	0.04	-	0.53
Nd	0.55	0.54	0.590	0.660	0.133	0.03	0.04	-
Sm	0.17	0.22	0.236	0.265	0.101	0.01	0.01	0.04
Eu	0.09	0.10	0.099	0.110	0.050	0.01	-	-
Gd	0.35	0.31	0.386	0.480	0.236	0.01	-	0.06
Tb	0.05	-	-	-	-	-	-	0.02
Ho	0.08	-	-	-	-	-	0.02	0.04
Yb	0.28	0.32	0.337	0.340	0.269	0.02	-	0.16
Lu	0.03	0.06	-	-	-	-	-	0.03

1. Othris (*Menzies*, 1976); 2. Lanzo (*Menzies*, 1976); 3. Beni Bouchera (*Loubet et al.*, 1976); 4. Lherz (*Loubet et al.*, 1976); 5. Tinaquillo (*Loubet et al.*, 1976); 6. Troodos (*Kay and Senechel*, 1976); 7. Othris (*Menzies*, 1976); 8. Othris (*Menzies*, 1976).

basaltic magma either through cumulus processes (*Thayer*, 1946) or via fusion processes (*Boudier*, 1972; *Menzies*, 1974; *Dick*, 1976). Conventional reasoning would therefore require that the isotopic composition of the peridotites be similar to that of basalts ($^{87}Sr/^{86}Sr$ = 0.702-0.7035), unless one invokes disequilibrium fusion (*Graham and Ringwood*, 1971). Much of the published data on alpine peridotites (*Hurley et al.*, 1964; *Roe*, 1964; *Roe et al.*, 1965; *Steuber*, 1965; *Steuber and Murthy*, 1966; *Steuber*, 1969) appear to invalidate any simple genetic correlation of alpine ultramafics and basalts. Consequently many authors (*Bonatti et al.*, 1970; *Bonatti*, 1971; *Lussia-Berdou and Allegre*, 1973) devised complex models to account for the differences in isotopic composition (alpine peridotites $^{87}Sr/^{86}Sr$ = 0.706-0.7029). Much of this early work concluded that alpine peridotites were not related to basalts in any way - either via partial fusion or precipitation. Recently *Graham and Ringwood* (1971) and *Ringwood* (1975) proposed that alpine peridotites are residua left after extraction of magma produced by disequilibrium melting, assuming that strontium isotopic differences exist between mineral phases in the peridotite.

The data outlined in sections (a) to (f) argues very strongly for a genetic relationship between alpine peridotites and basalts, as does the paragenetic association of alpine peridotites and ophiolites (*Davies*, 1969; *Gass*, 1968). Strontium isotopic analyses of ophiolites and cumulate alpine bodies (*Lanphere*, 1968; *Jones et al.*, 1973; *Chapman et al.*, 1975; *Davies and Lass*, 1975) further strengthens the arguments for a strong genetic relationship.

Recent studies of alpine lherzolites by the author (*Menzies and Murthy*, 1976a,b,c, 1977, in press) have revealed that much of the published data must be treated with caution. Major problems exist in the interpretation of much of the data from alpine massifs: (1) Many of the ultramafic rocks are highly serpentinized but the origin of the serpentine is unknown; (2) The analyzed ultramafics are all harzburgites and dunites.

Isotopic analyses of clinopyroxene, orthopyroxene and olivine attest to a mantle origin for the Lanzo, Ronda and Beni Bouchera lherzolites since the lherzolites have an isotopic composition similar to basalt. This obviates the requirement for the highly complex models outlined to date. The low melting fraction in all of the analyzed lherzolites would have a $^{87}Sr/^{86}Sr$ ratio in the range of oceanic tholeiites. Thus melting of these lherzolites would produce a liquid with the isotopic composition of a tholeiite.

$Sr^{87/86}$ ratios for whole-rock lherzolites calculated from analyses of mineral data range from 0.7025-0.7028 (*Menzies and Murthy*, 1977 in press). The highly radiogenic value in one olivine may result from introduction of radiogenic Sr, since the olivine from this particular lherzolite was highly serpentinized. Further investigations will attempt to ascertain whether or not apparent isochron relationships, reflecting past mantle events, exist in alpine lherzolites.

Summary

A partial fusion hypothesis adequately explains the following features within the considered alpine peridotite massifs:

1. The monotonous uniformity of alpine-type harzburgite on a local and world-wide scale.

2. The presence of segregations which in a modal (*Dick*, 1976) and normative (*Boudier*, 1972) fashion resemble cotectic melts.

3. The co-existence of harzburgite gradational into lherzolite, both containing in situ dikelets or segregations.

4. The limited compositional range of olivine, enstatite and diopside.

5. The Cr-Al variation in the spinel phase which may result from interaction with basaltic melt.

6. The refractory major and trace element chemistry of the harzburgite-Mg/Mg+Fe > 0.90 and the past presence of a tholeiitic type liquid as indicated by U liquid-solid partition coefficient studies.

7. The similarity of lherzolite to estimates of primary mantle composition - Mg/Mg+Fe = 0.88.

8. The REE similarities of alpine lherzolites and computed source material for oceanic tholeiites. Calculated REE contents of liquids derived from alpine lherzolites are similar to those of basalt.

9. The light REE depleted nature of the harzburgites resembles computed residues, assuming a chondritic parent. However, fine details of the REE chemistry are incompatible with such a simple model.

10. The strontium isotopic chemistry of certain alpine lherzolites. All recent clinopyroxene analyses indicate that the low melting fraction has an $^{87}Sr/^{86}Sr$ ratio similar to that of oceanic tholeiite. In some cases lherzolite data (recalculated from mineral isotopic compositions) attests to a simple mantle origin for alpine lherzolites, without the complex models invoked to date.

Alpine harzburgites and lherzolites are interpreted as residua left after variable degrees of melting. Lherzolite is believed to be the residue left after removal of a nephelinitic or alkalic melt (small percent melt), while harzburgites resemble the residue left after loss of a basalt fraction (large percent melt).

Acknowledgements

The author wishes to thank Drs. C. Allen, D. Blanchard, E.D. Jackson, P. Henderson, and V.R. Murthy for their comments, discussion and analytical assistance in relation to this study. Part of this work was supported by N.E.R.C. (London) in partial fulfillment of the requirements for a Ph.D. at the University of Cambridge, and subsequent studies at N.A.S.A. and the University of Minnesota were supported by the Lindemann Committee (E.S.U.). The author thanks both these organizations, and Drs. W. Leeman, I.D. MacGregor and D.M. Shaw for helpful comments on an earlier copy of this manuscript.

APPENDIX A

Listing of alpine peridotite localities throughout the world.

Asia - *Hutchinson** (1971, 1972, 1975); *Hutchinson and Donau* (1969)

Britain - *Green* (1964)

California, U.S.A. - *Himmelberg and Coleman* (1968); *Moores* (1970); *Loney et al.* (1971); *James* (1971); *Springer* (1974); *Ehrenberg* (1975)

Canada - *MacGregor* (1962); *Church and Stevens* (1970); *Upadhyay et al.** (1971); *Malpas and Strong** (1975)

Cuba - *Kozary* (1968)

Cyprus - *Gass** (1967); *George** (1975)

Elba - *Klemm and Lammerer** (1975)

France - *Conquere* (1971)

Greece - *Moores** (1969); *Menzies** (1973); *Menzies and Allen** (1974); *Nicolas and Jackson* (1972)

Italy - *Boudier* (1972); *Boudier and Nicolas* (1972); *Bezzi and Piccardo** (1971)

Morocco - *Kornprobst* (1969); *Dickey* (1970)

New Caledonia - *Rodgers* (1973); *Guillon* (1975)

New Guinea - *Davies** (1968, 1969)

New Zealand - *Challis* (1963); *Blake and Landis* (1973); *Mossman* (1973); *Coombs et al.* (1976); *Sinton* (1976a,b)

North Carolina, U.S.A. - *Hartley* (1972)

Norway - *Carswell†* (1968)

Oregon - *Medaris* (1972); *Medaris and Dott* (1970); *Dick* (1975, 1976); *Himmelberg and Loney* (1973)

Oman - *Glennie et al.** (1974); *Smewing et al.** (1977)

Russia - *Edel'sthein* (19a6)

Spain - *Dickey* (1970)

Syria - *Smewing et al.** (1977)

Turkey - *Juteau* (1971, 1975*); *Thayer* (1964)

---

* Intimately associated with ophiolitic rocks as the metamorphic peridotite basement to the plutonic and volcanic suite.
† Caledonian type peridotites.

Venezuela - *MacKenzie* (1960)

Washington, U.S.A. - *Ragan* (1967); *Raleigh* (1965); *Southwick* (1974); *Dungan* (1974)

Yugoslavia - *Pamic* (1971, 1972); *Nicolas and Jackson* (1972)

References

Aumento, F., and R.D. Hyndeman, Uranium content of the oceanic upper mantle, *Earth Planet. Sci. Letts., 12*, 373-354, 1971.

Benson, W.N., The tectonic conditions accompanying the intrusion of basic and ultrabasic igneous rocks, *Natl. Acad. Sci. Mem. 19, 1st Memoir*, 1-90, 1926.

Bezzi, A., and G.B. Piccardo, Structural features of the Ligurian ophiolites: petrologic evidence for the oceanic floor of the North Appenines geosyncline: a contribution to the problem of the alpine-type gabbro-peridotite associations, *Mem. Soc. Geol. Ital., 10*, 53-63, 1971.

Blake, M.C., and C.A. Landis, The Dun mountain ultramafic belt - Permian oceanic crust and upper mantle in New Zealand, *J. Res. U.S. Geol. Surv. Section, 1*, 529-534, 1973.

Bonatti, E., Ancient continental mantle beneath oceanic ridges, *J. Geophys. Res., 76*, 3825-3831, 1971.

Bonatti, E., J. Honnorez, and G. Ferrara, Equatorial Mid-Atlantic ridge - petrologic and Sr isotopic evidence for an Alpine type rock assemblage, *Earth Planet. Sci. Lett., 9*, 247-256, 1970.

Boudier, F., Relations lherzolite-gabbro-dunite dans le massif de Lanzo (Alpes piemontaises): Exemple de fusion partielle, *These presentee a l'Institut des Sciences de la Nature de l'Universite de Nantes*, janvier 29, 1972.

Boudier, F., and A. Nicolas, Fusion partielle gabbroique dans la lherzolite de Lanzo, *Schw. Min. und Petrol. Mitt., 52*, 39-56, 1972.

Carswell, D.A., Picritic magma - residual dunite relationships in garnet peridotite at Kalskaret near Tafjord, S. Norway, *Contr. Mineral. Petrol., 19*, 97-124, 1968.

Challis, G.A., The petrology of the New Zealand ultramafic belt, *Unpublished Ph.D. Thesis, University of Cambridge, England*, August 1963.

Chapman, H.J., E.T.C. Spooner, and J. Smewing, Sr^{87} enrichment of ophiolitic rocks from Troodos, Cyprus indicates seawater interaction, *Trans. Amer. Geophys. Union (EOS), 56*, 1074, 1975.

Church, W.R., and R.K. Stevens, Mantle peridotite and the early Palaeozoic ophiolite complexes of the Newfoundland Appalachians, *Dept. Geol. Univ. Western Ont., Prel. Rept. 175*, 3 p., 1970.

Church, W.R., and R.K. Stevens, Early Palaeozoic ophiolite complexes of Newfoundland Appalachians as mantle - ocean crust sequences, *J. Geophys. Res., 76*, 1460-1466, 1971.

Conquere, F., Les pyroxenolites a amphibolites associees aux lherzolite du gisement de Lherz (Ariege, France): un exemple du role de l'eau au cours de la cristallisation fractionee des liquides issue de la fusion partielle de lherzolites, *Contr. Mineral. Petrol.*, 32-61, 1971.

Coombs, D.S., C.A. Landis, R.J. Norris, J.M. Sinton, D.J. Borns, and D. Craw, The Dun mountain ophiolite belt, New Zealand, its tectonic setting, constitution and origin, with special reference to the southern portion, *Am. J. Sci., 276*, 561-603, 1976.

Davis, T.E., and G.L. Lass, Strontium isotope composition of plutonic and volcanic rocks from the Jurassic Point Sal ophiolite, *Trans. Amer. Geophy. Union (EOS), 57*, 162, 1976.

Davies, H.L., Peridotite gabbro basalt complex in Eastern Papua an overthrust plate of oceanic mantle and crust, *Unpublished Thesis, Stanford University*, 88 p., 1969.

Dick, H., The Josephine peridotite, a refractory residue of the generation of andesite, *Trans. Amer. Geophy. Union (EOS), 44*, 464, 1975.

Dick, H.J.B., The origin and emplacement of the Josephine peridotite of southwestern Oregon, *Ph.D. Thesis, Yale University*, 409 p., 1976.

Dickey, J.S., Partial fusion products in alpine type peridotites, *Mineral. Soc. Am. Spec. Paper 3*, 33-59, 1970.

Dickey, J.S., and M.S. Yoder, Partitioning of Cr and Al between clinopyroxene and spinel, *Carnegie Inst. Yrbk.*, 384-392, 1971-72.

Dostal, J., S. Capedri, and F. Aumento, U as an indicator of the origin of the Tethyan ophiolites, *Earth Planet. Sci. Letts., 26*, 345-352, 1975.

Dungan, M.A., The origin, emplacement, and metamorphism of the Sultan mafic ultramafic complex North Cascades Snohomish County, Washington, *Ph.D. Dissertation, Univ. of Washington, Seattle, U.S.A.*, 1974.

Dungan, M.A., and H.G. Avé Lallemant, Formation of small dunite bodies from harzburgite by metasomatic transformation in the Canyon Mountain ophiolite Oregon, *Proc. Chapman Conference on "Partial Melting in the Earth's Upper Mantle", Brookings, Oregon*, 1977.

Edel'sthein, I.L., Petrology and Ni content of ultrabasic intrusions in Tobol-Buryktul area of the southern Urals - Magmatizm, Metamorfizm, Mettalogeniya Urala, *Akad. Nauk. SSR Ural'sk Filal, Gorn - Geol. Inst. Tr Pervogo Ural'sk Petrogr. Soveshch, Sverdlovsk 961*, 319-323, 1963.

Ehrenberg, S.N., Feather river ultramafic body, Northern Sierra Nevada, California, *Geol. Soc. Amer. Bull., 86*, 1235-1243, 1975.

Faure, G., and J.L. Powell, *Strontium Isotope Geology*, 188 p., Springer-Verlag, New York, 1972.

Frey, F.A., Rare earth abundances in a high temperature peridotite intrusion, *Geochim. Cosmochim. Acta*, *33*, 1429-1477, 1969.

Frey, F.A., Rare earth abundances in alpine ultramafic rocks, *Phys. Earth Planet. Int.*, *3*, 323, 1970.

Frey, F.A., M.A. Haskin, and L.A. Haskin, Rare earth abundances in some ultramafic rocks, *J. Geophys. Res.*, *76*, 2057-2070, 1971.

Garmann, L.B., A.O. Brunfelt, K.G. Finstad, and K.S. Heier, Rare earth element distribution in basic and ultrabasic rocks from west Norway, *Chem. Geol.*, *15*, 103-116, 1975.

Gass, I., The ultrabasic volcanic assemblage of the Troodos massif, Cyprus, in *Ultramafic and Related Rocks*, edited by P. Wyllie, pp. 121-134, Wiley, New York, 1967.

George, D., The internal structure of the Troodos ultramafic complex, Cyprus, *Ph.D. Thesis, State University of New York, Stony Brook*, May 1975.

Graham, A.L., and A.E. Ringwood, Lunar basalt genesis: the origin of the europium anomaly, *Earth Planet. Sci. Lett.*, *13*, 105-115, 1971.

Green, D.H., A re-study and re-interpretation of the geology of the Lizard Peninsula, Cornwall, *Roy. Geol. Soc. of Cornwall*, 87-114, 1964.

Green, D.H., and A.E. Ringwood, The stability fields of aluminous pyroxene peridotite and garnet peridotite and their relevance in upper mantle structure, *Earth Planet. Sci. Lett.*, *3*, 151-160, 1967.

Griffin, W.L., and V.R. Murthy, Distribution of K, Rb, Sr and Ba in some minerals relevant to basalt genesis, *Geochim. Cosmochim. Acta*, *33*, 1389-1414, 1969.

Guillon, J.-H., Les massifs peridotitiques de Nouvelle-Caledonie, *Mem. ORSTOM*, *76*, 120 p., 1975.

Hartley, M.E. III, Ultramafic and related rocks in the vicinity of Lake Chatuge, Towns County, Georgia and Clay county, North Carolina, *Georgia Geol. Surv. Bull. 85*, 1972.

Henderson, P., Reaction trends shown by Cr-spinels of the Rhum layered intrusion, *Proc. of the Chromium Conf., Geophys. Lab., Carnegie Inst., Washington*, 1974.

Himmelberg, G.R., and R.G. Coleman, Chemistry of primary minerals and rocks from the Red Mountain del Puerto ultramafic mass, California, *Geol. Surv. Res. 1968 U.S.G.S. Prof. Paper 600-C*, C18-C26, 1968.

Himmelberg, G.R., and R.A. Loney, Petrology of the Vulcan Peak alpine-type peridotite, S.W. Oregon, *Bull. Geol. Soc. Amer. 84*, 1585-1600, 1973.

Hurley, P.M., H.W. Fairbairn, and W.H. Pinson, Rb-Sr relationships in serpentine from Mayaguez,Puerto Rico and dunite from St. Paul's rocks: a progress report, *NAS-NRC, 1188*, 149-151, 1964.

Hutchison, C., An alpine association of metabasites and ultrabasic rocks in Davel Bey, East Sabah, Borneo, *Overseas Geol. and Mineral. Resources, 10*, 289-308, 1971.

Hutchison, C., Alpine type chromite in North Borneo with special reference to Darvel Bay, *Amer. Mineralogist, 57*, 835-856, 1972.

Hutchison, C.S., Ophiolite in Southeast Asia, *Geol. Soc. Amer. Bull., 86*, 797-806, 1975.

Hutchison, C., and T.J. Dhonau, Deformation of an alpine ultramafic association in Darvel Bay East Sabah Malaysia, *Geologie en Mijnbouw, 48*, 481-494, 1969.

Irvine, T.N., Chromian spinel as a petrogenetic indicator. Part I: Theory, *Can. J. Earth Sci., 2*, 1965.

Irvine, T.N., Chromian spinel as a petrogenetic indicator. Part II: Petrogenetic applications, *Can. Jour. Earth Sci., 4*, 1967.

Irvine, T.N., and T.C. Findlay, Alpine type peridotite with particular reference to the Bay of Islands igneous complex, *Univ. of Ottawa, Earth Phys. Branch, Publ. 42*, 97-128, 1972.

Jackson, E.D., and T. Thayer, Some criteria for distinguishing between stratiform concentric, and alpine peridotite gabbro complexes, *Submitted to Section 2, Petrology, I.G.C. 24th, Montreal*, 1972.

James, O.B., Origin and emplacement of the ultramafic rocks of the Emigrant Gap area, California, *J. Petrol., 2*, 523, 1971.

Jones, L.M., M.E. Hartley, and R.L. Walker, Strontium isotope composition of Alpine type ultramafic rocks in the Lake Chatuge district Georgia N. Carolina, *Contrib. Mineral. Petrol., 38*, 321-327, 1973.

Juteau, T., Petrogenese des napes d'Antalya (Taurus lycien oriental, Turquie) Sci. de la Terre, *Nancy, 15*, 265-288, 1971.

Juteau, T., Les ophiolites des napes d'Antalya (Taurides occidentales Turquie) Sci. de la Terre, *Mem. 32, These, Universite de Nancy*, 692 p., 1975.

Kay, R., and R.G. Senechel, Rare earth geochemistry of the Troodos ophiolite, *J. Geophys. Res., 81*, 964-970, 1976.

Kays, M.A., Metamorphism and the occurrence of ultramafic-mafic complexes, western Palaeozoic and Triassic belt, northern Klamath mountains, Oregon and northern California, *Proc. Chapman Conference on "Partial Melting in the Earth's Upper Mantle", Brookings, Oregon*, 1977.

Klemm, D.D., and B. Lammerer, A basic to ultrabasic extrusion in East Elba, *Chem. Geology, 13*, 23-28, 1974.

Komarov, A.N., A.S. Zmitkov, L.V. Dmitriev, and L.L. Leonava, Uranium distribution in ultrabasics of Indian Ocean rift zones, *Geochem. International, 10*, 217-224, 1973.

Kornprobst, J., Le massif ultrabasique des Beni Bouchera (Rif interne, Maroc) etude des peridotites de haute temperature et de haute pression, et des pyroxenolites, a grenat et sans grenat, qui leur sont associes, *Contrib. Mineral. Petrol., 23*, 283, 1969.

Kozary, M.T., Ultramafic rocks in thrust zones of N.W. Oriente Province, Cuba, *Amer. Assoc. Petrol. Geol. Bull., 52*, 2298-2317, 1968.

Lanphere, M.A., Sr-Rb-K and Sr isotopic relationships in ultramafic rocks, S.E. Alaska, *Earth Planet. Sci. Lett., 4*, 185-190, 1968.

Lanphere, M., Strontium isotope relations in the Canyon Mountain, Oregon and Red Mountain, Cal., ophiolites, *Trans. Amer. Geophys. Union (EOS), 54*, 1220, 1973.

Lindsley Griffin, N., D.M. Rohr, J.R. Griffin, and E.M. Moores, Geology of the Lovers Leap area, Eastern Klamath Mountains, Cal., *Geol. Soc. Sacramento, Ann. Field Trip Gdbk.*, edited by D.F.R. McGeary, 1974.

Loney, R.A., G.R. Himmelberg, and R.G. Coleman, Structure and petrology of the alpine-type peridotite at Burro mountain, California, U.S.A., *J. Petrol., 12*, 245-309, 1971.

Loubet, M., N. Shimizu, and C.J. Allegre, Rare earth elements in alpine peridotites, *Contrib. Mineral. Petrol., 53*, 1-12, 1975.

MacGregor, I.D., Geology, petrology and geochemistry of the Mount Albert and associated ultramafic bodies of central Gaspe, Quebec, *Unpublished M.S. Thesis, Queen's University, Kingston, Ontario*, 288 p., 1962.

MacKenzie, D.B., High temperature alpine type peridotite from Venezuela, *Geol. Soc. Amer. Bull., 71*, 303-318, 1960.

Malpas, J., and D.F. Strong, A comparison of chrome spinels in ophiolites and mantle diapirs of Newfoundland, *Geochim. Cosmochim. Acta, 39*, 1045-1060, 1975.

Medaris, L.G., High pressure peridotites in southwestern Oregon, *Geol. Soc. Amer. Bull., 83*, 41-58, 1972.

Medaris, L.G., Coexisting spinels and silicates in alpine peridotites of the granulite facies, *Geochim. Cosmochim. Acta, 39*, 947-958, 1975.

Medaris, L.G., and R.H. Dott, Mantle derived peridotites in southwestern Oregon: relation to plate tectonics, *Science, 169*, 971-974, 1970.

Menzies, M.A., Mineralogy and partial melt textures within an ultramafic-mafic body, Greece, *Contrib. Mineral. Petrol., 42*, 273-285, 1973.

Menzies, M.A., Petrogenesis of the Makrirrakhi ultramafic complex (part of the Othris ophiolite), *Unpublished Ph.D. Thesis, Cambridge, England*, 1974.

Menzies, M.A., Spinel compositional variation in the crustal and mantle lithologies of the Othris ophiolite, *Contrib. Mineral. Petrol., 51*, 303-309, 1975.

Menzies, M.A., Rare earth geochemistry of fused alpine and ophiolitic lherzolites. Part I: Othris, Lanzo and Troodos, *Geochim. Cosmochim. Acta, 41*, 645-656, 1976.

Menzies, M.A., Oceanic lithosphere - evidence from the Mediterranean, *Trans. Amer. Geophys. Union (EOS), 57*, 342, 1976.

Menzies, M.A., and C.A. Allen, Plagioclase lherzolite residual mantle relationships within two eastern Mediterranean ophiolites, *Contrib. Mineral. Petrol.*, *45*, 197-213, 1974.

Menzies, M.A., D. Blanchard, J. Brannon, and R. Korotev, Mediterranean lherzolites: rare earth evidence of their primitive nature, *Trans. Amer. Geophys. Union (EOS)*, *72*, 29, 1975.

Menzies, M.A., and V.R. Murthy, Strontium isotopic compositions of clinopyroxenes from tectonite alpine lherzolites, *Geol. Soc. Amer. Abs. with Programs, Denver*, *8*, 1009, 1976a.

Menzies, M.A., and V.R. Murthy, Sr-isotopic composition of clinopyroxenes from some Mediterranean alpine lherzolites, *Geochim. Cosmochim. Acta*, *40*, 1577-1581, 1976b.

Menzies, M.A., and V.R. Murthy, Strontium isotope geochemistry of alpine tectonite lherzolites - compatible with a mantle origin, *Trans. Amer. Geophys. Union (EOS)*, *57*, 1025, 1976c.

Menzies, M.A., D. Blanchard, and J. Jacobs, Rare earth geochemistry of alpine tectonite lherzolites from northern California, *Geol. Soc. Amer. (abs.)*, *9*, 465, 1977a.

Menzies, M.A., D. Blanchard, J. Brennon, and R. Korotev, Rare earth geochemistry of fused alpine and ophiolitic lherzolites. Part II - Lanzo, Beni Bouchera and Ronda, *Cont. Mineral. Petrol.*, 1977b, in press.

Menzies, M.A., and V.R. Murthy, Strontium isotope geochemistry of the constituent minerals of alpine tectonite lherzolites, *Earth Planet. Sci. Letters*, 1977, in press.

Moores, E.M., Petrology and structure of the Vourinos ophiolitic complex of Northern Greece, *G.S.A. Spec. Paper 118*, 60 p., 1969.

Moores, E.M., Ultramafics and orogeny with models of the U.S. Cordillera and the Tethys, *Nature*, *228*, 837-842, 1970.

Mossman, D.J., Geology of the Greenhills ultramafic complex, Bluff peninsula, Southland, New Zealand, *Geol. Soc. Amer. Bull. 84*, 39-62, 1973.

Nicolas, A., and E.D. Jackson, Repartition en deux provinces des peridotites des chaines alpines logeant la Mediterranee: implications geotectonique, *Schw. Min. und Pet. Mitt.*, *52*, 479-495, 1972.

Page, B.M., Oceanic crust and mantle fragment in subduction complex near San Luis Obispo, California, *Geol. Soc. Amer. Bull.*, *83*, 957-972, 1972.

Raleigh, C.B., Structure and petrology of an alpine peridotite on Cypress Island, Washington, U.S.A., *Beitr. Miner. Petrogr.*, *11*, 719-741, 1965.

Ragan, D.M., The Twin Sisters dunite, Washington, in *Ultramafic and Related Rocks*, edited by P.J. Wyllie, pp. 160-167, Wiley, New York, 1967.

Ringwood, A.E., Chemical evolution of the terrestrial planets, *Geochim. Cosmochim. Acta*, *30*, 41-104, 1966.

Ringwood, A.E., Composition of the upper mantle (Chap. 3); The pyrolite model (Chap. 5), in *Composition and Petrology of the Earth's Mantle*, edited by Summersgill and Bradley, 618 p., McGraw-Hill, 1975.

Rodgers, K.A., Cr-spinels from the Massif du Sud, S. New Caledonia, *Min. Mag., 3a*, 326-339, 1973.

Roe, G.D., Rubidium-strontium analyses of ultramafic rocks and the origin of peridotites, *Ph.D. Thesis, Department of Geology and Geophysics, M.I.T. (University Microfilm)*, 1964.

Roe, G.D., W.H. Pinson, and P.M. Hurley, Rb-Sr evidence for the origin of peridotites, *Trans. Amer. Geophys. Union (Abst.), 46*, 186, 1965.

Schilling, J.G., Rare earth variations across normal segments of the Rekjanes ridge 60-53 N, Mid-Atlantic Ridge 29 S and East Pacific ridge 2-19 S and evidence of the composition of the underlying low-velocity layer, *J. Geophys. Res., 80*, 1459-1473, 1975.

Seitz, M.G., and S.R. Hart, Uranium and boron distributions in some oceanic ultramafic rocks, *Earth Planet. Sci. Letts., 21*, 97-105, 1973.

Shimizu, N., Trace element contents of clinopyroxenes from garnet lherzolites in kimberlites, *D.T.M. Ann. Rep. 1972-1973*, 272, 1973.

Shimizu, N., and S.R. Hart, Rare earth element concentrations in clinopyroxene from an ocean-ridge lherzolite, *Carnegie Inst. Yrbk. 73*, 964-967, 1974.

Sinton, J.M., Equilibration and partial re-equilibration of alpine peridotite, Red Mountain, New Zealand, *Trans. Amer. Geophys. Union (EOS), 57*, 597, 1976.

Smewing, J.D., I.M. Elboushi, J.-F. Parrot, and I.G. Gass, Similar ophiolite sequences from the Troodos massif, the Oman mountains and the Baer Bassit region of Syria, *Contr. Mineral. Petrol.*, 1977, in prep.

Southwick, D.L., Geology of the alpine type ultramafic complex near Mount Stuart, Washington, *Geol. Soc. Amer. Bull., 85*, 391-402, 1974.

Springer, R.K., Contact metamorphosed ultramafic rocks in the western Sierra Nevada foothills, California, *J. Petrol., 15*, 160-195, 1974.

Steinmann, G., Geologische Beobachtungen in den Alpen II: Die Schardt'sche Uberfantungstheorie und die geologische Bedeutung der Tiefseeabsatze und der ophiolithischen Massengesteine, *Ber. Nat. Ges. Freiburg 1, Bd. 16*, 44-65, 1905.

Steinmann, G., Die ophiolithische Zonen in dem mediterranean Keltengebirgen, *14th Intl. Geol. Cong. Madrid*, 638-667, 1927.

Steuber, A., A geochemical study of ultramafic rocks, *Ph.D. Dissertation, Geology, U.C. San Diego (University Microfilms, Inc.)*, 1965.

Steuber, A.M., Abundances of K, Rb, Sr, and Sr isotopes in ultramafic rocks and minerals from western North Carolina, *Geochim. Cosmochim. Acta, 33*, 543-552, 1969.

Steuber, A.M., and V.R. Murthy, Sr isotopic abundances and alkali element abundances in ultramafic rocks, *Geochim. Cosmochim. Acta, 30*, 1243-1259, 1966.

Stevens, R.K., D.F. Strong, and B.F. Kean, Do some eastern Appalachian ultramafic rocks represent mantle diapirs produced above a subduction zone?, *Geology, 2*, 175-178, 1974.

Thayer, T., Preliminary chemical correlation of chromite with the containing rocks, *Economic Geology, 41*, 202, 1946.

Thayer, T., Flow layering in alpine peridotite gabbro complexes, *Min. Soc. Amer. Spec. Paper 1*, 55-61, 1963.

Thayer, T., Principal features and the origin of podiform chromite deposits, and some observations on the Guleman-Soridag District, Turkey, *Econ. Geol. 59*, 1497, 1964.

Thayer, T., Chemical and structural relations of ultramafic and feldspathic rocks in alpine intrusive complexes, in *Ultramafic and Related Rocks*, edited by P.J. Wyllie, Wiley, New York, 1967.

Thayer, T., Gravity differentiation and magmatic reemplacement of podiform chromite deposits, in *Magmatic Ore Deposits*, edited by H.D.B. Wilson, *Econ. Geol. Mon. 4*, 132-146, 1969.

Thayer, T., Chromite segregations as petrogenetic indicators, *Geol. Soc. South Africa Spec. Publ. 1*, 380-396, 1970.

Upadhyay, H.D., J.F. Dewey, and E.P.W. Neale, The Betts cove ophiolite complex, Newfoundland, Appalachian Oceanic Crust and Mantle, *Geol. Assoc. Can. Proc. 24*, 27-34, 1971.

COMPARISON OF Rb/Sr, U/Pb, AND RARE EARTH CHARACTERISTICS OF SUB-CONTINENTAL AND SUB-OCEANIC MANTLE REGIONS

William P. Leeman*
Geology Department
Oregon State University
Corvallis, Oregon 97331

Abstract

Radiogenic isotope ratios and abundances of certain trace elements display systematic variations between ocean-floor and continental tholeiitic flood basalts. Mid-ocean ridge (MOR) tholeiites generally contain less radiogenic Pb and Sr, more radiogenic Nd, and display consistent depletion in light rare earth elements (REE) compared to continental tholeiites. In addition, significant variations in these parameters have been detected within each of these classes of tholeiitic basalts. Because these basalts are probably formed by relatively large degrees of melting, it is likely that they record significant isotopic and trace element differences between (and within) sub-oceanic and sub-continental mantle regions. On a gross scale it would appear that the differences noted above are consistent with relative depletions of U/Pb, Rb/Sr, and light REE in the sub-oceanic mantle that have persisted for times on the order of 10^9 years. The isotopic data in particular suggest profound implications regarding mantle dynamics -- namely, large volumes of sub-continental upper mantle material apparently have failed to "mix" by convective or other means with the more voluminous sub-oceanic mantle.

Sufficient data are not yet available to show conclusively that such differences are generally inherent to the respective source regions, and other processes, such as crustal contamination, may account in part for some of the observed differences between oceanic and continental tholeiites. However, in favorable cases where data are available for two or more isotopic systems (e.g., Rb-Sr and U-Pb), it can be shown that crustal contamination is probably not a significant factor. This review emphasizes the need for systematic study of several isotopic systems in additional suites of continental and MOR basalts from restricted geographic areas.

Introduction

Geochemical and petrological studies of basaltic lavas have been widely employed to understand the nature of upper mantle source regions of their parental magmas. Despite the strong possibility that during ascent to the surface many basaltic magmas have undergone polybaric crystallization and perhaps wall-rock reaction, which have modified their chemical compositions (*O'Hara*, 1977), certain elemental and isotopic ratios may be considered representative of primary magmas and can thus yield constraints on the composition of the upper mantle. This paper summarizes investigations of lead and strontium isotopic compositions and rare earth element

---

* Present address: Geology Department, Rice University, Houston, Texas 77001

(REE) relative abundances in basalts from oceanic basins and from the continental shields and contrasts some geochemical features inferred for sub-oceanic and sub-continental mantle regions.

Emphasis is placed on discussion of mid-ocean ridge (MOR) tholeiites and continental flood basalts because these lavas typically display only limited diversity in bulk composition (on a local scale) while being erupted in great volume and (or) over long periods of time. For these reasons such basalts are considered to have undergone minimal differentiation and they may approximate primary magmas. Geochemical studies of continental basalts still lag behind those of oceanic basalts because of the common prejudice that the former lavas have been modified by interactions with sialic material as they ascended through the continental crust. Crustal contamination must be regarded as a viable process, but in favorable cases, it can be shown to have had little or no significance. Detailed studies of basalts from the Snake River Plain and Columbia River Plateau, in the northwestern United States, for example, provide strong evidence that many of these lavas have not been contaminated by crustal material. Perhaps this is true for many, if not most, continental basalts elsewhere in the world. If the isotopic and trace element characteristics of basalts discussed herein are representative of the source regions for these lavas, it can be shown that sub-oceanic and sub-continental mantle materials are distinct in composition and that these differences have existed for at least 10^9 years.

Sr and Pb Isotopic Compositions

It is conventionally regarded that Sr and Pb isotopic compositions of primary magmas are representative of their mantle source regions (i.e., isotopic homogeneity is attained between melt and residue) because the small differences in mass between nuclides of these elements preclude any significant isotopic fractionation during formation of melt or its subsequent chemical differentiation. In any event, Sr isotopic ratios are routinely normalized to correct for mass fractionation that occurs during mass spectrometric analysis. Variations in isotopic composition of mantle-derived volcanic rocks are well documented (see discussion below) and can be attributed to contamination by crustal materials, mixing of magmas having different isotopic compositions, isotopic disequilibrium during partial melting, and heterogeneity in the mantle source regions. Of these possibilities, the last seems most viable.

Contamination models are discussed separately for oceanic and continental basalts in the next sections, and it is concluded that they are inadequate to explain isotopic variations in oceanic and many continental basalts. Magma mixing is strongly indicated for some localities (e.g., Iceland-Reykjanes Ridge; *Hart et al.*, 1973; *Sun et al.*, 1975), but the question still remains of how isotopic differences are generated in the respective magmas. Disequilibrium melting of mantle material that is isotopically inhomogeneous on a mineralogical scale has been suggested (*O'Nions and Pankhurst*, 1973, 1974; *Flower et al.*, 1975) as a way in which magmas having different isotopic compositions can be generated from mantle that is homogeneous on a regional scale. These authors suggest that phases having low melting temperatures (e.g., micas, amphiboles, apatite, etc.) could impart their isotopic compositions to early formed melts, and that as melting proceeds the isotopic composition of the liquid approaches that of the bulk source material. Isotopic inhomogeneities between constituent minerals in ultramafic xenoliths have been demonstrated for both Sr and Pb

(*Peterman et al.*, 1970; *Steuber and Ikramuddin*, 1974; *Dasch and Green*, 1975; *Zartman and Tera*, 1973; *Morioki and Kigoshi*, 1975) but it remains to be seen whether or not such heterogeneities can be preserved at the high temperatures required to produce basaltic melts. *Hofmann and Hart* (1975) and *Nelson and Dasch* (1976) suggest that isotopic disequilibrium between minerals is favored at subsolidus temperatures by the low solid diffusion rates expected for Sr (and possibly Pb), but that higher temperatures of melting will favor greatly increased diffusion rates and this factor plus the presence of a melt phase, which would act as a diffusion bridge, would result in rather effective isotopic homogenization over reasonably short periods of time. Furthermore, it is difficult to reconcile with the disequilibrium melting model the fact that on some oceanic islands tholeiitic, alkalic, and nephelinitic basalts, which form by different degrees of partial melting (*Gast*, 1968), have essentially the same $^{87}Sr/^{86}Sr$ ratio. Considerations such as these suggest that equilibrium melting is more likely involved in the production of basaltic magmas (though this question is not fully resolved) and this assumption is adopted in the following discussion.

Numerous authors have adopted the view that the mantle is heterogeneous with regard to Sr and Pb isotopic composition. Such heterogeneities reflect differences in Rb/Sr, U/Pb, and Th/Pb ratios that have existed in the mantle for sufficient time that different amounts of radiogenic Sr and Pb could accumulate from place to place. The Pb and Sr isotopic systematics discussed below indicate that such heterogeneities have existed for times on the order of 10^9 years, and may reflect a time of major chemical differentiation of the mantle. It is also possible that variations in Rb/Sr, U/Pb, and Th/Pb were established by continuous or multi-episodic processes that operated early in the Earth's history; if so, age information obtained from the Pb and Sr data corresponds to an "average" time since the mantle heterogeneities were established. It might be expected that volcanic rocks from different oceanic and continental regions might "sample" mantle regions of differing age and isotopic composition. The following sections discuss the isotopic data from these regions.

A. Oceanic Regions

Faure and Hurley (1963), *Hedge and Walthall* (1963) and *Gast, Tilton, and Hedge* (1964) first clearly showed that there are systematic differences in Sr and Pb isotopic composition in volcanic rocks from individual oceanic islands. Considerable subsequent work has confirmed this observation and recent high precision isotopic analyses (e.g., *O'Nions and Pankhurst*, 1973, 1974; *Hart et al.*, 1973; *Sun*, 1973; *Sun and Jahn*, 1975; *Grant et al.*, 1976; *Duncan and Compston*, 1976) have revealed previously undiscovered detail in these variations. The reported range in $^{87}Sr/^{86}Sr$ observed for oceanic island basalts is 0.7028 to 0.7082. *Hedge and Peterman* (1970) and *Hart* (1971) showed that MOR-type basalts (including ocean floor basalts sampled by deep sea drilling) have systematically lower $^{87}Sr/^{86}Sr$ ratios ranging from 0.7023 to 0.7035, with most less than 0.7030. Rb/Sr ratios measured in MOR basalts are too low to have produced their present-day $^{87}Sr/^{86}Sr$ ratios within 4.6 b.y., the accepted age of the Earth. Because Rb/Sr ratios are likely to *increase* in the liquid during partial melting, it seems probable that the residue from source regions for MOR basalt have been depleted in Rb (*Gast*, 1968). Note that residual phlogopite in the source region could result in a decrease in Rb/Sr in the melt, but for the degree of melting (about 30%) suggested for MOR basalts

(*Gast*, 1968) it is improbable that phlogopite would remain. The persistence of residual phlogopite has been suggested (e.g., *Beswick*, 1976). *Hofmann and Hart* (1975) have summarized the Sr isotopic data collected since 1970 for oceanic basalts, and they suggest that the mantle is compositionally inhomogeneous not only laterally but also vertically because "volcanoes situated near a mid-ocean ridge usually erupt lavas that differ in isotopic composition from the mid-ocean ridge material itself."

The Pb isotopic data for oceanic basalts (summarized by *Sun and Hanson*, 1975) support this hypothesis. As with the Sr data, MOR basalts display a much smaller range in Pb isotopic composition than do oceanic island basalts and MOR basalts have generally less radiogenic $^{206}Pb/^{204}Pb$ and $^{208}Pb/^{204}Pb$ ratios. Thus, it seems that source regions for MOR basalts have lower U/Pb and Th/Pb (also lower Th/U) ratios than source regions for most oceanic island basalts. This conclusion is supported by lower U/Pb and Th/U observed in MOR basalts (e.g., *Tatsumoto et al.*, 1965; *Church and Tatsumoto*, 1975) compared to oceanic island basalts (e.g., *Tatsumoto*, 1966a, 1966b; *Gast*, 1969; *Oversby and Gast*, 1970; *Oversby et al.*, 1971).

It is noteworthy that basalts (and differentiated lavas in some cases) from several oceanic islands have $^{87}Sr/^{86}Sr$ ratios in excess of 0.705 and as high as 0.7082 (*Hedge et al.*, 1972, 1973; *O'Nions and Pankhurst*, 1974; *White et al.*, 1975; *Duncan and McDougall*, 1976). These values are higher than $^{87}Sr/^{86}Sr$ ratios observed in many continental basalts (see next section), and indicate that the source regions for these lavas have higher time-averaged Rb/Sr ratios than source regions for many other oceanic island and MOR basalts. Such elevated $^{87}Sr/^{86}Sr$ ratios could perhaps also be attributed to some form of contamination involving crustal materials. However, this possibility seems unlikely in most cases because (1) sialic crust is generally absent in oceanic basins, (2) other potential contaminants such as oceanic sediments, altered rocks in the oceanic crust or in volcanic piles, and seawater have compositions that are inadequate to cause the observed variations in isotopic composition of oceanic volcanic rocks without obviously affecting other compositional characteristics of these lavas (e.g., Ba and alkali element contents, oxygen isotopic composition, etc.), (3) for some individual islands Sr isotopic compositions are consistent despite wide variation in bulk composition of the lavas (e.g., alkali basalt to phonolite). In addition, the Sr and Pb isotopic compositions are remarkably uniform for fresh MOR-derived basalts from all oceans and display no substantive change with age or geographic location, except possibly near such hot spots as Iceland (*Hart et al.*, 1973; *Sun et al.*, 1975) and the Azores (*White et al.*, 1975), where mixing of different magmas or source materials has been postulated.

If it is accepted that the sub-oceanic mantle is heterogeneous in isotopic and chemical composition, the question arises of how long such heterogeneities have existed. Some indication of this time can be derived from Pb isotopic studies. $^{207}Pb/^{204}Pb$ and $^{206}Pb/^{204}Pb$ ratios in oceanic island and MOR basalts are strongly correlated and define a linear trend that can be interpreted as a secondary isochron (*Gale and Musset*, 1973). In physical terms, such a relationship is readily attributed to derivation of these magmas from source regions having a continuum of different U/Pb ratios but uniform isotopic composition that were established at a common time, perhaps during some major chemical differentiation of the sub-oceanic mantle. It is unlikely that this trend reflects mixing of mantle-derived Pb with a crustal Pb component because oceanic sediments (and seawater) have Pb isotopic compositions that fall well off the trend for the volcanic rocks, having higher $^{207}Pb/^{204}Pb$ ratios for any given $^{206}Pb/^{204}Pb$ ratio (*Chow and Patterson*, 1962; *Church and Tatsumoto*, 1975; *Meijer*, 1976), and seawater has Pb contents at least four orders of magnitude lower than those

of MOR and other basalts. Secondary isochron interpretations of $^{207}Pb/^{204}Pb$-$^{206}Pb/^{204}Pb$ plots for individual oceanic islands or MOR segments yield ages ranging between 0.95 and 2.5 b.y. for the time since U/Pb variations were established in their respective source regions (*Sun*, 1973; *Sun et al.*, 1975; *Sun and Jahn*, 1975; *Church and Tatsumoto*, 1975; *Tatsumoto*, 1977). *Brooks et al.* (1976) postulated that averaged $^{87}Sr/^{86}Sr$ and Rb/Sr ratios for MOR and oceanic island tholeiitic basalts define a "mantle isochron" corresponding to an age of about 1.6 b.y. for the time since Rb/Sr heterogeneities were established in the sub-oceanic mantle. A similar Rb-Sr mantle isochron for basalts from French Polynesia suggests a minimum age of about 1.2 b.y. for their source region (*Duncan and Compston*, 1976). The similarity between the Rb-Sr and U-Pb systematics suggests that the isochron trends obtained have real age significance and do not represent, for example, some random mixing process.

In summary, the Sr and Pb isotopic data for oceanic volcanic rocks strongly suggest that the sub-oceanic mantle is heterogeneous in such ratios as Rb/Sr, U/Pb and Th/U and that all of these ratios are lower in the source regions for MOR basalts. These data are compatible with models involving a vertically stratified mantle with an upper "depleted" layer from which MOR basalts are generated and deeper, more fertile material from which oceanic island (especially alkalic) basalts are derived (e.g., *Sun and Hanson*, 1975; *Hofmann and Hart*, 1975). Other models are possible, of course, but the important conclusions are that oceanic basalts are derived from heterogeneous source regions and that such heterogeneities probably have existed for at least 10^9 years.

B. Continental Tholeiites

It has long been recognized (*Faure and Hurley*, 1963; *Hedge and Walthall*, 1963) that continental basalts differ from oceanic basalts in having generally higher $^{87}Sr/^{86}Sr$ ratios. There are comparatively few Pb isotopic analyses of these rocks, but *Doe* (1967, 1968) noted that basalts from cratonic regions of western North America apparently were derived from source regions having higher $^{238}U/^{204}Pb$ ratios than source regions for oceanic basalts.

Leeman and Manton (1971, Fig. 4) summarized most of the Sr isotopic data and suggested that initial $^{87}Sr/^{86}Sr$ ratios of continental tholeiites erupted over the last 3 b.y. consistently have been higher than those expected for MOR tholeiite source regions, assuming that the latter increased linearly (due to ^{87}Rb decay) from the primordial value of 0.69898 (*Papanastassiou and Wasserburg*, 1969) to the present-day values of about 0.703. Such a linear extrapolation requires that the time-integrated Rb/Sr ratio for the sub-oceanic mantle was about 0.025, whereas that inferred for continental tholeiite sources is at least 0.04. Because Rb/Sr ratios in the mantle may have varied throughout time in a more complicated manner (*Hart and Brooks*, 1970; *Faure and Powell*, 1972), the following discussion will be restricted to Mesozoic or younger basalts from which we can draw a comparison between "modern" sub-oceanic and sub-continental mantle regions. Initial $^{87}Sr/^{86}Sr$ ratios in some representative continental tholeiite suites are summarized in Table 1. Of these, Pb isotopic data are available for only the Snake River Plain-Yellowstone (*Leeman et al.*, 1978) and Columbia River Plateau (*Church*, 1977) basalts. Based on the decay constants and growth curve parameters adopted by *Tatsumoto et al.* (1973), the Pb in these basalts was derived from a source having a present-day $^{238}U/^{204}Pb$ value near 8.1; the corresponding value for oceanic basalt source regions is about 7.8, which is significantly distinct.

The differences in Sr and Pb isotopic compositions between oceanic and continental tholeiites can be attributed to (1) primary differences in composition between the respective source regions, or (2) contamination of the latter basalts by sialic crustal material. These alternatives will be examined below for the Snake River Plain-Yellowstone basalts which have been studied in the greatest detail.

At present, isotopic evidence against crustal contamination of continental tholeiites is rarely conclusive, and some rocks of probable hybrid origin have been described (e.g., *Pankhurst*, 1969; *Leeman and Manton*, 1971; *Faure et al.*, 1974). In the Snake River Plain-Yellowstone province, however, such evidence is seemingly incompatible with significant amounts of crustal contamination of the voluminous olivine tholeiites there. Briefly, the evidence is summarized as follows:

1. $^{87}Sr/^{86}Sr$ ratios vary only from 0.7055 to 0.7075 in the tholeiites, but over 80 percent of the analyzed samples are within 0.0005 of the mean value of 0.7065. This range is only about twice the two-sigma uncertainty in the individual analyses. In contrast, $^{206}Pb/^{204}Pb$ ratios vary from 16.10 to 18.84 (nearly 20 percent variation) and with $^{207}Pb/^{204}Pb$ ratios define a precise linear array (all samples lie within two sigma analytical error of the best-fit line) which is interpreted as a secondary isochron (*Leeman et al.*, 1978). The slope of this isochron indicates that heterogeneities in U/Pb ratio have existed in the mantle source region for about 2.5 b.y. This age is remarkably similar to ages of crystalline basement rocks exposed in the region. The small range in $^{87}Sr/^{86}Sr$ ratios observed in these tholeiites is consistent with the existence of small heterogeneities in Rb/Sr in a 2.5 b.y. old source region. Although the $^{87}Sr/^{86}Sr$ ratios are comparatively high, they lie within the range of values observed in basalts from oceanic islands.

2. There is no correlation between Pb and Sr isotopic compositions in the olivine tholeiites. However, hybrid lavas from the King Hill area and at Craters of the Moon lava field (*Leeman and Manton*, 1971; *Leeman*, in preparation) exhibit well-defined correlations between $^{87}Sr/^{86}Sr$ and $^{206}Pb/^{204}Pb$ which are consistent with contamination by crustal Sr and Pb. The olivine tholeiites display no such trends.

3. Correlations are lacking between the isotopic compositions and contents (or inverse contents) of Sr and Pb (e.g., see *Ewart and Stipp*, 1968; *Pushkar*, 1968; *Faure et al.*, 1974) in the olivine tholeiites. The absence of such correlations suggests that these magmas have not been contaminated by Sr or Pb of distinct isotopic composition, nor were they derived from a "mixed" mantle source such as has been postulated for Italian volcanoes (*Vollmer*, 1976). Hybrid lavas from the Snake River Plain do display such correlations that are interpreted as reflecting crustal contamination.

4. Crustal xenoliths of granulite facies gneiss, granitic rocks, and meta-igneous rocks which occur in some of the Snake River Plain hybrid lavas display wide ranges in $^{87}Sr/^{86}Sr$ (0.702 to 0.830) and Pb isotopic ratios ($^{206}Pb/^{204}Pb$ ranges from 13.4 to 24.7) (*Leeman*, in preparation) which are

characteristic of ancient crustal rocks (*Doe*, 1970; *Faure and Powell*, 1972). In view of the diversity of these ratios, it seems unlikely that random contamination by such rocks would be consistent with the narrow range in $^{87}Sr/^{86}Sr$ and precise linear array in $^{207}Pb/^{204}Pb$-$^{206}Pb/^{204}Pb$ space observed in the olivine tholeiites. Of course, little is known of the isotopic composition of lower crustal rocks and no firm conclusions can be drawn regarding their role in contamination or magma genesis.

5. Rhyolites from the Snake River Plain-Yellowstone province display essentially the same ranges in Pb isotopic ratios ($^{206}Pb/^{204}Pb$ ranges from 16.58 to 18.94) as the olivine tholeiites, although their Pb contents (about 30 ppm for most samples) are about ten times higher than those of the basalts (*Leeman*, unpublished data). Because the tholeiites contain appreciably less Pb, they should be more susceptible to crustal contamination than the rhyolitic magmas; thus, the overlap in Pb isotopic compositions would suggest that contamination of the basalts has not been significant. Furthermore, Pb isotopic ratios in the rhyolites display a consistent relationship with geographic setting. The ratios become less radiogenic from west to east and fall into three main groupings corresponding to western Snake River Plain, east-central Snake River Plain, and Yellowstone-Island Park subprovinces. The olivine tholeiites exhibit no such clear-cut trend, suggesting that the source regions for these two magma types are distinct. $^{87}Sr/^{86}Sr$ ratios in the rhyolites (0.709 to 0.712) are significantly higher than those of the tholeiites and preclude a cogenetic origin with the basalts (*Leeman*, unpublished data).

On the basis of these observations, and especially the contrasting trends found in the olivine tholeiites and the hybrid lavas of the Snake River Plain, it seems most reasonable to attribute the isotopic compositions of the tholeiites to derivation of these magmas from an old mantle region that is characterized by higher Rb/Sr and U/Pb than are typical of most sub-oceanic mantle regions.

More limited data from the Columbia River Plateau indicate that tholeiites there have Sr (*McDougall*, 1976; *Nelson*, personal communication) and Pb (*Church*, 1977) isotopic compositions that are consistent with such a model. A significant feature of these data is the uniformity of $^{87}Sr/^{86}Sr$ within different magma types (e.g., Picture Gorge, Grande Ronde and Imnaha, lower and middle Yakima), but persistence of significant differences in this ratio between magma types (see Table 1). The Pb isotopic data display similar groupings within magma types, as well as some overlap between types. The total range in $^{206}Pb/^{204}Pb$ for these magma types is comparatively small (18.66 to 19.04) and the Pb compositions are consistent with derivation of these basalts from a source with higher U/Pb than is typical of oceanic basalts. There is no correlation between Sr and Pb isotopic compositions for these rocks, nor is there any correlation between $^{87}Sr/^{86}Sr$ and Sr content (or 1/Sr) within individual magma types. The apparent uniformity in $^{87}Sr/^{86}Sr$ within the voluminous lower and middle Yakima basalt types, despite a very wide distribution of vents, suggests that crustal contamination is not significant. Upper Yakima basalts

TABLE 1. Initial $^{87}Sr/^{86}Sr$ Ratios in Representative Continental Tholeiitic Basalts

Name	Age (my)	$^{87}Sr/^{86}Sr_o$[a]	N	Ref.
Snake River Plain-Yellowstone				
olivine tholeiites	0-12	0.7065±5[b]	65	1
Craters of the Moon lavas	0	0.7075-0.7120	21	1
King Hill lavas	3	0.7104-0.7176	15	1
Columbia River Plateau				
Picture Gorge	~15	0.7037±1	10	2
Grande Ronde	"	0.7047±1	9	2
Imnaha	"	0.7045±2	9	2
Lower Yakima	"	0.7052±3	11	2
Middle Yakima	"	0.7053±1	5	2
Upper Yakima	8-14	0.7069±0.7092	8	2
Deccan, India				
tholeiitic basalts	~60	0.7059±3	3	3
Serra Geral, Brazil				
dolerites, basalts	120-150	0.7056±3	6	4
Antarctica				
Queen Maude Land basalts	~150	0.7053±20	12	5
Kirkpatrick Basalt	"	0.7093-0.7143	22	6
Ferrar Dolerites	"	0.7089-0.7142	22	4
Karroo, S. Africa				
dolerites, basalts	150-190	0.7056±9	6	4
Eastern N. America				
Palisades diabase	~200	0.7051±10	3	3
Brookville diabase	"	0.7058	1	7
N. and S. Carolina diabase dikes	"	0.7048 n.d.	11	8

[a] Initial ratio adjusted to $^{87}Sr/^{86}Sr = 0.7080$ in E & A Standard

[b] Error is one sigma uncertainty in last significant digit(s); n.d. = not determined

References

1. *Leeman and Manton* (1971) and *Leeman* (unpublished data)
2. *McDougall* (1976)
3. *Faure and Hurley* (1963)
4. *Compston et al.* (1968)
5. *Faure et al.* (1971)
6. *Faure et al.* (1974)
7. *Barker and Long* (1969)
8. *Ragland et al.* (personal communication, 1972)

display a wider range in major element (*Wright et al.*, 1973) and isotopic composition. $^{87}Sr/^{86}Sr$ ratios range from 0.707 to greater than 0.714 (*Nelson*, personal communication, 1976), but display no clearcut correlation with Sr content. $^{206}Pb/^{204}Pb$ ratios also display a wider range (18.14 to 19.11) than for the other Columbia River basalts and define a crude linear array with $^{207}Pb/^{204}Pb$ ratios that corresponds to a secondary isochron age of about 2.5 b.y. At present, complete Sr and Pb isotopic data are not available for all analyzed samples, nor have Pb contents been measured. Thus it is not possible to show that the Upper Yakima samples define a "mantle" isochron at this time.

Data of comparable quantity and/or quality are not yet available from most other continental tholeiite suites. However, *Brooks et al.* (1976) have pointed out the existence of correlations between observed Rb/Sr and initial $^{87}Sr/^{86}Sr$ ratios for some such suites. They interpret these trends as mantle isochrons that reflect the antiquity of the source regions for continental basalts. One important feature of some of these mantle isochrons is their comparatively high $^{87}Sr/^{86}Sr$ intercepts, which are incompatible with crustal contamination of mantle derived magmas that initially had $^{87}Sr/^{86}Sr$ ratios equivalent to those of most oceanic basalts. This conclusion supports the inference that sub-continental mantle regions may be enriched in Rb/Sr compared to sub-oceanic mantle regions.

In conclusion, analogy with the Snake River-Yellowstone tholeiites suggests that isotopic data for many continental tholeiites does not require that such magmas are necessarily contaminated by crustal Sr or Pb. Further work on such isotopic studies can potentially provide reliable criteria for assessing the effects of crustal contamination, magma mixing, etc. The available data raise the possibility that continental tholeiites appear to be derived from ancient (aeons old) mantle sources that have remained intact within the continental lithosphere, and that these source regions are characterized by higher Rb/Sr and U/Pb ratios than are typical for most sub-oceanic mantle regions (*Leeman*, 1975; *Brooks et al.*, 1976).

In certain continental areas that are characterized by extensional tectonics and uplift (e.g., Basin and Range Province, western United States) there are notable occurrences of predominantly alkalic basalts that have Sr and Pb isotopic compositions typical of many oceanic island basalts (*Leeman*, 1970, 1974a; *Zartman and Tera*, 1973). These magmas may have been derived largely from upwelling oceanic-type mantle (asthenosphere?)(*Leeman*, 1970), rather than from ancient sub-continental lithospheric mantle.

Rare Earth Element (REE) Compositions

REE contents in volcanic rocks have been used widely to evaluate such processes as partial melting and crystal fractionation and to infer compositional features of mantle source regions (e.g., *Gast*, 1968; *Schilling*, 1975a; *Leeman et al.*, 1977). To a first approximation, the content of a given trace element in a magma is governed theoretically by the nature of solid phases (either melt residue or precipitating crystals) with which it is equilibrated, and the values of mineral/liquid distribution coefficients (herein denoted as D values) for the relevant crystalline phases. D values for most minerals are dependent to some degree upon such variable factors as temperature, pressure, composition of the phases and, for some elements (e.g., Eu), oxygen fugacity (*Shaw*, 1977). Values of REE D's for important minerals that occur in the mantle or as phenocrysts in basaltic magmas have been estimated empirically from analyses of

phenocrysts and matrix separated from volcanic rocks or by experimental studies. *Leeman et al.* (1977) present a set of representative D values for several important minerals and discuss their reliability.

In the case of partial melting, calculated REE contents of liquids are somewhat model dependent. These models fall into three main classes (*Schilling and Winchester*, 1967; *Gast*, 1968; *Shaw*, 1970; *Harris*, 1957) as follows:

1. Batch equilibrium melting--liquid remains in equilibrium with bulk residual solid until its extraction.

2. Fractional equilibrium melting--liquid is separated continuously from residual solid with or without collection of liquid in a common magma chamber.

3. Zone melting--liquid reacts continuously with wall rocks during its ascent.

Variants of these models are discussed by *Shaw* (1970, 1977) and it can be shown that each process will result in different patterns of REE enrichment in the resulting partial melts relative to REE contents in a given source rock, with the differences increasing as the degree of melting increases. Most discussions of partial melting stress batch melting models (e.g., *Schilling*, 1975; *Leeman et al.*, 1977) because it seems unlikely that infinitesimal amounts of liquid could be continuously collected or extracted from the mantle; batch melting seems most realistic for formation of large volumes of magma of uniform composition.

Although most aspects of partial melting are only imperfectly understood, theoretical considerations of partial melting processes can establish some first order constraints on the nature of source materials that could be melted to produce REE patterns and other trace element distributions observed in basaltic rocks. In order to derive information about the mantle sources of such rocks, it is necessary to evaluate the extent to which trace element contents in the magmas have been modified by pre-eruptive processes. One of the most important processes, and certainly the best understood, is crystal fractionation. The effectiveness of this process in modifying trace element contents in a residual liquid depends upon the nature and amounts of precipitating phases, the relevant D values, and the type of equilibrium (or lack thereof) maintained between crystals and liquid (i.e., kinetics of crystal growth, diffusion rates of trace elements in crystals and liquid; see *Albarede and Bottinga*, 1972). Two end-member cases of crystal-liquid equilibrium have been discussed by *Gast* (1968):

1. Bulk or Nernst equilibrium--liquid remains in equilibrium with bulk cumulate crystals, which are homogeneous.

2. Surface of Rayleigh equilibrium--liquid remains in equilibrium only with surfaces of cumulate crystals, which display compositional zoning.

Enrichment factors for elements in residual liquids relative to their contents in a parental magma differ between these end-member cases for "excluded" elements (those that are preferentially incorporated in the melt phase). Under conditions of moderate to low pressure crystallization, the REE are not significantly incorporated into near-liquidus phases that typically precipitate from basaltic magmas. A notable exception is Eu which may be concentrated into plagioclase relative to basaltic liquid

(*Schnetzler and Philpotts*, 1970). Thus, under these conditions relative abundances of the REE, with possible exception of Eu, are not strongly modified by crystal fractionation (e.g., *Schilling*, 1975a), although absolute contents of the REE will be increased by this process. Therefore, REE relative abundances in basaltic lavas may be considered representative of those in the parental magmas where it can be demonstrated that crystallization has not been extensive or else the bulk cumulate phases do not significantly fractionate the REE. This appears to be the case for most MOR tholeiites (*Kay et al.*, 1970; *Schilling*, 1975a) and for some continental tholeiites (*Leeman*, 1976).

In the following sections it is shown that there are systematic differences in REE abundance patterns between MOR and continental tholeiites, and it is suggested that these differences arise primarily from partial melting of distinctly different source materials. The former must be depleted in light REE (LREE), whereas the latter may be characterized by chondritic (or possibly LREE-enriched) relative REE abundances. This distinction is supported by Nd isotopic ratios which indicate that differences in REE abundance patterns for sub-oceanic and sub-continental mantle regions may have persisted for more than 10^9 years (see below).

A. Oceanic Regions

It has long been recognized (*Frey et al.*, 1968; *Kay et al.*, 1970; *Schilling*, 1971) that MOR tholeiites are characterized by LREE-depleted abundance patterns (chondrite-normalized). Furthermore, *Schilling* (1975a) has shown that MOR tholeiites from normal ridge segments display a remarkable similarity in $(La/Sm)_{E.F.}$ (the chondrite-normalized La/Sm ratio is used as an indicator of LREE-depletion) regardless of spatial or temporal (during at least the past 70 m.y.) variations. Nearly all are LREE-depleted and average REE contents are similar for all extensively studied areas. Some variability in absolute REE contents exists within each locality, but this can be accounted for either by low pressure fractionation of olivine and plagioclase, or by small differences in the degree of partial melting. Although unique partial melting models cannot yet be formulated, it is apparent that the source regions for these basalts must also be depleted in LREE at least to the extent of the basalts themselves. In addition, there is little reason to believe that the source regions contain appreciable garnet. This mineral strongly incorporates the heavy REE relative to the LREE, and its presence in the residual solid would favor enrichment of the LREE in partial melts derived from such a source rock. More likely the REE profiles in these magmas resulted from fusion of lherzolitic source rocks, possibly containing some plagioclase. The REE data are consistent with large (10 to 30 percent) degrees of melting of such rocks at moderate pressures, in agreement with other petrologic models for the origin of MOR tholeiites (e.g., *Gast*, 1968; *Green*, 1971). An important conclusion from these studies is that the oceanic lithosphere is apparently underlain by an upper mantle zone that is essentially uniformly depleted in LREE.

Alpine ultramafic rocks that are believed to be remnants of oceanic upper mantle are also characterized by moderate to strong depletion in LREE and other large lithophile elements (*Frey et al.*, 1968; *Frey*, 1969; *Loubet et al.*, 1975; *Menzies*, 1976). These rocks have REE contents that are compatible with their being either source material for MOR tholeiites or residual material remaining after extraction of such basaltic magma.

Basalts from oceanic islands (and ridge segments near such islands) are typically enriched in LREE relative to MOR tholeiites, although MOR-like tholeiites occur on some islands (*O'Nions et al.*, 1976; *Lindstrom*, 1976). *Schilling* (1973, 1975b) has suggested that oceanic island basalts having $(La/Sm)_{E.F.}>1$ are derived from different source materials from that of the MOR tholeiites, which are characterized by distinct REE and isotopic compositions. In particular, he postulates their derivation from a deep mantle plume (or blob) that is relatively enriched in LREE, Rb/Sr, etc. This model is open to question, especially in the light of Nd isotopic studies. *DePaolo and Wasserburg* (1976a,b), *Richard et al.* (1976), and *O'Nions et al.* (1977) show that nearly all oceanic basalts, whether from ridges or islands, have $^{143}Nd/^{144}Nd$ ratios that developed in a source region with higher than chondritic $^{147}Sm/^{144}Nd$ ratio (i.e., LREE depleted). *Richard et al.* (1976) suggest that the minimum time that such conditions have existed is on the order of 1.1 b.y. The Nd isotopic constraints are critical in that, if the available analyses are typical and most oceanic basalts are derived from LREE-depleted mantle, the extreme enrichments of LREE in many alkalic basalts from oceanic islands (e.g., *Kay and Gast*, 1973) require segregation of extremely small (<<1 percent) batch melt fractions from the mantle. Alternatively, other melting or enrichment processes must be considered.

B. Continental Regions

Continental tholeiites are typically characterized by REE patterns that are enriched in the LREE relative to chondrites. Data for many such suites are summarized in Table 2; most of these basalts have $(La/Sm)_{E.F.}$ values greater than about 1.4, although two exceptions (chilled margin rocks from the Bushveld and Stillwater intrusions) are known. Variations in this ratio and in $(Yb)_{E.F.}$, especially within individual magmatic suites, may reflect differences in the degree of partial melting of similar source rocks having chondritic REE relative abundances. These variations cannot generally be related to low pressure crystal fractionation of parental magmas. Among the Snake River Plain tholeiites, for example, samples with the minimum (72-24) and maximum (D1651) REE contents display nearly a factor of two range in $(Yb)_{E.F.}$. This range would correspond to about 50 percent crystallization of olivine and plagioclase (the phenocryst minerals in these rocks) from the more primitive magma (72-24), yet major and trace element contents of these rocks preclude this possibility (*Leeman*, 1974b and in preparation). The wide range in REE contents and small range in $(La/Sm)_{E.F.}$ of the Snake River tholeiites also seems incompatible with their contamination by typical crustal rocks, which are characterized by much different REE relative abundances. The similarity in $(La/Sm)_{E.F.}$ between many continental tholeiites is consistent with their derivation from similar source materials. In this regard, *DePaolo and Wasserburg* (1977) find that most of the few analyzed continental tholeiites have Nd isotopic compositions that are consistent with chondritic relative REE abundances in their source regions. As in the case with Sr and Pb isotopic data, many more Nd isotopic analyses are needed to test this conclusion. The two exceptional tholeiitic rocks with $(La/Sm)_{E.F.}<1$, noted above, may have been derived from LREE-depleted source rocks; otherwise they are indeed enigmatic. Systematic studies of REE contents in typical continental tholeiites from many areas are needed to convincingly demonstrate that these rocks are derived from source materials that are distinct from those of the sub-oceanic mantle.

TABLE 2. Rare Earth Element Profile Characteristics For Continental Basalts

Locality	$(La/Sm)_{E.F.}$	$(Yb)_{E.F.}$	Ref.
Snake River Plain			
McKinney Basalt pillow glass	1.9	19	1
low REE tholeiite (72-24)	1.4	11.5	2
high REE tholeiite (D-1651)	1.9	20	2
Columbia River Plateau			
lower Picture Gorge	1.4	12.5	3
upper Picture Gorge	1.7	14.5	3
high-Mg lower Yakima	2.5	14	4
low-Mg lower Yakima	2.4	19	4
middle Yakima (Frenchman Springs)	2.3	17	4
Prineville	1.8	23	5
upper Yakima (Ice Harbor)	2.3	21	6
Steens Mountain			
avg. of 52	2.0	16.5	7
avg. groups 6 and 8	1.6	12	7
Deccan			
Mahabaleshwar (avg. of 10)	1.7	13	8
Miscellaneous (range of 18)	1.8-2.5	12-20	9
Keweenawan			
Duluth Gabbro	3.0	4.4	10
Northshore Volcanics basalts (range of 12)	1.6-3.1	8-20	11
Gabbroic intrusions - chilled margin			
Skaergaard	1.4	5.8	10
Stillwater	0.5	1.5	10
Bushveld	0.6	4.3	10
Palisade	2.0	10	10
W-1	1.9	10	12

References

(1) *Leeman* (1976), (2) *Leeman* (1974), (3) *Osawa and Goles* (1970), (4) *Nathan and Fruchter* (1974), (5) *Uppuluri* (1975), (6) *Leeman* (unpublished), (7) *Helmke and Haskin* (1973), (8) *Nakamura and Masuda* (1971), (9) *Goles* (personal communication, 1973), (10) *Frey et al.* (1968), (11) *Haskin and Green* (personal communication, 1975), (12) *Flanagan* (1973).

Conclusions

Sr and Pb isotopic data and REE patterns for oceanic and continental tholeiites suggest that these types of basalts are derived from chemically distinct mantle regions. These differences are consistent with the oceanic mantle having lower Rb/Sr and U/Pb ratios and LREE-depleted REE abundances relative to mantle source regions for continental basalts. The isotopic data are consistent in indicating that such differences have persisted for at least 10^9 years. If this interpretation is correct, then a significant conclusion is that source regions for continental tholeiites have not been involved to any significant extent in convective stirring or other mixing processes that would homogenize the upper mantle. Rather, they have remained an integral part of the continental lithosphere for at least 10^9 years. The depths to which such compositional differences between sub-oceanic and sub-continental mantle regions extend are not known; it seems reasonable, however, that such differences may extend at least to the depths of origin of continental tholeiites. A more fundamental question is how did such compositional differences arise in the first place? *Gast* (1968) suggested that sub-oceanic mantle, at least the source regions for MOR tholeiites, was depleted in large-ion lithophile elements on a world-wide scale by some previous melting event(s) that must have occurred prior to 10^9 years ago. (If so, where and what are the partial melt products of this event?) Alternatively, the earth's upper mantle may have been heterogeneous throughout much of geologic time, at least since the time that the continents were differentiated from the whole Earth. If this is the case, portions of the upper mantle must have been partially remixed or isotopically homogenized at various times so as to yield a range in apparent $^{207}Pb/^{206}Pb$ ages of source materials for different basaltic suites (*Leeman*, in preparation).

References

Albarede, F., and Y. Bottinga, Kinetic disequilibrium in trace element partitioning between phenocrysts and host lava, *Geochim. Cosmochim. Acta, 36*, 141-156, 1972.

Barker, D.S., and L.E. Long, Feldspathoidal syenite in a quartz diabase sill, Brookville, New Jersey, *Jour. Petrol., 10*, 202-221, 1969.

Beswick, A.E., K and Rb relations in basalts and other mantle derived materials. Is phlogopite the key?, *Geochim. Cosmochim. Acta, 40*, 1167-1183, 1976.

Brooks, C., D.E. James, and S.R. Hart, Ancient lithosphere: its role in young continental volcanism, *Science, 193*, 1083-1094, 1976.

Brooks, C., S.R. Hart, A.W. Hofmann, and D.E. James, Rb-Sr mantle isochrons from oceanic regions, *Earth Planet. Sci. Lett., 32*, 51-61, 1976.

Chow, T.J., and C.C. Patterson, On the occurrence and significance of lead isotopes in pelagic sediments, *Geochim. Cosmochim. Acta, 26*, 263-308, 1962.

Church, S.E., and M. Tatsumoto, Lead isotope relations in oceanic ridge basalts from the Juan de Fuca-Gorda Ridge area, N.E. Pacific Ocean, *Contrib. Mineral Petrol., 53*, 253-279, 1975.

Church, S.E., Lead isotopic data and their bearing on the genesis of basalts in the Columbia River Plateau, *Earth Planet. Sci. Lett.*, in press.

Compston, W., I. McDougall, and K.S. Heier, Geochemical comparison of the Mesozoic basaltic rocks of Antarctica, South Africa, South America and Tasmania, *Geochim. Cosmochim. Acta*, *32*, 129-149, 1968.

Dasch, E.J., and D.H. Green, Strontium isotopic geochemistry of lherzolite inclusions and host basaltic rocks, Victoria, Australia, *Amer. Jour. Sci.*, *275*, 461-469, 1975.

DePaolo, D.J., and G.J. Wasserberg, Nd isotopic variations and petrogenetic models, *Geophys. Res. Lett.*, *3*, 249-252, 1976a.

DePaolo, D.J., and G.J. Wasserberg, Inferences about magma sources and mantle structure from variations of $^{143}Nd/^{144}Nd$, *Geophys. Res. Lett.*, *3*, 743-746, 1976b.

Doe, B.R., The bearing of lead isotopes on the source of granitic magma, *Jour. Petrol.*, *8*, 51-83, 1967.

Doe, B.R., Lead and strontium isotope studies of Cenozoic volcanic rocks in the Rocky Mountain region - a summary, *Colorado School Mines Quart.*, *63*, 149-174, 1968.

Doe, B.R., *Lead Isotopes*, Springer-Verlag, New York, 137 pp., 1970.

Duncan, R.A., and W. Compston, Sr-isotopic evidence for an old mantle source region for French Polynesian volcanism, *Geology*, *4*, 728-732, 1976.

Ewart, A., and J.J. Stipp, Petrogenesis of the volcanic rocks of the Central North Island, New Zealand, as indicated by a study of Sr^{87}/Sr^{86} ratios, and Sr, Rb, K, U, and Th abundances, *Geochim. Cosmochim. Acta*, *32*, 699-736, 1968.

Faure, G., and P.M. Hurley, The isotopic composition of strontium in oceanic and continental basalts: application to the origin of igneous rocks, *Jour. Petrol.*, *4*, 31-50, 1963.

Faure, G., R.L. Hill, L.M. Jones, and D.H. Elliot, Isotope composition and silica content of Mesozoic basalt and dolerite from Antarctica, *SCAR Symposium, University Press, Oslo*, 1970.

Faure, G., J.R. Bowman, D.H. Elliot, and L.M. Jones, Strontium isotope composition and petrogenesis of the Kirkpatrick Basalt, Queen Alexandra Range, Antarctica, *Contrib. Mineral. Petrol.*, *48*, 153-169, 1974.

Faure, G., and J.L. Powell, *Strontium Isotope Geology*, Springer-Verlag, New York, 188 pp., 1972.

Flanagan, F.J., 1972 values for international geochemical reference samples, *Geochim. Cosmochim. Acta*, *37*, 1189-1200, 1973.

Flower, M.F.J., H.-U. Schminke, and R.N. Thompson, Phlogopite stability and the $^{87}Sr/^{86}Sr$ step in basalts along the Reykjanes ridge, *Nature*, *254*, 404-406, 1975.

Frey, F.A., Rare Earth Abundances in a high-temperature peridotite intrusion, *Geochim. Cosmochim. Acta, 33*, 1429-1447, 1969.

Frey, F.A., M.A. Haskin, J.A. Poetz, and L.A. Haskin, Rare earth abundances in some basic rocks, *Jour. Geophys. Res., 73*, 6085-6098, 1968.

Frey, F.A., L.A. Haskin, and M.A. Haskin, Rare earth abundances in some ultramafic rocks, *Jour. Geophys. Res., 76*, 2057-2070, 1971.

Gale, N.H., and A.E. Mussett, Episodic uranium-lead models and the interpretation of variations in the isotopic composition of lead in rocks, *Rev. Geophys. and Space Physics, 11*, 37-86, 1973.

Gast, P.W., Trace element fractionation and the origin of tholeiitic and alkaline magma types, *Geochim. Cosmochim. Acta, 32*, 1057-1086, 1968.

Gast, P.W., The isotopic composition of lead from St. Helena and Ascension Islands, *Earth Planet. Sci. Lett., 5*, 353-359, 1969.

Gast, P.W., G.R. Tilton, and C.E. Hedge, Isotopic composition of lead and strontium from Ascension and Gough Islands, *Science, 145*, 1181-1185, 1964.

Grant, N.K., J.L. Powell, F.R. Burkholder, J.V. Walther, and M.L. Coleman, The isotopic composition of strontium and oxygen in lavas from St. Helena, South Atlantic, *Earth Planet. Sci. Lett., 31*, 209-233, 1976.

Green, D.H., Composition of basaltic magmas as indicators of conditions of origin: application to oceanic volcanism, *Phil. Trans. Roy. Soc. London, Ser. A., 268*, 707-725, 1971.

Harris, P.G., Zone refining and the origin of potassic basalts, *Geochim. Cosmochim. Acta, 12*, 195-208, 1957.

Hart, S.R., K, Rb, Cs, Sr and Ba contents and Sr isotopic ratios of ocean floor basalts, *Phil. Trans. Roy. Soc. Lond. A., 268*, 573-587, 1971.

Hart, S.R., and C. Brooks, Rb-Sr mantle evolution models, *Carnegie Inst. Wash. Yearbook, 69*, 426-429, 1970.

Hart, S.R., J.-G. Schilling, and J.L. Powell, Basalts from Iceland and along the Reykjanes ridge; Sr isotope geochemistry, *Nature, 246*, 104-107, 1973.

Hedge, C.E., and F.G. Walthall, Radiogenic strontium-87 as an index of geological processes, *Science, 140*, 1214-1217, 1963.

Hedge, C.E., and Z.E. Peterman, The strontium isotopic composition of basalts from the Gorda and Juan de Fuca Rises, northeastern Pacific Ocean, *Contrib. Mineral. Petrol., 27*, 114-120, 1970.

Heier, K.S., W. Compston, and I. McDougall, Thorium and uranium concentrations, and the isotopic composition of strontium in the differentiated Tasmanian dolerites, *Geochim. Cosmochim. Acta, 29*, 643-659, 1965.

Helmke, P.A., and L.A. Haskin, Rare-earth elements, Co, Sc and Hf in the Steens Mountain basalts, *Geochim. Cosmochim. Acta, 37*, 1513-1529, 1973.

Hofmann, A.W., and S.R. Hart, An assessment of local and regional isotopic equilibrium in a partially molten mantle, *Carnegie Inst. Wash. Yearbook, 74*, 195-210, 1975.

Kay, R., N.J. Hubbard, and P.W. Gast, Chemical characteristics and origin of oceanic ridge volcanic rocks, *Jour. Geophys. Res., 75*, 1585-1613, 1970.

Kay, R.W., and P.W. Gast, The rare earth content and origin of alkali-rich basalts, *Jour. Geol., 81*, 653-682, 1973.

Leeman, W.P., The isotopic composition of strontium in late Cenozoic basalts from the Basin-Range province, western United States, *Geochim. Cosmochim. Acta, 34*, 857-872, 1970.

Leeman, W.P., Late Cenozoic alkali-rich basalt from the western Grand Canyon area, Utah and Arizona: isotopic composition of strontium, *Geol. Soc. Amer. Bull., 85*, 1691-1696, 1974a.

Leeman, W.P., Petrology of basaltic lavas from the Snake River Plain, Idaho: Part I, *Ph.D. Dissertation, Univ. of Oregon, Eugene*, 1-230, 1974b.

Leeman, W.P., Radiogenic tracers applied to basalt genesis in the Snake River Plain-Yellowstone National Park region -- evidence for a 2.7 b.y. old upper mantle keel, *Geol. Soc. Amer. Abst. with Programs, 7*, 1165, 1975.

Leeman, W.P., Petrogenesis of McKinney (Snake River) olivine tholeiite in light of rare-earth element and Cr/Ni distributions, *Geol. Soc. Amer. Bull., 87*, 1582-1586, 1976.

Leeman, W.P., and W.I. Manton, Strontium isotopic composition of basaltic lavas from the Snake River Plain, southern Idaho, *Earth Planet. Sci. Lett., 5*, 420-434, 1971.

Leeman, W.P., A.V. Murali, M.-S. Ma, and R.A. Schmitt, Mineral constitution of mantle source regions for Hawaiian basalts -- rare earth element evidence for mantle heterogeneity, this volume.

Leeman, W.P., B.R. Doe, and W.I. Manton, Lead isotopic analyses of basalts from the Snake River Plain-Yellowstone volcanic province: evidence for a 2.5 b.y. old sub-continental mantle source, *Earth Planet. Sci. Lett.*, in press, 1978.

Lindstrom, M.M., Geochemical studies of volcanic rocks from Pinzon and Santiago Islands, Galapagos archipelago, *Ph.D. Dissertation, Univ. of Oregon, Eugene*, 174 pp., 1976.

Loubet, M., N. Shimizu, and C.J. Allegre, Rare earths elements in alpine peridotites, *Contrib. Mineral Petrol., 53*, 1-12, 1975.

McDougall, I., Geochemistry and origin of basalt of the Columbia River Group, Oregon and Washington, *Geol. Soc. Amer. Bull., 87*, 777-792, 1976.

Meijer, A., Pb and Sr isotopic data bearing on the origin of volcanic rocks from the Mariana island-arc system, *Geol. Soc. Amer. Bull.*, *87*, 1358-1369, 1976.

Menzies, M.A., Rare earth geochemistry of fused alpine and ophiolitic lherzolites: Part 1, Othris, Lanzo and Troodos, *Geochim. Cosmochim. Acta*, *40*, 645-656, 1976.

Morioka, M., and K. Kigoshi, Lead isotopes and the age of Hawaiian lherzolite nodules, *Earth Planet. Sci. Lett.*, *25*, 116-120, 1975.

Nakamura, N., and A. Masuda, Rare earth elements in abyssal basalts and plateau basalts, *Nature*, *233*, 130-131, 1971.

Nathan, S., and J.S. Fruchter, Geochemical and paleomagnetic stratigraphy of the Picture Gorge and Yakima basalts (Columbia River Group) in central Oregon, *Geol. Soc. Amer. Bull.*, *85*, 63-76, 1974.

Nelson, D.O., and E.M. Dasch, Disequilibrium of strontium isotopes between mineral phases of parental rocks during magma genesis: a discussion, *Jour. Volcanol. and Geotherm. Res.*, *1*, 183-191, 1976.

O'Hara, M.J., Partial melting of upper mantle peridotites - a short summary, this volume.

O'Nions, R.K., and R.J. Pankhurst, Secular variation in the Sr-isotope composition of Icelandic volcanic rocks, *Earth Planet. Sci. Lett.*, *21*, 12-21, 1973.

O'Nions, R.K., and R.J. Pankhurst, Petrogenetic significance of isotope and trace element variations in volcanic rocks from the mid-Atlantic, *Jour. Petrol.*, *15*, 603-634, 1974.

O'Nions, R.K., R.J. Pankhurst, and K. Gronvold, Nature and development of basalt magma sources beneath Iceland and the Reykjanes Ridge, *Jour. Petrol.*, *17*, 315-338, 1976.

O'Nions, R.K., P.J. Hamilton, and N.M. Evensen, Variations in $^{143}Nd/^{144}Nd$ and $^{87}Sr/^{86}Sr$ ratios in oceanic basalts, *Earth Planet. Sci. Lett.*, *34*, 13-22, 1977.

Osawa, M., and G.G. Goles, Trace element abundances in Columbia River basalts, in *Preced. Second Columbia River Basalt Symposium*, edited by E.H. Gilmour and D. Stradling, Eastern Washington State College, Cheney, 173-175, 1970.

Oversby, V.M., and P.W. Gast, Isotopic composition of lead from oceanic islands, *Jour. Geophys. Res.*, *75*, 2097-2114, 1970.

Oversby, V.M., J. Lancelot, and P.W. Gast, Isotopic composition of lead in volcanic rocks from Tenerife, Canary Islands, *Jour. Geophys. Res.*, *76*, 3402-3413, 1971.

Pankhurst, R.J., Strontium isotope studies related to petrogenesis in the Caledonian basic igneous province of NE Scotland, *Jour. Petrol.*, *10*, 115-143, 1969.

Papanastassiou, D.A., and G.J. Wasserberg, Initial strontium isotopic abundances and the resolution of small time differences in the formation of planetary objects, *Earth Planet. Sci. Lett.*, *5*, 361-376, 1969.

Peterman, Z.E., I.S.E. Carmichael, and A.L. Smith, Strontium isotopes in Quaternary basalts of southeastern California, *Earth Planet. Sci. Lett.*, *7*, 381-384, 1970.

Peterman, Z.E., and C.E. Hedge, Related strontium isotopic and chemical variations in oceanic basalts, *Geol. Soc. Amer. Bull.*, *82*, 493-500, 1971.

Peterman, Z.E., C.E. Hedge, and W.R. Dickenson, Petrogenesis of lavas from western Samoa, *Geol. Soc. Amer. Bull.*, *83*, 2709-2714, 1972.

Philpotts, J.A., C.C. Schnetzler, and H.H. Thomas, Petrogenetic implications of some new geochemical data on eclogitic and ultrabasic inclusions, *Geochim. Cosmochim. Acta*, *36*, 1131-1166, 1972.

Pushkar, P., Strontium isotope ratios in volcanic rocks of three island arc areas, *Jour. Geophys. Res.*, *73*, 2701-2714, 1968.

Richard, P., N. Shimizu, and C.J. Allegre, $^{143}Nd/^{146}Nd$, a natural tracer; an application to oceanic basalts, *Earth Planet. Sci. Lett.*, *31*, 269-278, 1976.

Schilling, J.-G., Iceland mantle plume: geochemical study of Reykjanes ridge, *Nature*, *242*, 565-571, 1973.

Schilling, J.-G., Rare earth variations across 'normal segments' of the Reykjanes Ridge, 60°-53°N, Mid-Atlantic Ridge, 29°S, and East Pacific Rise, 2°-19°S, and evidence on the composition of the underlying low-velocity layer, *Jour. Geophys. Res.*, *80*, 1459-1473, 1975a.

Schilling, J.-G., Azores mantle blob: rare earth evidence, *Earth Planet. Sci. Lett.*, *25*, 103-115, 1975b.

Schilling, J.-G., and J.W. Winchester, Rare-earth fractionation and magmatic processes, in *Mantles of the Earth and Terrestrial Planets*, edited by S.K. Runcorn, Interscience, New York, 267-283, 1967.

Schnetzler, C.C., and J.A. Philpotts, Partition coefficients of rare-earth elements between igneous matrix material and rock-forming mineral phenocrysts, 2, *Geochim. Cosmochim. Acta*, *34*, 331-340, 1970.

Shaw, D.M., Trace element fractionation during anatexis, *Geochim. Cosmochim. Acta*, *34*, 237-243, 1970.

Shaw, D.M., Trace element behavior during anatexis, this volume.

Steuber, A.M., and M. Ikramuddin, Rubidium, strontium, and the isotopic composition of strontium in ultramafic nodule minerals and host basalts, *Geochim. Cosmochim. Acta*, *38*, 207-216, 1974.

Sun, S.-S., Lead isotope studies of young rocks from oceanic islands, mid-ocean ridges, and island arcs, *Ph.D. Dissertation, Columbia Univ., New York*, 139 p., 1973.

Sun, S.-S., and G.N. Hanson, Evolution of the mantle: geochemical evidence from alkali basalt, *Geology*, *3*, 297-302, 1975.

Sun, S.-S., and B. Jahn, Lead and strontium isotopes in post-glacial basalts from Iceland, *Nature*, *255*, 527-530, 1975.

Sun, S.-S., M. Tatsumoto, and J.-G. Schilling, Mantle plume mixing along the Reykjanes Ridge axis: lead isotope evidence, *Science, 190*, 143-147, 1975.

Tatsumoto, M., Genetic relations of oceanic basalts as indicated by lead isotopes, *Science, 153*, 1088-1093, 1966a.

Tatsumoto, M., Isotopic composition of lead in volcanic rocks from Hawaii, Iwo Jima, and Japan, *Jour. Geophys. Res., 71*, 1721-1733, 1966b.

Tatsumoto, M., Isotopic composition of Pb in oceanic basalt and its implication to mantle evolution, *submitted to Gast volume, Earth Plan. Sci. Lett.*, 1977.

Tatsumoto, M., C.E. Hedge, and A.E.J. Engel, Potassium, rubidium, strontium, thorium, uranium and the ratio of strontium-87 to strontium-86 in oceanic tholeiitic basalt, *Science, 150*, 886-888, 1965.

Tatsumoto, M., R.J. Knight, and C.J. Allegre, Time differences in the formation of meteorites as determined from the ratio of lead-207 to lead-206, *Science, 180*, 1279-1283, 1973.

Uppaluri, V.R., Prineville chemical type: A new chemical type in the Columbia River Group, *Geol. Soc. Amer. Bull., 85*, 1315-1318, 1974.

Vollmer, R., Rb-Sr and U-Th-Pb systematics of alkaline rocks: the alkaline rocks from Italy, *Geochim. Cosmochim. Acta, 40*, 283-295, 1976.

White, W.M., S.R. Hart, and J.-G. Schilling, Geochemistry of the Azores and the Mid-Atlantic Ridge: 29°N to 60°N, *Carnegie Inst. Wash. Yearbook, 74*, 224-234, 1975.

Wright, T.L., M.J. Grolier, and D.A. Swanson, Chemical variation related to the stratigraphy of the Columbia River basalt, *Geol. Soc. Amer. Bull., 84*, 371-386, 1973.

Zartman, R.E., and F. Tera, Lead concentration and isotopic composition in five peridotite inclusions of probable mantle origin, *Earth Planet. Sci. Lett., 20*, 54-66, 1973.

MINERAL CONSTITUTION OF MANTLE SOURCE REGIONS FOR HAWAIIAN BASALTS--RARE EARTH ELEMENT EVIDENCE FOR MANTLE HETEROGENEITY

W.P. Leeman*
Geology Department
Oregon State University
Corvallis, Oregon 97331

A.V. Murali, M.-S. Ma, and R.A. Schmitt
Chemistry Department and Radiation Center
Oregon State University
Corvallis, Oregon 97331

Abstract

Rare earth element (REE) contents were determined for Kilauea and Mauna Loa summit lavas that lie near low-MgO ends of olivine control lines. Except for removal or addition of olivine (and possibly orthopyroxene) these samples approximate mantle-derived partial melts. As removal of these minerals will not significantly fractionate the REE, the observed REE patterns likely represent *relative* REE abundances in the initial melts. Lavas of both volcanoes have light-REE enriched profiles relative to chondrites, but Mauna Loa basalt has a significantly less fractionated REE profile. A multi-linear regression method was used to determine mantle mineral proportions that yield a least-squares best fit between calculated and observed REE profiles in liquids produced by non-modal equilibrium melting at varying melt fractions (F). A range in F up to 0.18 (Kilauea) or 0.46 (Mauna Loa) is possible for olivine-orthopyroxene-clinopyroxene-garnet mantle; spinel peridotite models failed to yield acceptable fits (i.e., within experimental errors of our REE analyses).

For garnet-bearing mantle models, weight fractions of mantle garnet and clinopyroxene increase while those of olivine and orthopyroxene decrease regularly with increasing F. Also clinopyroxene/garnet ratios (5.7 for Kilauea and 1.6 for Mauna Loa) remain constant with varying F, indicating significant differences in composition between source regions for the two volcanoes. Garnet lherzolite or garnet pyroxenite lithologies are required as source materials. We emphasize that different degrees of melting of the same source material are not likely to account for the differences in REE patterns for these volcanoes.

Calculated modes for residual peridotite produced by extraction of Kilauea and Mauna Loa magmas are also distinct in clinopyroxene/garnet ratio (9.0 for Kilauea and 2.7 for Mauna Loa) and both must have light-REE depleted profiles relative to chondrites. Dunite or harzburgite residua are possible only for comparatively small degrees of melting ($F < 0.05$ for Kilauea and $F < 0.2$ for Mauna Loa); otherwise the residua will likely contain appreciable amounts of clinopyroxene and garnet.

Assuming that the source materials have chondritic relative REE abundances, our Kilauea models indicate that for $F = 0.01$ to 0.10, the source material has REE contents ranging from 0.8 to 6.1 times those in

---

* Present address: Geology Department, Rice University, Houston, Texas 77001

chondrites, respectively; for Mauna Loa models, we find that for F = 0.05 to 0.40, REE contents in the source material range from 1.8 to 13.3 times those in chondrites, respectively. Because REE contents in the analyzed lavas are probably enriched in an absolute sense (compared to the primary magmas) by olivine fractionation, our estimates of REE contents in the source materials are considered to be upper limits.

Introduction

A common approach toward an understanding of the Earth's upper mantle is through petrologic and geochemical studies of basaltic lavas. This approach is an indirect one and it is often difficult to ascertain the extent to which compositional variations among basaltic lavas reflect true variations in the composition of their source regions or result from differentiation of the ascending magmas. Before we can resolve such problems in a general way, it is necessary to understand how magmas evolve during their ascent from the point of generation to the surface.

In this paper we present rare earth element (REE) data for tholeiitic basalts from Hawaii. We have applied an "inversion" technique to infer the mineral constitution of mantle source regions that, upon melting, could produce liquids with REE abundance patterns consistent with those of the analyzed basalts. For Hawaii we can fortunately place rather close constraints upon the extent to which REE relative abundances are fractionated during ascent of the magmas from their source regions.

Kilauea and Mauna Loa volcanoes were selected for study because: (1) petrologic data and major element analyses are available for most twentieth century and many earlier eruptive phases; (2) geophysical and volcanological observations and petrochemical constraints provide comparatively detailed working models for differentiation and mixing processes that operate during ascent of magma to the surface; (3) these two volcanoes are spatially close (about 30 km apart) on a single island and both are currently active, thus tapping two close mantle source regions; and (4) their intra-oceanic plate location precludes contamination by "sialic" crust, although contamination by sea water, sediments, altered basalt, etc. cannot be ruled out *a priori*.

Wright and Fiske (1971) and *Wright* (1971) summarized much of the early work on Kilauea and Mauna Loa and presented petrogenetic models to explain spatial-temporal compositional variations among basalts from each volcano. Briefly, picritic to olivine tholeiitic summit lavas containing more than about 7% MgO display compositional variations controlled by addition or subtraction of olivine phenocrysts (and a trace of Cr-spinel); these are denoted as olivine-controlled lavas. Summit lavas containing less than about 7% MgO display compositional variations that result from low pressure fractionation of pyroxenes, plagioclase, and oxides, in addition to olivine. Rift lavas, which will not be considered here, display compositional variations that largely result from low pressure differentiation and magma mixing. Olivine-controlled summit lavas of a given eruptive phase are considered to represent deep-seated magma batches that largely are unmodified except for high level fractionation of olivine.

Superimposed on such trends are secular variations ranging over relatively long time periods (tens of years) in which magma compositions change in response to other less well understood processes. For Kilauea, *Wright* (1971, 1973) and *Wright et al.* (1975) relate some of these changes to high pressure fractionation of pyroxenes and spinel in addition to

olivine. In contrast, Mauna Loa lavas do not display any pronounced secular variation in composition, but *Wright* (1971) presents evidence for fractionation of small amounts of orthopyroxene from Mauna Loa magmas at intermediate to low pressure.

Small but significant differences in compositional trends, element ratios (e.g., K_2O/P_2O_5), and trace element contents exist between Kilauea and Mauna Loa lavas (*Jamieson*, 1970; *Wright*, 1971). These differences are reflected in the one-atmosphere melting behavior of these rocks as summarized by *Jamieson* (1970). Our trace element data further confirm these differences (*Murali et al.*, 1978; this paper). *Wright* (1971) suggested that compositional differences between Kilauea and Mauna Loa are similar in nature to the secular variations observed at Kilauea alone, and that they could arise as the result of high pressure fractionation involving ortho- and clinopyroxene, spinel, and olivine. We will show that *Wright's* (1971) model is not consistent with differences in the REE abundance patterns of Kilauea and Mauna Loa basalts. We will also demonstrate that the REE data are consistent with origin of these two magma types by partial melting of different mantle source regions.

Sampling and Analytical Results

In order to evaluate the nature of mantle source regions we analyzed a suite of twentieth century summit lavas from Kilauea that consisted of seven olivine-controlled basalts with low MgO and glasses separated from three high MgO picritic lavas; all of these samples lie near the low MgO end of the olivine-control line defined by twentieth century Kilauea summit lavas. We also analyzed a glass separated from a prehistoric picritic summit lava from Mauna Loa. The REE contents of the Kilauea samples are uniform within our analytical uncertainty and an average content is considered in the following discussion. The REE abundances for the Mauna Loa and the average Kilauea summit lavas and our analytical uncertainties are given in Table 1. All individual analyses and details of our INAA (instrumental neutron activation analysis) procedures are given in *Murali et al.* (1978).

The chondrite-normalized REE profiles for Kilauea and Mauna Loa basalts are contrasted in Fig. 1. The Kilauea samples display a more strongly fractionated REE profile with higher light REE and slightly lower heavy REE abundances than the Mauna Loa Sample. The shapes of the REE profiles also differ significantly. It will be noted that our REE profiles differ from those published by *Schilling and Winchester* (1969) in that theirs are characterized by chondrite-normalized La/Ce < 1. Their data for standard rock W-1 also shows this feature. Recent high precision data of *Taylor* (in press) for a Kilauea basalt (BHVO-1) are in excellent agreement with our average for Kilauea summit lavas.

Effects of Fractional Crystallization

Murali et al. (1978) have evaluated low pressure fractionation processes at Kilauea using the differentiation models of *Wright and Fiske* (1971) that were derived independently from considerations of major element data. The only relevant low pressure modification of the summit lavas is through fractionation of olivine and perhaps small amounts of spinel and orthopyroxene. All of these phases have very low REE

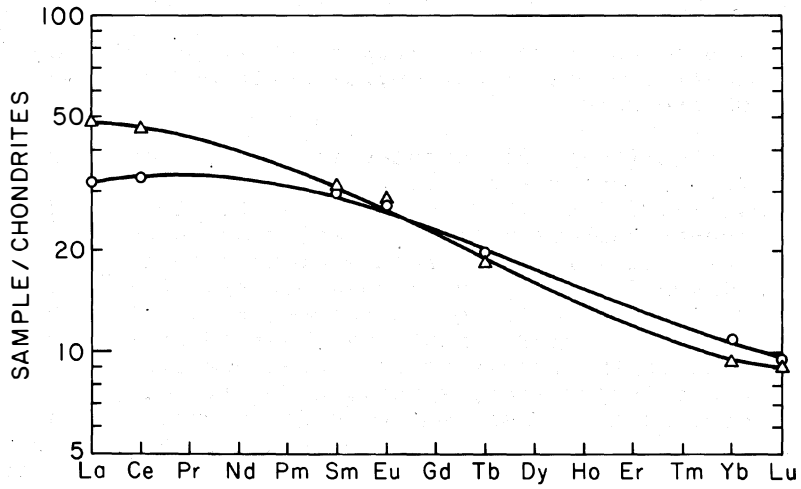

Fig. 1. Chondrite-normalized REE profiles for Mauna Loa (o) and Kilauea (Δ) summit lavas.

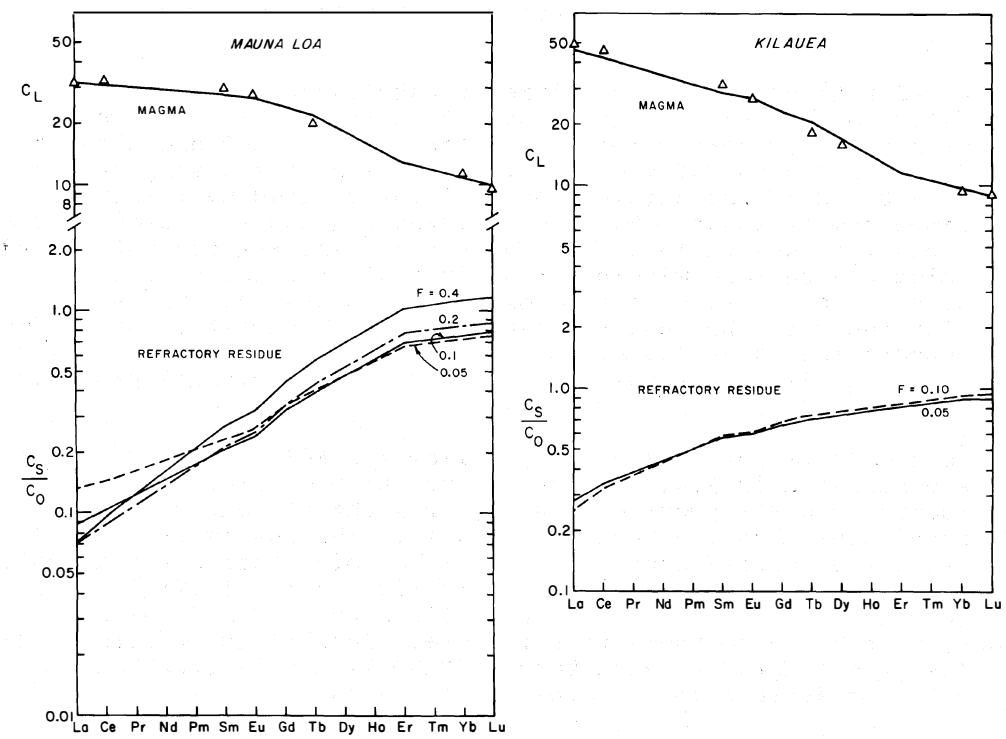

Fig. 2. Comparison between observed (Δ's) and calculated REE profiles in liquids (C_L) and calculated REE profiles for refractory residue (C_S/C_O) for Mauna Loa (A) and Kilauea (B). The computed chondrite-normalized liquid profiles (solid lines) are identical over the entire range of F values in models for each volcano. Melting models were considered satisfactory only if calculated values of C_L for each REE agreed within our analytical uncertainty with the observed values. Residue profiles (normalized to chondritic source with REE abundances C_O times those in chondrites) vary as a function of F; some representative patterns are shown. These profiles resemble those in many Alpine (ophiolitic) peridotites.

TABLE 1. Trace Element Content of Kilauea and Mauna Loa Summit Lavas (ppm)

	Kilauea[a]	Mauna Loa	Uncertainty[b] (%)
La	15.4 ± 0.9	10.0	5
Ce	38 ± 1.6	27	5
Sm	6.04 ± 0.16	5.69	2
Eu	2.00 ± 0.09	1.99	5
Tb	0.88 ± 0.06	0.94	5
Dy	5.2 ± 0.3	--	20
Yb	1.96 ± 0.11	2.33	5
Lu	0.29 ± 0.03	0.31	5
Ba	118 ± 21	--	20
Sc	31 ± 1.4	32	2
Cr	386 ± 54	420	5
Ni	171 ± 47	119	15
Co	46 ± 3.2	35	2

[a] Average of ten samples, except for La, Ce, and Cr (n = 9) and Dy (n = 5).
[b] Estimated counting statistical errors.

TABLE 2. Melting Proportions Used in Melting Calculations

Assemblage	Melting Proportions (p_i's)	Reference
oliv:cpx:gar	0.08:0.46:0.46	Davis & Schairer (1965)
oliv:opx:gar	0.05:0.20:0.75	Kushiro (1968)
oliv:opx:cpx	0.20:0.20:0.60	Kushiro (1968, 1969)
oliv:opx:cpx:gar	0.05:0.15:0.40:0.40	estimated
oliv:opx:cpx:spin	0.10:0.20:0.60:0.10	estimated

distribution coefficients (they strongly reject the REE compared with a coexisting silicate melt), and it is easily shown that removal of these phases will enrich the REE in the residual melt without significantly fractionating the light and heavy REE. Therefore, fractionation models involving these phases will not alter the relative abundances of the REE; that is, the REE profiles will remain representative of the undifferentiated precursor magmas. Insofar as high pressure fractionation involves these minerals, the same conclusion applies.

Wright (1971) postulated that the secular variations in composition of Kilauea summit lavas, and in principle the difference between Mauna Loa and Kilauea lavas, could arise as a result of high pressure fractionation of clinopyroxene in addition to the above mentioned minerals. REE distribution coefficients for clinopyroxene are significantly different for the light and heavy REE so that removal of this mineral will increase the light REE/heavy REE ratio in residual liquids. However, all the REE distribution coefficients for clinopyroxene are less than one (*Grutzeck et al.*, 1974; *Murali et al.*, 1978). Thus removal of clinopyroxene will also produce some enrichment of the heavy REE as well as the light REE and, therefore, cannot account for the difference in REE profiles for Kilauea and Mauna Loa. Explicit tests of *Wright's* (1971, Table 22) high pressure fractionation models using distribution coefficients given in *Murali et al.* (1978, Table 6) indicate that REE profiles of the resulting liquids will not be significantly fractionated. Calculated enrichments, assuming Rayleigh fractionation, range from 1.35 to 1.42 for La and 1.28 to 1.37 for Lu for Wright's models. In addition, these models would result in strong depletion of Cr, Ni and Co in the residual liquids, whereas the Kilauea glasses (containing no olivine) actually have higher Co and lower Cr and Ni than the Mauna Loa glass. Finally, it is impossible to account for the different K_2O/P_2O_5 ratios in the Kilauea (1.9-2.1) and Mauna Loa (1.76) lavas by Wright's models. It would be required that a phosphorus-bearing phase such as apatite be fractionated to account for such a difference, yet there is no petrographic or experimental support for this possibility. All of these considerations are at least consistent with, if not supportive of, the interpretation that the Kilauea and Mauna Loa magmas are not related by intermediate pressure fractionation processes as envisaged by *Wright* (1971).

We note that high pressure fractionation of Mauna Loa type magma may possibly yield magmas of the Kilauea type if garnet is involved. Garnet strongly excludes the light REE while strongly accepting the heavy REE (e.g., *Shimizu and Kushiro*, 1975) and may also incorporate significant amounts of P_2O_5 (*Thompson*, 1975). It remains to be seen whether or not garnet fractionation is compatible with variations in major element composition of the Kilauea and Mauna Loa lavas.

It is important to note that the secular variations in major element composition noted for Kilauea apparently are not reflected in the REE contents of those lavas. *Murali et al.* (1978) show that prehistoric and nineteenth century low MgO olivine-controlled summit lavas have REE profiles that resemble those for the twentieth century lavas, although the absolute REE contents are not identical. Therefore, these samples do not display any gradation in REE pattern toward the Mauna Loa type magma. This relationship also indicates that if secular variations at Kilauea do result from some high pressure fractionation process, that process does not significantly affect the REE relative abundances. Thus it seems likely that REE profiles in the summit lavas are similar to those in their parental magmas and can be employed to gain information about their mantle source region.

Swanson (1972) suggested that magma has been supplied to Kilauea volcano at a steady rate from 1952 to 1971, and perhaps throughout historic

time, based on (1) direct calculations of magma production rates for three major eruptions of sustained duration, (2) consideration of summit deformation related to high-level magma storage during periods of quiescence or of small volume eruptions, and (3) comparison of isostatic subsidence rates for Hawaii with rates of addition of magma (mass) to Mauna Loa and Kilauea. Swanson proposed that the observed rate of magma supply may be that from the mantle, and not simply from holding reservoirs within the volcanic edifice itself. If this model is correct, much of the magma erupted at Kilauea has undergone only minimal differentiation at intermediate depths.

In the next section we estimate, using a least-squares multilinear regression analysis (MRA), the modal mineralogy of mantle source regions that can generate magmas with REE abundance patterns like those in Kilauea and Mauna Loa summit lavas.

Effects of partial melting--theoretical considerations

We employ a rather simple model of partial melting in which magma accumulates in a single batch and remains in chemical equilibrium with residual minerals until the batch of magma is extracted. It is assumed that melting occurs at some invariant (i.e., eutectic or peritectic) composition that can be expressed in terms of the proportions (p_i's) in which each phase melts; for melting intervals in which none of the original phases is depleted, the values of p_i remain constant. This case seems more realistic than fractional melting models which involve continuous segregation of melt from the residual source rock, and lends itself to a straightforward mathematical treatment based on the non-modal batch melting equation of *Shaw* (1970):

$$\frac{C_L}{C_o} = \frac{1}{\bar{D}_o + F(1-P)}$$

where

C_L = trace element content in melt phase (chondrite-normalized)

C_o = trace element content in initial solid (chondrite-normalized)

F = fraction of original solid that is melted

$\bar{D}_o$ = initial bulk distribution coefficient weighted according to weight fraction (W_i) of phases initially present in the source rock ($= \Sigma W_i \cdot D_i$)

D_i = individual mineral/liquid distribution coefficient (= concentration of element in phase i/concentration in melt)

P = bulk distribution coefficient weighted according to weight proportions (p_i) in which the source phases melt ($= \Sigma p_i \cdot D_i$)

From the above equations we can derive two expressions for the initial bulk distribution coefficient for any given element as follows:

$$\bar{D}_o = \frac{C_o}{C_L} - F(1-P) = \Sigma W_i \cdot D_i \cdot$$

For the case of three phases in the source rock:

$$\frac{C_o}{C_L} - F(1-P) = W_a \cdot D_a + W_b \cdot D_b + W_c \cdot D_c \cdot$$

Considering that $W_c = (1 - W_a - W_b)$ this expression can be rearranged as follows:

$$W_a(D_c - D_a) + W_b(D_c - D_b) + C_o(\frac{1}{C_L}) = F(1-P) + D_c$$

In this equation all expressions in brackets and on the right hand side, except for F, can be treated as constants. For any arbitrary value of F a matrix of such equations (one for each REE) can be solved by MRA to yield optimal values for the dependent variables C_o, W_a, W_b, etc. As we have defined C_L to be chondrite-normalized, the C_o parameter obtained from the MRA solution is an estimate for enrichment of REE contents in the source region relative to chondritic abundances. This approach implicitly assumes that the source region is characterized by chondritic REE relative abundances. REE contents in several garnet pyroxenite and spinel lherzolite xenoliths from Oahu (*Nagasawa et al.*, 1969; *Reid and Frey*, 1971; *Philpotts et al.*, 1972) indicate that this assumption is reasonable to a first approximation. Preliminary models involving light REE depleted source material have not yielded satisfactory agreement between calculated and observed values of C_L for Mauna Loa or Kilauea. The chondritic abundances used by *Sun and Hanson* (1976) have been adopted for all calculations in this paper. Melting proportions have been estimated from phase diagrams of simplified mantle systems and are given in Table 2 with references. The calculations are not very sensitive to even rather large uncertainties in the p_i values used.

The mineral/liquid distribution coefficients (D's) adopted in this paper are given in Table 3. The D's for olivine, orthopyroxene, and even spinel are sufficiently low for the REE that uncertainties in these values will not greatly affect the outcome of partial melting calculations. On the other hand, uncertainties in the REE D's for garnet and clinopyroxene can significantly change the outcome of the calculations. Inasmuch as published estimates of REE D's are quite variable for these minerals (*Masuda and Kushiro*, 1970; *Grutzeck et al.*, 1974; *Arth and Hanson*, 1975; *Shimizu and Kushiro*, 1975; *Shaw*, 1977) we tested our models using most of the quoted estimates. We adopted the clinopyroxene D's of *Grutzeck et al.* (1974) because their experimental procedures were most straightforward and their measurements are suitable for the temperature range of interest (near 1300°C). Except for La and Ce their data also agree with one of the experimental results of *Masuda and Kushiro* (1970). However, the latter work involved difficult mineral separations in a small sample, so the higher D's reported by Masuda and Kushiro for La and Ce may reflect contamination of their clinopyroxene by glass. We adopted the garnet D's similar to those compiled by *Arth and Hanson* (1975) as a matter of necessity; their values were the only ones that could give us an acceptable fit between calculated and observed REE profiles for the Kilauea and Mauna Loa data. We checked all possible combinations with D's for other minerals. It is conceivable that the experimentally determined garnet D's of *Shimizu and Kushiro* (1975) may be in error, since they performed mineral separations using a differential dissolution procedure. If their garnets were zoned with increasing heavy REE content toward the rims (a possibility they did not check), then differential dissolution of garnet rims during mineral purification would result in low apparent D's for the heavy REE whereas D's for the light REE would not be significantly affected. Because the REE D's for olivine and orthopyroxene are so small and similar,

TABLE 3. Distribution Coefficients Used in Partial Melting Models

Element	Olivine	Opx	Cpx	Garnet	Spinel
La	0.007	0.005	0.069	0.004	0.03
Ce	0.007	0.006	0.098	0.008	0.032
Sm	0.007	0.013	0.26	0.21	0.053
Eu	0.007	0.014	0.26	0.42	0.055
Tb	0.009	0.021	0.31	1.6	0.092
Yb	0.014	0.056	0.29	9.3	0.17
Lu	0.016	0.068	0.28	10.5	0.091

Sources of data:

Olivine: *Arth and Hansen* (1975)
Orthopyroxene: *McKay and Weill* (1976)
Clinopyroxene: *Grutzeck et al.* (1974)
Garnet: *Philpotts et al.* (1972), calculated for sample GSFC-21
Spinel: *Kay and Gast* (1973)

NOTE: Where experimental data are available values of D appropriate for ∿ 1300°C were adopted. D's for some REE's were interpolated or extrapolated from measured values.

TABLE 4. Mantle Models for Kilauea and Mauna Loa

F	W_{OL-OPX}	W_{CPX}	W_{GAR}	C_o	R_{OL}	R_{OPX}	R_{CPX}	R_{GAR}	R_{OL+OPX}
Kilauea									
0.01	0.95	0.040	0.0082	0.81	0.72	0.24	0.037	0.0042	0. 6
0.05	0.75	0.21	0.042	3.1	0.59	0.19	0.02	0.023	0.78
0.10	0.49	0.43	0.084	6.1	0.40	0.12	0.43	0.049	0.52
Mauna Loa									
0.05	0.93	0.037	0.029	1.8	0.73	0.24	0.018	0.0099	0.97
0.10	0.85	0.087	0.060	3.4	0.71	0.22	0.052	0.022	0.93
0.20	0.69	0.19	0.12	6.7	0.64	0.18	0.13	0.051	0.81
0.30	0.53	0.29	0.18	10.0	0.55	0.13	0.24	0.088	0.67
0.40	0.37	0.39	0.24	13.3	0.43	0.005	0.38	0.14	0.49

W_i's are initial weight fractions of phases in source region.

R_i's are weight fractions of phases in residual solid after magma extraction; these are calculated using a ratio of OL:OPX = 3:1. These values are only approximate since they depend upon values of p_i's adopted.

p_i's used are as follows: oliv+opx:cpx:gar = 0.20:0.40:0.40.

treatment of these phases separately in the MRA calculations introduces large uncertainty into the estimation of W_{oliv} and W_{opx}. Therefore, we have treated these minerals as a single phase in our models, using D's weighted in the proportion oliv:opx = 3:1; the resulting MRA solutions give an estimate of the weight fraction of combined olivine and orthopyroxene in the original source region.

To model the mineral constitution in the mantle beneath Hawaii we assume that the mantle generally resembles some of the ultramafic xenoliths found in Hawaiian lavas (e.g., *Jackson*, 1968). The most common xenoliths of a non-cumulate nature are lherzolites and pyroxenites; on Oahu garnet-bearing lherzolites and pyroxenites are found, but these are not common there and they are not found elsewhere in the Hawaiian Islands. *Jackson and Wright* (1970) suggest that garnet lherzolite is a reasonable parental material for Hawaiian tholeiites and that the scarcity of this lithology among xenolith suites is to be expected as it is largely melted at depth or during ascent to the surface. Other constraints come from geophysical studies that show that major eruptive phases at Kilauea and Mauna Loa are preceded by intensified seismic activity with earthquake foci as deep as about 60 km (*Eaton and Murata*, 1960; *Koyanagi et al.*, 1975). If it is assumed that the magmas are derived from a melting zone below this depth (c.f., *Wright*, 1971), then the melting zone lies within the spinel or garnet peridotite stability field (*Green and Ringwood*, 1970). We have tested a variety of hypothetical source assemblages including the minerals olivine, ortho- and clinopyroxene, and either spinel or garnet. We have not considered models involving hydrous minerals such as mica or amphibole. In mafic magmas, REE D's for mica are small and those of amphibole are similar to clinopyroxene D's (*Arth and Hanson*, 1975) so involvement of these minerals will not materially alter the partial melting calculations.

Partial melting models - liquids

The inversion technique described above was applied to the data for Kilauea and Mauna Loa summit lavas. Of the several hypothetical mineral assemblages tested only that involving (oliv + opx)-cpx-gar yielded acceptable solutions for a wide range of F. All other assemblages (including spinel or plagioclase) tested either yielded negative weight fractions for one or more phases or yielded positive values only at very low degrees of melting ($F < 0.01$). Some representative solutions are given for each volcano in Table 4. These solutions are not unique. For a wide range in F (up to 0.18 for Kilauea and 0.46 for Mauna Loa), values of W_i and C_o can be found that will yield reasonable agreement between calculated and observed values of C_L (see Fig. 2). Plots of W_i's and C_o solutions versus F for each volcano (Fig. 3) show that these parameters vary smoothly with F. Furthermore, a unique melting model can be defined if any one of these variables can be determined independently. It is also apparent that C_o (enrichment of source in REE relative to chondrites) must increase with increasing melt fraction, but the <u>absolute</u> values of C_o cannot be precisely defined at any F value because REE contents in the analyzed summit lavas may have been enhanced by olivine fractionation. The calculated C_o values must be considered as upper limits.

Weight fractions of phases in the source material for Kilauea and Mauna Loa are displayed in a different way in Fig. 4a. At low degrees of melting the source materials for each volcano approach harzburgite, but as the degree of melting increases the source materials must become progressively richer in clinopyroxene and garnet. Also the clinopyroxene/garnet ratios remain constant for all degrees of melting, but differ significantly

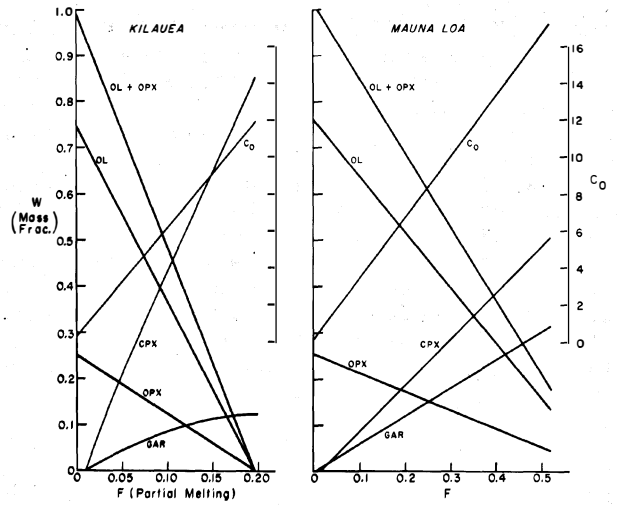

Fig. 3. Computed weight fraction models (scale on left) and C_o (scale on right) values for source rocks that, upon melting over a range of F values, can yield optimal agreement between calculated and observed REE abundance patterns. Results of calculations are given for both Kilauea (A) and Mauna Loa (B).

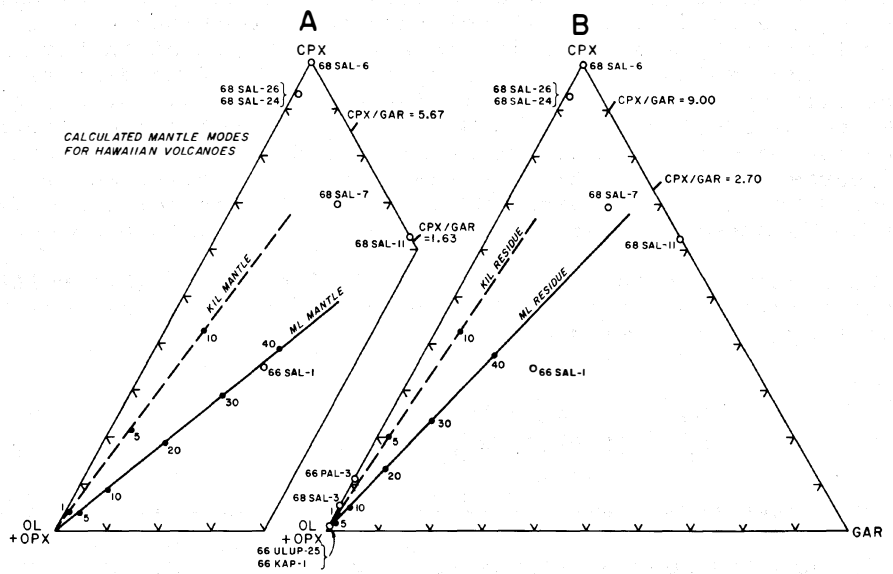

Fig. 4. Calculated modes of original source rocks (A) and refractory residua (B), for Mauna Loa and Kilauea melting models. Regardless of the postulated degree of melting, the source region for each volcano is characterized by a constant clinopyroxene/ garnet ratio. Modes of ultramafic xenoliths (*Jackson and Wright*, 1970) from Oahu are plotted for comparison (O's). Numbers by solid circles represent percentage of partial melting.

for the two volcanoes (5.7 for Kilauea versus 1.6 for Mauna Loa). Any systematic errors in the D_i's and p_i's used in the calculations will not alter the conclusion that a significant difference in the mineral constitution of the source regions is required if the REE patterns of the Kilauea and Mauna Loa lavas are representative of their parental magmas. We emphasize that different degrees of melting of the same source material cannot produce liquids with both the Kilauea and Mauna Loa REE profiles. REE profiles in picritic samples (up to 22% MgO) from Kilauea are essentially identical to those of the low-MgO summit lavas considered here, although absolute REE contents are lower as a result of olivine dilution (*Murali et al.*, 1978). Modes are plotted in Fig. 4 for several Oahu xenoliths studied by *Jackson and Wright* (1970). Of these xenoliths, the garnet lherzolites appear to be the most reasonable candidates as parental material for Hawaiian tholeiites, in which case the degree of melting required is moderately large ($F > 0.3$).

Partial melting models - refractory residue

The partial melting models for Kilauea and Mauna Loa can be further evaluated in terms of the mineral constitution and REE profiles predicted for the refractory residue left after extraction of magma. Weight fractions of residual minerals (R_i's) can be calculated by mass balance using the values of W_i's, p_i's, and F for each melting model. Because of our combined treatment of olivine and orthopyroxene, $W_{oliv+opx}$ was proportioned according to the arbitrary ratio oliv:opx = 3:1. Resulting values of R_i are given in Table 4 and displayed in Fig. 4b. Calculated residue modes vary regularly with F and define different trends of constant clinopyroxene/garnet ratio for each volcano. At any given value of F the residual material is depleted in garnet and clinopyroxene relative to the parent, but the extent of this depletion is uncertain largely because of uncertainties in the p_i's. Lherzolite and/or dunite residues would be consistent with our models, although for large degrees of melting it would seem likely that the residue would contain some garnet.

REE contents in the aggregate residual material (C_s) relative to those in the initial source rock (C_o) are given for the non-modal batch melting model by the following equation:

$$\frac{C_s}{C_o} = \frac{\bar{D}_o - PF}{(1-F)(\bar{D}_o + F(1-P))}$$

By our earlier definitions this ratio is chondrite-normalized. Some representative REE profiles calculated for refractory residua in the Kilauea and Mauna Loa source regions are given in Fig. 2. Partial melting of a source material with chondritic REE relative abundances should result in light REE depleted residua, that is, rocks similar to Alpine peridotites. Analyzed lherzolites and garnet pyroxenites from Oahu (*Reid and Frey*, 1971; *Philpotts et al.*, 1972) all display unfractionated or light REE enriched profiles, and do not appear to be residual with respect to Hawaiian tholeiite magmas. At present there are too few REE data for Hawaiian xenoliths to rigorously test our partial melting models.

Conclusions

The petrology and geochemistry of summit lavas from Kilauea and Mauna Loa volcanoes are sufficiently distinct to suggest that these lavas are not genetically related by crystal fractionation processes. Temporal-compositional relationships further suggest that REE abundance patterns for Kilauea and probably Mauna Loa magmas have not been significantly modified by differentiation processes during ascent to the surface. If these REE profiles are indeed representative of REE profiles in Kilauea and Mauna Loa primary magmas, then it seems likely that differences between the REE profiles of the two magma types could be produced only by partial melting of source regions having different mineral constitution. We are currently testing this conclusion by further analyses of samples from Mauna Loa. Because these two volcanoes are situated only 30 km apart, it seems most likely that their magmas are derived by melting at different depths. The higher garnet/clinopyroxene ratio inferred for the Mauna Loa source would seem to be compatible with melting at greater depth below this volcano. Until further work has been done on Hawaiian lavas and ultramafic xenoliths it seems premature to explore tectonic implications of our models; however, our approach, coupled with radiogenic isotope studies, may lead to a better understanding of mantle heterogenieties beneath the Hawaiian Islands.

The results of Pb (*Tatsumoto*, personal communication, 1977) and Sr and Nd (*O'Nions et al.*, 1977) isotopic studies of samples from Kilauea and Mauna Loa indicate that their respective source materials may be isotopically distinct, and that these isotopic heterogeneities in the Hawaiian mantle may have persisted for long periods of time.

Acknowledgements

We express our thanks to T.L. Wright for providing the samples used in this study, and M. Menzies, D.M. Shaw, and F.A. Frey for helpful reviews of the manuscript. This research has been supported by NASA Grant NGL-38-002-039 and NSF Grant 30-262-1711. We thank T.V. Anderson and W.T. Carpenter for irradiating samples in the O.S.U. TRIGA Reactor.

Note added in proof:

Twelve additional samples, containing about 7 wt.% MgO, from Mauna Loa have chondrite-normalized REE profiles that agree closely with that presented here for a single prehistoric lava, thus confirming a consistent difference in REE profiles between Kilauea and Mauna Loa. We also wish to emphasize that an important objective of this study is to evaluate simple melting models for Hawaiian basalts. Because certain parameters in these models (such as distribution coefficients and REE profiles in the postulated source material) are not well established, our models must be considered tentative. As an example, recently published Sm-Nd isotopic data seem to require a light-REE depleted source material for Hawaiian basalts. Preliminary models involving such a source yield calculated liquids with REE profiles similar to those observed in the Kilauea and Mauna Loa basalts. However, our conclusion that the respective source regions differ with respect to mineral constitution and(or) bulk composition still seems viable. Future modelling involving transition metals may help resolve additional details of the mantle beneath Hawaii.

References

Arth, J.G., and G.N. Hanson, Geochemistry and origin of the early precambrian crust of northeastern Minnesota, *Geochim. et Cosmochim. Acta, 39*, 325-362, 1975.

Davis, B.T.C., and J.F. Schairer, Melting relations in the join diopside-forsterite-pyrope at 40 kilobars and at one atmosphere, *Carnegie Institute Washington Yearbook, 64*, 123-134, 1965.

Eaton, J.P., and K.J. Murata, How volcanoes grow, *Science, 132*, 925-938, 1960.

Green, D.H., and A.E. Ringwood, Mineralogy of peridotitic compositions under upper mantle conditions, *Phys. Earth Planet. Interiors, 3*, 359-371, 1970.

Grutzeck, M., S. Kridelbaugh, and D.F. Weill, The distribution of Sr and REE between diopside and silicate liquid, *Geophys. Res. Letters, 1*, 273-275, 1974.

Jackson, E.D., and T.L. Wright, Xenoliths in the Honolulu volcanic series, *Jour. Petrology, 11*, 405-430, 1970.

Jamieson, B.G., Phase relations in some tholeiitic lavas illustrated by the system R_2O_3-XO-YO-XO_2, *Mineral. Magazine, 37*, 538-554, 1970.

Kay, R.W., and P.W. Gast, The rare earth content and origin of alkali-rich basalts, *Jour. Geology, 81*, 653-682, 1973.

Koyanagi, R.Y., E.T. Endo, and J.S. Ebisu, Reawakening of Mauna Loa volcano, Hawaii: A preliminary evaluation of seismic evidence, *Geophys. Res. Letters, 2*, 405-408, 1975.

Kushiro, I., Compositions of magmas formed by partial zone melting of the Earth's upper mantle, *Jour. Geophys. Research, 73*, 619-634, 1968.

Kushiro, I., The system forsterite-diopside-silica with and without water at high pressures, *Am. Jour. Sci., 267-A*, 269-294, 1969.

Masuda, A., and I. Kushiro, Experimental determination of partition coefficients of ten rare earth elements and barium between clinopyroxene and liquid in the synthetic silicate system at 20 kilobar pressure, *Contr. Mineralogy Petrology, 26*, 42-49, 1970.

McKay, G.A., and D.F. Weill, Petrogenesis of KREEP, *Proc. 7th Lun. Sci. Conf.*, 1976, in press.

Murali, A.V., W.P. Leeman, M.-S. Ma, and R.A. Schmitt, Evaluation of fractionation and hybridization models for Kilauea eruptions and probable mantle source of Kilauea and Mauna Loa tholeiitic basalts, Hawaii--A trace element study, *Jour. Petrology*, 1978, submitted.

Nagasawa, H., H. Wakita, H. Higuchi, and H. Onuma, Rare earths in peridotite nodules: an explanation of the genetic relationship between basalt and peridotite nodules, *Earth Planet. Sci. Letters, 5*, 377-381, 1969.

O'Nions, R.K., P.J. Hamilton, and N.M. Evensen, Variations in $^{143}Nd/^{144}Nd$ and $^{87}Sr/^{86}Sr$ ratios in oceanic basalts, *Earth Planet. Sci. Letters, 34*, 13-22, 1977.

Philpotts, J.A., C.C. Schnetzler, and H.H. Thomas, Petrogenetic implications of some new geochemical data on eclogitic and ultrabasic inclusions, *Geochim. et Cosmochim. Acta, 36*, 1131-1166, 1972.

Reid, J.B., and F.A. Frey, Rare earth distribution in lherzolite and garnet pyroxenite xenoliths and the constitution of the upper mantle, *Jour. Geophys. Research, 76*, 1184-1196, 1971.

Schilling, J.G., and J.W. Winchester, Rare earth contribution to the origin of Hawaiian lavas, *Contr. Mineralogy Petrology, 23*, 27-37, 1969.

Shaw, D.M., Trace element fractionation during anatexis, *Geochim. et Cosmochim. Acta, 34*, 237-243, 1970.

Shaw, D.M., Trace element behaviour in anatexis, or why make muddled models?, *Proceed. Chapman Conference: Partial Melting in the Earth's Upper Mantle*, 1977, in press.

Shimizu, N., Geochemistry of ultramafic inclusions from Salt Lake Crater, Hawaii and from Southern African Kimberlites, *Phys. Chem. Earth, 9*, 655-669, 1975.

Shimizu, N., and I. Kushiro, The partitioning of rare earth elements between garnet and liquid at high pressures: Preliminary experiments, *Geophys. Res. Letters, 2*, 413-416, 1975.

Sun, S.-S., and G.N. Hanson, Rare earth element evidence for differentiation of McMurado volcanics, Ross island, Antarctica, *Contr. Mineralogy Petrology, 54*, 139-155, 1976.

Swanson, D.A., Magma supply rate at Kilauea volcano, 1952-1971, *Science, 175*, 169-170, 1972.

Taylor, S.R., and M.P. Gorton, Geochemical application of spark source mass spectrography III: Element sensitivity, precision and accuracy (preprint), 1977.

Thompson, R.N., Is upper-mantle phosphorous contained in sodic garnet?, *Earth Planet. Sci. Letters, 26*, 417-424, 1975.

Wright, T.L., Chemistry of Kilauea and Mauna Loa lava in space and time, *U.S. Geol. Survey Prof. Paper, 735*, 40 p., 1971.

Wright, T.L., Magma mixing as illustrated by the 1959 eruption, Kilauea volcano, Hawaii, *Geol. Soc. America Bull., 84*, 849-858, 1973.

Wright, T.L., and R.S. Fiske, Origin of the differentiated and hybrid lavas of Kilauea volcano, Hawaii, *Jour. Petrology, 12*, 1-65, 1971.

CHEMICAL AND ISOTOPIC COMPOSITIONS OF LAVAS OF ISLA TORTUGA AND INDICATIONS OF PARTIAL FUSION OF ISOTOPICALLY DISTINCT MANTLE SOURCE IN THE VICINITY OF OCEANIC SPREADING CENTERS

Rodey Batiza*
Scripps Institution of Oceanography
La Jolla, California 92093

(Extended Abstract)

Isla Tortuga (Fig. 1) is a small (45 km^3) and young ($\leq$ 1.7 m.y.) tholeiitic oceanic central volcano. It is both structurally and petrologically linked to the actively spreading trough with which it is associated (the Guaymas basin). The significance of Tortuga and other small volcanoes located on young oceanic crust lies in the fact that if they remain active as they drift away from the ridge crest, the chemical and isotopic content of their lavas may help to elucidate several important petrogenetic problems. For example, these seamounts may provide a continuous petrologic record of the transition from LIL-depleted tholeiitic ridge-crest volcanism to more typically undepleted, alkalic "off-ridge" volcanism (*Batiza*, 1977a). Thus, they may help to determine the nature of changes either in the chemical or phase composition of the oceanic upper mantle and the processes of partial melting responsible for the production of these chemically different magma types. Results from the study of Tortuga bear on this particular problem.

The regional setting, geology, petrology, and geochemistry of Isla Tortuga are discussed by *Batiza* (1977b), and the results of Sr^{87}/Sr^{86} and rare-earth element (REE) abundance determinations will be presented by *Batiza et al.* (in prep.). Tortuga is composed of LIL-depleted tholeiitic basalt, abundance fractionated basalt and small volumes of icelandite. Numerical models of the major and trace element (including REE) contents of the lavas of this suite support the hypothesis that the more evolved lavas are related to the most Mg and Ni-rich Tortuga samples by simple fractional crystallization of a low-pressure phase assemblage. Furthermore, the most Mg and Ni-rich Tortuga lavas could evolve from a typical mid-ocean ridge tholeiitic liquid by subtraction of about 10 wt. % of Fo85 (*Batiza et al.*, in prep.). It is therefore concluded that the source of the Mg and Ni-rich Tortuga lavas is identical with that of the nearby spreading center lavas.

However, the Sr^{87}/Sr^{86} ratios of the Tortuga lavas ranges from 0.7024 to 0.7036 which is much larger variation than would be produced in a suite of comagmatic lavas produced by partial melting of an isotopically homogeneous source in the upper mantle. Further, the Sr^{87}/Sr^{86} ratios appear to be related to the chemical compositions of the lavas (but not to

---

* Present address: Department of Earth and Planetary Sciences, McDonnell Center for the Space Sciences, Washington University, St. Louis, Missouri 63130

Figure 1. Isla Tortuga.

their stratigraphic position). For example, the negative correlation between MgO and Sr^{87}/Sr^{86} of the lavas has $r^2 = 0.73$. This variation in Sr^{87}/Sr^{86} could be due to contamination of the lavas by a small amount (2-3 wt. %) of material having an Sr^{87}/Sr^{86} of 0.71 and Sr = 500 ppm, or by mantle heterogenieties in the source region of the Tortuga lavas. Production of the high Sr^{87}/Sr^{86} ratio in the crust by the radioactive decay of Rb^{87} in a magma chamber, for example, is precluded by the youth and low Rb/Sr of the lavas. Contamination of the lavas by material having high Sr content and low Sr^{87}/Sr^{86} is precluded by the low Sr abundance of the Tortuga lavas and lack of correlation between Sr content and Sr^{87}/Sr^{86} of the lavas after the removal of the effects of fractional crystallization on their Sr contents. It may be possible to determine whether contamination or mantle heterogeneities have caused the observed range of Sr^{87}/Sr^{86} on Tortuga examination of the Nd^{143}/Nd^{144} ratios of the lavas (determinations are in progress). If the range of Sr^{87}/Sr^{86} is not due to contamination, then it must be due to mantle heterogeneities in the source region of the lavas. Since the range of strontium isotope ratios on Tortuga is greater than that observed at the mid-ocean ridges, it may represent the mixing of two isotopically distinct mantle sources. However, these isotopically distinct mantle sources must be very similar in other respects, since the Tortuga lavas appear to be related by simple fractional crystallization. It is suggested that Tortuga may be representative of central volcanoes located over the narrow transition zone between the depleted mantle source of ridge crest tholeiites and the less-depleted mantle source of "off-ridge" volcanism.

References

Batiza, R., Geology, petrology and geochemistry of Isla Tortuga, a recent tholeiitic island in the Gulf of California, *submitted to Geol. Soc. Amer. Bull.*, 1977a.

Batiza, R., Age, volume, compositional and spatial relations of small isolated oceanic central volcanoes, *Marine Geology*, in press, 1977b.

Batiza, R., K. Futa, and C.E. Hedge, Rare-earth element and strontium isotope abundances in lavas of Isla Tortuga, in preparation.

TRACE ELEMENT BEHAVIOUR DURING ANATEXIS

Denis M. Shaw
Department of Geology
McMaster University
Hamilton, Ontario
Canada

Abstract

The behaviour of trace elements during anatexis has been thoroughly explored in recent years in algebraic and geometric applications of the Berthelot-Nernst partition rule. Experimental measurements are beginning to suggest the magnitudes and variabilities of partition coefficients.

Some of the factors which are often neglected are (a) inadequacies in the theory, (b) variability of D-values, (c) measurement difficulties for D-values, (d) role of accessory minerals, (e) role of volatile phase, (f) petrological controls, (g) dynamics of melt separation, (h) wall-rock interactions.

Trace element models are useful provided allowance is made for these factors and the geological base is sound.

Introduction

Development of the theory of trace element behaviour in heterogeneous phase equilibria has led to numerous studies of magmatic crystallisation over the last 30 years: adaptations of the theory to anatexis have been elaborated more recently. Quantitative applications in both fields have been hindered by a lack of measurements of the essential parameters, i.e. partition coefficients (D-values), but the situation is improving rapidly and in recent years many trace element models of mantle and crustal fusion have been proposed. This is a worthwhile activity, but should be moderated in view of the inherent pitfalls and present-day uncertainties: this paper will review some of these.

The basic theory will first be stated, using certain simplifying assumptions. The effects of variation of D-values will next be examined, followed by a statement of a more generalized theory. Lastly the effects of phase petrology, melt migration dynamics and zone-refining will be shown to provide inescapable constraints on the trace element theory.

Simple theory for trace element behaviour during partial melting

Schilling and Winchester (1967), *Gast* (1968) and *Shaw* (1970) developed equations to describe the behaviour of a trace element during

TABLE 1. Definitions

W_o	mass (g) of whole system
W or W^s	mass of solid phases
L	mass of liquid phase
W^f	mass of fluid (gaseous) phase
F	= L/W_o fraction of liquid
S	= W^s/W_o = 1-F = fraction of solid
w_{io}	mass of component i in the whole system
w_i^s	mass of component i in the solids
w_i^ℓ	mass of component i in the liquid
c_{io}	mass concentration of component in the whole system
c_i^s or c_i	mass concentration of component in the solids
c_i^ℓ	mass concentration of component in the liquid
R_{i-j}	mass concentration ratio for components i, j
X^ε	mass fraction of solid phase ε among the other solid phases
p^ε	mass fraction of solid phase ε which melts, expressed as a fraction of the liquid phase
n_i^ε	number of moles of component i in phase ε
x_i^ε	mole fraction or cation fraction of component i in phase ε
K	molar equilibrium constant (also called K_D)
$\Delta_i^{\alpha-\beta}$	molar partition coefficient of component i between phases α,β
$D_i^{\alpha-\beta}$	mass partition coefficient of component i between phases α,β
$d_i^{\alpha-\beta}$	apparent value of $D_i^{\alpha-\beta}$ (see text)

partial melting. More recently *Hertogen and Gijbels* (1976) and *Consolmagno and Drake* (1976) have written on these theoretical topics. Using the terminology of the third reference, summarized in Table 1, the point of departure is the Nernst-Berthelot principle, that the ratio of the molar concentrations (x) of a component (i) soluble ideally in two phases (α,β) coexisting at equilibrium is

$$\Delta_i^{\alpha-\beta} = x_i^{\alpha}/x_i^{\beta} \tag{1}$$

and $\Delta_i^{\alpha-\beta}$ may be taken as constant, for constant P, T, and other components x_j, provided that the x_i are small. In practice the difference between molar and weight concentration is often ignored (not always with justification: see *Mysen*, 1976), the chemical identity of the component i is ignored and taken to be simply a metallic element or cation, and the partition coefficient Δ is then written as D, so that eq. (1) becomes

$$D_i^{\alpha-\beta} = c_i^{\alpha}/c_i^{\beta} \tag{2}$$

If the coexisting phases are solid (s) and liquid (ℓ) we can write (neglecting i)

$$D^{s-\ell} = D = c^s/c^{\ell}, \tag{3}$$

but if several solids α,β,ε coexist in equilibrium with liquid, we can define a bulk distribution coefficient, D or D_{WR} where,

$$D_{WR} = X^{\alpha}D^{\alpha-\ell} + X^{\beta}D^{\beta-\ell} + \ldots = \Sigma X^{\varepsilon}D^{\varepsilon-\ell} \tag{4}$$

where the X^{ε} are the mass fractions of the different phases, and $\Sigma X^{\varepsilon} = 1$. The $D^{\varepsilon-\ell}$ will now be taken as constants, but this already depends on the several assumptions already mentioned.

If a multiphase solid having a bulk partition coefficient D is partially melted, in such a manner that each phase melts in the proportion which it has in the initial rock (modal melting), three expressions may be derived to describe the concentration of a trace element i after a fraction F (where $0<F<1$) of liquid has been produced (see *Shaw*, 1970):

$$c^{\ell} = \frac{c_o}{D}(1-F)^{(\frac{1}{D}-1)} \qquad \text{Rayleigh fractionation} \tag{5}$$

$$\bar{c}^{\ell} = \frac{c_o}{F}\left[1-(1-F)^{\frac{1}{D}}\right] \qquad \text{accumulated fractions} \tag{6}$$

$$c^{L} = \frac{c_o}{D+F(1-D)} \qquad \text{equilibrium fusion} \tag{7}$$

The first of these gives the instantaneous concentration of i in the liquid separating at F, where the melt is continuously removed from the residual

solid: this formula was first derived by *Rayleigh* (1896) and may correspond closely to some geological situations (e.g., where liquid is continually squeezed out of a solid). The second expression shows the average or accumulated concentration of all the liquid fractions: this may closely portray the accumulation of melt fractions in a magma reservoir. Equation 7 shows the concentration obtained where complete equilibrium is maintained between solids and melt: it implies that rates of material diffusion within crystals and between crystals and liquid are greater than the rate at which heat is supplied to cause melting. *Hoffman and Magaritz* (1976) have shown that cation diffusion rates in silicate melts are 10^5 to 10^7 times faster than in silicate solids, but nevertheless local equilibrium might obtain if the grain-size is coarse (> 1 cm) and the time available is about 10^5 yr: this supposes a static environment without convective mixing, which would of course aid equilibration.

The restriction that a rock will melt in its modal proportions is generally far from true except where the minerals happen to be present in eutectic or peritectic proportions, so equations 5, 6, 7 need to be modified for the case where the proportions of the minerals entering the molten phase are p^ε ($\Sigma\, p^\varepsilon = 1$). This is achieved by defining a new bulk distribution coefficient

$$P = \Sigma\, p^\varepsilon D^{\varepsilon-\ell}, \tag{8}$$

which permits calculation (*Shaw*, 1970) of modified equations for non-modal melting:

$$c^\ell = \frac{c_o}{D_o}\left(1-\frac{PF}{D_o}\right)^{\left(\frac{1}{P}-1\right)} \tag{9}$$

$$\bar{c}^\ell = \frac{c_o}{F}\left[1-\left(1-\frac{PF}{D_o}\right)^{\frac{1}{P}}\right] \tag{10}$$

$$c^L = \frac{c_o}{D_o+F(1-P)} \tag{11}$$

In these expressions zero values for p^ε are permissible, so long as at least one is in the range $0<p^\varepsilon<1$. Using these equations it is thus possible to calculate the effect of partial melting on an initial assemblage of, say, ol+opx+cpx+spin+phlog, where only opx+phlog enter the melt. Of course the constraint that $0<F<1$ is further restricted, and melting will cease (or change course) when some phase α is exhausted, which obtains when

$$F = X^\alpha/p^\alpha \tag{12}$$

Melting thus proceeds in a series of steps, each ending with the exhaustion of one phase, being renewed with a new set of p^ε: the final concentration may be calculated by making the end parameters of one step become the initial parameters for the next step. Explicit analytic expressions for this have been derived by *Hertogen and Gijbels* (1976).

If attention is to be focussed on the behaviour of the concentration ratio R for two elements, i and j, equations 5 through 12 may be readily adapted. Thus for the accumulated liquid during modal melting we find that

$$\bar{R} = R_o \cdot \frac{1-(1-F)^{1/D_i}}{1-(1-F)^{1/D_j}} \qquad (13)$$

where R_o is the element ratio in the initial solid assemblage.

The foregoing simple theory depends on assumptions of various kinds, including the constancy of $D_i^{\varepsilon-\ell}$ (or D_i), i.e. that

$$\frac{dD_i}{dT} = \frac{dD_i}{dP} = \frac{dD_i}{dx_j} = 0 \qquad (14)$$

It also depends on the assumption that the proportions of mineral melting do not change, or

$$\frac{dp^{\varepsilon}}{dF} = 0 \qquad (15)$$

The theory furthermore disregards the effect of incongruent melting, and the effect of a second fluid phase (volatile-rich) and of other constraints imposed by the phase petrology. In addition the geometry and dynamics of heat supply (diffusion, convection, etc.) and of magma movement (viscosity, surface tension, density, etc.) have not been considered, nor have the chemical effects of moving magma on wall rocks (zone refining). Some of these factors will now be examined.

Dependence of D on other components

This effect may be studied analytically or experimentally. First looking at theoretical aspects, consider a binary solid solution series such as the Mg-Fe olivines. The molar partition coefficient for forsterite (fo) between solid and coexisting liquid is expressed by

$$\Delta_{fo} = x^s_{fo}/x^{\ell}_{fo}$$

If we use n to represent number of moles of any component, then

$$x^s_{fo} = n^s_{fo}/(n^s_{fo} + n^s_{fa}) = n^s_{Mg}/(n^s_{Mg} + n^s_{Fe}) = x^s_{Mg}$$

and the partition coefficient Δ_{fo} will equal Δ_{Mg}. The mass action law will now express the equilibrium constant K and it is easy to show that

$$\Delta_{Mg} = \frac{x^s_{Mg}}{x^{\ell}_{Mg}} = \frac{x^s_{fo}}{x^{\ell}_{fo}} = \frac{K}{K+x^{\ell}_{fa}(1-K)} \qquad (16)$$

for ideal solutions.

The dependence of Δ_{Mg} on the other component (iron in fayalite) at a given P, T is shown in Figure 1. When x^{ℓ}_{Mg} is very small of course

$x^{\ell}_{fa} \cong 1$ and $\Delta_{Mg} \cong K$, which is the Nernst-Berthelot law, but otherwise x^{ℓ}_{fa} varies and consequently Δ_{Mg} is not constant.

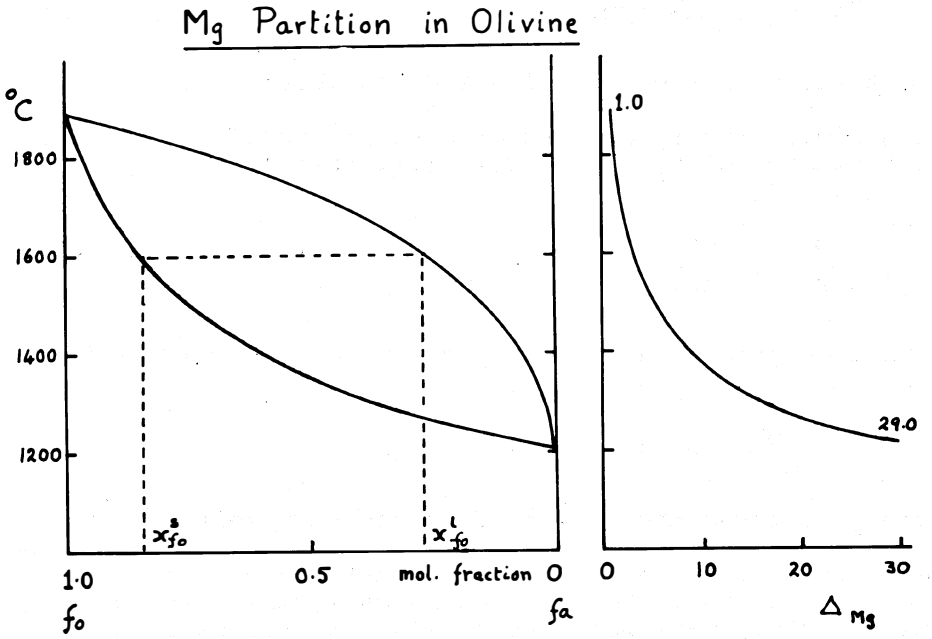

Fig. 1. Variation of partition coefficient Δ_{Mg} with T and composition under univariant conditions for the binary olivine system at constant pressure. The curves were calculated assuming an ideal molecular composition.

If we write the mass partition coefficient D for this system, we obtain

$$D^{s-\ell}_{Mg} = \Delta^{s-\ell}_{Mg} \cdot \frac{L}{W^s} \cdot \frac{\Sigma n^s_i}{\Sigma n^{\ell}_i}$$

or

$$D^{s-\ell}_{Mg} = \Delta^{s-\ell}_{Mg} \cdot \frac{M^{\ell}}{M^s} \qquad (17)$$

where M^{ℓ} (& M^s) is the weighted molecular (formula) weight) per component for all components (e.g. for Mg, Fe, Si, O or whatever combinations of these elements have been chosen as components). These are variables whose values will depend on the liquid fraction F, but will be of similar magnitude; so D will differ from Δ, but not by a great deal.

Passing to a ternary system, where a trace metal i may substitute at lattice sites occupied by two major metals, then as above we neglect the differences between molar and mass partition and equate

$$D^{\alpha-\beta}_i = x^{\alpha}_i / x^{\beta}_i .$$

Analysis of the effects of the major element (j or k) substitution leads to prediction of a linear relationship of the form

$$D^{\alpha-\beta}_i = a + bx^{\alpha}_j \qquad (18)$$

where a, b are constants, for the case where activity coefficients are close to unity. This means in practice that the partition of, for example, Ni between olivine and basalt should approximate a linear function of the forsterite fraction in the olivine.

The analysis may be extended to an r-component system, obtaining again a linear dependence:

$$D_i^{\alpha-\beta} = u_o + \sum_{j\neq i}^{r} u_j x_j^{\alpha} \qquad (19)$$

Turning now to experimental evidence for the dependence of D on bulk composition, many examples could be cited. A few have been chosen to illustrate different factors.

The first example is the effect of %An in plagioclase on the partition of Eu between plagioclase and liquid. Data compiled by *Zielinski* (1975, Fig. 4) and shown in Figure 2 indicates D-values ranging from 0.1 for calcic plagioclase to nearly 2 for albite.

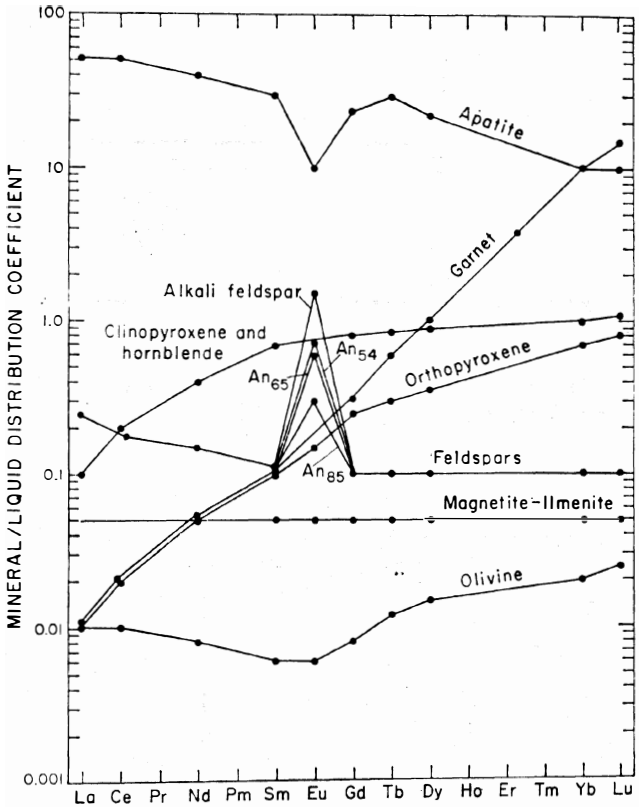

Fig. 2. Dependence of $D_{Eu}^{plag-melt}$ on plagioclase composition (*Zielinski*, 1975, Fig. 4).

Another example is the influence of the Ca-content of garnet on the partition of V between biotite and garnet. The original data (*Kretz*, 1959, Fig. 8) are shown in Figure 3a, and in Figure 3b they have been recalculated to show the approximate conformity with equation 18.

Numerous examples of non-Nernst partition of Rb, Cs, Sr, Ba between alkali feldspar of variable composition and aqueous solutions may be found in papers by *Iiyama* (1968), *Sabatier* (1971), *Lagache and Sabatier* (1973).

Iiyama (1965, 1970) also demonstrates how varying anion concentrations in the aqueous fluid may also affect D-values for alkali metals.

The influence of bulk melt composition is seen on measurements of partition between garnet and host lavas (*Irving and Frey*, 1976). With systematic increase in SiO_2 from basanite through hawaiite to andesite the range in values for Sm and Yb were:

$$D_{Sm} = 0.10 - 1.28$$

$$D_{Yb} = 6.5 - 56$$

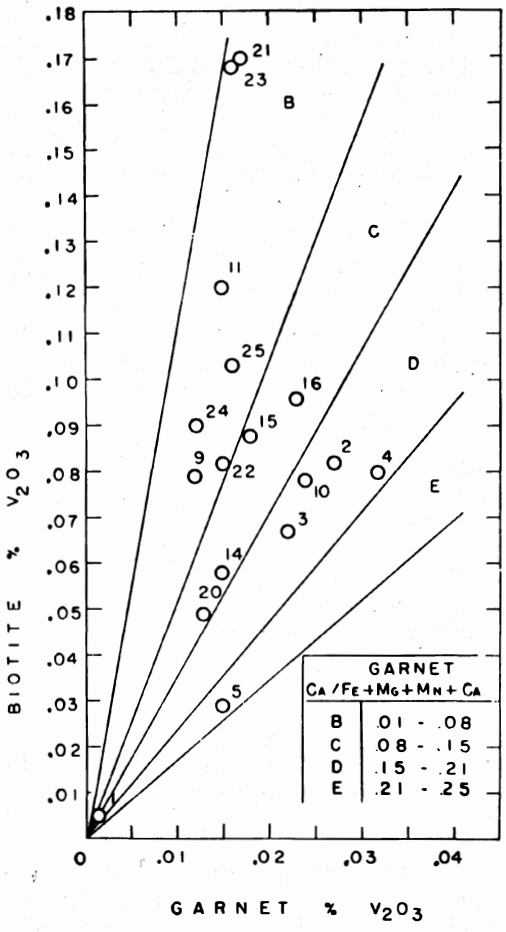

Fig. 3a. Partition of V_2O_3 between biotite and hornblende in relation to x_{Ca}^{gar}, original data (*Kretz*, 1959, Fig. 8).

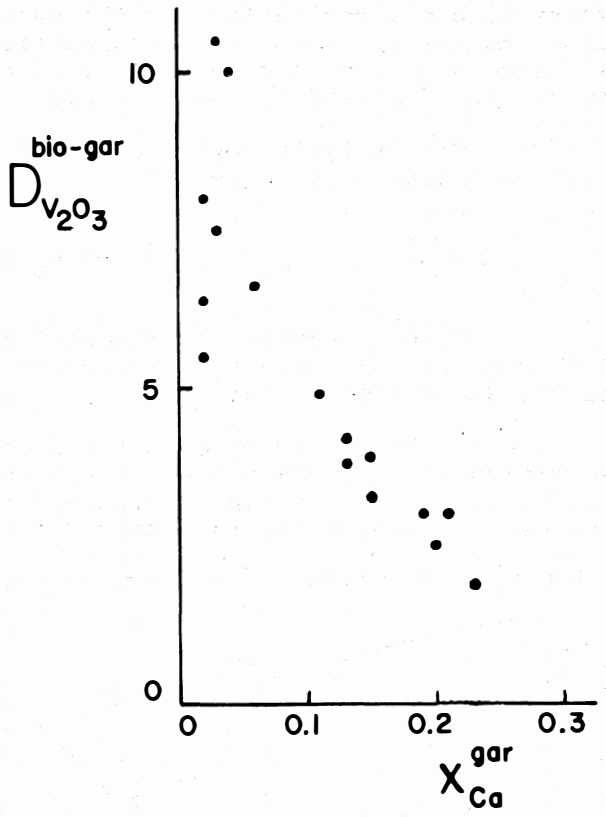

Fig. 3b. Partition of V_2O_3 between biotite and hornblende in relation to x_{Ca}^{gar}, data recalculated to show the approximately linear dependence predicted by equation 18.

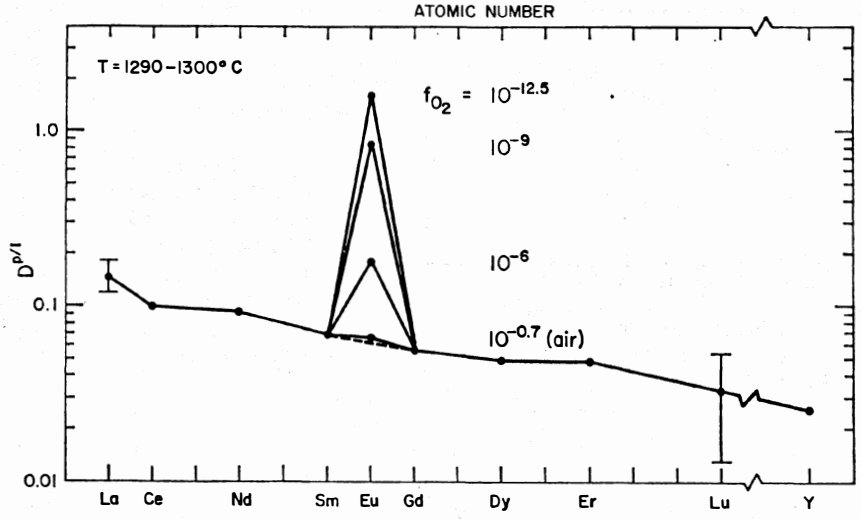

Fig. 4. Dependence of $D_{Eu}^{plag-melt}$ on oxygen fugacity (*Drake and Weill*, 1975, Fig. 6).

Oxidation state is often relevant to the partition of a polyvalent element. Variation of Eu partition between plagioclase and melt depends strongly on f_{O_2} and has been experimentally demonstrated by *Drake and Weill* (1975, Fig. 6) as shown in Figure 4.

The next and last example can best be described as a non-Nernst distribution for which no specific cause of the non-ideality is evident. Figure 5 shows an inflection in the Roozeboom plot of Sm in opx versus Sm in coexisting basaltic liquid, taken from *Mysen* (1976, Fig. 4). One is led inexorably to suspect the experimental results, and even though the analytical errors seem very small, small amounts of a rather incompatible element "inside" an orthopyroxene may have no thermodynamic significance.

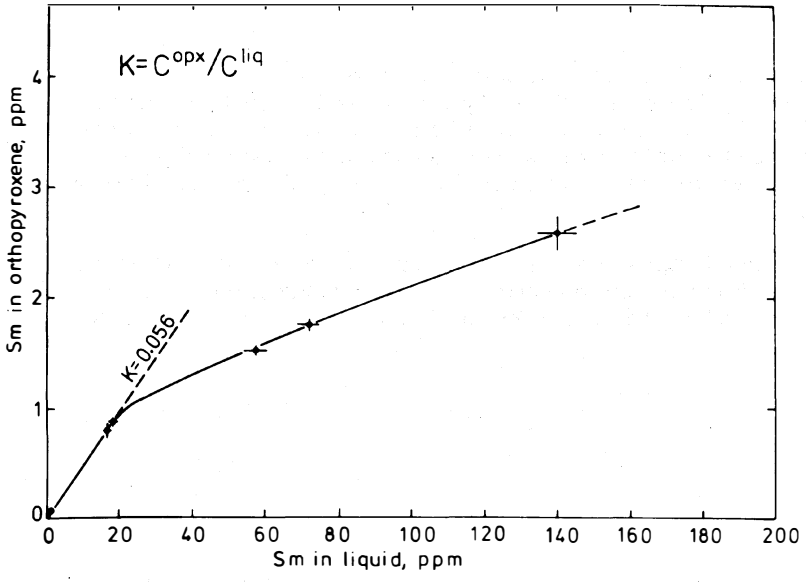

Fig. 5. Non-Nernst partition of Sm between orthopyroxene and melt (*Mysen*, 1976, Fig. 4).

Dependence of D on P and T

The theoretical basis for expecting element partition to be temperature and pressure dependent comes from the mass-action law. The equilibrium constant for a binary, two-phase (α,β), two cation (i,j) exchange, assuming unit activity coefficients is

$$D_i^{\alpha-\beta}/D_j^{\alpha-\beta} = K_D = \exp(-\frac{\Delta G}{RT})$$

(the usual symbol K could be used, but an anglo-saxon tradition not only to prefer K_D, but also to incorrectly call it a partition coefficient, is widespread), where ΔG is the free energy change at P,T. Variation of K_D will then be expressed by:

$$\ell n(K_{D1}/K_{D2}) = -\frac{\Delta H}{R}(\frac{1}{T_1} - \frac{1}{T_2}) \qquad (20)$$

$$\text{or} \quad \ell n\, K_D \propto \frac{1}{T} \qquad \text{for constant P,}$$

and

$$\ell n(K_{D1}/K_{D2}) = \frac{\Delta V}{RT}(P_1 - P_2) \qquad (21)$$

$$\text{or} \quad \ell n\, K_D \propto P \qquad \text{for constant T.}$$

Many examples could be cited of studies which purport to show natural systems for which equations 20, 21 apply. For some, major elements have been used, necessitating use of K_D, but for systems where component i is a trace element the equations, under adequate assumptions, reduce to:

$$\ell n\, D \propto \frac{1}{T} \quad \text{and} \quad \ell n\, D \propto P$$

Attempts to demonstrate these relations using rocks have often given ambiguous results, partly as a result of analytical and sampling problems (e.g. resulting from zoning in garnets), but also because of the difficulty of establishing the P,T conditions under which a natural assemblage crystallized. Recently, experimental studies have helped to provide more satisfactory calibrations.

An example of major element partition varying with P and T is given by the Mg, Fe^{2+} substitution in garnet and clinopyroxene (*Raheim and Green*, 1975) from basaltic (eclogitic) rocks and is shown in Figure 6.

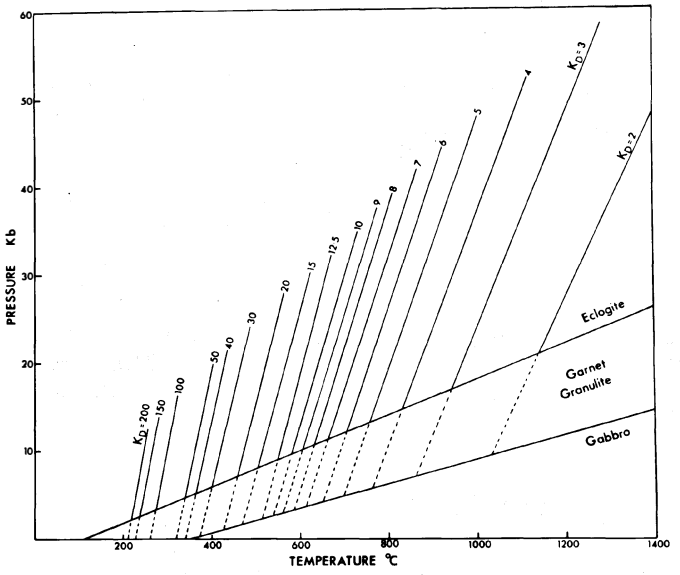

Fig. 6. The Mg-Fe exchange equilibrium constant for garnet-clinopyroxene (K_D) as a function of P and T (*Raheim and Green*, 1975, Fig. 1).

For trace element partition, the behaviour of Sr, Ba and REE has been investigated by many authors, and studies by *Sun et al.*(1974) and *Drake and Weill* (1975) show significant T-dependence for some elements in the plagioclase-basalt melt system[1]: an example from the last authors is seen in Figure 7. The REE also show significant T variations in partition between olivine and water (w): combining their experimental results from the equality

[1] In experiments of this kind the effects of T cannot strictly be distinguished from those of composition variation on the liquidus and solidus.

$$D^{oliv\text{-}cpx} = D^{oliv\text{-}w}/D^{cpx\text{-}w},$$

Cullers et al. (1973) obtained ol-cpx partition values applicable to natural rocks (at 1 kb pressure), which are compared with observed basaltic mineral partitions (Fig. 8). Geothermometric interpretations are clearly possible.

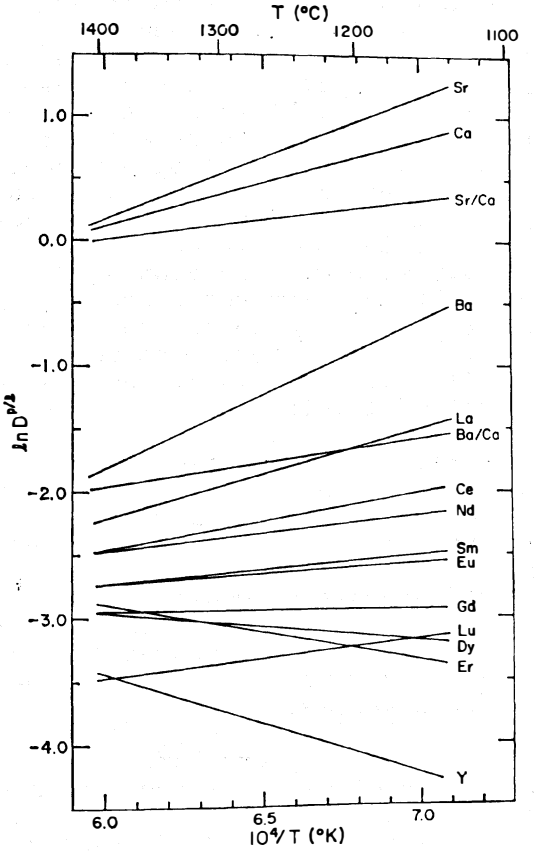

Fig. 7. Temperature dependence, at constant pressure, of $D^{plag\text{-}melt}$ for various elements (*Drake and Weill*, 1975, Figs. 2,3).

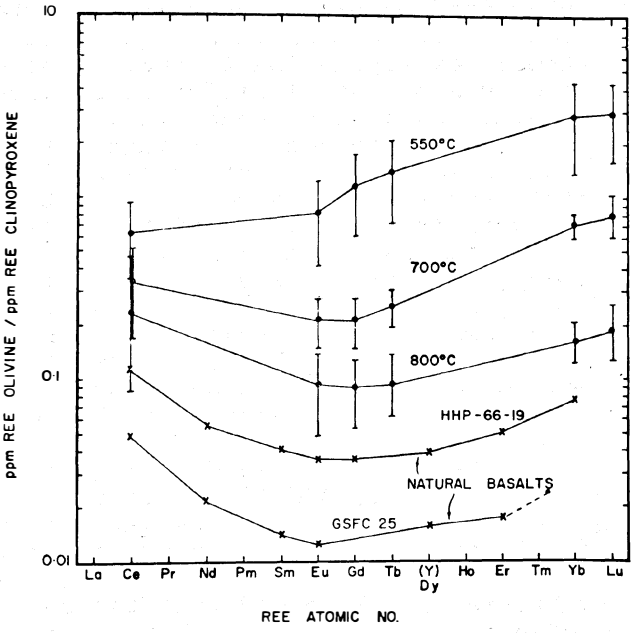

Fig. 8. Comparison of $D^{ol\text{-}cpx}$ for the REE as measured on natural rocks with experimental results at three temperatures (*Cullers et al.*, 1973, Fig. 6).

A number of other T-dependent partition coefficients for Ni, Co have been determined by *Leeman* (1973) and *Hart et al.* (1976): composition effects again are important. A summary of most available data is given by *Drake* (1976).

The effect of P on trace metal substitution is less well-known. *Shimizu and Akimoto* (1971) and *Shimizu* (1974) however showed that there was little change in $D^{cpx\text{-}basalt}$ between 15 and 50 kb for Sr, Ba, K, Rb, Cs. Preliminary results on $D^{gar\text{-}basalt}$ for REE at 30 kb have been obtained by *Shimizu and Kushiro* (1975), so information on P effects in this important system may be forthcoming soon.

There are numerous sources of uncertainty in values of partition coefficients used in melting models. These may somewhat artificially be divided into two groups, according to whether D is measured by laboratory experiment or on a quenched natural system.

Two of the problems in laboratory measurements are common to all experimental mineralogy. The first is that laboratory experiments are simpler than Nature, either in the external variables which have fewer degrees of freedom or in shorter time-periods, or in simpler chemical systems: extrapolation to real rocks may therefore be hazardous. The second is slowness of diffusion between grain interiors, grain surfaces, and melt. As a consequence it is difficult to establish whether equilibrium has been reached: a thoughtful study along these lines relevant to REE partition has been given by *Zielinski and Frey* (1974). Another experimental problem, more specific in nature, is that until recently analytical techniques frequently lacked the sensitivity required for precise analyses of trace metals on the (usually) small samples obtainable in controlled P,T experiments: it was consequently necessary to boost the abundance range by 2 to 4 orders of magnitude, hoping that the D-values thereby obtained would remain valid at lower concentrations. Radiochemical techniques are now available for some elements, to obviate these problems (see, for example, *Mysen and Seitz*, 1975; *Seitz and Hart*, 1973), and many D-values can now be measured at low concentration levels.

D-values obtained from quenched natural rocks have two main sources of error, additional to analysis problems. The first is impurities in mineral separates. This may take the form of surface or interior contamination, often of unknown nature, and is the most serious for minerals which are not preferred hosts for the element in question. Thus *Hart and Brooks* (1974) showed that two volcanic clinopyroxenes contained lower abundances of K, Rb, Cs, Sr, Ba than are normally reported, but only after the minerals had been subjected to ultra-meticulous sample separation and cleansing: as a consequence the phenocryst-matrix D-values were lower by factors of from 6x to 100x than other literature values.

This example nevertheless raises an interesting problem. If a clinopyroxene of this kind form part of a rock undergoing melting, which is being represented by a model such as given by equations 5-11, should the mineral be represented by a "clean" or a "dirty" D-value? Certainly the clean value is the only one which makes mathematical sense, but it is nevertheless the dirty pyroxene which is melting. This pyroxene partition paradox is unresolved.

Another troublesome form of impurity is the foreign inclusion. Sometimes its presence is clear, e.g. where Cr values in olivine are attributable to chromite inclusions. In other cases its presence may be suspected, as with the REE abundances in the biotite shown in Fig. 9. The abundance pattern mimics closely the pattern in the apatite, but at a level 10x lower: the almost universal occurrence of apatite inclusions in plutonic biotites suggests that the biotite is contaminated. Rare-earth D-values for other biotites may also be suspect.

The other source of error in D-values from quenched natural assemblages comes from having unknowingly analyzed inhomogeneous crystals. The most common inhomogeneity is zoning, which is seldom visible in thin section for minerals of higher symmetry: zoning of course reflects changes in major or minor elements, but often suggests parallel changes in trace elements. Zoning in garnet is seen in Fig. 10: if a D-value were to be

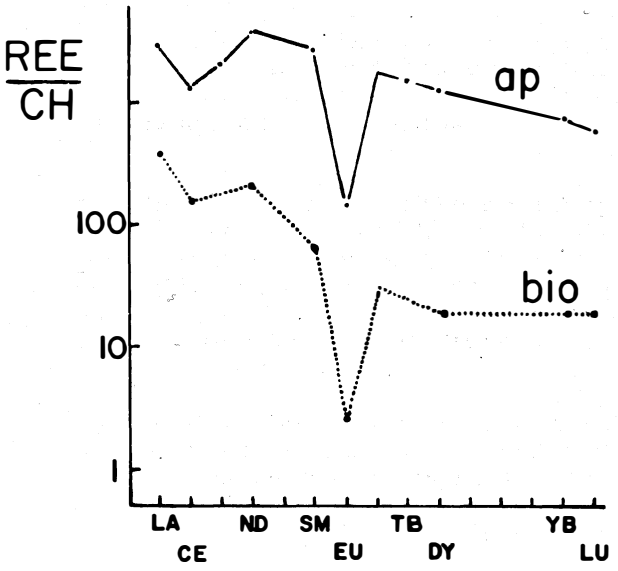

Fig. 9. Chondrite-normalized REE abundances in apatite and biotite from the Albtal granite (after *Puchelt and Emmermann*, 1976, Fig. 3). The distribution patterns are closely similar, but differ by an order of magnitude.

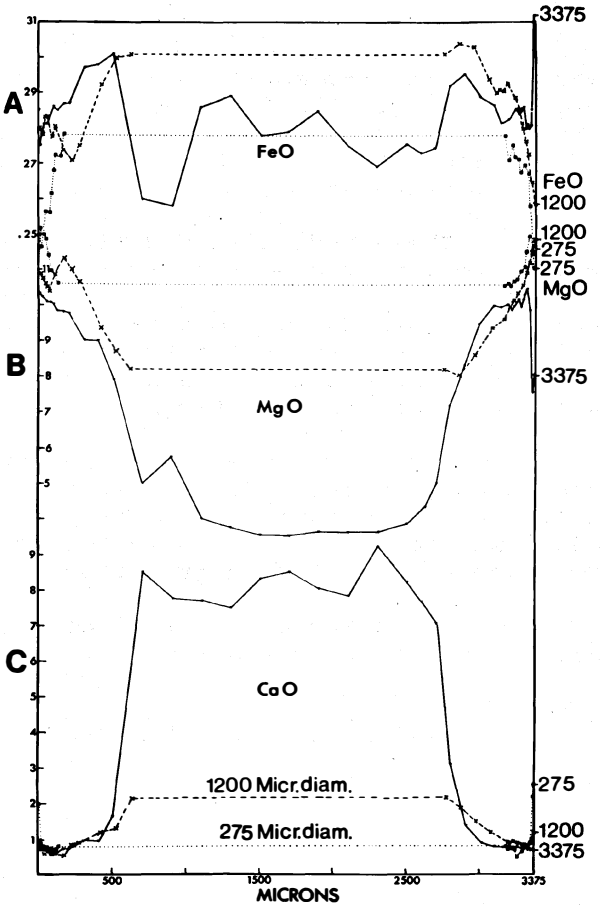

Fig. 10. Element profiles measured across garnet grains of various diameters, as indicated (*Råheim*, 1975, Fig. 10).

to be measured between such garnet and nearby pyroxene, using an REE or Ni, camouflaged by Ca and Mg, respectively, the meaning of "coexisting" would be ambiguous. At any stage during its growth, the outer rim of a garnet crystal might be in equilibrium with the outer rim of a nearby pyroxene grain, but it would not necessarily follow that either separated garnets or a polished section microprobe analysis would satisfactorily represent the concentration in the garnet.

If the system of study be a phenocryst (ph) which has crystallized from the surrounding igneous melt, now seen as fine-grained groundmass (gm), and if the phenocryst embodies extreme fractional crystallization (i.e. extreme zoning) sometimes referred to as Doerner-Hoskins or logarithmic fractionation, then analysis of the whole phenocryst and nearby groundmass will give a false partition coefficient d^{ph-gm}, expressed by

$$d = \frac{1-F^D}{F^{D-1}(1-F)} \tag{22}$$

where only mineral ph is crystallizing, with true partition coefficient D (or D^{ph-gm});

or

$$d = \frac{D}{D_{WR}} \cdot \frac{1-F^{D_{WR}}}{F^{(D_{WR}-1)}(1-F)} \tag{23}$$

where D_{WR} is from equation 4, for the case where several minerals are crystallizing. The difference between the false and true values can be very great. For example, if the true coefficient is 5, then application of equation 22 with 50 per cent crystallization would give an apparent phenocryst-groundmass partition of 31.

These and related diffusion-controlled effects have been studied theoretically by *Albarede and Bottinga* (1972). L.H. Haskin has pointed out in several papers (e.g. *Haskin et al.*, 1970), that the apparent coefficient between two coexisting zoned phenocryst species, e.g. $d^{phl-ph2}$ will equal the true value $D^{phl-ph2}$, from equation 23, but for this to be true it is necessary to know that the two minerals began and ended crystallization at the same times.

Probably the second greatest failing of D-values obtained from the phenocryst-matrix principle is however that it is seldom certain that the phenocrysts formed from the portion of the magma now seen as the adjacent groundmass: this factor is particularly critical when treating cumulate-trapped liquid fractionation (e.g. *Maaloe*, 1976).

There are a number of other drawbacks to measuring D-values from natural minerals, but space does not permit a complete discussion.

TABLE 2. Some Measured Partition Coefficient Ranges

$D_K^{cpx-\ell}$	0.00045-0.7
$D_{Ba}^{hb-\ell}$	0.1-8.0
$D_{Eu}^{p\ell-\ell}$	0.055-4.2
$D_{Rb}^{bio-\ell}$	0.7-5.75

To conclude the discussion of D-value variation, Table 2 records some ranges, culled from the available literature in recent years. All the values came from reputable laboratories and there is no reason to suspect gross errors of measurement. The liquid phases were in all cases silicate melt or magma, but varied considerably in bulk composition. It is clear that (a) there is no such thing as constancy in D-value for a trace element, (b) the effects of bulk composition, P, T and measurement problems must be given further attention, if partition coefficients are to be used effectively in petrological modelling. It must be added, however, that usable values are nevertheless available for some elements, provided that temperature and bulk composition is specified.

A Generalized Theory

The variability of partition coefficients outlined in the preceding sections makes a generalization of the theory presented at the beginning rather necessary. We may assume that the melting proportions p^ε also vary, at least initially.

Using the symbols in Table 1, mass-balance and the partition principle establish that (as in *Shaw*, 1970, and following the approach of *Greenland*, 1970)

$$\frac{dc}{c} = \frac{dS}{S}\left(\frac{1}{D} - 1\right) \qquad (24)$$

for the trace element of interest. This is the basic equation from which equations 5-13 are derived. S is used rather than F to avoid integration problems. If we now accept that variations in p^ε and $D^{\varepsilon-\ell}$ (see equation 8) can be expressed as functions of the degree of melting (S or F), which for convenience may be written as $p^\varepsilon(S)$, $D^\varepsilon(S)$, we may use equations 8, 24 to obtain

$$\ell n\ c/c_o = \frac{1}{S}\int_1^S dS/[D_o-(1-S)\sum_\varepsilon p^\varepsilon(S)D^\varepsilon(S)] \qquad (25)$$

Integration of equation 25 requires explicit knowledge of the functions $p^\varepsilon(S)$ and $D^\varepsilon(S)$ and the mathematics can be troublesome: solutions for an analogous expression have been given by *Hertogen and Gijbels* (1976). A solution which is realistic in many cases is to accept that the p^ε are constants and that the partition coefficients are linear in S:

e.g. $D^\varepsilon(S) = u^\varepsilon + v^\varepsilon S$

If then we write $U = \sum_\varepsilon p^\varepsilon u^\varepsilon$, $V = \sum_\varepsilon p^\varepsilon v^\varepsilon$ and

$T = 4V(D_o - U) - (U - V)^2$

the solution to equation 25 becomes:

$$\ell n\ c/c_o = \frac{2}{S\sqrt{T}}\left[\tan^{-1}(2VS + U - V)/\sqrt{T} - \tan^{-1}(U + V)/\sqrt{T}\right] \qquad (26)$$

The individual user must decide whether the uncertainties in assumptions warrant using expressions such as equation 26.

Another factor necessary in a generalized theory is incongruent melting, which is the rule rather than the exception in many rocks undergoing anatexis. The equations derived by *Hertogen and Gijbels* (1976) appear ambiguous and an alternative formulation has been proposed (*Shaw*, in press).

Choice of Phases for Melting Models

Another critical factor in the development of models for trace element behaviour during anatexis is the modal composition of the hypothetical initial rock.

Most models start with either mantle or crustal rocks, although other materials such as deep ocean sediments may play a role. For mantle melting the usual source materials are spinel, olivine, orthopyroxene, clinopyroxene, garnet, amphibole, phlogopite and plagioclase: for crustal anatexis more siliceous rocks are taken, containing quartz, plagioclase, K-feldspar, amphibole, pyroxene and micas. All these phases except quartz are more or less complex solid solutions, whose compositions determine not only the initial bulk composition but also affect (as seen above) the partition coefficients of trace elements as melting starts. The choice of such compositions and coefficients determines profoundly the composition of the resulting magmas. It should hardly need adding that there is little reason to believe the mantle to be at all homogeneous in lithology, let alone the crust, and models will therefore of necessity be too simple.

Additional problems arise with accessory phases and volatile phases.

To illustrate the first of these consider the ubiquitous accessory, apatite. In the Albtal granite already considered (Fig. 9), *Puchelt and Emmermann* (1976) report that apatite makes up only 1 per cent of the rock, but contains 27 per cent of all the REE present and shows a marked negative Eu anomaly. The whole rock analysis also shows a (smaller) negative Eu anomaly. If the apatite had not been analyzed it might have been concluded that the whole rock anomaly resulted from the parent magma being depleted in Eu as the consequence of earlier crystallization of feldspars, whereas the depletion may in fact reflect prior crystallization of apatite. Which of these (if either) is true is beside the point, which is that interpretation of REE behaviour in this granite would be different if the apatite had not been considered. Analogous considerations apply to melting.

Another aspect of this example is that *Puchelt and Emmermann* (1976) show that the REE fractionation pattern of apatite (from different rocks) varies considerably, some specimens showing marked enrichment of LREE compared with HREE. In a melting model involving apatite the variety chosen would strongly affect the REE distribution in the resulting magma. These effects would be more important still in melting a peridotite, whose major phases contain lower REE abundances than in a granite.

The importance of accessory minerals thus lies in the fact that they are commonly enriched in certain rare metals: e.g.

chromite	Cr, Ni, Zn, Ir
zircon	Zr, Hf, U, Th
rutile, sphene	Ti, REE, U, Th, Nb, Ta
sulphides	Ni, Co, Pb, Zn, Cu
apatite	P, REE
allanite	REE
opaque oxides	Cr, Ni, Co, V

Rarer accessories such as monazite, xenotime, etc., may also be present.

The other choice, as mentioned above, is whether the anatexis will involve a fluid (volatile-rich second liquid); this is important in (at

least) two ways. The first is the obvious one, namely that fluids determine phase stabilities in various ways. Apart from the fact that this will influence the choice of major mineral phases in the model, e.g. amphibole is unstable at pressures greater than 10 to 18 kb (*Green and Ringwood*, 1970; *Lambert and Wyllie*, 1970), the abundance of fluid also determines the melting behaviour. In the melting of dry or water-deficient granodiorite, biotite will probably be the first phase to melt (Fig. 11), whereas if excess water is present K-feldspar will be the first to go: owing to the different K/Rb ratios of these two minerals the resulting magmas, and rocks later formed from them, may bear the imprint of these differences.

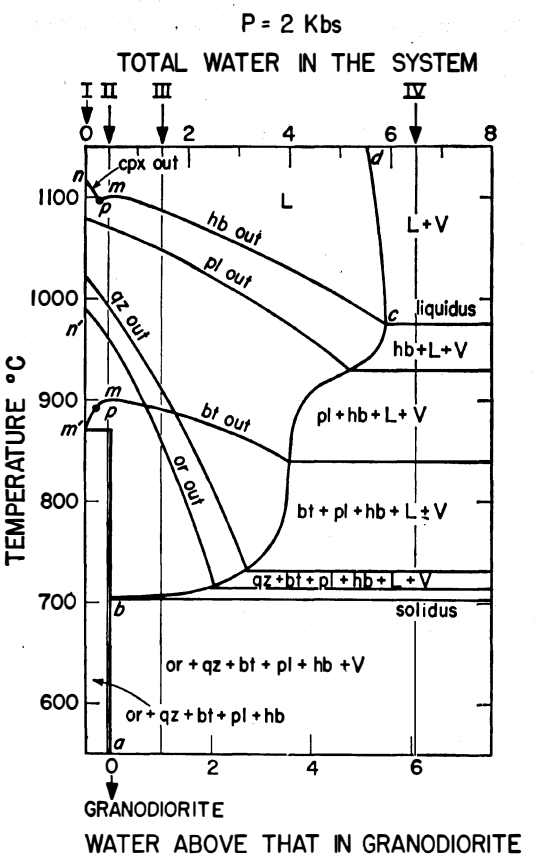

Fig. 11. Interpretation of phase stabilities during the melting of a granodiorite (no. 766-H_2O) in the presence of various relative amounts of water (*Robertson and Wyllie*, 1971, Fig. 4). The differing behaviour of biotite and K-feldspar could affect the K/Rb ratios of anatectic melt.

A second way in which a fluid phase is important is as a transient solution, holding some proportion of each element in the system. This additional phase differs from the other phases present in being less dense, less viscous and more volatile, so allowing a variety of possibilities for influencing trace element fractionation. A full theoretical treatment is impractical here, but a simplified approach will illustrate the possibilities, having in mind the subduction of wet sediments into a zone of anatexis.

Suppose a mass of W^s g of residual solids to be in equilibrium with W^l g of silicate melt, so that for the trace element of interest we have, as usual

$$c^s = D^{sl}c^L$$

where D^{sl} is the bulk partition coefficient. If we now add to the system W^f g of fluid, for which the bulk partition coefficient is D^{sf}, the concentration in the silicate magma will change to c^L, assuming equilibration. If we write $W^s/W^l = y$, $W^f/W^l = z$, then

$$\frac{C^L}{c^L} = \frac{D^{sf}(yD^{sl} + 1)}{zD^{sl} + D^{sf}(yD^{sl} + 1)}$$

$$\text{or} \quad \frac{C^L}{c^L} = \frac{yD^{sl} + 1}{zD^{fl} + yD^{sl} + 1} \qquad (27)$$

since $D^{sf}/D^{sl} = D^{fl}$.

Rather few values of solid-fluid, magma-fluid partition coefficients are known. However, experiments by *Cullers et al.* (1973) and *Zielinski and Frey* (1974) suggest that the REE are much more soluble in silicate melt than in (coexisting) water, in fact about two orders of magnitude more so than Rb (*Beswick*, 1973). Suppose for example we consider the

modal melting of a granodiorite consisting of two feldspars, quartz and a little biotite and hornblende. Using solid/magma partition coefficients from the literature for Rb and La, together with fluid/magma coefficients from the authors just quoted, we may use the following parameters:

$$D_{Rb}^{s\ell} = 0.24 \qquad D_{La}^{s\ell} = 0.09$$

$$D_{Rb}^{f\ell} = 1.03 \qquad D_{La}^{f\ell} = 0.05$$

If we now rewrite equation 27, putting the RHS equal to t, we can write

$$C^L = c^L t$$

for each element. The concentration ratios may be indicated by R

$$R = C_{Rb}^L / C_{La}^L \quad \text{and}$$

$$r = c_{Rb}^L / c_{La}^L$$

and then we have

$$R = r t_{Rb} / t_{La} \tag{28}$$

Remembering that $y = (1-F)/F$, equation 28 has been evaluated for different proportions of melting and three arbitrary values z equal to 1/10, 1 and 10 times the mass of liquid.

TABLE 3. Calculated Changes in Rb/La ratio R/r resulting from equilibration of a partial melt with water.

F	t_{Rb}/t_{La}		
	z=0.1	z=1	z=10
0.1	.96	.77	.30
0.3	.95	.63	.19
0.5	.92	.57	.16
0.7	.92	.54	.14

t = calculated concentration ratio in the (equilibrium) hydrous melt relative to dry melt.
z = mass fraction fluid relative to melt.

Two conclusions may be drawn from the results in Table 3. First of all, for a given z, the effect of different degrees of melting is not great: however, it should be borne in mind that the mass of fluid phase required in this model is proportional in each case to F. The second and more interesting conclusion is that for any F, increasing amounts of water decrease the concentration ratio markedly, attaining between 4 and 7 times decrease when the mass of water attains 10 times the mass of magma, compared with the dry system. This effect arises of course from the marked difference between $D^{f\ell}$ for the two elements, and is valid only so far as the values chosen may be accepted as realistic.

If in fact the $D^{f\ell}$ values <u>are</u> realistic, then ratios such as Rb/La might give information as to whether an anatectic magma was wet or dry.

Another model of obvious importance would include a relatively large mass of fluid phase at the onset of melting, thereafter disappearing to leave an already modified solid rock to undergo dry melting. This and other possibilities cannot be elaborated here (see *Shaw*, in press).

Phase Petrology Controls on Melting

The foregoing theory has mostly accepted implicitly the proposition that anatexis may be described in terms of a mathematically continuous function of F, the liquid fraction. This was because attention was focussed on trace elements, rather than major elements or the minerals which they form.

But the fractional melting of minerals, or their assemblages, may be a discontinuous process: after an initial (nearly isothermal) melting step, the further supply of heat may cause temperature to rise without further melting, until another invariant point is encountered, permitting melting to recommence. Such interpretations are not new, and follow directly from phase diagram topology (e.g. see *Presnall*, 1969). Depending on the solid solution relations and phase petrology of the particular system being considered, the first melting episode (ab, Fig. 12) may be nearly isothermal, yielding the same liquid composition from widely varying proportions of starting minerals: this is probably the reason why mid-ocean ridge basalt tends to have a globally uniform composition although the mantle source rocks are unlikely to be very uniform.

The first melting step ends upon exhaustion of one of the phases, whereupon the system has lost one of its effective components, the temperature is now below the solidus for the remaining components, and must rise to c (Fig. 12) before a new solidus is encountered and melting recommences, with a different composition. This behaviour is paralleled in practice, in rock-melting experiments, as shown in various studies by P.J. Wyllie and his colleagues, e.g. Fig. 13 (*Robertson and Wyllie*, 1971).

The major application of these considerations to trace element behaviour is to impose the restriction that the mineral proportions melting, the p^{ε}, may not be chosen arbitrarily. They must in fact be chosen to conform as closely as possible to the known phase petrology of the system. A second consequence is that the p^{ε} are nearly constant during a melting episode, and their variation in expressions such as equation 25 may often be ignored.

A final point in this connection is that the behaviour of accessory minerals may be of great importance in relation to the petrology of melting. Very little is known about this subject, except that Rosenbusch's rule (that euhedral crystal shape indicates early crystallization or late melting) is unreliable. Evidence from partially fused granulite and

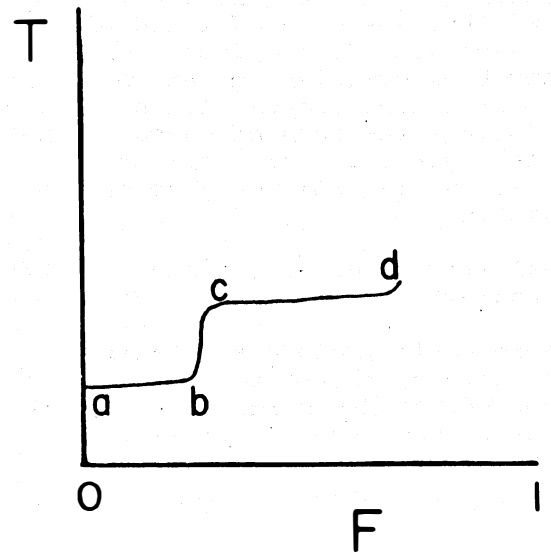

Fig. 12. Schematic illustration of discontinuous melting, after *Presnall* (1969) and *O'Hara* (1976). A step of nearly isothermal melting (ab) at an invariant point is followed by a period of heating (bc) with no melting, until the next invariant solidus is encountered, melting continuing isothermally (cd) and so on.

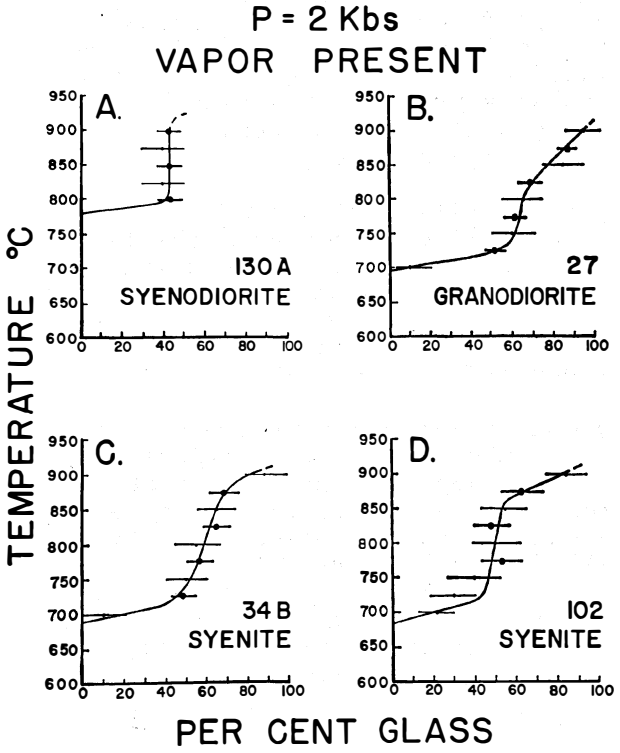

and anorthosite inclusions in lavas from Kilbourne Hole, N.M., shows enrichment of P (melting of apatite?) in glass (*E. Padovani*, pers. comm.), and it would be of great interest to know whether apatite melts early in peridotites: this is implied by *O'Hara* (1976) who points out that incompatible trace elements (i.e. for which $D \leq 0.01$) will be extensively liberated during the first one per cent melting of lherzolite. Of course small amounts of accessory minerals which melt early will only be diluted by subsequent melting. Of greater importance are accessory minerals which persist throughout a considerable melting interval (e.g. phlogopite, kaersutite, spinel): effects of this on REE behaviour have been discussed by *Sun and Hanson* (1975).

Zone-Refining

In the industrial process which bears this name, metals for which $D^{s-\ell} < 1$ become enriched in a zone of localized melting, as this zone of width h is made to pass along a rod of length t, traversing n (= t/h) zone lengths. The total enrichment is expressed by the final liquid relative concentration, c^z/c_o where

$$c^z = c_o \left[\frac{1}{D} + \left(1 - \frac{1}{D}\right)e^{-Dn}\right] \quad (29)$$

the first term in the RHS parentheses expresses the equilibrium partition, and the second is the added, cumulative effect of the refining process. This process has been considered to be important in mantle melting by *Harris* (1957), *Vinogradov and Yaroshevsky* (1965) among others.

It is not immediately clear that zone refining is relevant to models for anatexis. In the deep mantle it may well be a valid mechanism for enriching some trace

← Fig. 13. Melt percentage as function of temperature in experimental anatexis of several rocks (*Robertson and Wyllie*, 1971, Fig. 7).

elements in the interstitial melt persisting in the sub-lithospheric low-velocity zone: for if this interstitial melt be continually re-equilibrated with solids brought by convection from below, then the conditions for zone refining have been met. At higher levels the effect has often been invoked to describe the effect of an ascending silicate magma on its walls. As the magma rises along a conduit it will move down a thermal gradient: if it is dry, the pressure release will move the system further above the solidus and if the magma has entrained some of its source-rocks further melting may take place; if it is wet, volatiles will achieve saturation then second boiling will ensue until either the pressure release has been compensated or the system becomes solid with interstitial fluid.

In the second case the magma has little opportunity to incorporate material from wall-rocks, but in the former situation an ascending dry magma could melt appropriate wall-rocks, thereby enlarging its conduit and of course its mass. Those wall-rocks further away, beyond the supply of adequate heat for melting, might nevertheless supply any H_2O and CO_2 which they contained to the unsaturated magma: such a volatile fluid, if previously equilibrated with the wall-rocks, might then add to the magma's stock of the more soluble trace elements, perhaps the alkalis for example. The effect of these processes would depend greatly on the flow rate of rising magma, and heat diffusion rate into the wall-rock. It is clear that the effects are very small for many near-surface volcanic effects, or otherwise we would not find continental plateau basalts to have such similar compositions all over the world, after traversing the continental crust before effusion. At mantle depths more interaction is to be expected.

But these processes are not zone-refining, in which the essential element is a cyclicity, where solids repeatedly equilibrate with liquid. They are better described as wall-rock interaction or assimilation.

Conclusions

A number of factors have been considered which indicate that we should regard trace element anatexis models with some suspicion. These factors may be summarized as follows:

melting may be equilibrated, fractional or disequilibrated;

D-values are functions of P, T, bulk composition, f_{O_2};

experimental D-values are imprecise;

natural rock D-values are imprecise;

accessory minerals in source rocks are usually ignored;

volatile element influences;

phase petrology (geometric) effects;

zone-refining effects on wall-rocks.

Questions of a heterogeneous mantle and lower crust, non-isotopic T distribution at source and the dynamics of melt separation introduce further problems.

It should not, however, be supposed that trace element studies have therefore no value in solving geological problems, and that the construction of models should be abandoned. If an acceptable model has been constructed, using the geological evidence available in a given situation, then it is always desirable to test such a model with trace element data - such elements being much more sensitive than major elements to fractionationing mechanisms. Remarkable successes have been obtained in a few cases (Skaergaard complex, lunar basalts) in matching trace element analyses to fractionation models.

In the absence of geological supporting evidence, however, it appears unwise to construct geochemical models to explain the evolution of large segments of the earth's crust, often in the remote Precambrian, based only on a handful of analyses (however precise these may be), an assortment of partition coefficients as uncertain in quality as a used car, and an unbending faith in the integral calculus. Geology has not had very much quantitative theory to apply in the past, so let us use it remembering its limitations.

Acknowledgements

Permission to reproduce published diagrams which have appeared in the Journal of Geology, Earth and Planetary Science Letters, Geochimica et Cosmochimica Acta, was kindly given by The University of Chicago Press, Elsevier Publishing Company, Pergamon Press Ltd., respectively.

An earlier version of this article has benefited from reviews by S.R. Hart and H.J.B. Dick.

Financial support from the National Research Council of Canada is gratefully acknowledged. This is contribution no. 61 of the McMaster Isotopic, Nuclear and Geochemical Studies Group.

References

Albarede, F., and Y. Bottinga, Kinetic disequilibrium in trace element partitioning between phenocrysts and host lava, *Geochim. Cosmochim. Acta, 36*, 141-156, 1972.

Beswick, A.E., An experimental study of alkali metal distributions in feldspars and micas, *Geochim. Cosmochim. Acta, 37*, 183-208, 1973.

Consolmagno, G.J., and M.J. Drake, Equivalence of equations describing trace element distribution during equilibrium partial melting, *Geochim. Cosmochim. Acta, 40*, 1421-1422, 1976.

Cullers, R.L., L.G. Medaris, and L.A. Haskin, Experimental studies of the distribution of rare earths as trace elements among silicate minerals and liquids and water, *Geochim. Cosmochim. Acta, 37*, 1499-1512, 1973.

Drake, M.J., Evolution of major mineral compositions and trace element abundances during fractional crystallization of a model lunar composition, *Geochim. Cosmochim. Acta, 40*, 401-412, 1976.

Drake, M.J., and D.F. Weill, Partition of Sr, Ba, Ca, Y, Eu^{2+}, Eu^{3+}, and other REE between plagioclase feldspar and magmatic liquid: an experimental study, *Geochim. Cosmochim. Acta, 39*, 689-712, 1975.

Gast, P.W., Trace element fractionation and the origin of tholeiitic and alkaline magma types, *Geochim. Cosmochim. Acta, 32*, 1057-1086, 1968.

Green, D.H., and A.E. Ringwood, Mineralogy of peridotitic compositions under upper mantle conditions, *Phys. Earth Planet. Interiors, 3*, 359-371, 1970.

Greenland, L.P., An equation for trace element distribution during magmatic crystallization, *Amer. Mineral., 55*, 455-465, 1970.

Harris, P.G., Zone refining and the origin of potassic basalts, *Geochim. Cosmochim. Acta, 12*, 195-208, 1957.

Hart, S.R., and C. Brooks, Clinopyroxene-matrix partitioning of K, Rb, Cs, Sr and Ba, *Geochim. Cosmochim. Acta, 38*, 1797-1806, 1974.

Hart, S.R., K.E. Davis, I. Kushiro, and E.B. Watson, Partitioning of nickel between olivine and silicate liquid, *Geol. Soc. Amer. Abstr. with Programs, 8*, 906, 1976.

Haskin, L.A., R.O. Allen, P.A. Helmke, T.P. Paster, M.R. Anderson, R.L. Korotev, and K.A. Zweifel, Rare earths and other trace elements in Apollo 11 lunar samples, *Proc. Apollo 11 Lunar Sci. Conf., 2*, 1213-1231, 1970.

Hertogen, J., and R. Gijbels, Calculation of trace element fractionation during partial melting, *Geochim. Cosmochim. Acta, 40*, 313-322, 1976.

Hofmann, A.W., and M. Magaritz, Range of chemical equilibrium in partially molten rocks, *Proc. Chapman Conf., Partial Melting in the Earth's Upper Mantle, Oregon, September 1976*, 1977.

Iiyama, J.T., Influence des anions sur les équilibres d'échange d'ions Na-K dans les feldspaths alcalins à 600°C sous une pression de 1000 bars, *Bull. Soc. fr. Miner. Cristallogr., 88*, 618-622, 1965.

Iiyama, J.T., Experimental study of the distribution of trace elements between two feldspars. I. Distribution of Rb, Cs, Sr and Ba at 600°C, *Geochemistry International, 5*, 2, 433-442, 1968.

Irving, A.J., and F.A. Frey, Effect of composition on the partitioning of rare earth elements, Hf, Sc and Co between garnet and liquid: experimental and natural evidence, *EOS, 57*, 339, 1976.

Kretz, R., Chemical study of garnet, biotite, and hornblende from gneisses of southwestern Quebec, with emphasis on distribution of elements in coexisting minerals, *Jour. Geol., 67*, 371-402, 1959.

Lambert, I.B., and P.J. Wyllie, Melting in the deep crust and upper mantle and the nature of the low velocity layer, *Phys. Earth Planet. Interiors, 3*, 316-322, 1970.

Lagache, M., and G. Sabatier, Distribution des éléments Na, K, Rb et Cs à l'état de trace entre feldspaths alcalins et solutions hydrothermales à 650°C, 1 kbar: données expérimentales et

interprétation thermodynamique, *Geochim. Cosmochim. Acta, 37*, 2617-2640, 1973.

Leeman, W.P., Partitioning of Ni and Co between olivine and basaltic liquid: an experimental study, *EOS, 54*, 1222, 1973.

Maaloe, S., Quantitative aspects of fractional crystallization of major elements, *Jour. Geol., 84*, 81-96, 1976.

Mysen, B., Partitioning of samarium and nickel between olivine, orthopyroxene and liquid: preliminary data at 20 kbar and 1025°C, *Earth Planet. Sci. Lett., 31*, 1-7, 1976.

Mysen, B.O., and M.G. Seitz, Trace element partitioning determined by beta track mapping: an experimental study using carbon and samarium as examples, *Jour. Geophys. Res., 80*, 2627-2635, 1975.

O'Hara, M.J., Partial melting of upper mantle peridotites - a short summary, *Proc. Chapman Conf., Partial Melting in the Earth's Upper Mantle, Oregon, September 1976*, 1977.

O'Hara, M.J., M.J. Saunders, and E.L.P. Mercy, Garnet-peridotite, primary ultrabasic magma and eclogite: interpretation of upper mantle processes in kimberlite, *Phys. Chem. Earth, 9*, 571-604, 1975.

Presnall, D.C., The geometric analysis of partial fusion, *Amer. Jour. Sci., 267*, 1178-1194, 1969.

Puchelt, H., and R. Emmermann, Bearing of rare earth patterns of apatites from igneous and metamorphic rocks, *Earth Planet. Sci. Lett., 31*, 279-286, 1976.

Råheim, A., Mineral zoning as a record of P, T history of Precambrian eclogites and schists in western Tasmania, *Lithos, 8*, 221-236, 1975.

Råheim, A., and D.H. Green, P, T paths of natural eclogites during metamorphism - a record of subduction, *Lithos, 8*, 317-328, 1975.

Rayleigh, J.W.S., Theoretical considerations respecting the separation of gases by diffusion and similar processes, *Phil. Mag., 42*, 493-498, 1896.

Robertson, J.K., and P.J. Wyllie, Experimental studies on rocks from the Deboullie Stock, Northern Maine, including melting relations in the water-deficient environment, *Jour. Geol., 79*, 549-571, 1971.

Sabatier, G., Theorie de la distribution d'un élément en trace entre solution hydrothermale et solution solide. Application à la distribution du césium dans la serie des feldspaths alcalins, *Bull. Soc. fr. Mineral. Cristallogr., 94*, 451-455, 1971.

Schilling, J.-G., and J.W. Winchester, Rare-earth fractionation and magmatic processes, in *Mantles of the Earth and Terrestrial Planets*, edited by S.K. Runcorn, Interscience, pp. 267-283, 1967.

Seitz, M.G., and S.R. Hart, Uranium and boron distributions in some oceanic ultramafic rocks, *Earth Planet. Sci. Lett., 21*, 97-107, 1973.

Shaw, D.M., Trace element fractionation during anatexis, *Geochim. Cosmochim. Acta, 34*, 237-242, 1970.

Shaw, D.M., Trace element melting models, in *Proc. 2nd Symposium Origin and Distribution of the Elements, Paris, May 1977*, in press.

Shimizu, N., An experimental study of the partitioning of K, Rb, Cs, Sr and Ba between clinopyroxene and liquid at high pressures, *Geochim. Cosmochim. Acta, 38*, 1789-1796, 1974.

Shimizu, N., and S. Akimoto, Partitioning of strontium between clinopyroxene and liquid at high pressures: preliminary experiments, *Earth Planet. Sci. Lett., 13*, 134-138, 1971.

Shimizu, N., and I. Kushiro, The partitioning of rare earth elements between garnet and liquid at high pressures: preliminary experiments. *Geophys. Res. Letters, 2*, 413-416, 1975.

Sun, S.S., and G.N. Hanson, Origin of Ross Island basanitoids and limitations upon the heterogeneity of mantle sources for alkali basalts and nephelinites, *Contr. Mineral. Petrol., 52*, 77-106, 1975.

Sun, C.-O., R.J. Williams, and S.S. Sun, Distribution coefficients of Eu and Sr for plagioclase-liquid and clinopyroxene-liquid equilibria in oceanic ridge basalt: an experimental study, *Geochim. Cosmochim. Acta, 38*, 1415-1434, 1974.

Vinogradov, A.P., and A.A. Yaroshevsky, On the physical parameters of zone melting in the earth's mantle, *Geokhimiya*, 779-790, 1965.

Zielinski, R.A., Trace element evaluation of a suite of rocks from Reunion Island, Indian Ocean, *Geochim. Cosmochim. Acta, 39*, 713-734, 1975.

Zielinski, R.A., and F.A. Frey, An experimental study of the partitioning of a rare earth element (Gd) in the system diopside-aqueous vapour, *Geochim. Cosmochim. Acta, 38*, 545-566, 1974.

4. GEOPHYSICS OF PARTIAL MELTING

PARTIAL MELT IN REGIONS OF HIGH ELECTRICAL CONDUCTIVITY

T.J. Shankland
Los Alamos Scientific Laboratory
Los Alamos, New Mexico 87545

(Extended Abstract)

In many regions of the upper mantle, notably beneath the major rift systems and western North America, there exist regions of anomalously high electrical conductivity, 0.1 - 1 S/m, at depths of 30-300 km. To interpret such conductivities in terms of conduction measurements on olivine or pyroxene under mantle conditions would require temperatures several hundred degrees above the melting points of peridotites or lherzolites. Thus, it is reasonable to model mantle conductivity by treating a partial melt as an aggregate of a good conductor, the melt, mixed in a matrix of relatively insulating crystalline material.

The *Waff* (1974) model, which is functionally equivalent to the *Hashin-Shtrikman* (1962) upper bound, can provide a way to calculate the effective conductivity σ^* of a partial melt:

$$\sigma^* = \frac{\sigma_m + (\sigma_s - \sigma_m)(1 - \frac{2}{3} f)}{1 + \frac{f}{3}\left(\frac{\sigma_s}{\sigma_s} - 1\right)} \qquad (1)$$

where f is the fraction of partial melt and σ_s and σ_m are conductivities of the solid and melt phases, respectively. Fig. 1 shows the electrical conductivities used in the model as functions of temperature, T, and pressure, P. The olivine single-crystal curve at P = 0 comes from measurements of *Duba et al.* (1974) on Red Sea Peridot (RSP) and has been multiplied by a factor of 10 to accommodate the effect of a possible higher oxygen fugacity, f_{O_2}, under mantle conditions. The zero pressure melt conductivity is a composite of results from *Waff and Weill* (1975) for a variety of magmas. Not only are melt conductivities virtually independent of f_{O_2}, but they vary by only a factor of 2 over a wide range of compositions, as observed also by *Rai and Manghnani* (1977). The effects of pressure in Fig. 1 (*Shankland and Waff*, 1977) come from plausible values for activation volumes assuming the high temperature olivine and the melt conduction mechanisms to be ionic and the low temperature olivine mechanism to be electronic (*Shankland*, 1975). The activation volume ΔV_m allows for the effect of pressure on the activation energy for conduction in the melt; preliminary results (*H.S. Waff*, work in progress) are consistent with a value close to zero, but other values have also been considered. The great contrast between solid and melt conductivities means that only a small melt fraction can dominate the bulk conductivity, providing the melt forms a continuously interconnected phase as the model assumes, rather than isolated pockets.

Evidence for a well-interconnected melt at low melt fractions comes from laboratory (*Unger*, 1967) and field (*Boudier and Nicolas*, 1972;

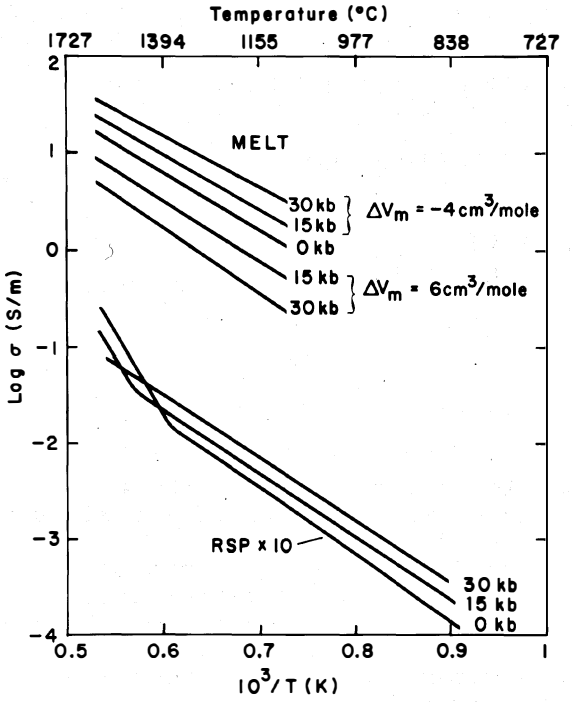

Fig. 1. Electrical conductivities in silicate melts (*Waff and Weill*, 1975) and olivine single crystals as functions of temperature and pressure; RSPx10 is the RSP curve of *Duba et al.* (1974) multiplied by 10 to allow for uncertainties of oxygen fugacity in the mantle. With increasing pressure the presumably electronic mechanism having a decreasing activation energy dominates the conduction process in olivine.

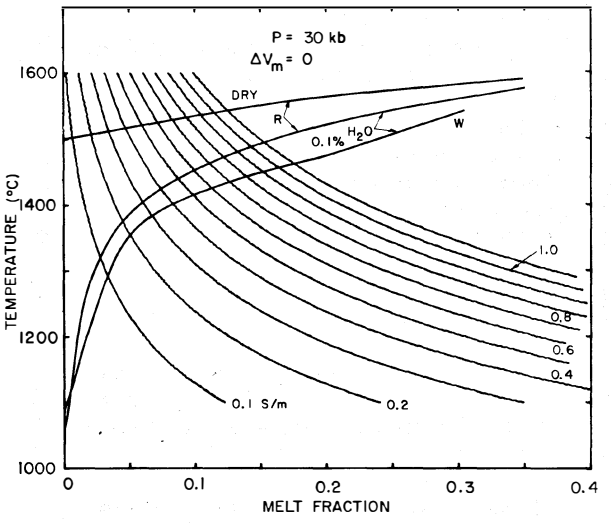

Fig. 2. Lines of equal effective conductivity σ* of a partial melt according to the upper bound formula Eq. (1) at 30 kb pressure. Conductivity data from Fig. 1; melting curves W from *Wyllie* (1971) and R from *Ringwood* (1975).

Padovani and Carter, 1977) studies. There is also a self-consistency argument: if the melt is not substantially interconnected, then it makes a negligible contribution to high conductivity anomalies until large melt fractions are attained.

A given effective conductivity in Eq. (1) can be attained at either a high temperature or a high partial melt fraction. The 30-kb curves of Fig. 1 have been used to calculate effective conductivities above 0.1 S/m in partial melts as illustrated in Fig. 2. Additional petrological information on partial melting exists; the curve W in Fig. 2 shows the temperature needed to yield a given melt fraction in peridotite containing 0.1% water, as taken from *Wyllie* (Fig. 8-20, 1971). The curves labeled R are taken from Fig. 4-8 of *Ringwood* (1975) for wet and dry pyrolite.

The electrical model given here together with petrological constraints allows the assignment of both a temperature and a melt fraction from the conductivity observed at a mantle depth; uncertainties about effects of water content in the lower crust make it more difficult to argue unambiguously for partial melt to explain conductivity anomalies there. Fig. 3 illustrates the calculation for a peridotite partial melt at 0, 15, and 30 kb (about 0, 50, and 100 km depth). It is seen that temperatures can be calculated with reasonable certainty as a result of the stabilizing influence of the melting curves. However, melt fraction, f, is more nearly proportional to σ^* and to σ_m and therefore is probably uncertain to a factor of 2 or 3 owing to uncertainties (a) in field measurements of σ^*, (b) in the effect of pressure on σ_m, and (c) in water

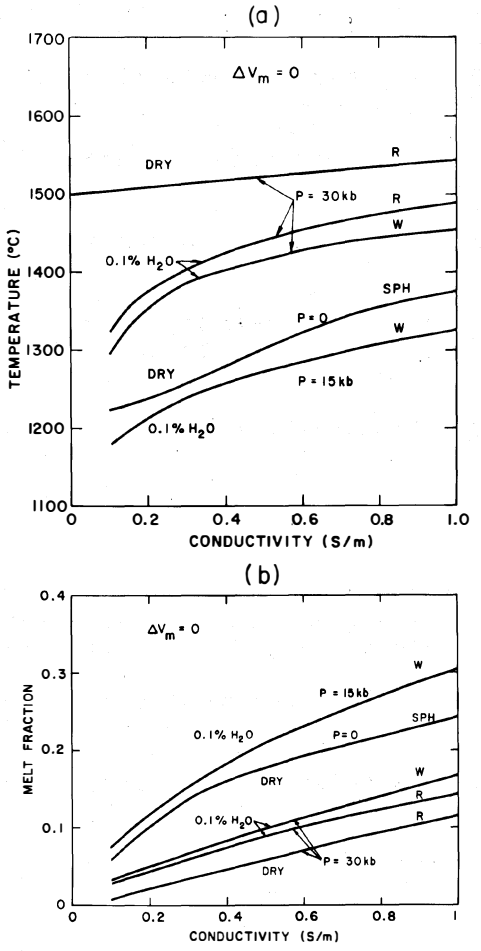

Fig. 3. (a) Temperature of a partial melt as calculated from its effective conductivity using data taken from Fig. 2 at 30 kb and a similar figure for 0 and 15 kb. Uncertainty in the water content of different mantle regions leads to uncertainty in the melting curves and therefore of temperatures inferred from conductivity. (b) Melt fraction in a zone of anomalous mantle conductivity as inferred from the conductivity model. Curves W and R use melting curves of *Wyllie* (1971) and *Ringwood* (1975) while SPH is based on data by *Scarfe et al.* (1972).

content in the mantle. In principle, however, the model is capable of improvement as these uncertainties decrease.

Conductivities above 0.1 S/m are seldom obtained at shallow mantle depths on either a global scale (*Banks*, 1972) or under shields (*Kurtz and Garland*, 1976). However, as *Gough* (1974) and *Garland* (1975) have pointed out, high conductivity anomalies in the mantle are found under the major continental and oceanic rift zones of the world, under hot spots like Yellowstone, and under much of western North America. This model affords a powerful technique to estimate temperatures and the present extent of partial melting in these zones. As seen in Fig. 3, the measured anomalies in the range of 0.1 to 1.0 S/m imply very substantial melt fractions. As a practical application, estimations of the geotherm using the model and further conductivity mapping should assist in improved mapping of geothermal resources.

References

Banks, R.J., The overall conductivity distribution of the earth, *J. Geomag. Geoelectr.*, *24*, 337-351, 1972.

Boudier, F., and A. Nicolas, Fusion partielle gabbroique dans la lherzolite de Lanzo (Alpes piemontaires), *Bull. Suisse Min. Petrogr.*, *52*, 39-56, 1972.

Duba, A., H.C. Heard, and R.N. Schock, Electrical conductivity of olivine at high pressure and under controlled oxygen fugacity, *J. Geophys. Res.*, *79*, 1667-1673, 1974.

Garland, G.D., Correlation between electrical conductivity and other geophysical parameters, *Phys. Earth Planet. Interiors*, *10*, 220-230, 1975.

Gough, D.I., Conductivity under western North America in relation to heat flow, seismology, and structure, *J. Geomag. Geoelectr.*, *26*, 105-123, 1974.

Hashin, Z., and S. Shtrikman, A variational approach to the theory of the effective magnetic permeability of multiphase materials, *J. Appl. Phys.*, *33*, 3125-3133, 1962.

Kurtz, R.D., and G.D. Garland, Magnetotelluric measurements in eastern Canada, *Geophys. J.*, *45*, 321-347, 1976.

Padovani, E.R., and J.L. Carter, Nonequilibrium fusion due to decompression effects in crustal mantle xenoliths, this volume, 1977.

Rai, C.S., and M.H. Manghnani, Electrical conductivity measurements on basalts, peridotite, garnet pyroxenite, and eclogite to 1500°C, this volume, 1977.

Ringwood, A.E., *Composition and Petrology of the Earth's Mantle*, McGraw-Hill, New York, 1975.

Scarfe, C.M., D.K. Paul, and P.G. Harris, Melting experiments at one atmosphere on two ultramafic nodules, *N. Jb. Miner. Mh.*, 469-476, 1972.

Shankland, T.J., Electrical conduction in rocks and minerals: parameters for interpretation, *Phys. Earth Planetary Int.*, *10*, 209-219, 1975.

Shankland, T.J., and H.S. Waff, Partial melting and electrical conductivity anomalies in the upper mantle, *J. Geophys. Res.*, in press, 1977.

Unger, J.D., Melting of granite under effective confining pressure, M.Sc. Thesis, Massachusetts Institute of Technology, 1967.

Waff, H., Theoretical consideration of electrical conductivity in a partially molten mantle and implications for geothermometry, *J. Geophys. Res.*, *79*, 4003-4010, 1974.

Waff, H.S., and D.F. Weill, Electrical conductivity of magmatic liquids; effects of temperature, oxygen fugacity and composition, *Earth Planet. Sci. Letters*, *28*, 254-260, 1975.

Wyllie, P.J., *The Dynamic Earth: Textbook in Geosciences*, Wiley, New York, 1971.

Electrical Conductivity of Basalts to 1550°C

C.S. Rai and M.H. Manghnani
Hawaii Institute of Geophysics
University of Hawaii
Honolulu, Hawaii 96822

Abstract

Using the loop technique (*Waff and Weill*, 1975), the a.c. electrical conductivity σ of ten Hawaiian basalts (tholeiitic, alkalic and nephelinic types), has been investigated in the temperature range 500-1500°C under known oxygen fugacity environments. Below the solidus temperatures, σ increases monotonically with 1/T, and at a given temperature alkalic basalts are most conductive and nephelinic least conductive. Premonitory decreases in σ observed before melting are probably caused by cracks formed by thermal stresses. The basalt σ values jump by 1 to 1 1/2 orders of magnitude during the melting interval ($\sim$ 200-250°C). At $T \geq$ 1200°C, the melt σ values for the basalts investigated fall in a narrow range, within half an order of magnitude. The ionic conduction in the liquid phase is found to be controlled principally by silica and alkali contents, $\Sigma M^{2+}/\Sigma M^{+}$ ratio, and to some extent by femic content. The σ values decrease with silica content and increase with the other parameters.

Introduction

High-conductivity anomalies observed in geomagnetic soundings of the upper mantle in the western United States (*Porath and Gough*, 1971) invoke temperatures significantly higher than those deduced for an olivine model using laboratory data on the electrical conductivity of olivine at high temperatures reported by *Duba et al.* (1974). Measurements of the electrical conductivity of basalts through the melting interval (e.g., *Watanabe*, 1970; *Presnall et al.*, 1972) show that on melting the conductivity of basalt increases by one to two orders of magnitude. The conductivity of basaltic melts above liquidus temperatures is about 3 to 4 orders of magnitude greater than that of olivine in the temperature range 1200-1550°C. On this basis, the observed high-conductivity anomalies in the upper mantle have been attributed to partial melting, especially when the depths of these anomalies match low seismic velocity zones and the conductivity structure strongly correlates with heat flow (*Porath*, 1971; *Chan et al.*, 1973; *Gough*, 1974).

Recently, *Shankland and Waff* (in press), in the spirit of *Waff's* (1974) theoretical approach, have explained anomalously high electrical conductivity zones (> 0.1 mho/m) within the upper mantle by partial melting of peridotite. Their calculations for the model consisting of basalt melt in a mainly olivine matrix show that accurate estimation of temperature and degree of partial melting depend critically not only on the amount of water and volatiles present in the mantle, but also on other factors, such as

geometry and wetting, that influence the bulk electrical conductivity of partially melted mantle rock. Nevertheless, knowledge of the two input parameters -- conductivities of the solid and liquid phases -- is essential for testing such theoretical models.

The purpose of this paper is to report the electrical conductivity of ten basalts, in the temperature range 500°C-1550°C under known oxygen fugacity environments, and to discuss the results in terms of the chemical variations.

Experimental Methods

Rock Samples

Electrical conductivity of ten Hawaiian basalts (3 tholeiites, 5 alkalic basalts, and 2 nephelinic basalts) have been investigated. All the ten Hawaiian basalts (C-series) were kindly provided by Professor G.A. Macdonald; their chemical and normative analyses have been reported by *Macdonald and Katsura* (1964) and *Macdonald* (1968). Table 1 lists the chemical analyses of the ten basalts employed in this study.

Electrical Measurements

The loop technique employed by *Waff and Weill* (1975) was used for measuring the a.c. electrical conductivity of the rock samples to melting temperatures and above. The powdered sample was mixed with acetone and made into paste which adhered inside the periphery of an open-ended circular loop, approximately 7 mm in diameter, made from 0.64 mm-thick 80% Pt-20% Rh wire. The other end of the loop wire was bent perpendicular to the plane of the loop to lend vertical support. The loop acts as one electrode; the other electrode consists of a straight 80% Pt-20% Rh wire of 0.241 mm diameter, centrally located inside the loop. Outside the loop, the central wire is supported and insulated by an alumina tube. Four such loop assemblies are attached to an alumina tube which is placed in a high-temperature furnace. The loops were heated to 1500°C and then cooled slowly to room temperature. The process was repeated twice in order to obtain homogeneous starting samples. The atmosphere surrounding the samples in the furnace was controlled by maintaining a constant flow of a mixture of CO_2 and H_2 (87.6% CO_2 and 12.4% H_2, by volume) in the entire range of temperature (500-1550°C). This mixture provided a variation in the f_{O_2} values from 10^{-6} to 1500°C to 10^{-23} at 500°C, based on the tables of *Deines et al.* (1974). The line representing the oxygen fugacity versus temperature in our experiments falls close to that denoting the wüstite-magnetite transition (*Nitsan*, 1974), between the oxidation and reduction lines for olivine (fo_{90}), as shown in Fig. 1. Temperature of the specimen was measured by means of Pt-13% Rh thermocouples, sheated in alumina tubing and placed adjacent to the specimen. The thermocouples were calibrated against the melting point of gold (1064.4°C).

The resistance of the sample was measured at 500 Hz with a phase-sensitive lock-in amplifier (Princeton Applied Research model HR-8) which enabled maximization of the signal-to-noise ratio and elimination of the unwanted polarization effects. The resistance values were converted to conductivity values by geometric scale-modeling (*Waff*, 1976). The

TABLE 1. Chemical Analyses* of Basalts

	Basalts									
	1	2	3	4	5	6	7	8	9	10
	Tholeiitic			Alkalic					Nephelinite	
	Thol. Olivine Basalt (C-50)	Olivine Thol. (C-214)	Thol. (C-8)	Hawaiite (C-42)	Alkalic Olivine Basalt (C-222)	Alkalic Olivine Basalt (C-70)	Mugearite (C-210)	Trachyte (C-128)	Nephelinite (C-195)	Basanite (C-90)
SiO_2	46.81	50.15	50.98	45.88	46.54	47.48	51.80	60.85	38.92	40.66
Al_2O_3	14.50	12.84	15.13	16.39	13.95	17.42	17.07	18.51	12.25	10.57
Fe_2O_3	2.45	2.52	2.48	3.39	3.16	3.59	3.12	3.10	5.33	2.95
FeO	8.98	9.36	7.55	10.00	9.97	8.10	6.93	2.08	7.88	9.74
MgO	10.66	9.29	8.15	5.92	9.40	6.74	3.10	0.58	12.95	15.75
CaO	8.96	10.37	9.01	8.90	10.74	8.54	6.01	1.77	13.21	11.37
Na_2O	2.21	2.10	2.22	3.30	2.69	3.12	5.78	7.20	3.92	1.48
K_2O	0.57	0.40	0.30	1.02	0.87	1.20	2.23	3.60	1.26	0.49
P_2O_5	0.40	0.25	0.26	0.59	0.29	0.36	1.54	0.29	1.11	0.36
Cr_2O_3	--	--	--	--	--	--	--	--	--	--
TiO_2	2.69	2.05	2.11	3.83	2.25	2.63	1.95	0.65	2.62	2.28
MnO	0.16	0.17	0.19	0.18	0.16	0.18	0.22	0.27	0.20	0.19
NiO	--	--	--	--	--	--	--	--	--	--
H_2O^+	0.97	0.41	0.94	0.29	0.41	0.40	0.48	0.47	0.33	2.52
H_2O^-	0.45	0.31	0.49	0.24	0.24	0.22	0.41	0.42	0.38	1.65
Total	99.81	100.22	99.81	99.93	100.67	99.98	100.64	99.79	100.36	100.01

* Sources of analyses: Basalts 1, 3, 4, 6, 8, 10, *Macdonald and Katsura* (1964), samples donated by G.A. Macdonald; basalts 2, 5, 7, 9, *Macdonald* (1968), samples donated by G.A. Macdonald.

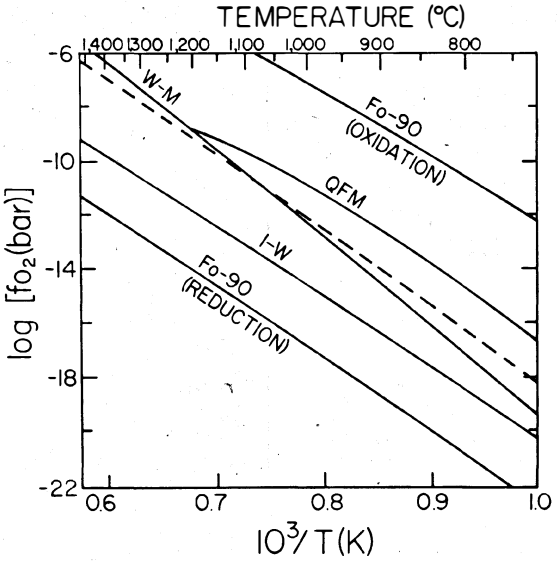

Fig. 1. Stability field of olivine with respect to oxidation and reduction at 1-atm. total pressure. The dotted line represents the oxygen fugacity at various temperatures in our experiment. I - iron, W - wüstite, Q - quartz, F - fayalite and M - magnetite (*Nitsan*, 1974).

measurements were made during both the heating and cooling cycles, at intervals of about 50°C. The heating/cooling rate was 300°C/hour. An interval of about 15 min was allowed between reaching a temperature and making the measurement. It is recognized that total equilibration of the sample with the atmosphere in the furnace did not occur during this 15-min interval. Durations of the order of several hours or days are required for reaching equilibration for Fe^{3+}/Fe^{2+} (*Presnall et al.*, 1972). The percentage of glass in the sample after making the run was estimated by examination of a polished section in reflected light.

Results and Discussion

Figures 2, 3, and 4 show the temperature dependence of the conductivity of the tholeiitic, alkalic and nephelinic basalts, respectively. The melt σ values, measured during both heating and cooling cycles, were reproducible within $\pm$ 1% in the case of all the basalts except for nephelinic basalts and a tholeiitic olivine basalt (C-50). In the latter cases the values were slightly higher for the cooling cycle. Below $\sim$ 900°C, the σ values for the cooling cycles for all the basalts are lower. For clarity here only the measurements taken during the heating cycles are presented in the figures. The previously published log σ versus 1/T curves for a synthetic basalt of tholeiitic composition (*Presnall et al.*, 1972) (denoted by P) and an olivine basalt (*Watanabe*, 1970) (denoted by W) are also shown. Below 1100°C, the W curve falls between the curves representing the completely crystalline (lower P) and predominantly glassy (upper P) curves for the synthetic tholeiitic basalt reported by *Presnall et al.*

Conductivity of basalts below melting temperatures. The relation of log σ to 1/T for the Hawaiian basalts is somewhat curvilinear; in most cases, the negative slope of the line first increases with increasing temperature in the 600-650°C range, and then decreases at $\sim$ 800°C. Just below the solidus temperatures ($\leq$ 1050°C), a premonitory decrease in σ is observed in most basalts, particularly in tholeiitic basalts. *Schloessin* (1976, and to be published) has also reported premonitory decreases in σ during the melting of mid-oceanic ridge basalts and has proposed three possible reasons: (1) formation of isolated melt pockets, (2) latent heat

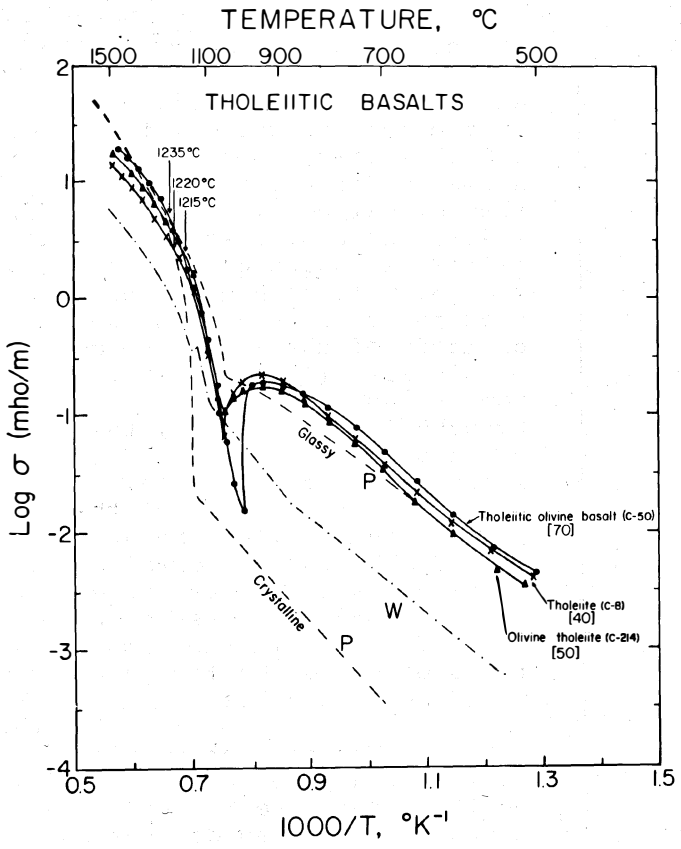

Fig. 2. Log σ versus 1/T for the three tholeiitic basalts. The values in brackets are the estimated percentages of the glass content. The data and the curves shown are for the heating cycles only.

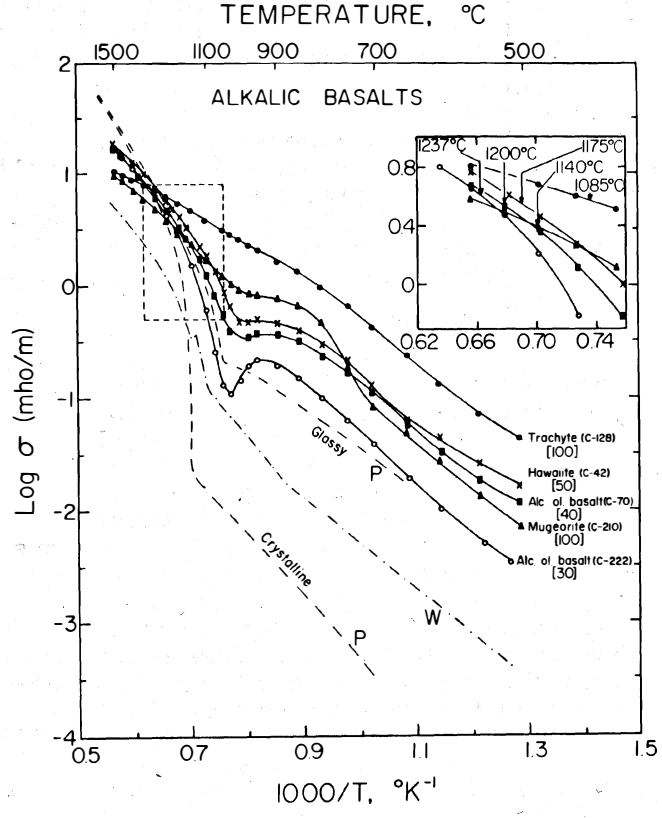

Fig. 3. Log σ versus 1/T for the five alkalic basalts. The values in brackets are the estimated percentages of the glass content. The data and the curves shown are for the heating cycles only. The insert in the upper right corner shows the curves in detail between 1050 and 1250°C and the liquidus temperature for each basalt.

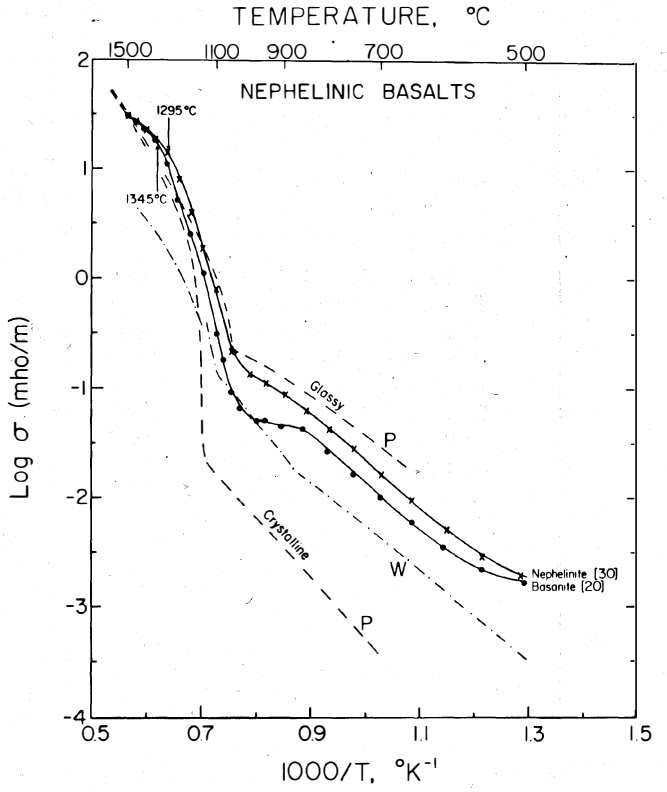

Fig. 4. Log σ versus 1/T for the two nephelinic basalts. The values in brackets are the estimated percentages of the glass content. The data and the curves shown are for the heating cycles only.

effects, and (3) change in the dominant mode of conduction from electronic in the solid to ionic in the melt phase. Of the three possibilities, the last one seems most reasonable. From theoretical consideration (*Waff*, 1974), the σ of a solid-liquid matrix, in which $\sigma_{liquid} > \sigma_{solid}$, will be higher than the σ of the solid phase for any geometry of the melt. Hence, possibility (1) cannot apply. Concerning the second hypothesis, we believe, the question of the latent heat effects should not arise. Because heat capacity of the furnace is high, and because an appreciable time interval is allowed between temperature increase and the measurement, the difference in the temperatures of solid and liquid phases would be negligible.

The present results suggest that the observed premonitory decrease in σ is time dependent and also depends on the rate of heating/cooling and on the composition of the rock. During the heating cycle, for the same rate of heating (300°C/hour), the decrease is most pronounced in the tholeiitic basalts and least in the nephelinic basalts. The premonitory decrease is least pronounced in basalt samples which are either predominantly glassy (trachyte, mugearite) or crystalline (nephelinite, basanite) (see Figs. 3 and 4). During the cooling cycle, the premonitory decrease in σ is dependent on the rate of cooling -- the lower the cooling rate the less conspicuous the decrease; although cooling curves are not shown in Figs. 3 and 4 the decrease is more pronounced in the alkalic basalts and least in the nephelinic basalts.

Fig. 5 shows the time dependency of the conductivity of mugearite and trachyte. During the heating cycle, the premonitory decrease is observed for mugearite but not for trachyte. During the cooling cycle, in both cases, the sample was held at 950°C, presumably below the solidus temperature, for 63 hours. As a result of devitrification of the glass, the conductivity of mugearite and trachyte is found to decrease about 2 and 2 1/2 orders of magnitude, respectively. Below 950°C the log σ versus 1/T relationships follow closely but slightly above the lower P curve.

In view of these observations, it appears that premonitory decrease in σ is probably caused by one or a combination of the two factors: (1) formation of cracks due to thermal stresses during the heating cycle (the number of cracks depending on the rate of heating and the ratio of glassy to crystalline phases present). A higher heating rate will

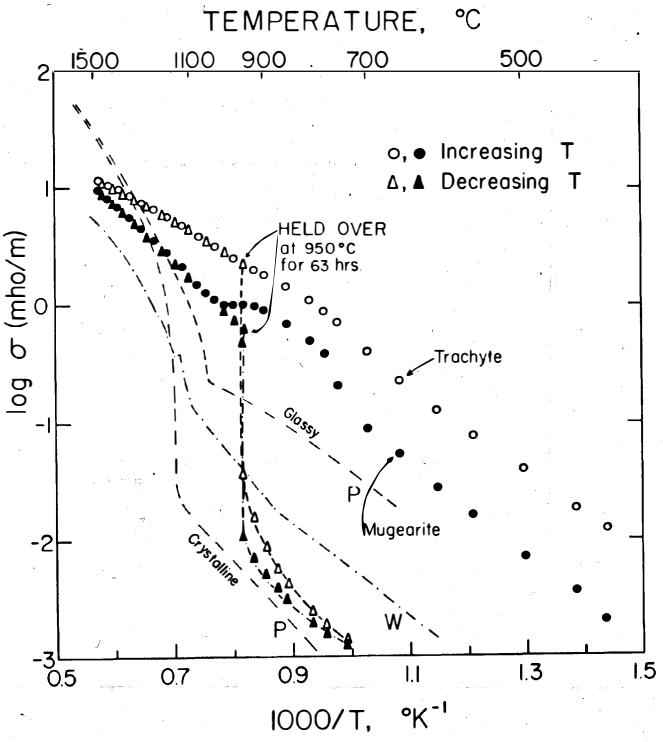

Fig. 5. Time dependence of the variation of σ with temperature for the two alkalic basalts.

promote the formation of more cracks and the predominance of crystalline or glassy phases will inhibit the crack formation and, hence, will suppress decrease in σ. (2) Devitrification of the glassy phase, at sufficiently low cooling rate, can also cause a decrease in σ (due to an increase in crystallinity) as evidenced by the data shown in Fig. 5.

The variations in σ of basalts, at a given temperature (Figs. 2, 3, and 4), seem to be related to differences in their chemical composition and glass content -- the higher the alkali ($Na_2O + K_2O$) and glass contents, the greater the σ. In general, the conductivities of the alkalic basalts below the solidus temperatures are highest (Fig. 3) and are, at a given temperature, about an order of magnitude greater than that reported for a predominantly glassy tholeiite (upper P curve); the conductivities of the two nephelinic basalts are lowest (Fig. 4) and fall slightly below the upper P curve. On the other hand, the conductivities of the three tholeiitic basalts are intermediate and are close to the upper P curve (Fig. 4).

Conductivity of basalts to melting temperatures and above. The approximate liquidus temperatures of the basalts, calculated from chemical composition (*Tilley et al.*, 1967), are indicated in Figs. 2, 3, and 4. The slope of the log σ versus 1/T curve decreases notably with increasing temperature in the vicinity of the liquidus temperatures. The temperature range of melting, estimated from the reported solidus and liquidus temperatures for tholeiitic and alkalic Hawaiian basalts (*Yoder and Tilley*, 1962), is approximately 200°-250°C. The σ of basalts, following the premonitory decrease, increases very rapidly -- by 1 1/2 to 2 1/2 orders of magnitude -- during the melting range. Such a sharp increase is probably due to ionic conduction in the liquid phase formed above solidus temperatures (*Waff*, 1975). It is interesting to note that the order of increasing σ for the basaltic melts is reversed as compared to the trend found below melting temperatures. The conductivities of nephelinic basalt melts are the highest and of alkalic basalt melts the lowest, just the opposite of what was observed in the solid state. The reversal in the order of increasing σ might not occur if the curves in the solid state were for completely glassy material. Fig. 6 shows the σ of basalt melts in more detail. Even for such a wide range of chemical composition, the melt conductivities at any temperature are within half an order of magnitude. The log conductivity varies linearly with reciprocal temperature for alkalic basalts (Arrhenius behavior) and curvilinearly (slope decreasing with increasing temperature) for tholeiitic and nephelinic basalts (non-Arrhenius behavior). The apparent activation energies E_o of melts as a function of temperature, calculated from the Arrhenius equation $\sigma = \sigma_o e^{-E_o/kT}$, are shown in Fig. 7.

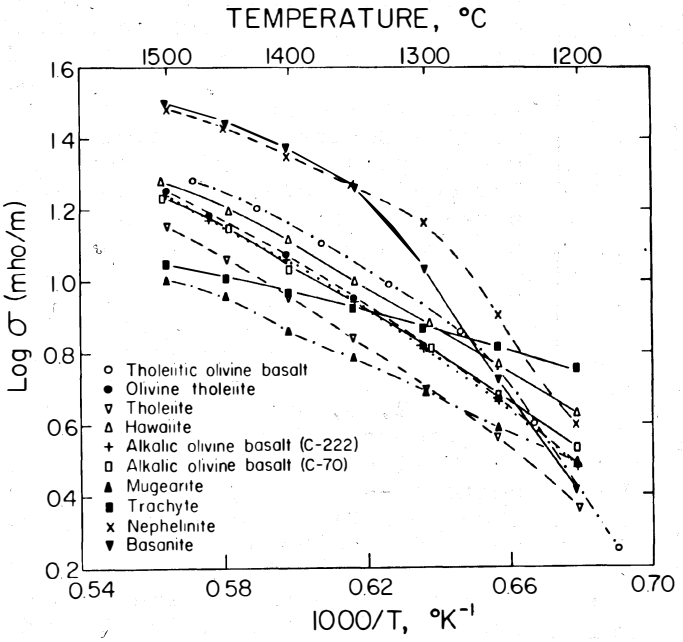

Fig. 6. Temperature dependence of the conductivities of basaltic melts.

Fig. 7. Temperature dependence of the apparent activation energies for electrical conduction in various basaltic melts.

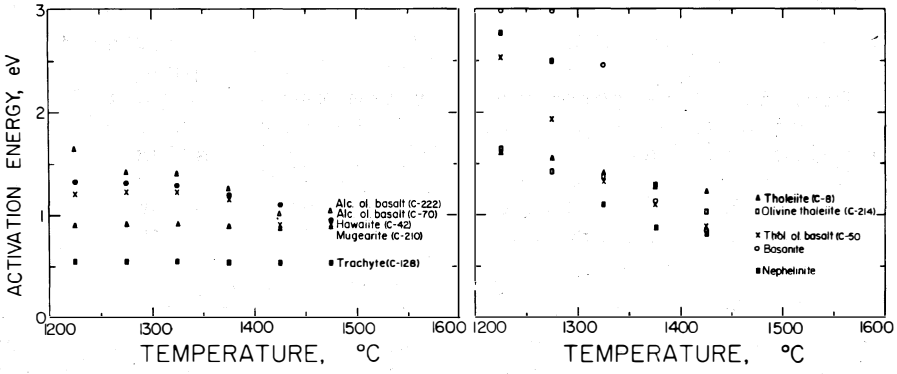

Nephelinitic and tholeiitic basalts are characterized by rapid decrease of activation energy with temperature. On the other hand, for alkalic basalts, which exhibit Arrhenius behavior, activation energies are approximately independent of temperature. Nephelinic and tholeiitic basalts have relatively higher $\Sigma M^{2+}/\Sigma M^{+}$ ratio than the alkalic basalts (Table 2). *Waff and Weill* (1975) also noted that melts with high $\Sigma M^{2+}/\Sigma M^{+}$ ratio depart from Arrhenius behavior, and have explained this on the basis of polymerization of the melts.

Composition dependence of melt conductivity of basalts. Relative atomic and cation concentrations, based on Niggli's scheme (*Niggli*, 1954), for the basalts are given in Tables 2 and 3. Fig. 8 shows that alkali ($Na_2O + K_2O$) content increases with increasing SiO_2 content in these rocks. The composition dependences of log σ (at 1400°C) are shown in the four plots in Fig. 9. The data for the five basalts reported by *Waff and Weill* (1975) are also included in the plots. As seen, σ increases with increasing MgO and CaO and decreases with increasing SiO_2 and alkali ($Na_2O + K_2O$) contents. The latter observation -- decrease in σ with increasing alkali content -- is misleading. The σ should increase with increase in alkali content if the other constituents remain the same (*Waff and Weill*, 1975); however, in the present case, because SiO_2 content increases with alkali content (see Fig. 8) and because the effect of increasing SiO_2 content is to decrease σ, we find an apparent decrease in σ with an increase in

TABLE 2. Relative Cationic Concentration Based on Niggli's Scheme for Basalts

	Basalts									
No.	1	2	3	4	5	6	7	8	9	10
Cations	Thol. Olivine Basalt	Olivine Thol.	Tholeiite	Hawaiite	Alkalic Olivine Basalt	Alkalic Olivine Basalt	Mugear.	Trachyte	Nephelin.	Basanite
Si^{4+}	44.1	47.1	48.3	43.4	43.3	44.5	47.9	55.8	35.5	38.8
Al^{3+}	16.1	14.2	16.9	18.3	15.3	19.2	18.6	20.1	13.2	11.9
Fe^{3+}	1.7	1.8	1.8	2.4	2.2	2.5	2.2	2.1	3.6	2.1
Fe^{2+}	7.2	7.4	6.2	8.1	7.9	6.6	5.5	1.8	6.2	8.0
Mg^{2+}	14.9	13.0	11.5	8.4	13.0	9.4	4.3	0.8	17.6	22.4
Ca^{+}	9.0	10.4	9.2	9.0	10.7	8.6	5.9	1.8	12.9	11.6
Na^{+}	4.1	3.8	4.1	6.0	4.8	5.6	10.3	12.8	6.9	2.7
K^{+}	0.7	0.5	0.3	1.3	1.0	1.5	2.7	4.2	1.4	0.6
Ti^{4+}	1.9	1.5	1.5	2.7	1.6	1.9	1.3	0.4	1.8	1.7
ΣM^{2+}	31.1	30.80	26.9	25.5	31.60	24.6	15.7	4.4	36.7	42.0
ΣM^{+}	4.8	4.3	4.4	7.3	5.8	7.1	13.0	17.0	8.3	3.3
$\frac{\Sigma M^{2+}}{\Sigma M^{+}}$	6.5	7.2	6.1	3.5	5.5	3.5	1.2	0.3	4.4	12.7

TABLE 3. Niggli Concentration Numbers for Basalts

	Basalts									
No.	1	2	3	4	5	6	7	8	9	10
	Thol. Olivine Basalt	Olivine Thol.	Tholeiite	Hawaiite	Alkalic Olivine Basalt	Alkalic Olivine Basalt	Mugearite	Trachyte	Nephelin.	Basanite
si	101.8	112.0	123.0	106.9	97.5	110.9	142.0	223.6	69.5	75.1
al	18.6	17.0	21.4	22.5	17.2	24.0	27.5	40.2	12.9	11.5
fm	55.0	52.9	49.6	46.3	52.1	45.9	35.6	18.8	53.6	62.7
c	20.9	25.0	23.3	22.2	24.2	21.3	17.6	7.1	25.3	22.5
alk	5.5	5.1	5.7	9.0	6.5	8.8	19.3	34.0	8.2	3.2
mg	62.7	58.4	59.1	44.4	56.3	51.1	35.6	16.5	64.2	69.1
ti	4.4	3.5	3.8	6.7	3.5	4.6	4.0	1.8	3.5	3.2

Note: si - denoted silica (SiO_2), al - aluminous (Al_2O_3), fm - femic (MgO, Fe_2O_3, FeO, MnO), c - calcic (CaO), alk - alkaline (Na_2O, K_2O), mg - MgO/fm ratio, ti - titanium (TiO_2).

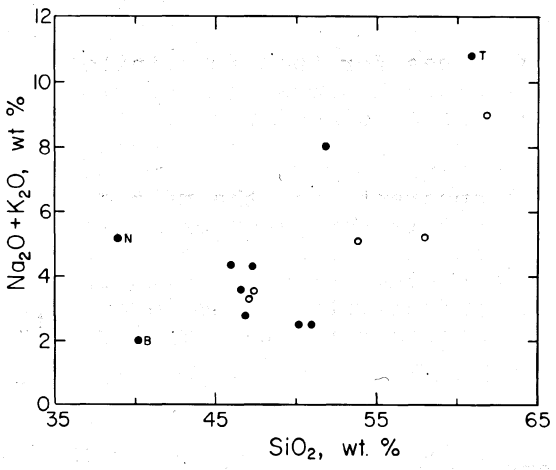

Fig. 8. Alkali ($Na_2O + K_2O$) content versus SiO_2 content for ten basalts studied. Included in the plot are also the data on five basalts (open circles) reported by *Waff and Weill* (1975). N denotes nephelinite, B basanite, T trachyte.

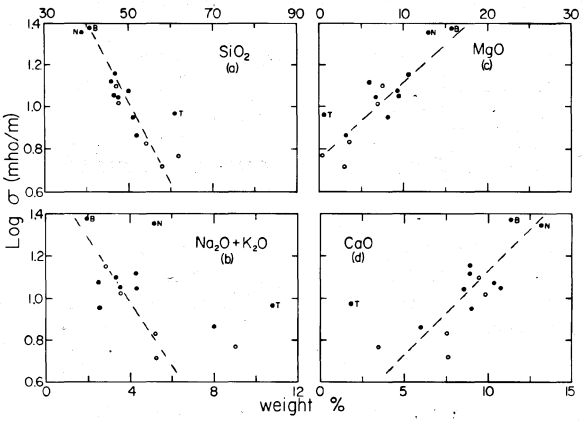

Fig. 9. Plots of log σ (at 1400°C) versus (a) SiO_2, (b) (Na_2O + K_2O), (c) MgO, and (d) CaO content. The explanation of the symbols is given in Fig. 8.

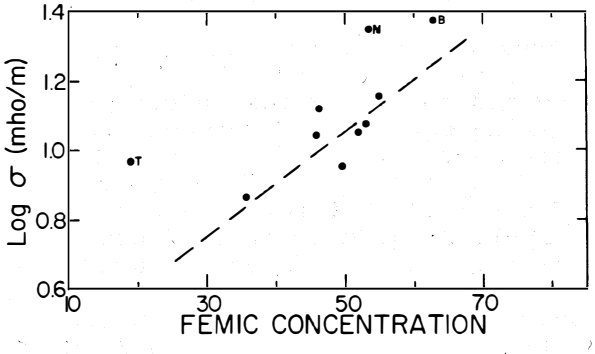

Fig. 10. Log σ (at 1400°C) versus femic concentration for ten Hawaiian basalts. The explanation of the symbols is given in Fig. 8.

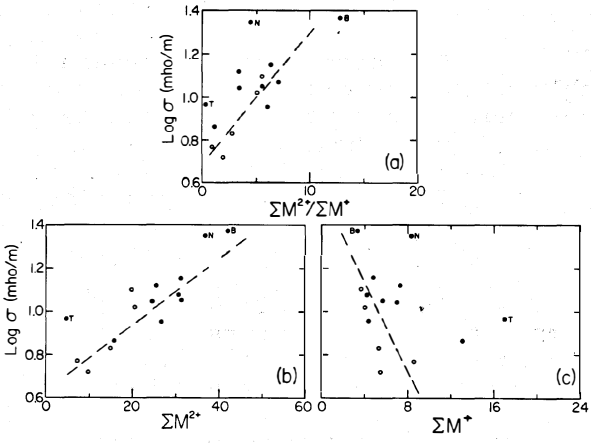

Fig. 11. Log σ (at 1400°C) versus (a) $\Sigma M^{2+}/\Sigma M^{+}$, (b) ΣM^{2+} and (c) ΣM^{+} for ten basalts studied. The explanation of the symbols is given in Fig. 8.

alkalic content. A consistent finding from all the four plots (Fig. 9) is that trachyte (T) has higher conductivity than the best-fit trend in each plot. The higher σ of trachyte is attributed to its highest alkali content. Similarly, the σ of nephelinite (N), which has very low silica content and high alkali content, is appreciably higher than the general trend found in Fig. 9b.

Fig. 10. shows the log σ versus femic concentration for all the rocks. There is a slight effect of increasing σ with femic concentration but the scatter in the data preclude a clear-cut conclusion about the effect of femic concentration on σ.

It is of interest to investigate the relationship between log σ (at 1400°C) and $\Sigma M^{2+}/\Sigma M^{+}$ (Fig. 11a). For basalts there is a systematic

increase in melt σ with $\Sigma M^{2+}/\Sigma M^{+}$. The σ values for the nephelinite (N) and trachyte (T) fall slightly above the trend. A comparison of plots on Fig. 11 shows that the melt σ seems to be related directly to ΣM^{2+} more so than to $\Sigma M^{2+}/\Sigma M^{+}$ or ΣM^{+}.

From the above observations it is apparent that the melt σ at a given temperature is a function of a number of factors such as silica, alkali, and femic contents and $\Sigma M^{2+}/\Sigma M^{+}$ ratio which are independent. For this reason, it is difficult to predict the conductivity of melts from chemical composition. Data on electrical conductivity of simple melts, consisting of two or three components, are needed first to simplify this problem.

Conclusions

The variations in the temperature dependence of conductivity of basalts are related, below solidus temperatures, to variations in chemical composition and glass content. Alkalic basalts are most conductive and nephelinic basalts least conductive. The conductivity of a rock in the solid state increases with glass content.

The premonitory decrease in σ below melting temperature is probably caused by crack formation due to the thermal stresses developed during heating. The σ values of basalts jump by 1 1/2 to 2 1/2 orders of magnitude through their melting, in a temperature range ∿ 250°C.

It is recognized that the heating and cooling rates in our experiments are not sufficiently small for attaining equilibrium between the solid and liquid phases at melting temperatures.

The rock melt σ is a function of a number of interdependent compositional parameters such as ($Na_2O + K_2O$), SiO_2, MgO, and CaO contents; the role of femic content is relatively minor. The melt σ values are highest for the nephelinic basalts and lowest for the alkalic basalts. The range of the melt σ values for all the basalts is less than half an order of magnitude at any temperature above melting (at 1400°C, σ varies from ∿ 7 to ∿ 24 mho/m). The alkalic basalts show Arrhenius-type temperature behavior, whereas the nephelinic tholeiitic basalts behave in non-Arrhenius manner.

The conductivity of basalt, during the cooling cycle, is found to be time dependent as a result of devitrification of glass.

Acknowledgements

Thanks are due Professor G.A. Macdonald for kindly providing the samples for this study. We are grateful to Professors H. Waff and Dean Presnall for their advice and guidance in the experimental work, and to Drs. T.J. Shankland and A. Duba for their review of the manuscript. We thank Mr. J. Balogh for his expertise in designing and maintaining the apparatus. This study was supported by the National Science Foundation (Grant EAR 74-22645) and by the Energy Research and Development Administration (Contract E(04-3)-1093). Hawaii Institute of Geophysics Contribution No. 854.

References

Chan, T., E. Nyland, and D.I. Gough, Partial melting and conductivity anomalies in the upper mantle, *Natur. Phys. Sci.*, *244*, 89-90, 1973.

Deines, P., R.H. Nafziger, G.C. Ulmer, and E. Woermann, Temperature-oxygen fugacity tables for selected gas mixtures in the system C-H-0 at one atmosphere total pressure, *Bull. Earth and Mineral Sciences Experimental Station*, The Pennsylvania State University, 1974.

Duba, A., H.C. Heard, and R. Schock, Electrical conductivity of olivine at high pressure and under controlled oxygen fugacity, *J. Geophys. Res.*, *79*, 1667-1673, 1974.

Gough, D.I., Electrical conductivity under western North America and relation to heat flow, seismology and structure, *J. Geomag. Geoelectr.*, *26*, 105-123, 1974.

Macdonald, G.A., Composition and origin of Hawaiian lavas, *Geol. Soc. Amer. Mem. 116*, Studies in Volcanology, edited by Coats, Hay and Anderson, Williams Volume, 447-522, 1968.

Macdonald, G.A., and T. Katsura, Chemical composition of Hawaiian lavas, *Jour. Petrol.*, *5*, 82-133, 1964.

Niggli, P., *Rocks and Mineral Deposits*, W.H. Freeman and Co., San Francisco, 1954.

Nitsan, U., Stability field of olivine with respect to oxidation and reduction, *J. Geophys. Res.*, *79*, 706-711, 1974.

Porath, H., Magnetic variation anomalies and seismic low-velocity zone in the western United States, *J. Geophys. Res.*, *76*, 2643-2648, 1971.

Porath, H., and D.I. Gough, Mantle conductive structures in the western United States from magnetometer array studies, *Geophys. J. Roy. Astron. Soc.*, *22*, 261-274, 1971.

Presnall, D.C., C.L. Simmons, and H. Porath, Changes in electrical conductivity of a synthetic basalt during melting, *J. Geophys. Res.*, *77*, 5665-5672, 1972.

Schloessin, H.H., High pressure studies of electrical conductivity variations through the melting points of basalts, *presented at the 29th Ann. Meet. Geol. Assoc. Canada*, 1976.

Schloessin, H.H., On the pressure dependence of solidus temperatures and electrical conductivity during melting of JOIDES Leg 37 samples, to be published.

Shankland, T.J., and H.S. Waff, Partial melting and electrical conductivity anomalies in the upper mantle, *J. Geophys. Res.*, in press.

Tilley, C.E., H.S. Yoder, Jr., and J.F. Schairer, Melting relations of volcanic rock series, *Carnegie Inst. of Washington Yearbook 65*, 260-269, 1967.

Waff, H.S., Theoretical considerations of electrical conductivity in a partially molten mantle and implications for geothermometry, *J. Geophys. Res.*, *79*, 4003-4010, 1974.

Waff, H.S., Electrical conductivity measurements on silicate melts using the loop technique, *Rev. Sci. Instrum.*, *47*, 877-879, 1976.

Waff, H.S., and D.F. Weill, Electrical conductivity of magmatic liquids: Effects of temperature, oxygen fugacity and composition, *Earth Planet. Sci. Lett.*, *28*, 254-260, 1975.

Watanabe, H., Measurements of electrical conductivity of basalt at temperatures up to 1500°C and pressures to about 20 kilobars, *Spec. Contrib., Geophys. Inst., Kyoto University*, *10*, 159-170, 1970.

Yoder, H.S., Jr., and C.E. Tilley, Origin of basalt magmas: An experimental study of natural and synthetic rock systems, *J. Petrol.*, *3*, 342-532, 1962.

SUBSOLIDUS DEFORMATION MECHANISMS AND HYPERSOLIDUS CREEP OF PERIDOTITE

Richard P. George, Jr.
Institute of Geophysics and Planetary Sciences
University of California
Los Angeles, California 90024

Abstract

Ductile deformation of crystalline materials generally involves several flow processes that operate at the microscopic or sub-microscopic level: (1) diffusion of point defects through the crystal lattice and along grain boundaries (diffusion creep), (2) conservative (non-diffusive) motion of curvilinear defects through the crystal lattice (dislocation glide flow), (3) non-conservative (diffusion-accompanied) motion of curvilinear defects through the crystal lattice (dislocation creep), (4) movement of arrays of dislocations (grain- and subgrain-boundary migration and subgrain coalescense), and (5) grain-boundary sliding. The first four mechanisms can operate independently but probably interact complexly during natural deformation of silicates. Grain-boundary sliding cannot operate independently, except for special conditions or special configurations of grains. During deformation of polycrystalline aggregates in which it accompanies one of the first four mechanisms, grain-boundary sliding can accommodate more than half of the total strain.

The mechanism that causes the highest flow rate will control the deformation and the resulting textures. Textures diagnostic of diffusion creep and of grain-boundary sliding are more subtle than and are easily overprinted by those of dislocation glide, dislocation creep, and grain-boundary migration (which include the processes commonly referred to as "plastic flow" and "syntectonic recrystallization"). Consequently, deformation by diffusion creep and grain-boundary sliding may be more common in naturally deformed silicates than is generally supposed.

Harzburgite tectonite in the basal portion of ophiolites is generally considered to be the residuum of partial melting of upper mantle peridotite. Partial fusion probably affects the relative contributions of the five flow mechanisms to the overall flow rate of hypersolidus harzburgite compared to those of subsolidus harzburgite. The most likely effect of partial melts, if distributed along grain boundaries, is to aid diffusion along grain boundaries and thus to promote the development of "magmatic pressure-solution and reprecipitation" textures. Another likely effect of grain-boundary melt is to reduce cohesion of grains and thereby to promote grain-boundary sliding and "magma-fracting". Dislocation glide and dislocation creep, the mechanisms currently believed to control the preferred orientation of crystallographic axes of olivine and the pyroxenes during subsolidus deformation of peridotite, would be relatively less important during hypersolidus deformation. Thus, the preferred orientations of olivine and the pyroxenes produced during hypersolidus creep would be weaker than or oriented differently from those produced during subsolidus creep at comparable strains.

Introduction

Harzburgite in the basal portion of ophiolites and in some non-ophiolitic alpine-type peridotites is generally considered to be the residuum of partial fusion of the upper mantle. The high temperatures attained during partial fusion are conducive to both ductile flow of the solid phases and crystal-mush flow, in which interstitial liquid accommodates the strain by allowing grain-boundary sliding to occur. Partial fusion perhaps can perturb intracrystalline flow mechanisms during penetrative deformation.

Deformation textures produced during high temperature flow of metals are complexly dependent on several deformation processes. Recent applications of transmission electron microscopy (TEM) techniques to geologic materials indicate that deformation mechanisms grossly similar to those in metals strongly influence deformation textures in rocks as well. Not surprisingly, attempts to categorize textures as resulting from either "plastic flow" or "syntectonic recrystallization" obscure and oversimplify the microscopic and sub-microscopic processes that control textures, and may inhibit recognition of other flow mechanisms.

Partial fusion of peridotites generally yields distinctive textures, termed "pyrometamorphic" by *Pike and Schwarzman* (1977). My purpose in writing this paper is to predict the textures that are diagnostic of syntectonic pyrometamorphism, by reviewing known solid-state deformation processes relevant to the three major silicate phases in harzburgite (olivine, OL; orthopyroxene, OPX; and clinopyroxene, CPX) and by suggesting possible perturbations of solid-state deformation mechanisms during partial fusion.

Terminology: A Caveat

The investigation of deformation processes of rocks has been approached from several different directions. One unfortunate result is the development of plastic terminology whose usage differs from one author to the next. The term "stress" means different things to theoreticians, engineers, and materials scientists, and its many meanings in the geologic literature encompass its many meanings in the non-geologic literature: the stress tensor σ_{ij}; the stress deviator (also known as the deviatoric stress or the non-hydrostatic component of the stress tensor) $\sigma_{ij}^* = \sigma_{ij} - \bar{\sigma}$, where $\bar{\sigma}$ is the mean stress (also known as the hydrostatic stress, lithostatic stress, or confining pressure); the differential stress $\sigma_1 - \sigma_3$; the shear stress $(\sigma_1 - \sigma_3)/2$ (commonly written as τ); or the "load" (the excess of σ_1 over the confining pressure extant before the load is imposed[1]). The term "plastic flow" in the geologic literature is used in two senses that reflect its different meanings in the materials science and physics (mechanics) literature respectively: (1) deformation of single crystals and polycrystalline aggregates by dislocation glide and, for some authors, by dislocation creep; and (2) deformation that causes permanent change in shape of a solid without failure by rupture. Dynamic or syntectonic recrystallization is a type of plastic flow under the second definition, but not under the restricted version of the first.

---

[1] Note that imposition of a uniaxial load σ_1 increases the mean stress by $\sigma_1/3$, since mean stress = $(\sigma_1 + \sigma_2 + \sigma_3)/3$.

Some terms that were borrowed from the metallurgists and ceramists have been applied imprecisely or inappropriately to rocks. Other terms had double meanings in the materials science literature when they were borrowed. Double meanings arise quite naturally, as epitomized in the development of deformation-mechanism maps by *Ashby* (1972) and his co-workers. Ashby related submicroscopic processes that are observed directly with the transmission electron microscope or that are inferred from optical and electron microscope observations of textures, to theoretical models that yield macroscopic flow laws. In turn, the theoretical flow laws have been related to experimentally-determined macroscopic flow laws (e.g., *Ashby and Verrall*, 1977). One result is that the term "dislocation glide" can mean either a certain submicroscopic deformation mechanism, or macroscopic flow in which the submicroscopic mechanism of dislocation glide dominates.

Other terms are ambiguous because they describe processes that are poorly understood. Some of these terms are discussed at appropriate places in the text below.

Deformation Mechanisms

High-temperature deformation processes can be divided into five types:

1) diffusion creep
2) dislocation-glide flow
3) dislocation creep
4) movement of arrays of dislocations
5) grain-boundary sliding

All five types may operate simultaneously, but the process that causes the highest flow rate will control the deformation textures. Whichever flow mechanism dominates for a given mineral is a complex function of temperature T, pressure or hydrostatic stress $\bar{\sigma}$, deviatoric stress σ^*_{ij}, strain ε_{kl}, strain rate $\dot{\varepsilon}_{kl}$, partial pressure of water P_{H_2O} (through the effect of hydrolytic weakening), and crystallographic orientation of the grains with respect to stress. Early dominance by one flow mechanism may yield to later dominance by another, if any of the above variables changes during the deformation.

Each mechanism involves several dependent steps. The slowest step will be rate-limiting for that mechanism and hence will determine whether that mechanism is the dominant, texture-controlling mechanism. Typically, some steps cause net transport of material, whereas others merely accommodate the mass transfer mechanism by readjusting the crystal sub-structure as to allow material transport to continue.

Diffusion Creep

Diffusion creep, dislocation creep, and movement of arrays of dislocations all require volume diffusion (diffusion through the crystal lattice) and/or grain-boundary diffusion. The term diffusion creep is reserved for deformation during which material is transported *solely* by diffusion of point defects.

Natural crystals contain several types of defects, one type being point defects. A common type of point defect is a vacancy, in which the crystal lattice is missing an atom or small molecular complex. When surface tractions are applied to a crystal, vacancies tend to diffuse towards the more compressed faces (or surfaces normal to the axis of maximum principal compressive stress σ_1; see Fig. 1). Their accumulation causes a net reduction of material at the compressed faces and acts to relieve the compressive stress. By the same token, the reduction of concentration of vacancies at other sites in the crystal, and particularly at crystal faces undergoing extension, will cause a net increase of material at those sites. The net effect is transport of material from relatively more to relatively less compressed faces.

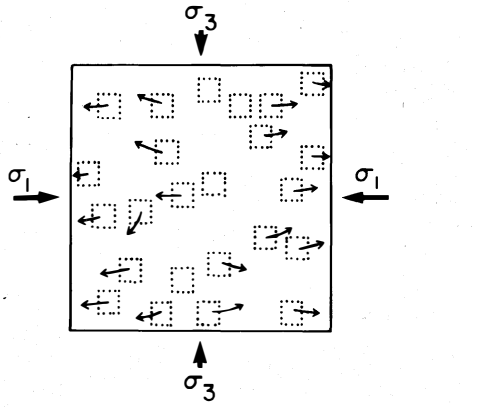

Fig. 1. Migration of vacancies in a stressed crystal. Direction of migration of vacancies (depicted by dotted squares) is shown by small arrows that emanate from each vacancy. Accumulation of vacancies at face normal to σ_1 results in net reduction of material along that face.

Diffusion creep is limited by the rate of diffusion of vacancies and by the availability of vacancies (vacancy sources) and of sites to which to move them (vacancy sinks). Although the interiors of natural crystals contain thermodynamically stable concentrations of vacancies, grain boundaries (and subgrain boundaries) are the largest source of vacancies and also serve as excellent sinks for vacancies, owing to the "looser" packing of atoms along grain boundaries.

Diffusion creep of an individual crystal in an aggregate entails no net change in size (volume) of the crystal or orientation of the lattice. Originally equant crystals become tabular or elongate, with their short axes parallel to σ_1 (Fig. 1). Diffusion creep of *polycrystalline* aggregates is more complicated for three reasons: 1) A vacancy at the edge of a grain may shift across a grain boundary to the edge of the neighboring grain. The shift causes a change in size of both the donor and the recipient. In effect, this shift transfers the location of the boundary between the two grains; this topic, grain-boundary migration, is discussed in the section on movement of arrays of dislocations. 2) Accumulation of vacancies along a grain boundary will create a void, unless sliding of grains along grain boundaries at high angles to the void closes it (*Lifshitz*, 1963; see Fig. 2 after *Cannon*, 1972). For arrays of polyhedra that approximate the shapes of polycrystals, *Stevens* (1971) and *Gates* (1975) calculated that grain-boundary *sliding* accommodates more than half of the total strain during diffusion creep! 3) Vacancies in a stressed polycrystal can diffuse along any of several paths (*Weertman*, 1968; *Elliott*, 1973): along cores of dislocations or linear defects in the crystal lattice, through the crystal lattice (volume-diffusion creep or Nabarro-Herring creep), along grain boundaries (grain-boundary-diffusion creep, known as Coble creep in metals) or subgrain boundaries,

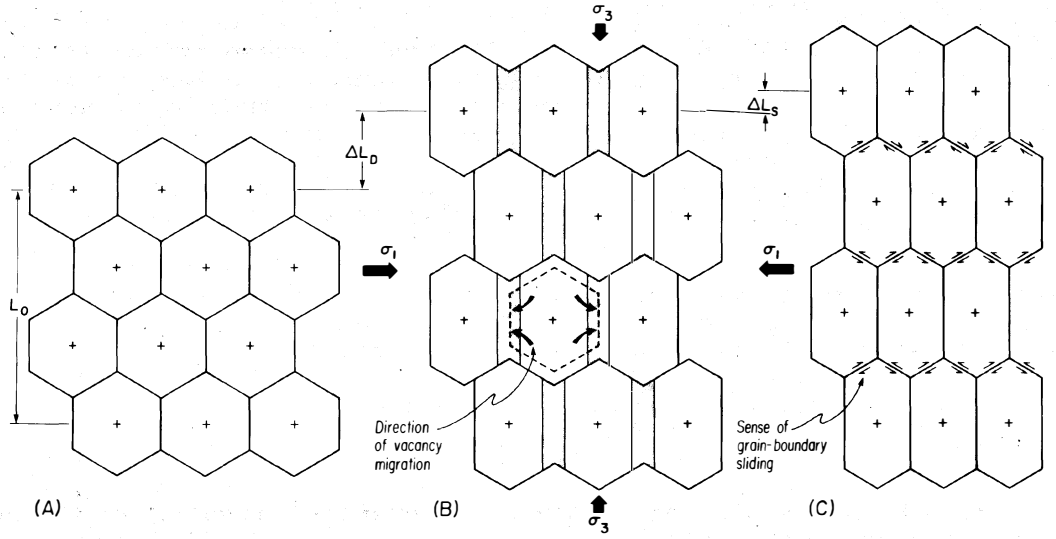

Fig. 2. Diffusion creep accompanied by grain-boundary sliding in idealized stressed polycrystal. (A) Initial undeformed state. (B) Intermediate state, in which diffusion of vacancies to grain boundaries opens voids (shaded areas) between grains. (C) Final state, in which grain-boundary voids have been closed by sliding of grains along boundaries at high angles to the voids. Lo = original length of three rows of crystals, center-to-center. ΔL_D = change in length from L_0 attributable to diffusion creep. ΔL_S = change in length from L_0 attributable to grain-boundary sliding. Center of mass of bottom row of three grains remains at same horizon in all three diagrams. (Modified after *Cannon*, 1972).

or through fluids along grain boundaries and pores. Microscopic textures are not diagnostic of diffusion paths (*Elliott*, 1973). Thus, all of these paths of diffusion yield geometrically equivalent deformation, which geologists term "pressure solution and precipitation[2]" (*Elliott*, 1973; *Rutter*, 1976; *Durney*, 1976).

The *macroscopic* flow laws of diffusion creep do depend on diffusion paths, and whether diffusion creep predominates over dislocation creep consequently can depend on the availability of paths of fast diffusion. Grain-boundary diffusion is generally faster than volume diffusion (*Barrer*, 1951), but most rocks are too coarse-grained (i.e., they have too low a density of grain boundaries per unit volume) for grain-boundary diffusion to dominate over volume diffusion[3]. Possible exceptions are mylonitic (i.e., very fine grained) peridotites. Diffusion creep, accompanied by grain-boundary sliding (see section on Grain-Boundary Sliding), might have produced the distinctive features of "SP" (superplastic) mylonites described by *Boullier and Gueguen* (1975) and *Gueguen and Boullier* (1975) and discussed further by *Twiss* (1976).

---

[2] Strictly speaking, diffusion creep is a solid state process; creep by fluid-phase transport of material along grain boundaries or "magmatic pressure-solution" is discussed in the section on Pyrometamorphism.

[3] In diffusion-creep flow laws, the Newtonian viscosity for grain boundary diffusion increases as the cube of the grain size; for volume diffusion, as the square of the grain size (*Gittus*, 1975, p. 22-23).

Diffusion creep dominates over dislocation creep and dislocation glide flow at low stresses, even at low temperatures (*Stocker and Ashby*, 1973; *Ashby and Verrall*, 1977). At low temperatures, though, strain rates for a given stress are extremely low: a rock deformed by diffusion creep (in the absence of fluids) at low temperatures is unlikely to be noticeably strained. Furthermore, since flow of the rock by diffusion creep is slow, it cannot relieve differential stress quickly; at low temperatures, stresses can build up rapidly to levels that allow dislocation creep and dislocation glide to dominate. Textures diagnostic of deformation by low temperature, solid-state diffusion creep are likely to be too subtle to recognize and probably are commonly overprinted by the more obvious textures of dislocation glide and dislocation creep.

Grain-Boundary Sliding and Superplasticity

Grain-boundary sliding involves differential movement of grains that slide past each other along their boundaries. At high pressures, porosity is forced to remain constant and near zero, and internal deformation of grains must accompany sliding in order to remove or reduce protuberances on grain boundaries that inhibit sliding (*Kirby and Raleigh*, 1973). The rate of deformation of a polycrystalline aggregate during grain-boundary sliding is limited by the rate of elimination of the slide-inhibiting protuberances by dislocation-glide flow, dislocation creep, grain-boundary migration, or diffusion creep.

Metallurgists describe materials that can deform in a ductile manner to large strains in tension without fracturing as being *superplastic*[4] (*Gittus*, 1975). The term "superplastic" is appropriate to materials deformed in *compression* (as in nature and in most rock deformation experiments) only if the same or analogous deformation mechanisms operate. Grain-boundary sliding is generally regarded as an important mechanism during superplastic flow of metals (*Edington et al.*, 1976). The essential feature of theories of superplasticity developed by *Ball and Hutchinson* (1969) and *Ashby and Verrall* (1973) is the switching of neighbors that grain-boundary sliding allows (Fig. 3). *Crossland and Wood* (1975) concluded that grains *must* switch neighbors, as well as undergo grain boundary sliding and internal deformation, to explain why grain-boundary denuded zones (*Squires et al.*, 1963) in Mg-.62 wt% Mn alloy that was extended to large strains are narrower than expected from extrapolations of moderate-strain models of *Stevens* (1971) and *Gates* (1975). *Twiss* (1976) emphasized that the diffusion-accommodated switching of neighbors can achieve nearly an order of magnitude more strain per unit of species diffused through unit distance than can Nabarro-Herring creep.

By its very nature, grain-boundary sliding *per se* produces no diagnostic textures (*Schmid et al.*, 1977), and consequently the study of superplasticity in geologic materials is in its infancy. *Boullier and Gueguen* (1975) proposed criteria for recognizing superplasticity in specimens of naturally deformed peridotite, anorthosite, and amphibolite, and *Schmid et al.* (1977) found many of these criteria applicable to limestone deformed experimentally in the superplastic regime. Textures

---

[4] Here I am discussing only so-called material superplasticity. *Sammis and Dein* (1974) have suggested that *transformational* super-plasticity may dominate flow textures in peridotites during the olivine-spinel inversion.

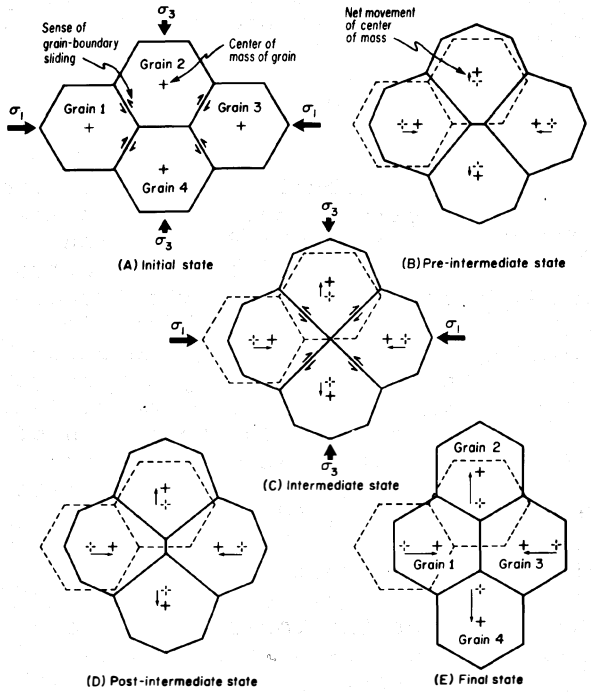

Fig. 3. Switching of neighbors in idealized polycrystal during superplastic flow by grain-boundary sliding. Grains 1 and 3 move towards each other during the deformation and ultimately become neighbors. Internal deformation of crystals accompanies sliding. (Modified after *Ashby and Verrall*, 1973.)

characteristic, although perhaps not diagnostic, of superplasticity are 1) equant grains, 2) very fine grain size (on the order of ten μm), and 3) moderate dislocation densities. *Boullier and Gueguen* (1975) suggested further that superplastic deformation of silicates destroys their preferred orientations and prevents formation of dislocation cells. (Dislocation cells are described in the next section.) On the other hand, *Schmid et al.* (1977) measured moderate preferred orientations and observed development of dislocation cells and subgrains in their specimens of limestone deformed experimentally, and they therefore warned that some of the textures observed by *Boullier and Gueguen* may not be generally characteristic of superplasticity.

Grain-boundary sliding at high temperatures and pressures is best viewed as a mechanism that accommodates other flow mechanisms: if porosity remains constant, then grain-boundary sliding necessarily accompanies both diffusion creep (*Lifschitz*, 1963) and dislocation creep[5]; otherwise, voids will form at sites of accumulation of vacancies.

Dislocation-Glide Flow

Mechanisms of flow by the movement of dislocations through crystals is the subject of extensive description and discussion in the materials science literature. For detailed reviews and references, see texts by *Cottrell* (1953), *Read* (1953), *McLean* (1962), *Weertman and Weertman* (1964), *Byrne* (1965), *Kelly and Groves* (1970), and *Gittus* (1975). Geologists should welcome the recently published text by *Nicolas and Poirier* (1976), which reviews deformation mechanisms in peridotites.

Dislocations are curvilinear defects in crystal lattices and occur in all natural crystals. There are three types of dislocations: edge, screw, and mixed. The edge dislocation can be best viewed as the edge of an extra half-plane of atoms inserted into the lattice (Fig. 4). The screw

[5] Grain-boundary sliding need not accompany *dislocation* creep, in the unlikely event that the Von Mises condition is fulfilled during high temperature creep of peridotite (see next section).

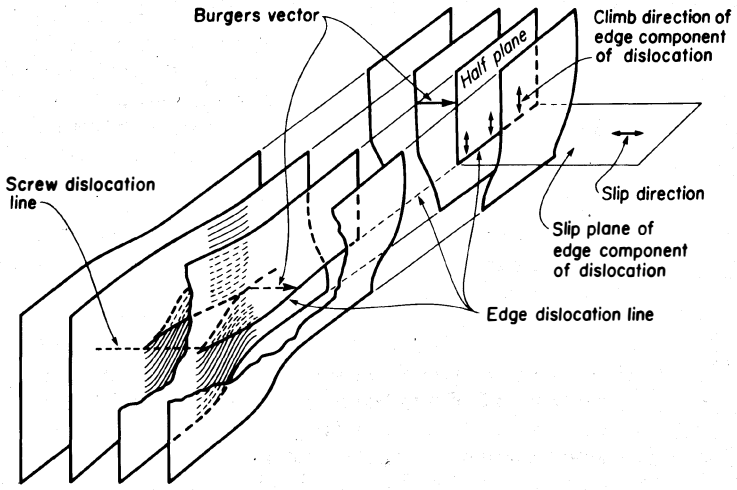

Fig. 4. Screw dislocation (lower left) and edge dislocation (upper right). Climb of edge component occurs by diffusion of vacancies to or away from the edge of the extra half-plane (shortening or lengthening the half--lane, respectively).

dislocation marks a line of shearing of one plane of atoms over another (Figs. 4, 5, and 7). Mixed dislocations are combinations of edge and screw dislocations.

Edge dislocations are strongly associated with a slip plane, the plane that contains the dislocation line (the edge of the extra half-plane) and the Burgers vector of the dislocation (Fig. 4). The dislocation moves most easily by glide, in the absence of obstacles. Glide entails the motion of the dislocation along the slip plane. The net effect of the glide of one dislocation through a region is to shift or slip the upper half of the crystal over the lower half by a distance of one Burgers vector.

Obstacles to glide include interstitial solutes, vacancies, or other dislocations in the same slip plane or in intersecting slip planes. Newly crystallized or annealed crystals have a low density (*ca.* $10^6/cm^2$) of free dislocations[6]. In such crystals, edge dislocations can glide freely along their slip planes with little chance of encountering barriers to glide, especially other dislocations. Small shear stresses can move the dislocations easily, and so the crystal is relatively weak. As progressive deformation creates and activates more and more dislocation sources, the density of free dislocations increases dramatically (to values of 10^8 to $10^{10}/cm^2$ in experimentally deformed olivine investigated by *Phakey et al.*, 1972). Dislocations on intersecting slip planes commonly become ensnarled and form chaotic tangles, some with dislocation densities greater than $10^{11}/cm^2$ (*Green and Radcliffe*, 1972), through which dislocation glide is impossible. The resulting network of dislocation tangles, which surround areas or "cells" of material that have moderate dislocation densities, gives rise to "dislocation-cell structure". Since higher stresses are now needed to move the edge and screw dislocations, the crystal becomes stronger: it work-hardens.

Flow by dislocation glide is in steady-state only when continued deformation causes no further work-hardening. Whether naturally deformed peridotites ever attain steady-state flow by dislocation glide is a moot point for two reasons: (1) In nature, peridotites are likely to be either at temperatures high enough to permit the dislocation substructure to recover (see section on Dislocation Creep) or, if at low temperatures, at pressures too low to suppress brittle behavior (fracturing) at high stresses. (2) For polycrystalline aggregates to deform homogeneously by

---

[6] Free dislocations are those dislocations that are in the interior of grains or subgrains and are distinct from dislocations in grain boundaries and subgrain boundaries. Free dislocations can be either glissile (mobile or free to move) or sessile (immobile and pinned by barriers to glide).

dislocation glide flow only, five independent slip systems are required (the Von Mises condition). For polycrystals to deform inhomogeneously (the grains deform compatibly but not uniformly) solely by dislocation-glide flow, four independent slip systems may suffice (*J.W. Hutchinson*, 1976, pers. comm. to *Ashby and Verrall*, 1977). Although as many as five slip systems have been identified by transmission electron microscopy of experimentally deformed olivine, only three are independent (*Phakey et al.*, 1972). In addition, the critical resolved shear stress[7] that is required to activate the different slip systems of olivine is different (and is a function of temperature and strain rate). It is unlikely that more than one or two slip systems of olivine and the pyroxenes are active at a given temperature and strain rate, and therefore the Von Mises condition is probably not fulfilled in peridotites. Furthermore, no combination of slip along the five slip systems of olivine permits a pure, homogeneous contraction along the [010]-axis by dislocation glide alone (*Phakey et al.*, 1972; *Kohlstedt and Goetze*, 1974). Thus, an olivine crystal compressed parallel to [010] can deform by dislocation glide only by *inhomogeneous* slip (kinking), which cannot produce steady-state flow by itself.

Dislocation-glide flow is probably only a transient phenomenon during natural deformation of peridotites. For most purposes the submicroscopic mechanism of dislocation glide need only be considered one of the dependent steps of dislocation creep.

Dislocation Creep: Plastic Flow

The dislocation mechanisms that are involved in the type of dislocation creep commonly called plastic flow or high-temperature plasticity include dislocation glide, cross-slip of screw components of dislocations, and climb of edge components.

Screw dislocations that have not dissociated into partial dislocations are not strongly associated with their slip planes, unlike edge dislocations. When a screw dislocation encounters a barrier to glide, it can move to another, parallel, unobstructed plane by *cross-slip* and then continue to glide (*Cottrell*, 1964, p. 275-279; Fig. 5). Cross-slip can occur along any plane (other than the original slip plane, by definition) that contains the Burgers vector. Cross-slip would be only slightly more difficult than glide, if constraints at the ends of a screw dislocation line could be ignored. Where the dislocation changes character from screw to mixed to edge, however, the dislocation cannot move out of its slip plane by cross-slip. Hence, cross-slip of screw dislocations is retarded by drag from edge components of the dislocation at the ends of the screw segment. Furthermore, if a screw dislocation dissociates into partial dislocations, it becomes strongly associated with the plane that contains the partials (see *Cottrell*, 1964, p. 275-276) and will not be able to cross-slip freely.

An edge dislocation that is pinned at a barrier can "recover" its freedom to glide by "climbing" from the obstructed slip plane to a slip plane with no barriers. An edge dislocation *climbs* by the *diffusion* of vacancies to or away from its extra half-plane. Similarly, screw

---

[7] The critical resolved shear stress is the minimum shear stress that is required to activate slip on a slip system optimally oriented with respect to stress (see *Nicolas and Poirier*, 1975, p. 40-42).

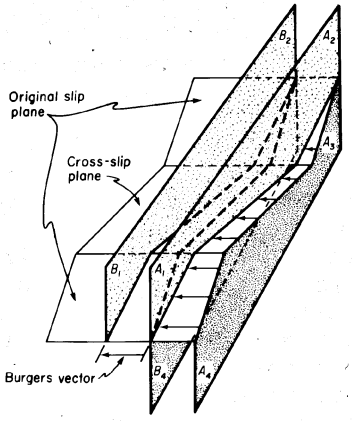

Fig. 5. Cross-slip of screw dislocation. Front of top half (corner A_1) of former vertical crystal plane A_1 - A_2 - A_3 - A_4 has been sheared to left, with respect to front of bottom half (corner A_4) of former plane A_1 - A_2 - A_3 - A_4. Cross-slip can occur on any plane in the zone for which the Burgers vector is the zone axis, except on the original slip plane.

dislocations that contain offsets or "jogs" (typically produced by two dislocations passing through each other on intersecting slip planes; see *Cottrell*, 1953, p. 173, or *Weertman and Weertman*, 1964, p. 131-139) can move their jogs only by diffusion. Mechanical data from deformation experiments on olivine undergoing steady-state dislocation creep are fit best by a power-law equation of the form:

$$\dot{\varepsilon} = A\sigma^n \exp(-Q_c/RT)$$

where $\dot{\varepsilon}$ is the strain rate, σ is the differential stress, Q_c is the activation energy for creep, T is the absolute temperate, R is the gas constant, A is a constant related to the structure of the mineral, and n is a constant in the range of 2 to 5 (*Carter and Avé Lallemant*, 1970; *Post*, 1973, 1977; see review by *Carter*, 1976). The form of this equation is consistent with that predicted from theory (*Weertman*, 1968; *Ashby*, 1972). The Arrhenius term, characteristic of thermally activated processes, suggests that diffusion-controlled climb is the rate-limiting step during steady-state dislocation creep (*Weertman*, 1968).

Dislocation climb softens a crystal, since the dislocations are once again free to glide: the crystal has undergone *recovery* of the mechanical behavior that it had in the original or annealed state. When generation and annihilation, and pinning and climb of dislocations all proceed at a rate that maintains a constant density of mobile dislocations, then recovery by cross-slip and climb occurs as quickly as work-hardening by dislocation entanglement, and the crystal undergoes steady-state dislocation creep by plastic flow (*Mitra and McLean*, 1966, 1967).

Dislocation climb manifests itself in optically observable textures by causing zones of broad undulatory extinction to change into strain-free areas that are separated by sharp kink band boundaries[8,9]. Dislocations are more stable in arrays that exert small long-range stresses than in arrays that exert large long-range stresses. The pile-up of many dislocations behind a barrier on the same slip plane generates a large long-range stress (Fig. 6A). Undulatory extinction reflects relatively homogeneous bending of the crystal lattice, which is caused by the relatively uniform distribution of dislocations that are piled-up behind

---

[8] Kink bands are called deformation bands by some authors. Kink bands should not be confused with deformation lamellae, which are photoelastic effects best seen in phase contrast illumination that are produced by the pile-up of dislocations in a plane parallel or sub-parallel to the slip plane (*Carter et al.*, 1964; *Christie and Ardell*, 1974).

[9] Sharp kinks are not of themselves diagnostic of dislocation climb; inhomogeneous slip along parallel slip planes can also produce sharp kinks, as in deformation of mica with the axis of compression parallel to the slip plane (e.g., *T. Tullis*, 1971).

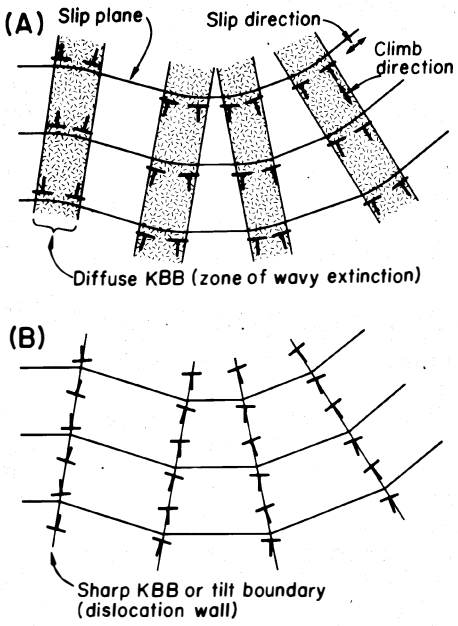

Fig. 6. Recovery by climb of edge dislocations. (A) Schematic representation of slip planes (sub-horizontal lines) that are gently curved where several dislocations are piled up (shaded regions); such regions would appear optically as zones of undulatory extinction. (B) Dislocations have formed stable arrays (tilt boundaries); curvature of crystal is concentrated at tilt boundaries, which thus will appear as sharp kink-band boundaries (KBB). (Modified after *Cottrell*, 1953).

barriers throughout the crystal. The long-range stress can be reduced through redistribution of the dislocations into other, more stable configurations by climb to other slip planes (Fig. 6B). (For a full discussion of this and the next paragraph, see *Weertman and Weertman*, 1964.)

Arrays that exert the smallest long-range stresses are tilt boundaries (also called dislocation walls), which are stable arrays of edge dislocations (Fig. 6b), and twist boundaries, which are stable arrays of screw dislocations (Fig. 7). Straight dislocation walls are energetically

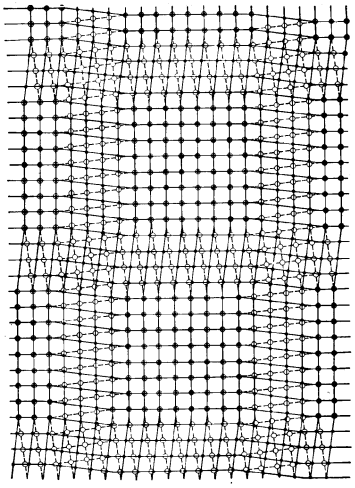

Fig. 7. Twist boundaries in a simple cubic lattice. Boundaries are formed by stable arrays of screw dislocations with two different Burgers vectors (one is horizontal, the other is vertical in this example). Dots connected by solid lines lie in a plane above the plane of the figure; open circles connected by dashed lines lie in a plane below the plane of the figure. Twist boundaries are parallel to the plane of the figure. (From *Dislocations in Crystals* by W.T. Read, Jr. Copyright 1953 by McGraw-Hill Book Company. Used with permission of McGraw-Hill Book Company.)

favored over curved walls (*Cottrell*, 1953, p. 46-49). Climb allows the dislocations to form straight walls, in planes normal to the slip direction. The crystal structure is slightly bent across a dislocation wall (Fig. 6b). The greater the concentration of edge dislocations in a wall, the greater the angle through which the crystal is bent[10]. If the angle is large enough, the wall is evident optically as a kink-band boundary.

[10] See bottom of next page.

Tilt and twist boundaries can connect to surround a portion of a grain and form a *subgrain* with a polygonal shape. The interior of a subgrain that forms during deformation may have a dislocation density as low as that expected for undeformed crystals ($10^6/cm^2$), if recovery keeps pace with dislocation generation. Well-recovered grains contain a mosaic of small, commonly rectangular subgrains (produced during "polygonization", one type of recovery process) whose lattice orientations differ from those of adjacent subgrains by less than 5° and commonly less than 1° (Fig. 9; also see photomicrographs by *Kirby and Raleigh*, 1973, Fig. 7, or *Carter*, 1976, Fig. 24).

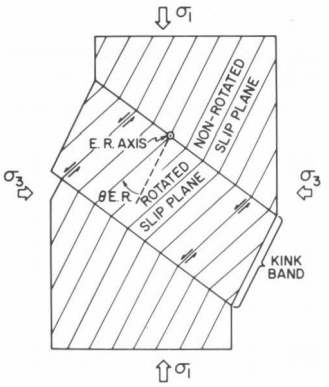

Fig. 8. Plastic flow by translation gliding. Inhomogeneous slip causes slip planes within the kink band to rotate about the axis of external rotation (E.R. axis) through an angle $\theta_{E.R.}$ to orientations that are at progressively higher angles to maximum principal compressive stress σ_1 than original (non-rotated) orientation of slip planes. As drawn, region of crystal within kink band will appear strain-free in thin section. (Modified after *Carter and Raleigh*, 1969.)

Fig. 9. Photomicrograph of subgrains in an olivine grain from specimen GB-517 deformed experimentally by *Post* (1973). Long direction = 1.15 mm. Crossed nicols. Subgrains are visible as small, rectangular patches. Various shades of gray indicate that some subgrains are closer to extinction than others. Fine-grained "veins" contain olivine neoblasts that developed during intracrystalline recrystallization.

---

10 This angle is known as the angle of external rotation. Two coordinate systems (crystal lattices) of differing orientations can be brought into the same orientation by rotation about a single axis (the axis of external rotation). The angle of rotation about this axis is the angle of external rotation (see Fig. 8).

In general, increasing the total strain by plastic flow increases the number of dislocations that are generated and that ultimately climb and glide into subgrain boundaries. Consequently, the angle through which undulatory extinction sweeps or which relates crystal lattices on the opposite sides of a kink-band boundary increases with increasing plastic strain (Table 1), in the absence of other complications discussed below. Similarly, the average aspect ratio[11] observed in thin section typically increases with increasing strain, as the movement of dislocations in the stress field causes a net flow of material away from crystal faces under compression and toward faces under extension (Table 2). However, any process that obscures or destroys the integrity of originally undeformed or annealed grains will invalidate conclusions drawn from blind applications of Tables 1 and 2 about the strain recorded by those grains. Recrystallization is the most common such process.

TABLE 1. Typical angles of external rotation

	Amount of Strain		
	Mild	Moderate	Strong
OL	0-5°	5-10°	10-30°
OPX	0-2°	2-5°	5-20°
CPX	0-2°	2-5°	5-10°

TABLE 2. Typical aspect ratios

	Amount of Strain		
	Mild	Moderate	Strong
OL	2:1	5:1	50:1
OPX	1.5:1	3:1	10:1
CPX	1.5:1	2:1	5:1

[11] Aspect ratios (length-to-width ratios) for grain shapes are usually measured in thin sections cut normal to foliation and parallel to lineation.

Recrystallization typically occurs along kink-band boundaries and grain boundaries of plastically deformed original grains (porphyroclasts of *Mercier and Nicolás*, 1975, and *Harte*, 1977), since those boundaries are sites of high strain energy (see next section). Trains of recrystallized grains (neoblasts) commonly completely transect porphyroclasts along former kink band boundaries. They divide the original grain into several parts that are relatively free of optical strain and whose individual aspect ratios may bear little relationship to the aspect ratio of the deformed original grain (*Nicolás*, 1976). Failure to recognize the subdivided parts of a partially recrystallized porphyroclast as components of the original porphyroclast can lead to a totally inaccurate estimate of not only the magnitude but the orientation of the finite strain.

During plastic flow, slip planes rotate towards becoming perpendicular to the axis of compression, and slip directions towards parallelism with the axis of extension (Fig. 8). The systematic rotation of slip planes and slip directions produces a crystallographic preferred orientation that ideally should increase with strain. Theoretical models predict that plastic flow of initially randomly oriented grains in a single-phase polycrystal can produce strong preferred orientations at small total strains (see discussion by *J. Tullis*, 1971, p. 250-300, of models by *Calnan and Clews*, 1950; *Schmid and Boas*, 1950; and *Bishop*, 1954). However, rock deformation experiments on quartzite (*J. Tullis*, 1971) and dunite (*Avé Lallemant*, 1975) show that plastic flow produces strong crystallographic preferred orientations only at large strains.

Movement of Arrays of Dislocations: Recrystallization

The processes discussed in this section all involve adjustments or movements of grain or subgrain boundaries. These boundaries can be modeled as arrays of dislocations (*Gleiter and Chalmers*, 1972). The behavior of an array of dislocations is sufficiently different from that of an individual dislocation to warrant separate discussion.

The distinction between recovery of plastically deformed grains and recrystallization is somewhat artificial, both in theory and practice. Both processes reduce elastic strain energy in small domains, which are called subgrains if produced by recovery, and neoblasts if produced by recrystallization. *Byrne* (1965, p. 33) defines recovery as constituting "all those annealing phenomena which occur before the appearance of new strain-free recrystallized grains, regardless of how refined the technique used to detect the new grains", and recrystallization as "the nucleation and growth of these new strain-free grains and the gradual consumption of the cold-worked matrix by the movement of large-angle grain boundaries". However, strain-free grains can originate by growth of strain-free material at sites other than new nuclei. *Beck and Sperry* (1950) observed a type of recrystallization, termed grain-boundary migration (or "bulge nucleation"), that involved no nucleation of strain-free grains (see below). Subgrains of whatever origin can enlarge to produce recrystallization textures, whether the subgrains be ill-defined cells bounded by dislocation tangles, well-defined polygons (formed during "polygonization") bounded by regular arrays of dislocations (tilt and twist boundaries), or embryo recrystallized nuclei (*Byrne*, 1965).

The distinction between subgrains and neoblasts in practice is based either on their size or on whether the lattice orientation of the relatively strain-free domain differs from that of the host porphyroclast by less than or more than, respectively, an arbitrarily chosen angle,

usually 5° or 10°. A subgrain is bounded by dislocation walls and/or twist boundaries. If continued deformation causes accumulation of more and more dislocations in the subgrain boundaries, the subgrain lattice will become progressively more rotated with respect to the host lattice. *Poirier and Nicolás* (1975) have proposed that one possible mechanism for generating olivine neoblasts in peridotite tectonites is the progressive rotation of subgrains during deformation, to angles greater than the arbitrary 5° or 10°.

Where recrystallization involves nucleation, an incubation period characterizes the recrystallization kinetics as it does for most processes than involve nucleation (*Cottrell*, 1953, p. 193; *Byrne*, 1965, p. 60). Embryo nuclei have a critical minimum size to be stable, which reflects the trade-off between decrease in free energy of strain-free nucleus relative to the strained matrix, and the increase in surface energy from creating the interface between the strain-free nucleus and the strained matrix. Thus nucleation occurs preferentially where reduction of lattice-strain energy will be greatest, namely in the most severely strained regions of a grain, as has been observed in metals (*Byrne*, 1965) and in olivine (*Lalley et al.*, 1976).

Subgrain coalescence can be viewed as a mechanism for either nucleation (*Byrne*, 1965, p. 76-85) or growth (*Hu*, 1962; *Li*, 1962) of a neoblast. As envisioned by *Hu* (1962), for two strain-free subgrains with slightly different lattice orientations to coalesce, one subgrain has to rotate slightly with respect to the other, in order to bring the lattice orientation of the two subgrains into coincidence (Fig. 10). In so doing, the subgrain also rotates with respect to all other neighboring subgrains. *Li* (1962) showed that the driving force for such a rotation is not only the elimination of the strain and surface energy associated with the interface between the two merging neighbors, but also the improved fit of the rotated subgrains with neighboring grains and subgrains along the newly adjusted boundaries. The finer the size of the cell structure (subgrain) and the more diffuse the boundaries between subgrains, the easier is coalescence (see discussion by *Byrne*, 1965, p. 76-85). A coalesced group of subgrains will be recognized as a neoblast only when it has grown to a critical size large enough for it to be distinguished from individual subgrains and for it to be able to grow by grain-boundary migration (see below). Because the period preceding the attainment of the critical size is in essense an incubation period, *Byrne* (1965) viewed the early stages of coalescence as a nucleation process.

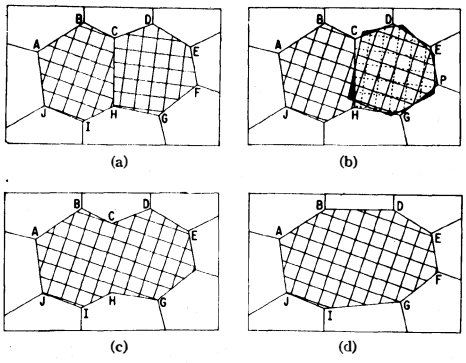

Fig. 10. Subgrain coalescence. Two subgrains with slightly different lattice orientations coalesce along their common boundary C-H by progressive rotation of the lattice of subgrain C-D-E-F-G-H into coincidence with that of subgrain A-B-C-H-I-J. (A) Initial subgrain structure. (B) Rotation of one subgrain. (C) Subgrain structure after coalescence. (D) Final subgrain structure after limited migration of subboundaries. (Reprinted from *J.C.M. Li*, Jour. Appl. Phys., v. 33, p. 2958-2965, 1962. Used with permission of J.C.M. Li and American Institute of Physics.)

At least two mechanisms contribute to the *growth* of neoblasts: subgrain coalescence (described above) and grain-boundary migration (*Beck*

and Sperry, 1950; *Bailey*, 1962). As implied by its name, grain-boundary migration involves the growth of a strain-free grain at the expense of its strained neighbor by migration of their common boundary into the strained neighbor. During primary recrystallization, the dominant driving force for migration is the elimination of lattice strain energy in the material through which the boundary passes. Even after primary recrystallization has eliminated all lattice strain energy, grain-boundary migration can continue, driven by the reduction of grain-boundary energy by eliminating fine grains. The coarsening of grain size that results is termed grain growth, if the larger grains from the primary recrystallization survive, or secondary recrystallization (exaggerated grain growth), if they do not (*Cottrell*, 1964, p. 286; *Byrne*, 1965, p. 106; see *Cotterill and Mould*, 1976, especially p. 271-274, for an excellent discussion of primary recrystallization, grain growth, and secondary recrystallization).

Recrystallization Textures

Discussion in the literature of recrystallization textures in ultramafic rocks is virtually limited to olivine (*Collee*, 1963; *Raleigh*, 1963; *Ragan*, 1969; *Brothers and Rodgers*, 1969; *Raleigh and Kirby*, 1970; *Avé Lallemant and Carter*, 1970; *Post*, 1973, 1977; *Kirby and Raleigh*, 1973; *Nicolás et al.*, 1973; *Mercier and Nicolás*, 1975; see review by *Carter*, 1976). Experimental work on orthopyroxene (*Raleigh et al.*, 1971; *Carter*, 1971; *Carter et al.*, 1972; *George*, 1975; *Ross*, 1977) and on clinopyroxene (*Etheridge and Kirby*, 1977; *Avé Lallemant*, 1977) and observations on natural peridotites (*Avé Lallemant*, 1967) indicate that the pyroxenes recover and recrystallize far less readily than does olivine (*Carter*, 1976), apparently because the low stacking fault energy of the pyroxenes inhibits dislocation climb (*Green and Radcliffe*, 1972; *Goetze and Kohlstedt*, 1973; see *Barrett and Massalski*, 1966, p. 387-390 for a discussion of stacking faults, partial dislocations, and their effect on climb in metals).

Completely recrystallized olivine in deformed peridotites typically displays a mosaic texture in which the straight boundaries of fine-grained, polygonal olivine commonly terminate in 120° junctions. The grains are equigranular but not necessarily equant. This texture is the equigrangular textures of *Mercier and Nicolás* (1975) and the granuloblastic texture of *Harte* (1977).

Completely recrystallized olivine with no relict plastically deformed parent grains is rare in both naturally and experimentally deformed olivine. More commonly, recrystallized grains have consumed only some of the parent grains. The resulting texture, *Mercier and Nicolás's* (1975) and *Harte's* (1977) porphyroclastic texture, consists of an imperfect mosaic of small, equigranular, nearly strain-free neoblasts that surrounds large, strained porphyroclasts (Fig. 11). The neoblasts have straight or slightly curved mutual boundaries that tend to terminate in 120° junctions. The very fine-grained equigranular texture of most peridotite mylonites (e.g., *Boullier and Gueguen*, 1975) is probably produced by recrystallization[12] (whether accompanied by grain boundary sliding or not).

---

[12] The very fine grain size of most mylonites is produced by recrystallization and *not* by the brittle process commonly termed cataclasis or granulation (c.f. discussion of quartz recrystallization textures by *Carter et al.*, 1964).

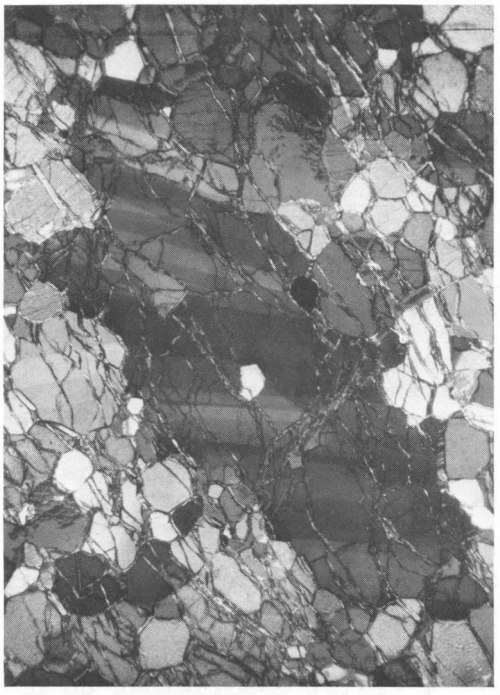

Fig. 11. Photomicrograph of naturally deformed, partially recrystallized dunite from North Carolina. Long direction = 4.6 mm. Large NW-trending olivine porphyroclast in center contains E-trending kink bands. Porphyroclast is surrounded by mosaic of olivine neoblasts, some of which are mildly kinked themselves. Neoblasts have a strong preferred orientation of [010]-axes normal to foliation defined by long dimensions of remnant porphyroclasts.

Two types of recrystallization are commonly discussed in the geologic literature: syntectonic recrystallization (hot-working) and annealing recrystallization of plastically deformed (cold-worked) specimens. Both types probably involve the same submicroscopic processes but operating to different extents, owing to three differences: 1) The dislocation and point defect substructures and their relative mobilities in host (non-recrystallized) grains of hot-worked material are different from those of cold-worked material. 2) The deviatoric (non-hydrostatic) component of stress can favor certain directions of atomic migrations or grain-boundary migrations, or certain orientations of newly crystallized nuclei over others during syntectonic recrystallization. 3) Neoblasts themselves become plastically deformed during syntectonic recrystallization but not during annealing recrystallization. These difficulties are probably sensitive to the magnitude of the stress deviator, and we should expect to see a range of recrystallization textures corresponding to a range of deviatoric stresses from infinitesimally low (i.e., annealing recrystallization) to intermediate ("typical" syntectonic recrystallization) to high (mylonites?).

In fact, in experimentally deformed peridotites we do see a range of textures that correlate roughly with deviatoric stresses. In experiments on olivine, recrystallized grains are more flattened, have more irregular boundaries, and define a stronger foliation in high-stress experiments than in low-stress ones (personal observation of specimens experimentally deformed by *Avé Lallemant and Carter*, 1970, and *Post*, 1973, 1977). *Post* (1973, 1977), *Kohlstedt et al.* (1976) and *Mercier et al.* (1977) observed a modest inverse correlation between stress and grain size in olivine, a relation previously reported for metals (*Luton and Sellars*, 1969; *Glover and Sellars*, 1973) and predicted from theory (*Barret and Nix*, 1965; *White*, 1976). However, more recent experimental work both on metals (*Gittus*, 1975; *T. Langdon*, pers. commun.) and on olivine (*Ross et al.*, 1977) suggested that the temperature of deformation also influences grain size and that grain size changes quickly during annealing of hot-worked dunite (*Zeuch and Green*, 1977). Thus, *Twiss* (1977) urged caution in application of grain size to interpretations of paleostress of natural deformations.

Development of crystallographic preferred orientation during recrystallization is poorly understood. Two possible mechanisms are:

(1) preferential nucleation of nuclei in a certain orientation, and (2) nucleation of nuclei with random orientations, followed by selective growth of only certain nuclei.

Dollinger (1973) and *Avé Lallemant* (1975) applied the *Green et al.* (1970) discussion of syntectonic recrystallization of quartz to recrystallization of olivine. *Avé Lallemant* (1975) argued that neoblasts that are oriented in the stress field least favorably for translation gliding on (010)[100](that is, neoblasts whose b-axes parallel σ_1) will acquire less stored strain energy than neoblasts in other orientations; consequently, neoblasts with b-axes parallel to σ_1 will be more stable than and will grow at the expense of their more highly strained neighbors. *Dollinger* (1973) found that *annealing* recrystallization of experimentally deformed olivine can also produce strong crystallographic preferred orientations, with the b-axes statistically parallel to the pre-annealing orientation of σ_1. During annealing, there is no deviatoric stress to influence the orientation of nuclei or the relative mobilities of differently oriented grain boundaries. However, subgrains whose b-axes paralleled σ_1 during the pre-annealing plastic deformation will have less stored strain energy than subgrains in other orientations, just as in the case for neoblasts during syntectonic recrystallization. Thus, *Dollinger's* (1973) and *Ave Lallemant's* (1975) results suggest that recrystallization fabrics are controlled by selective growth of subgrains (or nuclei from "bulge" nucleation) of certain orientations.

Dollinger's (1973) and *Avé Lallemant's* (1975) conclusions do not preclude the possibility that nuclei are nucleated with a preferred orientation. For example, neoblasts that are developed during intracrystalline recrystallization (as opposed to grain-boundary recrystallization) have a preferred orientation that is strongly controlled by the host grains, regardless of the orientation of the host, in experimentally deformed dunite (*Avé Lallemant and Carter*, 1970), experimentally deformed orthopyroxenite (*George*, 1975; *Etheridge and Kirby*, 1977) and naturally deformed orthopyroxenite (*Etheridge*, 1975). Their preferred orientation could arise either from oriented nucleation or from selective or "oriented" growth of those nuclei whose boundaries are most mobile because of a coincidence lattice relationship (see *Gleiter and Chalmers*, 1972). Acting individually, oriented nucleation and oriented growth can explain some, but not all, characteristics of development of preferred orientations during annealing recrystallization of metals (*McLean*, 1962, p. 282-284; *Barrett and Bassalski*, 1966, p. 579-583), and it is unlikely that both processes contribute to the development of oriented fabrics in silicates. Since both processes probably occur during both syntectonic and annealing recrystallization, fabric diagrams of preferred orientations of recrystallized grains are unlikely discriminators of annealed and hot-worked rocks.

Pyrometamorphism

Partial melts probably perturb solid-state deformation processes through two properties: 1) diffusion rates are five orders of magnitude greater through silicates melts than through crystalline silicates (*Hofman and Magaritz*, this vol.) and 2) silicate melts, even if polymerized, are less structured than solids. This section speculates on how melts can affect material properties and, in turn, on how a partially fused peridotite reacts to a deviatoric stress.

Diffusion is inferred to be the rate-limiting step during high-temperature creep of silicates, whether the dominant mode of deformation is diffusion creep or dislocation creep (*Carter*, 1976). If one makes the reasonable assumption that other dependent steps (if indeed they exist in melts) in the creep process, such as generation of vacancies, are no slower in silicate melts than they are in crystalline silicates, then the higher rates of diffusion through melts must lower the creep strength (or effective viscosity) of silicate melts relative to crystalline silicates. Indeed, *Kushiro et al.* (1976) report that the effective viscosity of basaltic magma at 1375-1400°C and 20 kb may be as low as 30-50 poises, in contrast to effective viscosities of the order of 10^{20} poises for dunite (*Carter and Avé Lallemant*, 1970; *Post*, 1973, 1977).

The rheologic properties of a multiphase aggregate are controlled dominantly by the flow properties of the phase that provides the structural framework. The most abundant phase (typically olivine in harzburgites) forms the structural framework for most geometries of polycrystals. In partially molten material, though, the melt will provide the structural framework, if it is penetratively distributed along grain boundaries and if it comprises a volume fraction large enough (10% or more?) to isolate grains of the solid phases from one another. Hypersolidus harzburgite that contains very large volume fractions (30% or more) of silicate melt can deform by "crystal mush flow" ("polygenic flow" of *Thayer and Jackson*, 1972), in which the melt accommodates the strain by bulk flow.

Experiments on hydrostatic melting of granite (*Brace et al.*, 1968; *Mehnert et al.*, 1973) and hypersolidus deformation experiments on peridotite (*Avé Lallemant and Carter*, 1970; *Boudier and Nicolás*, this volume) indicate that silicate melts do penetrate the host rock, both along grain boundaries and through finely spaced fractures (see Fig. 1D of *Avé Lallemant and Carter*, 1970). In *Mehnert et al.'s* (1973) experiments, grain-boundary melting was initiated at multiphase nodes and interfaces (e.g., quartz/feldspar boundaries); as the volume fraction of the melt increased, the thickness of the melt remained greater at multiphase interfaces than along boundaries between grains of the same phase. Granitic melts are highly viscous, though, and their behavior along grain boundaries is probably quite different from the behavior of basaltic melts. Indeed, in view of the low viscosity observed by *Kushiro et al.* (1976) for basaltic magma, one wonders whether any melt but the thinnest coating along grain boundaries would be retained during *syntectonic* partial fusion of mantle peridotite, and thus whether "crystal mush flow" would be a common mode of flow of harzburgite tectonite.

A small percent of grain-boundary melt perhaps will profoundly affect deformation processes in another way, however. One mechanism of deformation by pressure solution is creep by grain-boundary diffusion (Coble creep). Grain-boundary-diffusion creep apparently contributes little to total strain under most geologic conditions (*Stocker and Ashby*, 1973), since deformation of crystalline silicates is typically dominated by dislocation creep at intermediate to high temperatures and moderate stresses, and by Nabarro creep (lattice diffusion) at high temperatures and low stresses. At hypersolidus temperatures, though, grain-boundary diffusion is effectively enhanced by five orders of magnitude (*Hofman and Magaritz*, this volume). The singular increase in the rate of grain-boundary diffusion at the melting temperature perhaps is sufficiently large to permit "magmatic pressure solution" to dominate the flow mechanisms. Magmatic pressure solution is conceptually identical to pressure solution of quartzites by aqueous solutions (*H. Dick*, 1973, oral comm.; see the excellent discussion by *Elliott*, 1973), the only difference being the distinction between silicate melt and metamorphic fluid as the transporting agent.

A change in dominant deformation mechanisms should cause a change in strength of a rock. Preliminary experiments at confining pressure (*Goetze*, 1977) demonstrated no drastic weakening (within an order of magnitude) of hypersolidus peridotite containing up to 10 volume percent of melt, compared to subsolidus peridotite. However, since diffusional flow should be relatively favored over dislocation creep as stresses and strain rates are lowered to approach those of natural deformation (*Stocker and Ashby*, 1973), Goetze's experiments do not preclude magmatic pressure solution as a dominant flow mechanism of naturally deformed harzburgite (*Goetze*, 1977). At the very least, grain-boundary-diffusion creep by magmatic pressure solution should be expected to dominate to larger grain sizes than predicted by *Stocker and Ashby* (1973) for subsolidus grain-boundary-diffusion creep.

Partial melt along grain boundaries of crystalline silicates will affect the process of grain-boundary migration, but in what way is dependent on several factors. In partially fused alloys and ceramics, one important factor is the distribution of the melt: if melt is distributed along grain boundaries as small spherical droplets (as one would expect for melts whose interfacial energy against the solid phase is greater than half the interfacial energy of the solid-solid grain boundary; see *Kingery et al.*, 1976, p. 290-314), the melt droplets act as any dispersed particles along grain boundaries would, to inhibit grain-boundary migration (*Burke*, 1959; *Gleiter and Chalmers*, 1972, p. 143-146).

If melt "wets" the grain boundary (as one would expect for melts whose interfacial energy against the solid phase is less than half the interfacial energy of the solid-solid grain boundary), the affect of melt on grain-boundary migration depends on other factors (*Burke*, 1959): During growth of one grain at the expense of its neighbor by migration of their common boundary, the radius of curvature of the face of the growing grain is negative (as viewed from inside that grain) and that of the shrinking grain is positive. The contribution that the large difference in radii of curvature of the two grains makes to the driving force for grain-boundary migration will be large (see *Cotterill and Mould*, 1976, p. 271-274; *Kingery et al.*, 1976, p. 452). A melt that coats the grain boundary will tend to round both grains, however, and will give both grains a positive radius of curvature. Thus, the driving force for grain-boundary migration will be reduced in the presence of a good "wetting" agent.

Grain growth in the presence of a grain-boundary fluid phase by *solution-precipitation* can be faster or slower than grain-boundary migration, again depending on several factors (*Burke*, 1959; *Gleiter and Chalmers*, 1972, p. 143-144; *Kingery et al.*, 1976, p. 407-413 and 498-501). For example, polycrystalline halite undergoes no grain growth at temperatures below several hundred degrees centigrade, but salt crystals in a cold-pressed aqueous slurry of sodium chloride do undergo grain growth. In contrast, grain-growth in partially fused, high-alumina ceramic is slower than in alumina ceramic that is sintered in the solid-state (*Barlett and Schwartzwalder*, 1949, cited in *Burke*, 1959, p. 115). *Vallon* (in *Lliboutry*, 1971, p. 16) reported that the size of ice crystals in a temperate alpine glacier was smaller (presumably because of lower growth rates), the higher the local water content. Lower rates of grain growth in the presence of grain-boundary melt are observed in systems that contain two solid phases than in the corresponding systems that contain just one of the two solid phases (*Gleiter and Chalmers*, 1972, p. 144). The above observations suggest that grain growth by solid-precipitation is controlled by the kinetics of dissolution and mass transport through the melt, of components from the solid phases. Since the problem of solution-precipitation is beyond the scope of this paper, I refer the reader to papers by *Rutter* (1976) and *Durney* (1976) for further discussion.

In the absence of pertinent experimental data on the kinetics of melting and melt-transfer in peridotites, I must rely on *Mercier and Nicolás's* (1975) interpretation of textures in ultramafic xenoliths. Mercier and Nicolás inferred that ultramafic xenoliths that have protogranular texture (large grain size, unstrained or nearly unstrained minerals, and olivine grains having gently curved boundaries) recrystallized in the presence of melt. Thus, I conclude that partial fusion of peridotites can promote grain growth through solution-precipitation.

Imposing a deviatoric stress on a partially fused peridotite will alter the distribution of grain-boundary melt, through mechanical and thermodynamic effects, and may thereby control preferred directions of grain growth. The hydrostatic pressure of the melt P_m can never exceed the least principal compressive stress σ_3 on the rock by more than the tensile strength of the rock; otherwise, the melt will escape from the rock by "magmafracting" (analagous to hydrofracting; *Yoder*, 1976)[13]. Thus P_m will be less than σ_1, and the melt will tend to be squeezed from grain boundaries normal to σ_1 to grain boundaries normal to σ_3 (Fig. 12; for examples see *Ode*, 1957; *Nye*, 1967; or *Durney*, 1976).

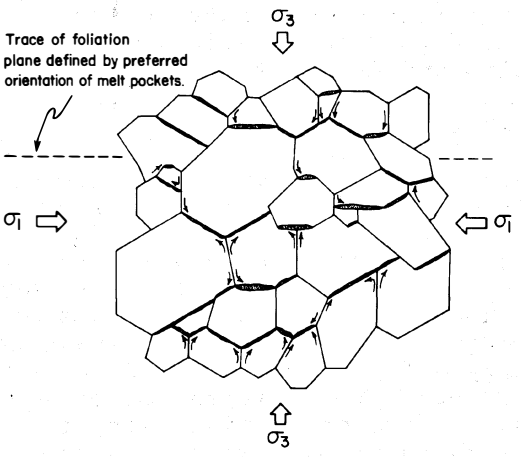

Fig. 12. Migration of partial melt in an idealized stressed polycrystal. Other factors being equal, melt (shaded regions) is forced from grain boundaries at high angles to maximum principal compressive stress σ_1. Foliation defined by melt pockets parallels σ_1, in contrast to "solid-state" foliation (defined by flattened or sheared porphyroclasts or tabular neoblasts that remain crystalline during deformation), which typically lies at high angles to σ_1.

Thermodynamical effects will complicate the picture. The slope of the peridotite solidus in temperature-pressure space is positive for melting that produces water-undersaturated melts ("dry" melting) and is negative for water-saturated melts ("wet" melting; see *Yoder*, 1976, p. 4-20). Interfaces normal to σ_1 will be at a slightly higher pressure than those normal to σ_3. During "dry" melting, grain boundaries normal to σ_3 should have a slightly lower melting temperature than those normal to σ_1. Thus, during "dry" syntectonic melting, grain boundaries normal to σ_3 should melt preferentially over those normal to σ_1, and one might therefore expect "dry" grain boundary melts to be preferentially aligned in grain boundaries normal to σ_3 (i.e., in the same orientation as expected from mechanical considerations).

During "wet" melting, however, grain boundaries normal to σ_1 should have a slightly lower melting temperature than those normal to σ_3. Thus during "wet" syntectonic melting, grain boundaries normal to σ_1 should melt preferentially over those normal to σ_3. If the kinetics of transfer of melt are slow relative to the rate of melting, one would expect grain-boundary melts to be preferentially aligned in grain

[13] See *Nye and Mae* (1972) for an example of the similar problem of relating the mean stress in temperate ice to the pressure on intergranular water.

boundaries normal to σ_1 (i.e., perpendicular to the orientation expected from mechanical considerations). Indeed, experiments on stressed ice (for which dT_m/dP is also negative) at its melting temperature show that "lenses" of water are preferentially aligned normal to σ_1 (*Nye and Mae*, 1972). On the other hand, if the deviatoric stress forces the melt to migrate quickly from sites of formation (faces normal to σ_1) to faces normal to σ_3, rapid dissolution along faces normal to σ_1 and rapid precipitation of melt onto faces normal to σ_3 could quickly cause grains to become elongate parallel to σ_3 during "wet" syntectonic partial fusion. In that case, one would expect phases that contribute disproportionately more to the melt (i.e., clinopyroxene and orthopyroxene for tholeiitic melts) to become more elongate than relatively refractory phases (typically olivine in tholeiitic melts).

Conclusions

In a field area containing both pyrometamorphic and deformation textures, there are only three ways in principle to demonstrate that pyrometamorphism was syntectonic: 1) accurate determination of the equivalence of the absolute ages of melting and deformation; 2) demonstration that the stress field that caused the deformation also caused preferred orientation of former partial melt and indigenous dikes; and 3) identification of deformation textures unique to pyrometamorphic deformation. The first approach is generally impracticable, in view of the uncertainties introduced by the post-deformational thermal history.

The second approach, the subject of the paper by *Boudier and Nicolás* (this volume) and discussed in the previous section of this paper, is currently the only practicable approach. However, its usefulness will generally be limited to rocks in which large percentages of melt have been trapped. In such rocks, interfacial energy effects could not have overwhelmed the expected mechanical control of preferred orientation of melt pockets. In addition, the greater the percentage of partial melt, the more likely the melt was undersaturated with respect to water. Since the slope of the melting curve of water-undersaturated melts in P-T space is positive, the thermodynamically favored sites for melting (grain boundaries normal to σ_3) will be in harmony with the mechanically favored sites for collection of melt (planes normal to σ_3).

The focus of this final section is the third approach, based solely on the textures of residual (non-melted) phases. Because of the paucity of experimental data or pertinent observations on natural peridotites, the discussion of deformation mechanisms and melting in the previous sections is the basis for my speculations on textures expected from pyrometamorphic deformation:

1) The edges of clinopyroxene grains in some peridotite xenoliths have a spongy appearance that *Kleeman et al.* (1969) and *Pike and Schwarzman* (1977) attributed to corrosion during partial melting. If partial fusion occurred while the rock was stressed, one might expect to find a preferred orientation of the spongy borders of residual clinopyroxene.

2) A grain-boundary melt that coats most grain boundaries will "insulate" most grain boundaries from deviatoric stresses that are any greater than those the melt itself can support. Deviatoric stresses will be concentrated along the remaining grain boundaries at point-to-point contacts where no melt is present. Thus, for a given deviatoric stress on the entire aggregate, one should expect a greater chance of local stress

concentrations in a partially fused polycrystalline aggregate (in which the melt coats boundaries) than in a subsolidus polycrystalline aggregate. Since local stress concentrations will produce local strain concentrations, one should expect that recrystallization will occur at lower values of *total* strain of the rock (although at the same value of local strain) in a hypersolidus rock than in a subsolidus rock. In addition, the tendency for recrystallization to occur at grain boundaries rather than in the interior of grains should be enhanced.

3) For a given amount of total strain, a hypersolidus peridotite will appear "less deformed" than a subsolidus peridotite. For example, *George* (1975, 1977) found that harzburgite tectonite with trapped interstitial melt from the Troodos ophiolite has weak preferred orientations of olivine crystallographic axes and appears almost undeformed in thin section, even in specimens that display a pronounced foliation defined by flattened orthopyroxene and spinel grains. The "deformation" or flow of interstitial melt is not recorded by the products of post-tectonic crystallization of the melt. Thus, if the melt accommodated much of the strain during "crystal mush flow", the now-solid rock preserves little textural evidence of its strain history.

4) Since magmatic pressure solution and precipitation is merely another type of diffusion creep, it will produce textures analogous to pressure shadows in deformed quartzites (*Elliott*, 1973) or grain-boundary denuded zones in metals (*Gittus*, 1975, p. 27-28). One should expect the presence of pressure shadows at the long ends of grains in any strongly foliated peridotite whose grains bear little evidence of dislocation-creep deformation textures. Pressure shadows in olivine would probably be subtle features, since metamorphic olivine is rarely zoned compositionally and is relatively free of inclusions of other phases. However, pressure shadows in the pyroxenes should be more obvious for two reasons: a) the pyroxenes tend to be compositionally inhomogeneous and to contain more inclusions (witness the "clouded" appearance of the pyroxenes as observed in thin section in plane polarized light, compared to olivine); and b) the peritectic composition in the OL-EN-DI system is decidedly more pyroxene-rich than the bulk composition of the typical alpine-type harzburgite or lherzolite (*Yoder*, 1976, Chapters 2 and 4), and so the pyroxenes (especially clinopyroxene) contribute disproportionately more to melting (and therefore to reprecipitation) than does olivine.

Acknowledgments

Critical reviews of an earlier draft of this paper by John Christie, Tom Foster, and Rick Stocker materially improved my understanding of deformation and metamorphism. I wish to thank them and also Jan Tullis, Steve Kirby, and Steve Ehrenberg for their general comments, which made me better appreciate the different perspectives of students of structural petrology. I am grateful to Henry Dick for stimulating discussions on partial fusion, and to Chris Goetze for comments and information on specific topics in this paper. My participation in the Chapman Conference was supported by the U.S. Geological Survey project, "Fabrics of Deformed Ultramafic Rocks" (project number 9940-01487) awarded to Dale Jackson. The research for this paper was supported by N.S.F. Grant DES 7502905.

References

Ashby, M.F., A first report on deformation-mechanism maps, *Acta Metal.*, *20*, 887-897, 1972.

Ashby, M.F., and R.A. Verrall, Diffusion-accommodated flow and superplasticity, *Acta Metal.*, *21*, 149-163, 1973.

Ashby, M.F., and R.A. Verrall, Micromechanisms of flow and fracture, and their relevance to the rheology of the upper mantle, *Univ. of Cambridge, Dept. of Engin. Mat/TR30*, 66 p., 1977.

Avé Lallemant, H.G., Structural and petrofabric analysis of an "Alpine-type" peridotite: the lherzolite of the French Pyrenees, *Leidse Geol. Med.*, *42*, 1-57, 1967.

Avé Lallemant, H.G., Mechanisms of preferred orientations of olivine in tectonite peridotite, *Geology*, *3*, 653-656, 1975.

Avé Lallemant, H.G., Experimental deformation of clinopyroxene (abstr.), *Trans. Amer. Geophys. Union*, *58*, 513, 1977.

Avé Lallemant, H.G., and N.L. Carter, Syntectonic recrystallization of olivine and modes of flow in the upper mantle, *Geol. Soc. Amer. Bull.*, *81*, 2203-2220, 1970.

Bailey, J.E., Electron microscope observations on recovery and recrystallization processes in cold-worked metals, in *Electron Microscopy and Strength of Crystals: Proceedings of the First Berkeley Internat. Mater. Confer., July 5-8, 1961*, edited by G. Thomas and J. Washburn, Interscience Publ., John Wiley and Sons, New York, 535-574, 1962.

Ball, A., and M.M. Hutchinson, Superplasticity in the aluminum-zinc eutectoid, *Metal. Sci. Journ.*, *3*, 1-7, 1969.

Barlett, H., and K. Schwartzwalder, Trends in the constitution of spark plug insulators, *Bull. Amer. Ceram. Soc.*, *28*, 462, 1949.

Barrer, R.M., *Diffusion In and Through Solids*, Cambridge University Press, 1951.

Barrett, C.S., and T.B. Massalski, *Structure of Metals: Crystallographic Methods, Principles, and Data*, McGraw-Hill, New York, 654 p., 1966.

Barrett, C.R., and W.D. Nix, A model for steady state creep based on the motion of jogged screw dislocations, *Acta Metal.*, *13*, 1247-1258, 1965.

Beck, P.A., and P.R. Sperry, Strain induced grain boundary migration in high purity aluminum, *Journ. App. Phys.*, *21*, 150-152, 1950.

Bishop, J.F.W., A theory of the tensile and compressive textures of face centered cubic metals, *Journ. Mech. Physics of Solids*, *3*, 130-142, 1954.

Boudier, F., and A. Nicolás, Structural controls on partial melting in the Lanzo peridotites, *this volume*, 1977.

Boullier, A.M., and Y. Gueguen, S.P. mylonites: origin of some mylonites by superplastic flow, *Contrib. Mineral. Petrol., 50*, 93-104, 1975.

Brace, W.F., W.C. Luth, and J.D. Unger, Melting of granite under an effective confining pressure (abstr.), *Geol. Soc. Amer. Spec. Pap. 115*, 21, 1968.

Brothers, R.N., and K.A. Rodgers, Petrofabric studies of ultramafic nodules from Auckland, New Zealand, *J. Geol., 77*, 452-465, 1969.

Burke, J.E., Grain growth in ceramics, in *Kinetics of High Temperature Processes*, edited by W.D. Kingery, Technology Press of Massachusetts Inst. Tech. and John Wiley & Sons, N.Y., 109-116, 1959.

Byrne, J.G., *Recovery, Recrystallization, and Grain Growth*, Macmillian Company, New York, 179 p., 1965.

Calnan, E.A., and C.G.B. Clews, Deformation textures in face-centered cubic metals, *Philos. Mag., 41*, 1085-1100, 1950.

Cannon, W.R., The contribution of grain-boundary sliding to axial strain during diffusion creep, *Phil. Mag., 25*, 1489-1497, 1972.

Carter, N.L., Static deformation of silica and silicates, *Jour. Geophys. Res., 76*, 5514-5540, 1971.

Carter, N.L., Steady state flow of rocks, *Rev. Geophys. Space Phys., 14*, 301-360, 1976.

Carter, N.L., and H.G. Avé Lallemant, High temperature flow of dunite and peridotite, *Geol. Soc. Amer. Bull., 81*, 2181-2202, 1970.

Carter, N.L., D.W. Baker, and R.P. George, Jr., Seismic anistropy, flow, and constitution of the upper mantle, in *Flow and Fracture of Rocks*, edited by H.C. Heard, I.Y. Borg, N.L. Carter, and C.B. Raleigh, Amer. Geophys. Union, Geophys. Monogr. Series, 16, 167-190, 1972.

Carter, N.L., J.M. Christie, and D.T. Griggs, Experimental deformation and recrystallization of quartz, *Jour. Geol., 72*, 687-733, 1964.

Carter, N.L., and C.B. Raleigh, Principal stress directions from plastic flow in crystals, *Geol. Soc. Amer. Bull., 80*, 1231-1264, 1969.

Christie, J.M., and A.J. Ardell, Substructures of deformation lamellae in quartz, *Geology, 2*, 405-408, 1974.

Collée, A.L.G., A fabric study of lherzolites with special reference to ultrabasic nodular inclusions in the lavas of Auvergne (France), *Leidse Geol. Med., 28*, 1-102, 1962.

Cotterill, P., and P.R. Mould, *Recrystallization and Grain Growth in Metals*, John Wiley & Sons, New York, 409 p., 1976.

Cottrell, A.H., *Dislocations and Plastic Flow in Crystals*, Oxford Univ. Press, Amen House, London, 223 p., 1953.

Cottrell, A.H., *The Mechanical Properties of Matter*, John Wiley & Sons, New York, 430 p., 1964.

Crossland, I.G., and J.C. Wood, Microstructural observations on specimens deformed by diffusion creep, *Philos. Mag., 31*, 1415-1419, 1975.

Dollinger, G.L., The development of preferred orientation in experimentally deformed synthetic dunite (abstr.), *Trans. Amer. Geophys. Union, 54*, 452, 1973.

Durney, D.W., Pressure-solution and crystallization deformation, *Philos. Trans. Royal Soc. London, A283*, 229-240, 1976.

Edington, J.W., K.N. Melton, and C.P. Cutler, Superplasticity, in *Prog. in Mater. Sci., 21*, edited by B. Chalmers, J.W. Christian, and T.B. Massalski, Pergamon Press, Oxford, 61-170, 1976.

Elliott, D., Diffusion flow laws in metamorphic rocks, *Geol. Soc. Amer. Bull., 84*, 2645-2664, 1973.

Etheridge, M.A., Deformation and recrystallization of orthopyroxene from the Giles complex, central Australia, *Tectonophys., 25*, 85-114, 1975.

Etheridge, M.A , and S.H. Kirby, Experimental deformation of rock-forming pyroxenes: recrystallization mechanisms and preferred orientation development (abstr.), *Trans. Amer. Geophys. Union, 58*, 513, 1977.

Gates, R.S., The effects of creep strain on grain boundary sliding during diffusion creep, *Philos. Mag., 31*, 367-385, 1975.

George, R.P., Jr., The internal structure of the Troodos ultramafic complex Cyprus, *Ph.D. Thesis, State Univ. of New York, Stony Brook*, 223 p., 1975.

George, R.P., Jr., Structural petrology of the Olympus ultramafic complex in the Troodos ophiolite, Cyprus, *Geol. Soc. Amer. Bull.*, in press, 1977.

Gittus, J., *Creep, Viscoelasticity and Creep Fracture in Solids*, John Wiley and Sons, New York-Toronto, 725 p., 1975.

Gleiter, H., and B. Chalmers, High-angle grain boundaries, in *Progress in Mater. Sci., 16*, edited by B. Chalmers, J.W. Christian, and T.B. Massalski, 1-272, 1972.

Glover, G., and C.M. Sellars, Recovery and recrystallization during high temperature deformation of α-iron, *Metal. Trans., 4*, 765-775, 1973.

Goetze, C., A brief summary of our present day understanding of the effect of volatiles and partial melt on the mechanical properties of the upper mantle, in *High-Pressure Research*, edited by M.H. Manghani and S.-I. Akimoto, Academic Press, Inc., New York, 3-23, 1977.

Goetze, C., and D.L. Kohlstedt, Laboratory study of dislocation climb and diffusion in olivine, *Journ. Geophys. Research, 78*, 5961-5971, 1973.

Green, H.W., D.T. Griggs, and J.M. Christie, Syntectonic and annealing recrystallization of fine-grained quartz aggregates, in *Experimental and Natural Rock Deformation*, edited by P. Paulitsch, Springer-Verlag, Berlin, 272-335, 1970.

Green, H.W., II, and S.V. Radcliffe, Deformation processes in the upper mantle, in *Flow and Fracture of Rocks*, edited by H.C. Heard, I.Y. Borg, N.L. Carter, and C.B. Raleigh, American Geophys. Union Monograph Series, v. 16, 139-156, 1972.

Gueguen, Y., and A.M. Boullier, Evidence of superplasticity in mantle peridotites, in *Physics and Chemistry of Minerals and Rocks*, edited by R.G.J. Strens, John Wiley and Sons, New York, 19-33, 1975.

Harte, B., Rock nomenclature with particular relation to deformation and recrystallization textures in olivine-bearing xenoliths, *Journ. Geol., 85*, 279-288, 1977.

Hofman, A.W., and M. Magaritz, Range of chemical equilibrium in partially molten rocks, this volume, 1977.

Hu, H., Recrystallization by subgrain coalescence, in *Electron Microscopy and Strength of Crystals: Proceedings of the First Berkeley Internat. Mater. Confer., July 5-8, 1961*, edited by G. Thomas and J. Washburn, Interscience Publ., John Wiley and Sons, New York, 564-574, 1962.

Kelly, A., and G.W. Groves, *Crystallography and Crystal Defects*, Addison-Wesley Publ. Co., Reading, Massachusetts, 428 p., 1970.

Kingery, W.D., H.K. Bowen, and D.R. Uhlmann, *Introduction to Ceramics: 2nd Edition*, John Wiley and Sons, New York, 1032 p., 1976.

Kirby, S.H., and C.B. Raleigh, Mechanisms of high-temperature, solid-state flow in minerals and ceramics and their bearing on the creep behavior of the mantle, *Tectonophys., 19*, 165-194, 1973.

Kleeman, J.D., D.H. Green, and J.F. Lovering, Uranium distribution in ultramafic inclusions from Victorian basalts, *Earth Planet. Sci. Letters, 15*, 449-458, 1969.

Kohlstedt, D.L., and C. Goetze, Low-stress high-temperature creep in olivine single crystals, *Journ. Geophys. Research, 79*, 2045-2051, 1974.

Kohlstedt, D.L., C. Goetze, and W.B. Durham, Experimental deformation of single crystal olivine, in *The Physics and Chemistry of Minerals and Rocks*, edited by R.G.J. Strens, J. Wiley and Sons, 35-49, 1976.

Kushiro, I., H.S. Yoder, Jr., and B.O. Mysen, Viscosity of basaltic and andesitic liquids at high pressures, *Carnegie Inst. Washington Yearbook 75*, 614-618, 1976.

Lally, J.S., J.M. Christie, G.L. Nord, Jr., and A.H. Heuer, Deformation, recovery, and recrystallization of lunar dunite 72417, *Proc. Lunar Sci. Conf. 7th*, 1845-1863, 1976.

Li, J.C.M., Possibility of subgrain rotation during recrystallization, *Journ. App. Phys., 33*, 2958-2965, 1962.

Lifshitz, I.M., On the theory of diffusion -- Viscous flow of polycrystalline bodies, *Soviet Physics, JETP, 17*, 909-920, 1963.

Lliboutry, L., Permeability, brine content and temperature of temperate ice, *Journ. Glaciol.*, *10*, 15-29, 1971.

Luton, M.J., and C.M. Sellars, Dynamic recrystallization in nickel and nickel-iron alloys during high temperature deformation, *Acta Metal.*, *17*, 1033-1043, 1969.

McLean, D., *Mechanical Properties of Metals*, John Wiley and Sons, Inc., New York, 403 p., 1962.

Mehnert, K.R., W. Busch, and G. Schneider, Initial melting at grain boundaries of quartz and feldspar in gneisses and granulites, *Neues Jahrb. Mineral. Monatsh.*, 165-183, 1973.

Mercier, J.-C., D.A. Anderson, and N.L. Carter, Stress in the lithosphere: inferences from steady state flow of rocks, *Pure and Applied Geophys.*, *115*, 199-226, 1977.

Mercier, J.-C.C., and A. Nicolás, Textures and fabrics of upper-mantle peridotites as illustrated by xenoliths from basalts, *Journ. Petrol.*, *16*, 454-487, 1975.

Mitra, S.K., and D. McLean, Work hardening and recovery in creep, *Proc. Royal Soc. London*, *A295*, 288-299, 1966.

Mitra, S.K., and D. McLean, Cold work and recovery in creep at ostensibly constant structure, *Metal Science Journ.*, *1*, 192-198, 1967.

Nicolás, A., Flow in upper mantle rocks: some geophysical and geodynamical consequences, *Tectonophys.*, *32*, 93-106, 1976.

Nicolás, A., F. Boudier, and A.M. Boullier, Mechanisms of flow in naturally and experimentally deformed peridotites, *Am. J. Sci.*, *273*, 853-876, 1973.

Nicolás, A., and J.P. Poirier, *Crystalline Plasticity and Solid State Flow in Metamorphic Rocks*, John Wiley and Sons, London, 444 p., 1976.

Nye, J.F., Theory of regelation, *Philos. Mag.*, *16*, 1249-1266, 1967.

Nye, J.F., and S. Mae, The effect of non-hydrostatic stress on intergranular water veins and lenses in ice, *Journ. Glaciol.*, *11*, 81-101, 1972.

Odé, H., Mechanical analysis of the dike pattern of the Spanish Peaks area, Colorado, *Geol. Soc. Amer. Bull.*, *68*, 567-575, 1957.

Phakey, P., G. Dollinger, and J. Christie, Transmission electron microscopy of experimentally deformed olivine crystals, in *Flow and Fracture of Rocks*, edited by H.C. Heard, I.Y. Borg, N.L. Carter, and C.B. Raleigh, Amer. Geophys. Union, Geophys. Mongr. Series, 16, 117-138, 1972.

Pike, J.E. Nielson, and E.C. Schwarzman, Classification of textures in ultramafic xenoliths, *Journ. Geol.*, *85*, 49-61, 1977.

Poirier, J.P., and A. Nicolás, Deformation-induced recrystallization by progressive misorientation of sub-grain boundaries, with special reference to mantle peridotites, *Journ. Geol.*, *83*, 707-720, 1975.

Post, R.L., Jr., The flow laws of Mt. Burnett dunite, *Ph.D. Thesis, Univ. of Calif., Los Angeles*, 272 p., 1973.

Post, R.L., Jr., High temperature creep of Mt. Burnet dunite, *Tectonophys.*, 1977.

Ragan, D.M., Olivine recrystallization textures, *Mineral. Mag., 37*, 238-240, 1969.

Raleigh, C.B., Fabrics of naturally and experimentally deformed olivine, *Ph.D. Dissertation, Univ. Cal. Los Angeles*, 215 p., 1963.

Raleigh, C.B., and S.H. Kirby, Creep in the upper mantle, *Miner. Soc. Am. Spec. Pap. 3*, 113-121, 1970.

Raleigh, C.B., S.H. Kirby, N.L. Carter, and H.G. Avé Lallemant, Slip and the clinoenstatite transformation as competing rate processes in enstatite, *Journ. Geophys. Res., 76*, 4011-4022, 1971.

Read, W.T., *Dislocations in Crystals*, McGraw-Hill, New York, 228 p., 1953.

Ross, J.V., Experimental deformation of enstatite, in preparation, 1977.

Ross, J.V., H.G. Avé Lallemant, and N.L. Carter, Neoblast and subgrain sizes in experimentally deformed olivine (abstr.), *Trans. Amer. Geophys. Union, 58*, 512-513, 1977.

Rutter, E.H., The kinetics of rock deformation by pressure solution, *Philos. Royal Soc. London, A283*, 203-219, 1976.

Sammis, C.G., and J.L. Dein, On the possibility of transformational superplasticity in the earth's mantle, *Jour. Geophys. Res., 79*, 2961-2965, 1974.

Schmid, E., and W. Boas, *Plasticity of Crystals*, F.A. Hughes, London, 353 p., 1950.

Schmid, S.M., J.M. Boland, and M.S. Paterson, Superplastic flow in fine grained limestone, in press, 1977.

Squires, R.L., R.T. Weiner, and M. Phillips, Grain boundary denuded zones in a magnesium, 1/2 wt. % zirconium alloy, *Journ. Nucl. Mat., 8*, 77-80, 1953.

Stevens, R.N., Grain-boundary sliding and diffusion creep in polycrystalline solids, *Philos. Mag., 23*, 265-283, 1971.

Stocker, R.L., and M.F. Ashby, On the rheology of the upper mantle, *Rev. Geophys. Space Phys., 11*, 391-426, 1973.

Thayer, T.P., and E.D. Jackson, A classification of igneous rocks by their history of crystallization and emplacement, *U.S. Geol. Surv. Prof. Paper 800-B*, B79-B83, 1972.

Tullis, J.A., Preferred orientations in experimentally deformed quartzites, *Ph.D. Thesis, Univ. California, Los Angeles*, 342 p., 1971.

Tullis, T.E., Experimental development of preferred orientation of mica during recrystallization, *Ph.D. Thesis, Univ. California, Los Angeles*, 262 p., 1971.

Twiss, R.J., Structural superplastic creep and linear viscosity in the earth's mantle, *Earth and Planet. Sci. Letters, 33*, 86-100, 1976.

Twiss, R.J., Theory and applicability of a recrystallized grain size paleopiezometer, *Pure and Appl. Geophys., 115*, 227-244, 1977.

Weertman, J., Dislocation climb theory of steady-state creep, *Trans. Amer. Soc. Metal., 61*, 681-694, 1968.

Weertman, J., and J.R. Weertman, *Elementary Dislocation Theory*, Macmillan Company, Collier-Macmillan Limited, London, 213 p., 1964.

White, S., The effects of strain on the microstructures, fabrics, and deformation mechanisms in quartzites, *Phil. Trans. Royal Soc. London, A283*, 69-86, 1976.

Yoder, H.S., Jr., *Generation of Basaltic Magma*, National Academy of Sciences, Printing and Publishing Offices, Washington, D.C. 20418, 1976.

Zeuch, D.H., and H.W. Green, II, Syntectonically recrystallized grain size and dislocation density in olivine (abstr.), *Trans. Amer. Geophys. Union, 58*, 513, 1977.

A MODEL FOR PARTIAL MELTING OF UPPER MANTLE ROCKS BY LOCAL INSTABILITY AND ITS CYCLICAL STRESS-RELIEF

H. Koide
Brooklyn College of the City University of New York
Brooklyn, New York 11210

S. Bhattacharji*
Department of Geological and Geophysical Sciences
Princeton University
Princeton, New Jersey 08540

Abstract

Deep and intermediate earthquakes indicate mechanical instability of the upper mantle rocks. Velocity anisotropy of elastic wave propagation also suggests that mantle rocks can sustain differential stress and stress gradients at least over a short time interval. Release of those stresses due to sudden reduction of rigidity, volume expansion due to local inhomogeneity, and lowering of rigidity due to dehydration of hydrous minerals or phase transformations can induce onset of partial melting of upper mantle materials.

The estimation of stress around inhomogeneities or pockets of pressurized fluid of various aspect ratios indicates that a thin, lenticular or spheroidal inhomogeneity induces the greatest pressure reduction around its tips. The maximum thermo-mechanical stress (σ_{max}) due to phase transformation around such inhomogeneities or pockets of pressurized fluids is obtained by:

$$\sigma_{max} = 1/2(\sigma_t + \sqrt{\sigma_t^2 + b^2\tau^2}) + \sigma_L,$$

where stress release (σ_t) by volume expansion ($\Delta\nabla'$) due to phase transformation is $\sigma_t = 8/D[1-\nu(G'/G)k'\Delta\nabla']$, ν and G are Poisson's ratio and rigidity of mantle, K' and G' are bulk modulus and rigidity of inhomogeneity or inclusion, D and b are coefficients, σ_L is the lithostatic stress, τ is the shearing stress across the plane of inhomogeneity or inclusion at infinity.

A model for development and propagation of physical inhomogeneities (fractures or flaws) in the upper mantle, and possible onset of partial melting and its transport by cyclical stress release is postulated. Theoretical equations and examples are presented to show that phase transformations of stable and metastable phases in areas of tectonic instability and upper mantle thermal anomalies can produce rapid volume change and reduction of rigidity in upper mantle rocks. Such changes can propagate further physical inhomogeneities, pockets of partial melt and volatiles, and create conditions for rapid or explosive emplacement of volatile-rich magmas and diatremes.

* Present address: Brooklyn College of the City University of New York, Brooklyn, New York 11210

INTRODUCTION

Active ridge-rift systems, intraplate hot spots, tectonically active regions such as island arcs and subduction zones are areas of magma generation by partial melting of the upper mantle, magmatic uprise or diapirism and volcanicity. The presence of volatiles like CO_2, H_2O, etc., has been thought to play an important role in melting processes, segregation and emplacement of magmas from the upper mantle in subduction zones (*Lambert and Wyllie*, 1968; *Kushiro*, 1968; *Wyllie*, 1971a; *Eggler*, 1975). Various petrological, geochemical and geophysical models for equilibrium and disequilibrium melting of upper mantle crystalline materials, role of fluids and magma generation processes are excellently reviewed by *Wyllie* (1971b) and *Yoder* (1976b).

Recently the presence of interstitial fluids (such as CO_2 and H_2O) has also been attributed to the physical characteristics of the low-velocity zone, which represents the inhomogeneous nature of the mantle (*Anderson*, 1962; *Wyllie*, 1971a; *Brey and Green*, 1976; *Eggler*, 1976). Physical and chemical inhomogeneities of varying magnitudes in the upper mantle have been established from geophysical (*Bullen*, 1947; *Anderson*, 1962), geochemical and isotopic studies (*Hart et al.*, 1970; *Hart*, 1976; *O'Nions and Pankhurst*, 1974; *Schilling*, 1975; *Sun and Hanson*, 1975; and others). 1975; *Sun and Hanson*, 1975; etc.).

Upper mantle rocks commonly show various degrees of fracturing. In Griffith's theory (1925) of fracture propagation, fractures, cracks or flaws are physical inhomogeneities or inclusions in a rock. *Griggs and Handin* (1960) suggested that after such homogeneities exist, release of stress (i.e., stored elastic energy) from the flaw or crack can propagate additional cracks, and shear melting can generate deep-seated earthquakes. *Griggs and Baker* (1969) expanded this concept and considered the energy required to melt a mass from a propagating crack.

The stress relief hypothesis and generation of magma by partial melting of the upper mantle were considered by *Yoder* (1952), *Uffen* (1959), *Uffen and Jessop* (1963), and elaborated by *Yoder* (1976a; 1976b).

Bott (1965) and *Roberts* (1970) emphasized that to produce an appreciable amount of partial melting requires large stress differences which cannot normally be maintained if large plastic creep occurs in the upper mantle. However, as deformation by plastic creep is generally a slow process (*Carter and Avé Lallemant*, 1970), high elastic stress can be maintained over a short time period. Mantle material can deform elastically if there is expansion by volume change or if there is loss of rigidity due to phase transformation. Under such conditions large stress differences can be maintained, at least locally, for a time duration sufficient for formation and rapid propagation of fractures or inhomogeneities with generation of earthquakes and local melting spots (*Koide*, 1974; *Koide and Bhattacharji*, 1974).

In this paper we will present briefly the theoretical basis and a few examples of phase transformations of stable and metastable phases which may trigger mechanical instability in the upper mantle. We will show that the magnitude of stress release by rapid phase transformations and nucleation and concentration of stress around mantle inhomogeneities have the potential to produce deep-seated fractures, deep-focus earthquakes, the onset of melting and propagation of fluids through grain boundaries and existing anisotropies.

STRESS RELEASE BY RAPID VOLUME CHANGE RELATED TO PHASE TRANSFORMATION

Many types of phase transformation can occur in the mantle. Due to the relative motion of the lithospheric plate and the mantle, materials cross phase stability boundaries. They may not, however, transform continuously at the equilibrium depth. Nucleation of the new phase originates in relatively small areas at appreciable deviation from equilibrium (*Vaisnys and Pilbeam*, 1976). As the phase transformation is generally accompanied by a large volume change, differential volume change causes stress disturbance along the boundary between the phase-transformed portion and the nearby unchanged mantle material (Fig. 1). The phase-transformed portion may consist of an inhomogeneous region, an inclusion, flaws or fractures of different mechanical properties from the surrounding mantle material, or a phase with physical properties (such as shearing strength) different from the surrounding mantle material.

In addition to the volume of the phase-transformed region, its shape has a significant effect on the stress disturbance and mechanical characteristics around it (*Koide*, 1974; *Koide and Bhattacharji*, 1975a). However, the stress distribution of the inhomogeneous region or inclusion can be adequately estimated if the inclusion is assumed to be of the shape of a spheroid of various aspect ratios.

The exact analytical solution for statistical stress distribution in and around a spheroidal inclusion embedded in an infinite homogeneous elastic body has been obtained by *Edwards* (1951). *Koide* (1970, 1972), *Bhattacharji and Koide* (1974), and *Koide and Bhattacharji* (1975a) have developed the solution into forms more convenient for calculation of stress and have applied the solution to study the development of various fracture patterns and to fracture propagation around diapir intrusions in the elastic lithospheric plate.

The complete equation for stress distribution around a phase transformed inclusion or inhomogeneity is highly complex (*Koide*, 1970); an approximate value of maximum stress at the tip can be determined from the equation given by *Koide* (1976). Stress (σ_T) at the tip of an inhomogeneous spot or inclusion which acts on the mantle host in a transverse direction is obtained from the equation:

$$\sigma_T = \frac{8}{D}\left(1 - \nu\frac{G'}{G}\right)K'\Delta\nabla' + \sigma_L \qquad (1)$$

$$\text{the coefficient } D = \frac{2\pi}{S} + \frac{4(1-\nu)K'}{G} + 16\,(1-\nu)\frac{G'}{G} \qquad (2)$$

where S is the aspect ratio of the inhomogeneity, G and ν are respectively rigidity and Poisson's ratio of the mantle, K' and G' are bulk modulus and rigidity of the inhomogeneity after phase transformation, $\Delta\nabla'$ is relative volume change of the inhomogeneity by the phase transformation, and σ_L is lithostatic stress (*Koide*, 1970, 1976). The first term of equation (1) expresses the magnitude of stress release ($\sigma_t = \sigma_T - \sigma_L$). The stress release ($\sigma_t$) occurs by volume expansion due to phase transformation in a transverse direction.

In the case of an extremely thin lenticular or oblate shaped inhomogeneity, the first term of equation (2) becomes negligible, because the aspect ratio (S) is very large. Thus, as the shape effect (determined by aspect ratio) becomes negligible, the coefficient D becomes almost constant.

For an inhomogeneity of very small aspect ratio, the transverse stress (σ_T) of equation (1) can be expressed as:

$$\sigma_T = \frac{2(G-\nu\, G')}{(1-\nu).\ (K' + 4G'/3)} .\ K'\ \Delta\nabla' + \sigma_L \qquad (3)$$

The maximum value of stress release ($\sigma_t = \sigma_T - \sigma_L$) by volume change due to phase transformation of a large, narrow inhomogeneous zone of the mantle can also be estimated by equation (3).

In many cases, the elastic constants of the phase-transformed materials or inclusion are not known. The elastic constant of the phase-transformed inclusion or zone is commonly assumed to be almost equal to the surrounding mantle material (Case I in Table 1). Thus when G' = G in equation (3),

$$\sigma_T = \frac{2\ (1 + \nu)}{3\ (1 - \nu)} .\ G\ \Delta\nabla' + \sigma_L \qquad (4)$$

Stress distribution at the tip of a thin lenticular or spheroidal melted rock zone or inclusion can be calculated by using the same solutions.

Another possible case is a phase transformation in which the inclusion is fluid after transformation (G'=0) (Case II in Table 1). The equation (3), for such a case, can be expressed as:

$$\sigma_T = \frac{2G}{1-\nu}\ \Delta\nabla' + \sigma_L \qquad (5)$$

The stress induced by the volume change of the spheroidal inclusion or inhomogeneity due to phase transformation is obtained by the three dimensional theory of elasticity (*Koide*, 1970, 1972; *Koide and Bhattacharji*, 1975a).

An example of stress distribution around an inhomogeneous spot or inclusion of coesite surrounded by mantle material due to a volume expansion of 10 percent by a phase transformation of coesite→quartz under the compressive pressure of 36 kb (corresponding to a depth of about 120 km, Table 1) is shown in Fig. 2. *Smyth and Hatten* (1977) have recently identified inclusions of crystals of coesite in grospydite from the Robert Victor Kimberlite pipe, South Africa. The shape of the inhomogeneous spot or inclusion of coesite in the mantle is assumed to be a stretched oblate spheroid or lenticular protuberance of aspect ratio 1:100. The stress contours in such a case (Fig. 2) indicate the potential of a large stress release around the tip. The large volume expansion (Table 1) by phase transformation at or around the tip of the inclusion, therefore, can induce large tensile stress around it.

Although uniform isotropic compressive stress of about 36 kb due to overlying lithostatic load is expected at a depth of 120 km, a 10 percent volume expansion of a lenticular inclusion of aspect ratio 1:100 due to phase transformation theoretically has the potential to create a maximum absolute tensile stress as high as 20 kb.

No rock can sustain such high tensile stress, which would cause a large deviatoric stress (*Yoder*, 1976b). The tensile strength of the upper mantle is estimated to be about 0.5 kb by *Roberts* (1970). Any greater release of tensile stress by rapid phase transformation can potentially initiate tensile fracturing from the areas of highest stress concentration (Figs. 1 and 2) and partial melting by pressure release. However, if enthalpy of melting is low (such as ΔH = 135 cal/gm) at 0.5 kb, pressure release would not produce appreciable melting.

TABLE 1. The minimum volume expansion of a lenticular penny-shaped inclusion about which fractures or a melting spot can form in the pyrolite mantle.

DEPTH	PRESSURE	ELASTIC PROPERTIES OF THE MANTLE		THE MINIMUM VOLUME EXPANSION TO INDUCE TENSION (%)	
		Rigidity	Poisson's Ratio		
(Km)	(Kb)	G(Mb)		Case I	Case II
100	-31	0.642	0.266	4.2	1.8
200	-64	0.674	0.285	7.9	3.4
300	-98	0.756	0.286	10.8	4.6
400	-133	0.871	0.283	12.8	5.5

	FORMATION OF MELTING SPOT IN THE OCEANIC CONDITION					FORMATION OF MELTING SPOT IN THE SHIELD CONDITION				
DEPTH	TEMP.	MELTING PRESS.	REQUIRED STRESS RELEASE	THE MINIMUM VOLUME EXPANSION (%)		TEMP.	MELTING PRESS.	REQUIRED STRESS RELEASE	THE MINIMUM VOLUME EXPANSION (%)	
(Km)	(°C)	(Kb)	(Kb)	Case I	Case II	(°C)	(Kb)	(Kb)	Case I	Case II
100	1150	-4.5	26.5	3.6	1.5	860	--	--	--	--
200	1420	-23	42	5.2	2.2	1200	7.5	56.5	7.0	3.0
300	1570	-34	64	7.0	3.0	1420	23	75	8.3	3.5
400	1680	-44	89	8.6	3.7	1570	34	99	9.5	4.1

Case I: Elastic constants of inclusion are equal to those of the mantle.
Case II: The inclusion is fluid after transition.
The values for pressure, temperature and elastic moduli are after *Clark and Ringwood* (1964). The melting pressures of dry pyrolite are after *Ringwood* (1975).

Note: Compressional pressure is indicated with negative sign.

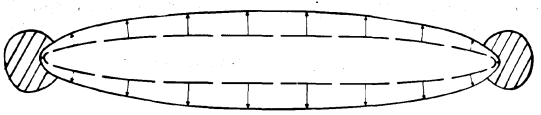

Fig. 1. Schematic diagram of an inclusion or inhomogeneous spot showing areas of stress release (hatched areas) by volume expansion.

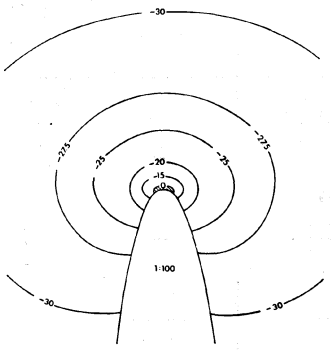

Fig. 2. Development of maximum stress around the tip of a penny-shaped or thin lenticular inclusion of aspect ratio 1:100, which has undergone a volume expansion of 10 percent due to coesite→quartz phase transformation under lithostatic, compressive pressure of 36 kb (corresponding to a depth of about 120 km). The contours indicate the distribution of maximum compressive stress component (negative and in kb). The bulk modulus and rigidity of quartz are respectively 0.377 Mb and 0.443 Mb (*Akimoto*, 1972). The Poisson's ratio and rigidity of the mantle are assumed to be 0.3 and 0.658 Mb respectively (after *Bucher and Smith*, 1971).

The propagation of elastic fracturing can be extremely fast under the above mantle conditions (*Griggs and Handin*, 1960; *Orowan*, 1960); release of stored elastic stress in rocks by such sudden tensile fracturing can generate earthquakes.

In Fig. 3, the coesite→quartz transformation curve (*Takahashi*, 1963; *Boyd*, 1964; *Akimoto*, 1972), the solidus of eclogite (*Ito and Kennedy*, 1971), and the oceanic geotherm (*Clark and Ringwood*, 1964) are superimposed. If the transition of coesite→quartz occurs at point A (i.e., under 36 kb lithostatic pressure and at about 1240°C, corresponding to approximately 120 km depth), the pressure is released (A→A') around the tip of the inclusion (Fig. 2). Although the temperature may be slightly lowered momentarily due to adiabatic expansion, the line A→A' crosses the solidus at about 13 kb compressive pressure, and the sudden pressure release can initiate melting around the tip of the inclusion (hatched area in Fig. 2). If coesite is not present in sufficient quantity as an inhomogeneity in the upper mantle, such transformation may not result in a general melting process.

The relation between shape ratio of the spheroidal inclusion and magnitude of maximum possible stress release is shown in Fig. 4. In this calculation a spheroidal inclusion of spinel is assumed to undergo phase transformation into olivine with a volume expansion of 10.8 percent (*Akimoto and Fujisawa*, 1968; *Akimoto*, 1972).

The stress release due to phase transformation is minimal for a

Fig. 3. The coesite→quartz transition (after *Takahashi*, 1963; *Boyd*, 1964; *Akimoto*, 1972) basalt-eclogite phase relation (after *Ito and Kennedy*, 1971), and the oceanic geotherm (after *Clark and Ringwood*, 1964) are superimposed. EC: eclogite: PL-EC: plagioclase; GA-GR: garnet granulite; BA: basalt; TZ: transition zone. The line A→A' indicates the path of stress release by phase transformation at the tip of the inclusion.

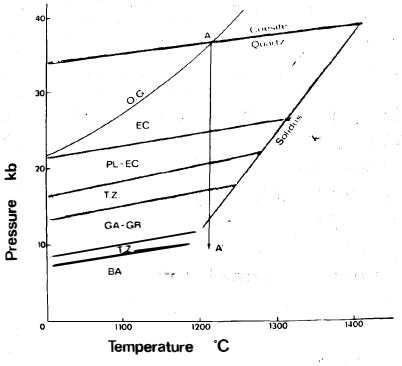

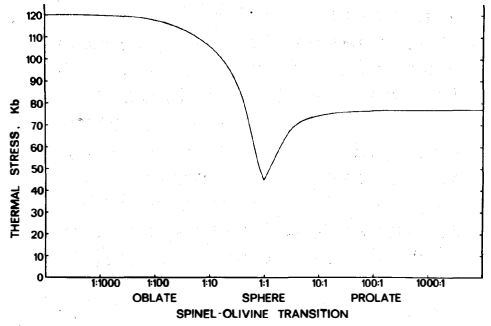

Fig. 4. Theoretical values of maximum possible stress release due to a volume expansion of 10.8 percent (after *Akimoto and Fujisawa*, 1968; *Akimoto*, 1972) for the phase transition spinel→olivine. The magnitude of the maximum possible thermal tensile stress release (kb) is shown as a function of the shape ratio of oblate-spheroidal-prolate inclusions. The bulk modulus and rigidity of olivine are assumed to be respectively, 1.63 Mb and 0.83 Mb (after *Kumazawa and Anderson*, 1969). The Poisson's ratio and rigidity of the mantle are assumed to be 0.283 Mb and 0.871 Mb respectively (after *Clark and Ringwood*, 1964). If such a high thermal tensile stress release occurs, one, or the following combination of energy dissipation processes may take place in the upper mantle: fracturing, phase transformation, fluid migration, diffusion and plastic flow (in order of time rate).

spherical inclusion but increases with the aspect ratio for both prolate and oblate inclusions (Fig. 4). The magnitude of stress release at the tip of an oblate inclusion is larger than at that of a prolate one and maximum stress release occurs at the tip of a very thin, oblate or lenticular inclusion. Our estimation shows that for such an extremely thin inclusion, stress release becomes almost constant beyond a certain aspect ratio.

The maximum possible stress release due to spinel→olivine transition is estimated theoretically to be about 120 kb (Fig. 4). If spinel→olivine transition can occur under lithostatic compressive stress of about 120 kb in the mantle (*Akimoto and Fujisawa*, 1968; *Ringwood*, 1975, p. 403), the stress at the tip of the phase-transformed inclusion would become practically zero (i.e., the tensile stress virtually equals the lithostatic load).

As fracturing in rocks can occur under very small tensile stress (*Brace*, 1964), fractures can form when stress release by phase transformation (i.e., tensile stress) would just overcome the lithostatic stress.

A positive increment of such a stress differential is most likely to occur in areas of tectonic instability. This can trigger the onset of local partial melting by the propagation of fracturing through grain boundaries and interconnecting the zones of weaknesses (such as lenses of melt), which also show a high degree of interconnectedness during experimental partial melting of pyrolite (*Waff and Bulau*, 1977). The presence of interstitial glass in pyroxenite from Williams, Arizona (*Pike and Schwarzman*, 1977) suggests that melts form along grain boundaries. Such interstitial fluids can act as "Griffith's" inhomogeneities or inclusions which become effective loci for stress concentration. *Savage* (1969) has shown that when stress affects the melting process, lenses of melt tend to propagate perpendicular to the direction of minimum tension. The "liquid-bonded aggregate" concept of rock melting along grain boundaries has been discussed by *Yoder* (1976b, p. 164).

Where inhomogeneities or fluid inclusions of various aspect ratios exist in the upper mantle (as discussed later), our analysis indicates that the inhomogeneity or inclusion with lowest aspect ratio is the probable locus for the initiation of fracturing and the onset of local melting. Thus, the magnitude of actual tensile stress relieved, is in actuality, much less than the theoretical maximum values shown in Fig. 4.

Yoder (1976b, p. 162) has suggested that the very first melt may actually begin with inclusions or involve minor phases interstitial to the major phases. If large volume changes by phase transformations of meta-minor phases continue (shown earlier), melting can initiate from inclusions or minor phases and proceed with cyclical process of stress concentration and tensile stress relief (discussed later). However, without the space requisite for volume expansion, melting will stop. The rate at which the deviatoric stress is relieved largely determines whether this melting continues or freezes. Interestingly, zones of frozen melt can act as further inhomogeneities or paths along which future propagation of melt can occur (*Bhattacharji and Koide*, in preparation).

STRESS RELEASE BY THE REDUCTION OF RIGIDITY RELATED TO PHASE TRANSFORMATION

In ridge centers, subduction zones, and intraplate areas of convective plume uprise, differential stress in the mantle can be maintained over a considerable period of time, and reduction of rigidity due to phase transformation can produce substantial stress release under shear deformation (Figs. 5 and 6). *Vaisnys and Pilbeam* (1976) have shown that phase transformation in a region of mantle material that is initially in locally stable, mechanical motion can induce extensive shear deformation associated with a thermal catastrophe.

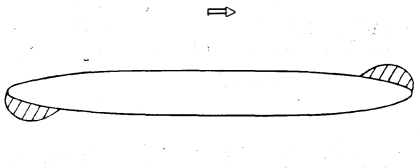

Fig. 5. Schematic diagram of an inclusion or inhomogeneity showing areas of stress release (hatched) by reduction of rigidity due to a phase change under shearing stress.

The fracturing from inclusions or inhomogeneous spots in the mantle due to phase transformation would reduce the apparent rigidity of rocks as fracture zones become significantly weaker under shearing stress, especially when it is associated with a thermal catastrophe. The reduction of rigidity and Young's modulus of rocks have also been observed with phase transformation in experiments (*Volarovich and Gurvich*, 1957).

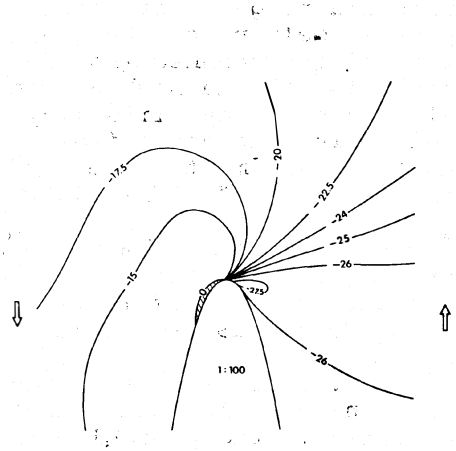

Fig. 6. Development of maximum stress release around the tip of a penny-shaped or thin lenticular fluid inclusion or fracture with pressurized fluid (of aspect ratio 1:100) due to melting under the compressive lithostatic pressure of 25 kb and 0.5 kb shearing stress. The bulk modulus and rigidity of the inclusion or fracture are, respectively, 0.645 Mb and OMb. The Poisson's ratio and rigidity of the mantle are assumed as 0.3 and 0.658 Mb respectively.

Total loss of rigidity may occur in the case of solid→fluid transformation (i.e., G' = 0). For such a phase transformation, inhomogeneities or inclusions can be considered as weak zones, or as fractures filled with fluid. Stress release by shear deformation generally occurs near the tip of the fracture boundary (Fig. 6). However, when volume expansion due

to phase transformation to fluid (melt) is large, the stress release magnitude also increases.

The effects of the additional stress release due to volume expansion by melting should be considered for mantle material which has undergone phase transformation by shear deformation. The maximum stress (σ_{max}) on the boundary of an inclusion or fracture which can produce volume change (due to melting as well as shear deformation) can be expressed by the equation (*Koide*, 1972, 1976):

$$\sigma_{max} = 1/2 \; (\sigma_t + \sqrt{\sigma_t^2 + b^2 \tau^2}) + \sigma_L \qquad (6)$$

where stress release by volume expansion (σ_t) is $\sigma_t = \sigma_T - \sigma_L$, and stress concentration coefficient (b) is

$$b = 8 \; (1 - G'/G) \Big/ \{\frac{(2 - \nu) \; \pi}{S} + 4 \; (1 - \nu) \; \frac{G'}{G} \} \qquad (7)$$

In equation (7), G' is the rigidity after phase transformation.

If the inhomogeneity or inclusion becomes fluid after transformation, rigidity G' = 0, and $b = 8S/(2-\nu)\pi$. Therefore, even a small shearing stress can cause high stress concentration around a fluid-filled inclusion or fracture.

According to the Griffith theory of fractures (*Griffith*, 1925), new fractures are formed where the maximum stress (σ_m) exceeds the tensile strength of materials. Although Griffith's energy criteria (*Griffith*, 1921) are not directly applicable under compression, the tensile stress criteria can describe the propagation of cracks under compression (*Brace and Bombolakis*, 1963).

The equation for the criterion for melting can be written as the equation of criterion for fracture formation from Griffith's inclusion or inhomogeneity (*Koide*, 1972) in which $P_m^{(t)}$, representing melting pressure (as a function of temperature) is substituted for the ideal tensile strength of a rock

$$\tau = \frac{2(P_m^{(t)} - \sigma_L)}{b} \cdot \sqrt{1 - \frac{\sigma_t}{P_m^{(t)} - \sigma_L}} \qquad (8)$$

Therefore, the propagation of melting spots may be described by the analogy of the propagation of fractures through grain boundaries and the process of interconnectedness of lenses of melt by fractures.

DISCUSSION

Volume changes caused by phase transformation, whether solid-solid or solid-fluid, migration of phase transformation zones with melting, and magma formation in the upper mantle have considerable effect on the elevation of the crustal surface and on tectonic disturbances in the earth's crust, depending on how the volume expansion is accommodated.

Various models related to the tectonic effects of phase transitions and volume changes within the first 100 km of the mantle have been discussed and summarized by *Wyllie* (1971b, p. 233-253). The minimum volume expansion necessary to initiate fracturing, stress release and probable onset of melting around a thin linear or spheroidal inclusion or inhomogeneity for depths of 100 to 400 km in the mantle has been estimated from pressure, temperature and elastic moduli data from the pyrolite model of *Clark and Ringwood* (1964) and *Ringwood* (1975) (Table 1).

In the case of a solid-fluid transformation (Case II), the required minimum volume expansion can be calculated from equation (5). In the case of a solid-solid transformation (Case I), the rigidity and bulk modulus of the inclusion or inhomogeneity must be known to calculate the volume expansion that can produce melting or fracturing. In this case it is assumed that the elastic properties of the inclusion are practically the same as those of the surrounding mantle material. As mentioned earlier, the rigidity of the inclusion is often reduced at the time of phase transformations; hence for many solid-solid phase transformations, the magnitude of stress release should be between Case I and Case II (Table I).

Volume expansion greater than 4.2 percent by solid-solid phase transformation (Case I) can cause fracturing at a depth of 100 km (Table I). Because melting causes larger stress release, volume expansion by melting greater than 1.8 percent can form fractures at 100 km.

Under the oceanic crust, at 100 km depth, the estimated temperature is about 1150°C (*Clark and Ringwood*, 1964) and the melting pressure of pyrolite is about 4.5 kb (*Ringwood*, 1975). Therefore, a volume expansion above 1.5 percent should initiate propagation of a melted inclusion (Case II), and a volume expansion above 3.6 percent should cause a melting spot at the tip of the inclusion in Case I. However, under the Shield, the temperature is too low to produce melting of dry pyrolite at such a depth.

As examples, we calculate that the transition of coesite→α-quartz with about 10 percent volume expansion and jadeite + quartz→albite with 19.8 percent volume expansion (calculated from *Clark*, 1966) can trigger propagation of fractures and the onset of melting at depths between 75 - 100 km.

The spinel→olivine transition resulting in a volume expansion of 10.8 percent at a depth of 300 km can initiate partial melting. The fosterite + pyrope→enstatite + spinel transition with 5.2 percent volume expansion which occurs at 20-25 kb pressure, corresponding to a depth of 70-80 km, and about 1100°C (*MacGregor*, 1964) can also trigger onset of local melting through the propagation of fractures along grain boundaries and existing cracks. It is interesting that *Ito and Kennedy* (1971), from their experimental study, noted a sudden volume expansion of about 4 percent for the transition of plagioclase eclogite to garnet granulite under a pressure of 19-23 kb at 1200°C, and a sudden volume expansion of about 4.9 percent from garnet granulite to basalt under a pressure of 11-13 kb at 1200°C (Fig. 3).

Areas in the mantle of uprising convection currents, thermal plumes, or diapirs of subduction zone, all under adiabatic conditions, are the most favorable sites for fractional melting by phase transformation (*Green and Ringwood*, 1967) and stress release, as the lithostatic pressure can be released more readily. Thus, in areas of uprising currents or diapirs, mantle material is more likely to be less viscous (a non-Newtonian

crystal mush or Newtonian melt) or plastic compared to the surrounding, more elastic, solid mantle material.

An example of the nature and effect of stress release in areas of viscous diapiric uprise is shown in Fig. 7. High Poisson's ratio (0.4) and reduced rigidity (0.5 Mb) values were used to represent a viscous core of a diapir or a rising current. All other parameters for calculations are identical to Fig. 2.

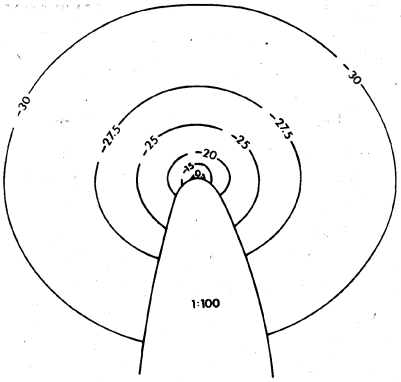

Fig. 7. Development of maximum stress release around the tip of a thin lenticular inclusion or inhomogeneity of aspect ratio 1:100 which has undergone a volume expansion of 10 percent due to coesite→quartz transition under a compressive pressure of 36 Kb. The Poisson's ratio and apparent rigidity of the less viscous mantle are assumed as 0.4 and 0.5 Mb respectively. Other parameters are the same as in Fig. 2.

The results (Fig. 7) indicate that the magnitude of the stress release is somewhat decreased due to the reduction of rigidity, but the effects of the reduction of lithospheric load due to diapiric rise dominate, creating an increased potential for melting by stress concentration, and the propagation of melt from the top of the diapir by gravitational instability (*Ramberg*, 1972, Fig. 10). The viscous strain rate (creep) or the rate of uprise of the diapir or current is also an important controlling factor. The effect is similar to Green and Ringwood's mantle pyrolite model of fractional melting (1967) under adiabatic conditions.

Phase equilibria studies suggest that under high pressure hydrous minerals (amphibole, muscovite, phlogopite) break down below the solidus, and dehydration temperature becomes lower with increasing pressure (*Wyllie*, 1971b). The breakdown of such minerals and concentration of water in thin films in intergranular boundaries or localized pockets may develop weak zones of reduced effective rigidity in the upper mantle at the level where the hydrous minerals become unstable.

The discharge of volatiles from the deeper levels of the mantle and their concentration in thin films along grain boundaries can also drastically reduce the effective rigidity of the surrounding mantle material.

Dehydration of hydrous minerals can occur in the sinking slab of a subduction zone under high pressure and low temperature conditions. Although melting at lower temperature is unlikely, propagation of fluid-filled fractures can readily occur (see below). This creates conditions favorable for the migration of volatiles along existing and newly formed passages.

Green and Radcliff (1975) have shown that CO_2-rich fluid may exsolve, precipitate, and concentrate along crystal defects and grain boundaries of mantle rocks during increasing deformation. *Francis* (1976) has also shown that interstitial amphibole in lherzolite zenolith from Nunivak Island, Alaska, was formed by infiltration of alkaline fluids in the upper mantle. These observations suggest that the discharge of volatiles or fluids into grain boundaries or stress released fractures is significant in mantle deformation. The continuous process of propagation

of fluid-filled cracks or pockets of melt by fracturing with maximum stress concentration at the tip followed by stress release (i.e., cyclical stresses and failures) can, therefore, be an important process for magma generation (*Uffen*, 1959; *Yoder*, 1976b) in regions of rising temperature and tectonic instability as well as in its migration in the direction of stress release.

A MODEL FOR PROPAGATION OF FLUID-FILLED FRACTURES BY PHASE TRANSFORMATIONS IN THE UPPER MANTLE

An area of controversy still surrounds the initial stage of melt formation through the processes of coalescence and melt removal from the asthenosphere (*Fedotov*, 1975; *Yoder*, 1976b). The most important remaining problem concerns the migration of melt from the asthenosphere (*Turcotte and Ahern*, 1977). While many consider that melts from the upper mantle rise as large drops (*Beloussov*, 1966; *Ringwood*, 1974), others think that at least basic magma rises to the surface in long magma channels or columns with the base at depths of several tens or hundreds of kilometers (*Fedotov*, 1975).

If a swarm of micro-fractures and grain boundaries filled with volatiles and melt, crystal-mush filled with interstitial fluid,or small pockets of melt are formed as inhomogeneities of a weak zone of lower effective rigidity, they may become important passages for melt migration due to mantle deformation.

Rock mechanics experiments (*Mogi*, 1971) have also shown that the concentration of micro-fractures in a weak (shear) zone leads to the development of large brittle fractures under confining pressure. The propagation of fluid-filled fractures in the mantle, which is similar to brittle fracture propagation under confining pressure (*Brace*, 1972), is essentially controlled by effective stress (σ_e): that is, normal tectonic stress minus fracture fluid pressure.

When swarms of fluid-filled fractures formed in the upper mantle due to phase changes become connected by cyclic stress relief into a continuous system for a vertical distance (h) (Fig. 8), the effective stress (σ_e') at the upper tip of the propagating fracture can be expressed as

$$\sigma_e' = \sigma_e + \Delta\rho gh \qquad (9)$$

where σ_e is the effective stress at the lower end, $\Delta\rho$ is the difference in density between the fluid and the host mantle rock,

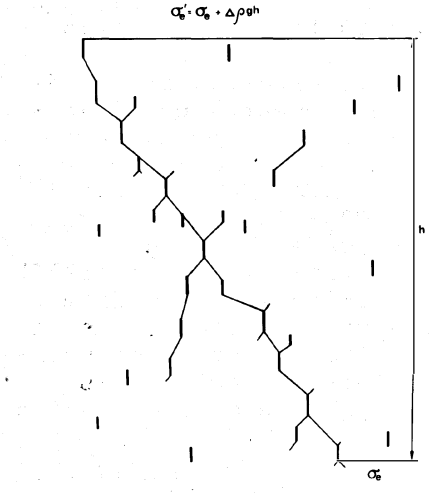

Fig. 8. Diagramatic sketch showing the probable propagation of fluid-filled fractures in the upper mantle due to phase and volume change(s). σ_e' and σ_e: the effective stress at the upper and lower tips respectively of the fluid-filled fracture(s), h: the vertical extent of a continuous fracture zone or fracture swarm, and $\Delta\rho$: the difference in density between the fluid and the host mantle rock, and g: acceleration due to gravity.

and g is acceleration due to gravity.

As the mantle rock is denser than the fluid (i.e., magma with volatiles) in the fracture system, fractures (with fluid) propagate upwards because of higher effective stress. The upward propagation of fluid-filled fractures is accelerated as the vertical distance (h) of fractures becomes larger. Thus rapid concentration of thin films of pressurized melt or volatiles (such as CO_2, H_2O) in weak, shear or deep fault zones can lead to the shattering of more rigid, surrounding rocks with numerous fluid-filled fractures. If fluid pressure in fracture zones under shear is lowered due to dilatancy, more fluid flows into deep fault or shear zones (*Frank*, 1965; *Nur*, 1972). Thus the accelerated propagation of pressurized fractures with increasing length and higher effective stress can lead to rapid or explosive emplacement of volatile-rich magmas and diatremes.

Rapid brittle fracture propagation, rather than viscous diapiric uprise, is more likely to result when the pressure of the partially melted mush with increasing volatile content at the roof approaches or exceeds the lithostatic load. Rates of uprise of such partially melted materials from the low velocity layer of the upper mantle or from the potentially unstable hotter boundary zone comprising both mantle and lower lithosphere are controlled primarily by compressive and differential stresses in the upper mantle, fluid pressure, effective kinematic viscosity and rate and volume supply of the fluid. Island arc, subduction zone and plate collision boundary are most suited for the development of such conditions.

The effects of the diapiric and forceful uprise of partially melted mantle material on the elastic lithospheric plate and the development of fracture geometry in both oceanic and continental crust due to diapirism have been discussed earlier (*Bhattacharji and Koide*, 1975, 1976; *Koide and Bhattacharji*, 1975a, 1975b).

ACKNOWLEDGEMENTS

This research was financially supported by (a grant from the) City University of New York faculty research award to S. Bhattacharji. The authors are thankful to Brooklyn College of the City University of New York for providing computer facilities, to Lee Bhattacharji for helping with the manuscript, to Professor Harve S. Waff, Yale University, Conn., and Drs. H.S. Yoder, Jr., and D.H. Eggler, Geophysical Laboratory, Washington, D.C., for valuable suggestions for improvement of the manuscript. The junior author (S.B.) is particularly grateful to Professor Sheldon Judson, Princeton University, N.J., for providing facilities for the completion of this manuscript, to Jayne Bialkowski, Princeton University, N.J., for typing it, and to Neville L. Carter, State University of New York at Stony Brook, N.Y., for the review of the manuscript.

REFERENCES

Akimoto, S., The System MgO-FeO-SiO_2 at high pressures and temperatures - phase equilibria and elastic properties, in *The Upper Mantle*, edited by A.R. Ritsema, Tectonophysics, 13, 161-187, 1972.

Akimoto, S.I., and H. Fujisawa, Olivine-spinel solid solution equilibria in the system Mg_2SiO_4 - Fe_2SiO_4, *J. Geophys. Res.*, *73*, 1467-1479, 1968.

Anderson, D.L., The Plastic layer of the Earth's mantle, in *Continental Adrift*, Sci. Amer. Pub. 28-35, 1962.

Beloussov, V.V., *The Earth's Crust and Upper Mantle of Continents*, Nauka, Moscow, 190 pp. (in Russian), 1966.

Bhattacharji, S., and H. Koide, Fracturing in lithospheric plates by magma induced pressure, *EOS, Trans. Amer. Geophys. Un.*, *55*, 439, 1974.

Bhattacharji, S., and H. Koide, Mechanistic model for triple junction fracture geometry, *Nature, Lond.*, *255*, 21-24, 1975.

Bhattacharji, S., and H. Koide, Partial melting, diapiric magnetic wedging and formation of Rift Valley System in the lithosphere, *25th Inter. Geol. Congress. Sec. 3A*, *1*, 75-76, 1976.

Bott, M., Formation of oceanic ridges, *Nature, Lond.*, *207*, 840, 1965.

Boyd, F.R., Jr., The system enstatite-pyrope, *Carnegie Inst. Washington Year Book*, *63*, 157-161, 1964.

Brace, W.F., and E.G. Bombolakis, A note on brittle crack growth in compression, *J. Geophys. Res.*, *68*, 3709-3713, 1963.

Brace, W.F., Brittle fractures of rocks, in *State of Stress in the Earth's Crust*, edited by W.P. Judd, Am. Elsevier Publ. Co., Inc., N.Y., 111-118, 1964.

Brace, W.F., Pore pressure in geophysics, in *Flow and Fracture of Rocks*, edited by Heard et al., Am. Geophys. Union, Geophys. Monograph 16, 265-273, 1972.

Brey, G., and D.H. Green, The role of CO_2 in the Earth's mantle, *25th Inter. Geol. Congress (Abstr. vols.), Sec. 10A*, 415, 1976.

Bucher, R.L., and R.B. Smith, in *The Structure and Physical Properties of the Earth's Crust*, Am. Geophys. Union, Geophys. Monograph 14, 59, 1971.

Carter, N.L., and H.G. Ave'Lallemant, High temperature flow of dunite and peridotite, *Bull. Geol. Soc. Am.*, *81*, 2181-2202, 1970.

Clark, S.P., Jr., Handbook of Physical Constant, *Mem. Geol. Soc. Am.*, 97, 1966.

Clark, S.P., and A.E. Ringwood, Density distribution and constitution of the mantle, *Rev. Geophys.*, *2*, 35-88, 1964.

Edwards, R.H., Stress concentrations around spheroidal inclusions and cavities, *Jour. Applied Mechanics*, *18*, 19-30, 1951.

Eggler, D.H., CO_2 as a volatile component of the mantle: the system Mg_2SiO_4-SiO_2-H_2O-CO_2, *Phys. Chem. Earth*, *9*, 869-881, 1975.

Eggler, D.H., Does CO_2 cause partial melting in the low-velocity layer of the mantle, *Geology*, *2*, 69-72, 1976.

Fedotov, S.A., Mechanism of magma ascent and deep feeding channels of Island Arc volcanoes, *Bull. Volcan., 39*, 1-14, 1975.

Francis, D.M., The origin of amphibole in lherzolite xenoliths from Nunivak Island, Alaska, *J. Petrol., 17*, 357-378, 1976.

Frank, F.C., On dilatancy in relation to seismic sources, *Rev. of Geophysics, 3*, 485-503, 1965.

Green, D.H., and A.E. Ringwood, The genesis of basaltic magmas, *Contr. Mineral. Petrology, 15*, 103-190, 1967.

Green, H.W., and S.V. Radcliff, Fluid precipitates in rocks from the earth's mantle, *Bull. Geol. Soc. Am. 86*, 846-852, 1975.

Griffith, A.A., The phenomena of rupture and flow in solids, *Philos. Trans. Roy. Soc. Lond. (Ser. A), 221*, 163-198, 1921.

Griffith, A.A., The theory of rupture, *Internal. Cong. Applied Mechanics, 1St, Delft, Proc.*, 53-63, 1925.

Griggs, D., and D.W. Baker, The origin of deep-focus earthquakes, in *Properties of Matter Under Unusual Conditions*, edited by H. Mark and S. Frenbach, Interscience Pub., New York, 23-42, 1969.

Griggs, D.T., and J. Handin, Observations on fracture and hypothesis of earthquakes, in *Mem. Geol. Soc. Am., 79*, edited by D. Griggs and J. Handin, 347-364, 1960.

Hart, S.R., C. Brooks, T.E. Krogh, G.L. Davis, and D. Nava, Ancient and modern volcanic rocks; a trace element model, *Earth and Planetary Sci. Letters, 10*, 17-28, 1970.

Hart, S.R., Magma genesis: what can you learn from trace elements and isotopes, *Geol. Soc. Am. (Abstr.), 8*, 906, 1976.

Ito, K., and G.C. Kennedy, An experimental study of the basalt-garnet, granulite-eclogite transition, in *The Structure and Physical Properties of the Earth's Crust*, Am. Geophys. Union, Geophys. Monograph 14, 303-314, 1971.

Koide, H., Condition for fracture formation from inclusion, I. soft inclusion and pore, *J. Mat. Sci. Soc. Japan, 7*, 252-263, 1970.

Koide, H., Fracture initiation in brittle polycrystalline material such as rocks, Mechanical Behavior of Materials, *Proc. Int. Conf. ICM, 6*, 455-463, 1972.

Koide, H., Brittle fracturing by a partial phase change - a mechanism of deep-earthquake, *EOS, Trans. AGU (Abstr.), 55*, 430, 1974.

Koide, H., Fracturing of heterogeneous materials by thermally induced residual stress with special reference to rocks, *Proc. Second Int. Conf. Mechanical Behavior of Materials: Boston (Abstr.)*, 1345-1348, 1976.

Koide, H., and S. Bhattacharji, Mantle inhomogeneity, partial melting and diapiric intrusion of magma from the mantle to lithospheric plates, *Geol. Soc. Am. (Abstr.), 6*, 829, 1974.

Koide, H., and S. Bhattacharji, Formation of fractures around magmatic intrusions and their role in ore localization, *Econ. Geol., 70*, 781-799, 1975a.

Koide, H., and S. Bhattacharji, Mechanistic interpretation of rift valley formation, *Science, 189*, 791-793, 1975b.

Kumazawa, M., and O.L. Anderson, Elastic moduli, pressure derivatives, and temperature derivatives of single-crystal olivine and single-crystal forsterite, *J. Geophys. Res., 74*, 5961-5971, 1969.

Kushiro, I., Composition of magmas formed by partial zone melting of the Earth's upper mantle, *J. Geophys. Res., 73*, 619-634, 1968.

Lambert, I.G., and P.J. Wyllie, Stability of hornblende and a model for the low-velocity zone, *Nature, 219*, 1240-1241, 1968.

Macgregor, I.D., The reaction 4 enstatite + spinel = forsterite + pyrope, *Carnegie Inst. Washington Yearbook 63*, 156-157, 1964.

Mogi, K., Fracture and flow of rocks, in *The Upper Mantle*, edited by A.R. Ritsema, Tectonophysics, 13, 1-4, 541-568, 1971.

Nur, A., Dilatancy, pore fluids, and premonitary variation of $^{ts}/_{tp}$ travel times, *Bull. Seism. Soc. Am., 62*, 1217-1222, 1972.

O'Nions, R.K., and R.J. Pankhurst, Secular variations in the Sr-isotope composition of Icelandic volcanic rocks, *Earth and Planetary Sci. Letters, 21*, 13-21, 1973.

Orowan, E., Mechanism of seismic faulting, *Geol. Soc. Am., Mem. 79*, 323-345, 1960.

Pike, J.E.N., and E.C. Schwarzman, Classification of textures in ultramafic xenolith, *J. Geol., 85*, 49-61, 1977.

Ramberg, H., Mantle diapirism and its tectonics and magmagenetic consequences, *Phys. Earth Planet. Inter., 5*, 45-60, 1972.

Ringwood, A.E., The petrological evolution of Island Arc Systems, *J. Roy. Geol. Soc., 130*, 3, 183-204, 1974.

Ringwood, A.E., *Composition and Petrology of the Earth's Mantle*, McGraw-Hill, New York, 618 p., 1975.

Roberts, J.L., The intrusion of magma into brittle rocks, in *Mechanism of Igneous Rocks*, edited by G. Newall and N. Rast, 287-338, 1970.

Savage, J.C., The mechanics of deep focus faulting, *Tectonophysics, 8*, 115-127, 1969.

Schilling, J.-G., Rare-earth variations across "normal" segments of the Reykjanes Ridge, 60°-53°N, Mid-Atlantic Ridge, 29°S, and S. Pacific Rise, 2°-19°S, and evidence for the composition of the underlying low velocity layer, *J. Geophys. Res., 80*, 1459-1973, 1975.

Smyth, J.R., and C.J. Hatton, A coesite-sanidine grospydite from the Roberts Victor kimberlite, *Earth Planet. Sci. Letters, 34*, 284-290, 1977.

Sun, S.S., and G.N. Hanson, Evolution of the mantle: Geochemical evidence from alkali basalt, *Geology, 3*, 297-302, 1975.

Takahashi, T., Discussion, in *High-Pressure Measurement*, edited by A.A. Giardini and E.C. Lloyd, Butterworths, Washington, D.C., 240-244, 1963.

Turcotte, D.H., and J.L. Ahern, A porous flow model for magma migration in the asthenosphere, *EOS, Trans. AGU (Abstr.), 58*, 535, 1977.

Uffen, R.J., On the origin of rock magma, *J. Geophys. Res., 64*, 117, 1959.

Uffen, R.J., and A.M. Jessop, The stress release hypothesis of magma formation, *Bull. Volcan., 26*, 57, 1963.

Vaisnys, J.R., and C.C. Pilbeam, Deep-earthquake initiation by phase transformations, *J. Geophys. Res., 81*, 985-988, 1976.

Volarovich, M.P., and A.S. Gurvich, A study of elastic moduli of rocks related to temperature: (issledovannie dinamicheskogo modulya uprugosti gornykh porod v zavusinosti ot temperatury) Izvestiya akagemii nauk USSR, *Seriya geofzicheskaya, No. 4* (after Japanese translation by Y. Konishi), *Bull. Geol. Surv. Japan, 8*, 535-541, 1957.

Waff, H.F., and J.R. Bulau, Fluid distribution in partially molten "pyrolite", *EOS, Trans. AGU (Abstr.), 58*, 535, 1977.

Wyllie, P.J., The role of water in magma generation and initiation of diapiric uprise in the mantle, *J. Geophys. Res., 76*, 1328-1338, 1971a.

Wyllie, P.J., *The Dynamic Earth*, Wiley, New York, 416 pp., 1971b.

Yoder, H.S., Jr., Change of melting point of diopside with pressure, *J. Geol., 60*, 364, 1952.

Yoder, H.S., Jr., Tectonophysics of melting in the mantle and thermo-chemical implications for basalt, *Geol. Soc. Am. (Abstr.), 8*, 6, 1179, 1976a.

Yoder, H.S., Jr., *Generation of Basaltic Magma*, National Acad. Sciences, Washington, D.C., 265 pp., 1976b.

TELESEISMIC TECHNIQUE TO LOCATE MAGMA IN THE CRUST AND UPPER MANTLE

H.M. Iyer and R.M. Stewart
U.S. Geological Survey
345 Middlefield Road
Menlo Park, California 94025

Abstract

Relative traveltime residuals, measured using a large number of teleseismic P-waves recorded in three volcanic areas (Long Valley and The Geysers, California; Yellowstone National Park, Wyoming), show that seismic compressional velocities are lower by 5 to 15% in large volumes beneath each area. In Yellowstone the teleseismic delays are about 1.5 sec inside the caldera. They also remain high over a 100-km wide area around the caldera. The spatial distribution of the delays and their magnitudes indicate the presence of a large body of low-velocity material with horizontal dimensions corresponding to the size of the caldera (40 km x 80 km) near the surface and extending to a depth of about 150 to 250 km under the caldera. Using ray tracing and inversion techniques, it is estimated that the compressional velocity inside the anomalous body is lower than the surrounding rock by 15 to 20% in the upper crust, and by 5% in the upper mantle. In Long Valley and The Geysers the delays are about 1 sec with a spatial distribution for teleseisms from different azimuths that indicates the presence of a low-velocity body in the upper crust. The diameter of the body in each area is estimated to be about 10 km and the velocity contrast to be lower than normal by 10 to 15%. Recent volcanism, surface geothermal phenomena, high heat flow, and gravity data suggest that hot rock is present under these areas, and the low seismic velocities are presumably caused by the hot rock. However, laboratory data demonstrate that to obtain the observed 10 to 15% reduction in compressional wave velocities, complete or partial melting of the rock is required. Hence, we postulate that the low velocity bodies at Long Valley, The Geysers, and Yellowstone are magma chambers responsible for the observed volcanism.

Introduction

Seismic techniques are ideally suited for detecting and delineating zones of partial melt. Both P-waves and S-waves can be expected to travel through magmatic material with lower than normal velocities. Attenuation is likely to occur for both types of waves and may be particularly severe for S-waves (*Kubota and Berg*, 1967; *Matumoto*, 1971). Both active and passive seismic techniques can be used to explore magma chambers and partially molten zones in the crust and upper mantle of the earth. In the active technique, controlled seismic sources such as explosions and Vibroseis are used to carry out conventional refraction and reflection surveys. Unfortunately this powerful technique has been used very little in the United States for geothermal and volcanological studies, presumably

because it is very expensive. The technique called "deep seismic sounding" has been extensively used in the USSR to study the deep structure of volcanoes in the Kamchatka area (*Utnasin et al.*, 1976). In the passive seismic technique earthquakes are used as seismic sources. Local and regional earthquakes can be used to study partial melts in the crust, and distant earthquakes (teleseisms) are useful to delineate magma bodies in the crust and upper mantle. In this paper we shall discuss only the teleseismic technique of exploring for magma.

Our main interest in partial molten zones is in connection with efforts to study heat sources in geothermal areas and is part of the U.S. Geological Survey's seismic monitoring program of geothermal areas. *Iyer* (1975) found that teleseismic P-waves recorded by a USGS seismic network in Yellowstone National Park were significantly delayed as they traveled under the Yellowstone caldera. *Steeples and Iyer* (1976a,b) studied teleseisms in Long Valley, California (a potential geothermal area) and found P-wave delays there, though present in a much less spectacular fashion than in Yellowstone. *Steeples and Iyer* (1976b) and *Iyer and Hitchcock* (1975) have also found that a similar phenomenon may be present at The Geysers, California, the only place in the United States where geothermal electric power is currently being generated. In this paper we shall briefly discuss the teleseismic technique to locate and delineate magma bodies, and the observations and their interpretation at Long Valley, Yellowstone, and The Geysers. The Geysers results are preliminary and we shall discuss them only briefly.

The Technique

The main advantage of using teleseisms to locate magma in the crust and upper mantle arises from the fact that teleseismic waves travel to the recording station almost vertically from underneath. Thus, if a recording station located in a volcanic area detects an anomalous velocity decrease for teleseisms from several azimuths, the material causing the anomaly can be constrained to a cone bounded by the rays. The anomalous increase or decrease in velocity encountered by a seismic ray along its travel path is estimated by a quantity termed the traveltime residual, which is obtained by subtracting from the observed traveltime (TO) between the source and recording station a theoretical time (TT) computed from a known earth model. The definition of traveltime residual can be represented by the following equation:

$$R = TO - TT \qquad (1)$$

The observed travel time TO is simply the difference between the arrival time at the recording station of the appropriate seismic phase (in the present case the P-phase which is the first arrival) and the origin time of the seismic event as determined by the National Earthquake Information Service of the U.S. Geological Survey. To calculate the theoretical traveltime (TT), the available information on the station coordinates and the coordinates of the earthquake hyopcenter are used to compute the angular distance (Δ) between the station and event in degrees. The traveltime TT is then calculated from the traveltime table using Δ and the event depth. The choice of the actual traveltime table is relatively unimportant as long as the study involves interpretation of variation of residuals in a small area. In practice we have found it convenient to use the traveltime table for P-phases compiled by *Herrin* (1968a). R contains, in addition to the crust and mantle effects under investigation immediately

beneath the recording station, effects due to mislocation of hypocenter of the event, errors in origin time and anomalous velocity structure along the path of propagation. In order to minimize contributions from both source and path effects to the residual R, we compute a quantity called relative residual (RR). It is assumed that there is at least one seismic station in our network which does not "see" any anomaly under it and can be considered to be a "normal" station. Relative residual RR is obtained by subtracting from the observed residual R at any station the residual RREF at the reference station.

$$RR = R - RREF \qquad (2)$$

The spatial variation of the final number RR over a seismic network for events from various azimuths and distances, contains the required information on the velocity structure in the crust and upper mantle under the network. Note that a positive value of RR (delay) means that the seismic ray reaching the station is slowed down by travel through material with lower than normal velocities. The teleseismic residual technique outlined here has been extensively used in seismology to study regional crust and upper mantle structure (*Tryggvason*, 1964; *Bolt and Nuttli*, 1966; *Iyer and Healy*, 1972). For a comprehensive list of references on studies using traveltimes of seismic waves see *Hales and Herrin* (1972). We shall discuss the method of inverting this type of data, using qualitative and quantitative techniques to delineate the shape and structure of anomalous bodies, in the discussion of specific case histories given below.

Case Histories

Long Valley, California

Long Valley caldera, a 17 x 32 km elliptical depression located on the east front of the Sierra Nevada about 30 km south of Mono Lake, is a collapse feature formed as a result of voluminous rhyolitic ash flow eruptions which occurred about 0.7 m.y. ago (*Bailey et al.*, 1976). The presence of surface geothermal phenomenon and higher than normal heat flow (*Lachenbruch et al.*, 1976) suggest that a magma chamber may be present under the Long Valley caldera. *Steeples and Iyer* (1976a,b) analyzed teleseismic data collected at Long Valley, using a portable seismic network deployed in the area for nine weeks in 1973 to record microearthquakes and seismic noise. The following three figures taken from *Steeples and Iyer* (1976a) summarize the main findings.

Fig. 1 is intended to show that the region outside the Long Valley caldera is normal. The average relative residuals (based on 3 or more readings) with respect to reference station LVC (shown by triangle) for events along three azimuths are shown at each station. Note that for the southeast and northwest azimuths we have earthquake sources at distances in the range of 20 to 90 degrees (1 degree = 111.19 km), whereas, for the southwest azimuth the events occur within a distance range of 85 to 95 degrees. In terms of our study this means that for southeast and northwest azimuths the angles of incidence at the surface, measured from vertical, of the seismic rays vary from 15 to 35 degrees, whereas, for the southwest azimuth the angles of emergence are in a narrow range around 16 degrees. The main feature to note in Fig. 1 is that the relative residuals are quite small outside the Long Valley caldera, thus justifying our choice of LVC as the reference station. Figures 2a and b show relative residuals

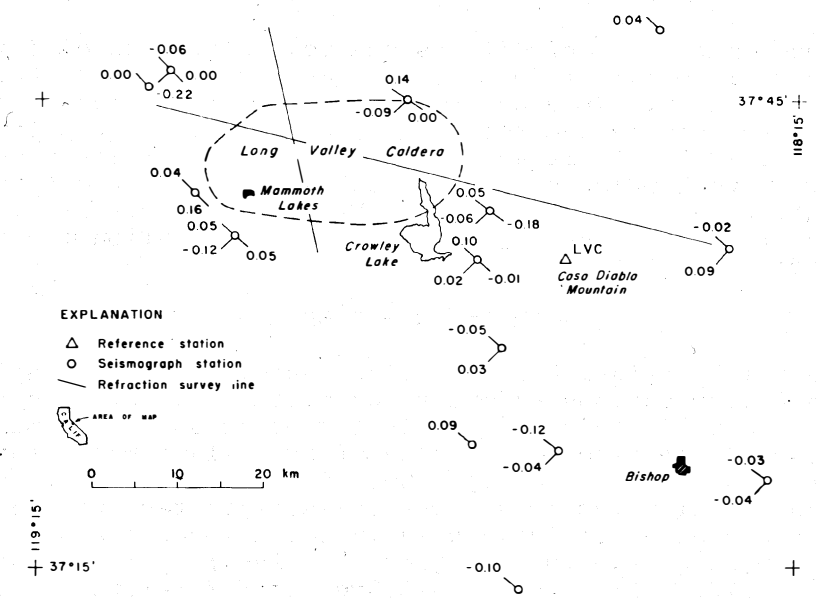

Fig. 1. Relative residuals at stations surrounding the Long Valley caldera. Reference station LVC, shown by triangle, is at Casa Diablo Mountain. The short radial lines from the stations show the three primary azimuths of the teleseisms used. Caldera boundary, from geological evidence, is shown by dashed lines. The two long lines show *Hill's* (1976) refraction profile. Figure is taken from *Steeples and Iyer* (1976a).

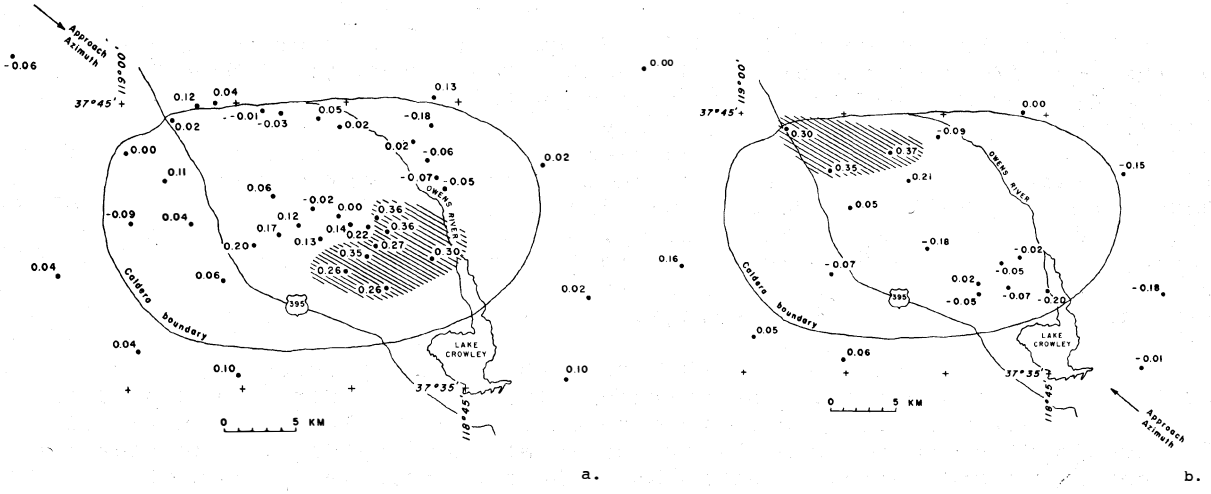

Fig. 2. Average relative residuals inside and just outside Long Valley caldera. Dots indicate station locations where the residual values are shown in seconds. The values are corrected for velocity structure in the top 6 km of the crust. Zones where delays exceed 0.25 sec are hachured. (a) Northwest teleseisms, (b) Southeast teleseisms. Figure adapted from *Steeples and Iyer* (1976a).

at caldera stations for events along the northwest and southeast azimuths, respectively. These values have been corrected for surface effects using a model for the upper 6 km of the crust obtained by *Hill* (1976) from a seismic refraction experiment. The correction is -0.2 sec at all stations except one location over the Owens River Valley where the value is -0.35 sec. The main features to observe in Figs. 2a and b are the zones of positive residuals (delays) in which the values are 0.25 sec. These zones, indicated by the hachured regions in the figures, occur on the sides of the caldera opposite to that where the seismic rays enter the caldera. In other words, the zone of large delays occurs inside the caldera near the southeast boundary for northwest events and near the northwest boundary for the southeast events. As we shall show below, the most likely cause of this reversal of the spatial pattern of delays for sources at opposite azimuths is a low-velocity anomaly deep under the center of the caldera.

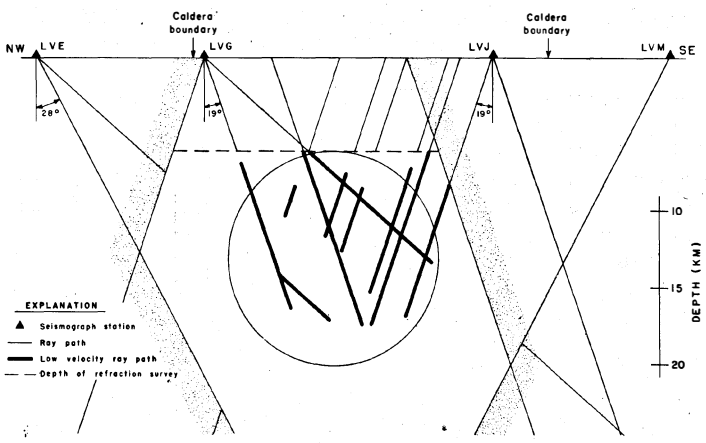

Fig. 3. A model for the low-velocity body under Long Valley caldera assuming a 15% decrease. Heavy lines indicate required path lengths of rays to produce the observed delays at the surface. Velocities outside the stippled zones are normal. The circle is a sectional view of a sphere of 14 km diameter required to contain the anomalous rays. Figure adapted from *Steeples and Iyer* (1976a).

Figure 3 shows an approximate northwesterly vertical cross-section of the Long Valley caldera in which the ray paths for events in opposite azimuths are shown. The delays observed at the surface (corrected for near-surface effects) are converted into equivalent path lengths in a medium in which the P-wave velocity is lower than normal by 15%. These path lengths are shown by the heavy lines in the figure. The rays along which the delays are negligible confine the anomalous ray paths to within the stippled zone in the figure. From the refraction survey by *Hill* (1976) it is known that anomalous low-velocity zone does not occur above 7 km in the crust, and the interaction of the normal rays that reach station LVE and LVM outside the caldera on the northwest and southeast sides, respectively, (see Fig. 3) shows that the low-velocity zone occurs above 40 km depth. Using these contraints, the maximum dimensions of the body can be restricted. The 15% velocity decrease which we have assumed makes the diameter of the anomalous body smaller than the diameter of the available zone. If we use 5% velocity contrast the anomalous ray paths become much larger than the zone bounded by the stippled bands. Hence, we conclude that the actual velocity decrease is somewhere between 5 and 15%. The projection of the body in a horizontal plane is almost directly under the post-caldera resurgent dome of about 10 km diameter in the central part of the western half of the caldera.

From the volcanism, heat flow, and surface geothermal phenomena in Long Valley it seems reasonable to assume that the low-velocity body is the magma chamber which is the geothermal heat source. As we shall show in the section on interpretation of low-velocity data, it is difficult to uniquely estimate from P-wave velocity reduction alone the state of partial melt in the magma chamber.

The spectacular geothermal phenomena for which Yellowstone is world famous is a result of recent volcanism. The volcanic evolution of Yellowstone is discussed in detail by *Christiansen and Blank* (1972) and summarized by *Eaton et al.* (1975). According to them, the most recent episode of volcanism in Yellowstone began about 150,000 years ago, and the youngest flows are only about 70,000 years old. The existence of a voluminous Quaternary rhyolite plateau, a large collapse caldera (70 km x 45 km), and the ongoing evidence for high conductive and convective heat flow (*Morgan et al.*, 1976; *Fournier et al.*, 1976) provide adequate evidence that a heat source is still present under Yellowstone. Indirect evidence from other geophysical data such as gravity and aeromagnetic data also indicates that magma may be present in the upper crust under Yellowstone (see *Smith et al.*, 1974; *Eaton et al.*, 1975; *Bhattacharyya and Leu*, 1975). A preliminary study of P-wave delays from data collected using a 12-station, telemetered, seismic network in Yellowstone National Park showed the presence of a large body of low-velocity material underlying the caldera. The horizontal dimensions of the body were found to be at least as large as those of the caldera, and the body extended to a depth of at least 100 km (*Iyer*, 1975). In order to obtain a detailed definition of the low-velocity body, the seismic network was extended to have 26 stations and was supplemented with field measurements using portable seismic stations. A summary of the detailed findings is given below.

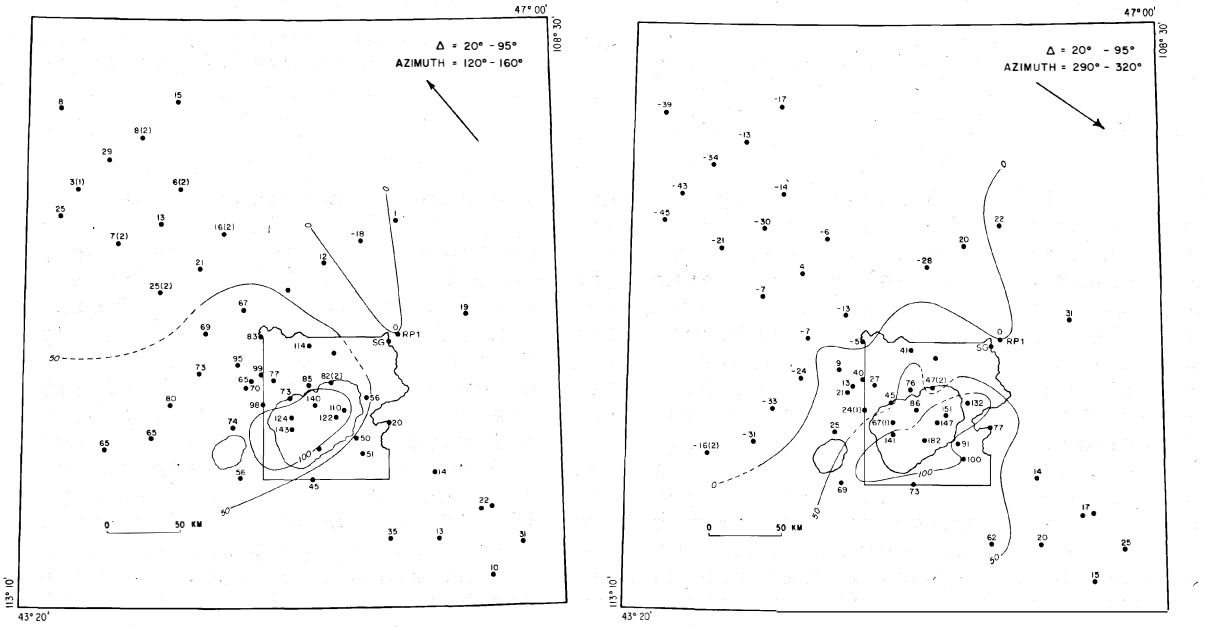

Fig. 4. Relative residuals in units of hundredths of a second in the Yellowstone region are shown near dots which indicate station locations. Numbers in parentheses indicate number of values used in estimating average when less than 3 readings were available. The contour interval is 0.5 sec (50 units). The Yellowstone National Park boundary is shown by straight and zigzag lines, and the caldera boundary is shown within the park. Island Park caldera is shown in the southwest of Yellowstone caldera. (a) Events from the southeast azimuth , (b) Events from the northwest azimuth.

Figures 4a and b show the average relative residuals for events in the distance range of 25 to 95 degrees and located approximately along southeast and northwest azimuths from Yellowstone. The values are in units of hundredths of a second. Reference stations SG and RP1 (not identified in the figure), located at the northeast boundary of the Park, are used to compute relative residuals. Most of the averages are based on 5 or more readings. However, there are a few stations where only 1 or 2 readings are available. The number of values at these stations are indicated in parentheses. Contours of average residuals for southeast events are shown in Fig. 4a. Note that the 0.5 sec (50 unit) contour extends to a distance of about 100 km outside the caldera boundary in the northwest direction, whereas to the southeast and northeast the delays decrease rapidly with distance. This is exactly the surface delay pattern to be expected from the presence of a deep low-velocity body situated underneath the caldera. The one sec (100 unit) contour gives an almost faithful shadow of the caldera, the slight northwesterly offset from the geologically mapped caldera boundary being due to the angle of emergence of teleseismic waves (about 20° to the vertical) at the surface. Note the persistence of delays $\geq$ 0.5 sec in the southwesterly direction indicating that a low-velocity anomaly is present under the Island Park caldera and the Snake River Plain. This is interesting because it is believed that Yellowstone is the present day manifestation of volcanism which migrated along the Snake River Plain. K-Ar dating of rocks by *Armstrong et al.* (1975) shows that volcanism progressed at the rate of approximately 2.5 cm/yr along the Snake River Plain towards Yellowstone. If the 0.65 sec delay seen about 100 km to the southwest of Yellowstone is any indication, it looks as if low velocity material may be present in the deep crust and upper mantle under the Snake River Plain.

Results for the northwest events (Fig. 4b) show a spatial delay pattern which is quite the opposite from that of southeast events (Fig. 4a). The 0.5 sec contour extends to a distance of about 100 km to the southeast of the caldera edge, and the one sec contour appears like an elongated picture of the caldera with a southeasterly offset. Note how the delays become quite small on the northwest side of the caldera in the region where large delays were seen for the southeast events. Available data show persistence of more than 0.5 sec delays to the south of Yellowstone National Park, an effect which may be due to low-velocity structure in the crust and upper mantle under the Snake River Plain.

A plausible interpretation of the patterns shown in Fig. 4a and b is that they are not caused by upper crustal effects such as caldera fill but by the existence of a deep low-velocity body underneath the caldera. To obtain a qualitative estimate of the horizontal and vertical dimensions of the low-velocity body, we have projected the observed relative residuals onto a vertical plane striking northeast and passing through the center of the caldera (Fig. 5). In doing this we make the *ad hoc* assumption that delays associated with events on the caldera side of a station are caused by ray paths through anomalous material under the caldera. Rays reaching the station are traced backwards toward the event, and the delays are projected on the plane at a point whose horizontal position depends on the event azimuth and the vertical position depends on the event distance. (The farther the event, the steeper is the angle of emergence of the seismic ray at the surface, and the deeper its travel path under the caldera.) A spherical earth model and Herrin's velocity distribution for the crust and upper mantle (*Herrin*, 1968b) are assumed in the ray path computations. We would like to emphasize that the ray path computations do not take into account the complicated velocity structure which we are proposing. This exercise is intended only to give an approximate idea of the shape and of the low-velocity body under Yellowstone. The results are shown in Fig. 5

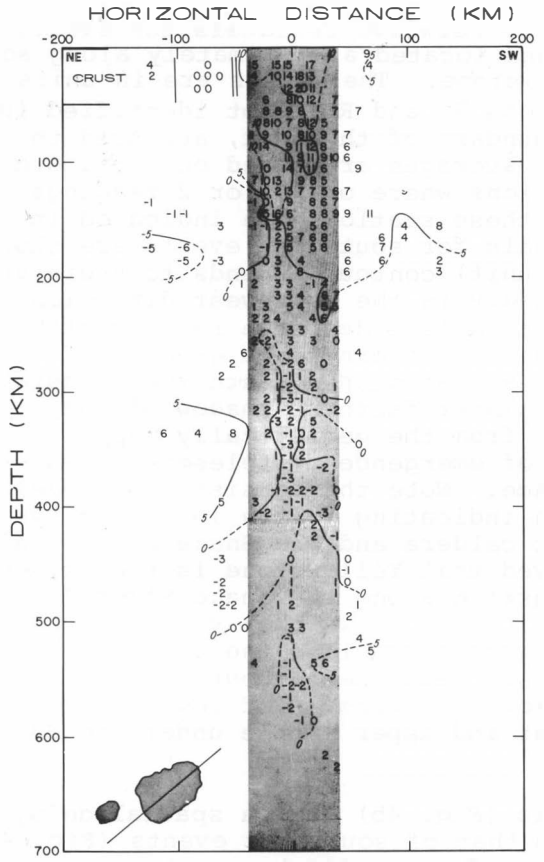

Fig. 5. Projection of relative residuals (shown by numbers in units of tenth of a second) on a northeast striking vertical plane passing through the center of Yellowstone caldera (see inset at the bottom left hand corner). Horizontal distance from the caldera center is shown as negative to the northeast and positive to the southwest. Each value is an average using available data in cells of 10 km x 10 km. Contour interval is 0.5 sec (50 units). The shaded vertical column is the projection of the caldera into the crust and upper mantle.

in which numbers are relative residuals in units of tenth of a second, averaged over 10 km x 10 km cells. The projected residuals, in a gross sense, give a picture of the northeast-southwest cross-section of the low-velocity anomaly under the Yellowstone caldera. Most of the values of one sec and over are confined to the crust, 0.7 to one sec are found up to a depth of about 150 km, and the 0.3 to 0.7 sec up to 250 km. At depths greater than 250 km the residuals decrease to slightly negative values. Since the negative residuals are, in general, quite small it is difficult to be certain whether the change in sign of the residuals is real or not, but the depth at which this occurs indicates the lower detectable boundary of the body. On the northeastern half of the plane the positive residuals are mostly inside the caldera boundary projected into the upper mantle. On the southeast side, however, delays at high as 0.5 sec can be observed up to a depth of 200 km as far as 100 km outside the caldera boundary. If we assume that the delays are directly related to velocity under the caldera from the surrounding normal rock, the following picture of the southeast-northwest cross-section of the low-velocity body emerges.

(i) A large velocity contrast from the surroundings in the crust and sub-crustal regions, the contrast becoming less with depth and disappearing around 250 km.

(ii) A possible well-defined northeast boundary which almost coincides with the extension of the caldera wall into the upper mantle.

(iii) An ill-defined southwest boundary with indication that lower-than-normal velocities persist under the Snake River Plain.

A similar cross-section was made along the northwest-southeast direction. Because available data for this line were mostly from southwest events in a narrow distance and azimuth range, the definition of the body was poor. The data, however, agree with the definition of the body along the northwest cross-section discussed under (i).

We would like to emphasize that the estimate of 250 km depth to the bottom of the anomalous body, obtained using the cross-section plot, is an approximation and, therefore, should be considered only as a possible upper limit. This is because the data used to delineate the deeper parts of the body are from stations which are at least 100 km away from the caldera boundary, and no corrections for the contribution to the residuals from possible crustal thickness and structure variations in the region have been applied. Also, we have not taken into consideration the refraction effects, inevitable in a complex body of this type which we propose here. Using an inversion technique for modeling the three-dimensional structure of the crust and upper mantle under Yellowstone, we shall show below that the low-velocity body can be seen even at a depth of 100 km. Using all available data, our conservative estimate for the lower limit to the depth of the body is approximately 150 km.

It was possible to invert the residual data from the 26 permanent stations to obtain a three-dimensional velocity model of the crust and upper mantle in the Yellowstone region using a technique developed by *Aki, Christoffersson, and Husebye* (1977). This technique requires data from a large number of teleseisms with good azimuth and distance distribution in order to provide adequate statistical stability in the final results. Therefore, it was not possible to use data from the portable stations for this analysis. This limitation restricts the depth of modeling to about 100 km since the horizontal dimensions of the permanent array were adequate to "see" only up to this depth.

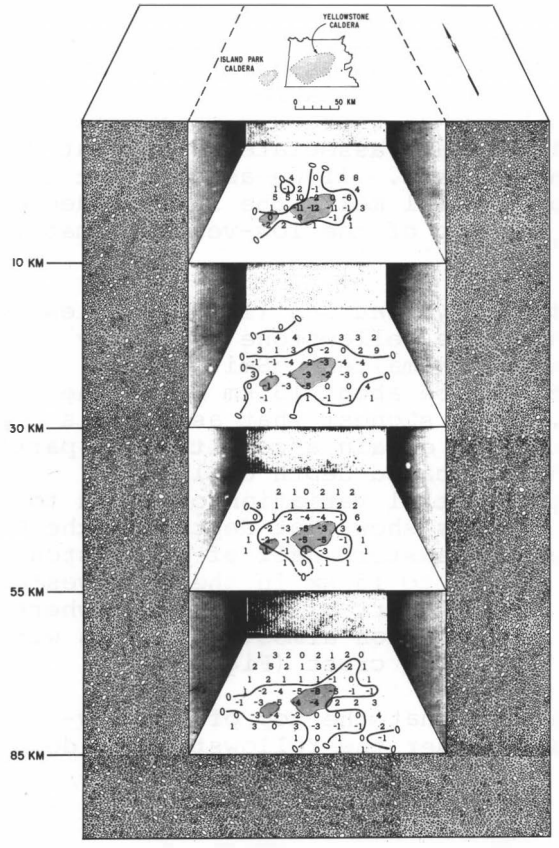

Fig. 6. A three-dimensional model for the crust and upper mantle in the Yellowstone region. The numbers show percentage variation of P-wave velocity from an average earth-model at four mean depths indicated along the ordinate. The 0% contour is shown at each level. An outline of Yellowstone National Park together with Yellowstone and Island Park caldera boundaries and the horizontal scale are shown at the surface. The vertical scale is arbitrary.

Figure 6 shows results of the three-dimensional inversion in the form of a shelf-diagram. The program computes horizontal variation of velocity in 4 layers located at depths 0 to 20, 20 to 40, 40 to 70, and 70 to 100 km. Velocity variations are plotted on horizontal "shelves" located at the mean depth of each layer. The numbers represent percentage change in velocity from the initial layer velocity. Because we are using relative residuals with respect to a reference residual obtained by averaging values from all stations for each event, the numbers do not reflect an absolute velocity change from any specific earth model. Thus, the zero

contour shown in the figure does not indicate that velocities are higher than the normal earth on one side and lower than normal on the other side in an absolute sense. Rather, it is only a guideline to indicate the relative changes in velocity occurring across the horizontal plane. The following observations can be made from Fig. 6.

(i) The highest velocity contrasts occur in the top 20 km of the crust as indicated by the values shown at the average level of 10 km in the shelf diagram. The velocities within the caldera seem to be less than the surrounding velocities by about 15¢.

(ii) Velocity contrast decreases to about 7% between 20 and 100 km depths.

(iii) The area within the zero contour, an approximate indicator of the horizontal size of the low-velocity body at various depths, seems to be much larger in the lower crust and upper mantle than the caldera size.

The results discussed above using the cross-section and shelf-diagrams (Figs. 5 and 6) taken together give us a conceptual picture of the shape and dimensions of the low-velocity body and the velocity contrast within it. One question we are unable to answer using teleseisms is the depth to the top of the low-velocity body. In the absence of a detailed refraction survey across Yellowstone, we can only speculate on this using other available geophysical data. Two lines of evidence are available to us. *Smith et al.* (1974) notice a lack of earthquakes at depths greater than 5 km under the Yellowstone caldera. *Pitt and Weaver* (oral communication) have not observed earthquakes deeper than 8 km. *Smith et al.* (1974) suggest that the absence of deeper earthquakes can be explained by abnormal pore pressures and temperatures favoring stable sliding instead of brittle fracture. It is quite possible that increased pore pressures are caused by a high degree of partial melt and associated fluids at depths greater than 5 km under the Yellowstone caldera. If we assume that the low-velocity body is a manifestation of partial melt, the lack of deeper earthquakes may be an indication that the top of the low-velocity material is located deeper than about 5 km.

Smith et al. (1974) and *Bhattacharyya and Leu* (1975) have estimated the depth to the Curie isotherm under the Yellowstone region by spectral analysis of residual aeromagnetic anomalies. Smith et al. estimate the depth of the Curie isotherm to be about 13 km below the surface under the Yellowstone caldera. They suggest that assuming a Curie Point temperature of 575°C it is possible to obtain a condition of partial melt for water-saturated granite at the indicated depth of 13 km. Bhattacharyya and Leu have contoured the spatial variation of depth to the Curie isotherm in Yellowstone. Their results show that depths to the Curie isotherm are 8 to 10 km in most of the southeastern half of Yellowstone National Park, including the caldera, and 10 to 15 km in the northwestern half. There is a clear region in the central part of the caldera where the isotherm is most shallow (7 to 9 km). This region almost coincides with the lower seismic velocities found in the upper crust (Fig. 6).

From the above studies we conclude that the top of the low-velocity body is at a depth of 5 to 13 km under the Yellowstone caldera.

The Geysers, California

The Geysers area is very interesting from several points of view. The Geysers-Clear Lake volcanic field is young (2.5 to 0.3 m/yr) and overlies rocks of the Franciscan assemblage and Great Valley sequence (*Hearn, Donnelly, and Goff*, 1976). The high heat flow in the region and presence of a large, almost circular, negative gravity anomaly have been interpreted as due to a shallow, crustal magma chamber (*Isherwood*, 1976). The Geysers is one of a few dry-stream geothermal systems in the world and the only place in the United States where electric power is being generated from geothermal energy.

Preliminary results using teleseismic residual data collected by a seismic network operated by U.S. Geological Survey indicate that delays greater than 1 sec may be present over The Geysers-Clear Lake volcanic field in the region defined by the gravity anomaly (*Iyer and Hitchcock*, 1975). The data are not adequate to delineate in detail the magma body if, indeed, the delays are due to a magma body. We have completed a detailed teleseismic survey using a portable network in the area to see if a magma chamber is present under The Geysers-Clear Lake volcanic field.

Interpretation

It is required to interpret a decrease of compressional velocity of about 10% in the upper crust in the case of Long Valley (and probably The Geysers) and in the lower crust and mantle in the case of Yellowstone. Wave velocities in rocks depend upon temperature, stress, mineralogy, chemistry, fabric, crack and pore properties, and the nature of fluid inclusions. Variation of any of these quantities will cause a velocity change. In estimating the extent to which these possible causes may actually account for observed velocity decreases, we consider first solid, uncracked or slightly cracked rocks.

The presence of extensive volcanism, surface geothermal phenomena, and high heat flow indicate that higher-than-normal tempratures are present under each of the geothermal areas discussed above. Measurements of temperature derivatives of compressional wave velocity in rocks and single crystals indicate that a 10% velocity decrease requires a temperature increase in excess of 1200°C (*Simmons and Wang*, 1971; *Anderson et al.*, 1968; *Stewart and Peselnick*, 1976; *Peselnick et al.*, 1977; *Fielitz*, 1971). Phase diagrams for lower crustal and upper mantle rocks (*Wyllie*, 1971) show that a temperature increase of this order would cause a large degree of melting in the crust and mantle. A maximum temperature increase of some 800°C above normal geothermal temperatures is permitted if melting is not to occur. Thus, no plausible case can be made for a 10% velocity decrease due strictly to temperature effects unaccompanied by melting. The sensitivity of velocity to stress is rather low in intact rocks and lower in single crystals. A negligible velocity change can be attributed to any plausible stress difference in the absence of cracking or recrystallization. We will deal with these phenomena below. Variations in mineralogy resulting in density changes and changes in chemistry as expressed by mean atomic weight changes will also affect velocity. These effects can be estimated using Birch's law (*Birch*, 1961). A 10% velocity decrease requires a density decrease of the order of 0.25 g/cm^3, or an increase of mean atomic weight of about 1.0, or some combination of the two. Density reduction would result in gravity decrease and an increase in elevation if isostatic compensation is complete. A density decrease of 0.25 g/cm^3

distributed over a body the size of the Yellowstone anomaly would result in a gravity decrease of several hundred mgal and an elevation increase approaching 10 km if compensation were complete. An elevation excess of 400 m and a Bouguer anomaly of -100 mgal have been observed in Yellowstone. At Long Valley a decrease in density of 0.25 g/cm^3 within the low-velocity zone (Fig. 3) would give rise to a gravity decrease of about 10 mgal, which is compatible with the observed anomaly attributable to a deep body (*Kane et al.*, 1976). Thus, the Yellowstone velocity anomaly cannot reasonably be attributed solely to density changes, while that of Long Valley perhaps can be. Insufficient data exist at this point to draw conclusions concerning density anomalies at The Geysers. As far as chemical changes are concerned, injection and subsequent solidification of basaltic magma could raise the mean atomic weight of graniitc rocks by 1 if almost total replacement occurred. Lower crustal rocks are commonly taken to be basaltic and would not suffer a change in chemistry because of intrusion of basaltic magma. The upper mantle, if it consisted of forsterite, would have to have added 50% by weight of basaltic material to have mean atomic weight change by one. Larger amounts of basaltic material would be required for peridotites. It should be remembered that mean atomic weight changes of 1 lead to velocity decreases of the required magnitude (10%) only if density is constant. Thus, the volume of basic material injected must not only be substantial; there must also be some process operating that prevents any increase in density associated with increased mean atomic weight. We know of no plausible combinations of mineralogical changes that will simultaneously cause higher mean atomic weight and/or decrease density throughout the wide range of temperatures, pressures, and compositions found in the mantle and crust. For this reason such changes seem an unlikely sole cause of the Yellowstone anomaly. On a more localized scale, such as at Long Valley, one may speculate that perhaps changes in mineralogy due to heating and fluid circulation have resulted in a velocity decrease. Preferred orientation of minerals in rocks can lead to velocity anisotropy exceeding 10% (*Birch*, 1960, 1961; *Peselnick et al.*, 1974). However, since there is strong evidence that the magnitude of the observed teleseismic delays are azimuthally independent, in order to explain the velocity anomaly, one requires an anisotropy figure symmetric about a vertical axis with velocity such that waves arriving nearly vertically have 10% lower velocity than waves that travel horizontally. In Yellowstone we have evidence from Nevada Test Site nuclear explosions that large delays are observed for seismic waves that travel at much shallower angles to the vertical than teleseisms (*C.S. Weaver*, oral communication). Hence anisotropy is an unlikely explanation for the observed anomaly.

The brief treatment above deals with uncracked or slightly cracked rock. It has been well established that introducing cracks or voids into an elastic matrix will lower velocity (*Birch*, 1960; *O'Connell and Budiansky*, 1974). Stresses associated with observed volcanism, combined with high fluid pressures in ascending liquids, may possibly contribute to cracking in rocks in the upper crust and could, perhaps, contribute to the Long Valley velocity anomaly. At greater depths, however, the high confining stress and temperatures present would seem likely to eliminate dry cracks through simple closure, creep and healing processes.

Partial Melting. Combinations of the effects mentioned above are, perhaps, quantitatively sufficient to account for the observed low-velocity anomalies. However, all of the effects of the recent volcanism in these areas depend upon transfer of hot, chemically reactive material from the mantle to the surface. In view of this it seems quite reasonable to explain the observed anomalies in terms of partial melting in the upper mantle and the injection of melt or associated fluids into the crust, particularly in the case of Yellowstone. Partial melting has been postulated

as the probable cause of the upper mantle seismic low-velocity zone by several authors (*Anderson and Sammis*, 1970; *Spetzler and Anderson*, 1968; *Hales and Doyle*, 1967). This mechanism seems to us the most direct, simple, and plausible mechanism to explain observed P-wave velocity decreases.

Even though experimental data on velocity in partially melted rocks are scarce, the qualitative behavior of seismic waves in partially melted rocks is fairly well understood. Partially melted and saturated media can be considered as two-phase aggregates. *Gassman* (1951) and *Biot* (1956) developed equations for wave velocity and attenuation in a porous elastic medium in which fluid may flow between pores. In another approach to understanding elastic properties of two-phase aggregates *Eshelby* (1957) considered the effect of introducing an inclusion into a solid medium. He showed that inclusions of ellipsoidal shape produced effects that could be calculated with relative ease. The concepts introduced by Biot and Eshelby have been amplified by many workers (*O'Connell and Budiansky*, 1974; *Geertsma and Smit*, 1961; *Kuster and Toksoz*, 1974a,b; *Walsh*, 1968, 1969; *Wu*, 1966). The important inference that can be made from available information is that different theories arrive at many similar conclusions that are important with respect to partially melted rock. In particular, wave velocity and attenuation in a solid medium with liquid inclusions are predicted to depend upon the wave velocity of the solid, compressibility and viscosity of the fluid, the relative volume of the fluid, the shapes of the fluid inclusions, and the frequency of the elastic wave. The exact effect of any one of these quantities upon seismic wave propagation depends upon the value assigned to each quantity, but the following generalizations can be made. Wave velocity in the aggregate varies *directly* with wave velocity in the solid, *inversely* with fluid compressibility, *inversely* with fluid concentration and flatness of the fluid inclusions. Tests of the theoretical predictions have been made by several laboratory experiments. The largest body of experimental data results from examining the role of water and hydrocarbons in porous rocks (*Hughes and Cross*, 1951; *Hughes and Kelly*, 1952; *Wyllie et al.*, 1956, 1958).

The results for saturated rocks in general agree with theoretical predictions and enable us to interpret results in partially melted systems. Melting experiments are hampered by difficulties inherent in simultaneous high temperature, high pressure measurements. As a result most work has been done on non-geologic systems at relatively low temperature, and high pressure has generally been avoided. *Takeuchi and Simmons* (1973) investigated compressional and shear velocities in rocks saturated with ice and water with confining pressures to 2 kb. Small concentrations (1%) of flat cracks lead to a velocity decrease of 3 to 6% for compressional waves and 3 to 9% for shear waves as the water in the cracks passed from solid to liquid. *Spetzler and Anderson* (1968) investigated partial melting in brine systems. They found that 3.5% liquid by volume leads to a decrease of 9.5% in compressional velocity and 13.5% in shear velocity and that 7% of liquid cause corresponding decreases of 28% and 40%. Melting and Woods' metal has been investigated by *Mizutani and Kanamori* (1964). The sample was of eutectic composition and quantitative relations between melt volume and velocity were undetermined. It was found that compressional velocity rapidly decreased by 10% and shear velocity by 40% as the melting point was approached. The total decrease in compressional velocity upon complete melting was 20%. *Pokorny* (1965) also reported results for Woods' metal whose composition was not specified but was not eutectic. The onset of melting produced a sharp compressional velocity decrease and a peak in attenuation of compressional waves. *Stocker and Gordon* (1975) examined the effects of partial melting in Cu-Pb and Cu-Ag alloys of varying composition. Sharp velocity decrease was observed at the eutectic temperature

for each alloy as melting occurred. They showed that velocity and attenuation in their partially melted alloys were functions of volume fraction of melt and melt-pocket geometry. *Murase and McBirney* (1973) measured compressional and shear velocities, attenuation, viscosity, and density in several rocks passing through melting. The behavior of velocity is quite similar to that described for systems above. As partial melting commences, shear and compressional velocities decrease rapidly. No estimate could be made of the relative volume of fluid at a given temperature. Thus, for a wide spectrum of materials experiments have demonstrated qualitatively similar behavior of wave velocity when fluid inclusions are introduced. The common effect of partial melting in materials is to rapidly decrease velocity, and the studies of velocity in water saturated rocks indicate that the process is dominated by the presence of small volumes of fluid in flat inclusions. Consistency from experiment to experiment and agreement between theory and observation is less pronounced in the case of attenuation measurements. In summary it can be said that the behavior of velocity in partially melted systems is qualitatively well understood, while attenuation is less so, and that data on physical properties of rocks and their melts at high pressure would be welcome for quantitative purposes.

The question arises, is it possible to compute the percentage of partial melt using measurements of P-wave velocity decrease? *Anderson et al.* (1972) using *Walsh's* (1969) equations for elastic wave velocities in a two-phase material composed of randomly oriented, penny-shaped partially melted zones, plotted curves for compressional and shear velocities as a function of melt concentration for various aspect ratios of the zones. The material was supposed to be solid olivine matrix containing ellipsodial pockets of basalt melt. Since we have only P-wave measurements, it can be seen from the curves (see their Fig. 6) that aspect ratio is a critical factor, and estimates of partial melt percent can vary by almost two orders of magnitude for a given velocity contrast. However, if it is possible to obtain P-wave and shear-wave measurements simultaneously, theories such as the above can be used to estimate percentage of partial melt. An ideal seismic experiment designed towards partial melt estimations should involve velocity and attenuation measurements of P and S waves.

Conclusions

Presence of positive P-wave residuals (delays) of about 0.5 sec in Long Valley caldera and their spatial variation have been interpreted as evidence for the presence of a low-velocity body under the central part of the caldera. The body is approximately a sphere of about 14 km radius, and its top is at a depth of 7 km from the surface.

In Yellowstone large delays are seen within the caldera and somewhat smaller delays are seen outside the caldera as far as 100 km away from the boundary. Qualitative interpretation of these delays is consistent with the existence of a deep, low-velocity body extending to a depth of 150 to 250 km fron the surface. A quantitative inversion of the teleseismic residual data shows that a 15 to 20% decrease of compressional velocity may be present in the upper crust, the contrast decreasing to about 3 to 5% in the upper mantle. The horizontal dimensions of the low-velocity body are about the same as those of the caldera at the top but may be much larger at depth.

Preliminary P-residual results from The Geysers-Clear Lake volcanic field show that a low-velocity body may be present underneath the area as well.

Compressional wave velocity decrease can be caused by various factors. Our preferred explanation, in view of the high heat flow and evidence for vertical transport of magma in these areas, is that the velocity decrease is caused by partial melt. It is not possible to uniquely determine the degree of partial melt using P-wave data alone. However, the teleseismic delay data provides an important clue in understanding the size and shape of magma bodies in geothermal areas.

Acknowledgements

The authors are indebted to their colleagues, John Coakley and Jeffrey Roloff for doing the field work; John Evans and Tim Hitchcock for processing the data; George Zandt for computing a three-dimensional velocity model for Yellowstone using a matrix inversion program; and Craig Weaver and Bill Bakun for their critical review of the manuscript.

References

Aki, K., A. Christoffersson, and E.S. Husebye, Determinations of the three-dimensional seismic structure of the lithosphere, *J. Geophys. Res.*, *82*, 277-296, 1977.

Anderson, D.L., and C. Sammis, Partial melting in the upper mantle, *Phys. Earth Planet. Interiors*, *3*, 41-50, 1970.

Anderson, D.L., C. Sammis, and T. Jordon, Composition of the mantle and core, in *The Nature of the Solid Earth*, edited by E.C. Robertson, McGraw-Hill, New York, 41-66, 1972.

Anderson, O.L., E. Schreiber, and R.C. Lieberman, Some elastic sonstant data on minerals relevant to geophysics, *Rev. Geophys.*, *6*, 491-524, 1968.

Armstrong, R.L., W.P. Leeman, and H.E. Malde, K-Ar dating, Quaternary and Neogene volcanic rocks in the Snake River Plain, Idaho, *Am. J. of Science*, *275*, 255-261, 1975.

Bailey, R.A., G.B. Dalrymple, and M.A. Lamphere, Volcanism, structure and geochronology of Long Valley caldera, Mono County, California, *J. Geophys. Res.*, *81*, 725-744, 1976.

Bhattacharyya, B.K., and L. Leu, Analysis of magnetic anomalies over Yellowstone National Park: Mapping of Curie Point isothermal surface for geothermal reconnaissance, *J. Geophys. Res.*, *80*, 4461-4465, 1975.

Biot, M.A., Theory of propagation of elastic waves in a fluid-saturated porous solid. I. Low-frequency range, *J. Accous. Soc. Amer.*, *28*, 168, 1956.

Birch, F., The velocity of compressional waves in rocks to 10 kilobars, part 1, *J. Geophys. Res.*, *65*, 1083-1102, 1960.

Birch, F., The velocity of compressional waves in rocks to 10 kilobars, part 2, *J. Geophys. Res., 66*, 2199-2224, 1961.

Bolt, B.A., and O.W. Nuttli, P-wave residuals as a function of azimuth, 1. Observations, *J. Geophys. Res., 71*, 5977-5985, 1966.

Christiansen, R.L., and H.R. Blank, Jr., Volcanic stratigraphy of the Quaternary rhyolite plateau in Yellowstone National Park, *U.S. Geological Survey Professional Paper 729-B*, U.S. Government Printing Office, Washington, D.C., 18 p., 1972.

Eaton, G.P., R.L. Christiansen, H.M. Iyer, A.M. Pitt, D.R. Mabey, H.R. Blank, Jr., I. Zietz, and M.E. Gettings, Magma beneath Yellowstone National Park, *Science, 188*, 787-796, 1975.

Eshelby, J.D., The determination of the elastic field of an ellipsoidal inclusion and related problems, *Proc. Roy. Soc. London, A, 241*, 376-396, 1957.

Fielitz, K., Elastic wave velocities in different rocks at high pressure and temperatures up to 750°C, *Zeit. für Geophys., 37*, 943-956, 1971.

Fournier, R.O., D.E. White, and A.H. Truesdell, Convective heat flow in Yellowstone National Park, *Proceedings of the Second United Nations Symposium on the Development and Use of Geothermal Resources, 1*, U.S. Government Printing Office, Washington, D.C., 731-739, 1976.

Gassman, F., Ueber die elastizität poröser medien, *Vierteljahrsschrift der Naturforschenden Gesellschaft in Zürich, 1*, 1951.

Geertsma, J., and D.C. Smit, Some aspects of elastic wave propagation in fluid-saturated porous solids, *Geophysics, 26*, 169-191, 1961.

Hales, A.L., and H.A. Doyle, P and S travel time anomalies and their interpretation, *Geophys. J.R. Astr. Soc., 13*, 403-415, 1967.

Hales, A.L., and E. Herrin, Travel times of seismic waves, in *The Nature of the Solid Earth*, edited by E.C. Robertson, McGraw-Hill, New York, 172-215, 1972.

Hearn, B.C., J.M. Donnelly, and F.E. Goff, Geology and geochronology of the Clear Lake volcanics, California, *Proceedings of the Second United Nations Symposium on the Development and Use of Geothermal Resources, 1*, U.S. Government Printing Office, Washington, D.C., 423-428, 1976.

Herrin, E., Seismological tables for P, *Bull. Seism. Soc. Am., 58*, 1196-1219, 1968a.

Herrin, E., P-wave velocity distribution in the mantle, *Bull. Seism. Soc. Am., 58*, 1223-1225, 1968b.

Hill, D.P., Structure of Long Valley caldera, California, from a seismic refraction experiment, *J. Geophys. Res., 81*, 745-753, 1976.

Hughes, D.S., and J.H. Cross, Elastic wave velocities in rock at high pressures and temperatures, *Geophysics, 16*, 577-593, 1951.

Hughes, D.S., and J.L. Kelly, Variation of elastic wave velocity with saturation in sandstone, *Geophysics, 17*, 739-752, 1952.

Isherwood, W.F., Gravity and magnetic studies of The Geysers-Clear Lake geothermal region, California, USA, *Proceedings of the Second United Nations Symposium on the Development and Use of Geothermal Resources, 2*, U.S. Government Printing Office, Washington, D.C., 1065-1073, 1976.

Iyer, H.M., Anomalous delays of teleseismic P-waves in Yellowstone National Park, *Nature, 253*, 425-427, 1975.

Iyer, H.M., and J.H. Healy, Teleseismic residuals at the Lasa-USGS extended array and their interpretation in terms of crust and upper-mantle structure, *J. Geophys. Res., 77*, 1503-1527, 1972.

Iyer, H.M., and T. Hitchcock, Teleseismic residuals at The Geysers geothermal area (abstract), *EOS Trans. Am. Geophys. Union, 56*, 1020, 1975.

Kane, M.F., D.R. Mabey, and R. Brace, A gravity and magnetic investigation of the Long Valley caldera, Mono County, California, *J. Geophys. Res., 81*, 754-762, 1976.

Kubota, S., and E. Berg, Evidence for magma in the Katmai volcanic range, *Bull. Volcanology, 31*, 175-214, 1967.

Kuster, G., and M.N. Toksoz, Velocity and attenuation of seismic waves in two-phase media: Part 1. Theoretical Formulation, *Geophysics, 39*, 587-606, 1974a.

Kuster, G., and M.N. Toksoz, Velocity and attenuation of seismic waves in two-phase media: Part 2. Experimental Results, *Geophysics, 39*, 607-618, 1974b.

Lachenbruch, A.H., J.H. Sass, R.J. Munroe, and T.H. Moses, Jr., Geothermal setting and simple heat conduction models for the Long Valley caldera, *J. Geophys. Res., 81*, 769-784, 1976.

Matumoto, T., Seismic body waves observed in the vicinity of Mount Katmai, Alaska, and evidence for the existence of molten chambers, *Geol. Soc. Am., Bull., 82*, 2905-2920, 1971.

Mizutani, H., and H. Kanamori, Variation of elastic wave velocity and attenuative property near the melting temperature, *J. Phys. Earth, 12*, 43-49, 1964.

Morgan, P., D.D. Blackwell, R.E. Spafford, and R.B. Smith, Evidence from heat-flow measurements for laterally extensive geothermal fluid systems in the Yellowstone caldera, Yellowstone National Park, Wyoming, USA, *Proceedings of the Second United Nations Symposium on the Development and Use of Geothermal Resources, 2*, U.S. Government Printing Office, Washington, D.C., 1155-1159, 1976.

Murase, T., and A.R. McBirney, Properties of some common igneous rocks and their melts at high temperatures, *Bull. Geol. Soc. Amer., 84*, 3563-3592, 1973.

O'Connell, R.J., and B. Budiansky, Seismic velocities in dry and saturated cracked solids, *J. Geophys. Res., 79*, 5412-5426, 1974.

Peselnick, L., J.P. Lockwood, and R. Stewart, Anisotropic elastic velocities of some upper mantle xenoliths underlying the Sierra Nevada batholith, *J. Geophys. Res.*, *82*, 2005-2010, 1977.

Peselnick, L., A. Nicolas, and P.R. Stevenson, Velocity anisotropy in a mantle peridotite from the Ivrea Zone: Application to upper mantle anisotropy, *J. Geophys. Res.*, *79*, 1175-1182, 1974.

Pokorny, M., Variation of velocity and attenuation of longitudinal waves during the solid-liquid and liquid-solid transition in Wood's alloy, *Studia Geoph. et Geod.*, *9*, 250-258, 1965.

Simmons, G., and H. Wang, *Single Crystal Elastic Constants and Calculated Aggregate Properties*, MIT Press, Cambridge, Mass., 1971.

Smith, R.B., R.T. Shuey, R.O. Freidline, R.M. Otis, and L.B. Alley, Yellowstone hot spot: New magnetic and seismic evidence, *Geology*, *2*, 451-455, 1974.

Spetzler, H., and D.L. Anderson, The effect of temperature and partial melting on velocity and attenuation in a simple binary system, *J. Geophys. Res.*, *73*, 6051-6060, 1968.

Steeples, D.W., and H.M. Iyer, Low-velocity zone under Long Valley as determined from teleseismic events, *J. Geophys. Res.*, *81*, 849-860, 1976a.

Steeples, D.W., and H.M. Iyer, Teleseismic P-wave delays in geothermal exploration, *Proceedings of the Second United Nations Symposium on the Development and Use of Geothermal Resources*, *2*, U.S. Government Printing Office, Washington, D.C., 1199-1206, 1976b.

Stewart, R., and L. Peselnick, Compressional and shear velocities in westerly granite at high pressure and temperature (abstract), *EOS, Trans. Am. Geophys. Union*, *57*, 1001, 1976.

Stocker, R.L., and R.B. Gordon, Velocity and internal friction in partial melts, *J. Geophys. Res.*, *80*, 4828-4836, 1975.

Takeuchi, S., and G. Simmons, Elasticity of water-saturated rocks as a function of temperature and pressure, *J. Geophys. Res.*, *78*, 3310-3320, 1973.

Tryggvason, E., Arrival times of P waves and upper mantle structure, *Bull. Seism. Soc. Am.*, *54*, 727-736, 1964.

Utnasin, V.K., A.I. Abdurakhmanov, G.I. Anosov, Yu. A. Budyansky, V.I. Fedorchenko, and Ye. K. Markhinin, Types of magma foci of island arc volcanoes and their study by the method of deep seismic sounding in Kamchatka, in *Volcanoes and Tectonosphere*, edited by Hitoshi Aoki and Susumu Iizuka, Tokai University Press, Japan, 123-137, 1976.

Walsh, J.B., Attenuation in partially melted material, *J. Geophys. Res.*, *73*, 2209-2216, 1968.

Walsh, J.B., New analysis of attenuation in partially melted rock, *J. Geophys. Res.*, *74*, 4333-4337, 1969.

Wu, T.T., The effect of inclusion shape on the elastic moduli of a two-phase material, *Int. J. Solids Structures*, *2*, 1-8, 1966.

Wyllie, M.R.J., A.R. Gregory, and L.W. Gardner, Elastic wave velocities in heterogeneous and porous media, *Geophysics*, *21*, 41-70, 1956.

Wyllie, M.R.J., A.R. Gregory, and G.H.F. Gardner, An experimental investigation of factors affecting elastic wave velocity in porous media, *Geophysics*, *23*, 459-493, 1958.

Wyllie, P.J., Experimental limits for conditions for melting in the earth's crust and upper mantle, in *The Structure and Physical Properties of the Earth's Crust*, edited by J.G. Heacock, Geophysical Monograph 14, American Geophysical Union, Washington, D.C., 279-302, 1971.

Nd ISOTOPIC CONSTRAINTS ON THE PARTIAL MELTING HISTORY OF THE MANTLE AND BASALT PETROGENESIS

D.J. DePaolo and G.J. Wasserburg
Division of Geological and Planetary Sciences
California Institution of Technology
Pasadena, California 91125

The decay of ^{147}Sm to ^{143}Nd ($\tau 1/2 = 1.06 \times 10^{11}$ yr) causes $^{143}Nd/^{144}Nd$ in a rock reservoir to increase with time at a rate proportional to its Sm/Nd. Rock types representative of the crust and mantle have widely varying Sm/Nd and therefore presently possess characteristic $^{143}Nd/^{144}Nd$. Thus $^{143}Nd/^{144}Nd$ of young igneous rocks can indicate if they are derived from the crust or mantle. Recent mantle-derived rocks can be used to study variations of $^{143}Nd/^{144}Nd$ in the mantle, and thereby determine its chemical structure and the time that heterogeneities formed.

$^{143}Nd/^{144}Nd$ and Sm/Nd have been measured in young basalts and in granitic crustal rocks with ages up to 3.6 AE. Measured $^{143}Nd/^{144}Nd$ are given here as fractional deviations in parts in 10^4 (ε_o^{CHUR}) from the value expected in a chrondritic Sm/Nd reservoir today. A value of $\varepsilon_o^{CHUR} = 0$ in a rock of zero age indicates that it has been derived from a source which has remained unfractionated relative to chrondrites over the history of the earth. $\varepsilon_o^{CHUR} > 0$ indicates a source with Sm/Nd higher than chrondritic, and $\varepsilon_o^{CHUR} < 0$ indicates a source with Sm/Nd lower than chrondritic.

ε_o^{CHUR} of young basalts ranges from 0 to +10, and is drastically different from that of ancient continental crustal material. A composite of North American shale has $\varepsilon_o^{CHUR} = -14.4$ while Archean granitic rocks fall in the range -25 to -40. Variations of $^{143}Nd/^{144}Nd$ in young basalts indicate that significant differences of Sm/Nd are preserved in the mantle for times > 1 AE. Oceanic tholeiitic basalts are derived from mantle which is distinct from that yielding oceanic alkali basalts; and there is indication that the mantle beneath oceanic areas is grossly different from that underlying the continents. Continental basalt has $\varepsilon_o^{CHUR} = 0$, consistent with deviation directly from mantle with chrondritic Sm/Nd. Oceanic tholeiites have $\varepsilon_o^{CHUR} \approx +10$, indicating that the mantle from which they are derived has had Sm/Nd $\sim$ 10% greater than chrondritic averaged over the age of the earth. The chemical layering of the mantle indicated by these data may have formed very early in the earth's history or it may have evolved gradually as a result of continuing large-scale differentiation processes such as upward transport of material to form continental crust. This problem will be discussed in light of the Nd isotopic data, which may place strict limits on the timing of mantle differentiation.

Alkali basalts and nephelinities have REE patterns which are highly fractionated relative to chrondrites. It has been suggested that they may be derived from unique mantle regions which are themselves highly fractionated. If alkali basalt is derived from an ancient, fractionated mantle source, then it would be expected to have a large negative ε_o^{CHUR} similar to that of North American shale. Alkali basalt from the mid-Atlantic ridge, however, has $\varepsilon_o^{CHUR} = +5.4$, indicating that it has been derived from a source with an essentially chrondritic REE pattern. Thus the REE patterns of these basalts must be the result of fractionation occurring during partial melting and extraction of the melts from the mantle.

THE GENERATION OF ULTRAMAFIC AND TRONDHJEMITIC MAGMAS ALONG THE EASTERN MARGIN OF THE SOUTHERN APPALACHIAN BLUE RIDGE

Jeffrey Greenberg and Stephen Kish
Department of Geology
University of North Carolina
Chapel Hill, North Carolina 27514

Since the late Precambrian rifting of the southern Appalachian Blue Ridge, this region was affected by two separate episodes of magmatic activity. One was related to the rifting and involved the ascent of ultramafics from the mantle, and the other, coming much later, resulted from crustal convergence producing high soda granitic intrusions. At present, these intrusions are represented by two belts; that of the ultramafics extends from Alabama to Maryland and lies to the northwest of the felsic pluton belt. Dunites, peridotites, and more altered lithologies such as serpentinite and soapstone are included in the hundreds of Blue Ridge ultramafics. The linear trend of the felsic plutons contains outcrops from central Alabama through central Virginia and includes large trondhjemite-granodiorite bodies as well as associated dikes and sodic pegmatites.

Attenuation and the ultimate rupture of the Blue Ridge 700 or 800 my ago allowed the formation and ascent of ultramafic diapirs to a position in the lower crust. Y olivine petrofabrics, igneous flow and recrystallization textures, and isoclinal folding support the diapiric mode of intrusion. As a consequence of flow, any possible cumulative textures were obliterated. Many of the peridotites are characterized by the association of forsterite (Fo_{92} average) with variable amounts of chromium-diopside and bronzeite (En_{95} average). High Cr/Al spinel is a minor constituent. Mineral paragenesis indicates early crystallization of the peridotites under spinel lherzolite conditions with subsequent changes occurring as plagioclase lherzolite stability is attained. In the specific case of the Webster-Addie dunite, incipient partial fusion of spinel lherzolite is exemplified by clinopyroxenite melt veinlets which have intruded across the primary flow lamination.

Associated with some of the better preserved ultramafic masses are marginal rims of amphibolite, troctolite, and forsterite-amphibole-plagioclase rock. Because previous ideas have held that the southern Appalachian ultramafites existed as deformed ophiolites, the plagioclase and amphibole bearing margins were considered as gabbroic portions of ophiolites. It is more likely that the mineralogy and small volume of these rocks represent outer zones of relatively low temperature, hydrous crystallization. No evidence currently exists for the production of volcanism consanguineous with the intrusion of ultramafic material. However, if the intrusions were indeed generated during rifting, then they may be related to parental material of the Catoctin rift volcanics and associated felsic plutons.

It was apparently not until the general time of tectonic deformation that the ultramafics were emplaced into late-Precambrian clastics and

alongside the basement gneisses. Their present tectonic position is not far removed horizontally from the original fracture line of intrusion.

Tectonic deformation intensified after ultramafic emplacement and culminated in a dynamothermal peak during which a great volume of high sodium felsic magma was intruded through deformed metasediments. It is odd that no more mafic or more potassic igneous lithologies of the same age exist in the region. In addition, no volcanics are now preserved from the Taconic subduction episode. However, Ordovician bentonites are found in the foreland sedimentary units of the folded Appalachians.

A majority of the rock types of the sodic series have Rb-Sr ages in the range of 390-450 my. All samples with the exception of a few pegmatites possess low Sr^{87}/Sr^{86} initial ratios (.704 - .706). This fact, together with the linear arrangement of the plutonic bodies, leads to the conclusion that these rocks were the result of partial melting of subducted "oceanic" material of quartz tholeiite composition. It is conceivable that a rather small degree of partial melting of quartz normative eclogite under mantle pressures could produce the high sodium, low calcium and low potassium bulk chemistries observed. The eclogite mineralogy also might explain the retention of mafic components from the crystallizing melt.

THEORETICAL AND EXPERIMENTAL ASPECTS OF PARTIAL MELTING

M.J. O'Hara
Grant Institute of Geology
University of Edinburgh
Edinburgh, Scotland EH9 3JW

Concepts which are important to the interpretation of field relationships in peridotite complexes which have undergone partial melting are listed and methods of establishing the compositions of the liquids extracted are summarized. Potentially confusing chemical and field relationships may result from interactions between residual peridotites and the partial melts as they cool. Fossilized partial melting processes from constructive and destructive plate margins, and several mid-plate environments, are reviewed together with the evidence they yield about extent of melting and magmas produced.

A COMPARISON OF PARTIAL MELTING PROCESSES BENEATH HAWAII AND THE SOUTHERN RIO GRANDE RIFT

J.B. Reid, Jr.
Q21, LASL
Los Alamos, New Mexico 87545

G.A. Woods
School of Natural Sciences
Hampshire College
Amherst, Massachusetts 01002

Large suites of spinel lherzolite inclusions from Salt Lake Crater, Hawaii, and Kilbourne Hole, New Mexico, have been analyzed in detail for the major elements of their four phases, and for their modal compositions.

The nodules of each suite were divided into three groups -- "undepleted parent"(A), "intermediate"(B), and "refractory residue"(C) -- on the basis of $Cr/(Cr+Al+Fe^{+3})$ spinel, a parameter shown to be a highly sensitive measure of a rock's relative degree of depletion in fusible constituents (*Reid*, 1972, E&S, *53*, 536). Average bulk compositions for groups A, B and C have been used to determine hypothetical melt compositions as functions of the percentage of partial melting, and the choice of parent and residue materials. The remarkably close similarities between the continental and oceanic settings are shown in the following table. Columns 3 and 6 show that similar olivine tholeiites could be produced with similar degrees of partial melting in each case.

	Kilbourne Hole			Salt Lake Crater		
	A	C	melt 22% A-C	A	C	melt 24% A-C
SiO_2	44.50	44.28	45.23	44.41	43.44	47.04
TiO_2	.11	.01	.45	.08	.03	.24
Al_2O_3	3.54	1.02	12.44	3.72	.99	12.13
Cr_2O_3	.43	.54	.05	.54	.50	.66
FeO	8.16	7.52	10.40	8.09	7.52	9.79
MnO	.12	.10	.18	.08	.08	.08
MgO	39.17	45.41	17.03	39.47	46.46	17.52
CaO	3.62	1.01	12.85	3.26	.68	11.20
Na_2O	.35	.07	1.36	.39	.08	1.34
Total	100.00	99.96	99.99	100.04	99.79	100.00
olivine	60	74		60	75	
opx	20	22		24	21	
cpx	18	3		13	3	
spinel	2	1		3	1	

OXYGEN FUGACITY OF THE MANTLE ENVIRONMENT

Motoaki Sato
U.S. Geological Survey
959 National Center
Reston, Virginia 22092

Knowledge of the range of oxygen fugacities prevailing in the upper mantle is essential in conducting partial melting experiments designed to simulate magma generation. Results of the direct determination of the intrinsic oxygen fugacities of minerals of mantle origin by the solid-electrolyte method indicate that these minerals probably formed in a reducing environment where graphite was stable. In some cases, the presence of submicroscopic graphite trapped within a mineral was indicated by a slow downward shift of $\underline{f}O_2$ at temperatures above 1100°C. The auto-reduction pattern was duplicated by adding a minute quantity of synthetic graphite to silicates formed in the upper crust, which normally do not show the reduction behavior.

In view of the measured $\underline{f}O_2$ values of mantle minerals, common occurrence of graphite or diamond in kimberlite-type nodules, predominance of CO_2 in fluid inclusions found in mantle-derived minerals, and the low solubility of CO_2 relative to the solubility of H_2O in magmatic melts, I propose that the oxygen fugacity of the upper mantle is essentially buffered by the graphite-CO_2 system. With increasing depth, eventually the diamond-carbonate system would replace the graphite-CO_2 system.

Partial melting of the mantle buffered by the graphite-CO_2 system would produce a magma of low Fe^{3+}/Fe^{2+} ratio. The reaction of C with H_2O during the ascent of the magma would produce CO_2 and H_2. Hydrogen would escape rapidly toward the surface because of its very high mobility, whereas less mobile CO_2 would largely be suspended in the magma as highly compressed bubbles and be partly trapped as fluid inclusions in liquidus minerals. Hydrogen would continue to escape even after carbon is exhausted, as H_2 can be produced also by the thermal dissociation of H_2O, thus accounting for the origin of most of the Fe^{3+} in a terrestrial magma. The hydrogen loss would also account for the undersaturation of magma with respect to H_2O in some cases. The strong contrast in the oxidation state between terrestrial magmas and lunar magmas can be explained by assuming that H_2O was scarce in the lunar interior and that the reduction by carbon predominated over the oxidation by hydrogen loss in the dry lunar magma in spite of probable similarity in $\underline{f}O_2$ in the source regions.

LITHOLOGIC DIVERSITY AND PARTIAL FUSION IN THE RED MOUNTAIN, NEW ZEALAND ALPINE PERIDOTITE

John M. Sinton
Smithsonian Institution
Washington, DC 20560

Olivine-orthopyroxene assemblages in the Red Mountain alpine peridotite range from dunite to olivine-orthopyroxenite with accessory Cr-spinel (1-3 vol. %) and clinopyroxene (1-5 vol. %). Compositional layering is locally well-developed; elsewhere only a pyroxene foliation is preserved. Mg/Fe of silicates and spinels increases with olivine/pyroxene ratio regardless of position in the mass. The main compositional variations are in Al_2O_3 (opx: 0.9-3.6 wt.%; cpx: 1.0-3.5 wt.%; spinel: 11-45 wt.%) and Cr_2O_3 (opx: 0.1-0.8 wt.%); cpx: 0.2-1.2 wt.%; spinel: 26-62 wt.%). (Al)px varies sympathetically with (X_{Al}) spinel but these variables can be shown to be functions of T, possibly of P, and also of bulk compositional variations, where T and P refer to conditions of subsolidus equilibration. However, layering and other bulk compositional variations are pre-equilibration in origin and probably formed during partial fusion.

Some of the layering is clearly secondary in origin; partially transposed earlier orientations are locally preserved. Microtextures are cataclastic or recrystallized, with the most pervasive cataclasis in pyroxenite layers. The evidence is consistent with an origin of the layering by forceful segregation of pyroxene in near solid peridotite. Differential movement within the peridotite mass facilitated layer formation and consequent squeezing off of interstitial liquid. The lithologic diversity at Red Mountain can be accounted for by two processes operating during partial fusion: (1) a physico-chemical process whereby different degrees of partial melting left a residuum variably depleted in Ca, Na and Ti, and (2) a mechanical process which tended to segregate olivine from pyroxene within the mass.